Design, Synthesis and Applications of Three-Dimensional Building Blocks for Fragment-Based Drug Discovery

Stephen Y. Yao

Doctor of Philosophy

University of York

Chemistry

September 2023

Abstract

Chapter 1 provides an overview of fragment-based drug discovery and its role in the development and discovery of pharmaceutical agents. In Chapter 2, the design and synthesis of an initial set of 3-D cyclopropyl building blocks **A**–**C** are described. Key features include the addition of a cyclopropane, a BMIDA group and a Boc-protected amine moiety, with the overall structure of building blocks following Astex's 'rule of two'. Next, Chapter 3 details the application of the 3-D cyclopropyl building blocks by demonstrating the scope of the Suzuki-Miyaura cross-coupling reaction to medicinally relevant fragment-like aryl or heteroaryl bromides. The functionalisation at the amine moiety is carried out in the synthesis of methanesulfonamides, such that the elaboration vectors of 3-D cyclopropyl building blocks could be determined using X-ray crystallography. Chapter 4 investigates the design and attempted synthesis of a second generation cyclobutyl 3-D building block **D**.

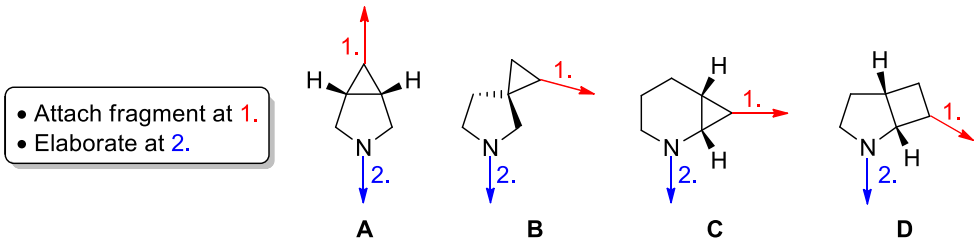

The next part of the thesis details the potential use of 3-D cyclopropyl building blocks in the generation of covalent fragments. A summary of covalent groups in drug development is provided in Chapter 5. This chapter also includes the preliminary studies for generating a library of covalent fragments using 3-D cyclopropyl building blocks. Finally in Chapter 6, the synthesis of JAK3 inhibitors *via* scaffold hopping using 3-D cyclopropyl building blocks is presented. The results from this chapter were formulated from a collaborative effort between researchers at AstraZeneca and the O'Brien group. Overall, compound **E** was designed and synthesised; compound **E** had nanomolar potency which rivals that of a licenced drug (Litfulo™).

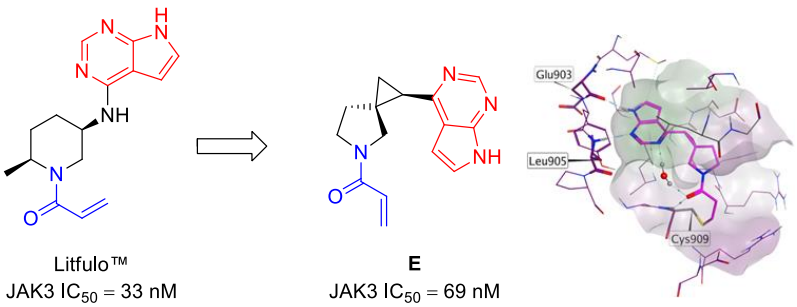

Table of Contents

List of Tables

List of Figures

Acknowledgements

The completion of this PhD thesis has been a tremendous journey, and it is with immense gratitude that I acknowledge the many individuals and institutions that have supported me along the way. This work represents not just my own efforts but also the collective contributions of several colleagues throughout the duration of my PhD.

First and foremost, I would like to thank Dr Anthony Wild and the Department of Chemistry at the University of York for funding my PhD through the Platinum Wild Scholarship. My academic journey would not have been possible without the steadfast financial support. I am also grateful to the University's administrative staff, especially Rachel Crooks, Alice Duckett, Sharon Stewart, and the rest of the Chemistry Graduate Office, for their efficiency, patience, and continuous assistance.

I would also like to express my gratitude to Professor Ian Fairlamb as my IPM who has greatly supported me through all of my TAP meetings. Their insightful feedback, constructive critique, and generous investment of time have been instrumental in refining the quality and depth of my research. My gratitude also extends to Dr. Adrian Whitwood and Theo Tanner for their support in X-ray crystallography.

Beyond the academic and professional sphere, I want to extend my heartfelt gratitude to my immediate family: Li Zhang, Katie Zhang, and Johnny Ooi. Their unwavering belief in me and their support and patience in allowing me to move to the UK to study for a postgraduate degree, I will be forever grateful. Their sacrifices and understanding have made it possible for me to focus on my studies and research with the peace of mind that comes from knowing I am supported at home.

Next, I would like to extend a heartfelt acknowledgment to my current partner Chloe Howman, whom I met during my PhD in the O'Brien group. I thank them for their encouragement, support, and company throughout a significant part of my PhD.

I owe a profound debt of gratitude to my fellow colleagues and lab mates who have been my companions throughout various points of this academic journey. The exchange of ideas, shared experiences, scientific discussions, social events, conferences, night outs, lab music, and board games within our research group have not only fostered a vibrant and intellectually stimulating environment but have also played a pivotal role in the memories I take away from my PhD experience. To this end, I would like to thank

Andres Gomez Angel, Matthew Gill, Giordaina Hartley, Ben Trowse, Lucy Tomczyk, Hannah Smith, Stuart McHale, Hannah Kemp, Will Butler, Hanna Klein, Jake Walder, Tom Downes, Nico Seling and Xinyu Wang. Their camaraderie and unwavering support have made the hours in the laboratory and technical challenges of chemistry much more manageable. Of course, my acknowledgments extends to non- and 'part-time' O'Brien group members including, Nick Rose & Kleo Palate (Portugal Dream Team™), Jerry Tam, Jack Wootton, Dominic Spurling, Ryan Epton and Fraiser Arnold.

In addition to everything mentioned, the post-doctoral researchers of the O'Brien group throughout my time: James Firth, James Donald, and Kevin Kasten deserves a special mention for their knowledge, diverse perspectives, and orchestration of SD sessions, which have been instrumental in my learning and development.

Finally, my deepest appreciation goes to Professor Peter O'Brien. Their unwavering guidance and immeasurable learning support has allowed me to join the group as a MSc by research student and finish with a PhD. Their tireless dedication to research, and boundless enthusiasm for chemistry have been the cornerstones of my academic development. I have been truly fortunate to have had the opportunity to work under their guidance. Their mentorship has not only shaped the research direction of this thesis but has also significantly influenced my growth as a chemist.

In closing, I want to acknowledge the countless individuals who are not named here but have played a role in shaping my academic and personal journey. From mentors and colleagues to friends and family, your contributions, no matter how small, have left an indelible mark on this thesis and on my life as a whole.

As I reflect on the completion of this thesis, I am humbled by the collective support and friendships that have defined this academic experience. It is with immense gratitude and a profound sense of accomplishment that I submit this work.

Stephen Y. Yao,

Written and signed on my 27th birthday.

19/09/2023, 23:44

Author's Declaration

The research presented in this thesis is, to the best of my knowledge, original unless clearly indicated by citation. This work has not previously been presented for an award at this or any other university.

Stephen Y. Yao

Abbreviations

3-D	Three-dimensional
Ac	Acetyl group
Ala	Alanine
Aq	Aqueous
Ar	Aryl group
AT	Aminotransferase
ATP	Adenosine triphosphate
BCB	Bicyclo[1.1.0]butane
Bn	Benzyl group
Boc	*tert*-Butyloxycarbonyl
BOP	Benzotriazol-1-yloxytris(dimethylamino)-phosphonium hexafluorophosphate
br	Broad
BuLi	Butyllithium
Cbz	Benzyloxycarbonyl
CDK7	Cyclin-dependent kinase 7
ClogP	Calculated logP
cm^{-1}	Wavenumber
COSY	2-D Correlated Spectroscopy
COVID-19	Coronavirus disease 2019
CSP	Chiral Stationary Phase
Cy	Cyclohexyl group
Cys	Cysteine
Cz	Carbazole group
D or *d*	Deuterium or Deuterated
DEA	Diethanolamine

DIBAL-H	Diisobutylaluminium hydride
DIPEA	*N*,*N*-Diisopropylethylamine
DMA(c)	Dimethylacetamide
DMAP	4-Dimethylaminopyridine
DME	Dimethoxyethane
DMF	Dimethylformamide
DMSO	Dimethyl sulfoxide
DPP	Dipeptidyl peptidase
dr	Diastereomeric ratio
$E1_CB$	Elimination unimolecular conjugate base
EDG	Electron donating group
EMA	European Medicines Agency
Enz	Enzyme
Eq	Equivalent
ESI	Electron spray ionisation
Et	Ethyl group
EWG	Electron withdrawing group
FBDD	Fragment-based drug discovery
FBLD	Fragment-based ligand discovery
FDA	U.S. Food and Drug Administration
Fsp^3	Fraction of sp^3 carbons
GABA	Gamma aminobutyric acid
GLP	Glucagon-like peptide
Glu	Glutamic acid
H^+/ K+ ATPase	Hydrogen potassium adenosine triphosphatase
HBA	Hydrogen bond acceptor
HBD	Hydrogen bond donator

His	Histidine
HRMS	High resolution mass spectrometry
HTS	High-throughput screening
IC_{50}	The half maximal inhibitory concentration
IPN	Isophthalonitrile
i-Pr	Isopropyl group
IR	Infrared
JAK	Janus kinase
JAKnib	Janus kinase inhibitor
K_D	Dissociation constant
KRAS	Kirsten rat sarcoma virus
LED	Light-emitting diode
Leu	Leucine
LG	Leaving group
Lys	Lysine
M	Molar concentration
m-	Meta position on a phenyl ring
m/z	Mass to charge ratio
M^+	Molecular ion
Mcl-1	Myeloid cell leukemia-1
Me	Methyl group
MIDA	*N*-Methylimidodiacetic acid
M^{pro}	Main protease
MS	Mass spectrometry
MW	Molecular weight
NAPBQI	*N*-Acetyl-*p*-benzoquinone imine
NBS	*N*-Bromosuccinimide

NHCs	*N*-heterocyclic carbenes
NK Cell	Natural killer cell
nM	Nanomolar concentration
NMR	Nuclear magnetic resonance
Ns	*ortho*-Nitrobenzenesulfonamide
o-	Ortho position on a phenyl ring
p-	Para position on a phenyl ring
P-450	Cytochrome P-450
pan-	Non-selective
Ph	Phenyl
pIC_{50}	Negative log of IC50
pin	Pinacol
PLP	Pyridoxal phosphate
PMI	Principal moments of inertia
ppm	Parts per million
RA	Rheumatoid arthritis
R_F	Retention factor
RO3 or RO5	Rule of three or Rule of five
rt	Room temperature
SAR	Structure activity relationship
SARS-CoV-2	Severe acute respiratory syndrome coronavirus 2
sec	Secondary
Ser	Serine
S_N2	Substitution nucleophilic bimolecular
S_NAr	Nucleophilic aromatic substitution
STAT	Signal transducer and activator of transcription
SuFEx	Sulfur(VI) fluoride exchange

SuTEx	Sulfur(VI) triazole exchange
T3P	Propylphosphonic anhydride
tert	Tertiary
TFA	Trifluoroacetic acid
THF	Tetrahydrofuran
Thr	Threonine
TLC	Thin layer chromatography
TM	Transition metal
TMEDA	Tetramethylethylenediamine
TMPhen	3,4,7,8-Tetramethyl-1,10-phenanthroline
TMS	Trimethylsilane
Ts	Toluenesulfonyl group
TYK	Tyrosine kinase
Tyr	Tyrosine
Val	Valine
VKOR	Vitamin K epoxide reductase
δ	Chemical shift in ppm

Chapter 1: Introduction

High-Throughput Screening *Versus* Fragment-Based Drug Discovery

Two of the main approaches in drug discovery are high-throughput screening (HTS) and fragment-based drug discovery (FBDD). HTS aims to screen larger and more complex lead-like structures according to Lipinski's 'rule of five' (RO5)[1] where common physiological properties were observed in the successful compounds following HTS.[2] Lead compounds typically have molecular weights of < 500 Da, ClogP ≤ 5, number of hydrogen bond donors ≤ 5 and number of hydrogen bond acceptors ≤ 10.[1] Due to the size of the molecules, HTS campaigns need to screen libraries that could contain millions of compounds. Once HTS hits are found, optimisation studies such as SAR (structure-activity relationship), can be conducted to turn lead-like molecules into potential drug candidates (Figure 1.1).[3]

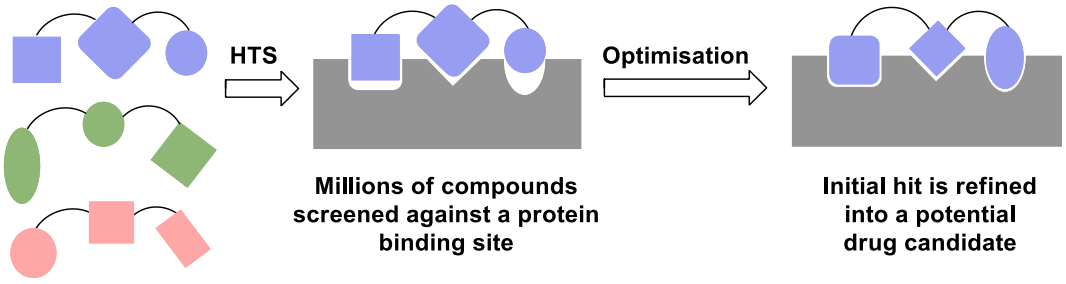

Figure 1.1 – Summary of high-throughput screening

Historically, HTS was the dominant lead-discovery approach and, to date, has led to numerous drugs in the market.[4] While HTS still remains as a commodity in the pharmaceutical industry, recent criticism has sparked debate among researchers.[4,5] An early estimation in 1996 by Guida and co-workers stated that the total number of possible lead-like molecules was well in excess of 10^{60} and would steeply rise with increasing molecular weight.[6] Therefore, the brute force approach adopted by HTS was argued by Lahana to be "a gamble", rather than scientific.[7] In addition, HTS hits have also been reported to show false-positives, resulting in the futile development of peculiar lead-like hits into drug candidates destined for failure.[8]

An alternative approach, fragment-based drug discovery, was first demonstrated by Fesik and co-workers, who developed a method to detect low molecular weight molecules with weak binding affinities to the immunosuppressant FK506 binding protein by NMR

spectroscopy. Using this technique, a library of compounds was screened in order to identify suitable fragments, before optimising them to produce a high affinity lead-like compound (Figure 1.2).[9] The pioneers of this target-directed drug discovery approach coined the phrase "SAR by NMR" to describe this process; we now call this process FBDD.[10]

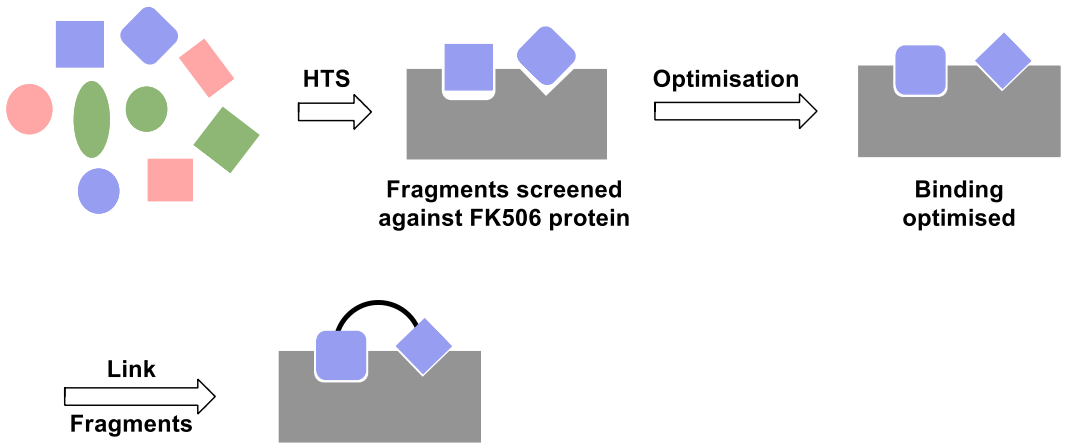

Figure 1.2 – Summary of fragment-based drug discovery

Another milestone in the development of FBDD was first conceptualised by Jhoti *et al.* in 2003, where results from Astex's preliminary work indicated that typical fragment hits seemed to obey a 'rule of three' (RO3).[11] The study was carried out by analysing a diverse set of fragments that showed binding to a series of protein targets. The physicochemical properties of fragment hits had commonalities including molecular weights of < 300 Da, ClogP ≤ 3 and number of hydrogen bond donors and acceptors ≤ 3.[11] Ten years later, the authors offered an update to their initial observations after many research groups continued to challenge the RO3.[12] For example, Klebe *et al.* successfully designed a fragment library without strictly adhering to the RO3.[13] While there are limitations to the RO3, the core concept of screening simpler compounds to allow for more efficient sampling of chemical space still holds true.[12] Another reason to screen smaller compounds is the concept of 'molecular complexity' introduced by Hann and co-workers.[14] The principle is based on the fact that as molecules become more complex, the chance of observing a hit towards a protein target decreases. This is because molecules can have both favourable and unfavourable binding interactions with their targets. Thus, the more complex a molecule becomes, the greater the chance of a negative interaction. This means that a molecule entirely complementary to a specific protein target could not be identified as a hit because of an unfortunately placed functional group.[14] Of course,

this concept should also be considered without too much emphasis as researchers from GlaxoSmithKline described ten years later.[15] In contrast, the identification of fragment hits in FBDD does not encounter these issues, as fragments are less complicated and often interact with just one protein pocket at a time.[16] In summary, fragments are capable of producing superior drugs than HTS as they start small and are elaborated to enhance optimal pharmaceutical properties.[17] This is coupled with the smaller fragment libraries involved with the screening of inherently smaller fragments.

Today, the development and application of FBDD has become mainstream and has even been deployed towards finding starting points for drugs against SARS-CoV-2. During the coronavirus pandemic, researchers were continuously engaged in the discovery of drugs and vaccines to combat this deadly disease. In February-March 2020, a fragment screening campaign was carried out on the main protease (M^{pro}) of SARS-CoV-2, using combined mass spectrometry and X-ray crystallography techniques.[18] The crystallographic screen scanned a total of 1250 fragments from a national fragment library, of which 71 (5.7%) were identified as "high value fragment hits".[18] Of those identified, two were fragments previously designed and synthesised within the O'Brien group (Figure 1.3). Both fragments are shown to follow Astex's RO3.

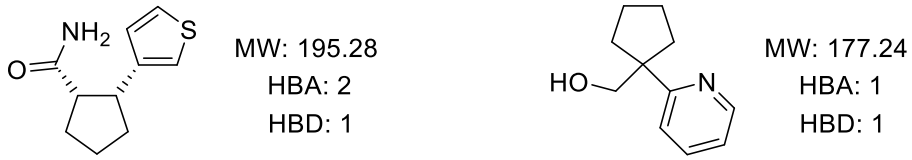

Figure 1.3 – Fragment hits against SARS-CoV-2 M^{pro}

Fragment Elaboration in Drug Development

1.1.1 Development of Fragment Libraries

As discussed previously, the general principles for fragment library design is that compounds typically follow a RO3.[11] In addition to this, a library should be structurally diverse in order to sample greater chemical space.[19] In this regard, Waring *et al.* developed a series of minimal halogenated fragments termed 'FragLites' (a portmanteau of 'fragment' and 'lite' – to mean particularly small fragments).[20] A total of 31 FragLites were reported (selected examples shown in Figure 1.4), which have various combinations of hydrogen bond donors and acceptors. FragLites have a pair of pharmacophore doublets and a heavy halogen atom (Br or I) incorporated into their structure. Due to the small nature of the fragments, the inclusion of bromine or iodine increases signal detection in X-ray crystallography.[20] Therefore, the various binding modes of protein pockets could be determined and visualised. This information on the druggability of the protein allowed for the methodical design and elaboration of fragments.[21]

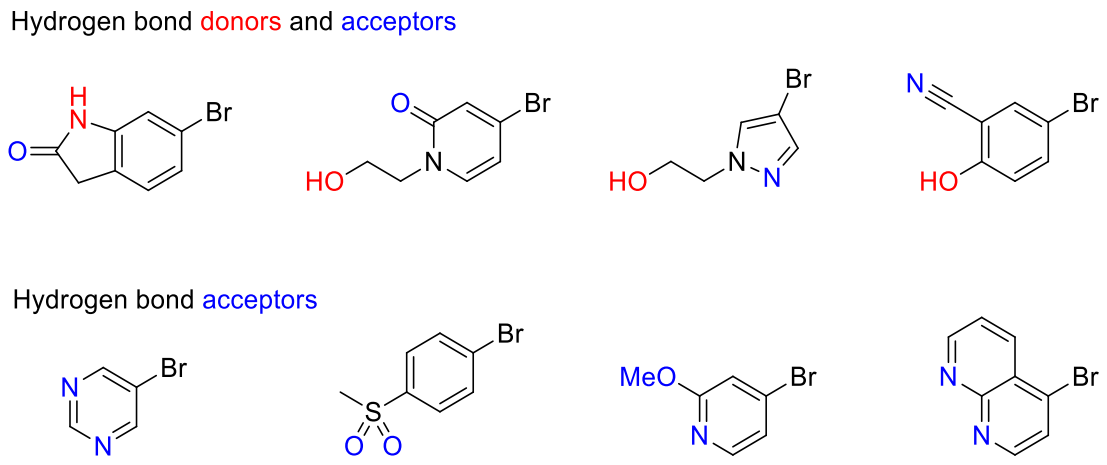

Figure 1.4 – Selected examples of FragLite fragments

As an example, Waring and co-workers mapped six allosteric and orthosteric binding sites in the cyclin-dependent kinase-2 (CDK2) receptor using FragLites.[20] Of the 31 FragLites, nine showed binding to the protein (29% hit rate), which is a far higher hit rate than that of typical fragment screens (~5%).[15] Waring *et al*. also showed the possibilities for the elaboration of FragLites (Scheme 1.1). Pyridone **4** was synthesised by the etherification of pyridine **1**, a FragLite, with phenyl alcohol **2**, CuI, TMPhen and Cs_2CO_3 in toluene at 110 °C for 24 h. Subsequent ester hydrolysis and demethylation was carried out on intermediate **3** using pyridine hydrochloride at 180 °C to afford pyridone **4** in 37%

yield. The elaborated fragment was found to have good binding to Lys[129] of the CDK2 protein.[20]

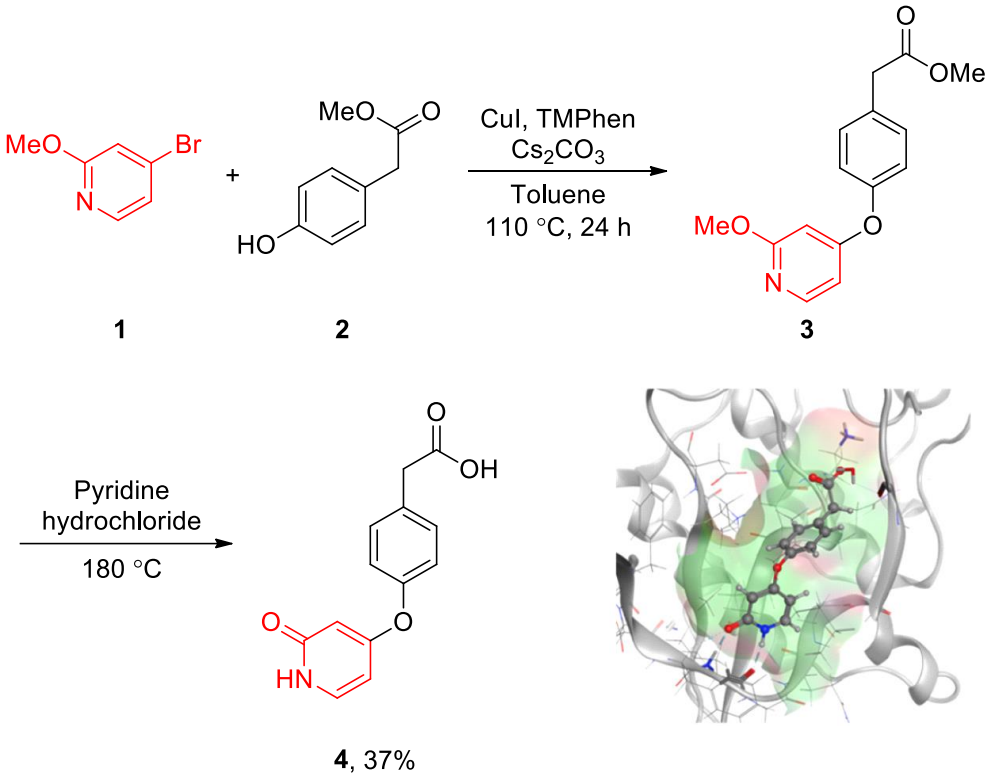

Scheme 1.1

The use of FragLites in mapping the protein site of interest was described to be comparable to a full fragment screen in identifying the key interactions.[22] Therefore, Waring and co-workers followed-up their initial library of 31 FragLites with additional fragments derived from amino acids coined 'PepLites' (derived from Peptide and Lite).[22] The addition of PepLites was proposed to mimic the interactions of peptides such that mapping of two bromodomains, BRD4 (bromodomain-containing protein 4) and ATAD2 (ATPase family AAA domain containing 2), could be carried out.[22] In a similar approach to the fragment elaboration of FragLites against the CDK2 protein, pyridone **5** was identified in binding to ATAD2 with an IC_{50} value of 377 μM. From the binding modes determined by the X-ray crystallographic structures of PepLites bound to ATAD2, Waring *et al.* proposed that elaboration of the 3- and 4-positions of pyridone **5** would potentially be productive (Scheme 1.2), therefore, compound **6** was explored.[22] Although the introduction of a fused piperazine actually gave a higher IC_{50} value of 822 μM, compound **6** provided additional vectors for elaboration. This ultimately led to further optimisation studies with compound **7** being synthesised (IC_{50} = 543 μM). Eventually,

compound **8** was discovered to have a significant improvement in potency (IC_{50} = 55 μM), where a 10-fold increase in the IC_{50} value from **7** to **8** was observed.[22]

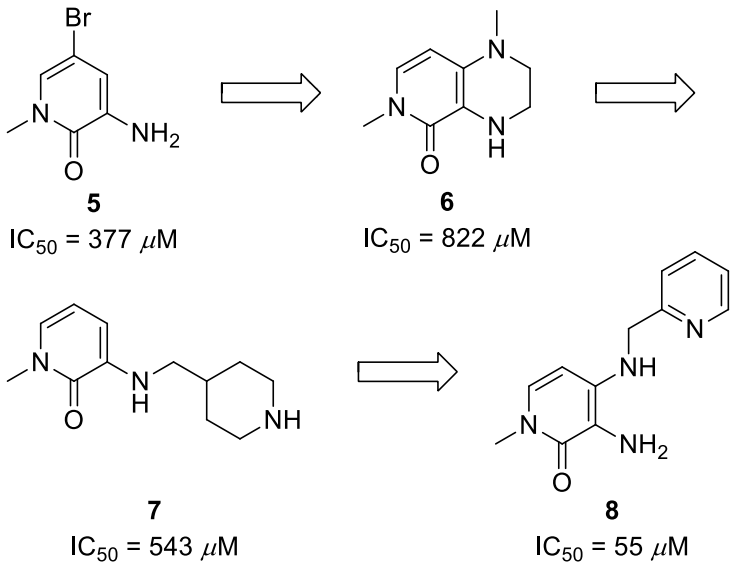

Scheme 1.2

Another fragment library designed to target bromodomains was developed by von Delft and Brennan *et al.*, where the PHIP2 (Pleckstrin homology domain interacting protein 2) protein was targeted due to its link in the progression of cancers and diabetes.[23] To this end, the authors introduced a series of 'poised fragments' **9**, **10**, and **11** (Scheme 1.3), which were defined as fragments that were synthesised from a robust methodology and can have a library of analogues generated from them using parallel chemistry.[23] From the synthons of the poised fragments **9**, **10**, and **11**, variation of the R^1 group, and where applicable, R^2, R^3, and R^4, can lead to the rapid generation of poised fragment analogues, effectively elaborated fragments, using single-step synthesis.[23]

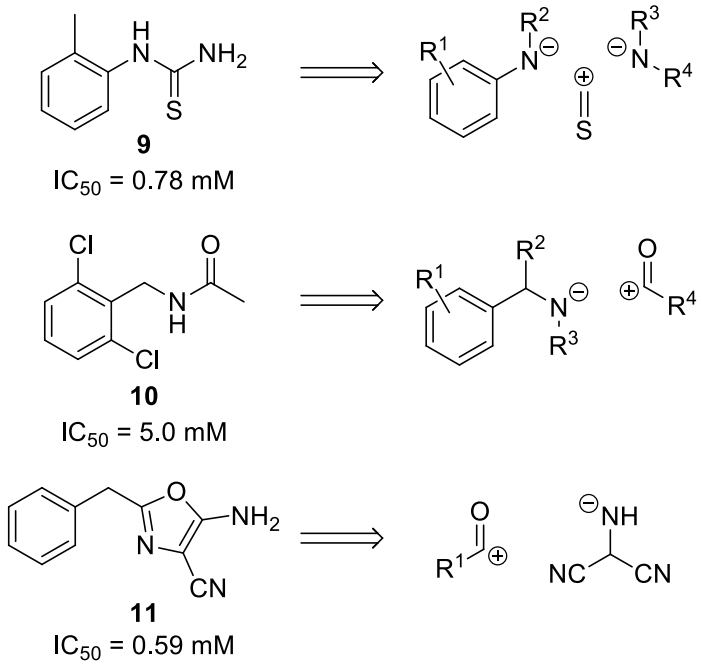

Scheme 1.3

By using X-ray crystallography, libraries generated from poised fragments provide detailed information on the ligand binding site as well as improving the binding affinity in some cases.[23] Selected examples of poised library entries are shown in Figure 1.5; these structures along with many others are commercially available as the Diamond SGC Poised Library 2.0 (DSPL2) through a supplier (Enamine Ltd).

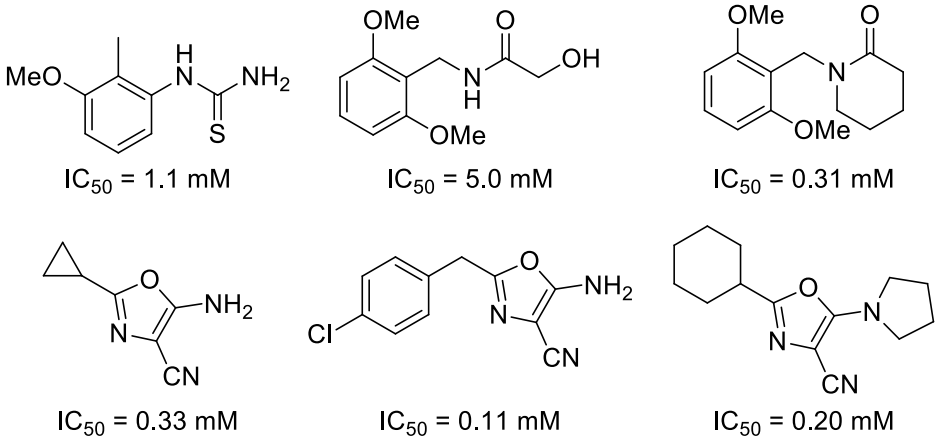

Figure 1.5 – Selected examples from the diamond SGC Poised Library 2.0 (DSPL2)

In 2021, Denis *et al.* introduced the concept of 'fragment sociability', to analyse existing fragment libraries.[24] A 'sociable fragment' was proposed to be supported by robust synthetic methodologies enabling fragment elaboration in multiple growth vectors. In addition, a number of commercially available analogues must also be accessible under

Denis' definition.[24] In contrast, 'unsociable fragments' are those that have limited synthetic methodology and few commercially available analogues. Under these definitions, fragment libraries can be analysed and grouped into two categories (sociable or unsociable). By doing so, sociable fragments can be prioritised in elaboration programmes, while unsociable fragments can lead to inspiration for the development of new synthetic methodologies.[24] In a FBDD screening campaign against the HCV NS3 (hepatitis C virus NS3) protease-helicase, fragments **12** and **14** were identified with IC_{50} values of 160 μM, and 31% @ 1 mM (Scheme 1.4). The sociable fragment **12** was elaborated by facile introduction of an ethyl group at the benzylic stereocentre together with amine substitution. Further SAR studies modified the substituents on the phenyl ring to afford compound **13** with high potency (IC_{50} = 0.1 μM) against HCV NS3.[24] Although fragment **14** itself was commercially available, analogues of fragment **14** were limited. Moreover, elaboration at the essential growth vectors (highlighted in red) was not possible and would require lengthy linear synthesis and thus it was deprioritised over fragment **12**.[24]

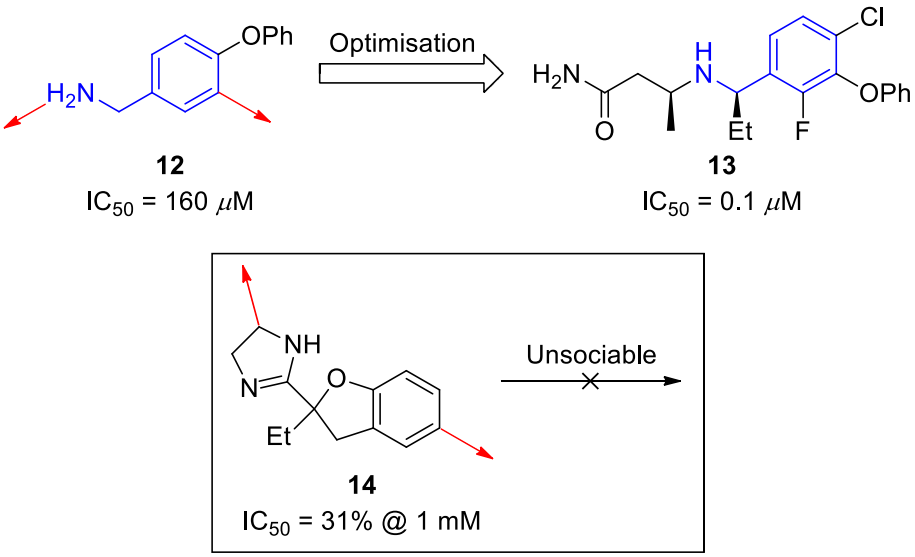

Scheme 1.4

1.1.2 Strategies for Fragment Elaboration

The most common and intuitive way to elaborate a low-potency fragment into a high-potency lead-like compound is by 'fragment growing'.[19,25] In order to achieve this, it is necessary to first establish the growth vectors.[26] Typically, the X-ray crystal structures of

the bound fragment to the target protein pocket are analysed to determine the growth vectors.[27] Then, by attaching additional atoms or functional groups at the point of growth, additional protein interactions can be picked up.[28] In scenarios where X-ray crystallographic data is not available, information of the binding modes on the target protein is important to grow the fragment effectively.[29] These properties can be determined by NMR and molecular docking studies.[30] The first inhibitors against the latency-associated nuclear antigen (LANA) were reported by Empting *et al.* The authors identified fragment **15** during a FBDD campaign where a 25% inhibitory effect at 1 mM concentration was observed.[31] Early development of fragment **15** identified two notable analogues, fragments **16** and **17** (Scheme 1.5). It was discovered that when the aniline was substituted for a benzoic acid in fragment **16**, improvement in the IC_{50} value was noted.[31] Similarly, for fragment **17**, the addition of a methyl group on the imidazole ring gave an improved inhibitory effect of 91% at 1 mM concentration.[31] Using the information generated from fragments **15**, **16** and **17**, further optimisation studies were conducted with a combinatorial chemistry approach using click chemistry to afford the final lead compound **18**.[31] Of note, addition of the pyridine was introduced along with the triazole core (replacing the imidazole ring), and the substituent position of the benzoic acid changed from *ortho* to *para*.

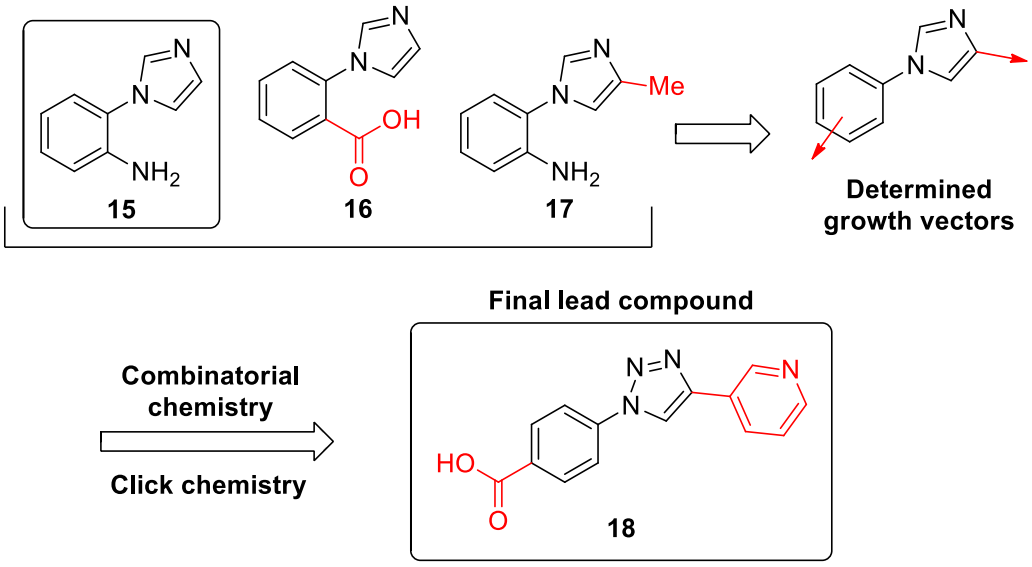

Scheme 1.5

Another strategy for the elaboration of fragments is the merging of two or more fragments into one compound. Unlike the previous fragment growing method, structural information of the bound ligand–protein is essential for this type of fragment elaboration strategy. In

2013, Hartmann and co-workers reported a series of inhibitors against the *P*qsD (*Pseudomonas* quinolone signal–D) enzyme, which is an attractive strategy in the fight against antimicrobial resistance.[32] In this sense, fragment **19** and compound (*R*)-**20** were identified (Scheme 1.6) in binding to the *P*qsD enzyme through a common benzyl alcohol moiety (highlighted in red). Although compound (*R*)-**20** is not a typical fragment, for example it does not follow Astex's RO3, as discussed previously, these larger structures can still be used in FBDD approaches.[12] By themselves, fragment **19** and compound (*R*)-**20** were shown to have IC_{50} values of 3 μM and 0.14 μM, respectively.[33] However, when merging of the two structures was carried out to generate compound (*R*)-**21**, an IC_{50} of 0.36 μM was obtained.[33,34] Although a better potency value was hoped for, the significance of several functional groups in binding to the *P*qsD enzyme was clarified. In 2015, Hartmann *et al.* concluded that the ureidothiophene carboxylic acid backbone (highlighted in blue, Scheme 1.6) was not suitable for use in the development of *P*qsD inhibitors.[34]

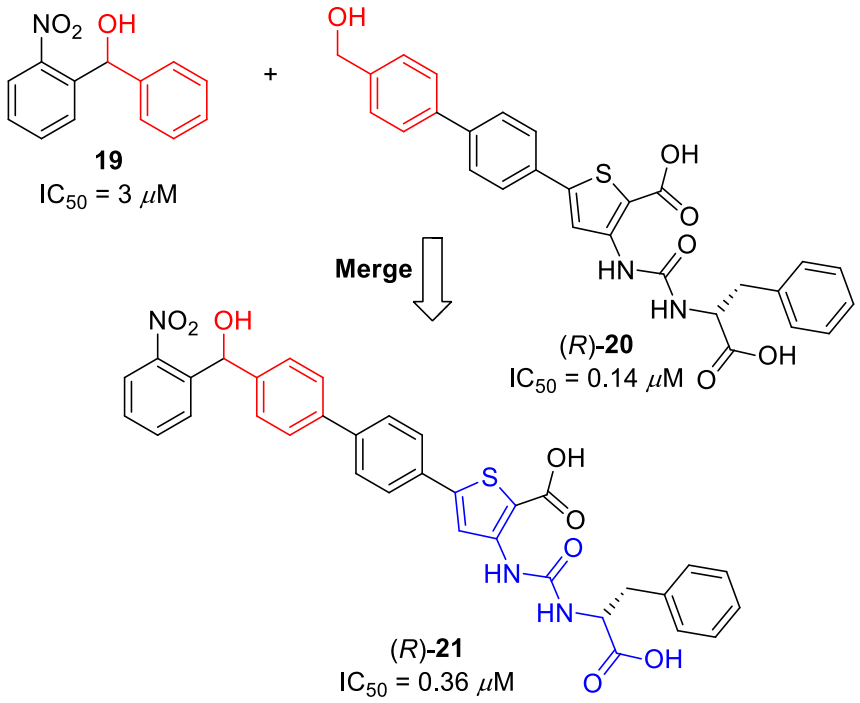

Scheme 1.6

Fragment linking is widely considered a powerful strategy in fragment elaboration.[25,35] As the name suggests, this approach aims to link together two or more fragment hits, which bind to different areas of the protein pocket.[36] However, unlike fragment merging, this method employs a linker moiety to connect the fragments of interest.[35] Due to the introduction of a linker to the ligand system, one of the biggest challenges is the

identification of a suitable linker structure that has no negative impact on the binding affinity toward the target site.[36] In addition, linkers must orient the fragments in the correct geometry; while at the same time, be rigid enough to not introduce too much flexibility.[19] A successful fragment linking strategy was demonstrated by Abell and co-workers in the discovery of inhibitors against TBPS (*mycobacterium tuberculosis* pantothenate synthetase).[37] Originally, fragments **22** and **24** were identified in binding to the TBPS enzyme with dissociation constants (K_D) of 1000 μM and 1100 μM, to their respective binding sites (Scheme 1.7). Following constructive modifications of fragment **24**, the resulting acetic acid derived fragment **23** possessed a K_D value of 500 μM.[37] Eventually, fragments **22** and **23** were linked by an alkyl ester and a methylene sulfonamide linker, to give compounds **25** (K_D 75 μM) and **26** (K_D 50 μM).[37] Finally, it was discovered that the acyl sulfonamide linker in compound **27** was more conformationally constrained. Thus, compound **27** was found to bind to the TBPS enzyme with significantly increased potency, achieving a K_D of 1.8 μM.[37]

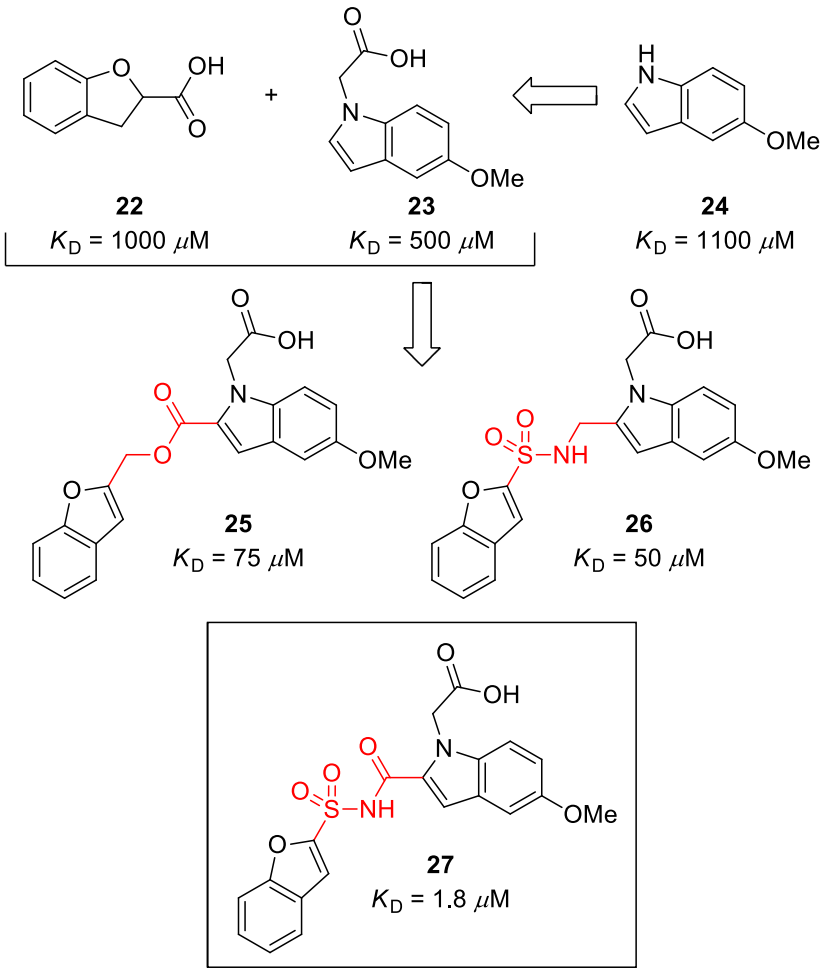

Scheme 1.7

1.1.3 FDA Approved Drugs from FBDD-Derived Origins

In a 2016 review entitled 'the impact of fragments on drug discovery' by Jhoti *et al*., the number (> 30) of FBDD-derived drugs approved or currently in clinical trials were highlighted.[3] Most of the reported drugs have progressed since then and advanced to the next stage of clinical trials or have been approved already. Currently, there are six FBDD-derived drugs on the market which have been approved by the FDA for treatment of disease and the original fragment precursors are indicated in red (Figure 1.6).

Venclexta® is a competitive antagonist inhibitor against the Bcl-2 (B-cell lymphoma-2) protein and was approved for the treatment of chronic lymphocytic leukaemia (CLL).[38] Similarly, in 2019, Balversa™ was approved for the treatment of urothelial carcinomas after 13 years of development.[39] Zelboraf® received plenty of media coverage due to its role in cancer treatments. By targeting a mutant form of the BRAF gene, patients with severe forms of skin cancers had a dramatic extension of their life. Zelboraf® represents the first FBDD-derived drug approved by the FDA.[40] Turalio® is an inhibitor of CSF1R (colony stimulating factor 1 receptor), the receptor suspected to be related to the growth of the tenosynovial giant-cell tumour.[41] In 2021, the FDA approved Lumakras® for the treatment of non-small cell lung cancer. The development of Lumakras® originated from two fragments linked, then optimised, leading to its final structure.[42,43] Lumakras® is an example of a covalent drug and will be discussed further in Chapter 5. The groundbreaking drug targets the $KRAS^{G12C}$ oncogene, previously considered an 'undruggable' target.[43] More recently, Scemblix® entered the market to treat patients with chronic myeloid leukemia. By using NMR and X-ray crystallography methods to identify fragments, the development of Scemblix® began with the linkage of two fragments similar to Lumakras®.[44] To date, Scemblix® remains the only inhibitor of the allosteric BCR-ABL1 oncogene.[44]

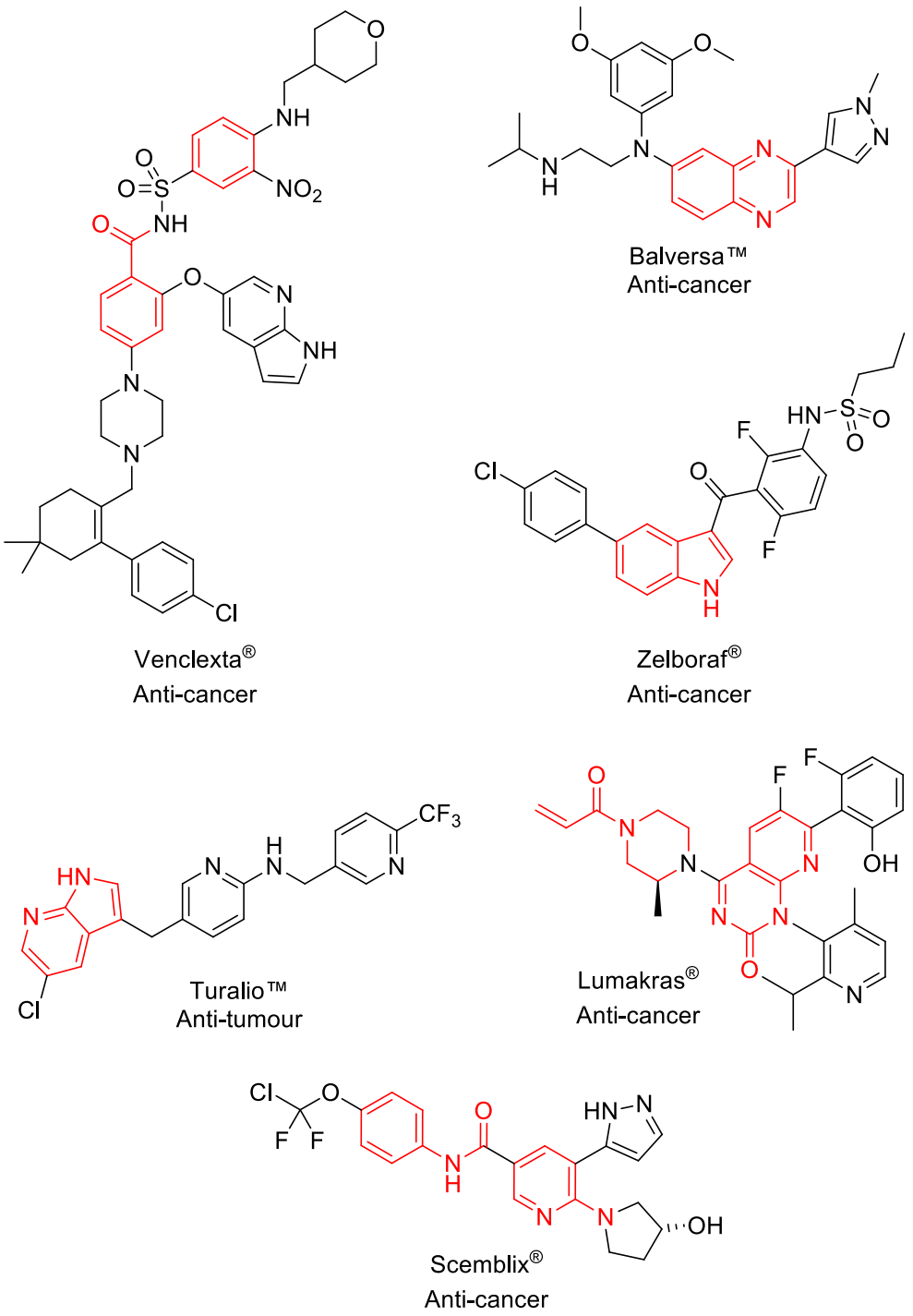

Figure 1.6 – Examples of FBDD-derived drugs

FBDD is commonly practiced in academia, biotech companies, and the pharmaceutical industry. Therefore, it was a collaboration between these organisations which led to the FDA approval of the fibroblast growth factor receptor (FGFR) inhibitor, erdafitinib (Balversa™), in late 2019. The original development of erdafitinib began in 2006 from a collaboration between Astex Pharmaceuticals and the Northern Institute of Cancer Research (NICR). During this time, the activation of FGFRs was known to be associated

with the development of cancers including lung, ovarian, breast, prostate, gastric, myeloma, rhabdomyosarcoma and urothelial.[39] However, the main complication in targeting FGFR for inhibition was the selectivity required for a pharmaceutical agent. Most FGFR inhibitors at the time also inhibited the vascular endothelial growth factor receptor (VEGFR2) causing undesirable hypertension and other side effects.[39] Two years later, a FBDD screening campaign was performed on a series of imidazopyridine-containing fragments for selective inhibition of FGFR. This work ultimately enticed Janssen Pharmaceuticals to join the collaboration and, not long after this, quinoxaline fragment **28** was identified. By using X-ray crystallography, the binding between quinoxaline fragment **28** and the FGFR was mapped. This ultimately led to the elaboration of the initial fragment **28** to choropyrazole **29** (Scheme 1.8). With further virtual screening efforts, **30** was identified and later improved to **31** by replacement of the substituted benzyl group with a substituted aniline substituent. Finally, substitution on the aniline gave erdafitinib (Balversa™).[39]

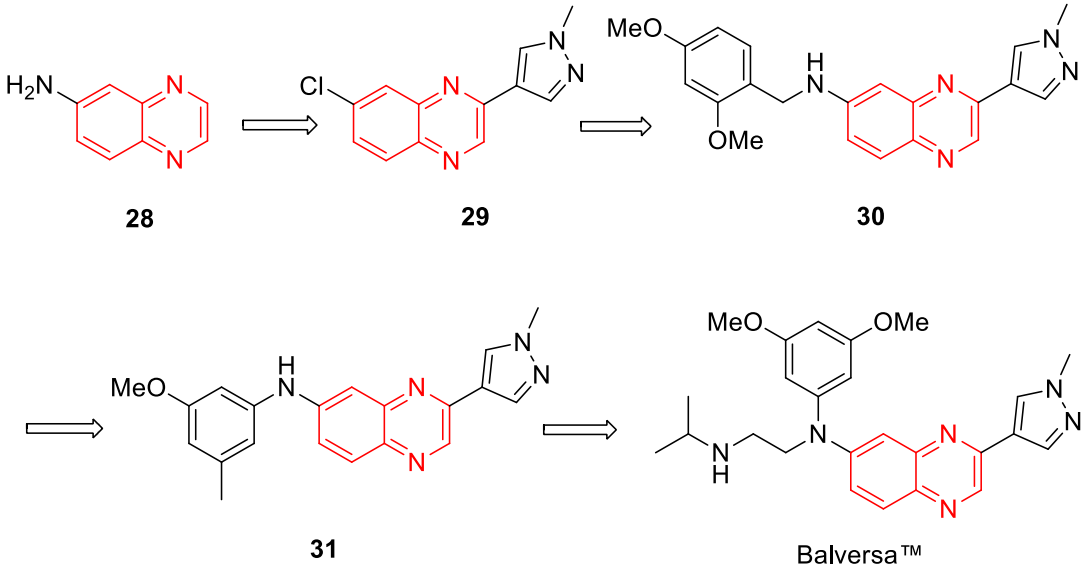

Scheme 1.8

In the same year as Fesik and co-workers published their work on 'SAR by NMR', Fesik *et al.* also used this technique to map the structure of the human BCL-xL (B-cell lymphoma-extra-large) protein.[45] Following this, a FBDD screening programme identified fragments **32** and **33** in binding to the BCL-xL protein with dissociation constants (K_D) of 300 μM and 6 mM respectively (Scheme 1.9).[46] Using a fragment linking strategy, fragments **32** and **33** were linked *via* a vinyl linker to give compound **34** with an inhibition constant (K_i) of 1.4 μM.[46] Later efforts to optimise compound **34**,

generated analogue **35** (K_i < 500 pM), before the final structure of venetoclax was determined.[46] In 2016, the FDA granted the approval of this drug for patients with chronic lymphocytic leukemia (sold under the brand name: Venclexta®).[46]

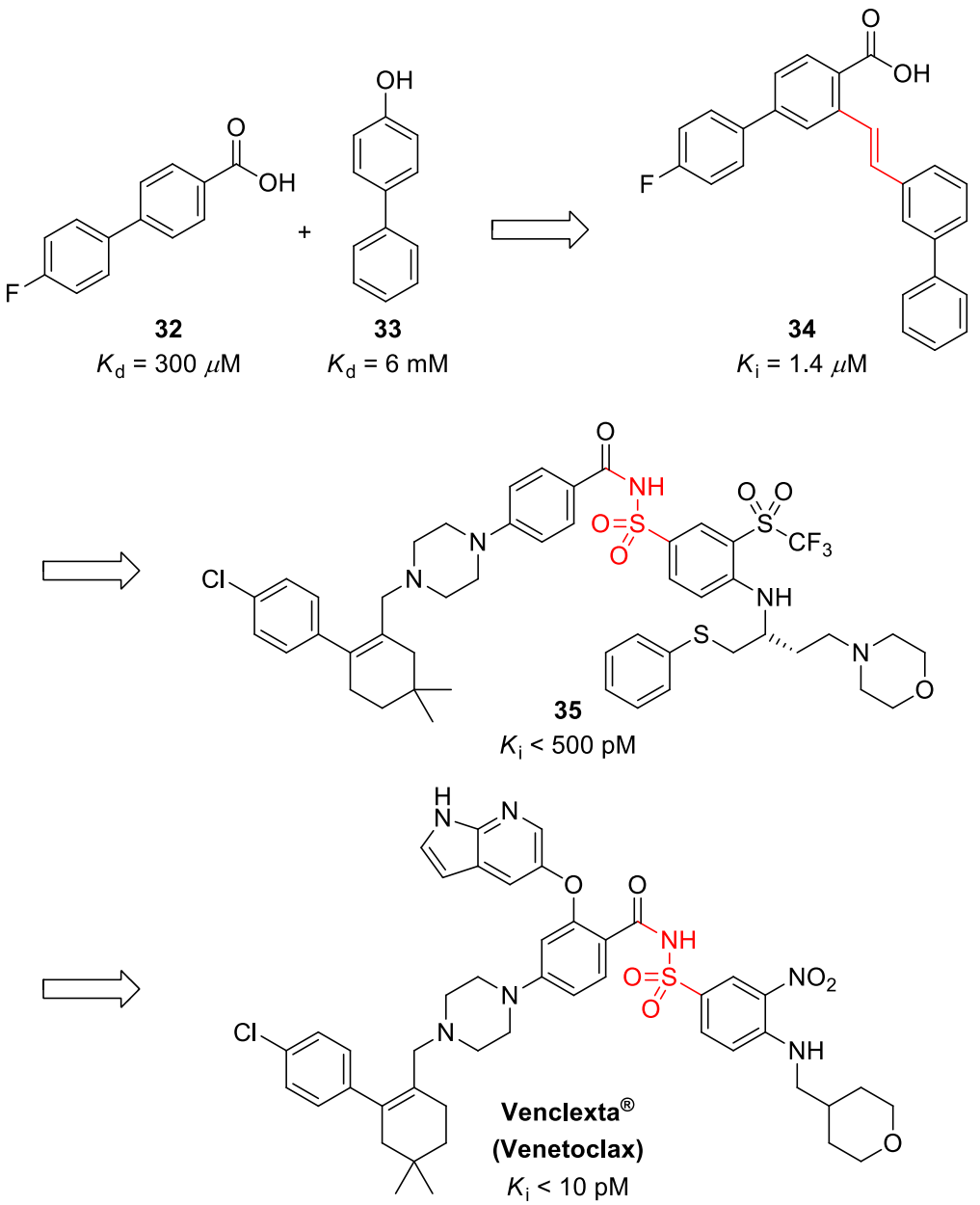

Scheme 1.9

Project Outline

The central theme of this thesis discusses the positive impacts of fragments in modern-day drug discovery. However, the challenge associated with synthesis and elaboration of fragments is an increasingly important issue within this field.[2] Firstly, one of the key aims of this project was to design a library of sp^3-rich and structurally diverse 3-D building blocks with distinct vectors in 3-D space. Previous members of the O'Brien group helped in the initial studies on the synthesis of *exo*-**36** and **37**, in addition to generic methodology development.[47–50] Our plan was to develop the gram-scale synthesis of *exo*-**36** and **37** along with five uniquely designed novel building blocks, pyrrolidine cyclopropanes *trans*-**38**, *cis*-**38**, *exo*-**39** and *endo*-**39**, together with pyrrolidine cyclobutane alcohol *endo*-**40** (Figure 1.7). The use of *N*-Boc amino alcohol *endo*-**40** for the cyclobutane scaffold is due to the use of a different method of cross-coupling, and this is explained fully in Chapter 4.

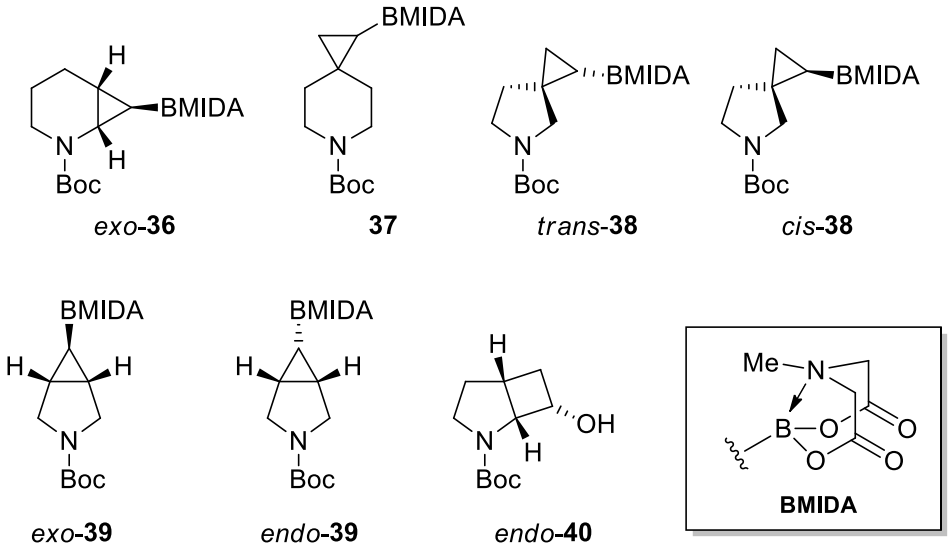

Figure 1.7 –York 3-D building blocks explored herein

Secondly, another key aim was to demonstrate that the proposed York 3-D building blocks could be applied to fragment elaboration with pre-determined synthetic methodology already in place. Traditionally, fragment elaboration often occurs in a stepwise fashion by growth from synthetic handles derived from the original screened fragment. In the illustrative example of a CK2 fragment inhibitor shown in Figure 1.8, elaboration of this fragment can be performed through derivatisation of the amine and functionalisation at the 3- or 4-position of the phenyl ring. Besides these, the linker

between the amine and aromatic core can also be varied to provide enhanced binding to target receptors.[51]

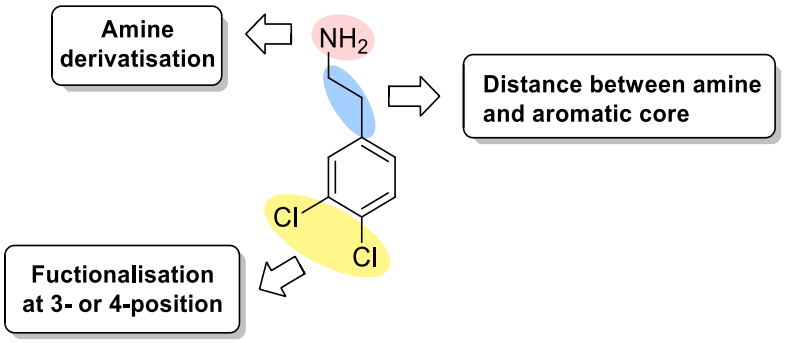

Figure 1.8 – Demonstration of traditional fragment elaboration

Unfortunately, not all fragment elaboration projects and plans are this trivial. To highlight some of the challenges, an example identified by a previous member of the O'Brien group illustrated that the target elaborated analogue **42** could have potentially improved binding features with respect to the original fragment **41** (Scheme 1.10).[47] However, diastereoselective arylation at the 3-position of fragment **41** still remains an unsolved synthetic challenge. For that reason, an entirely new bespoke synthesis of elaborated fragment **42** would be needed to obtain elaborated fragment **42**, slowing down and increasing the cost of fragment elaboration.

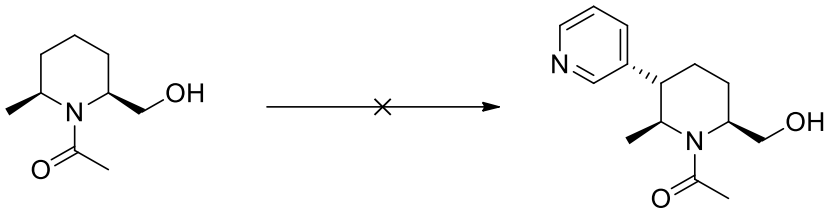

41 **42**

Scheme 1.10

Recently, a drive from researchers within the pharmaceutical industry describes the final technical challenge for fragment discovery is 'knowing how to optimise fragments to leads'.[3] This issue is focused on synthetic organic chemistry being the rate limiting step in the fragment elaboration stage.[2] A solution proposed by Murray and Rees discusses that 'practitioners of FBDD need to shift from thinking that productivity is about screening and synthesising more compounds, towards using a more design-led and lower-throughput approach'.[52] Hence, the goal in the O'Brien group is to address some of the

issues highlighted by attempting to elaborate fragments in 3-D using methodology already developed prior to any fragment screening. To begin dissemination of using a modular synthetic platform for fragment elaboration, fragment hits identified *via* X-ray crystallographic screening campaigns are targeted. Taking the aryl halide counterparts of such fragments (FragLites[20] could also be used), we propose to use a diverse library of 3-D building blocks (see Figure 1.7), which ideally would be eventually commercially available. With the aid of cross-coupling chemistry, attachment of the 3-D building blocks can be achieved to demonstrate successful elaboration of a fragment within a vector defined by the stereochemical properties processed by the chosen building block (Scheme 1.11). By possessing a library of unique 3-D building blocks, X-ray guided vector analysis of a fragment bound in a protein can elicit information on which 3-D building block would be most suitable to a specific fragment bound to a protein pocket. Although beyond what is discussed in this thesis, total automation for the elaboration of fragments using 3-D building blocks may not be too far-fetched. This would be especially useful for fragments without X-ray crystallographic data. Instead, automated synthesis of elaborated fragments by attachment of 3-D building blocks is possibly a solution to the bottleneck in fragment elaboration.[53,54]

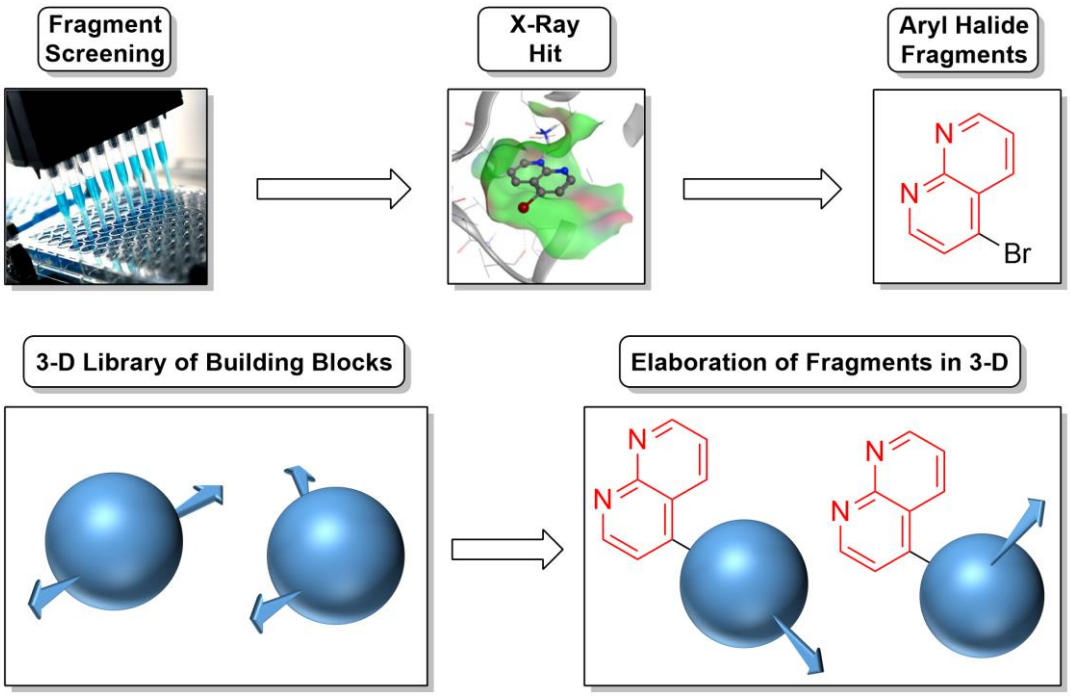

Scheme 1.11

Lastly, a final key aim in the work described in this thesis was to apply the existing set of 3-D building blocks in the synthesis of a library of 3-D covalent fragments. For this project, we proposed methodology to be designed such that the derivatisation of both synthetic handles (boron and amine) of 3-D building blocks occurs with the lowest possible number of reaction steps, mitigating the need for multiple chromatography. With this methodology in place, an example of approximately ten medicinally relevant aryl or heteroaryl bromides could be attached to cyclopropyl building blocks **43** in a single step to output an equal set of covalent fragments **44** (Scheme 1.12). It was envisaged that covalent fragment libraries generated from a number of building blocks may be achieved. These subsequent fragments could be submitted into globally accessible fragment libraries for screening in drug discovery programmes.

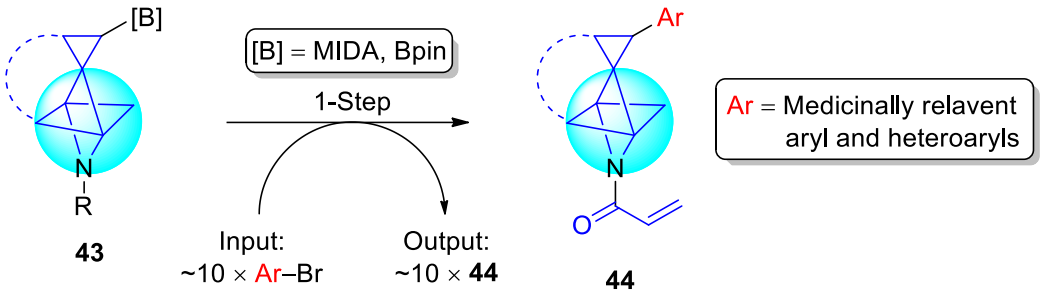

Scheme 1.12

In summary, the new 3-D building blocks will add to the existing set of 3-D building blocks synthesised by past and present members of the group. The synthesis of novel building blocks *exo*-**36**, *trans*-**38**, *cis*-**38**, and *exo*-**39**, and their ability to elaborate fragments in 3-D is discussed in Chapters 2 and 3. Chapter 4 illustrates the progress made in the synthesis of a second generation 3-D cyclobutyl building block *endo*-**40**. Methodology development for the synthesis of a covalent fragment library using the 3-D building blocks is presented in Chapter 5. This methodology attempts to demonstrate uses of York 3-D building blocks beyond fragment elaboration. Finally, Chapter 6 illustrates a practical example of using 3-D building blocks *exo*-**36** and *cis*-**38** to elaborate a fragment into a potential drug molecule.

Chapter 2: Design and Synthesis of Cyclopropyl 3-D Building Blocks for Fragment Elaboration

One of the limitations with fragment-based drug discovery is the lack of systematic approaches to elaborate low binding affinity fragments (typically mM to μM) into high binding affinity lead-like compounds (nM).[55] Moreover, fragment elaboration is not only time-consuming but also challenging to perform in 3-D. The need for complex (high Fsp^3) molecules was discussed in a landmark publication from Lovering *et al*.[56] Benefits of lower promiscuity from accessing greater chemical space can significantly increase the potential for pharmaceutical candidates to advance and excel in the clinic.[56] Thus, a solution to both areas of concern is desired.

In this chapter, we describe a synthetic platform that has been developed by the O'Brien group through the combined efforts of various past and present members. Such work should ultimately allow the elaboration of fragment hits into lead-like compounds using specially designed 3-D building blocks. Chapter 2.1 aims to outline our unique approach to tackle the synthetic problem associated with elaboration of fragments in 3-D using building blocks. The design criteria for the building blocks are summarised in Chapter 2.2. Here, we encapsulate the idea of the design choices which gives York 3-D building blocks the ability to elaborate fragments in various vectors around the fragment's 3-D space (Figure 2.1). Chapter 2.3 recounts the synthesis of cyclopropyl 3-D building blocks previously investigated in the group in conjunction with the methodology development and subsequent synthesis of some novel cyclopropyl 3-D building blocks.

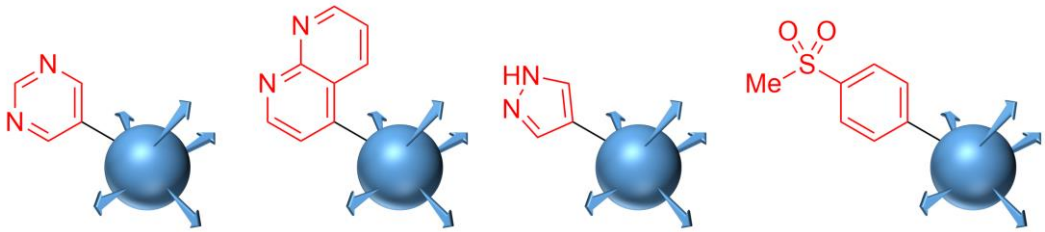

Figure 2.1 – Elaboration of fragments in 3-D vectors

2.1 Criteria for the Design of York 3-D Building Blocks

The design of a successful building block will rely on its ability to traverse unique 3-D vectors around a fragment's chemical space relative to other building blocks. As building

blocks would ultimately form the main backbone of a clinical drug candidate, focus on 3-dimensionality in the building blocks is pivotal towards the ultimate versatility of any subsequent pharmaceutical agent it generates to explore chemical space.[57] The building blocks are designed to have a high fraction of sp^3 hybridised carbons (Fsp^3) and it is anticipated that this could help future drug programmes to 'escape from flatland' as described by Lovering *et al*.[56] With the overall vision of 3-D building blocks defined, a set of common criteria were applied to the design process for 3-D building blocks.

Firstly, it was proposed that the initial set of 3-D building blocks would contain a cyclopropane moiety. The strain exerted by the three-membered ring makes the interactions of cyclopropanes with neighbouring π-systems resemble that of a vinyl group.[58] In drug discovery, the double bond character in alkenes may form an important feature in a drug molecule. However, the reactivity of such alkenes can lead to complications such as undesired metabolic instability.[59] Therefore, the less reactive cyclopropyl moiety can act as a bioisostere for unsaturated alkenes in potential drug molecules.[60] Cyclopropanes are also known to benefit drug molecules in terms of enhancing potency, increasing permeability across the blood-brain barrier, conformational restriction and decreasing plasma clearance.[61] Of note, the cyclopropyl moiety features in 18 different FDA approved drugs, some of which are shown in Figure 2.2.[62] For instance, Mekinist® is an inhibitor of the mitogen-activated protein kinase kinase enzymes MEK1 and MEK2. Its subsequent approval by the FDA was granted for treatment of mutated metastatic melanomas.[63] The development of Victrelis™ into a protease inhibitor for the treatment of hepatitis C was approved by the FDA in 2011.[64] However, in early 2015, Merck voluntarily withdrew the drug from the market for the more superior Harvoni®. Harvoni® is the trade name for a combination of two drugs: ledipasvir and sofosbuvir.[65] The collaboration between AstraZeneca and Bristol-Myers Squibb resulted in the development of Onglyza® – a dipeptidyl peptidase-4 (DPP-4) inhibitor for the treatment of type II diabetes.[66] Slynd™ is an oral contraceptive originally patented in 1976; it is also used as an ingredient as part of other licensed drugs (Yasmin®, Angeliq®).[67] In 2013, Fetzima® was approved for the treatment of major depressive disorder (MDD). The drug belongs to a family of serotonin-norepinephrine reuptake inhibitors (SNRIs) to restore hormonal balance in the brain.[68]

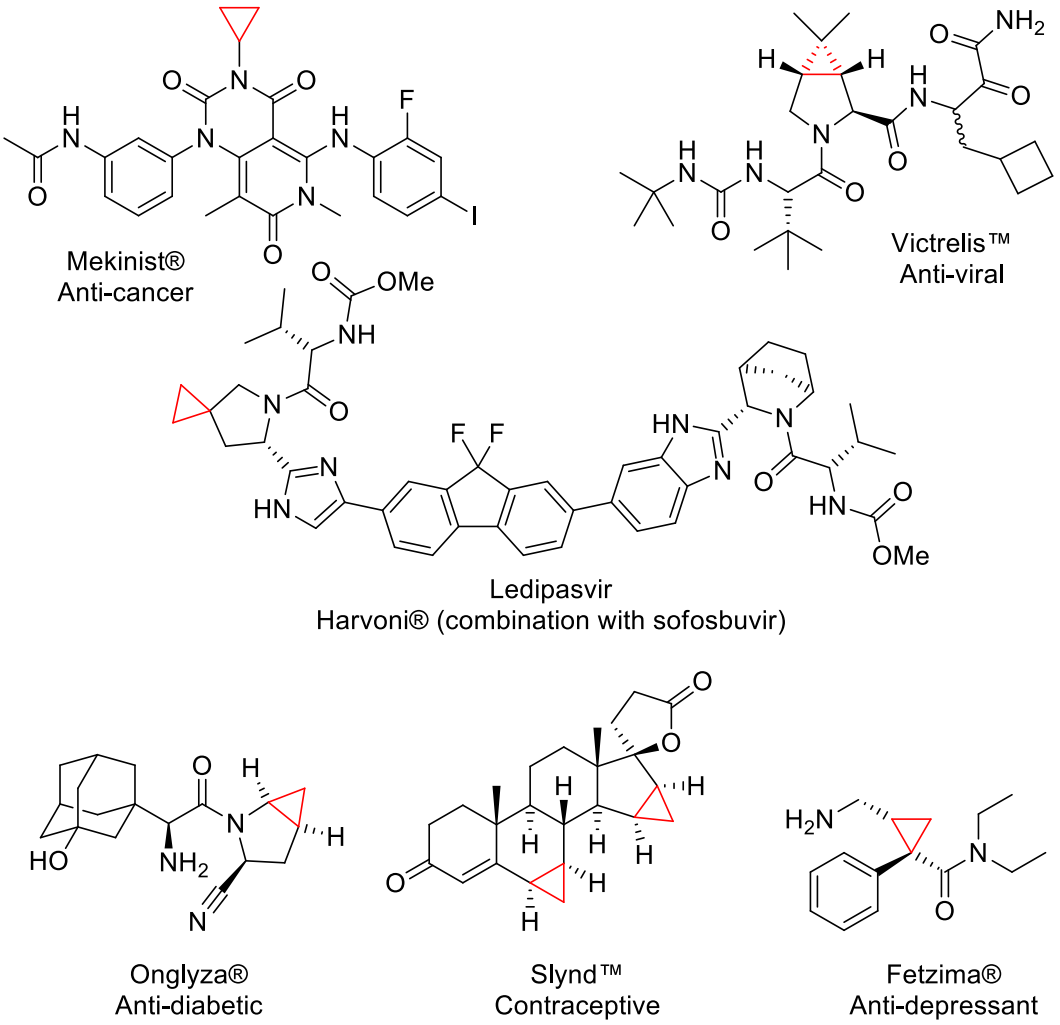

Figure 2.2 – Examples of approved drugs containing the cyclopropyl moiety

Another design element of cyclopropanes is the 3-dimensionality that this group adds. Incorporation of cyclopropanes allows saturated heterocycles to become bicyclic *via* a spiro or fused arrangement. The exemplar drugs featured in Figure 2.2 show this character with the exception of Mekinist® and Fetzima®. For building blocks, this component would give rise to unique 3-D vectors (illustrated in Figure 2.3).

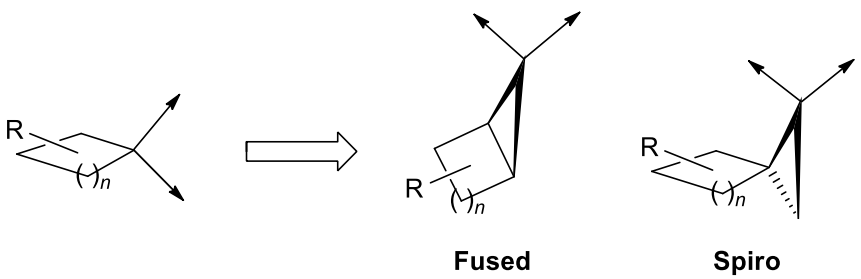

Figure 2.3 – Unique vectors arising from fused and spiro cyclopropyl bicycles

Secondly, it was decided that the 3-D building blocks will follow AstraZeneca's 'rule of two' guidelines described by Goldberg *et al*.[69] According to the team at AstraZeneca, building blocks with physiochemical properties of MW < 200, *c*logP < 2, HBD ≤ 2 and HBA ≤ 4 (Table 2.1) are the most useful for applications in drug discovery projects.

Table 2.1 – Preferred physicochemical properties observed in building blocks

Property	'**RO2**' **Guideline**[11]
Molecular Weight (MW)	< 200 Da
*c*logP	≤ 2
# H-bond donors (HBD)	≤ 2
# H-bond acceptors (HBA)	≤ 4

Thirdly, it was planned that the 3-D building blocks would contain a cyclopropyl BMIDA group (structure shown in Figure 2.4). While other cross-coupling enabled boron groups exist, the trivalent *N*-methyliminodiacetic acid (MIDA) group initially studied and developed by Burke *et al*. possesses several advantages over its competitors such as pinacol boronates (Bpin) and potassium trifluoroborate salts (BF_3K). Unfortunately, pinacol boronates can be unstable on silica and are often oils. Although potassium trifluoroborate salts are free flowing solids, purification and insolubility in common laboratory solvents remain a limitation. In contrast, MIDA boronates are reported to be air-stable, silica-gel compatible, free flowing solids and can undergo Suzuki-Miyaura cross-coupling *via* slow hydrolysis of the MIDA group under basic conditions to generate potentially unstable boronic acids *in situ*.[70] Thus, by having slow release of the boronic acid, decomposition may be prevented, and this could improve the overall yield for Suzuki-Miyaura cross-couplings for the attachment of fragments.[71]

Fourthly, the handle for elaboration of an attached fragment to a building block through an exit vector will be a Boc-protected amine. This versatile point of diversification allows for prevalent amine chemistry to be used. Some examples include, but are not limited to, amide formations, sulfonamide formations, S_NAr *N*-arylations, Buchwald-Hartwig *N*-arylations and reductive aminations. All of the four design criteria are captured visually in Figure 2.4.

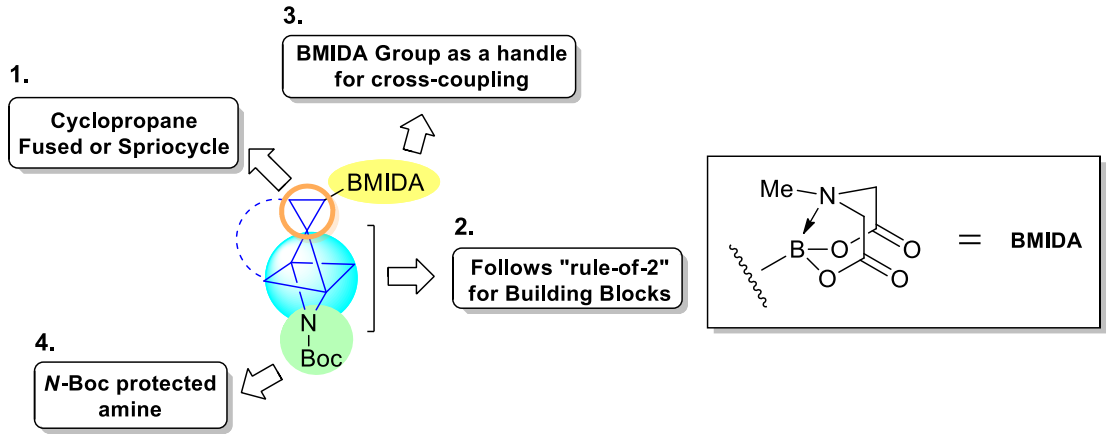

Figure 2.4 – Features of York 3-D Building Blocks

2.2 Cyclopropyl Boronate Building Blocks in Drug Discovery

Goldberg and co-workers from AstraZeneca suggested that the design of novel building blocks is an overlooked strategy for improving the quality of drug-like compounds.[69] It is thought that access to, and use of, a collection of high-quality building blocks can be directly correlated with the serendipitous discoveries made in drug discovery projects.[69] Detailed examination of serendipity in drug discovery was discussed by Ban, who disputed that luck in the drug discovery process should not be understated.[72] In practice, AstraZeneca researchers have reported significant 'big-steps' forward in drug development projects by screening accessible building blocks. They also indicated that the relatively large changes made by the use of building blocks were not capable of being replicated through conventional iterative design and synthesis.[69] Goldberg and co-workers finally concluded that a global effort to synthesise quality building blocks could be a successful strategy to enhance drug discovery programmes.[69]

More recently, Harris *et al*. from Pfizer reported the synthesis of azabicyclohexyl trifluoroborate salts such as **47** (Scheme 2.1).[73] A Simmons-Smith cyclopropanation reaction of pyrrolidinyl vinyl boronate **45** with diethylzinc, diiodomethane and TFA in CH_2Cl_2 at –40 °C formed the unprotected azabicyclohexyl boronate due to Boc removal by the TFA. Subsequent amine reprotection with Boc_2O was carried out to give *N*-Boc azabicyclohexyl boronate **46**. Unfortunately, the cyclopropanation of pyrrolidinyl vinyl boronate **45** did not go to completion and, additionally, product and starting material were inseparable by column chromatography. Therefore, a clean-up reaction was performed which involved reacting remaining alkene **45** with *N*-bromosuccinimide and H_2O in THF at rt for 2 h to form the more polar, and thus separable, *trans*-bromohydrin.[73] Overall, from this one-pot, three-step process, azabicyclohexyl boronate **46** was isolated in 46% yield on gram-scale batch synthesis.[73] In the next step, azabicyclohexyl boronate **46** was reacted with excess KHF_2 in order to generate the trifluoroborate salt **47** in 85% yield.[73]

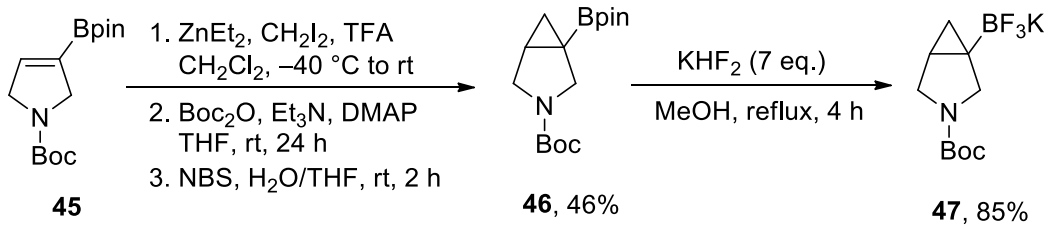

Scheme 2.1

In addition to the trifluoroborate salt **47**, Harris and co-workers also prepared a selection of 5- and 6-membered ring examples by using the same approach (Figure 2.5).[73] The two additional pyrrolidine examples **48** and **49** contained different protecting groups on the amine. As for the piperidines, these two isomers **50** and **51** differed based on the position of the BF_3K group.

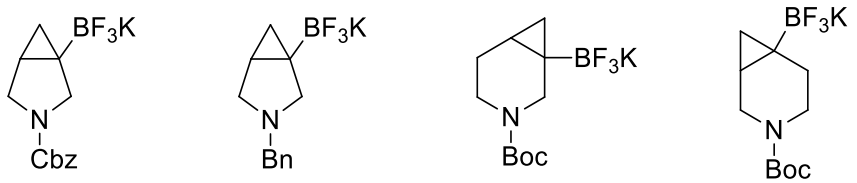

48 **49** **50** **51**

Figure 2.5 – Cyclopropyl boronates synthesised by the group at Pfizer

Recently, Gutiérrez–Bonet and co-workers demonstrated the asymmetric cyclopropanation of enantioenriched alkenyl boronic esters using a chiral auxiliary and *L*-leucine derivative (*S*)-**52** as a Lewis base.[74] The researchers found that the reaction of vinyl boronates under Simmon's Smith conditions ($ZnEt_2$, CH_2I_2 and (*S*)-**52** in THF at –20 °C) gave the *anti*-diastereomer. Using these conditions, (*S*,*S*)-**53** and (*S*,*S*)-**54** were synthesised in a 63% (8:1 dr) and 69% (20:1 dr) yield respectively. When the opposite

enantiomer (*R*,*R*) starting material was used, (*R*,*R*)-**55** was synthesised in 79% (8:1 dr) yield.[74]

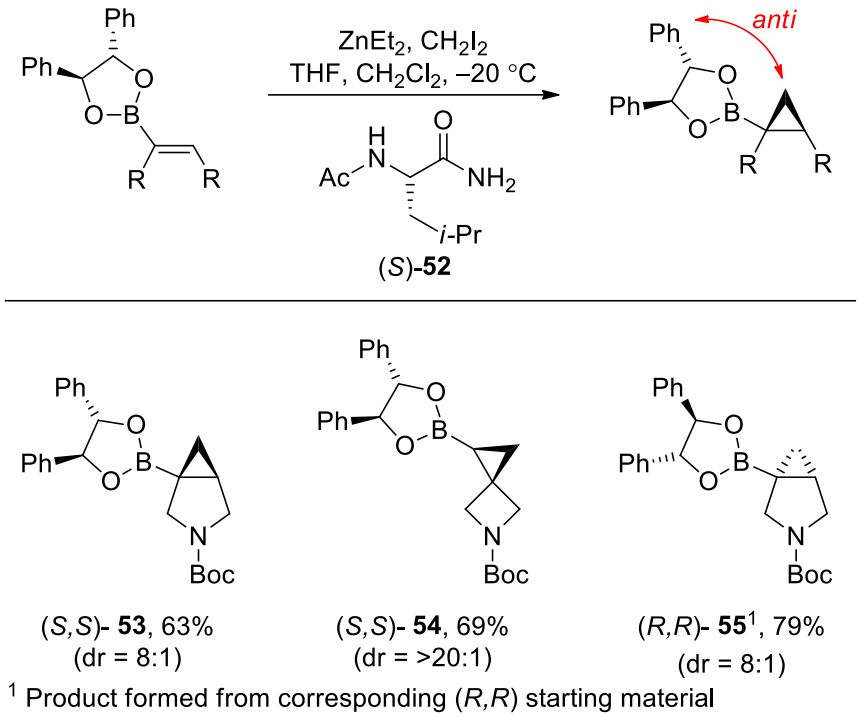

Scheme 2.2

In 2020, Grygorenko and co-workers reported on an alternative synthesis route to access Harris' trifluoroborate salts **49**, **50** and **51** previously shown in Figure 2.5. Instead of using the Simmons Smith cyclopropanation reaction, Grygorenko utilised diazomethane and $Pd(OAc)_2$ to form the cyclopropane. Vinyl-Bpin was reacted with diazomethane and $Pd(OAc)_2$ in *t*-BuOMe at –10 °C for 1 h before subsequent trifluorination with KHF_2 and MeOH in MeCN at rt for 2 h, provided cyclopropyl trifluoroborate salts **49** (94%), **50** (92%) and **51** (99%).[75] Despite the exceptional yield obtained, the potentially explosive

nature of diazomethane solutions heavily impacts on the scalability and practicality of the route.[75]

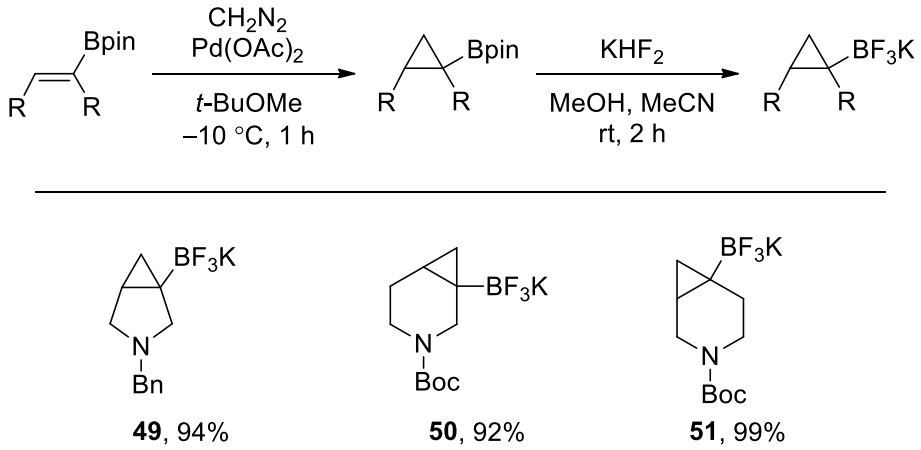

49, 94% **50**, 92% **51**, 99%

Scheme 2.3

Other concepts in the development of building blocks were proposed by Grygorenko *et al.* in the synthesis of geminal difluorocyclopropanes (Scheme 2.4).[76] Reaction of TMS–CF_3 and NaI in THF at refluxing temperatures generated the key difluorocarbene *in situ*. Then, reaction with vinyl trifluoroborates **56** salts gave difluorocyclopropyl trifluoroborate salts **57**. With this reaction, Grygorenko *et al.* managed the synthesis of **58**, **59**, **60** and **61** in excellent yields. The methodology was also demonstrated by preparation of 50 g of **60** from a single batch synthesis.

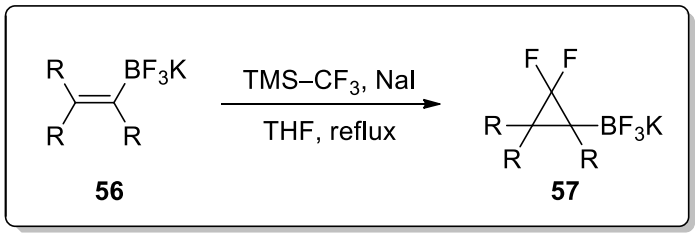

56 **57**

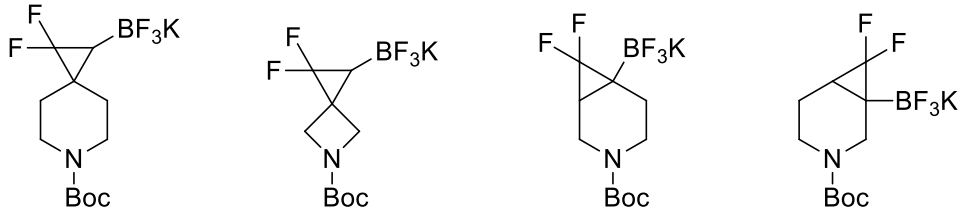

90%, **58** 75%, **59** 84%, **60** 70%, **61**

Scheme 2.4

The transformation of dichlorocyclopropane **62** into cyclopropyl catecholborane *exo*-**63** was reported by Renslo *et al*.[77] based on methodology that had previously been developed

by Danheiser and Savoca.[78] Based on Danheiser's findings, bromine–lithium exchange of dibromocyclopropane **62** was performed with *n*-BuLi in THF at low temperature (– 95 °C to –100 °C) for 10 min. The lithiated species was then trapped with catecholborane before being heated to 50 °C for 16 h to generate cyclopropyl catecholborane *exo*-**63** (Scheme 2.5). Cyclopropyl catecholborane *exo*-**63** was then treated with H_2O_2 and NaOH to give cyclopropanol **64** in a 15% overall yield.[78]

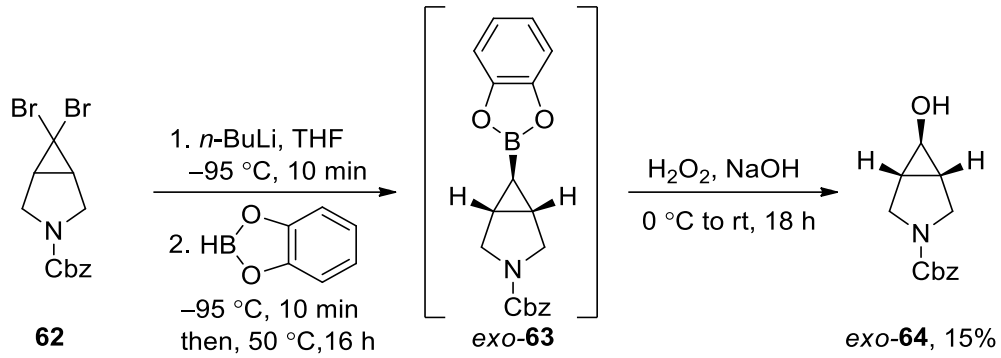

Scheme 2.5

The proposed mechanism and stereochemical outcome for this transformation is shown in Scheme 2.6. First, bromine–lithium exchange occurs on the *endo* bromine to place the remaining bromine atom in the least sterically hindered position (*exo*). The lithiated intermediate **65** is then trapped with catecholborane to afford boronate **66**. A 1,2-migration (Matteson–Pasto rearrangement) of the hydride of the boronate then gives cyclopropyl catecholborane *exo*-**63** with inversion of stereochemistry.

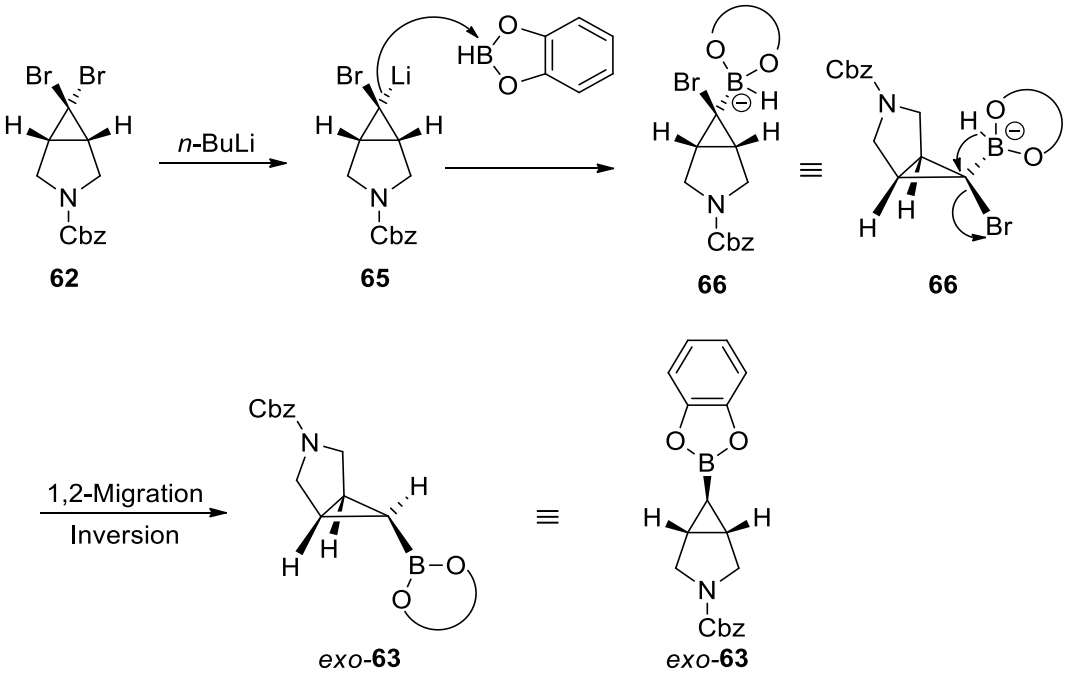

Scheme 2.6

Another comparative building block can be found in the patent literature. In 2022, Nasveschuk and co-workers described the use of tricyclic ligands for degradation of IKZ2 or IKZF4 genes.[79] Although the exact synthesis of cyclopropyl BF_3K salt *exo*-**71** was not disclosed in the patent, the authors suggested that the synthesis was carried out based on the work of Charette *et al*.[80] Therefore, a synthetic route whereby alkene **67** could undergo cyclopropanation with *gem*-dizinc carbenoid **68** to give cyclopropyl zinc iodide *exo*-**69** can be envisaged (Scheme 2.7). With no stereochemical outcome given for this reaction, we can assume preferential formation of the least sterically hindered *exo* diastereomer. Cyclopropyl zinc iodide *exo*-**69** would then be trapped with trimethylborate to produce cyclopropyl boronic acid *exo*-**70** from which cyclopropyl BF_3K salt *exo*-**71** could be formed.

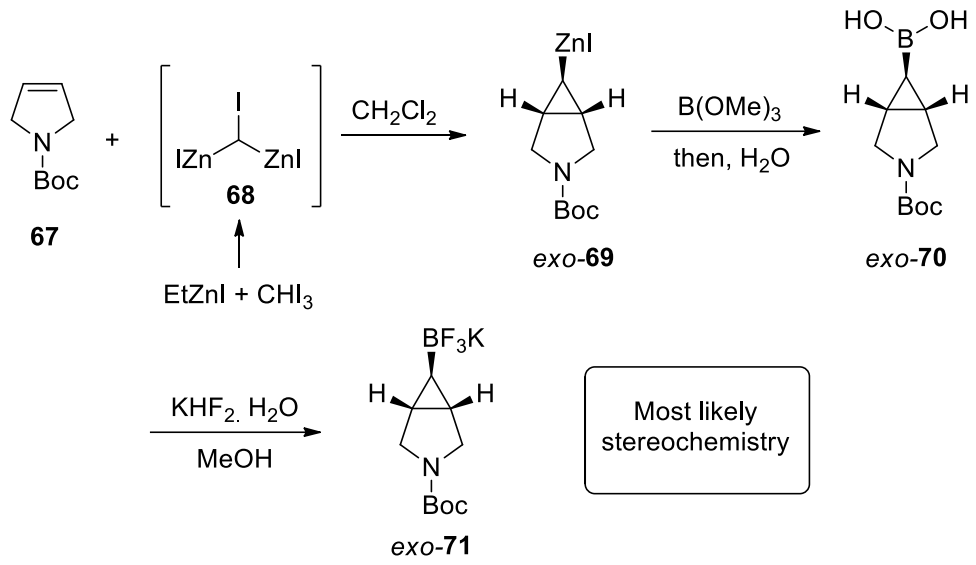

Scheme 2.7

The synthesis of geminal Bpin diborylalkanes has been developed.[81,82] Reaction of bromoform, potassium hydroxide and benzyltrimethylammonium chloride in CH_2Cl_2 generates a dibromocarbene *in situ*, and then reaction with alkene **67** gave the corresponding dibromocyclopropane in 52% yield (Scheme 2.8). Lithiation of dibromocyclopropane with *n*-BuLi, followed by trapping with B_2pin_2 in THF at – 78 °C for 12 h afforded geminal diboronpinacolato alkane **72**. Masarwa and co-workers later produced geminal Bpin–BF_3K diborylalkanes by subjecting diboronpinacolato alkane **72** to KF, CsF and *L*-tartaric acid in MeOH, MeCN and H_2O. Use of this approach produced diborylcyclopropane *exo*-**73** in high yield (90%) and diastereoselectivity (99:1 dr).[81]

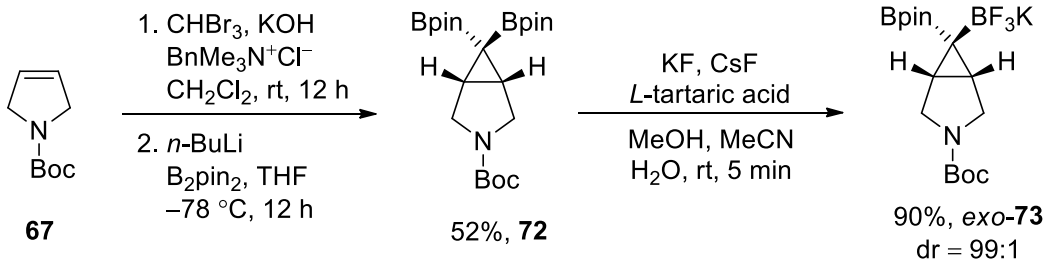

Scheme 2.8

The proposed mechanism for the synthesis of geminal diboronpinacolato alkane **72** involved a bromine-lithium exchange and Bpin trapping to give cyclopropyl boronate **75**. The subsequent transfer of Bpin proceeds *via* a Matteson–Pasto rearrangement to afford geminal diboronpinacolato alkane **72** (Scheme 2.9). Sequential fluorination of the least sterically hindered *exo* boron allows for increasing electrophilicity due to the greater

electronegativity of the fluorine displacing the oxygen atom. Thus, the selective repeated fluorination of the *exo* boron allows for the generation of diborylcyclopropane *exo*-**73**. It was also suggested that donation of a pair of electrons from fluorine into the empty *p*-orbital of boron stabilises the final product.[81]

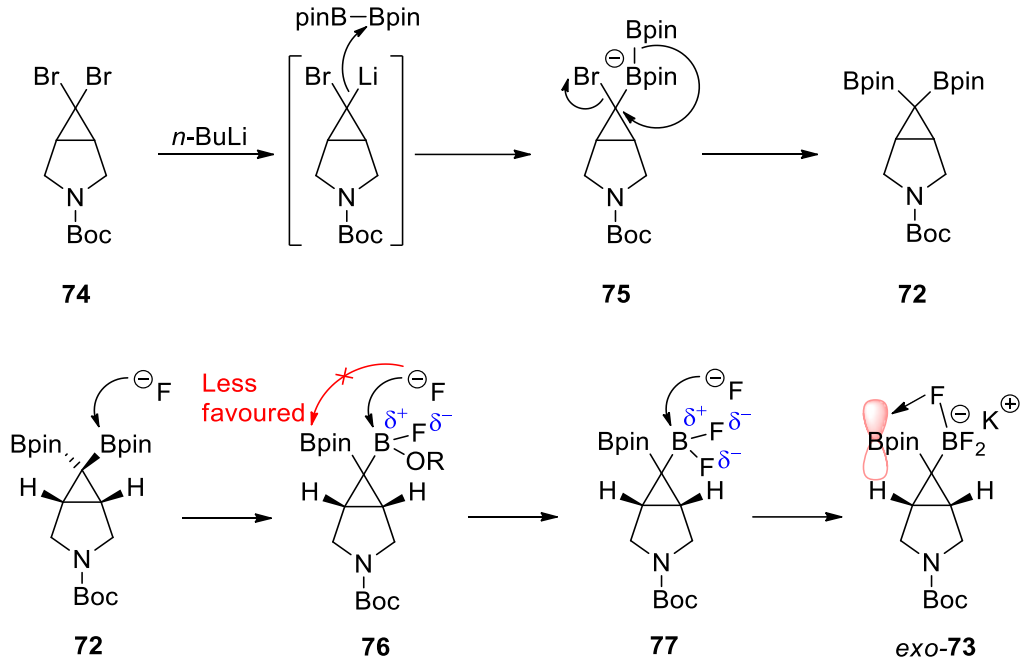

Scheme 2.9

Although the building blocks highlighted in this section represent similarities to the set of York 3-D building blocks (see Figure 1.7), none of the compounds were designed for use in the elaboration of fragments in 3-D. Nonetheless, they remain the closest examples to the work that will be discussed in the subsequent chapters.

2.3 Synthesis of Cyclopropyl 3-D Building Blocks

Previous members of the O'Brien group had developed key methodology for the synthesis of the York 3-D building blocks.[47] One of the routes involved dibromocyclopropanes **79** as an intermediate (Scheme 2.10). Starting from commercially available alkenes **78**, cyclopropanation *via* dibromocarbene generated from bromoform and NaOH gave dibromocyclopropane **79**. Removal of one bromine using dimethylphosphite and KO*t*-Bu generated monobromocyclopropanes **80** (the mechanism of this reaction is discussed later). Subsequent bromine-lithium exchange with *n*-BuLi and then trapping with *i*-PrO–Bpin afforded cyclopropyl Bpin derivatives **81**. Transformation into cyclopropyl BMIDAs **82** occurred using MIDA and triethyl orthoformate.

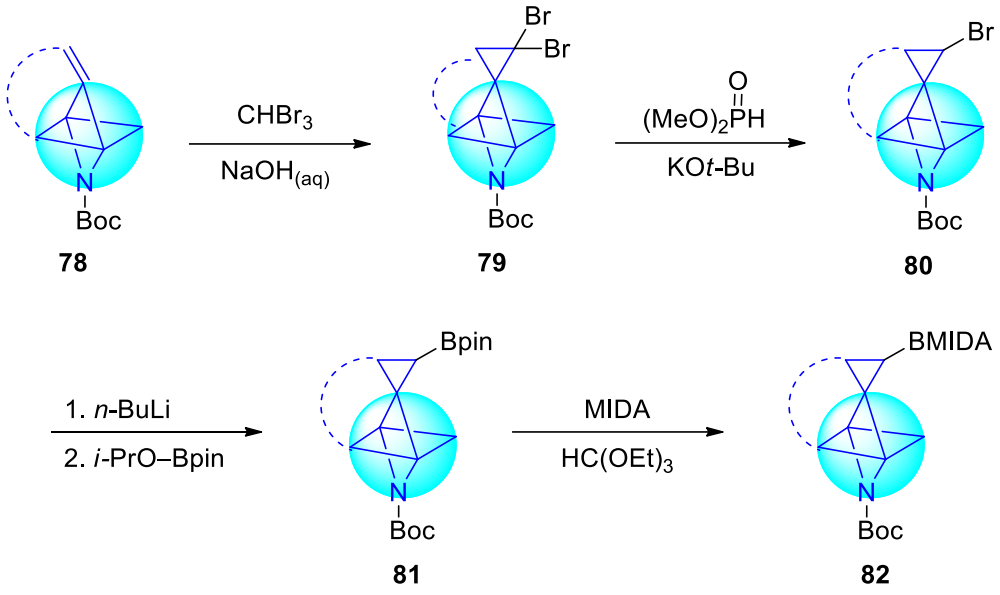

Scheme 2.10

The second synthetic methodology used for the synthesis of the York 3-D building blocks involves a boronate rearrangement from a dichlorocyclopropane intermediate, which effectively utilises the Danheiser methodology discussed in the previous section (see Schemes 2.5 and 2.6). The mechanism for the key step is shown in Scheme 2.11 using conditions that were developed by James Donald.[48] Thus, it was proposed that dichlorocyclopropanes **83** underwent lithium-chlorine exchange; trapping of the lithiated species **84** with H–Bpin generated the boronate intermediates **85**. Nucleophilic displacement of chloride with the boronate hydride then gave cyclopropyl Bpin derivatives **86**.

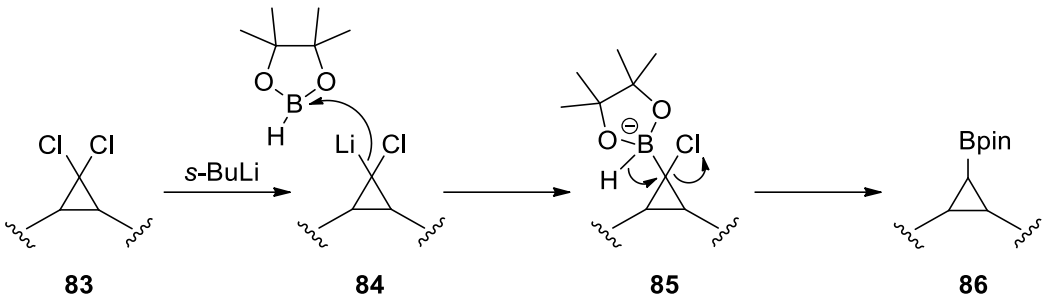

Scheme 2.11

Starting from the same type of starting material as the dibromocyclopropane route, dichlorocyclopropanes **87** were synthesised by reaction of alkenes **78** with chloroform and NaOH. Chlorine-lithium exchange with *s*-BuLi in the presence of H–Bpin and then rearrangement gave cyclopropyl Bpins **81**. Transformation of cyclopropyl Bpins **81** using MIDA and triethyl orthoformate to give cyclopropyl BMIDAs **82** finalises this route (Scheme 2.12).

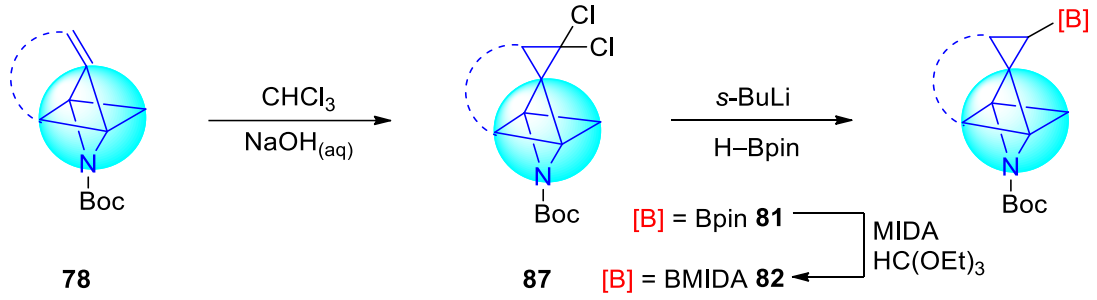

Scheme 2.12

In the rest of this chapter, the synthesis of five cyclopropyl 3-D building blocks *exo*-**36**, **37**, *trans*-**38**, *cis*-**38**, and *exo*-**39** are described. The objectives for these synthetic studies were: (*i*) to develop the synthetic routes to each building block and (*ii*) to scale up the synthetic routes to enable multi-gram quantities of each building block to be prepared. The results of these parts are described in subsequent sections.

2.3.1 2,3-Fused Piperidine 3-D Building Block

The approach for the synthesis of 2,3-fused piperidine cyclopropyl BMIDA *exo*-**36** follows the dibromocyclopropane route as highlighted in Scheme 2.10. This synthesis was developed by previous members of the group and the yields reported are from the previous studies.[47,49] Using a procedure by Six *et al.*, lactam **88** was reduced with

DIBAL–H resulting in the corresponding alcohol intermediate. Subsequent dehydration using *p*-toluenesulfonic acid gave enamide **89**.[83] The dibromocyclopropanation of alkenes has been reported in several studies. By adapting conditions from Six *et al*. and Yamazaki *et al*., alkene **89** was treated with dibromocarbene generated from bromoform and NaOH.[83,84] As a result, formation of dibromocyclopropane **90** occurred in 48% yield.[47] Monodebromination of dibromocyclopropanes with dimethylphosphite and KO*t*-Bu was a procedure originally reported by Meijs and Doyle.[85] Using these conditions, monodebromination of dibromocyclopropane **90** yielded 80% of monobromocyclopropane *exo*-**91**.[47] With conditions from Echavarren *et al.*,[86] sequential lithiation using *n*-BuLi and trapping with *i*-PrO–Bpin and transformation to MIDA with conditions from Wang *et al.*[87] gave cyclopropyl Bpin *exo*-**92** (70% yield) and cyclopropyl BMIDA *exo*-**36** (47% yield) respectively.[49]

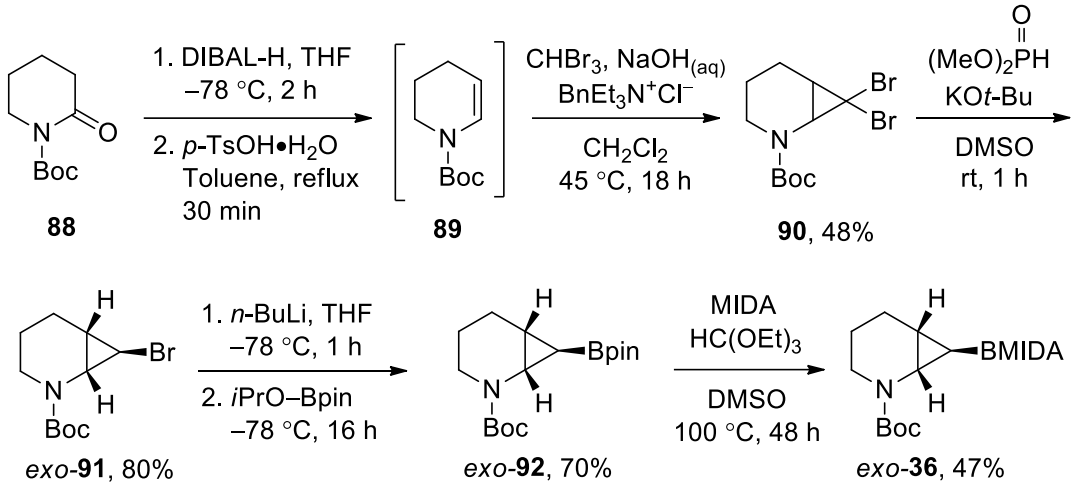

Scheme 2.13

With the methodology for the synthesis of cyclopropyl BMIDA *exo*-**36** already established by former members of the group, a scale-up of this route to obtain multiple grams of cyclopropyl BMIDA *exo*-**36** was carried out. To start, lactam **88** was converted into dibromocyclopropane **90** *via* reduction, dehydration and dibromocyclopropanation (Scheme 2.14).[83] Reduction of lactam **88** with DIBAL–H in THF at –78 °C, followed by work-up and addition of *p*-toluenesulfonic acid (0.2 mol%) in toluene at refluxing temperatures gave enamide **89** in varying yields between 53–70%. Dibromocyclopropanation of enamide **89** using $NaOH_{(aq)}$ (10 M aqueous solution) and benzyltriethylammonium chloride (phase transfer catalyst) in bromoform at rt gave dibromocyclopropane **90** in 68–76% yields.[83,84]

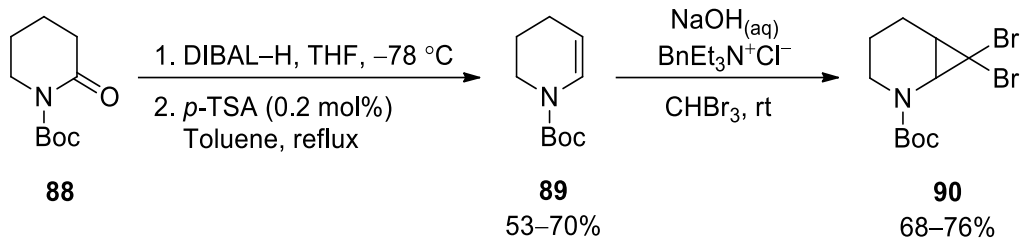

88 **89** 53–70% **90** 68–76%

Scheme 2.14

Slight adaptation to the route reported by Six *et al*. was proposed by former members of the group.[47] It was discovered that work-up and isolation of crude alcohol **93**, before dehydration and dibromocyclopropanation led to a significant increase in yield. Thus, the adapted conditions were used on 14.3 g (72 mmol) of lactam **88** by first treating it with DIBAL–H in THF at –78 °C for 2 h. Quenching with a saturated aqueous solution of potassium sodium tartrate (Rochelle salt) in THF initially at –78 °C and then warming to rt for 16 h gave crude alcohol **93**. Dehydration was accomplished using *p*-toluenesulfonic acid and Dean-Stark apparatus in toluene for 30 min and this gave crude enamide **89** after work-up. Without any purification, crude enamide **89** was subjected to dibromocyclopropanation using phase transfer catalysis conditions[88] to afford 20.2 g of dibromocyclopropane **90** in 81% yield across all three steps (Scheme 2.15). On this large scale, it was found that the work-up of the dibromocyclopropanation reaction was challenging since an emulsion readily formed when washing the organic solvent with H_2O. However, removal of the reaction solvent (CH_2Cl_2) by evaporation upon completion of the reaction and carrying out the extractions with Et_2O reduced the formation of an emulsion and made the overall work-up more straightforward. This was a key discovery for all such dibromocyclopropanation reactions.

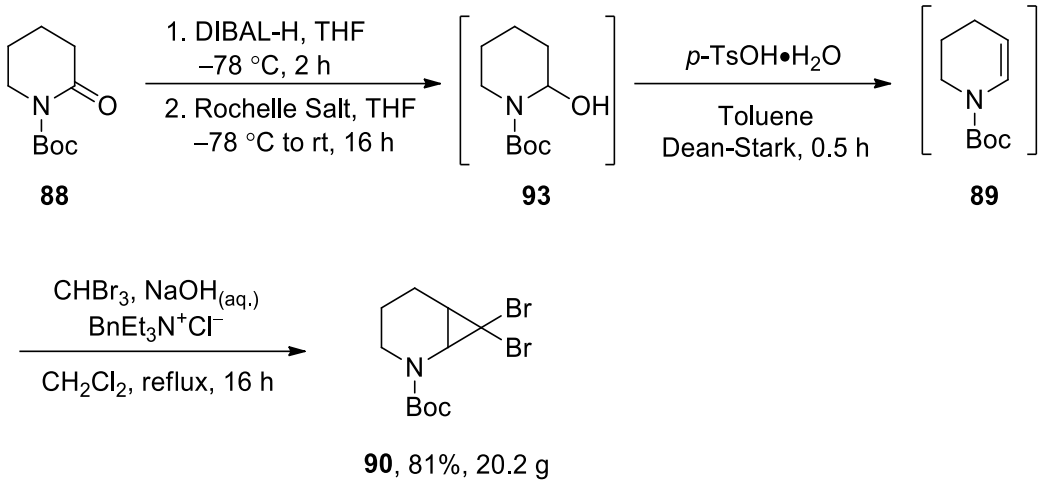

Scheme 2.15

The reduction of dihalocyclopropanes to monohalocyclopropanes was a transformation reported by Seyferth *et al*. in 1962 using organotin hydrides.[89] Reaction of tributyltin hydride with dibromocyclopropanes gave monobromocyclopropanes. However, over-reduction of the monobromocyclopropanes by tributyltin hydride was also possible. In addition to this, the high toxicity of tin compounds was a major drawback for this method. Therefore, various alternative monodebromination reactions were explored. Shimizu *et al.* and Jefford *et al.* demonstrated that monodebromination could be achieved using reducing agents such as $LiAlH_4$.[90,91] Taking dibromocyclopropane **94**, reaction with $LiAlH_4$ and 10 mol% of $AgClO_4$ in THF at –20 °C for 15 min gave monobromocyclopropanes *exo*-**95**, *endo*-**95**, and cyclopropane **96** in 4%, 77% and 17% yields respectively (Scheme 2.16).[90] It was noted that longer reaction times resulted in the increased formation of cyclopropane **96**. Although a radical mechanistic pathway was proposed for the transformation, no explanation for the observed diastereoselectivity was proposed.[90]

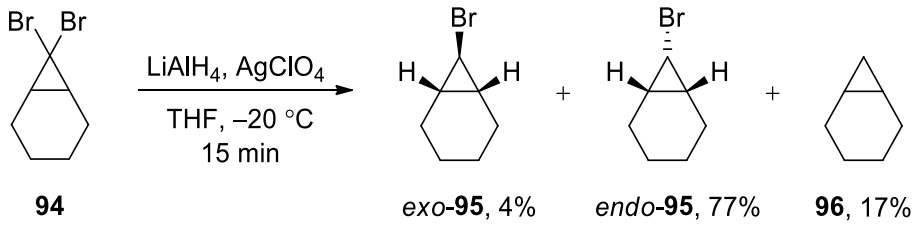

Scheme 2.16

Other approaches for monodebromination using Grignard reagents have also been well reported.[92,93] Unlike the previous examples, monodebromination using Grignard reagents

seems to avoid the further reaction of monobromocyclopropanes. For example, treatment of dibromocyclopropane **94** with ethyl magnesium bromide and titanium *iso*-propoxide (2 mol%) in Et_2O (rt, 20 min) gave monobromocyclopropanes *exo*-**95** and *endo*-**95** in 90% yield and 20:80 dr respectively (Scheme 2.17). The authors offered no explanation for the observed diastereoselectivity.[93]

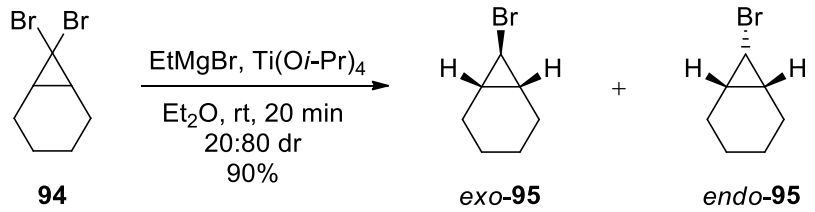

Scheme 2.17

However, research from Al Dulayymi *et al.* illustrated a proposal for the mechanism of monodebromination of dibromocyclopropanes using titanium *iso*-propoxide and ethylmagnesium bromide (Scheme 2.18).[94] The accepted mechanism for the activation of titanium *iso*-propoxide to titanacyclopropane **100** follows that of the Kulinkovich reaction,[95] such that nucleophilic substitution of *iso*-propoxy with ethyl groups occurs to give diethyltitanium **97**. Loss of ethane from diethyltitanium **97** affords titanacyclopropane **98**. This reactive species is proposed to undergo reaction with dibromocyclopropane **99** *via* a radical pathway to give cyclopropyl titanium complex **100** which is protonated on work-up to give monobromocyclopropane **101**.

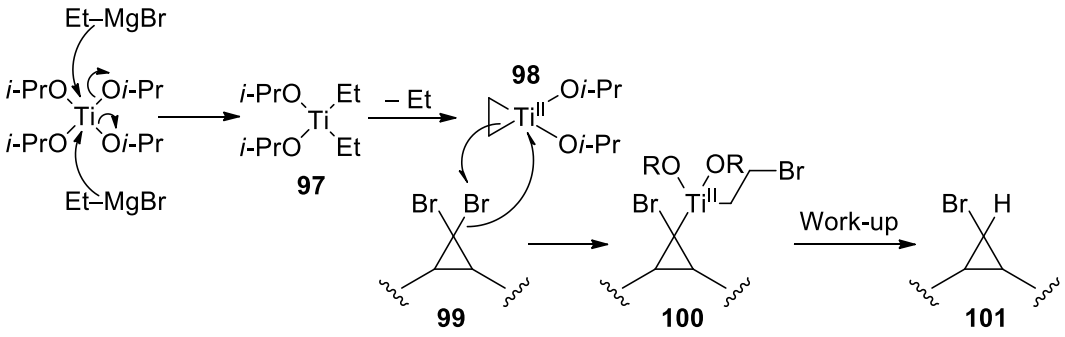

Scheme 2.18

In 1994, Harada and co-workers reported the diastereoselective monodebromination of dibromides using *n*-BuLi. As an example, dibromocyclopropane **94** was treated with *n*-BuLi in THF and hexane at –85 °C for 15 min. Then, addition of aqueous acetic acid

yielded monobromocyclopropanes *exo*-**95** and *endo*-**95** in 98:2 dr (Scheme 2.19, yield not reported).[96]

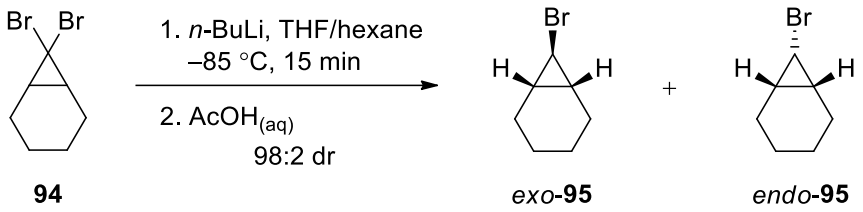

Scheme 2.19

Most of the reaction conditions documented above possess disadvantages including reagent toxicity, poor diastereoselectivity, reactions at low temperatures with reactive reagents or instances of double reduction of dibromocyclopropanes. Fortunately, Meijs and Doyle discovered that the mono-debromination of dibromocyclopropanes could be performed selectively and in high yields using dimethylphosphite and KO*t*-Bu in DMSO at rt for 1 h. For example, dibromocyclopropane **94** gave monobromocyclopropane *exo*-**95** in 96% yield along with monobromocyclopropane *endo*-**95** in 1% yield (Scheme 2.20).[85]

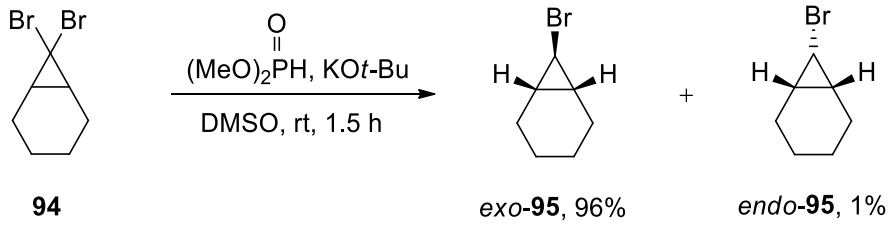

Scheme 2.20

The mechanism of monodebromination using dialkylphosphite has been investigated and an ionic or radical mechanism can both be imagined. The first mechanistic proposal for this reaction was by Hirao *et al*. who claimed an ionic pathway involving initial deprotonation of dialkylphosphite to give phosphorus anion **102**.[97] Next, halophilic attack of dibromocyclopropane **99** by anion **102** results in the formation of cyclopropyl anion **103**. Subsequent protonation affords monobromocyclopropanes **101** although an explanation for the diastereoselectivity was not proposed (Scheme 2.21).[98]

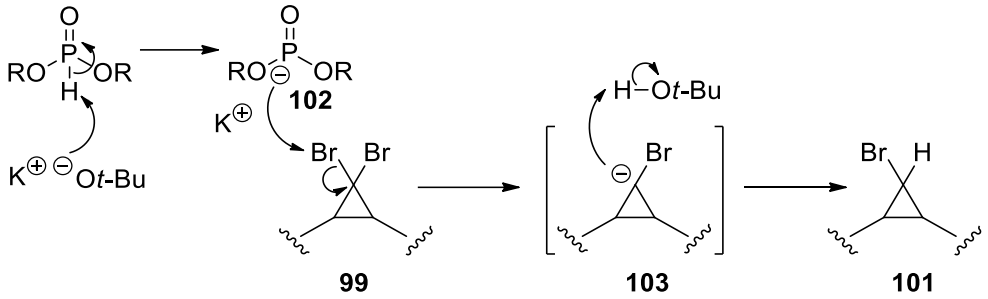

Scheme 2.21

Later, Meijs and Doyle challenged Hirao's mechanistic proposal by investigating the possibility of single electron transfer or homolytic pathways.[85] Two experiments were designed to probe this. First, monodebromination of dibromocyclopropane **94** was carried out in the dark and under an atmosphere of oxygen to inhibit any initiation of radical pathways.[85,99] Second, monodebromination of dibromocyclopropane **94** was carried out in the presence of radical traps such as di-*t*-butyl nitroxide (20 mol%) or *m*-dinitrobenzene (20 mol%). In both cases, no definitive impact on the yield of the monodebromination reaction was observed, suggesting that single electron transfer is not an important process in this transformation.[85,99] Confirmation that the reducing hydrogen does not originate from the methoxy groups on dimethylphosphite was investigated by a monodebromination reaction using deuterated dimethylphosphite. Data suggested that no incorporation of deuterium was present in the final product. Based on all of this, Meijs and Doyle proposed the mechanism shown in Scheme 2.22. Thus, following Hirao's mechanism, anions *exo*-**104** or *endo*-**104** would be formed *via* a reversible debromination process. This would set up an equilibrium between dibromocyclopropane **94** and anions *exo*-**104** or *endo*-**104**. Seyferth and Lambert reported evidence which suggests that anion *exo*-**104** was thermodynamically more favoured than the sterically hindered *endo*-**104**.[100] Protonation of anion *exo*-**104** by *t*-BuOH would give monobromocyclopropane *exo*-**95**. Thus, Meijs and Doyle indicated that formation of *endo*-**95** occurs but equilibration to *exo*-**95** occurs faster than protonation of anions *exo*-**104** and *endo*-**104**.[85]

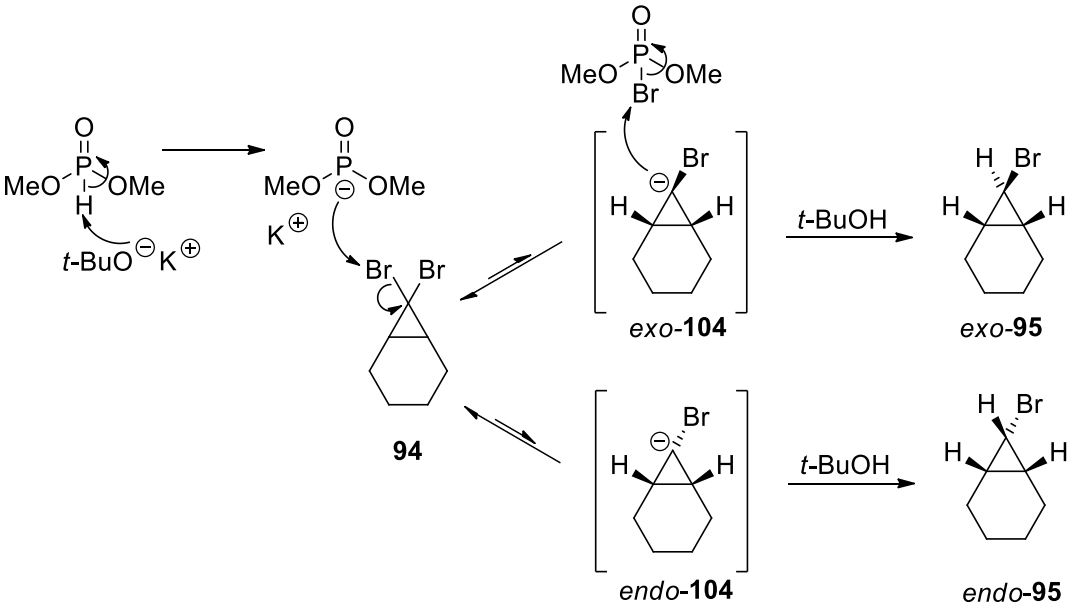

Scheme 2.22

The monodebromination conditions from Meijs and Doyle have proved very useful in the synthesis of the York 3-D building blocks and previous work from both Hanna Klein and Cameron Palmer demonstrated the successful removal of a bromine from dibromocyclopropane **90**.[49] Thus, we repeated their reactions on a larger scale. Dibromocyclopropane **90** was reacted with dimethyl phosphite and potassium *tert*-butoxide in DMSO at rt for 1.5 h to give 20.2 g of monobromocyclopropane *exo*-**91** in 86% yield after chromatography (Scheme 2.23).

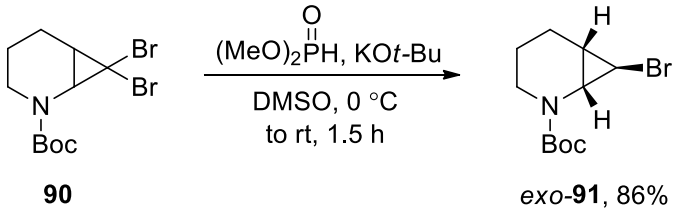

Scheme 2.23

The stereochemistry of monobromocyclopropane *exo*-**91** was assigned using diagnostic ^{3}J values around the cyclopropane ring. In 1964, Hutton and Schaefer reported trends in ^{3}J values for protons in a cyclopropane ring. If the protons are *trans* to each other, then the ^{3}J value is in the 2.0 – 7.0 Hz range. In contrast, for *cis*-cyclopropane protons, ^{3}J values of 7.1 – 11.0 Hz are observed.[101] The ^{3}J values for coupling between protons H_A and H_B and of H_A and H_C (both *trans* couplings) in monobromocyclopropane *exo*-**91** are

shown in Figure 2.8. For *exo*-**91**, proton H_A has a ^3J value of 2.0 Hz to proton H_B and 4.5 Hz to proton H_C. These values clearly indicate the *exo*-stereochemistry.

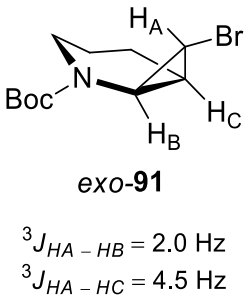

exo-**91**

$^3J_{HA-HB} = 2.0$ Hz
$^3J_{HA-HC} = 4.5$ Hz

Figure 2.6 – Assignment of stereochemistry using ^3J values

It was proposed that conversion of monobromocyclopropane *exo*-**91** into cyclopropyl Bpin *exo*-**92** would be performed using bromine-lithium exchange followed by trapping with *i*-PrO–Bpin. An example of this reaction was reported on a cyclopropyl phenanthrene by Echavarren *et al*.[86] Echavarren's lithiation was carried out using *n*-BuLi in THF at –78 °C for 1 h and the lithiated species was trapped with *i*-PrO–Bpin. These conditions were scalable and an example on a 4.0 g scale was described.[86] Using conditions adapted from this example, monobromocyclopropane *exo*-**91** was reacted with *n*-BuLi before the trapping of the lithiated species with *i*-PrO–Bpin was carried out. Work-up and purification by chromatography gave cyclopropyl Bpin *exo*-**92** in 60% yield (Scheme 2.24). The $^3J_{trans}$ and $^3J_{cis}$ values of 3.5 and 8.0 Hz for the cyclopropyl NCH proton of cyclopropyl Bpin *exo*-**92** established the *exo* stereochemistry.

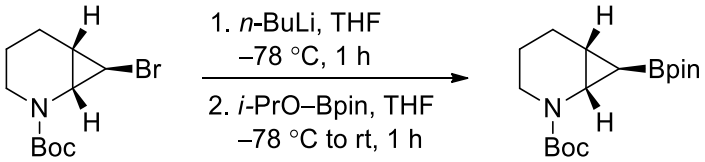

exo-**91** *exo*-**92**, 60%

Scheme 2.24

In the last step, the conversion of Bpin into BMIDA was required to complete the synthesis of 3-D building block *exo*-**36**. For this, conditions were taken from the conversion of a vinyl boronic pinacol ester into a BMIDA group, reported by Wang *et al*.[87] In their example, MIDA and triethyl orthoformate were reacted with a vinyl Bpin in anhydrous DMSO at 100 °C for 12 h to give the vinyl BMIDA compound, *via* a reaction that was scalable up to the gram-scale.[87] Based on these findings, cyclopropyl BMIDA

exo-**36** was synthesised by reaction of cyclopropyl Bpin *exo*-**92** with MIDA and triethyl orthoformate in DMSO at 100 °C for 48 h. The extended reaction time for synthesis of cyclopropyl BMIDA *exo*-**36** was required to allow the reaction to go to completion. After chromatography, cyclopropyl BMIDA *exo*-**36** was isolated in 90% yield (Scheme 2.25). The $^{3}J_{trans}$ and $^{3}J_{cis}$ values of 4.0 and 8.0 Hz for the cyclopropyl NCH proton of cyclopropyl BMIDA *exo*-**36** confirmed the *exo* stereochemistry.

exo-**92**, 60% *exo*-**36**, 90%

Scheme 2.25

The stereochemistry of cyclopropyl BMIDA *exo*-**36** was also definitively proven by an X-ray crystal structure (Figure 2.9). In the three-dimensional structure, it can be seen that the BMIDA group is pointing in the same face as the two vicinal cyclopropyl protons and thus farthest from the piperidine ring. Therefore, an *exo* configuration can be assigned.

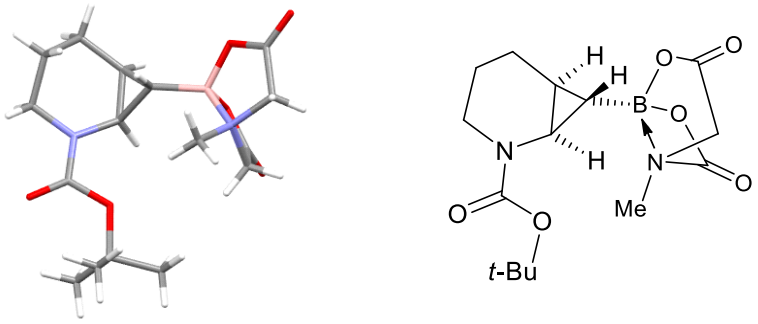

Figure 2.7 – X-ray crystal structure of MIDA boronate building block exo-**36**

Overall, this synthesis afforded 3.6 g of MIDA building block *exo*-**36** and 5.2 g of cyclopropyl Bpin *exo*-**92** prepared from commercially available lactam **88**. The synthesis of cyclopropyl BMIDA *exo*-**36** proceeded over five steps. The overall yield was a satisfactory 42% for synthesis of cyclopropyl Bpin *exo*-**92**, with only a 4.0 g batch of cyclopropyl Bpin *exo*-**92** being converted into cyclopropyl BMIDA *exo*-**36**.

2.3.2 4-Spiro Piperidine 3-D Building Block

The methodology for the synthesis of cyclopropyl BMIDA **37** has been thoroughly examined by former group member Hanna Klein.[47] It was found that synthesis of cyclopropyl BMIDA **37** could be achieved through monodebromination of dibromocyclopropane **106** (Scheme 2.26), as well as boronate rearrangement of dichlorocyclopropane **109** (Scheme 2.27). The dibromocyclopropane route consisted of a dibromocyclopropanation reaction of alkene **105** using bromoform, NaOH and benzyl triethylammonium chloride, which gave dibromocyclopropane **106** in 65% yield. Monodebromination *via* conditions from Al Dulayymi *et al.*,[93] namely reaction with ethyl magnesium bromide and titanium *iso*-propoxide in THF at rt for 3 h, were employed in the synthesis of monobromocyclopropane **107** (73% yield). Lithiation of monobromocyclopropane **107** with *n*-BuLi, then trapping with *i*-PrO–Bpin yielded cyclopropyl Bpin **108** in 86% yield (Scheme 2.26).[47]

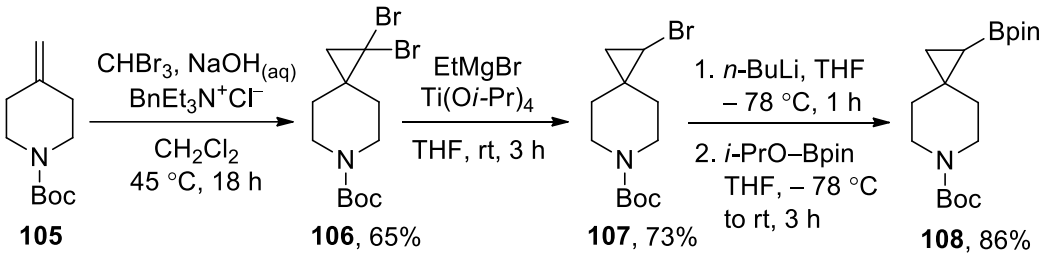

Scheme 2.26

The dichlorocyclopropanation route is shown in Scheme 2.27. Reaction of alkene **105** with NaOH and a phase-transfer catalyst in chloroform at 45 °C for 18 h yielded dichlorocyclopropane **109** (89% yield). Treatment of dichlorocyclopropane **109** with *s*-BuLi and H–Bpin in THF initially at –78 °C for 30 min and then rt for 1 h gave cyclopropyl Bpin **108** in 58% yield. Transformation of Bpin into BMIDA afforded cyclopropyl BMIDA **37** in 48% yield.[47]

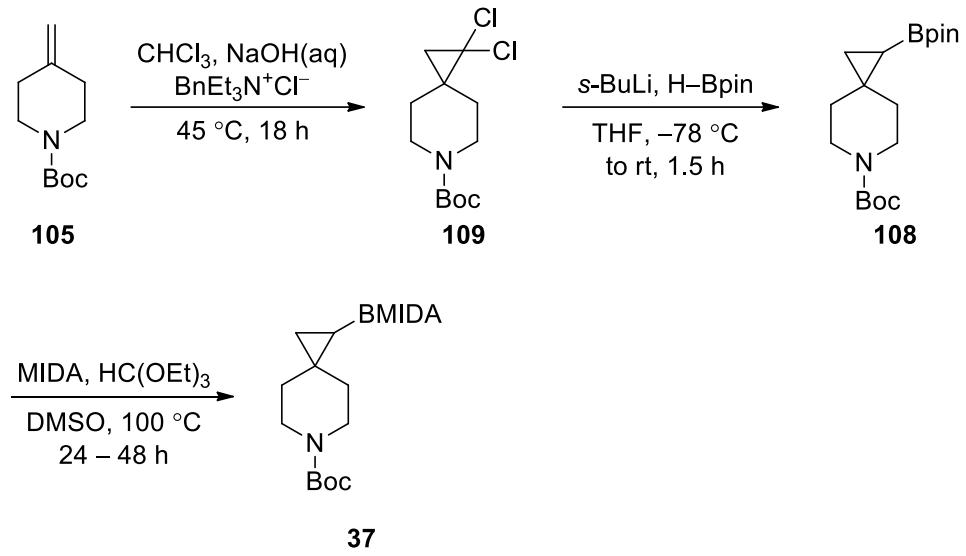

Scheme 2.27

As described in Chapter 5, building blocks cyclopropyl Bpin **108** and cyclopropyl BMIDA **37** were used as model systems for carrying out methodology development for the potential synthesis of a 3-D covalent fragment library. Therefore, it was necessary to synthesise gram quantities of each of these building blocks for our studies. After considering the two previous routes developed in the group, it was decided that the dichlorocyclopropane route was favoured due to its shorter synthesis as well as the potential to avoid the difficult work-up for dibromocyclopropanations on multi-gram reaction scales. First, reaction of alkene **105** with NaOH and benzyltriethylammonium chloride in chloroform at 45 ℃ for 16 h was carried out. This proceeded uneventfully and gave dichlorocyclopropane **109** in 75% yield (10.7 g prepared) (Scheme 2.28).

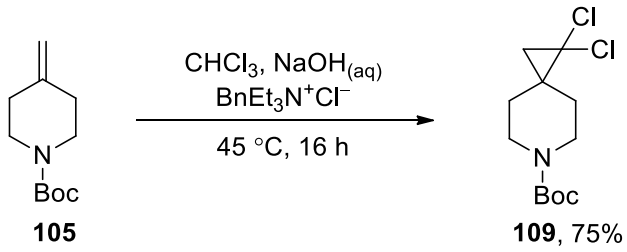

Scheme 2.28

Following a set of conditions developed by previous members of the group,[47,48] dichlorocyclopropane **109** was reacted with *s*-BuLi and H–Bpin in THF at – 78 ℃ for 30 min and then warming to rt over 1 h. After chromatography, cyclopropyl Bpin **108** was obtained in 64% yield (4.3 g prepared). Final transformation of some of the cyclopropyl Bpin **108** into cyclopropyl BMIDA **37** was performed with MIDA and triethyl

orthoformate in DMSO at 100 °C for 72 h. This afforded cyclopropyl BMIDA **37** in 61% yield (1 g prepared) (Scheme 2.29).

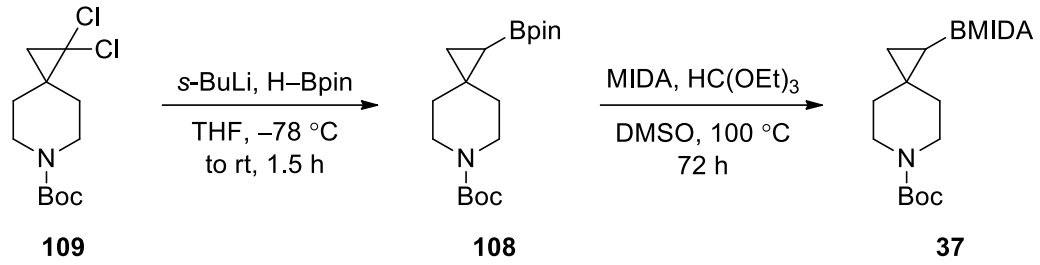

Scheme 2.29

2.3.3 3,4-Fused Pyrrolidine 3-D Building Block

The synthesis of cyclopropyl BMIDA building blocks *exo*-**39** and *endo*-**39** was unprecedented. Thus, we envisaged that the synthesis route for cyclopropyl BMIDAs *exo*-**39** and *endo*-**39** would follow the dibromocyclopropane pathway, as per the synthesis of cyclopropyl BMIDA *exo*-**36** previously described (see Scheme 2.13). It was anticipated that dibromocyclopropane **74** would be synthesised *via* a dibromocarbene generated from bromoform and aqueous NaOH. Then, removal of a bromine from dibromocyclopropane **74** may give both monobromocyclopropanes *exo*-**110** and *endo*-**110**. Subsequent halogen–lithium exchange, electrophile trapping with *i*-PrO–Bpin and transformation into BMIDA of each diastereomer would give cyclopropyl BMIDA building blocks *exo*-**39** and *endo*-**39** (Scheme 2.30).

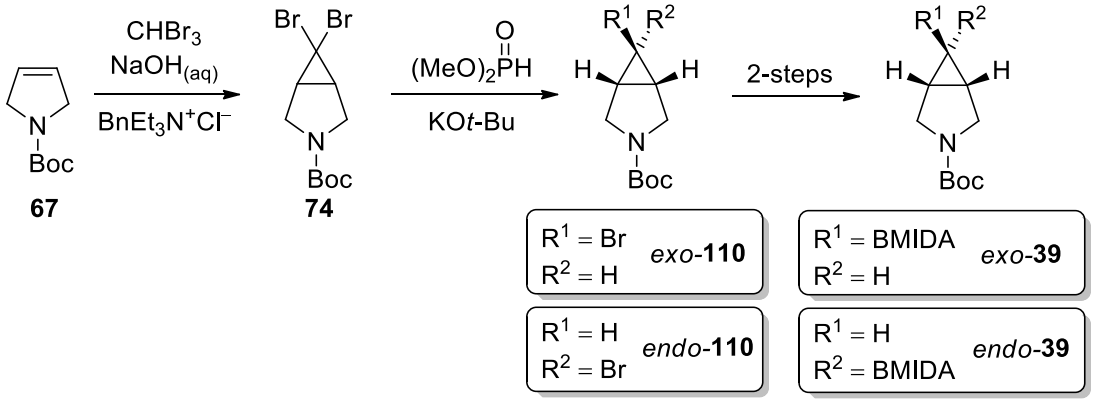

Scheme 2.30

For the first step in the synthesis of cyclopropyl BMIDAs *exo*-**39** and *endo*-**39**, dibromocyclopropanation of pyrroline **67** was proposed. Using standard conditions for dibromocyclopropanation (bromoform, NaOH and benzyltriethylammonium chloride in CH_2Cl_2 at 50 °C for 16 h), pyrroline **67** was converted into dibromocyclopropane **74**. The ^{1}H NMR spectrum of the crude product indicated a 60:40 mixture of pyrroline **67** and dibromocyclopropane **74**. Unfortunately, separation of dibromocyclopropane **74** from unreacted pyrroline **67** was challenging and a significant portion of dibromocyclopropane **74** co-eluted with *N*-Boc pyrroline **67**. After careful chromatography, dibromocyclopropane **74** was isolated in 39% yield (Scheme 2.31). Under these conditions, there was remaining pyrroline **67** after the reaction.

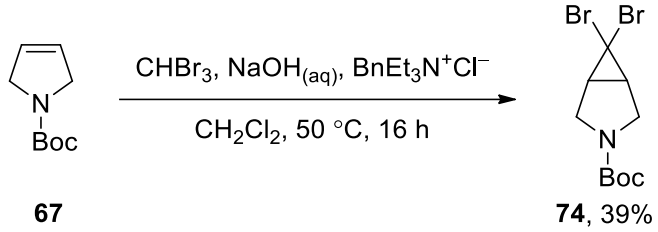

67 **74**, 39%

Scheme 2.31

Due to the incomplete conversion of pyrroline **67** into dibromocyclopropane **74**, other conditions for cyclopropanation were explored. In 2018, Mengwei *et al.* described the exact transformation of pyrroline **67** into dibromocyclopropane **74** in a patent. It was reported that reaction of pyrroline **67** with bromoform and sodium *tert*-pentoxide in *n*-heptane at rt for 4 h gave dibromocyclopropane **74** in 93% yield on a kilogram-scale.[102] Therefore, our starting point was to use this procedure on a smaller scale. Thus, following their procedure, pyrroline **67** was suspended with sodium *tert*-pentoxide in *n*-heptane at −10 °C and bromoform was slowly added over 1 h. The reaction was then stirred at rt for 5 h. After work-up, the crude product was analysed by ^{1}H NMR spectroscopy which indicated a 60:40 mixture of pyrroline **67** and dibromocyclopropane **74**. After careful chromatography, dibromocyclopropane **74** was obtained in 29% yield and the ^{1}H NMR spectroscopic data matched those reported in the literature[103] (Scheme 2.32).

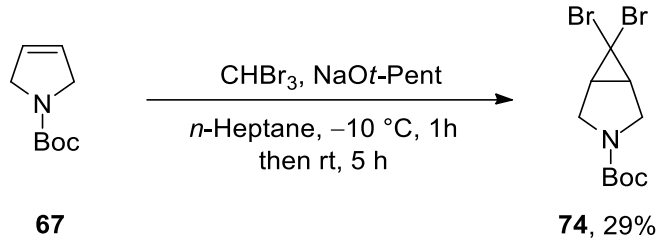

67 **74**, 29%

Scheme 2.32

In order to improve the conversion and ultimately yield of dibromocyclopropanation reactions, Dailey and Lynch reported the use of substoichiometric amounts of pinacol and dibenzo-18-crown-6 in combination with $NaOH_{(aq)}$ and bromoform.[104] Pleasingly, reports of high yields and facile work-ups were shown when reactions were carried out in the presence of pinacol and dibenzo-18-crown-6. The authors proposed that pinacol is responsible for accelerating the phase-transfer deprotonation of substrates up to pK_a 27.[104] In addition, the effects of crown ethers in phase-transfer catalysis was investigated by Dehmlow and Fastabend.[105,106] It was found addition of dibenzo-18-crown-6 at elevated temperatures gave the optimal reaction conditions for dibromocarbene addition.[104–106] Therefore, their reaction conditions were attempted. The reaction was carried out by the slow addition of a chilled 50% aqueous solution of $NaOH_{(aq)}$ to pyrroline **67**, bromoform, pinacol, and dibenzo-18-crown-6 in CH_2Cl_2 at rt before the mixture was refluxed for 16 h. The ^1H NMR spectrum of the crude product indicated a 45:55 mixture of pyrroline **67** and dibromocyclopropane **74** (Scheme 2.33). The yield of dibromocyclopropane **74** was determined using an internal standard (1,3-benzodioxole) and this gave a 26% NMR yield of dibromocyclopropane **74**; chromatography was not carried out.

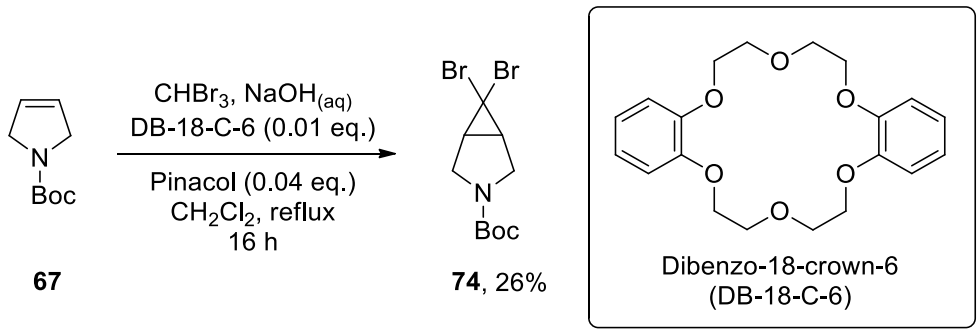

67 **74**, 26%

Scheme 2.33

After attempting several dibromocyclopropanation reactions, it appeared that the complete consumption of pyrroline **67** was unattainable. The most promising cyclopropanation reaction conditions so far were with bromoform and sodium *tert*-pentoxide in *n*-heptane (see Scheme 2.32). The cleaner reaction profile of using these conditions paved the way for an idea used by Harris *et al*. where a second reaction was used to react any remaining pyrroline **67** to bromohydrin *trans*-**111** (see Scheme 2.1). The increased polarity of bromohydrin *trans*-**111** meant that it could therefore be readily separated from dibromocyclopropane **74** by column chromatography.[73] Fortunately, synthesis of bromohydrin *trans*-**111** from pyrroline **67** had been reported by Bull *et al*. using NBS and H_2O in DMSO at rt for 16 h.[103] Thus, reaction of pyrroline **67** with sodium *tert*-pentoxide and bromoform was carried out in the usual way and gave the crude product. Then, the crude product was treated with NBS and H_2O in DMSO using Bull's procedure. Upon work-up, analysis of the ^{1}H NMR spectrum of the crude product showed complete conversion of pyrroline **67** to bromohydrin *trans*-**111**. Purification by chromatography gave dibromocyclopropane **74** in 47% yield and bromohydrin *trans*-**111** in 30% yield, indicating that at least 30% of pyrroline **67** had not reacted (Scheme 2.34). By utilising this approach, access to multi-gram quantities of pure dibromocyclopropane **74** (45-47% yield) was possible.

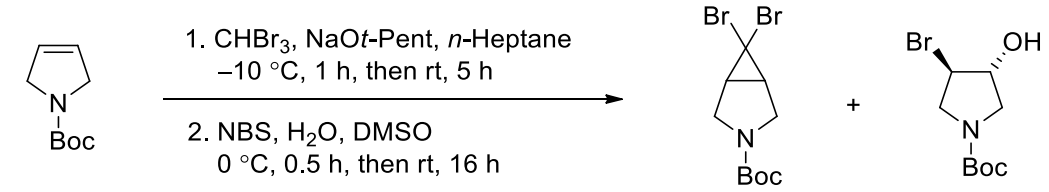

67	**74**	*trans*-**111**
30 mmol	47%	30%
45 mmol	45%	-

Scheme 2.34

Previously, the conditions reported by Meijs and Doyle successfully gave monobromocyclopropane *exo*-**91** diastereoselectivity (see Scheme 2.23). Therefore, it was anticipated that debromination of dibromocyclopropane **74** would also proceed with *exo* selectivity. Initially, a small-scale reaction was carried out using dibromocyclopropane **74** (0.44 mmol), potassium *tert*-butoxide and dimethyl phosphite in DMSO at rt for 1.5 h. Work-up and ^{1}H NMR spectroscopy of the crude product showed that a 70:30 mixture of monobromocyclopropanes *exo*-**110** and *endo*-**110** were formed.

The diastereomers were separable by chromatography and monobromocyclopropanes *exo*-**110** and *endo*-**110** were isolated in 55% and 22% yield respectively (Scheme 2.35). The scale-up of this monodebromination reaction to 3, 15 and 20 mmol proceeded with the same diastereoselectivity and gave combined yields of 83%, 69% and 81% for monobromocyclopropanes *exo*-**110** and *endo*-**110**.

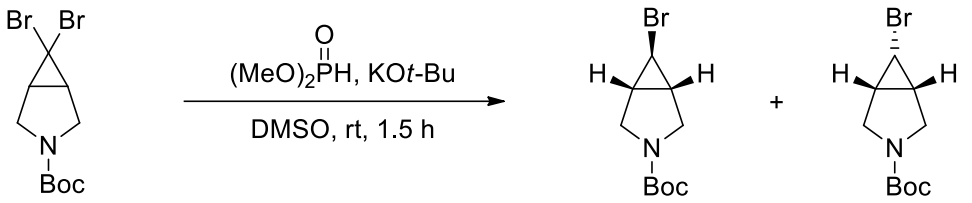

74	*exo*:*endo**	*exo*-**110**	*endo*-**110**
0.44 mmol	70:30	55%	22%
3 mmol	70:30	65%	18%
15 mmol	70:30	48%	21%
20 mmol	70:30	58%	23%

*Diasteromeric ratio determined by 1H NMR spectroscopy of the crude product

Scheme 2.35

The $^{3}J_{trans}$ value of 2.5 Hz for the cyclopropyl CHBr proton of monobromocyclopropane *exo*-**110** established the *exo* stereochemistry. In contrast, the $^{3}J_{cis}$ value of 7.5 Hz for the cyclopropyl CHBr proton of monobromocyclopropane *endo*-**110** established the *endo* stereochemistry. The stereochemistry of monobromocyclopropanes *exo*-**110** and *endo*-**110** were also confirmed by an X-ray structure of the crystalline monobromocyclopropane *endo*-**110** (Figure 2.10). In the three-dimensional structure, it can be seen that all three hydrogen atoms are on the same face of the cyclopropane, therefore assigning *endo*-configuration.

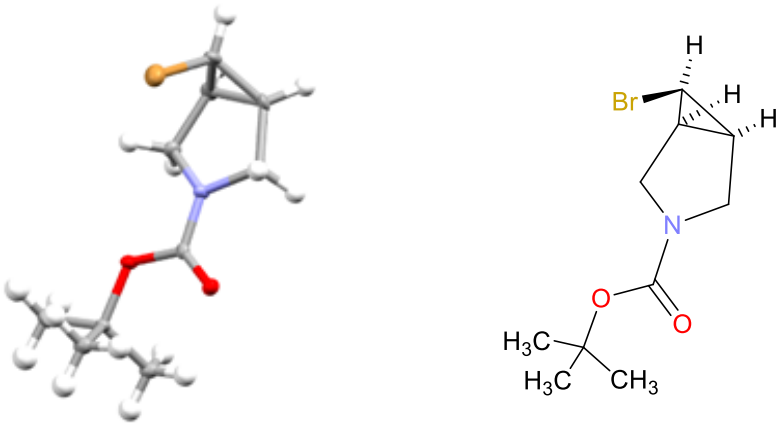

*Figure 2.8 – X-ray crystal structure of monobromocyclopropane endo-***110**

In 2015, Zhao and co-workers reported on the *endo*-selective reduction of geminal dibromides with dimethyl phosphite and a carbonate base.[107] As opposed to using dimethyl phosphite with potassium *tert*-butoxide and DMSO, their reaction conditions involved the use of dimethyl phosphite with potassium carbonate and dioxane at 80 °C for 16 h to generate monobromocyclopropane *endo*-**95** in 94% yield and 99:1 dr (Scheme 2.36).[107] However, close inspection of their ^{1}H NMR spectroscopic data clearly indicates that *endo*-stereochemistry was incorrectly assigned. The ^{3}J value of 3.6 Hz for the cyclopropyl CHBr proton on what they claimed to be monobromocyclopropane *endo*-**95** suggests *trans* coupling which indicates that their product was in fact *exo*-**95**.[101]

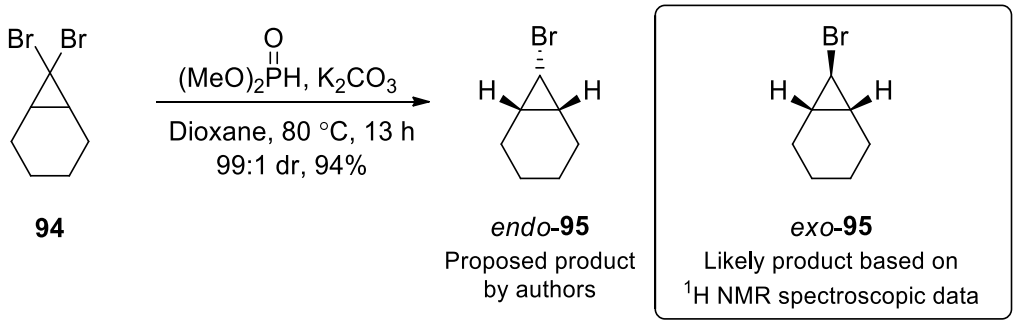

Scheme 2.36

Despite the erroneous assignment of *endo*-selectivity, for comparison, we decided to explore the reaction conditions reported by Zhao and co-workers for the debromination of dibromocyclopropane **74**. Thus, reaction of dibromocyclopropane **74** with dimethyl phosphite and potassium carbonate was carried out in dioxane at 80 °C for 16 h. This gave monobromocyclopropanes *exo*-**110** (12%) and *endo*-**110** (10%) after

chromatography (Scheme 2.37). As a result, these conditions were not further investigated nor used going forwards.

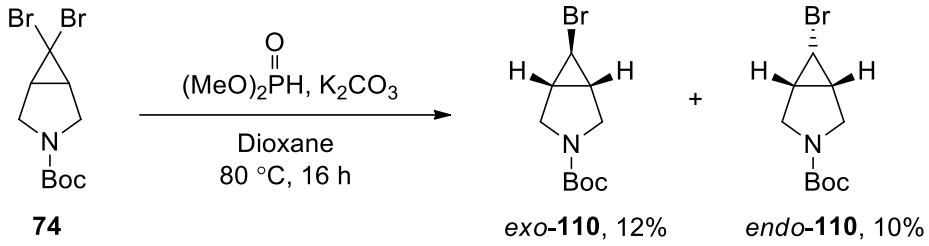

Scheme 2.37

The last two steps of the synthetic route would follow those typically used in the group. Thus, conversion of monobromocyclopropane *exo*-**110** into cyclopropyl Bpin *exo*-**112** using bromine-lithium exchange followed by trapping with *i*-PrO–Bpin would be carried out next. Monobromocyclopropane *exo*-**110** was reacted with *n*-BuLi before trapping of the lithiated species with *i*-PrO–Bpin. Work-up and purification by chromatography gave cyclopropyl Bpin *exo*-**112** in 80% yield on a small scale (1.6 mmol), and 73% yield on a large scale (16 mmol) (Scheme 2.38). The formation of cyclopropyl Bpin *exo*-**112** was confirmed by a $^{3}J_{trans}$ value of 4.5 Hz for the coupling of cyclopropyl C*H*–Bpin proton in the ^{1}H NMR spectrum. This showed that the reaction proceeded with retention of stereochemistry, as expected.

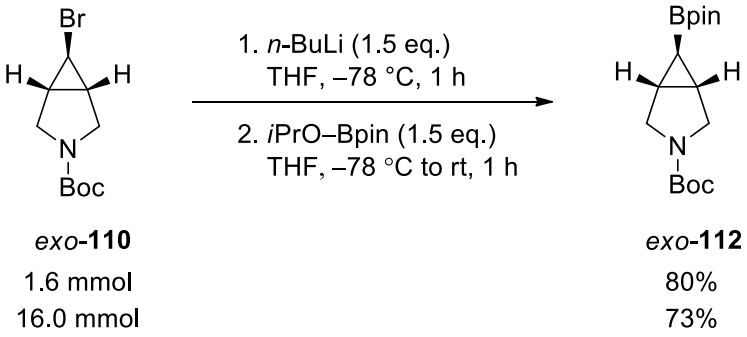

Scheme 2.38

The conversion of Bpin into BMIDA was required to conclude the synthesis of cyclopropyl BMIDA *exo*-**39**. Reaction of cyclopropyl Bpin *exo*-**112** with MIDA and triethyl orthoformate gave cyclopropyl BMIDA *exo*-**39** in 79% yield (2.97 g) post-chromatography on an 11 mmol scale (Scheme 2.39). The stereochemistry of cyclopropyl BMIDA *exo*-**39** was confirmed by a $^{3}J_{trans}$ value of 4.5 Hz in the ^{1}H NMR spectrum and by X-ray crystallography (Figure 2.11).

Scheme 2.39

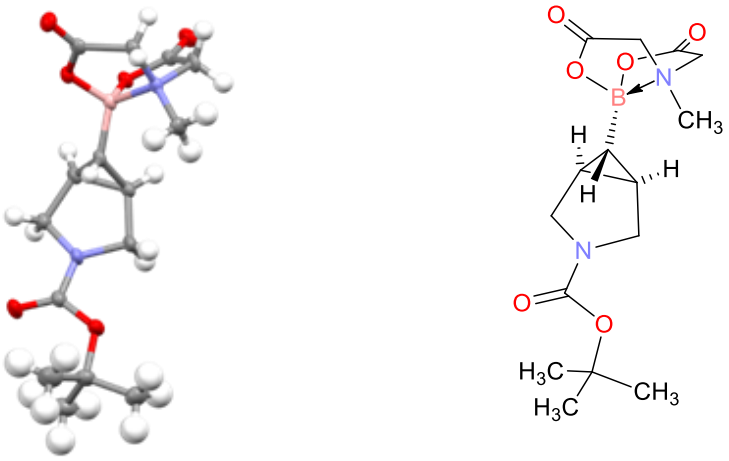

*Figure 2.9 –X-ray crystal structure of MIDA boronate building block exo-***39**

At this stage, we were also interested in trying to access cyclopropyl BMIDA *endo*-**39** as another potential 3-D building block. Two routes were envisaged, namely the usual bromine-lithium exchange and BMIDA formation but starting from the diastereomeric monobromocyclopropane *endo*-**110** or the dichlorocyclopropane boronate rearrangement route. The standard bromine-lithium exchange route was explored first. Unfortunately, subjecting monobromocyclopropane *endo*-**110** to bromine-lithium exchange then trapping with *i*PrO–Bpin was unsuccessful (Scheme 2.40). It is possible that the *endo* bromide is too sterically hindered to undergo bromine-lithium exchange. However, it may be the case that the *endo* position is too sterically hindered to trap with the relatively bulky *i*PrO–Bpin electrophile. Therefore, a slightly smaller boron electrophile was attempted. Bromine-lithium exchange on monobromocyclopropane *endo*-**110**, followed by addition

of H–Bpin was carried out. However, this too failed to give cyclopropyl Bpin *endo*-**112** (Scheme 2.40).

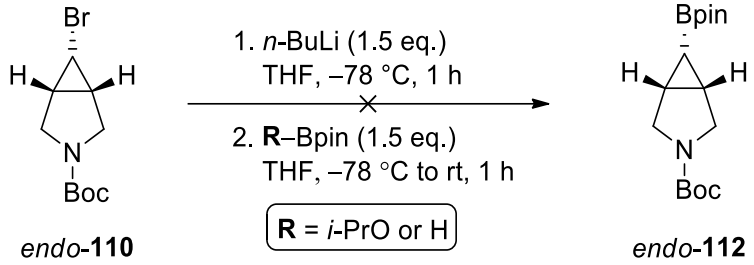

Scheme 2.40

Next, the dichlorocyclopropane route was explored as a potential way of synthesising cyclopropyl Bpin *endo*-**112** selectively (Scheme 2.41). First, dichlorocyclopropanation of alkene **67** with chloroform, phase-transfer catalyst and aqueous NaOH gave dichlorocyclopropane **113** in 52% yield. Then, lithiation of dichlorocyclopropane **113** with *s*-BuLi and trapping with H–Bpin gave evidence for the formation of the desired cyclopropyl Bpin *endo*-**112** after chromatography, although it could not be isolated pure. An approximate yield (5%) was determined from the ^{1}H NMR spectrum of the impure product (Scheme 2.41).

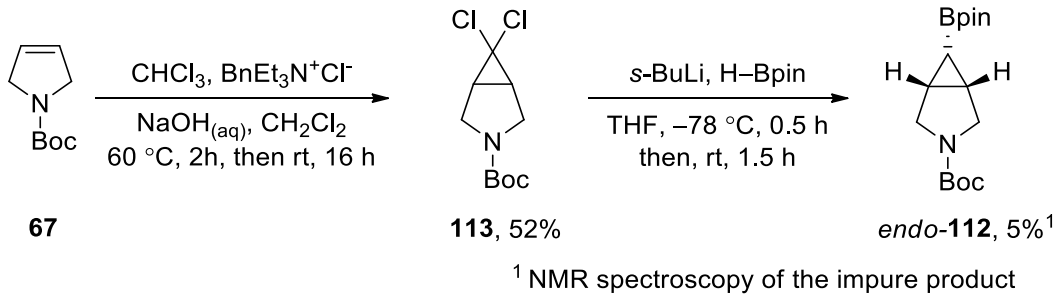

Scheme 2.41

Although plans to trap the lithiated species (generated by bromine-lithium exchange) with even smaller electrophiles such as borane•THF were considered, it is possible to hypothesise that introduction of the sterically hindered BMIDA group would also be problematic. Therefore, the attempts to prepare cyclopropyl BMIDA *endo*-**39** were halted at this point.

In summary, a 2.97 g batch of a new cyclopropyl BMIDA building block *exo*-**39** was prepared starting from pyrroline **67**. The synthesis proceeded over four steps. The overall yield was only 15% due to an inefficient dibromocyclopropanation step (47% yield of

dibromocyclopropane **74**) and a moderately *exo*-selective debromination reaction (58% yield of monobromocyclopropane *exo*-**110**).

2.3.4 3-Spirocyclic Pyrrolidine 3-D Building Blocks

The synthesis of novel cyclopropyl BMIDA building blocks *trans*-**38** and *cis*-**38** was proposed as outlined in Scheme 2.42. Similar to the synthesis of cyclopropyl BMIDA *exo*-**36** and *exo*-**39**, this synthetic route would also involve the dibromocyclopropane intermediate. First, a known Wittig reaction of pyrrolidinone **117** would yield alkene **114,**[108] which would then be reacted with bromoform and a base to form dibromocyclopropane **115**. Subsequent removal of bromine would generate monobromocyclopropanes *trans*-**116** and *cis*-**116**. Individual reactions of monobromocyclopropanes *trans*-**116** and *cis*-**116** with *n*-BuLi and then *i*-PrO–Bpin should generate cyclopropyl Bpin *trans*-**119** and *cis*-**119**. Completion of the synthesis of cyclopropyl BMIDA *trans*-**38** and *cis*-**38** would be performed by reaction of cyclopropyl Bpin *trans*-**119** and *cis*-**119** with MIDA.

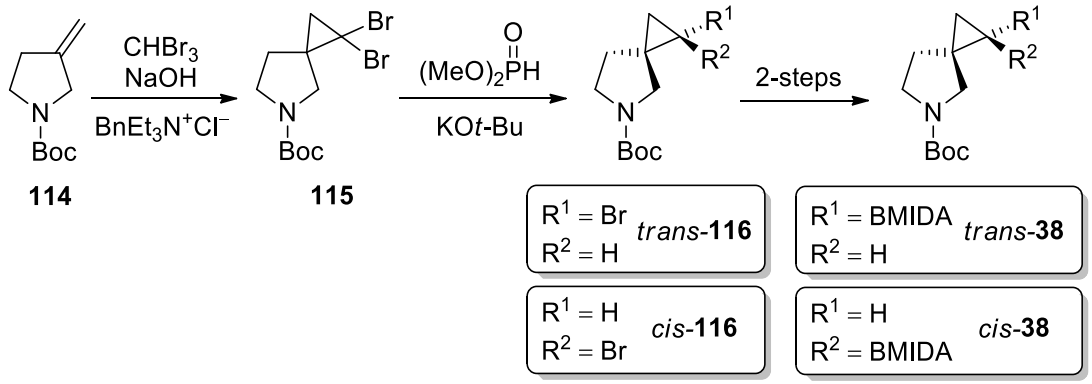

Scheme 2.42

In the first step of the route, alkene **114** would be synthesised by a Wittig reaction of pyrrolidinone **117** as reported by De Kimpe *et al.*[108] Thus, methyl triphenylphosphonium bromide was deprotonated using potassium *tert*-butoxide in THF at 0 °C to generate the methyl triphenylphosphonium ylide *in situ*. The non-stabilised ylide was then reacted with pyrrolidinone **117** at rt for 16 h to form alkene **114**. On a 5.0 mmol scale, alkene **114** was obtained in 66% yield after chromatography (Scheme 2.43). Subsequent reactions were performed on increased scales of 10 mmol, 27 mmol, and 130 mmol to give alkene **114** in 59%, 79%, and 56% yield respectively after chromatography (Scheme 2.43).

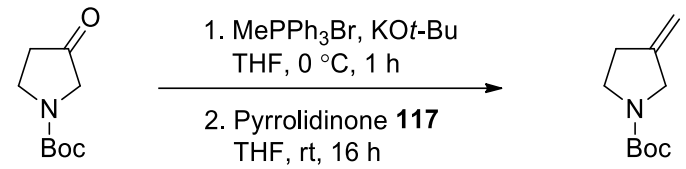

117	**114**
5 mmol	66%
10 mmol	59%
27 mmol	79%
130 mmol	56%

Scheme 2.43

Next, dibromocyclopropanation was performed *via* a dibromocarbene in the usual way (using bromoform, $NaOH_{(aq)}$ and benzyltriethylammonium chloride in CH_2Cl_2 at 50 °C for 16 h). Initially, a 3.0 mmol reaction was performed which gave dibromocyclopropane **115** in 53% yield. Subsequently, larger scale reactions using 21.0 mmol and 2.34 mol of alkene **114** were carried out to afford dibromocyclopropane **115** in 62% and 69% yield after purification by chromatography (Scheme 2.44).

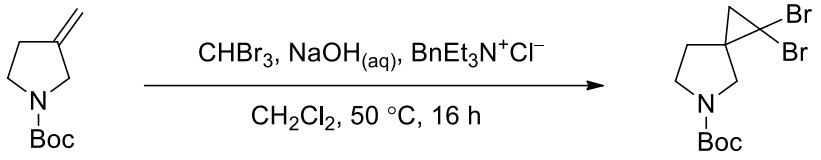

114	**115**
3.0 mmol	53%
21.0 mmol	62%
2.34 mol	69%

Scheme 2.44

The removal of one bromine from dibromocyclopropane **115** would generate diastereomeric monobromocyclopropanes *trans*-**116** and *cis*-**116**. For this, dibromocyclopropane **115** (44 mmol), dimethyl phosphite and potassium *tert*-butoxide in DMSO at rt for 1.5 h gave a 55:45 mixture of monobromocyclopropanes *trans*-**116** and *cis*-**116** based on the ^{1}H NMR spectrum of the crude product. Separation of monobromocyclopropanes *trans*-**116** and *cis*-**116** by chromatography was challenging. However, monobromocyclopropanes *trans*-**116** and *cis*-**116** were isolated in 48% and 35% yield respectively, together with a 5% yield of mixed fractions. The total yield was 88% (Scheme 2.45).

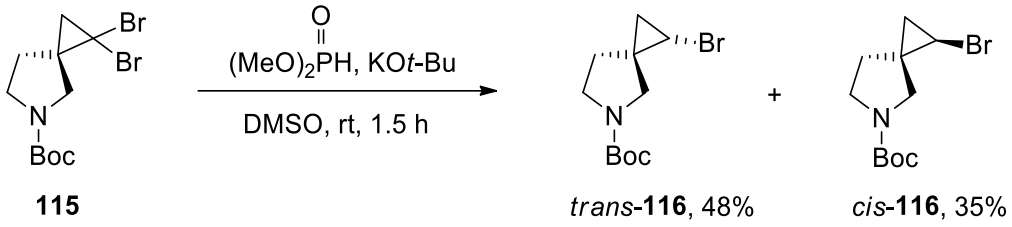

Scheme 2.45

In the debromination of dibromocyclopropane **115**, there was little diastereoselectivity observed, and this can be rationalised by applying the mechanism proposed earlier. Debromination of dibromocyclopropane **115** would produce anionic intermediates *trans*-**118** and *cis*-**118** (Scheme 2.46). In this instance, both anions had no obvious steric interactions to preferentially favour the formation of one diastereomer over the other, as the chemical environment around the bromine atom is very similar. Apparently, a minor preference for the *trans* diastereomer over the *cis* diastereomer was observed.

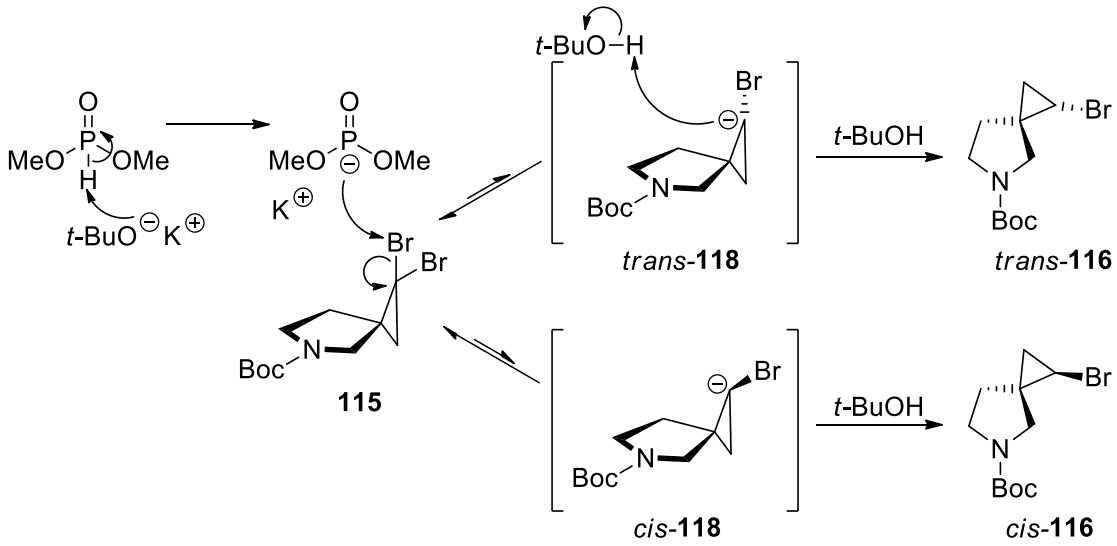

Scheme 2.46

The stereochemistry of monobromocyclopropanes *trans*-**116** and *cis*-**116** were determined by an X-ray structure of the crystalline monobromocyclopropane *cis*-**116** (Figure 2.12). In the three-dimensional structure, it can be seen that the bromine atom is pointing towards the same face as the CH_2 group that is adjacent to the nitrogen, and therefore a *cis* configuration can be assigned.

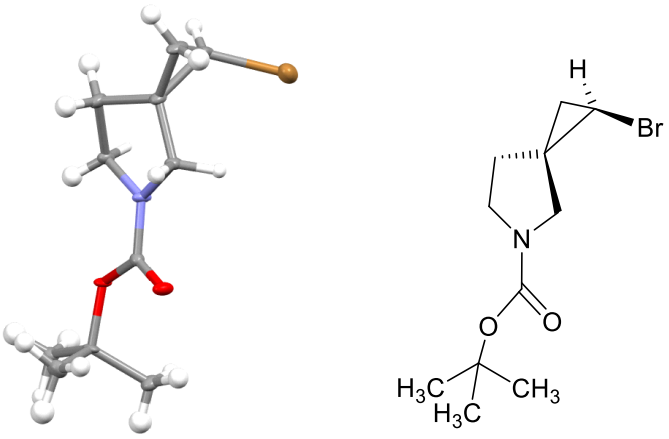

*Figure 2.10 – X-ray crystal structure of monobromocyclopropane cis-***116**

For the next step, the bromine-lithium exchange of each of monobromocyclopropanes *trans*-**116** and *cis*-**116** were carried out using the same procedure as in the synthesis of building blocks *exo*-**36** and *exo*-**39**. Thus, monobromocyclopropane *trans*-**116** was treated with *n*-BuLi in THF at –78 °C for 1 h and then reacted with *i*-PrO–Bpin. Work-up and purification by chromatography gave cyclopropyl Bpin *trans*-**119** in 71% yield on a small scale and 41–59% on a large scale (Scheme 2.47). Under the same conditions, monobromocyclopropane *cis*-**116** gave a 71% yield of cyclopropyl Bpin *cis*-**119**. The MIDA boronates were subsequently prepared on small and large scale using MIDA and triethyl orthoformate in DMSO at 100 °C for 48 h. Work-up and purification by chromatography gave cyclopropyl BMIDA *trans*-**38** (81% yield, 284 mg and 74% yield, 4.27 g) and *cis*-**38** (85% yield, 300 mg and 90%, 3.92 g), both as off-white solids (Scheme 2.47).

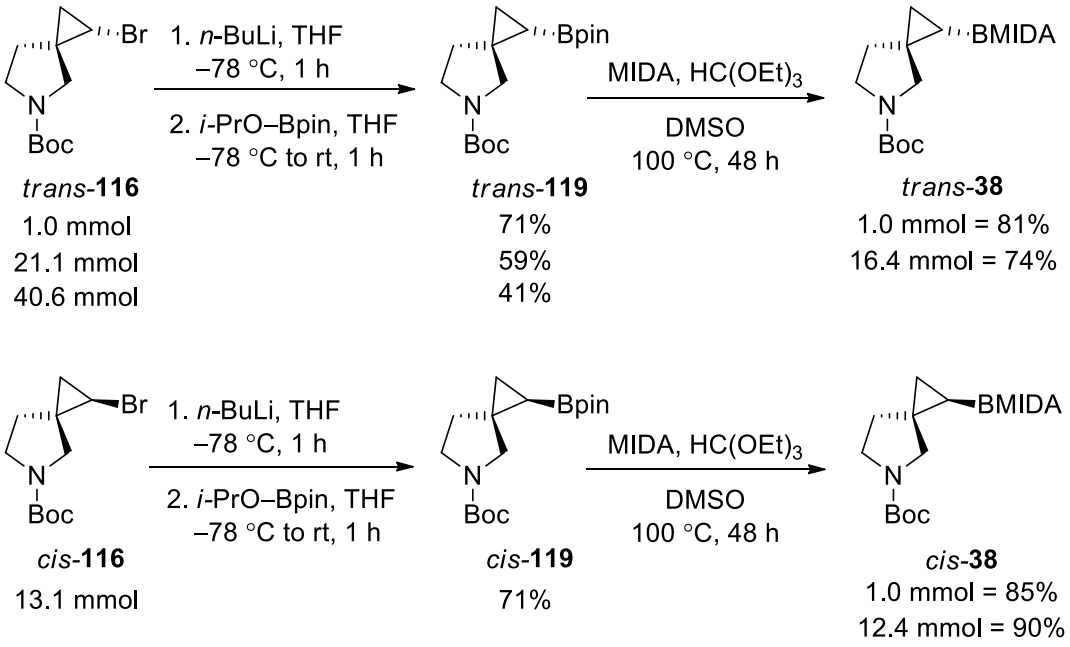

Scheme 2.47

In an attempt to decrease the number of synthetic steps to obtain cyclopropyl BMIDAs *trans*-**38** and *cis*-**38**, the dichlorocyclopropane route was explored. Thus, dichlorocyclopropanation of alkene **114** under the standard conditions gave dichlorocyclopropane **120** in a 72% yield (Scheme 2.48). In the next step, boronate rearrangement by lithiation and trapping of dichlorocyclopropane **120** was carried out to give an undetermined mixture of cyclopropyl Bpin *trans*-**119** and *cis*-**119**. The ^{1}H NMR spectrum of the crude product could not be used to determine the ratio of cyclopropyl Bpins *trans*-**119** and *cis*-**119**, as the chemical shifts in the diagnostic signals of both diastereomers were too similar. Separation of the diastereomers by column chromatography was also unsuccessful, and a mixture of cyclopropyl Bpins *trans*-**119** with *cis*-**119** was isolated in 70% combined yield over 2 steps (Scheme 2.48).

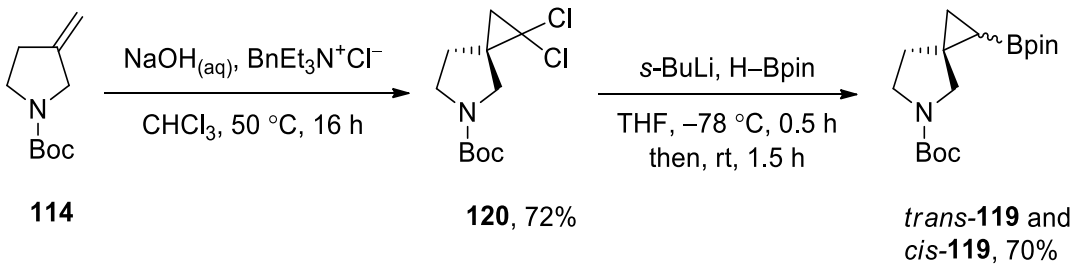

Scheme 2.48

In summary, 4.27 g, and 3.92 g batches of cyclopropyl BMIDAs *trans*-**38** and *cis*-**38** respectively were prepared, starting from pyrrolidinone **117** using the dibromocyclopropane route. The synthesis proceeded over five steps and could not be shortened to four steps *via* the dichlorocyclopropane route due to inseparable diastereomers at the cyclopropyl Bpin stage. The overall yield of the dibromocyclopropane route was only 11% and 10% for cyclopropyl BMIDAs *trans*-**38** and *cis*-**38** respectively due mainly to the lack of diastereoselectivity in the monodebromination step (48% yield of monobromocyclopropane *trans*-**116** and 35% yield of monobromocyclopropane *cis*-**116**). In this regard, the diastereomeric monobromocyclopropanes *trans*-**116** and *cis*-**116** were difficult to separate on large scale (43.5 mmol) and three purification attempts were required. However, an advantage of this method is that it provides a ready and direct access to both cyclopropyl BMIDAs *trans*-**38** and *cis*-**38**.

2.4 Conclusion

In conclusion, the successful synthesis of cyclopropyl BMIDAs *exo*-**36**, **37**, *exo*-**39**, *trans*-**38** and *cis*-**38** on a gram-scale has been accomplished. The synthesis of cyclopropyl BMIDAs *exo*-**36** and **37** were the most straightforward with no issues upon scale-up and subsequent purification of intermediates and final product. Although the route for cyclopropyl BMIDA *exo*-**39** was amongst the shortest (four steps), issues persist in the dibromocyclopropanation of pyrroline **67** with bromoform and a base, due to the presence of unreacted starting material that is difficult to separate by chromatography. The synthesis of cyclopropyl BMIDAs *trans*-**38** and *cis*-**38** remains the most challenging for multi-gram batch production. This is mainly due to the non-diastereoselective monodebromination of dibromocyclopropane **115** with dimethyl phosphite and potassium *tert*-butoxide which gave a 55:45 mixture of monobromocyclopropanes *trans*-**116** and *cis*-**116**. Separation of *trans*-**116** and *cis*-**116** on large scale (43.5 mmol) *via* chromatography remains a challenge. Nevertheless, a total of nine cyclopropyl BMIDA building blocks (Figure 2.13), including the five presented in this Chapter, are accessible through robust and scalable methodology. Only cyclopropyl BMIDA **121** requires a bespoke synthetic route. The nine cyclopropyl BMIDA building blocks (Figure 2.13) are commercially available from Key Organics Ltd thanks mostly to previous efforts of Redbrick Molecular before they unfortunately closed down.

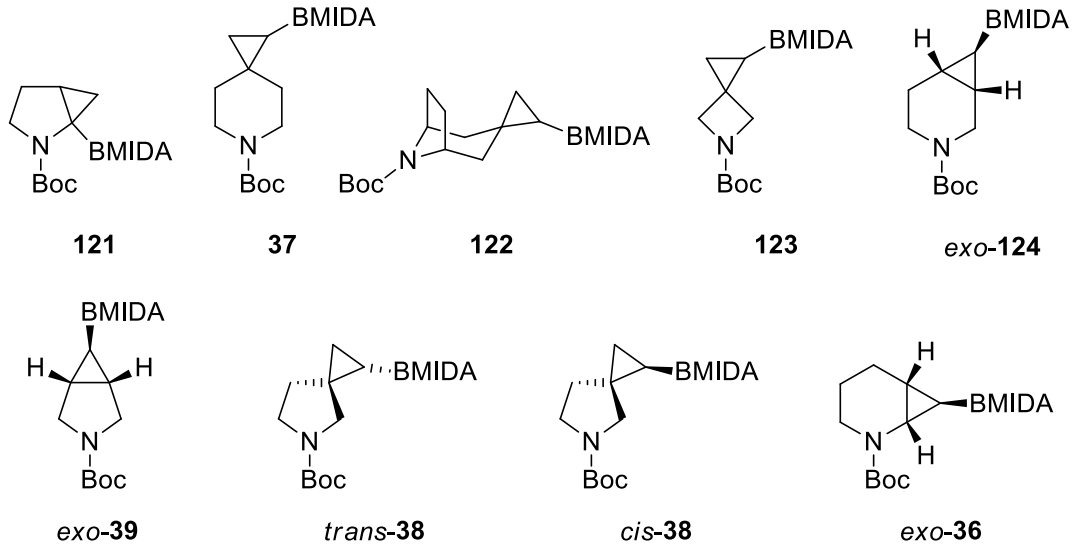

Figure 2.11 – Present library of York 3-D building blocks

Chapter 3: Elaboration of Fragments Using York 3-D Building Blocks

In order to successfully demonstrate fragment elaboration using cyclopropyl 3-D building blocks, first, the attachment of building blocks to fragment-like structures must be accomplished. Then, building blocks must be subsequently functionalised at the nitrogen terminus. This way, the initial fragment hit can be grown to provide additional binding interactions to a protein target of interest.

In this section, previous examples of the Suzuki-Miyaura cross-coupling of cyclopropanes are discussed in Chapter 3.1. An overview of cyclopropane cross-coupling, development and optimisation of cross-coupling conditions were performed (Chapter 3.2). Next, the functionalisation of cyclopropyl BMIDAs *exo*-**39**, *trans*-**38**, *cis*-**38**, and *exo*-**36** are described. In each case, the plan was to prepare a range of aryl cyclopropanes using Suzuki-Miyaura cross-coupling of the cyclopropyl boronate functionality with a medicinally relevant and structurally diverse set of aryl bromides (Chapter 3.3). Of these, cyclopropyl pyrimidines were selected and converted into cyclopropyl pyrimidine methanesulfonamides (Scheme 3.1) (Chapter 3.4). The plan was to characterise each elaborated pyrimidine fragment by X-ray crystallography. In that way, in addition to showing fragment elaboration using the building blocks, it would be possible to show that each building block had distinct 3-D vectors between the two elaboration groups. Chapter 3.5 discusses the concept of 3-D vectors in more detail with exit vector analysis of methanesulfonamides being illustrated.

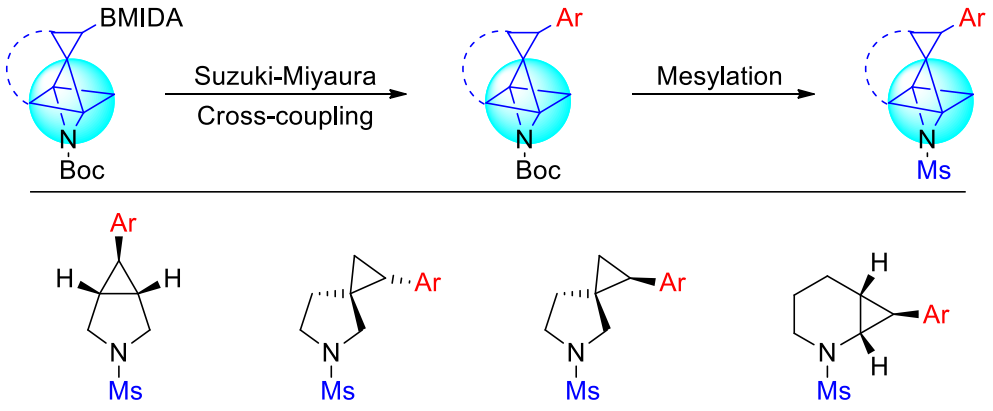

Scheme 3.1

Overview of Suzuki-Miyaura Cross-Coupling on Cyclopropanes

One of the most powerful carbon–carbon bond formation reactions in a synthetic chemist's toolbox is Suzuki-Miyaura cross-coupling.[109] First reported in 1979,[110] the palladium-catalysed reaction typically uses boronic acids and organohalides as synthetic handles to achieve cross-coupling. The reaction is common in drug discovery and plays an important role in the formation of aryl–aryl bonds in various medicinal chemistry projects.[111–114] For example, Graham *et al*. reported a kilogram scale synthesis of the ATR inhibitor Ceralasertib in which the new and adapted synthetic route used Suzuki-Miyaura cross-coupling at a key stage in the scale-up process. The attachment of a heteroaromatic boronic pinacol ester to a complex-substituted chloropyrimidine precursor for Ceralasertib was achieved with a yield of 70% to conclude its synthesis.[114] Suzuki-Miyaura reactions can be achieved using boronate esters (Bpin, BMIDA) or trifluoroborate salts (BF_3K) as well as using boronic acids. In this section, because of its relevance to our project, we will cover all of the limited examples of the Suzuki-Miyaura cross-coupling of cyclopropanes containing the *N*-methyliminodiacetyl (MIDA) group. In addition, a few selected examples of the cross-coupling of cyclopropyl boronic acids, pinacol boronates and trifluoroborate salts will be presented.

In 1996, Marsden and Hildebrand presented one of the first examples of the Suzuki-Miyaura cross-coupling of cyclopropanes.[115] By using 10 mol% of $Pd(PPh_3)_4$, it was shown that simple cyclopropanes could be cross-coupled to aryl iodides. For mono substituted alkyl cyclopropane *trans*-**125**, cross-coupling with iodobenzene was achieved by reaction with $Pd(PPh_3)_4$ and KO*t*-Bu in DME at 85 °C for 48 h to produce aryl cyclopropane *trans*-**126** in 74% yield (Scheme 3.2).[115] The reaction was stereospecific and proceeded with retention of configuration.

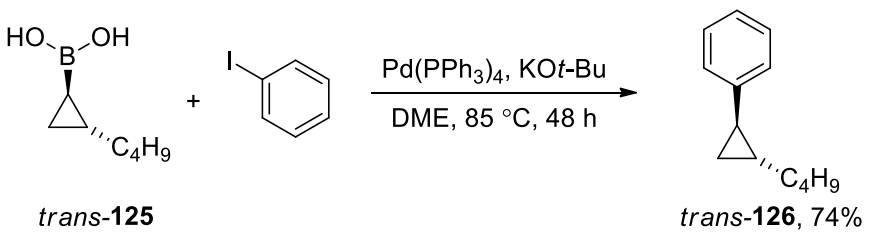

trans-**125** *trans*-**126**, 74%

Scheme 3.2

More complex di-substituted geminal cyclopropyl boronic acids were synthesised and used in cross-coupling by Gevorgyan *et al*.[116] A summary of the cross-coupling products are illustrated in Scheme 3.3. The stereospecific nature of the Suzuki-Miyaura cross-

coupling reaction was demonstrated upon characterisation of the products. When *cis*-**127** was reacted with an aryl iodide, Pd(*t*-$Bu_3P)_2$ and CsF in benzene at 80 °C for 1 h, arylated cyclopropanes *cis*-**128** (76%), *cis*-**129** (85%) and *cis*-**130** (77%) were synthesised in excellent yields (Scheme 3.3).[116]

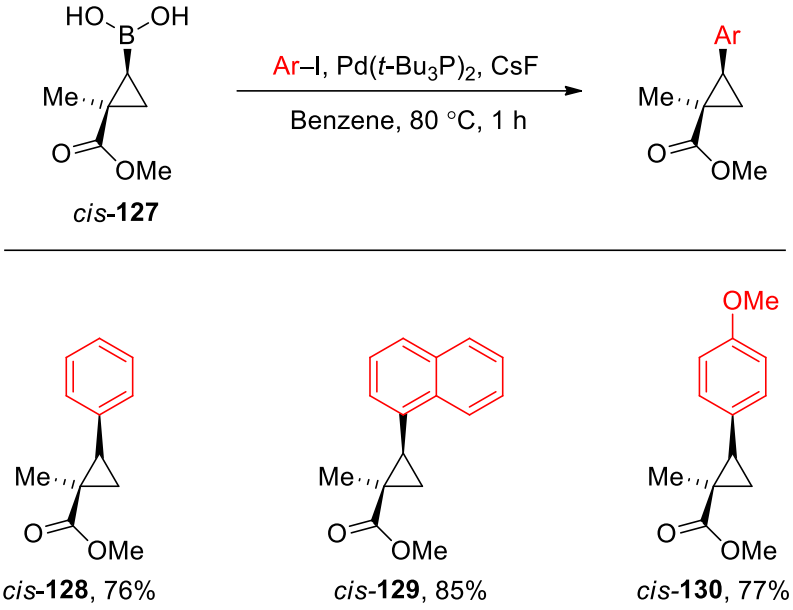

Scheme 3.3

Later, Wallace and Chen at Merck further developed the scope of halide substrates for the Suzuki-Miyaura cross-coupling to cyclopropanes. In addition to medicinally relevant aryl bromides being cross-coupled, a series of heteroaryl bromides were also included (Scheme 3.4).[117] Instead of using a Pd^0 precatalyst, it was found that using $Pd(OAc)_2$ and PCy_3 as the catalyst–ligand combination worked best in their cross-coupling reactions.[117] The unsubstituted cyclopropyl boronic acid **131** was cross-coupled to aryl or heteroaryl bromides using $Pd(OAc)_2$, PCy_3 and K_3PO_4•$3H_2O$ in toluene and H_2O at 100 °C for 3 h to afford a series of aryl and heteroaryl cyclopropanes (Scheme 3.4). Of note, examples included *o*-acetophenone **132** (65%), 2-pyridine **133** (49%), di-substituted furan **134** (81%), and isoquinoline **135** (95%).[117]

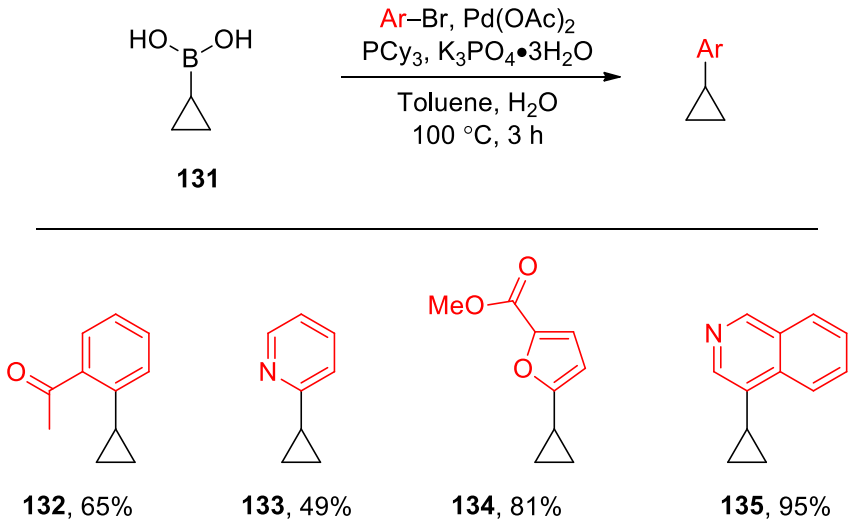

Scheme 3.4

One of the most common boron groups used in Suzuki−Miyaura cross-coupling is the boronic pinacol ester (Bpin) group. The use of Bpin in the cross-coupling of cyclopropanes was demonstrated by Charette and Benoit, where two examples of di-substituted cyclopropyl pinacol esters were cross-coupled to aryl and heteroaryl halides using $Pd(dba)_2$ and PCy_3.[118] For cyclopropyl Bpin *cis*-**136**, cross-coupling with iodobenzene with $Pd(dba)_2$, PCy_3 and KOH in toluene at 115 °C for 20 h gave aryl cyclopropane *cis*-**137** in 81% yield (Scheme 3.5). Under the same conditions, cyclopropyl Bpin *cis*-**138** and 3-bromopyridine were converted into heteroaryl cyclopropane *cis*-**139** in 99% yield. A stereoretentive pathway was also observed for cyclopropyl Bpin compounds.

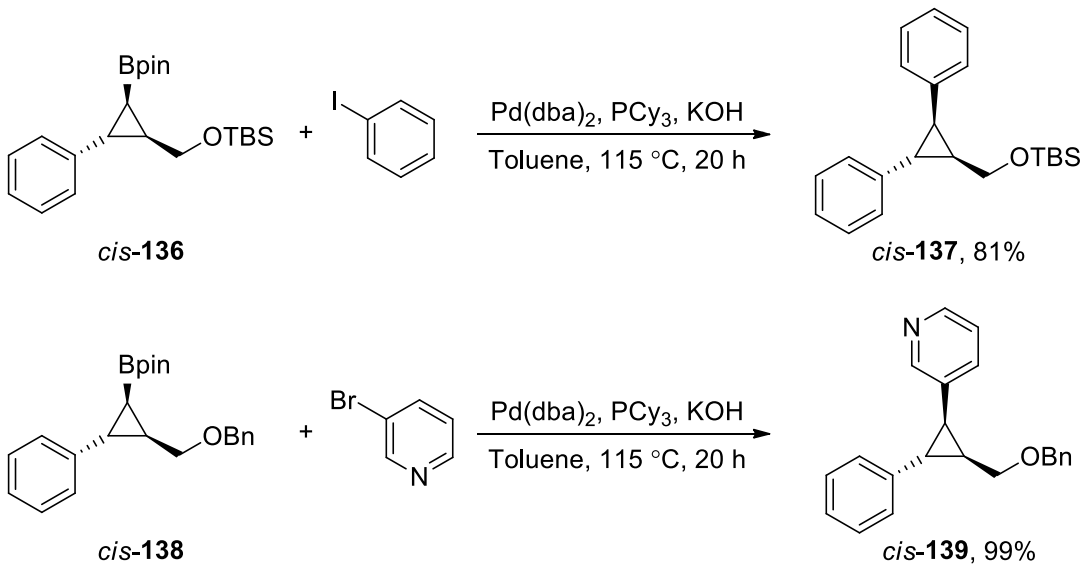

Scheme 3.5

Other examples shown by Takai *et al.* demonstrated *trans*-**140** being cross-coupled with iodo-toluene using $Pd(OAc)_2$, SPhos and KO*t*-Bu in *t*-BuOH and DME at 80 °C for 20 h to give aryl cyclopropane *trans*-**141** in 100% yield (Scheme 3.6).[119] Similarly, Pérez *et al.*[120] showed the cross-coupling of di-substituted *trans*-**142** with iodo-trifluoromethylbenezene using $Pd(OAc)_2$ and XantPhos and Cs_2CO_3 in *t*-BuOH and H_2O at 120 °C for 24 h to afford aryl cyclopropane **143** in 74% yield (Scheme 3.6).[120]

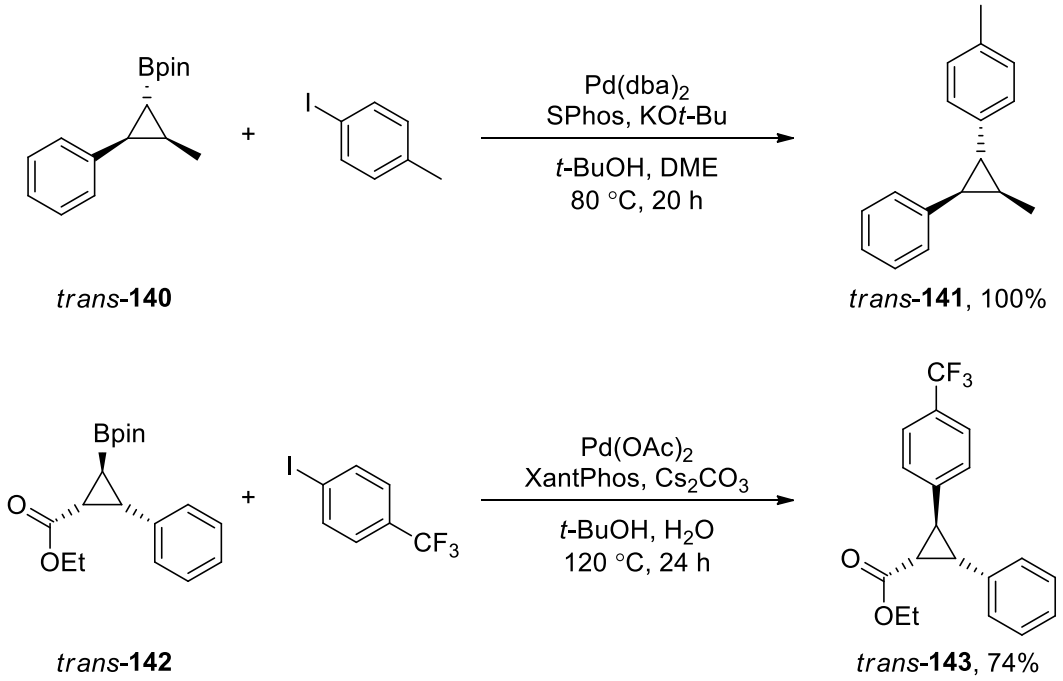

Scheme 3.6

In 2018, Harris and co-workers reported on the synthesis and Suzuki-Miyaura cross-coupling of geminal di-Bpin substituted cyclopropanes.[82] After careful optimisation of the reaction conditions, cross-coupling of cyclopropyl Bpins with aryl and heteroaryl bromides were achieved using cataCXium® A Pd G3 and Cs_2CO_3 in dioxane and H_2O at 100 °C for 24 h to give aryl and heteroaryl cyclopropanes *endo*-**144** (37%, >20:1 dr), *endo*-**145** (92%, >20:1 dr) and *trans*-**146** (31%, >20:1 dr) (Scheme 3.7).[82] Of note, these conditions were successful in the cross-coupling of unprotected anilines as well as heteroaromatics.

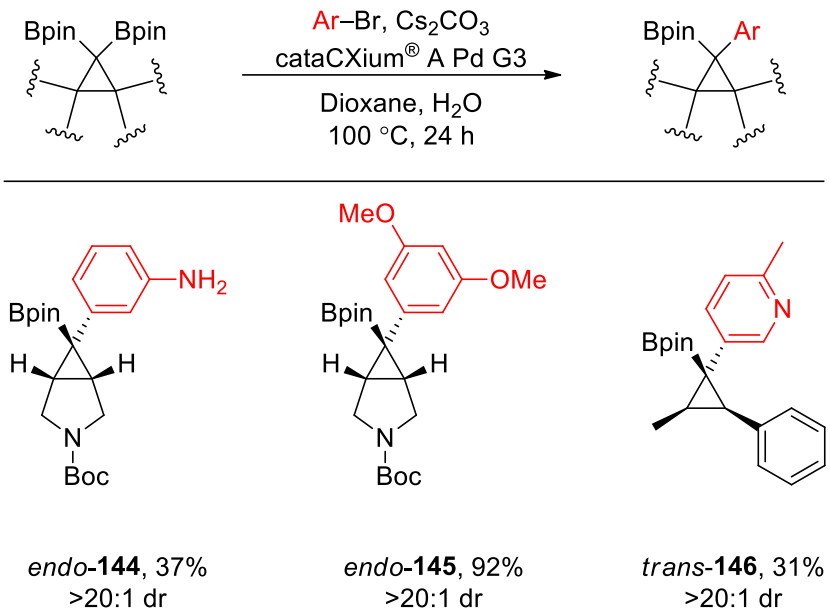

endo-**144**, 37%
>20:1 dr

endo-**145**, 92%
>20:1 dr

trans-**146**, 31%
>20:1 dr

Scheme 3.7

Much attention has been focused on the preparation and Suzuki-Miyaura cross-coupling of organotrifluoroborate (BF_3K) salts first reported by Molander and Ito.[121] For example, Deng and co-workers used BF_3K salts in cyclopropane cross-couplings.[122] Reaction of *cis*-**147** with aryl bromides using $Pd(PPh_3)_4$ and K_3PO_4•$3H_2O$ in toluene and H_2O at 100 °C for 20 h gave aryl cyclopropanes *cis*-**148**, *cis*-**149** and *cis*-**150** in 88%, 76% and 80% yields respectively (Scheme 3.8). The conditions used by Deng are comparable to those reported for cyclopropyl boronic acids.

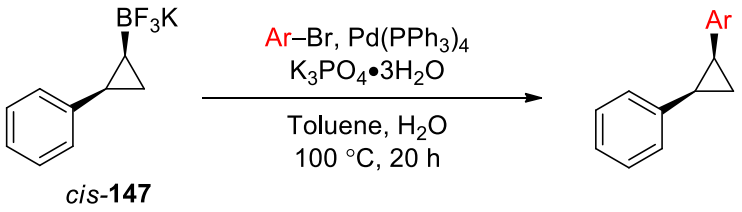

cis-**147**

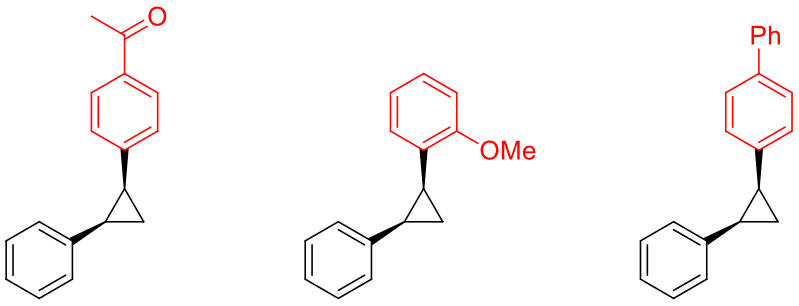

cis-**148**, 88%

cis-**149**, 76%

cis-**150**, 80%

Scheme 3.8

A detailed study on the Suzuki-Miyaura cross-coupling of cyclopropyl BF_3K **47** with aryl chlorides was reported by Harris *et al.*[73] Using cataCXium® A Pd G3 (5 mol%) and Cs_2CO_3 (3.0 eq.) in toluene and H_2O at 90 °C for 18 h, pyridine-*N*-oxide, methyl pyrazole, *o*-phenylacetonitrile, *iso*indolinone and others were successfully cross-coupled to cyclopropyl BF_3K **47** in excellent yields (Scheme 3.9).[73] Cyclopropyl BF_3K **47** can actually be considered as a potential 3-D building block for our fragment elaboration methodology and would provide different 3-D vectors to the other building blocks we are studying (*vide infra*).

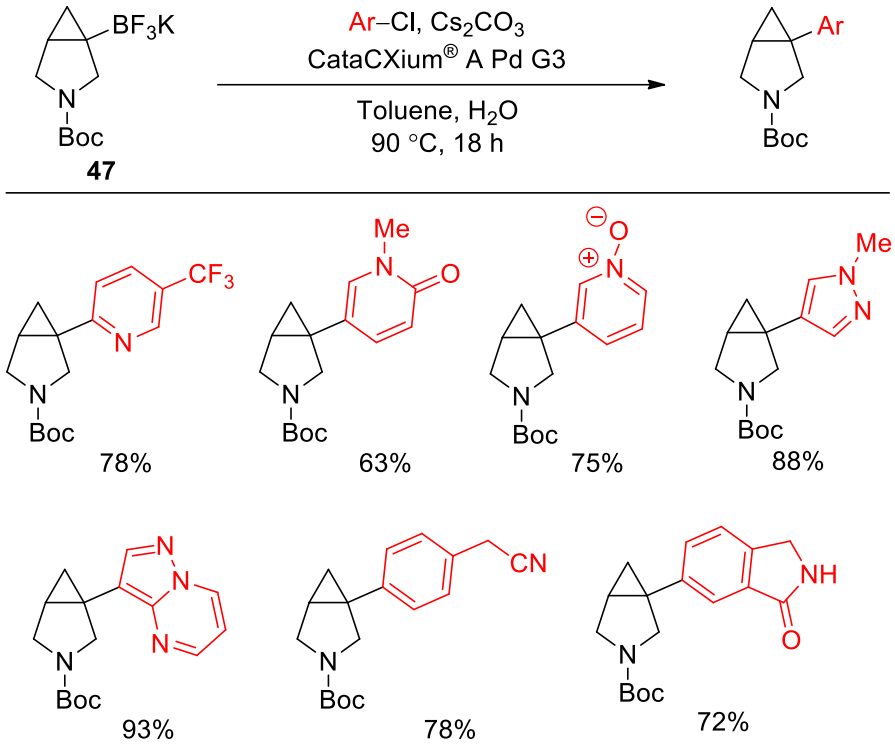

Scheme 3.9

In 2020, Grygorenko and co-workers reported on the synthesis of various sp^3-enriched compounds.[123] The 3-D scaffolds of the reported compounds are related to our cyclopropyl 3-D building blocks. By using conditions adapted from those previously reported by Harris (cataCXium® A Pd G3 (5 mol%) and Cs_2CO_3),[73] Grygorenko produced the cross-coupling examples illustrated in Scheme 3.10.[123] The corresponding cyclopropyl BF_3K salt was individually cross-coupled to complex and medicinally relevant aryl or heteroaryl bromides using cataCXium® A Pd G3 and Cs_2CO_3 in dioxane and H_2O at 100 °C for 14 h to generate aryl and heteroaryl cyclopropanes **151**, **152**, **153**, *exo*-**154**, and **155**.[123]

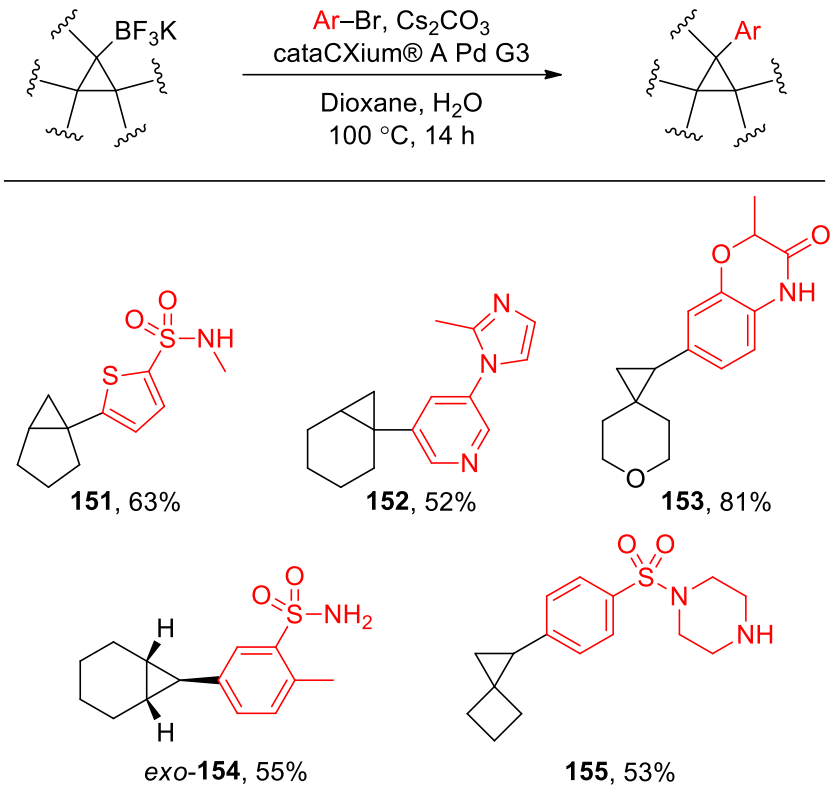

Scheme 3.10

In 2009, Burke and co-workers first reported the use of MIDA boronates as a general solution to stability problems observed with certain boronic acid derivatives, including trifluoroborate salts, trialkoxy / trihydroxyborate salts, diethanolamine adducts, bulky boronic esters and boroxines.[70,124] Burke focused primarily on 2-heterocyclic, vinyl and cyclopropyl MIDA boronates with aryl and heteroaryl chlorides. The attractiveness of MIDA boronates comes from their ability to promote slow release of unstable boronic acids *in situ*. Under the basic conditions required for Suzuki-Miyaura cross-coupling, the MIDA boronate ester can be slowly hydrolysed to the reactive boronic acid used in the transmetalation step.[125] To test the bench stability of MIDA boronates, Burke *et al.* subjected pre-prepared samples of various aryl, heteroaryl and cyclopropyl BMIDA compounds to bench-top conditions. As a control, the boronic acid counterparts were studied concurrently. After 15 days, the boronic acid samples were found to have decomposed and lost at least 20% of their original mass, with electron-rich heteroaromatics giving up to 90% decomposition. With cyclopropyl boronic acid, only 31% of the original mass was recovered after 15 days.[126] In contrast, the BMIDA samples were bench-stable with all samples showing no decomposition detectable by ^{1}H NMR spectroscopy even after 60 days.

As a result of the increased stability, the cross-coupling reactions of the BMIDA derivatives were much improved in comparison to those of their boronic acid versions. For example, cross-coupling reactions of cyclopropyl BMIDA **156** with three aryl chlorides were described. Reactions used $Pd(OAc)_2$ (5 mol%), SPhos (10 mol%), K_3PO_4 (7.5 eq.) in dioxane/H_2O at 100 °C for 6 h and aryl cyclopropanes **157**, **158** and **159** were isolated in yields of 79 – 97% (Scheme 3.11).[126] Overall, Burke's work showed that cross-coupling of cyclopropyl BMIDA **156** is possible for deactivated electron-rich aromatics as well as *ortho*-substituted aryl groups. This was the first study to report on MIDA boronates as a masked boronic acid in cross-coupling reactions with cyclopropanes, although an extensive study of the scope of the reaction was not reported any further.

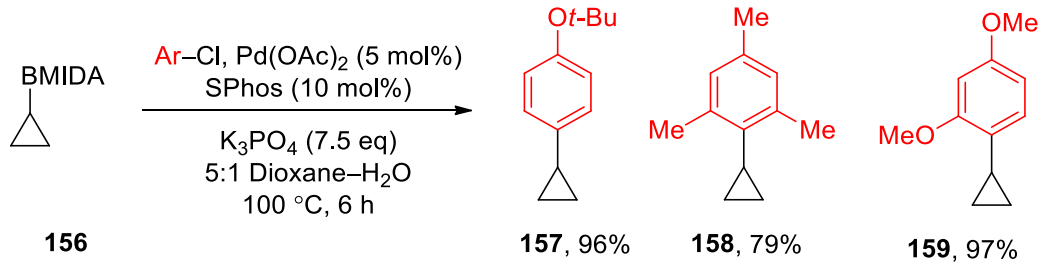

156 **157**, 96% **158**, 79% **159**, 97%

Scheme 3.11

In 2013, Duncton and Singh reported a method for attaching the medicinally-relevant 2-(trifluoromethyl) cyclopropyl group to a variety of aryl and heteroaryl coupling partners.[127] The strategy proposed involved synthesis of trifluoromethyl cyclopropyl BMIDA *trans*-**160** and its subsequent use in cross-coupling to aryl bromides. Palladium-catalysed Suzuki-Miyaura cross-coupling of trifluoromethyl cyclopropyl BMIDA *trans*-**160** with aryl- and heteroaryl bromides proceeded stereospecifically to give aryl trifluoromethyl cyclopropanes *trans*-**161**. A selection of examples is shown in Scheme 3.12. Generally, $Pd(OAc)_2$ (10 mol%) and electron-rich ligands such as PCy_3 or RuPhos (20 mol%) were used. The reactions proceeded at high temperatures of 80 – 115 °C in the presence of Cs_2CO_3 or K_2CO_3. These reaction conditions afforded a diverse array of electron-rich and electron-deficient heteroaromatic examples with yields varying depending on the substrate. Overall, Duncton and Singh identified and demonstrated the synthesis of a wide range of medicinally relevant heterocycles using robust methodology.

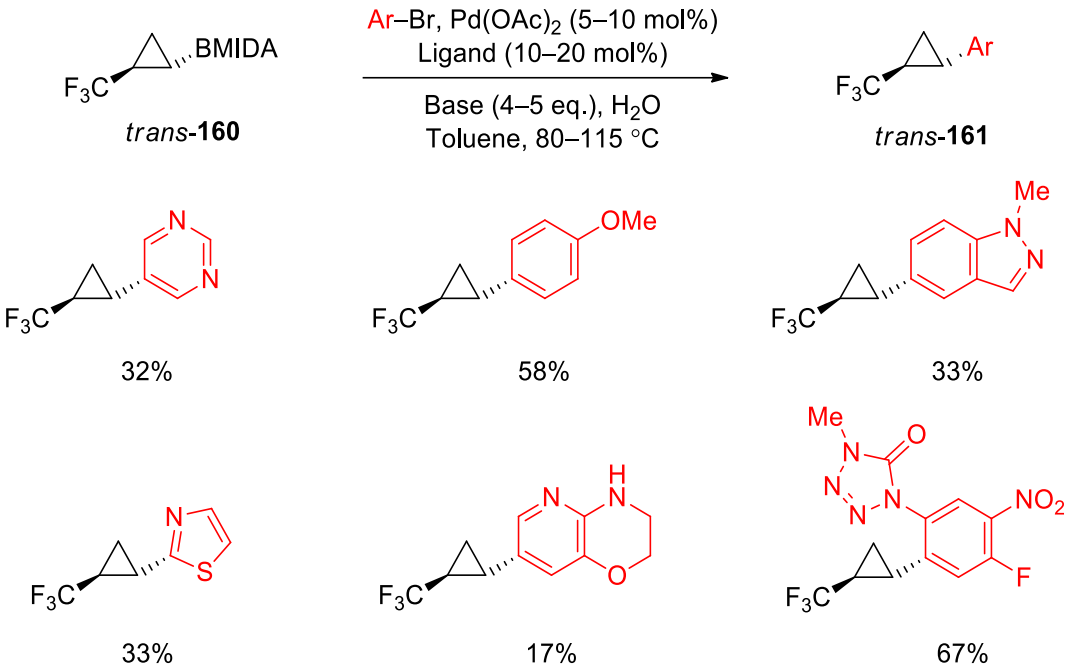

Scheme 3.12

In a patent from 2017, de Man *et al*. reported the use of 3-hydroxyimidazolidin-4-one derivatives for use in cancer prevention and treatment of disease.[128] The synthesis of 3-hydroxyimidazolidin-4-one **162** using cross-coupling conditions similar to Burke and Duncton's examples was reported. For the transformation shown in Scheme 3.13, reaction of cyclopropyl BMIDA **156** with the appropriate aryl bromide using $Pd(OAc)_2$ (15 mol%), PCy_3 (30 mol%), Cs_2CO_3 (6.0 eq.) in toluene and H_2O at 100 °C for 3 h gave aryl cyclopropane **162** in 63% yield.

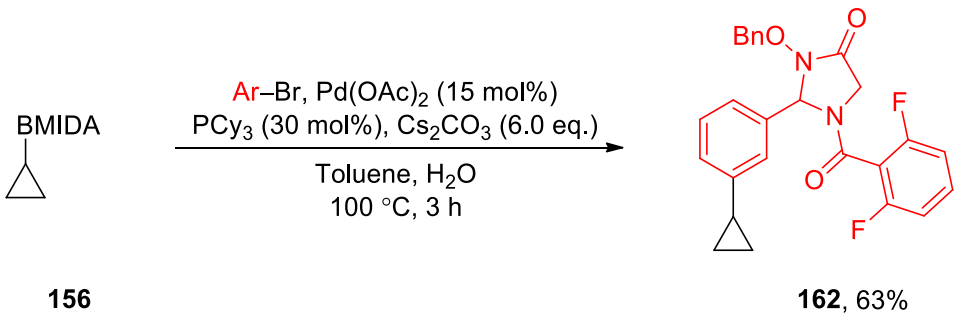

Scheme 3.13

During a study on inhibitors of protein kinase C, Singh and co-workers reported the cross-coupling of cyclopropyl BMIDAs with a set of aryl bromides in two patents (Scheme 3.14).[129,130] For these reactions, cyclopropyl BMIDA **156** was reacted with an aryl bromide, $Pd(OAc)_2$ (15 mol%), PCy_3 (30 mol%) and Cs_2CO_3 (6.0 eq.) in toluene and H_2O

at 100 °C overnight to give the respective products (Scheme 3.14). Of note, aryl cyclopropane **163**, required higher loadings of $Pd(OAc)_2$ (20 mol%), PCy_3 (40 mol%) and Cs_2CO_3 (18 eq.) to give a satisfactory (69%) yield.[130] An additional example using trifluoromethyl cyclopropyl BMIDA was used to give aryl cyclopropane *trans*-**164** in 54% yield, with the standard $Pd(OAc)_2$ (15 mol%), PCy_3 (30 mol%) and Cs_2CO_3 (6.0 eq.) conditions.

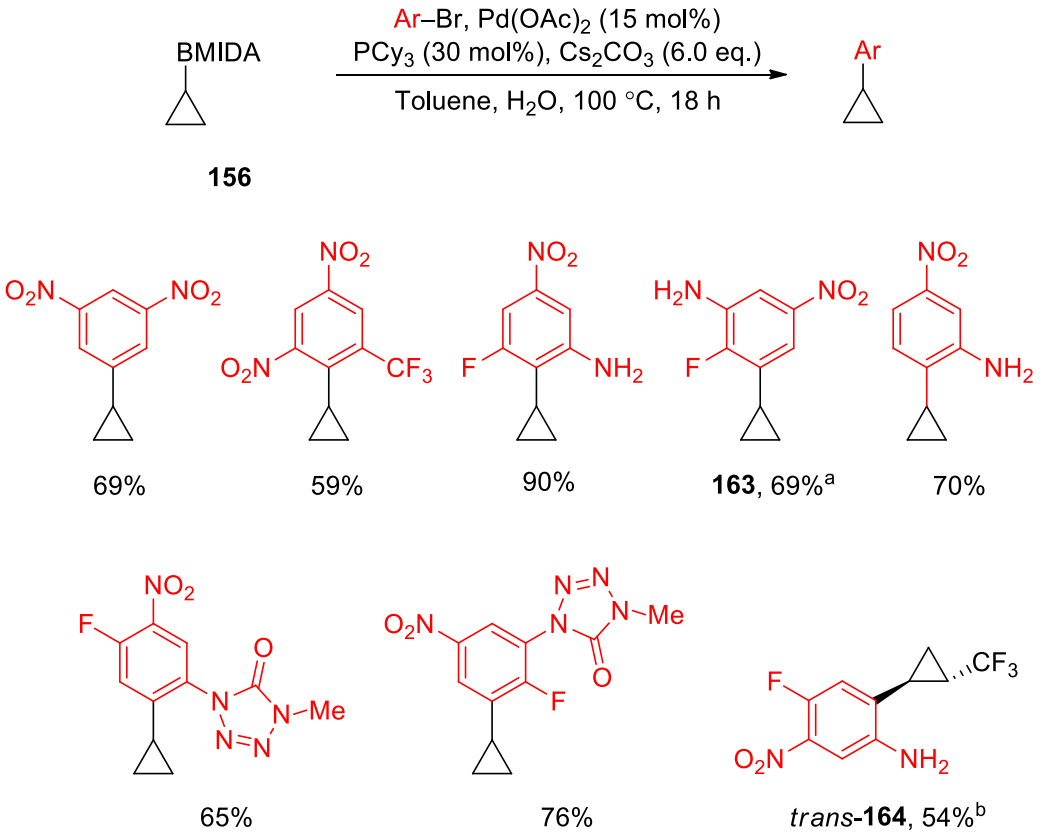

[a] Reaction conditions: $Pd(OAc)_2$ (20 mol%), PCy_3 (40 mol%), Cs_2CO_3 (18 eq.),
[b] *trans*-2-(trifluoromethyl)cyclopropyl-BMIDA was used for coupling to aryl bromide.

Scheme 3.14

In conclusion, there are a number of reports on the Suzuki-Miyaura cross-coupling of cyclopropyl boronates, some of which have been presented here. Of the examples described, Pd^0 catalysts such as $Pd(PPh_3)_4$ and $Pd(t\text{-}Bu_3P)_2$ were favoured for cross-coupling of boronic acids and simple BF_3K salts (precursor to boronic acid). When more complex aryl and heteroaryl halides were studied by Wallace and Chen, Pd^{II} catalyst–ligand-based systems ($Pd(OAc)_2$ / PCy_3) were favoured. The closest examples of Suzuki-Miyaura cross-coupling that are most relevant to our 3-D cyclopropyl building blocks were the examples reported by Harris and co-workers. In these examples, the Pd pre-

catalyst: cataCXium® A Pd G3 was used to access to a wide array of diverse functional groups and heterocycles.[73,82]

$Pd(OAc)_2$ and $Pd(dba)_2$ were the popular choices of pre-catalyst for the cross-coupling of cyclopropyl Bpins and BMIDAs with ligands such as PCy_3, XantPhos, SPhos, or RuPhos. One of the common trends observed with the cross-coupling conditions was the high palladium and ligand loadings of 5 – 20 mol% and 10 – 40 mol% respectively. Although Burke's original work presented excellent yields with the lowest catalyst loadings (5 mol%), there were no examples with heteroaryl bromides. Duncton and Singh's work on functionalised trifluorocyclopropyl BMIDA *trans*-**160** successfully utilised palladium cross-coupling to attach different heteroaryl bromides with a range of catalyst loadings (5 – 10 mol%) (see Scheme 3.12). In the example from de Man *et al*. (see Scheme 3.13), the Suzuki-Miyaura cross-coupling of cyclopropyl BMIDA **156** with a complex aryl bromide was shown. The high catalyst and ligand loadings of 15 mol% and 30 mol% used by de Man *et al.* were directly comparable to the conditions from patents by Singh *et al*. where the same catalyst and ligand loadings were used. In one exceptional example (aryl cyclopropane **163**), 20 mol% of $Pd(OAc)_2$ and 40 mol% of PCy_3 were used.

Optimisation of the Suzuki-Miyaura Cross-Coupling Reaction on Cyclopropyl MIDA Boronates

The Suzuki-Miyaura cross-coupling of cyclopropyl BMIDA building blocks with aryl bromides was initially explored by previous members of the group.[47,48,131,132] The initially preferred reaction conditions were based on those reported by de Man *et al*. (see Scheme 3.13) and included a high loading of $Pd(OAc)_2$ (15 mol%) and PCy_3 (30 mol%). Initial examples carried out in the group using these conditions with 5-bromopyrimidine (1.4 eq.), Cs_2CO_3 (6.0 eq.) in toluene and H_2O at 100 °C for 16 h are shown in Scheme 3.15. With high palladium catalyst and ligand loadings, cyclopropyl pyrimidines **165**, *exo*-**166**, *exo*-**167** and **168** were synthesised in excellent yields (73 – 85%).[47,132]

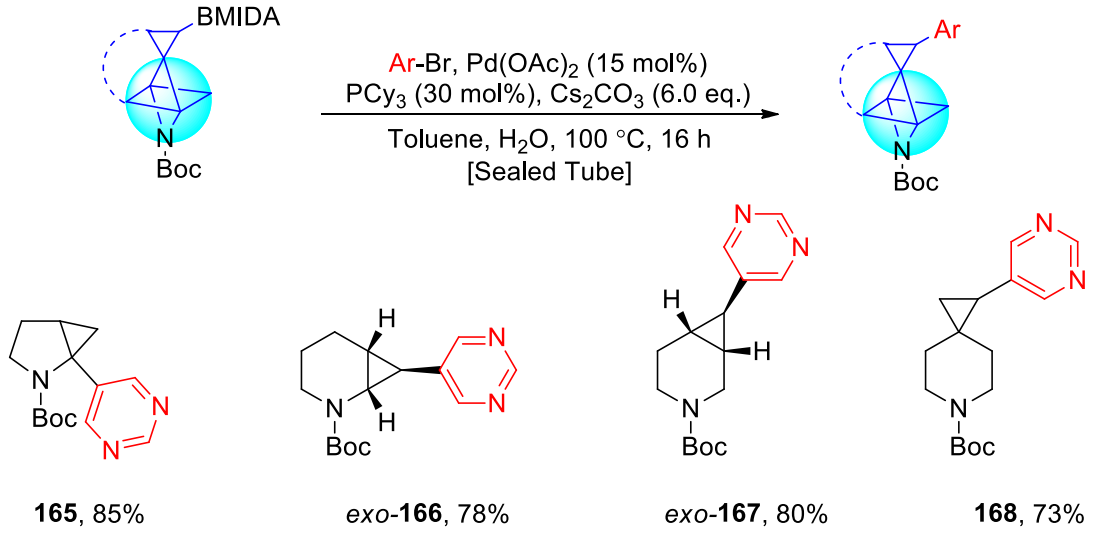

165, 85% *exo*-**166**, 78% *exo*-**167**, 80% **168**, 73%

Scheme 3.15

Before investigating the Suzuki-Miyaura cross-coupling scope further with the new building blocks, it was decided to briefly explore whether the amount of catalyst, ligand and base could be reduced, whilst maintaining good yields. For this study, 3-D building blocks *exo*-**36** and **37** were selected as representative examples of fused and spirocyclic systems respectively. I carried out the reactions with cyclopropyl BMIDA *exo*-**36** (Table 3.1) while another member of the group, Andres Gomez Angel, worked on cyclopropyl BMIDA **37** (Table 3.2).[131] The results from palladium cross-coupling between cyclopropyl BMIDA *exo*-**36** and **37** with 5-bromopyrimidine at different loadings are shown in Tables 3.1 and 3.2.

To carry out the Suzuki-Miyaura cross-coupling reactions, cyclopropyl BMIDAs *exo*-**36** and **37** were added to a pressure tube containing $Pd(OAc)_2$, PCy_3, Cs_2CO_3 and 5-

bromopyrimidine (1.4 eq.). 10:1 Toluene-H_2O (deoxygenated) was added and this mixture was then sealed and stirred at 100 °C for 16 h. To start, using cyclopropyl BMIDA *exo*-**36**, a reaction using 15 mol% $Pd(OAc)_2$ and 30 mol% PCy_3 was carried out which gave cyclopropyl pyrimidine *exo*-**166** in 78% yield (Table 3.1, entry 1). A similarly high yield (73%) of cyclopropyl pyrimidine *exo*-**166** was obtained using 5 mol% $Pd(OAc)_2$ and 10 mol% PCy_3 (Table 3.1, entry 2). Surprisingly, with only 2.5 mol% $Pd(OAc)_2$ and 5 mol% PCy_3, an excellent yield of 87% was observed (Table 3.1, entry 3). Repeating these conditions, a similar 84% yield was observed again (Table 3.1, entries 4). At 1 mol% $Pd(OAc)_2$ and 2 mol% PCy_3, a 58% yield of cyclopropyl pyrimidine *exo*-**166** was obtained (Table 3.1, entry 5). With the palladium loading threshold determined to be ≥ 2.5 mol% from this brief study, we then attempted to lower the amount of Cs_2CO_3. Using 5 mol% $Pd(OAc)_2$, 10 mol% PCy_3 and 3 eq. of Cs_2CO_3, a 73% yield of cyclopropyl pyrimidine *exo*-**166** was observed (Table 3.1, entry 6). Finally, when attempting to use 2.5 mol% $Pd(OAc)_2$ and 5 mol% PCy_3, cyclopropyl pyrimidine *exo*-**166** was isolated in a moderate 52% yield (Table 3.1, entry 7).

*Table 3.1 – Suzuki-Miyaura cross-coupling of cyclopropyl BMIDA exo-***36**

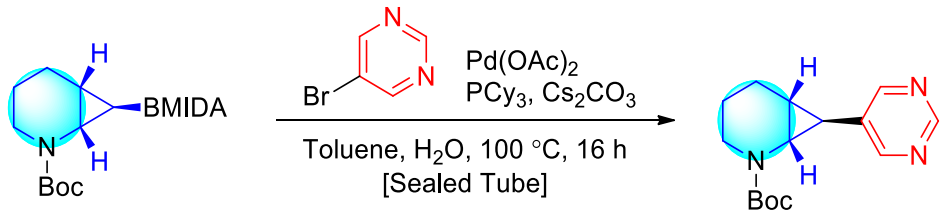

exo-**36** *exo*-**166**

Entry	$Pd(OAc)_2$ (mol%)	PCy_3 (mol%)	Cs_2CO_3 (eq.)	Yield (%)[a]
1	15	30	6	78
2	5	10	6	73
3	2.5	5	6	87
4	2.5	5	6	84
5	1.0	2	6	58
6	5	10	3	73
7	2.5	5	3	52

[a] *% yield after chromatography*

Alongside the study described in Table 3.1, a similar study on spirocyclic cyclopropyl BMIDA **37** was carried out by Andres Gomez Angel with the results shown in

Table 3.2.[131] Using the same general procedure, the high loading of 15 mol% $Pd(OAc)_2$ and 30 mol% PCy_3 gave cyclopropyl pyrimidine **168** in 55% yield (Table 3.2, entry 1). This was in fact slightly lower than expected as Hanna Klein had obtained a 73% yield of cyclopropyl pyrimidine **168** under these conditions.[47] When using 10 mol% $Pd(OAc)_2$ and 20 mol% PCy_3 (Table 3.1, entry 2), cyclopropyl pyrimidine **168** was obtained in only 30% yield. Use of lower loadings of 5 mol% $Pd(OAc)_2$ and 10 mol% PCy_3 gave cyclopropyl pyrimidine **168** in 59% yield (Table 3.2, entry 3), comparable to that obtained using 15 mol% $Pd(OAc)_2$ and 30 mol% PCy_3 (Table 3.2, entry 1). The conclusion drawn from these results was that the result from the 10 mol% $Pd(OAc)_2$ and 20 mol% PCy_3 conditions (Table 3.2, entry 2) could be considered as an outlier. When performing cross-coupling using 2.5 mol% $Pd(OAc)_2$ and 5 mol% PCy_3, a yield of 62% was observed for cyclopropyl pyrimidine **168** (Table 3.2, entry 4). Lowering the amount of Cs_2CO_3 to 3 eq. at 5 mol% $Pd(OAc)_2$ and 10 mol% PCy_3 showed no negative impact on the yield (70%) of cyclopropyl pyrimidine **168** (Table 3.2, entry 5). Unlike with cyclopropyl BMIDA *exo*-**36**, even at 2.5 mol% $Pd(OAc)_2$, 5 mol% PCy_3, and 3 eq. of Cs_2CO_3, the yield of cyclopropyl pyrimidine **168** remained consistently good (68%) (Table 3.2, entry 6).

Table 3.2 – Suzuki-Miyaura cross-coupling of cyclopropyl BMIDA **37**

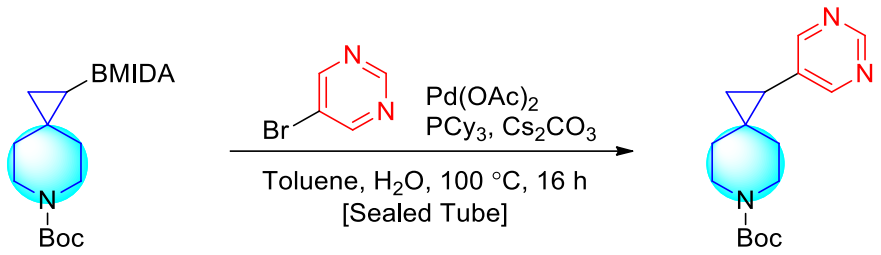

37 **168**

Entry	$Pd(OAc)_2$ (mol%)	PCy_3 (mol%)	Cs_2CO_3 (eq.)	Yield (%)[a]
1	15	30	6	55
2	10	20	6	30
3	5	10	6	59
4	2.5	5	6	62
5	5	10	3	70
6	2.5	5	3	68

[a] *% yield after chromatography*

In summary, taking all of the results from Tables 3.1 and 3.2, it can be concluded that Suzuki-Miyaura cross-couplings of spirocyclic cyclopropyl BMIDA **37** were less affected at lower catalyst, ligand and base loadings compared to fused cyclopropyl BMIDA *exo*-**36**. At 2.5 mol% $Pd(OAc)_2$, 5 mol% PCy_3, and 3 eq. of Cs_2CO_3 (Table 3.1, entry 7), coupling of 5-bromopyrimidine with cyclopropyl BMIDA *exo*-**36** was 21% lower yielding in comparison to the use of 5 mol% $Pd(OAc)_2$, 10 mol% PCy_3, and 3 eq. of Cs_2CO_3 (Table 3.1, entry 6). In contrast, cyclopropyl BMIDA **37** retained relatively consistent yields when switching from 5 mol% $Pd(Oac)_2$, 10 mol% PCy_3, and 3 eq. of Cs_2CO_3 (Table 3.2, entry 5) to the lower $Pd(Oac)_2$ (2.5 mol%) and PCy_3 (5 mol%) loadings (Table 3.2, entry 6). Ultimately, it was decided that 5 mol% $Pd(Oac)_2$, 10 mol% PCy_3, and 3 eq. of Cs_2CO_3 (Table 3.1, entry 6 and Table 3.2, entry 5) would be the most versatile conditions as good consistent results were observed for both cyclopropyl BMIDA *exo*-**36** and **37**. These were therefore selected as our standard cross-coupling conditions, with the idea that the 15 mol% $Pd(Oac)_2$, 30 mol% PCy_3 and 6 eq. of Cs_2CO_3 conditions would be explored if there were aryl bromides that proved more problematic.

Aryl Bromide Scope of the Suzuki-Miyaura Cross-Coupling Reaction with Cyclopropyl MIDA Boronates

Functionalisation of the cyclopropyl BMIDA moiety with a diverse range of aryl and heteroaryl groups was important in order to demonstrate the versatility of cross-coupling across all nine 3-D building blocks. To show this, we proposed to functionalise all nine cyclopropyl BMIDA building blocks with 5-bromopyrimidine using Suzuki-Miyaura cross-coupling under the conditions identified in Chapter 3.2 (5 mol% $Pd(Oac)_2$, 10 mol% PCy_3, and 3.0 eq. of Cs_2CO_3) and compare them with the original conditions (15 mol% $Pd(Oac)_2$, 30 mol% PCy_3, and 6 eq. of Cs_2CO_3). The choice of 5-bromopyrimidine was derived from the work on FragLites by Waring *et al.* where a set of 2-D halogenated fragments were reported (see Figure 1.4).[20]

To this end, cyclopropyl BMIDA building blocks were reacted with 5-bromopyrimidine and a summary of the cross-coupling results from this work and from others in the group is shown in Scheme 3.16. For the piperidine cyclopropyl pyrimidines *exo*-**166**, *exo*-**167** and **168**, yields were only slightly lower using loadings of 5 mol% $Pd(Oac)_2$, 10 mol% PCy_3 and 3.0 equivalents of Cs_2CO_3. By comparison, the pyrrolidine cyclopropyl pyrimidines *exo*-**170**, *trans*-**171** and azetidine cyclopropyl pyrimidine **172** showed similar reductions in yield at lower loadings of catalyst, ligand, and base. In particular, cyclopropyl pyrimidines *exo*-**170** and **172** were impacted the most with a yield difference of > 20% using the two sets of conditions. Special circumstances with cyclopropyl pyrimidines **169** and **165** were identified by other members of the group. For cyclopropyl BMIDA **122**, solubility issues were observed leading to incomplete hydrolysis of the BMIDA functionality to the boronic acid *in situ*. However, the problem was resolved by first treating cyclopropyl BMIDA **122** with 1.0 M solution of $NaOH_{(aq)}$ in THF at rt for 30 min before performing the cross-coupling with 5 mol% $Pd(Oac)_2$, 10 mol% PCy_3 and 3 eq. Cs_2CO_3. This gave cyclopropyl pyrimidine **169** in 58% yield.[131] With the most sterically hindered cyclopropyl BMIDA **121**, Andres Gomez Angel observed a protodeborylated by-product when attempting to use the reduced loadings.[47,131] This was especially problematic as the by-product could not be separated from cyclopropyl pyrimidine **165**. Under lower loadings, a 41% yield of cyclopropyl pyrimidine **165** was obtained (isolated as a 70:30 mixture of cyclopropyl pyrimidine **165** with the protodeborylated product).[131]

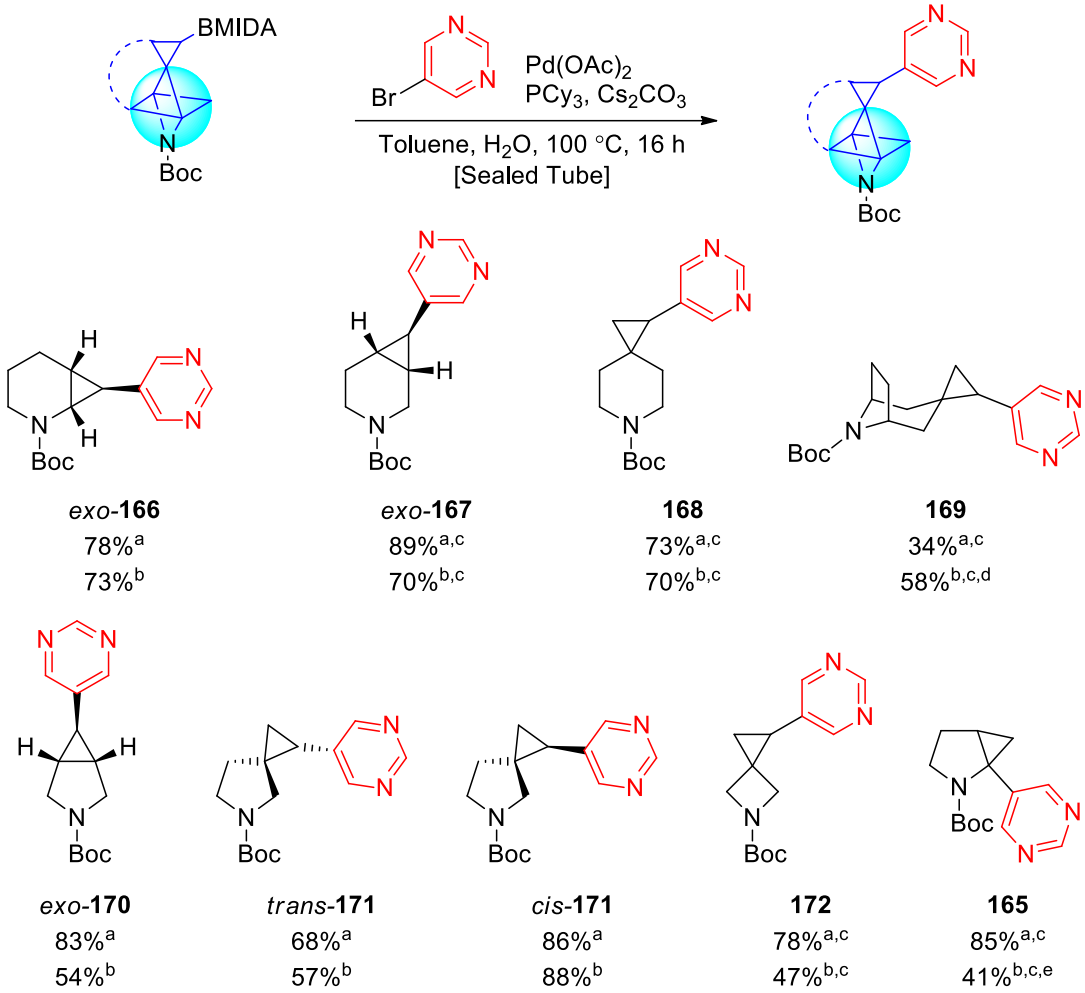

[a] $Pd(OAc)_2$ (15 mol%), PCy_3 (30 mol%), Cs_2CO_3 (6 eq.), [b] $Pd(OAc)_2$ (5 mol%), PCy_3 (10 mol%), Cs_2CO_3 (3 eq.), [c] Result obtained from other members of the group, [d] Suzuki-Miyaura cross-coupling performed using pre generated boronic acid, [e] Isolated as a 70:30 mixture of **165** with the protodeborylated product.

Scheme 3.16

To explore the scope and limitations of the Suzuki-Miyaura cross-coupling, reactions of all nine cyclopropyl BMIDA building blocks with various aryl and heteroaryl bromides were proposed. In this report, the reactions of cyclopropyl BMIDAs *exo*-**39**, *trans*-**38**, *cis*-**38**, and *exo*-**36** are described. The cross-coupling results on the other building blocks (~50 examples) were obtained by other members of the group. For each example shown in Scheme 3.17, cyclopropyl BMIDAs *exo*-**39**, *trans*-**38**, *cis*-**38**, and *exo*-**36** were individually cross-coupled with a diverse range of aryl- and heteroaryl bromides in a pressure tube containing 5 mol% $Pd(Oac)_2$, 10 mol% PCy_3 and 3.0 eq. of Cs_2CO_3 in 10:1 toluene–H_2O at 100 °C for 16 h.

To demonstrate that our 3-D building blocks were compatible with a range of aryl- and heteroaryl coupling partners in the Suzuki-Miyaura cross-coupling reactions, a selection

of medicinally relevant aryl- and heteroaryl bromides were taken from recent literature examples. To this end, the work of Harris and co-workers from Pfizer served as inspiration (see Scheme 3.9).[73,82] The selected aryl- and heteroaryl bromides were purposely diverse and included a series of five- or six-membered electron-rich and electron-deficient aromatics. The results of the cross-coupling reactions are shown in Scheme 3.17. Notable examples included the di-*meta*-methoxyphenyl cyclopropane *exo*-**177** (56%), methyl pyrazole cyclopropane *cis*-**185** (30%), *ortho*-methylbenzoate cyclopropane *trans*-**181** (64%), *para*-chlorophenyl cyclopropane *exo*-**189** (83%), furan cyclopropane **186** (61%), and thiophene cyclopropane *exo*-**175** (59%). These selected examples represent five-membered and six-membered rings with different substitution patterns of electron-withdrawing and donating groups around the aromatic ring. For the remaining examples, the yields ranged from 39-86%. In all cases, no evidence of protodeborylation was observed in the ^{1}H NMR spectra of the crude products, although it would be expected that such products may have a reasonable degree of volatility.

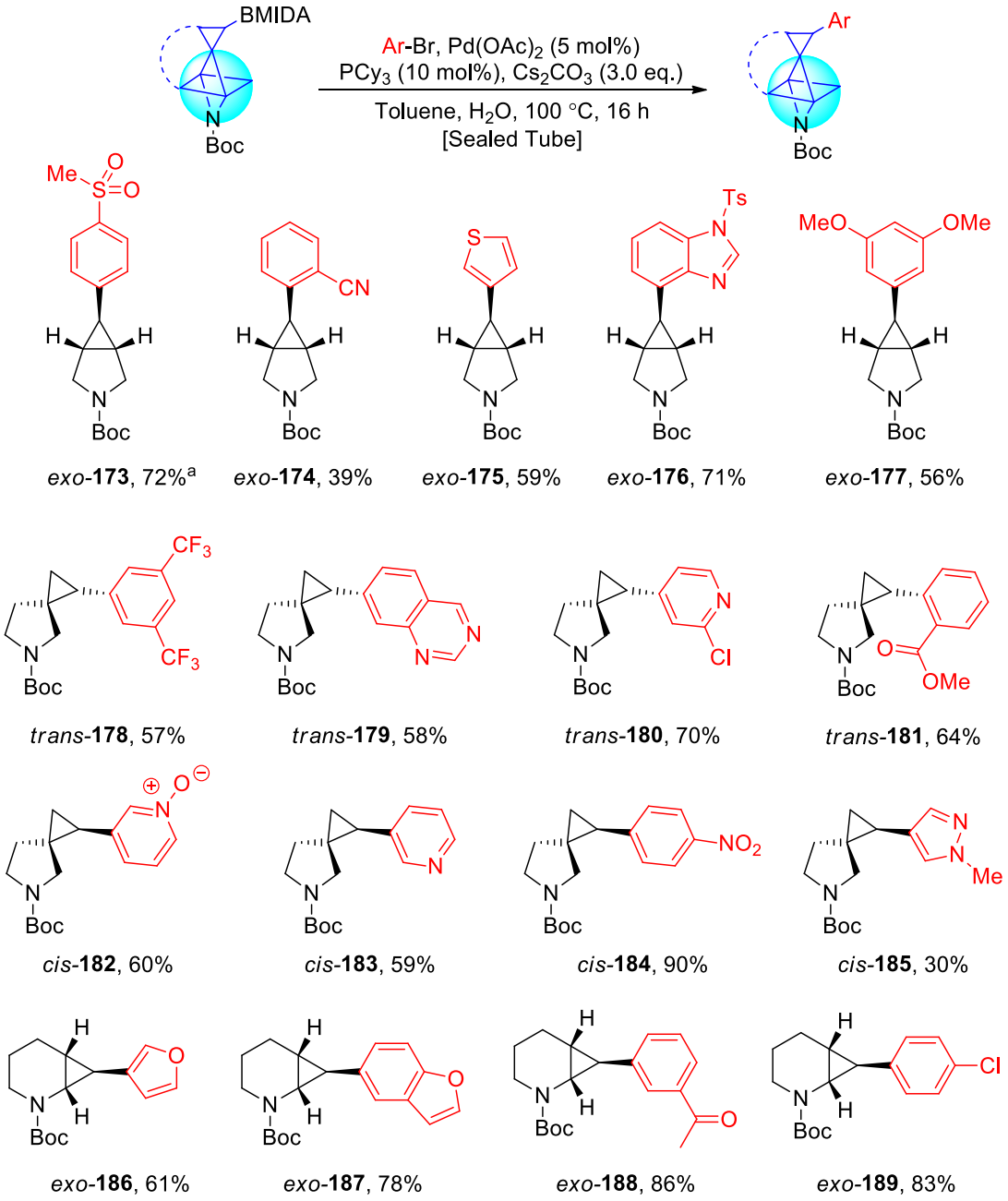

[a] Reaction performed using $Pd(OAc)_2$ (15 mol%), PCy_3 (30 mol%), Cs_2CO_3 (6.0 eq.)

Scheme 3.17

The stereochemistry of aryl and heteroaryl cyclopropanes *exo*-**173**–**177** and *exo*-**186**–**189** was confirmed using the characteristic ^3J values around the cyclopropane ring. The ^3J values for coupling between protons H_A and H_B / H_C in cyclopropyl aryl and heteroaryl cyclopropanes *exo*-**174** and *exo*-**188** are shown in Figure 3.1. For aryl cyclopropane *exo*-**174**, the ^3J values for coupling between protons H_A and H_B / H_C are 3.5 and 3.5 Hz. For the piperidine scaffold, acetophenone cyclopropane *exo*-**188**, the ^3J values for coupling between protons H_A and H_B / H_C are 3.0, 6.5 Hz. Thus, both cross-coupled

products have *exo* stereochemistry. The other cyclopropyl aryl and heteroaryl cyclopropanes *exo*-**173**–**177** and *exo*-**186**–**189** showed similar trends in their $^{3}J_{trans}$ values, measured from the C*H*Ar proton, in their respective ^{1}H NMR spectra.

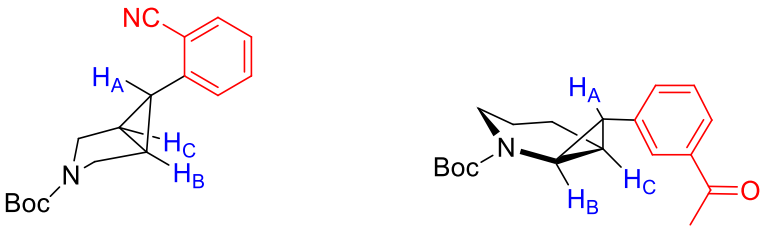

exo-**174**
$^{3}J_{HA–HB}$ = 3.5 Hz
$^{3}J_{HA–HC}$ = 3.5 Hz
$^{3}J_{HB–HC}$ = 7.5 Hz

exo-**188**
$^{3}J_{HA–HB}$ = 3.0 Hz
$^{3}J_{HA–HC}$ = 6.5 Hz
$^{3}J_{HB–HC}$ = 8.5 Hz

*Figure 3.1 – Examples of ^{3}J values of cyclopropyl aryl exo-***174** *and exo-***188**

For aryl and heteroaryl cyclopropanes *trans*-**178–181** and *cis*-**182–185**, the stereochemistry was assigned based on the X-ray crystal structure of the *trans*-cyclopropyl monobromide precursor. The transformation from the cyclopropyl monobromides (*trans* and *cis*) into cyclopropyl BMIDAs *trans*-**38** and *cis*-**38** involved the well-known stereospecific bromine–lithium exchange followed by trapping with *iso*-propoxypinacolborane. The transformation from the cyclopropyl Bpins (*trans* and *cis*) into cyclopropyl BMIDAs *trans*-**38** and *cis*-**38** does not break the carbon–boron bond, thus retaining stereochemistry. This was also correlated with the X-ray crystal structures of the pyrimidine cross-coupled methanesulfonamides *trans*-**191** and *cis*-**191**, which will be described in the next Chapter (see Scheme 3.18).

Overall, functionalisation *via* Suzuki-Miyaura cross-coupling of the cyclopropyl BMIDA group in 3-D building blocks *exo*-**39**, *trans*-**38**, *cis*-**38**, and *exo*-**36** has been demonstrated. The other 3-D building blocks have been investigated by co-workers. Ultimately, our goal is to demonstrate the versatility of the cyclopropyl BMIDA group in Suzuki-Miyaura cross-coupling across all nine building blocks. To date, we have carried out a total of ~70 examples of cross-coupling across the nine scaffolds, of which 20 are examples that I have carried out (see Schemes 3.15 and 3.17).

N-Functionalisation: Synthesis of Methanesulfonamides

In this Chapter, fragment elaboration towards lead-like compounds using four of the cyclopropyl pyrimidines cross-coupled products, *exo*-**170**, *trans*-**171**, *cis*-**171** and *exo*-**166**, is described. One of the design criteria for the 3-D building blocks was the ability for each to be elaborated through a distinct vector in 3-D chemical space. To demonstrate this, each of the nine 3-D building blocks (including the four described in this thesis) would be elaborated to a lead-like compound by functionalising the cyclopropyl BMIDA group (*via* Suzuki-Miyaura cross-coupling with 5-bromopyrimidine) and then the amino group (*via* Boc removal and mesylation of the amine). It was hoped that each of the lead-like cyclopropyl pyrimidine methanesulfonamides would be crystalline and, if so, their 3-D shape could be analysed in the solid-state using X-ray crystallography. This would allow a visual representation of the 3-D shape of the building blocks to be determined and would allow vector angles/distances between the *N*–SO_2Me and carbon–aryl bonds to be determined.

For our initial proof-of-concept examples of *N*-functionalisation, cyclopropyl pyrimidines *exo*-**170**, *trans*-**171**, *cis*-**171** and *exo*-**166** were subjected to Boc removal and *N*-mesylation (Scheme 3.18). First, the Boc group was removed under anhydrous conditions using 4 M HCl in dioxane at rt for 1 h. After solvent evaporation, the crude amine•HCl salts were mesylated using freshly distilled Et_3N and mesyl chloride in CH_2Cl_2 at rt for 16 h. Work-up and purification by chromatography afforded cyclopropyl pyrimidine methanesulfonamides *exo*-**190**, *trans*-**191**, *cis*-**191** and *exo*-**192** in 95%, 78%, 86% and 72% yields respectively (Scheme 3.18).

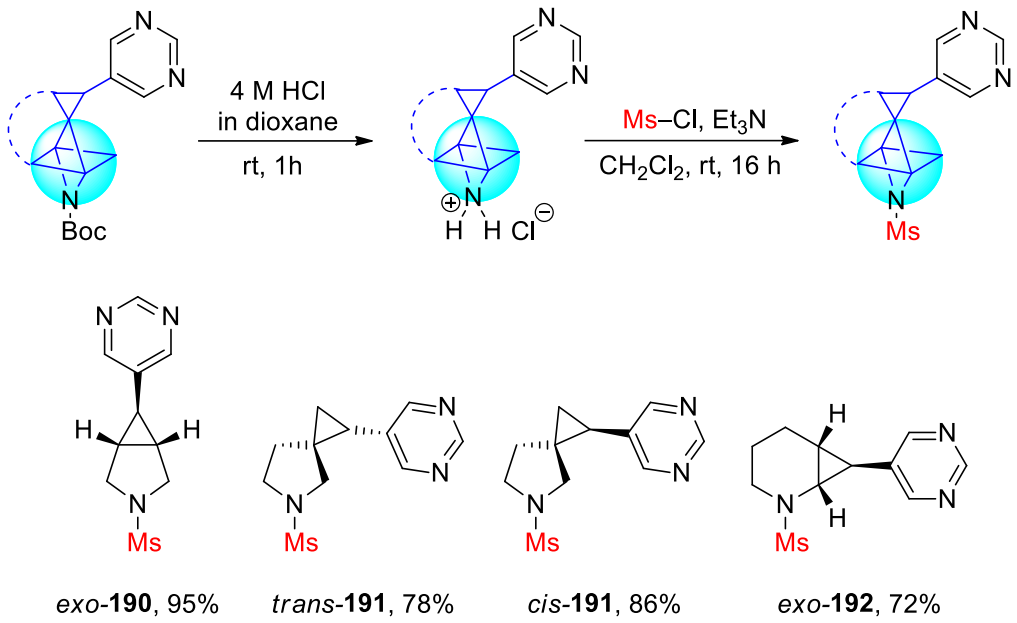

Scheme 3.18

To date, with results from other members of the group, all nine cyclopropyl building blocks shown in Figure 2.13 have been synthesised and elaborated to the corresponding cyclopropyl pyrimidine methanesulfonamides. Furthermore, each methanesulfonamide proved to be crystalline and suitable crystals were grown and analysed in the solid-state using X-ray crystallography (Figure 3.2). The 3-D shape diversity is clearly visible on inspection.

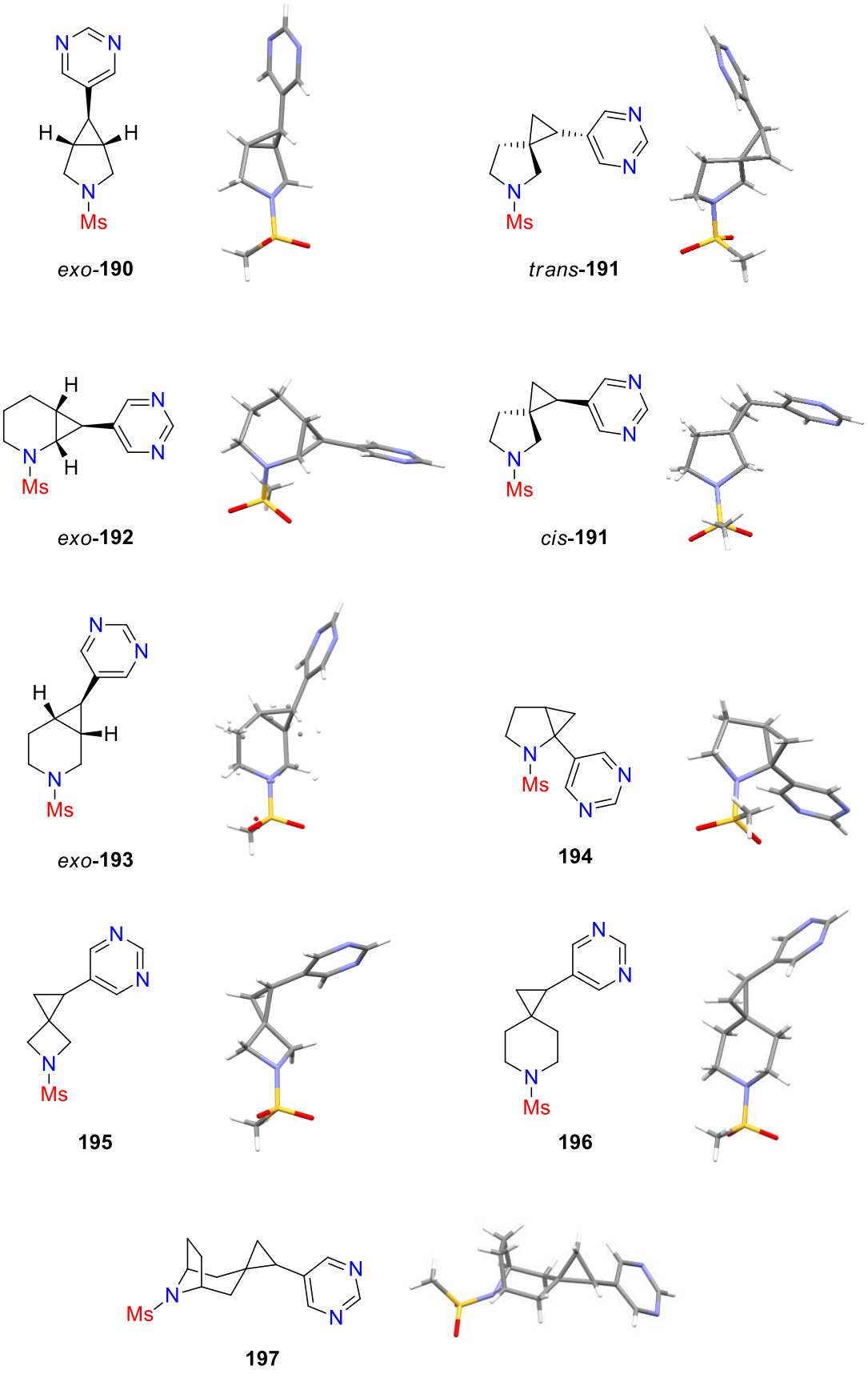

Figure 3.2 – X-ray crystal structure of various cyclopropyl-methanesulfonamides

Exit Vector Analysis

It is well-established that the design of drug-like molecules has shifted towards 3-D non-planar scaffolds.[56] So far, a number of approaches to quantitatively assess the three-dimensionality of molecules have been described. Concepts such as the fraction of sp^3 carbon atoms (Fsp^3) and principal moments of inertia (PMI) plots have been traditionally adopted to quantify the overall shape of the molecule.[56,133] However, the relative orientation of functional groups connected to the central scaffold can be an important factor overlooked by these methods of analysis.[134] In 1994, Bartlett and Lauri developed a program which facilitated the design of organic molecules called CAVEAT.[135] The premise of this software was to focus on the orientation of the functional groups (exit vectors) (Figure 3.3, A) rather than the location of the atoms (Figure 3.3, B).[135]

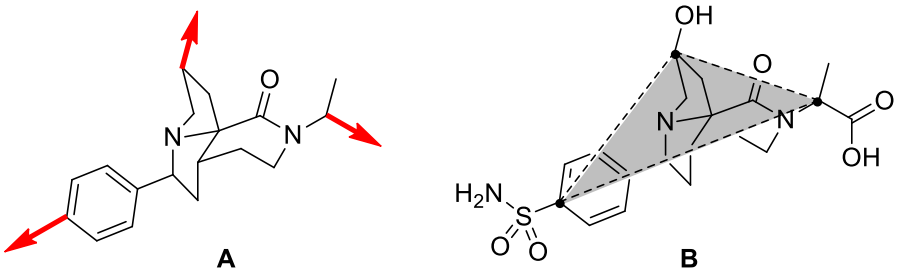

Figure 3.3 – Illustration of the orientation of exit vectors

More recently, Grygorenko and co-workers adopted this "exit vector" approach and expanded Bartlett and Lauri's idea.[136] Using 1,4-disubstituted cyclohexane as an example, vectors n_1 and n_2 can be defined for the substituents (Figure 3.4). The carbon atoms C1 and C2 are the starting points of the vectors n_1 and n_2, with r as the distance between C1 and C2. The dihedral angle θ, is defined by vectors n_1, C1–C2 and n_2. Finally, the plane angles φ_1 and φ_2 are measured from the angle between the vectors n_1 and C1–C2, and n_2 and C1–C2 respectively.[134,136,137]

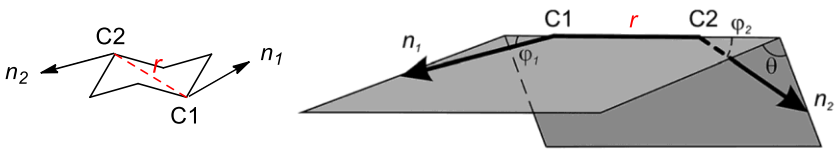

Figure 3.4 – Grygorenko's quantification of exit 3-dimensionality

Analysis of 3-D scaffolds in terms r and θ is especially useful to determine the effectiveness in the molecular design of our 3-D building blocks. Whereas r can be used

to determine the size of the scaffold, the value of the dihedral angle (θ) allows visualisation of the relative spatial orientation of the exit vector (Figure 3.5). For linear planar scaffolds such as 1,2-disubstituted benzenes **198**, the angles φ_1 and φ_2 would be zero with θ being undefined.[134] For non-linear planar molecules **199**, the values of φ_1 and φ_2 would be greater than zero, however, the value of θ would be close to zero or 180°. Finally, non-planar 3-D molecules **200**, would have all three angles far from 0°or 180°.[134]

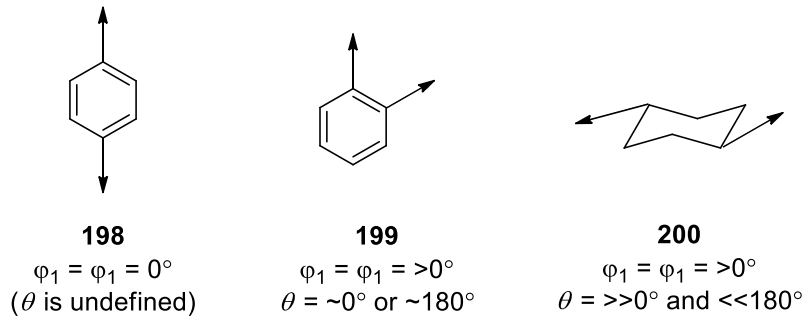

Figure 3.5 – Visualisation of relative spatial orientation based on φ_1, φ_2 and θ

The use of Grygorenko's exit vector analysis was applied to our current library of 3-D building blocks using the X-ray crystal structures of the pyrimidine methanesulfonamides. We calculated the distance between the cyclopropyl and amino variation points (r) as well as the dihedral angle of the two substituents (θ). These values were then mapped onto a r versus θ plot for each respective building block. Overall, our building blocks cover a wide variety of chemical space (Figure 3.6). The distance between variation points (r) ranges from 1.5 to 4.4 Å, and the spatial orientation between the different variation groups (θ) is also diverse across the various scaffolds.

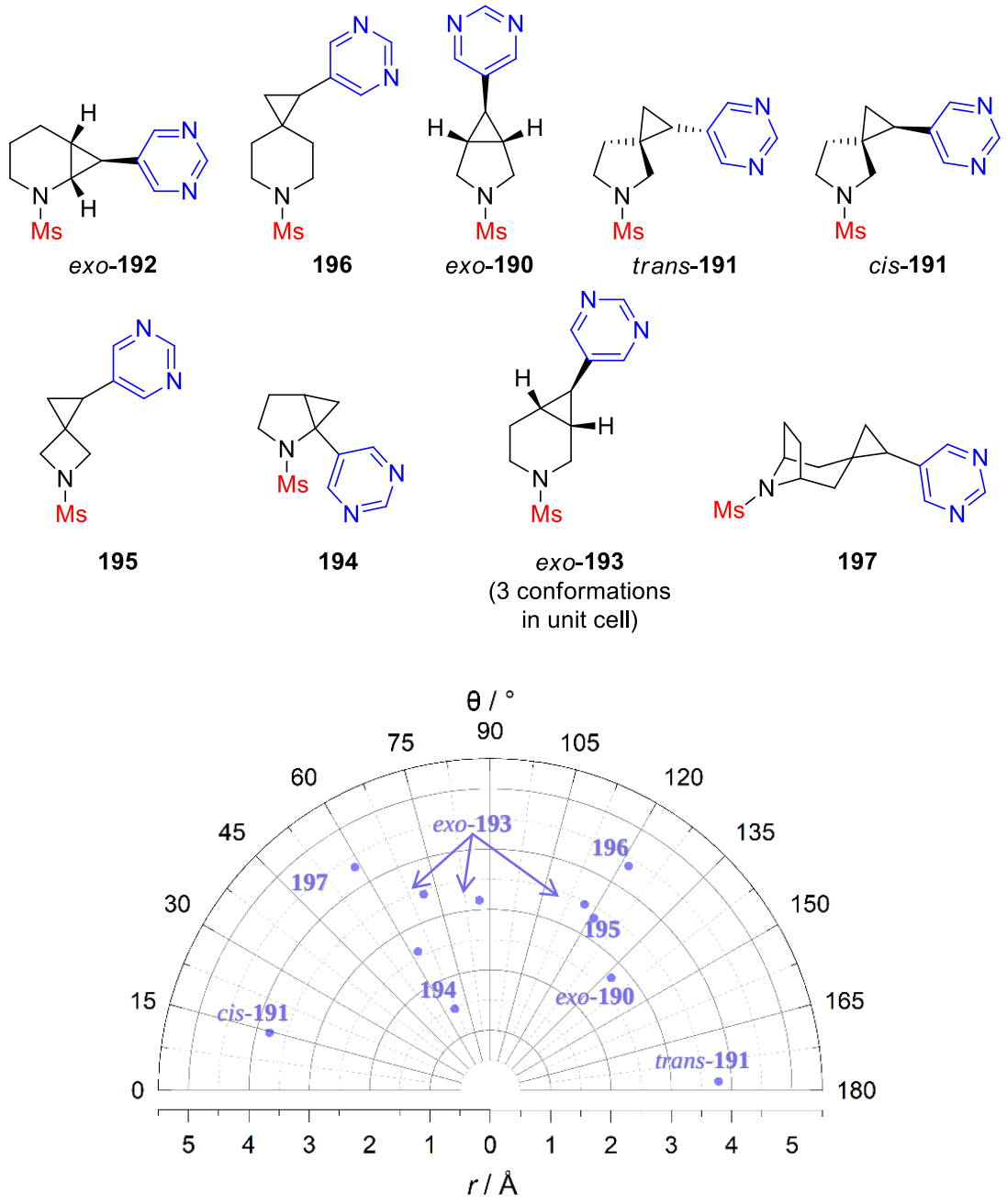

Figure 3.6 – Vector analysis of nine cyclopropyl 3-D building blocks

Conclusion

In conclusion, the successful demonstration of the Suzuki-Miyaura cross-coupling of cyclopropyl BMIDA building blocks *exo*-**39**, *trans*-**38**, *cis*-**38**, and *exo*-**36** has been accomplished. Despite the somewhat limited examples of Suzuki-Miyaura cross-coupling of cyclopropyl BMIDAs reported in the literature, the O'Brien group have successfully optimised cross-coupling conditions to tolerate a large range of medicinally relevant aryl bromides. In addition, lower Pd-loadings (5 mol%) were also achieved in contrast to the high loadings previously reported (10% – 15%). In the examples in this chapter, 21 cross-coupling examples were described in good yields ranging from 30% – 90%.

Following the successful Suzuki-Miyaura cross-coupling of cyclopropyl 3-D building blocks with 5-bromopyrimidine, reaction of the cross-coupled product with mesyl chloride afforded crystalline lead-like compounds. The X-ray crystal structures of the pyrimidine methanesulfonamides were obtained. To quantify the diversity of our library of 3-D building blocks, we adopted Grygorenko's exit vector analysis and applied it to the X-ray crystal structures of the pyrimidine methanesulfonamides. Delightfully, we observed good coverage of chemical space from just nine building blocks in our library so far.

Chapter 4: Preliminary Studies on the Synthesis and Cross-Coupling of Second-Generation Cyclobutyl 3-D Building Blocks

The most significant observation emerging from the vector analysis on the cyclopropyl 3-D building blocks in the previous chapter was the success in reaching a wide range of chemical space with just nine examples. Naturally, we envisaged the design of additional 3-D building blocks to access further areas of 3-D space. To this end, 3-D bifunctional cyclobutyl building blocks such as *N*-Boc amino alcohol *endo*-**40** were proposed (Figure 4.1). This could take advantage of the unique 3-D 'puckered' structure inherent in cyclobutane rings. The slightly increased *s*-character and chemical inertness, when compared to cyclopropanes, is another factor in favour of choosing the under-represented yet attractive cyclobutyl 3-D scaffold.[138,139] Cyclobutanes have been reported to improve metabolic stability and to reduce planarity, as well as being employed as aryl isosteres.[56,140,141] In all instances, the characteristics of cyclobutanes are favourable for the design of second-generation York 3-D cyclobutyl building blocks. In building block *N*-Boc amino alcohol *endo*-**40**, the cross-coupling handle will be the alcohol group and the plan was to make use of Dong and MacMillan's iridium and nickel catalysed photoredox cross-coupling reaction.[142]

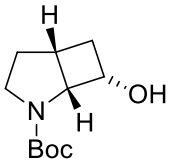

endo-**40**

Figure 4.1 – Target cyclobutyl building block for synthesis

Chapter 4.1 sets out design criteria for the cyclobutyl building blocks. Then, in Chapter 4.2, the attempted synthesis of a second generation cyclobutyl building block *endo*-**40** is described. The synthetic work was based on a [2+2] cycloaddition to incorporate the cyclobutane ring which is discussed in more detail in Chapter 4.2.1 and Chapter 4.2.2. Subsequent reaction of cyclobutanols with aryl bromides has been carried out by other members of the group and one example is presented in Chapter 4.2.3.

Criteria for the Design of York 3-D Cyclobutyl Building Blocks

The design criteria for the synthesis of second generation cyclobutyl 3-D York building block were proposed to follow those previously described for the cyclopropyl building blocks (see Chapter 2). Thus, 3-D building blocks would possess either a spiro or fused cyclobutyl ring, remain in accordance with the 'rule of two'[69] and be bifunctional, possessing both an amine and a cross-coupling handle (alcohol group in this case, *vide infra*). From these design restrictions, cyclobutyl building blocks *endo*-**40**, *exo*-**201** and **202** were identified and targeted for synthesis (Figure 4.2).

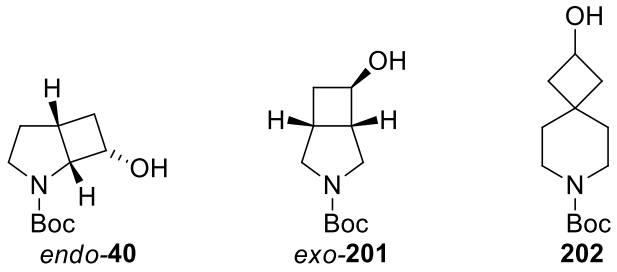

Figure 4.2 – Target cyclobutyl 3-D building blocks for synthesis

One key difference with the cyclobutyl building blocks in contrast to the cyclopropyl building blocks is the somewhat limited knowledge on the palladium-catalysed Suzuki-Miyaura cross-coupling of sp^3-hybridised cyclobutanes. Some examples of the Suzuki-Miyaura cross-couplings of simple cyclobutyl boronates have been reported[143–145] but we were concerned that the scope might not be reliable enough for our fragment elaboration purposes. More reliable routes to aryl and heteroaryl cyclobutanes from cyclobutyl boronates or their derivatives (*e.g.* BF_3K salts) typically involve iridium and nickel catalysed photoredox cross-coupling reactions.[146] One variant of these cross-coupling reactions that attracted our attention was reported by Dong and MacMillan in 2021 and involved the use of secondary alcohols.[142] Thus, we planned to use this methodology for arylation of the cyclobutane motif. An advantage of this approach is that alcohol building blocks such as *endo*-**40**, *exo*-**201** and **202** should be easier to synthesise than the corresponding BF_3K salts. The methodology development for the synthesis of cyclobutyl building block *exo*-**40** is reported in this chapter whereas cyclobutyl building blocks *exo*-**201** and **202** were explored by other members of the group.[131,147]

Synthesis and Photoredox Cross-Coupling of Fused 3-D Cyclobutanol Building Blocks

4.1.1 Overview of Ghosez's Route to Fused Cyclobutanones

To begin the synthesis of cyclobutyl building block *endo*-**40**, strategies for cyclobutanation were considered. Traditional synthesis of the cyclobutane moiety would typically involve a photochemical [2+2] cycloaddition.[148,149] However, other strategies were considered. In particular, we were attracted to Ghosez and Gobeaux's report on the intramolecular [2+2] cycloaddition of keteniminium ions. Analogous to ketenes and isocyanates, the use of keteniminium ions provides thermally-allowed [2+2] cycloaddition reactions.[150,151] An example of the Ghosez methodology to afford the scaffold present in 3-D building block *endo*-**40** is shown in Scheme 4.1. Through the action of triflic anhydride and 2,4,6-collidine in DCE at 90 °C for 2 h, carboxamide **203** was converted into keteniminium ion **204** (Scheme 4.1). Subsequent [2+2] cycloaddition, and reaction with H_2O in CCl_4 at refluxing temperatures for 2 h afforded cyclobutanone **205** in 56% yield.[150]

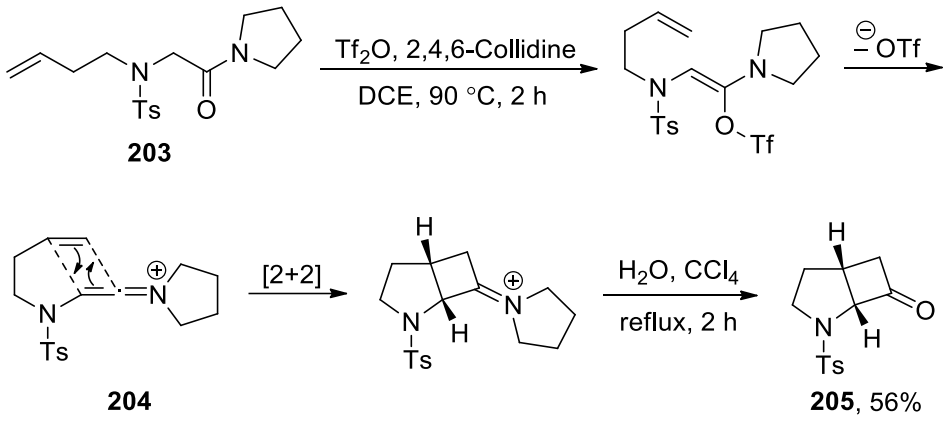

Scheme 4.1

In addition to cyclobutanone **205**, Ghosez and Gobeaux further explored two other scaffolds by varying the position of the cyclobutyl ring as well as the ring-size of the nitrogen heterocycle. Both variables were able to be controlled by the chain length of the carboxamide (*y*) or the alkene group (*x*) (Scheme 4.2).

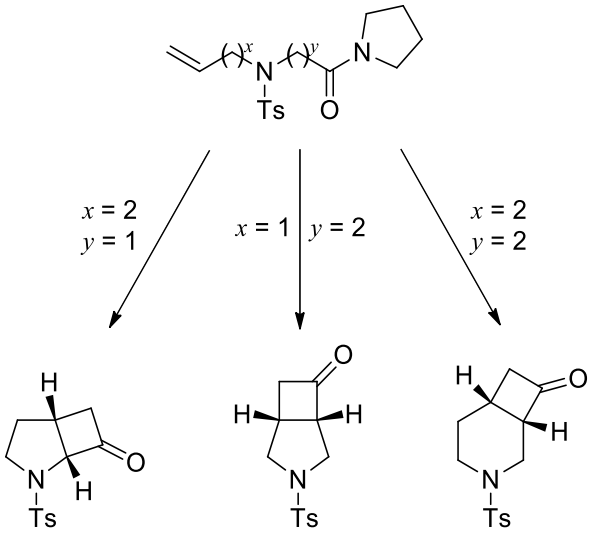

Scheme 4.2

The Ghosez cyclobutanation was later used by Dart *et al*. in a patent that described the synthesis of medicinally relevant azabicyclic compounds. Dart and co-workers were able to obtain cyclobutanone **206** directly from Ghosez's conditions (Tf_2O, 2,4,6-collidine, then H_2O). However, Dart *et al*. further demonstrated that the tosyl group could be removed and successfully replaced with a Boc group. First, the reduction of cyclobutanone **206** with $NaBH_4$ (exact conditions not specified) gave cyclobutanol *endo*-**207**. Then, a pre-mixed suspension of sodium metal and naphthalene in DME afforded the free amine *in situ*. Subsequent addition of Boc_2O provided Boc-protected cyclobutanol *endo*-**208** in an 81% yield (Scheme 4.3).

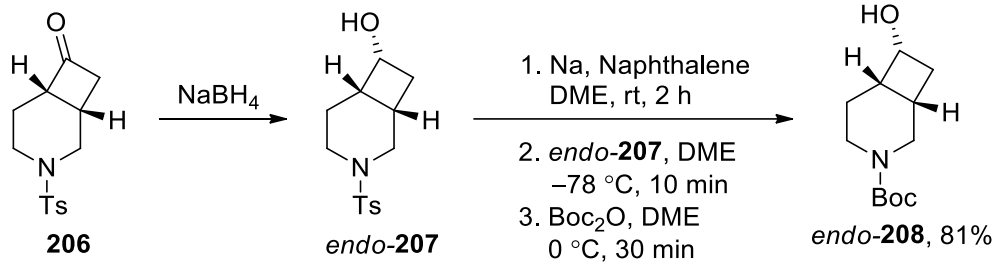

Scheme 4.3

4.1.2 Attempted synthesis of 2,3-Fused Cyclobutyl Pyrrolidine 3-D Building Block

A synthetic route for the synthesis of the Ghosez starting material, *N*-protected alkene pyrroloamide, was envisaged by utilising two alkylation reactions. To begin, bromopyrroloamide **209** was prepared by following a preparation from Manthorpe and

co-workers.[152] Using the reported procedure, bromoacetyl bromide was reacted with pyrrolidine in CH_2Cl_2 at 0 °C, before being warmed to rt and stirred for 4 h. The resulting bromopyrroloamide **209** was purified by chromatography and isolated in 70% yield (Scheme 4.4).

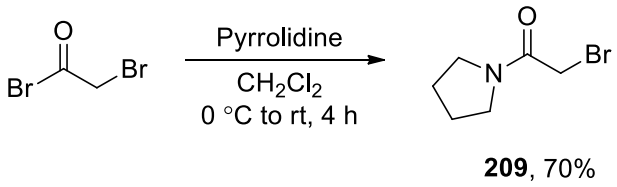

Scheme 4.4

For the purposes of using building blocks to elaborate fragments, the nitrogen protecting group would ideally be easy to remove using mild conditions. Given the success of Boc carbamates for cyclopropyl building blocks described in Chapter 2 and 3, we would ideally have Boc as the amine protecting group for cyclobutyl building blocks. To this end, amino alkene **210** was first reacted with Boc_2O, $NaHCO_3$ in THF and H_2O at rt for 16 h. The Boc protected intermediate was then added to NaH and bromopyrroloamide **209** at 0 °C and stirred at rt for 18 h to afford dialkylcarbamate **211** in 59% yield (Scheme 4.5).

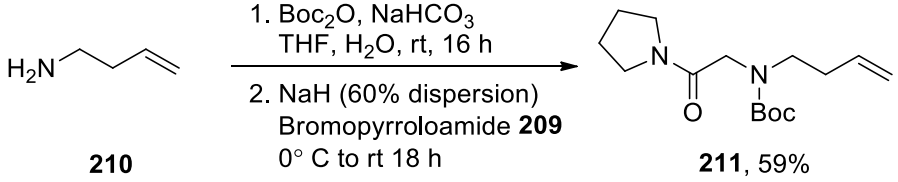

Scheme 4.5

The Ghosez cyclobutanation of dialkylcarbamate **211** was carried out by adapting the original preparation.[150] Substituting CCl_4 with CH_2Cl_2 allowed for safer hydrolysis conditions to access cyclobutanone **212**. Thus, dialkylcarbamate **211** was initially mixed with Tf_2O and 2,4,6-collidine in DCE at 80 °C for 2 h, before H_2O and CH_2Cl_2 were added and stirred at 60 °C for 2 h (Scheme 4.6). Unfortunately, the presence of cyclobutanone **212** was not detected in the ^1H NMR spectrum of the crude product.

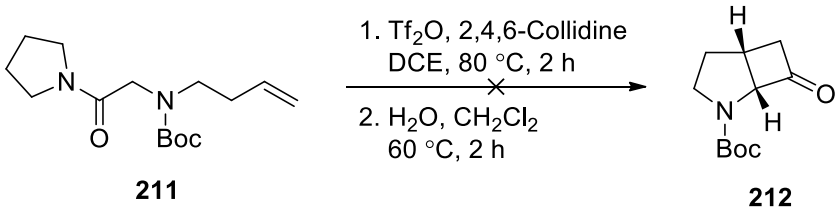

Scheme 4.6

The proposed challenge with using Boc carbamates is presumably the competing triflation of the Boc carbonyl group and the desired amide (Figure 4.3). While we hoped that the use of one equivalent of Tf_2O was sufficient to circumvent the possible side reaction, the failure of the reaction led to the conclusion that Boc carbamates are not compatible with Ghosez cycloaddition reactions.

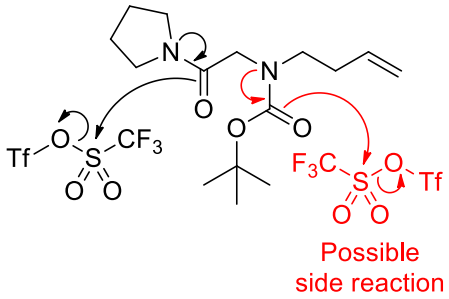

Figure 4.3 – Proposed side reaction when using Boc carbamates

Next, we attempted to use tosyl as the protecting group as this was the preferred choice in the original report from Ghosez and Gobeaux[150] as well as Dart *et al.*[153] The plan would be to modify the *N*-tosyl group to a *N*-Boc group at some later stage. To do this, the synthetic route to dialkylcarbamate **203** was modified. First, tosyl amine was reacted with bromo alkene **213** and K_2CO_3 in MeCN at 80 °C for 16 h to obtain alkylsulfonamide **214** in 96% yield after chromatography (Scheme 4.7). In the second step, previously prepared bromopyrroloamide **209** was reacted with alkylsulfonamide **214** in MeCN at 80 °C for 16 h to afford dialkylsulfonamide **203** in 51% yield (Scheme 4.7).

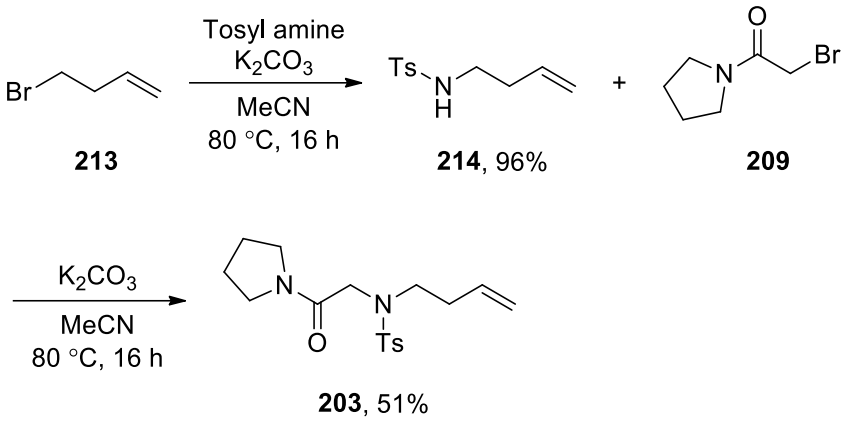

Scheme 4.7

For the Ghosez cycloaddition, after successful trials on a small scale, dialkylsulfonamide **203** (7.35 g) was first reacted with Tf_2O and 2,4,6-collidine in DCE at 80 °C for 2 h, before the iminium ion was hydrolysed with H_2O in CH_2Cl_2 at 60 °C for 2 h. This gave cyclobutanone **205** in 65% yield (3.74 g) after chromatography (Scheme 4.8). Subsequent reduction of cyclobutanone **205** was carried out by reacting cyclobutanone **205** with $NaBH_4$ in MeOH at rt for 4 h to afford cyclobutanol *endo*-**215** in 80% yield.

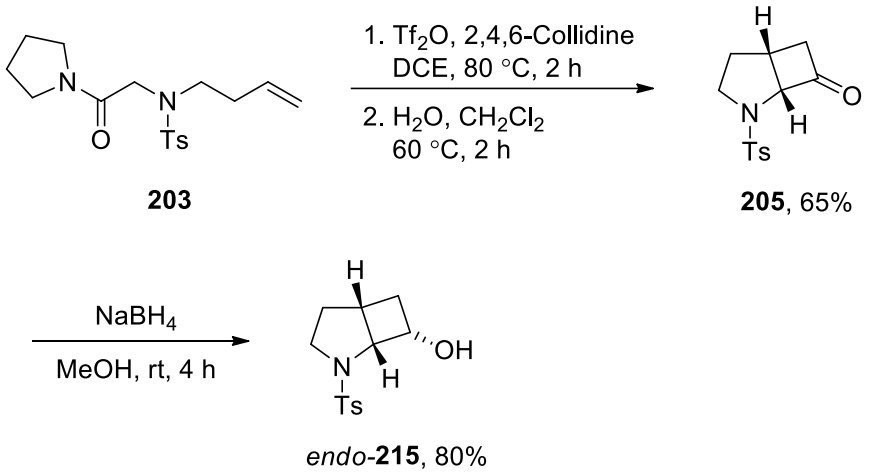

Scheme 4.8

The *endo* stereochemical outcome for the reduction of cyclobutanone **205** is explained by the approach of $NaBH_4$. In the key step, the hydride is proposed to be delivered from the less hindered *exo* face of the cyclobutyl ring. The resulting *exo* addition of the hydride would place the hydroxy group in the *endo* position (Scheme 4.9). Support for the assignment of *endo* stereochemistry is provided by an X-ray crystal structure of the

corresponding *N*-*p*-nitrobenzenesulfonyl cyclobutanol *endo*-**219**, which was synthesised in an analogous way (see Scheme 4.11 and Figure 4.4).

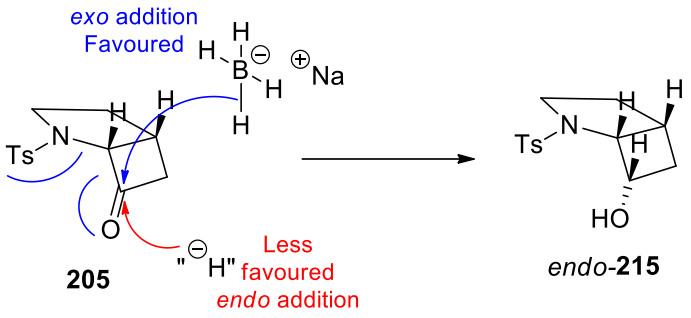

Scheme 4.9

In order to prepare the *N*-Boc amino alcohol with a convenient *N*-Boc protecting group, the plan was to transform the *N*-tosyl group into *N*-Boc. Using the conditions reported by Dart *et al.*,[153] sodium and naphthalene were reacted in DME at rt for 2 h, before this mixture was added to cyclobutanol *endo*-**215** at –78 °C. Upon addition, H_2O and Boc_2O were immediately added and the reaction was stirred for 30 min (Table 4.1, entry 1). Unfortunately, no evidence of *N*-Boc amino alcohol *endo*-**40** was observed by analysis of the ^{1}H NMR spectrum of the crude product. The same outcome was observed when the reaction was repeated and the deprotected cyclobutanol *endo*-**215** was allowed to stir with Boc_2O for 16 h (Table 4.1, entry 2). Attempts to isolate the free amine and hydrochloride salt were also unsuccessful when using sodium and naphthalene (Table 4.1, entry 3), magnesium and 1,2-dibromoethane (Table 4.1, entry 4), sodium and naphthalene then HCl (Table 4.1, entry 5), or HBr and 4-hydroxbenzoic acid (Table 4.1, entry 6). Although we have no definitive proof, based on Dart *et al.*'s precedent,[153] it seems reasonable to propose that removal of the *N*-tosyl group was occurring. This is consistent with the fact that there was no starting material remaining. If the subsequent Boc protection was not successful then isolation of the potentially volatile and water-soluble amino alcohol would be challenging and could account for the lack of evidence of anything characterisable in the ^{1}H NMR of the crude products. A similar issue would occur for reactions where we tried to isolate the free amine or hydrochloride salt.

Table 4.1 – Unsuccessful attempts towards the removal of the tosyl group

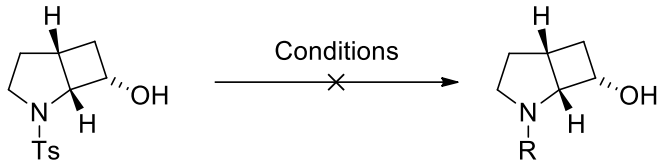

endo-**215**

Entry	**R**	**Conditions**
1	Boc	Na, Naphthalene, DME, rt, 2 h then, H_2O, Boc_2O, –78 °C, 30 min
2	Boc	Na, Naphthalene, DME, rt, 2 h then, H_2O, Boc_2O, –78 °C to rt, 16 h
3	H	Na, Naphthalene, DME, rt, 2 h then, H_2O, –78 °C, 10 min
4	H	Mg, 1,2-dibromoethane MeOH, rt, 2 h
5	H•HCl	Na, Naphthalene, DME, rt, 2 h then, HCl (in dioxane), –78 °C, 5 min
6	H	HBr (33% wt in AcOH) 4-hydroxybenzoic acid, rt, 72 h

Given that the conversion of the *N*-tosyl group into a *N*-Boc group was unsuccessful, the next plan was to explore a different sulfonyl group that could be removed *via* a different set of reaction conditions. It was decided that *p*-nitrobenzenesulfonyl (Ns) would be attempted as the amine protecting group. By adapting the previous synthetic route for synthesis of tosyl dialkylsulfonamide **203**, tosyl amine was replaced by nosyl amine. In this way, nosyl alkylsulfonamide **216** (11.27 g) was generated in 25% yield after 168 h at 60 °C (Scheme 4.10). This reaction also afforded dialkylsulfonamide **217** which was isolated in a 21% yield. Fortunately, nosyl alkylsulfonamide **216** and dialkylsulfonamide **217** were separable by column chromatography. Therefore, nosyl alkylsulfonamide **216** was subsequently reacted with bromopyrroloamide **209** to give dialkylsulfonamide **218** in 77% yield after 96 h at 60 °C (Scheme 4.10).

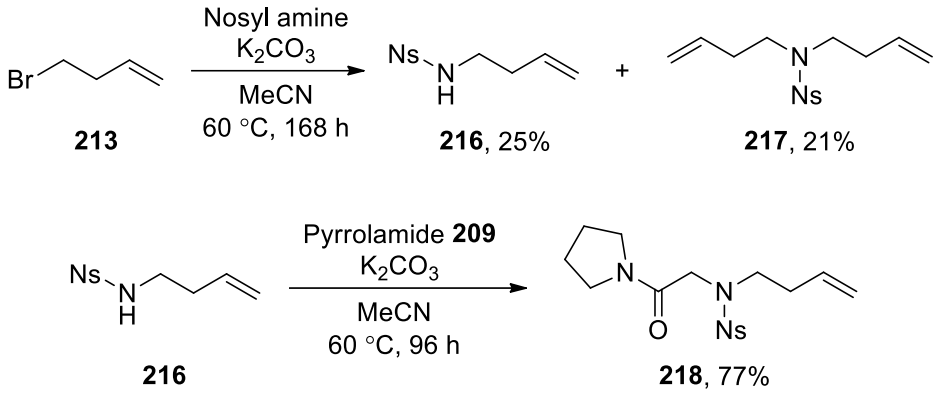

Scheme 4.10

The Ghosez cycloaddition of dialkylsulfonamide **218** using Tf_2O, 2,4,6-collidine and H_2O gave nosyl cyclobutanone **219** in 82% yield after purification by chromatography (Scheme 4.11). Reduction of cyclobutanone **219** with $NaBH_4$ afforded cyclobutanol *endo*-**220** in 91% yield. The crystalline cyclobutanol *endo*-**220** was analysed by X-ray diffraction and an X-ray crystal structure was obtained (Figure 4.4). In the 3-D structure of nosyl cyclobutanol *endo*-**220**, the hydroxy group is *trans* to the cyclobutyl bridgehead protons, therefore, assigning *endo* stereochemistry. Similarly, for tosyl cyclobutanol *endo*-**215**, the stereochemistry was also assigned by analogy. [20]

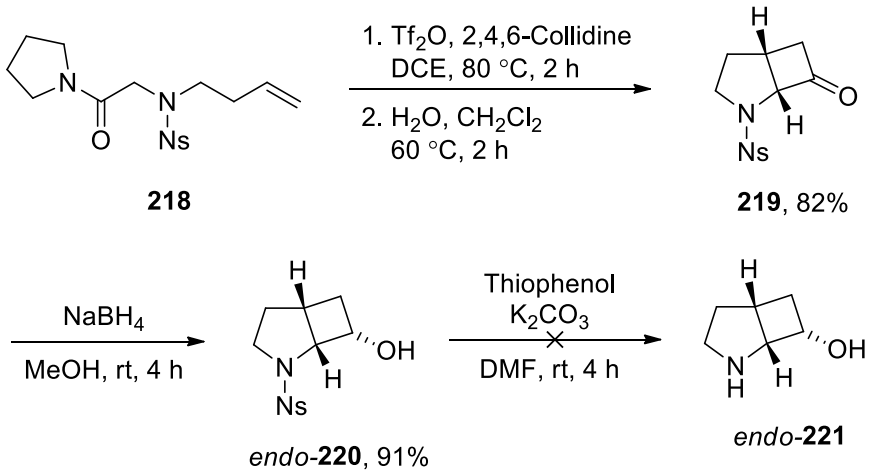

Scheme 4.11

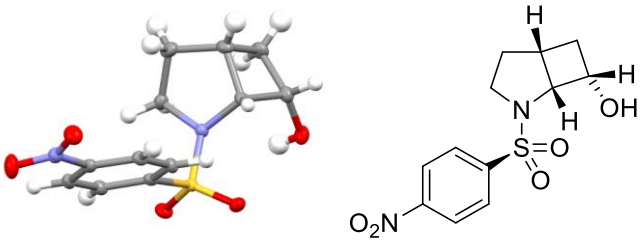

*Figure 4.4 – X-ray structure of nosyl cyclobutanol endo-***220**

Attempted removal of the nosyl group with reaction conditions reported by Hanamoto *et al.*[154] was carried out. Therefore, nosyl cyclobutanol **220** was reacted with thiophenol and K_2CO_3 in DMF at rt for 4 h. Analysis of the ^{1}H NMR spectrum of the crude product failed to show any signs of amino alcohol *endo*-**221** and starting material after work-up (Scheme 4.11). This further supports the difficulty in isolating the amino alcohol as observed in the synthesis of tosyl cyclobutanol *endo*-**214** (Table 4.1).

4.1.3 Photoredox cross-coupling of cyclobutyl 3-D building block *endo*-215

In 2021, Dong and MacMillan reported on the metallaphotoredox-enabled deoxygenative arylation of alcohols by activation using alcohol adducts **222** to facilitate homolytic cleavage of the C–O bond to form a cyclobutyl radical (Figure 4.5).[142] The resulting cyclobutyl radical is proposed to feed into the iridium–nickel catalyst system, whereby photoredox cross-coupling to aryl bromides can occur.[142]

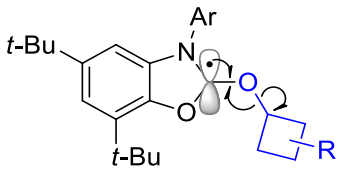

222

Figure 4.5 – Alcohol activation via homolytic cleavage of the C–O bond

The closest example reported by Dong and MacMillan which follows our envisaged design criteria for elaboration of fragments using 3-D building blocks is cyclobutanol **223**. Upon activation using benzoxazolium salt **224** and pyridine in *t*-BuOMe at rt for 5 min, the resulting cyclobutane radical undergoes photoredox coupling with an aryl bromide using $(Ir(ppy)_2(dtbbpy))PF_6$, $NiBr_2$•dtbbpy and quinuclidine in

t-BuOMe and DMAc mixture under illumination of blue LEDs at rt for 2 h gave aryl cyclobutane **225** in 83% yield (Scheme 4.12).[142]

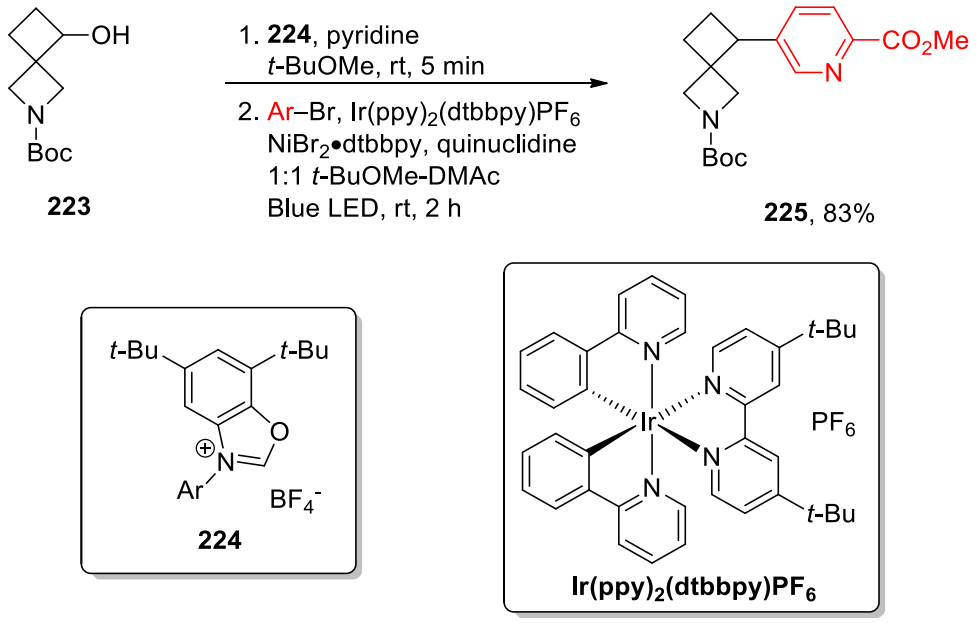

Scheme 4.12 – Photoredox cross-coupling of a spiro cyclobutanol

Members of the O'Brien group have investigated the variation of the aryl group attached to benzoxazolium salt **224** to provide optimised conditions for the cross-coupling of cyclobutanols **226**.[131] It was discovered that activation of cyclobutanols using benzoxazolium salt **227** and pyridine in trifluorotoluene at 0 °C for 1 h, followed by reaction with an aryl bromide, (Ir[dF(CF_3)ppy]$_2$(dtbpy))PF_6, $NiBr_2$•DME, dtbbpy and quinuclidine in DMAc under illumination of blue LEDs at rt for 18 h gave a series of cross-coupled aryl cyclobutanes **228** (Scheme 4.13).[131] These conditions are proposed to be the standard set that will be used to carry out fragment elaboration *via* cyclobutyl cross-coupling on second generation York 3-D cyclobutyl building blocks.

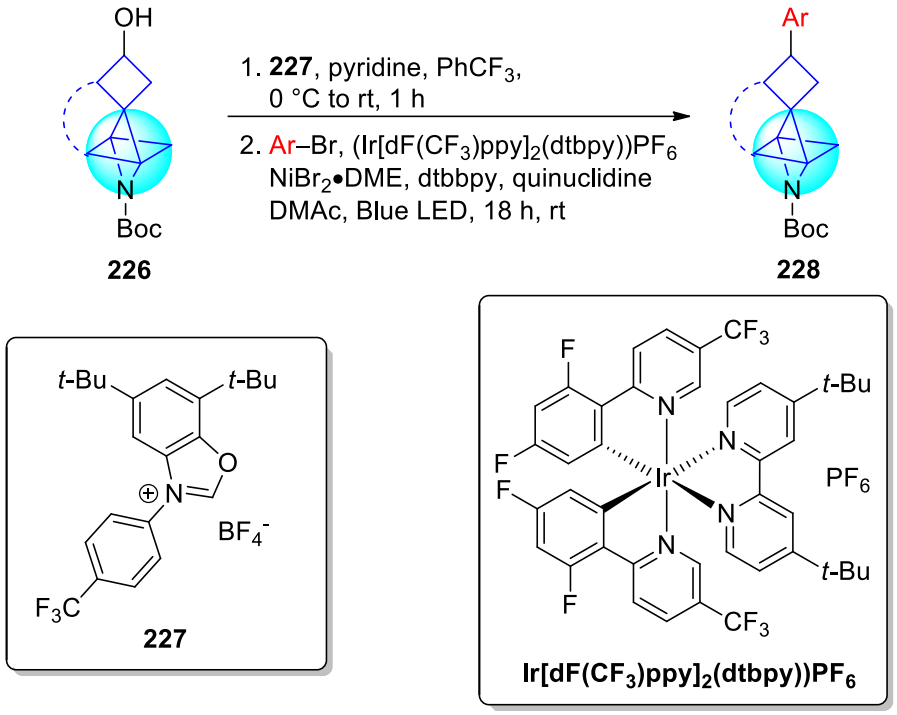

Scheme 4.13

With nosyl and tosyl cyclobutanols *endo*-**220** and *endo*-**215** in hand, it was proposed to investigate the MacMillan cross-coupling method in order to attach an aryl group onto the alcohol cross-coupling handle. However, nosyl cyclobutanol *endo*-**220** would not be compatible with photoredox cross-coupling as Doyle *et al.* had proposed that nitro groups would be readily reduced by the photocatalyst.[155] However, it was felt that the demonstration of photoredox cross-coupling on tosyl cyclobutanol *endo*-**215** was still important despite the challenges we had faced in removing the tosyl group. Therefore, Andres Gomez Angel of the O'Brien group explored the photoredox cross-coupling of cyclobutanol *endo*-**215**. First, cyclobutanol *endo*-**215** was activated by a reaction with benzoxazolium salt **227** and pyridine in trifluorotoluene at 0 °C for 1 h to afford cyclobutanol adduct *endo*-**229**. In the next step, cyclobutanol adduct *endo*-**229** was reacted with 5-bromopyrimidine under iridium and nickel photocatalysis with dtbbpy and quinuclidine in DMAc under the illumination of blue LEDs at rt for 18 h to give cyclobutyl pyrimidine *exo*-**230** in 41% yield (single diastereoisomer formed). The stereochemistry proposed in *exo*-**230** is currently an assumption but presumably arises from the planar radical intermediate reacting on the less sterically hindered *exo*-face of the fused bicyclic system. This demonstration of arylation of building block *endo*-**215** is important for the future development of cyclobutane-based 3-D building blocks.

However, a method to access the Boc-protected building block is still required and will be the subject of future work in the group.

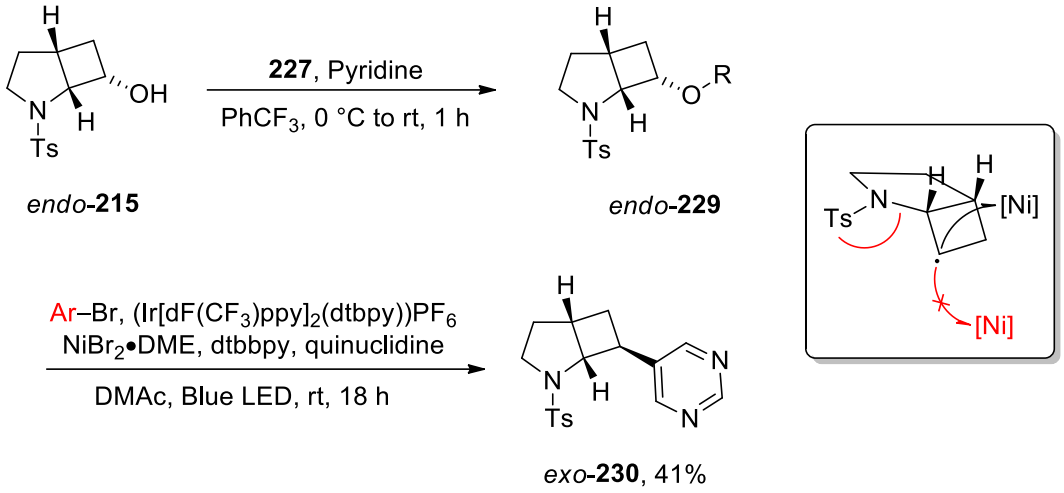

Scheme 4.14

Conclusion and Future Work

In conclusion, the successful synthesis of tosyl cyclobutanol *endo*-**215** and nosyl cyclobutanol *endo*-**220** on a gram-scale was achieved. Unfortunately, the direct synthesis of Boc protected cyclobutanes were unsuccessful due to incompatibility of carbamates in the Ghosez cycloaddition. Moreover, the removal of tosyl and nosyl groups and subsequent isolation of the amino alcohol or Boc protected version were also challenging, with numerous unsuccessful attempts made using various reaction conditions. Overall, the Ghosez cyclobutanation was an effective cyclobutanation strategy for the synthesis of fused cyclobutyl 3-D building blocks. However, the incompatibility of easily removable nitrogen protecting groups may hinder its usefulness.

The photoredox cross-coupling of tosyl cyclobutanol *endo*-**215** was achieved by Andres Gomez Angel to successfully demonstrate the cross-coupling potential of the cyclobutanol scaffold. Similarly to cyclopropane 3-D building blocks discussed in the previous chapter, cyclobutanol 3-D building blocks could also be attached to a fragment hit, then the fragment could be elaborated by subsequent functionalisation at the amino terminus.

Future work should continue to focus on the transformation of either tosyl or nosyl cyclobutanols *endo*-**215** or *endo*-**220** into *N*-Boc amino alcohol *endo*-**40**. As an alternative, a sulfinamide could also be investigated for the protection of the amino group. The use of a sulfinyl group could allow for facile removal using acid (*e.g.* HCl), a protocol that has been demonstrated by Aggarwal *et al.* for example.[156] Therefore, we envisage that Ghosez cycloaddition of sulfinamide **231** using standard conditions (Tf_2O and 2,4,6-collidine) would form cyclobutyl sulfinamide **232**. The reduction and subsequent transformation into *N*-Boc amino alcohol *endo*-**40** could be carried out with $NaBH_4$

before treating the resulting cyclobutanol *endo*-**233** with HCl and then Boc_2O (Scheme 4.15).

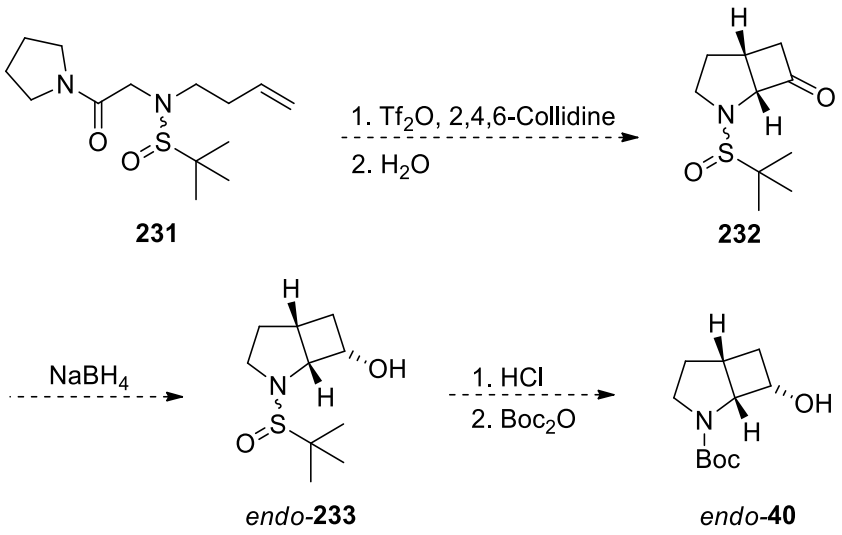

Scheme 4.15

Once the *N*-Boc amino alcohols are accessible, the scope of the Ghosez cycloaddition could generate a series of fused cyclobutanols (some samples shown in Figure 4.7). This would expand the coverage of exit vectors beyond those presented by the cyclopropyl 3-D building blocks described in Chapter 3 (see Figure 3.6).

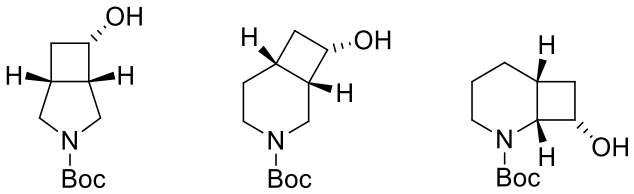

Figure 4.6 – Potential fused cyclobutanols synthesised from Ghosez cycloaddition

Chapter 5: Investigation of Methodology for the Synthesis of a 3-D Covalent Fragment Library

The studies in this Chapter aim to build on the use of York 3-D building blocks in drug discovery through the synthesis of building block-derived 3-D covalent fragments. As discussed in Chapter 3, the methodology for fragment elaboration included Suzuki-Miyaura cross-coupling of cyclopropyl BMIDA building blocks. Upon removal of the Boc group, amine derivatisation gave the elaborated fragment in two steps. Until now, a proposal for the synthesis of, for example, ten acrylamide fragments **44** would involve ten separate cross-coupling reactions with cyclopropyl BMIDA **234** and then ten Boc group removals and acrylamide formations (Scheme 5.1).

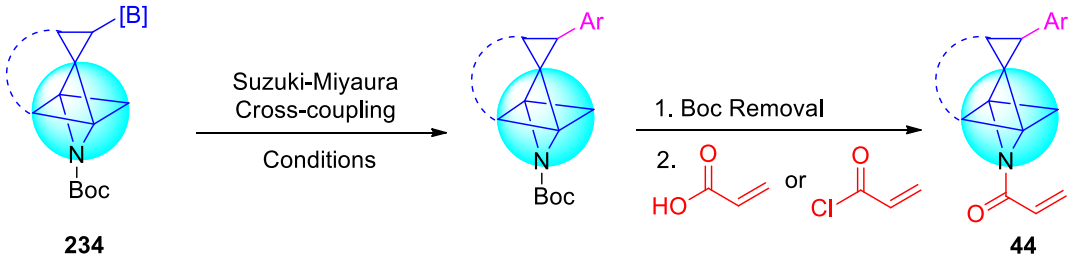

Scheme 5.1

A new methodology was envisaged that would allow for the single-step synthesis of acrylamides **44** from *β*-sulfonyl amides **236**. By first removing the Boc group in cyclopropyl BMIDAs **234**, *β*-sulfonyl amides **236** would be prepared (gram-scale). Then, under the basic Suzuki-Miyaura cross-coupling conditions, it is hoped that the boronate moiety could be functionalised with an aryl or heteroaryl halide in tandem with the elimination of methylsulfinate to reveal acrylamide fragments **44** (Scheme 5.2). This would represent a more efficient way of preparing a set of ten acrylamide fragments **44** than the linear synthesis shown in Scheme 5.1. Thus, a large-scale reaction to generate *β*-sulfonyl amides **236** could first be performed. Then, cross-coupling to various aryl and heteroaryl bromides of our choosing could be carried out in a single-step to give acrylamide fragments **44** (Scheme 5.2). In general, it was envisaged that this methodology could greatly reduce the synthetic workload required in the efficient and rapid generation of 3-D acrylamide fragments **44**.

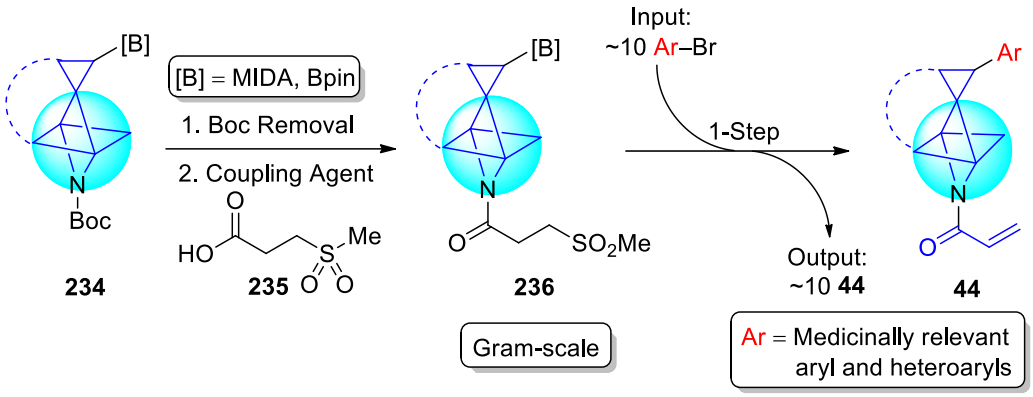

Scheme 5.2

In this regard, the mechanism of action of several covalent groups and drugs are discussed in Chapters 5.1 and 5.2, respectively. The methodology for the synthesis of a covalent fragment library using cyclopropyl 3-D building blocks begins in Chapter 5.3.1, by first investigating a model piperidine system. Next, in Chapter 5.3.2, the synthesis of *β*-sulfonyl amides was carried out on cyclopropyl 3-D building blocks with considerations being made for the boronic acid protecting group. Finally, the Suzuki-Miyaura cross-coupling of *β*-sulfonyl amides are investigated in Chapter 5.3.3. In this final section, compatible Suzuki-Miyaura cross-coupling conditions are discussed to ultimately enable the tandem elimination–cross-coupling of *β*-sulfonyl amides.

Chemistry of Covalent Warheads and Their Modes of Binding

A covalent drug is defined as a pharmaceutical agent that carries a bond-forming functional group which is commonly referred to as the 'covalent warhead'.[157,158] Examples of simple covalent warheads include electron-deficient alkenes and nitriles. For most covalent drugs, an *α,β*-unsaturated amide-type Michael acceptor is adopted as the covalent warhead.[159] With such warheads, covalent capture of the sulfhydryl group on cysteine, or the amine group on lysine, by conjugate addition forms the covalent bond.[160] For activated or unactivated alkynes, only cysteine residues are capable of forming covalent bonds to this type of warhead (Scheme 5.3).[161]

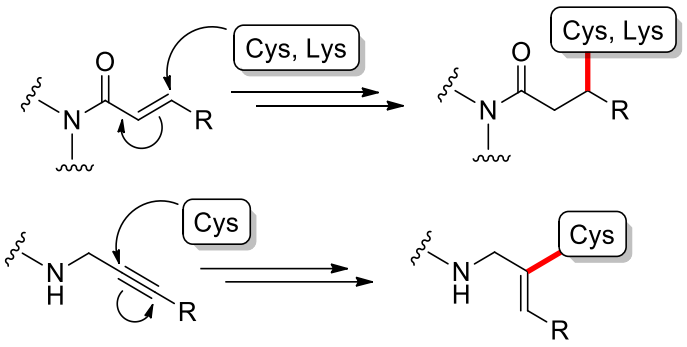

Scheme 5.3

Haloacetamides are another class of warheads commonly used to target cysteine residues.[162] Recently, London, von Delft, and Walsh *et al.* reported on the use of haloacetamides in a fragment-based ligand discovery screening campaign to identify new covalent inhibitors against SARS-CoV-2 M^{pro}.[163] The X-ray crystallography study identified 71 hits, covering the entire active site. These results enable the future development of more potent pharmaceutical agents that contain the haloacetamide warhead.[163] The haloacetamides undergo reaction with the sulfhydryl group on cysteine residues *via* an S_N2 mechanism, resulting in the formation of the desired covalent bond (Scheme 5.4). Similarly, developments in click chemistry have allowed the synthesis of sulfur(VI) fluoride exchange (SuFEx) warheads.[164] The arylsulfonyl fluoride group has good stability under aqueous conditions.[165] Furthermore, it has been demonstrated that SuFEx warheads can be deployed to target varies proteins through selective covalent interactions involving serine, threonine, lysine or tyrosine residues (Scheme 5.4).[166–168] Substitution of fluorine with an amino acid through a nucleophilic substitution mechanism results in the formation of a stable covalent adduct.

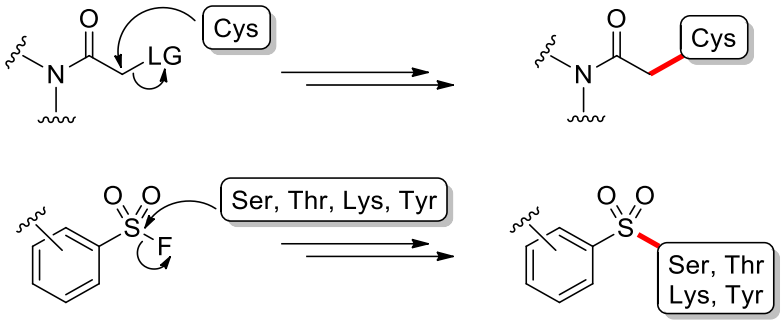

Scheme 5.4

In an effort to find new protein-reactive electrophiles, Weerapana *et al.* reported on the reactivity of aryl halides through the nucleophilic aromatic substitution reaction (S_NAr).[169] Interestingly, it was discovered that when *p*-chloronitrobenzene was subjected to complex proteomes, high cysteine selectivity was observed (Scheme 5.5). In the same way, dichlorotriazine was reported to be lysine selective.[169] The results of this study demonstrate the use of electron-deficient aryl halides as potential covalent warheads. As previously discussed in Chapter 1, Waring *et al.* reported on a series of halogenated fragments (FragLites) where a selection of the electron deficient FragLites could potentially undergo S_NAr with amino acid residues to form covalent bonds.[20,160]

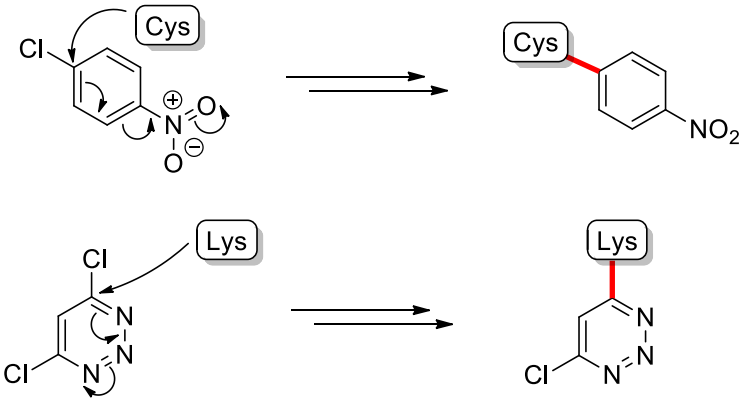

Scheme 5.5

Classical drugs such as aspirin and *β*-lactam antibiotics were the first examples of pharmaceuticals to undergo covalent bond formation.[160] Through an acylation mechanism, cysteine, lysine, and tyrosine residues can react to form a covalent bond with esters, amides, carbamates and ureas (Scheme 5.6). Alternatively, aldehydes, ketones, and nitriles are capable of undergoing 1,2-addition reactions with cysteine, threonine and serine residues (Scheme 5.6).[160]

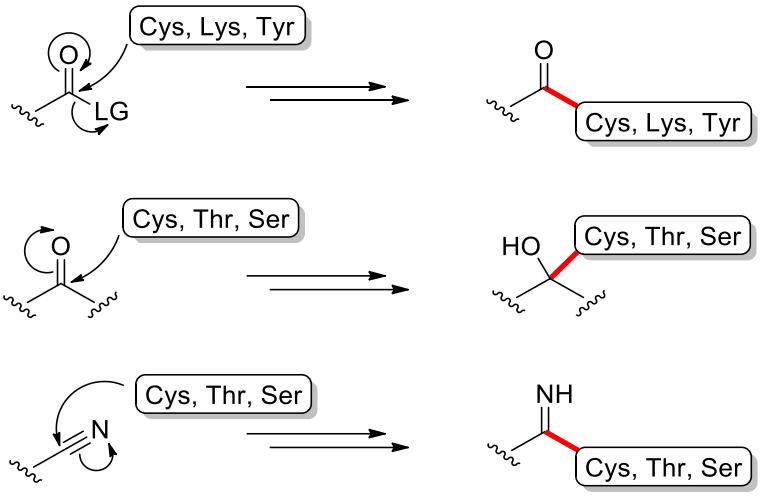

Scheme 5.6

In the past, strained molecules such as epoxides and bicyclo[1.1.0]butanes (BCBs) have been identified as biological hazards. Despite the controversy, recent advancements on our knowledge of epoxides and BCBs have shown the true potential of these moieties in drug design, with both groups being exploited for their ability to form covalent bonds with nucleophilic amino acid residues.[170,171] Detailed examination of epoxide-containing molecules by Gomes *et al.* demonstrated that this warhead has a significant impact on anticancer agents, among other drug-classes, and deserves to be better explored.[170] Functionally, the amino acids cysteine, lysine, threonine, and histidine possess the ability to ring-open the epoxide by nucleophilic attack (Scheme 5.7).[172] Moreover, Baran and co-workers have shown that BCB sulfones are susceptible to strain-release by addition of cysteine residues *via* nucleophilic addition (Scheme 5.7).[173] In the same way, the BCB warhead could be used as an important group in future drug design and development.[160]

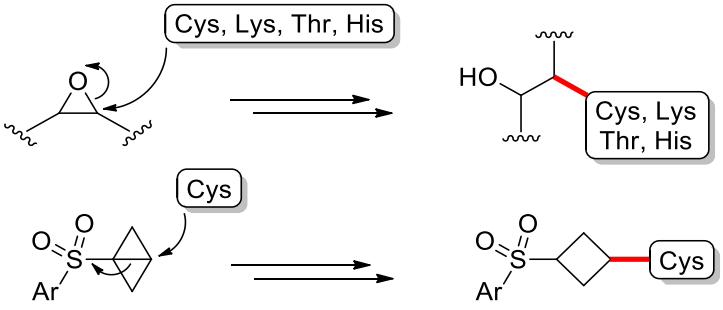

Scheme 5.7

In addition to their use in Suzuki-Miyaura cross-coupling reactions, boronic acids can also play a role in the formation of covalent bonds with proteins. In the first example, a boronic acid in the *ortho* position can accelerate the formation of an imine with a lysine

amino residue (Scheme 5.8).[174,175] In 2016, researchers at AstraZeneca used this covalent warhead strategy to design the first set of reversible covalent inhibitors against myeloid cell leukemia-1 (Mcl-1). The boronic acid is proposed to stabilise the imine lone pair by donation into the boron *p*-orbital.[176] Naturally, nucleophilic addition of the hydroxy groups present in serine and threonine, to the empty boron *p*-orbital could also serve as a covalent warhead strategy (Scheme 5.8). This is exactly the mode of action of Velcade® and Ninlaro® for the treatment of multiple myeloma (white blood cell cancer) in inhibiting the threonine residue on the 20*S* proteasome.[177]

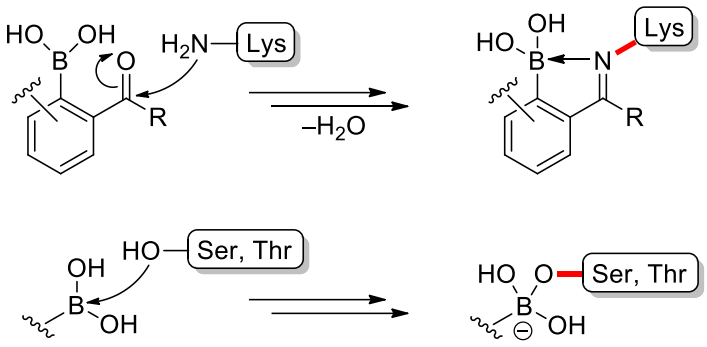

Scheme 5.8

Summary of Covalent Drugs and Their Mechanism of Action

Traditionally, the development of covalent pharmaceuticals was disfavoured due to concerns about off-target reactivity *in vivo*.[157,178] This opinion was supported by studies from the mid-1980s that revealed the hepatotoxicity (drug-induced liver injury) of paracetamol.[179,180] Despite being one of the most used medications worldwide, paracetamol is also responsible for the leading cause of acute liver failure.[181] Xenobiotic metabolism of paracetamol by cytochrome P450 enzymes allows for *N*-hydroxylation and subsequent dehydration of intermediate **237** to give *N*-acetyl-*p*-benzoquinone imine (NAPBQI) (Scheme 5.9). This toxic by-product usually conjugates with glutathione in the liver before it is excreted. However, depletion of glutathione can allow the conjugation of NAPBQI with off-target proteins and nucleic acids in the liver to give **238**, potentially causing fulminant liver damage or failure.[182]

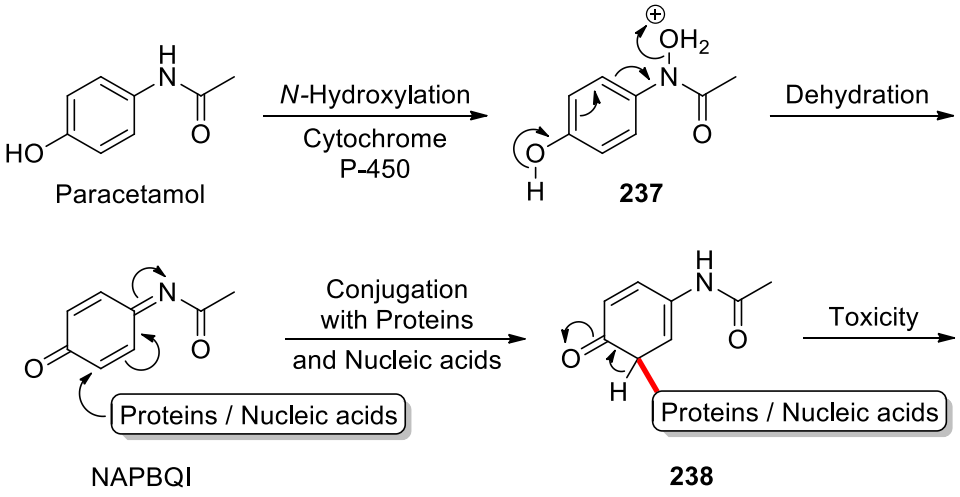

Scheme 5.9

Unsurprisingly, for many years, hits from screening campaigns that contained potentially reactive functionality such as covalent warheads, were ignored.[183] Today, however, the presence of covalent warheads in pharmaceutical agents has become mainstream and very popular with acrylamides and *α,β*-unsaturated carbonyl compounds as the predominant covalent warheads of choice.[160,184,185] In 2021, the FDA granted approval to Lumakras™ (developed by Amgen Inc.) for the treatment of metastatic non-small cell lung cancer (Figure 5.1).[186] Of note, Lumakras™ is one of the six marketed drugs that have been discovered using an FBDD approach (see Figure 1.6). The mechanism of action involves the nucleophilic cysteine residue present only in the mutated form of the KRAS gene that is responsible for cancer. This occurs by conjugate addition of cysteine to the *β*-carbon of

the acrylamide to give the covalent adduct (Scheme 5.10). Therefore, the covalent warhead in Lumakras™ makes it possible to selectively target mutated forms of the KRAS gene resulting in cell apoptosis, a target that was previously considered 'undruggable'.[187]

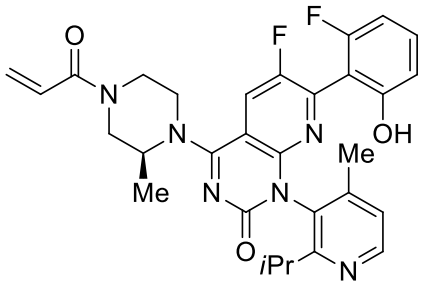

Lumakras™

Figure 5.1 – Chemical Structure of Lumakras™

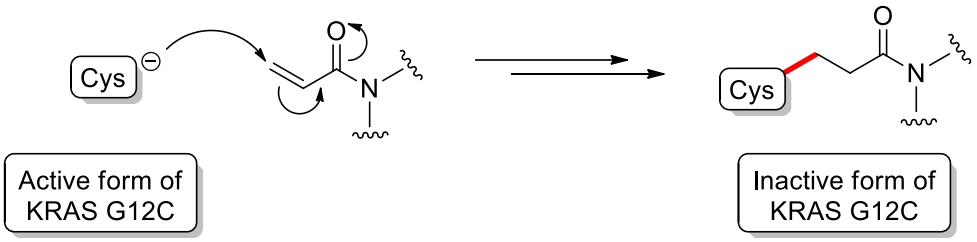

Scheme 5.10

Inhibition of the Vitamin K epoxide reductase (VKOR) enzyme is an important strategy for the prevention of thromboembolic disease (blood clots). Currently, one of the most prevalent inhibitors on the market against VKOR is Coumadin® (Warfarin).[183,188] Although the exact mechanism of inhibition of VKOR remains elusive, Silverman proposed a mechanism which is summarised in Scheme 5.11.[189] Tautomerisation of Coumadin® to intermediate keto-ester **239** allows the nucleophilic addition of a VKOR-cysteine residue to ring-open the coumarin heterocycle. The result of this reaction is an irreversible covalent bond formed to successfully inhibit the VKOR enzyme.

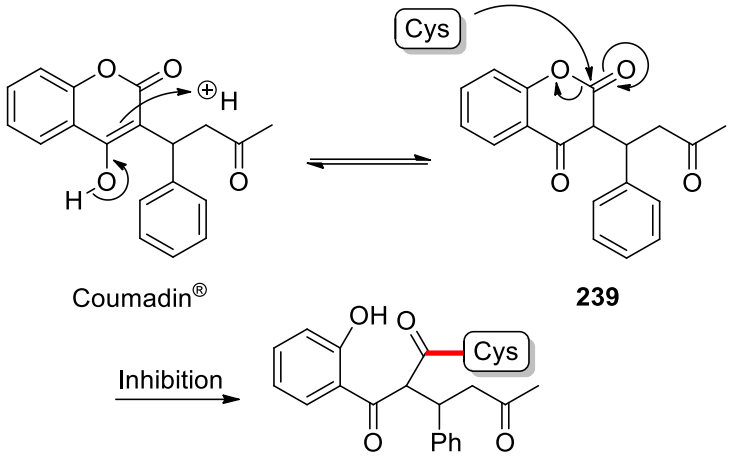

Scheme 5.11

In 2008, the EMA granted approval for the oral anti-hyperglycemic drug Galvus® developed by Novartis. Galvus® has a covalent warhead in the form of a nitrile group. This allows selective inhibition of dipeptidyl peptidase-4 (DPP-4) which prevents glucagon-like peptide-1 (GLP-1) degradation, reducing glycaemia in patients with type two diabetes mellitus.[190] The mechanism of action consists of a Pinner reaction with the Ser^{630} residue of DPP-4. Addition of the hydroxy moiety on Ser^{630} to the protonated nitrile *via* 1,2-addition, results in the formation of a covalent bond (Scheme 5.12).[191]

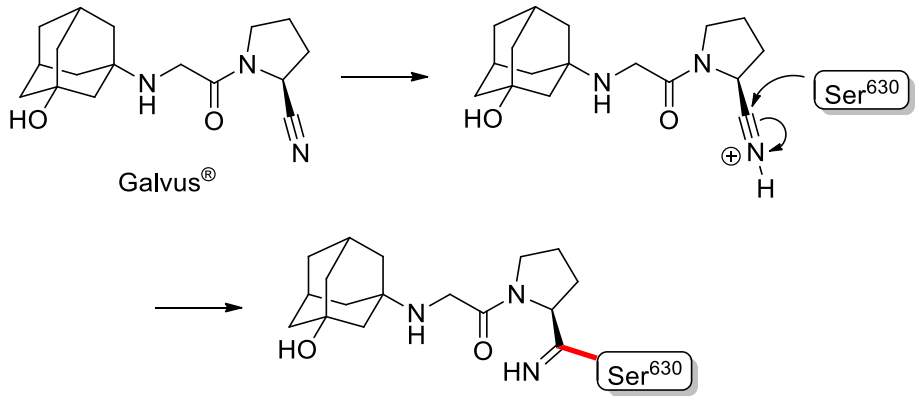

Scheme 5.12

Overall, the development of covalent drugs has resolved complex obstacles in drug design. Previously classed ‘undruggable’ protein targets were successfully targeted such as the case of Lumakras™. The development and approval of the selected covalent drugs outlined in this section showcases the potential and successes in this field.[178]

Synthesis, Cross-Coupling and Elimination of Masked Acrylamides

5.1.1 The Masked Acrylamide Strategy

There is the opportunity to adopt a vast number of covalent warheads into our 3-D set of building blocks. However, for this preliminary study, we decided to target the acrylamide warhead as the basis for covalent fragment library synthesis. Unlike the previous strategy for *N*-functionalisation in which Suzuki-Miyaura cross-coupling occurs before *N*-functionalisation, the proposed masked acrylamides would be synthesised as a precursor. Then under palladium-catalysed Suzuki-Miyaura cross-coupling conditions, unmasking of the acrylamide warhead can be performed in tandem with cross-coupling (Scheme 5.13).

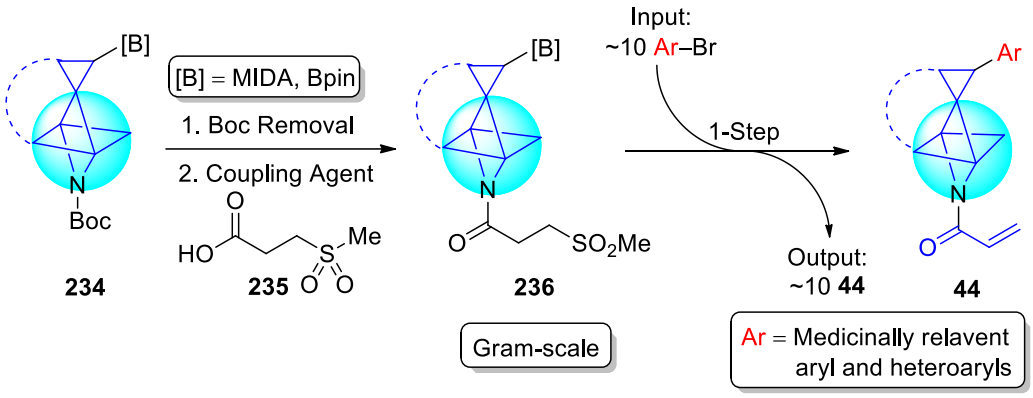

Scheme 5.13

In 2022, Janssen Pharmaceuticals filed a patent for tricyclic pyrimidines as cyclin-dependent kinase 7 (CDK7) inhibitors. As one of their examples, *β*-sulfonyl amide (*S*)-**240** was transformed into acrylamide (*S*)-**241** under basic conditions.[192] The reaction of *β*-sulfonyl amide (*S*)-**240** with a 2.0 M solution of sodium *tert*-butoxide in THF initially at 0 °C for 20 min, then rt for 1 h, gave acrylamide (*S*)-**241** in 50% yield (Scheme 5.14).[192] Although tandem synthesis was not demonstrated in this example, the study still managed to demonstrate the use of a masked acrylamide strategy for synthesis of acrylamides using relatively mild basic conditions. The elimination of methylsulfinate proceeds *via* an $E1_CB$ mechanism as per Scheme 5.15.

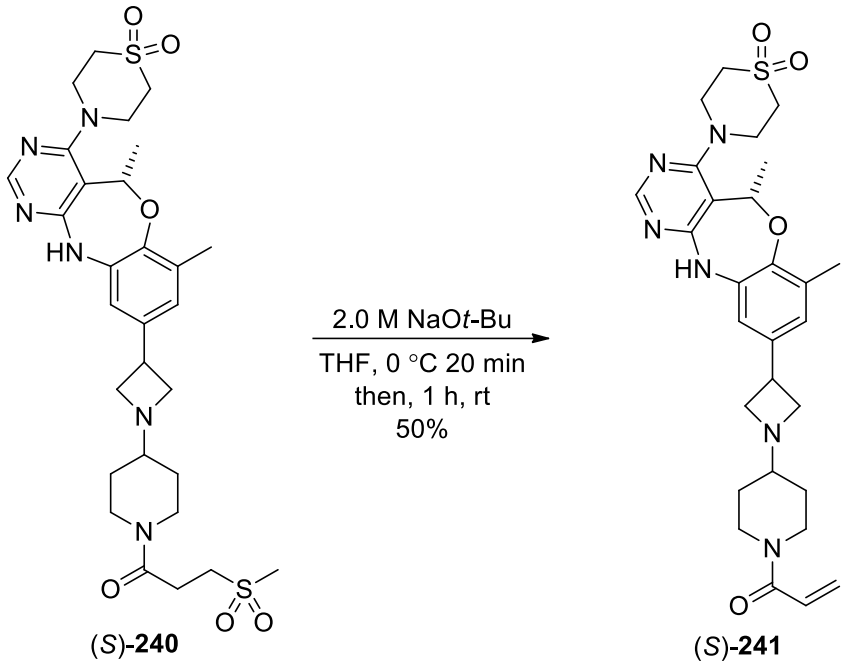

Scheme 5.14

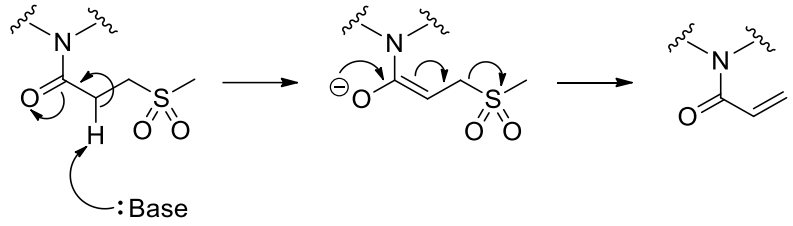

Scheme 5.15

The tandem Suzuki-Miyaura–elimination reaction has been demonstrated in the patent literature for the synthesis of a range of heteroaryl compounds that inhibit G12C mutant RAS proteins. Researchers at AstraZeneca reported the transformation of (*S*)-**242** into (*S*)-**243**, by cross-coupling with aryl boronic acids using substoichiometric amounts of $PdCl_2$(dtbpf) and Cs_2CO_3 (3.0 eq.) in 10:1 dioxane–H_2O at 100 °C for 16 h.[193] Overall, a total of 48 compounds were synthesised this way, using a diverse range of aryl boronic acids. Presumably, under the cross-coupling conditions, the *β*-sulfonyl amide functionality can undergo elimination *via* an $E1_CB$ mechanism to expel methylsulfinate and generate the acrylamide (Scheme 5.16). Unfortunately, all products were characterised by mass spectrometry and no isolated or calculated yields were reported.[193]

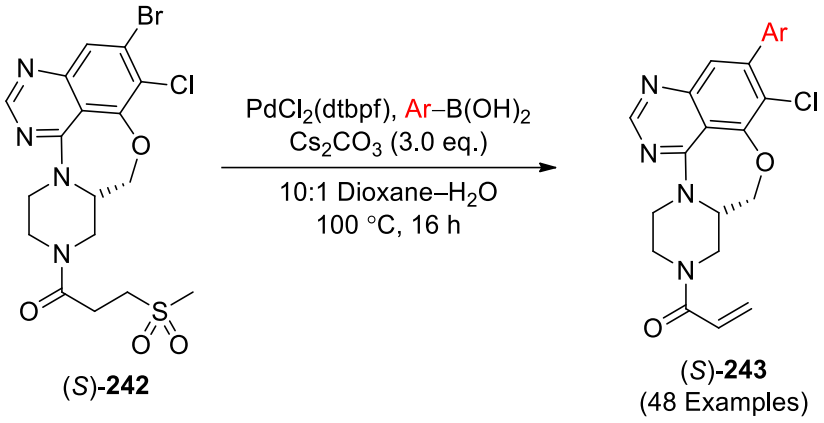

Scheme 5.16

The application of a masked acrylamide strategy to the cyclopropyl 3-D building blocks is attractive due to the potential stability of the amido sulfone. By utilising this group, control over each step could be achieved. Ideally, Suzuki-Miyaura cross-coupling could be initially carried out at low temperatures. Then, the temperature could be raised to carry out the elimination step. However, this would need to be explored. In addition, it may be necessary to investigate the effect of the boron protecting group in the synthesis of *β*-sulfonyl amides as well as mild cross-coupling conditions to make a tandem Suzuki-Miyaura–elimination reaction possible.

5.1.2 Model Studies on a Piperidine System

To begin exploring the masked acrylamide strategy, initial studies on a cheap and commercially available model system were carried out. To this end, 4-phenylpiperidine **244** was chosen as a representative amine to investigate the initial reactions for synthesis of acrylamide **246**. Firstly, it was proposed to attach 4-phenylpiperidine **244** to *β*-sulfonyl acid **235** using a coupling agent. Then, by treating *β*-sulfonyl amide **245** under basic conditions (probably at high temperature), elimination of methylsulfinate should give acrylamide **246** (Scheme 5.17).

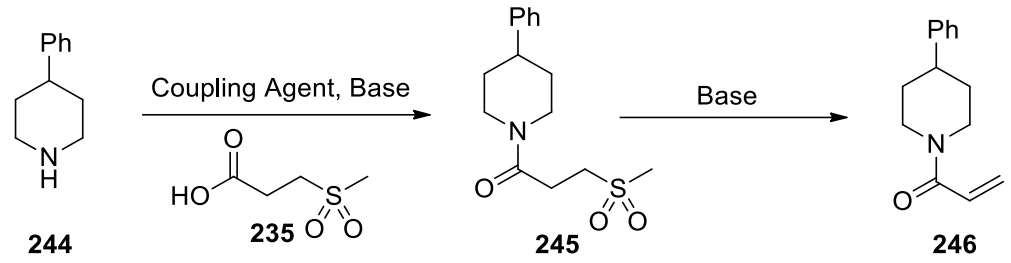

Scheme 5.17

To begin, it was necessary to access *β*-sulfonyl acid **235**. Thus, the synthesis previously reported by Kishton *et al*. was followed in order to obtain *β*-sulfonyl acid **235** on a multi-gram scale.[194] Oxidation of *β*-sulfido acid **247** was performed by reaction with acetic anhydride, acetic acid and H_2O_2 at 0 °C before further reaction at rt for 16 h. Excess H_2O_2 was quenched with substoichiometric amounts of MnO_2. Purification of crude *β*-sulfonyl acid **235** was performed by hot filtration using EtOAc to give *β*-sulfonyl acid **235** in 99% yield (9.46 g prepared) (Scheme 5.18).

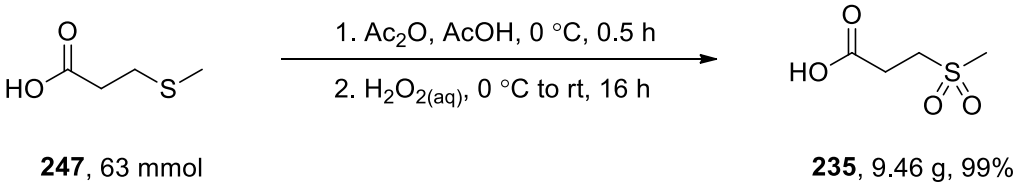

Scheme 5.18

Next, amide formation using *β*-sulfonyl acid **235** was explored. With a plentiful choice of amide bond forming reactions and conditions in the literature,[195] T3P was chosen due to its lack of toxicity, facile removal of by-products in aqueous washing and its compatibility with large-scale industrial synthesis.[196] Therefore, using the conditions adapted from Dunetz *et al*.,[196] 4-phenylpiperidine **244** was reacted with *β*-sulfonyl acid **235**, pyridine and T3P in EtOAc at rt for 16 h. Work-up and chromatography gave *β*-sulfonyl amide **245** in 62% yield (Scheme 5.19).

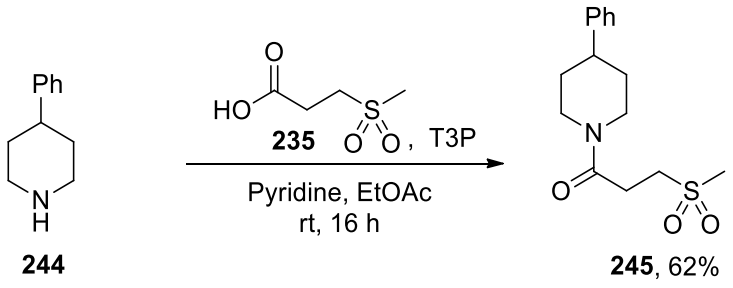

Scheme 5.19

The synthesis of acrylamide **246** from *β*-sulfonyl amide **245** was proposed to be carried out by screening basic conditions. With the ultimate goal of performing the elimination of the methylsulfinate in tandem with the Suzuki-Miyaura cross-coupling reaction, *β*-sulfonyl amide **245** was reacted with Cs_2CO_3 suspended in a sealed tube containing 10:1 toluene–H_2O at 100 °C for 16 h, as these conditions were used in the Suzuki-Miyaura cross-coupling reactions of the BMIDA building blocks, as discussed in Section 3.2. Work-up and purification by chromatography gave acrylamide **246** in only 16% yield, with all of unreacted *β*-sulfonyl amide **245** recovered (84%) (Table 5.1, entry 1). In order to improve the conversion and ultimately yield of acrylamide **246**, other conditions were explored. *β*-Sulfonyl amide **245** was treated with a 2.0 M aqueous solution of NaOH in a sealed tube containing DMF at 100 °C for 16 h. Work-up and purification by chromatography gave acrylamide **246** in 16% yield (Table 5.1, entry 2). Given the low yield of both reactions, it was speculated that poor solubility of the inorganic bases in the organic phase might be responsible. As a result, the use of a phase transfer catalyst was adopted in order to facilitate migration of carbonate from the water into toluene. Therefore, *β*-sulfonyl amide **245** was reacted with Cs_2CO_3 and substoichiometric amounts of $BnEt_3N^+Cl^-$ in a sealed tube containing 10:1 toluene–H_2O at 100 °C for 16 h. Pleasingly, work-up and purification by chromatography gave acrylamide **246** in 96% yield (Table 5.1, entry 3).

Table 5.1 – Conditions for elimination of methylsulfinate

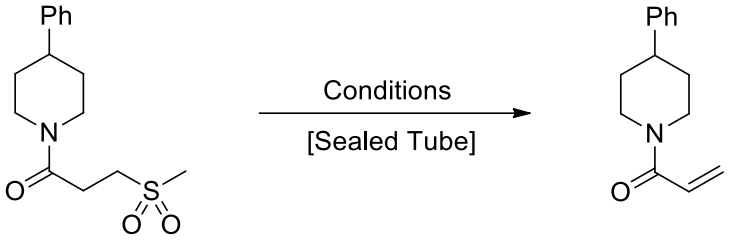

245 **246**

Entry	Conditions	Yield of **245** (%)[a]	Yield of **246** (%)[a]
1	Cs_2CO_3, Toluene, H_2O, 100 °C, 16 h	84	16%
2	2.0 M $NaOH_{(aq)}$, DMF, 100 °C, 16 h	-	16%
3	Cs_2CO_3, $BnEt_3N^+Cl^-$, Toluene, H_2O, 100 °C, 16 h	-	96%

[a] *% yield after chromatography*

In summary, acrylamide **246** was successfully synthesised from *β*-sulfonyl amide **245**. Amide bond formation using T3P and pyridine was used to attach *β*-sulfonyl acid **235** to 4-phenyl piperidine **244**. Although elimination of methylsulfinate was partly successful (16%) using aqueous NaOH or Cs_2CO_3, it was found that addition of a phase transfer catalyst allowed for the reaction to proceed to give acrylamide **246** in an excellent 96% yield.

5.1.3 Synthesis of *β*-Sulfonyl Amides

With the success of preparing acrylamide **246** starting from 4-phenyl piperidine **244**, demonstration of synthesis, cross-coupling and elimination of a masked acrylamide starting from cyclopropyl BMIDA *trans*-**38** was planned. Cyclopropyl BMIDA *trans*-**38** would have the Boc group removed and the so-generated amine would be coupled to *β*-sulfonyl acid **235** using a coupling agent to give *β*-sulfonyl amide *trans*-**247**. Then, under Suzuki-Miyaura cross-coupling conditions, arylation of BMIDA and elimination of methylsulfinate could be achieved in tandem to give 3-D acrylamide fragments *trans*-**248** (Scheme 5.20).

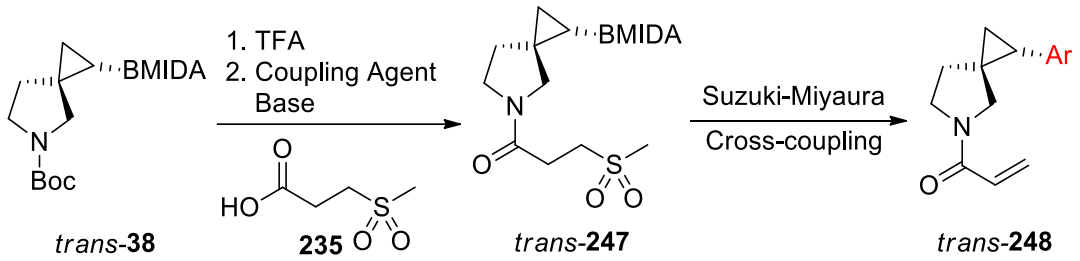

Scheme 5.20

For the first step of the synthesis, conditions were needed for removal of the Boc protecting group from cyclopropyl BMIDA *trans*-**38**. Previously in the group, for the synthesis of methanesulfonamides, the Boc group was removed using HCl in dioxane (see Scheme 3.18). Therefore, cyclopropyl BMIDA *trans*-**38** was treated with 4.0 M HCl in dioxane at rt for 30 min. After solvent evaporation, the crude amine•HCl salt *trans*-**249** was characterised by ^{1}H NMR spectroscopy. This showed that impure product had been generated (Table 5.2, entry 1). This is consistent with a mechanistic study reported by Lloyd-Jones *et al*. where the BMIDA group was shown to be susceptible to cleavage by HCl.[125] Based on this result, we set out to find milder conditions for removal of the Boc group whilst maintaining the sensitive BMIDA moiety. Awuah and co-workers recently reported the deprotection of *N*-Boc using oxalyl chloride and methanol.[197] Thus, using their procedure, cyclopropyl BMIDA *trans*-**38** was reacted with oxalyl chloride in methanol at rt for 1 h. After solvent evaporation, the ^{1}H NMR spectrum of the crude amine•HCl salt *trans*-**249** showed an impure product (Table 5.2, entry 2). The mechanism proposed by Awuah *et al*. generates chloride ions *in situ*[197] which could have a similar issue to using HCl in dioxane. Next, TFA in CH_2Cl_2 was attempted for the Boc group removal. Cyclopropyl BMIDA *trans*-**38** was treated with TFA in CH_2Cl_2 at rt for 30 min. After solvent evaporation, ^{1}H NMR spectroscopy of amine•TFA salt *trans*-**249** showed clean removal of the Boc group (Table 5.2, entry 3). However, in an attempt to isolate the free amine, work-up with 1.0 M $NaOH_{(aq)}$ and ^{1}H NMR spectroscopy indicated that impure amine had been produced, possibly by base-mediated MIDA ester hydrolysis. As a result, the plan was to remove the Boc group using TFA to give amine•TFA salt *trans*-**249** and then take this on to amide forming conditions.

Table 5.2 – Conditions for removal of the Boc group

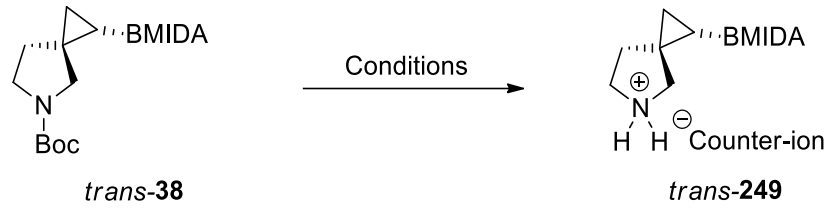

trans-**38** *trans*-**249**

Entry	Conditions	Observations[a]
1	4.0 M HCl (in dioxane), rt, 30 min	Impure
2	Oxalyl chloride, MeOH, rt, 1 h	Impure
3	TFA, CH_2Cl_2, rt, 30 min	Pure

[a] *By analysis of ^{1}H NMR spectrum of the crude amine salt*

To attach *β*-sulfonyl acid **235** to amine•TFA salt *trans*-**249**, the conditions used previously for 4-phenyl piperidine **244** (see Scheme 5.19) were attempted. Thus, cyclopropyl BMIDA *trans*-**38** was treated with TFA in CH_2Cl_2 at rt for 30 min to give amine•TFA salt *trans*-**249** after solvent evaporation. Then, amine•TFA salt *trans*-**249** was subjected to pyridine, *β*-sulfonyl acid **235** and T3P in EtOAc at rt for 16 h. Work-up and purification by chromatography failed to give *β*-sulfonyl amide *trans*-**247** (Scheme 5.21). Although excess pyridine was used, it is possible that not enough of the free amine was generated for the coupling to occur. Therefore , use of 1.0 eq. DIPEA together with pyridine was investigated. Removal of Boc group was performed before amine•TFA salt *trans*-**249** was subjected to pyridine, DIPEA, *β*-sulfonyl acid **235** and T3P in EtOAc at rt for 16 h. In this case, work-up and chromatography gave *β*-sulfonyl amide *trans*-**247** in 10% yield (Scheme 5.21).

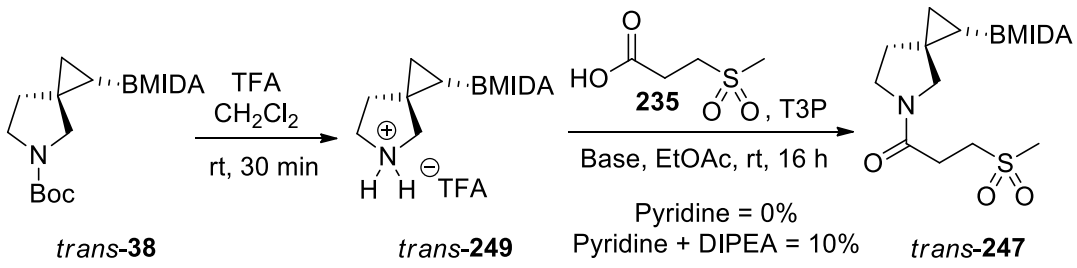

trans-**38** *trans*-**249** *trans*-**247**

Scheme 5.21

As the reactions with DIPEA gave only a 10% yield of *β*-sulfonyl amide *trans*-**247**, it was decided to omit pyridine altogether and different conditions using Et_3N were attempted. For these experiments, crude amine•TFA salt *trans*-**249** was formed in the usual way in each case. Then, amine•TFA salt *trans*-**249** was initially treated with Et_3N (4.0 eq.), *β*-sulfonyl acid **235** (1.1 eq.) and T3P (2.0 eq.) in EtOAc at rt for 16 h. This gave *β*-sulfonyl amide *trans*-**247** in 19% yield (Table 5.3, entry 1). Increased equivalents of reagents were then explored. Reaction of amine•TFA salt *trans*-**247** with Et_3N (5.0 eq.), *β*-sulfonyl acid **235** (1.5 eq.) and T3P (3.0 eq.) in EtOAc at rt for 16 h gave *β*-sulfonyl amide *trans*-**247** in 35% yield (Table 5.3, entry 2). A similar yield (31%) of *β*-sulfonyl amide *trans*-**247** was obtained using Et_3N (6.0 eq.), *β*-sulfonyl acid **235** (2.0 eq.) and T3P (4.0 eq.) (Table 5.3, entry 3).

Table 5.3 – Reaction optimisation for T3P coupling using Et_3N

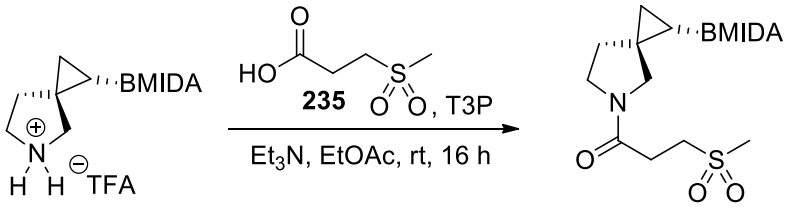

trans-**249** *trans*-**247**

Entry	Acid 235 (eq.)	T3P (eq.)	Et_3N (eq.)	Yield (%)[a]
1	1.1	2.0	4.0	19
2	1.5	3.0	5.0	35
3	2.0	4.0	6.0	31

[a] *% yield after chromatography over two steps of Boc removal and amide formation*

The attachment of the masked acrylamide to the diastereomeric cyclopropyl BMIDA *cis*-**38** was also attempted. Taking the best conditions previously established (Table 5.3, entry 2), amine•TFA salt *cis*-**249** (generated from *cis*-**38** using TFA) was reacted with Et_3N

(5.0 eq.), *β*-sulfonyl acid **235** (1.5 eq.) and T3P (3.0 eq.) to give *β*-sulfonyl amide *cis*-**247** in 24% yield over the 2 steps (Scheme 5.22).

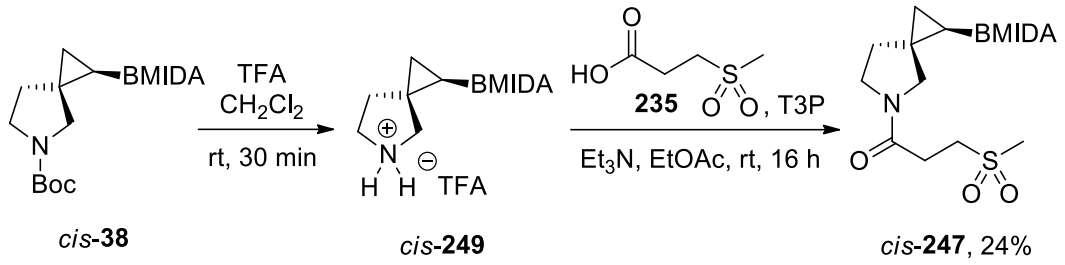

Scheme 5.22

The most successful result obtained with T3P coupling gave a 35% yield of amide *trans*-**247** (see Table 5.3, entry 2). Given the moderate yielding nature of T3P reactions observed thus far, other coupling reagents were attempted. Use of CDI yielded only trace amounts of *β*-sulfonyl amide *trans*-**247** (Table 5.4, entry 1). In 2018, researchers at AstraZeneca reported the use HATU for the attachment of *β*-sulfonyl acid **235** to a substituted piperazine intermediate.[193] Thus, we attempted these conditions by reacting amine•TFA salt *trans*-**249** with Et_3N, *β*-sulfonyl acid **235** and HATU in DMF at rt for 16 h but only trace amounts of *β*-sulfonyl amide *trans*-**247** were formed (Table 5.4, entry 2). Researchers from Janssen Pharmaceuticals had reported the attachment of *β*-sulfonyl acid **235** to 3-substituted pyrrolidine intermediates using EDCI.[198] However, use of two different sets of EDCI conditions yielded only trace amounts of *β*-sulfonyl amide *trans*-**247** (Table 5.4, entries 3 and 4).[198]

Table 5.4 – Screening of amine–carboxylic acid coupling agents

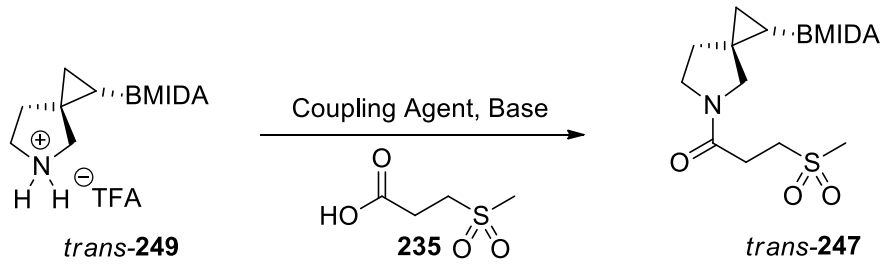

trans-**249** *trans*-**247**

Entry	Conditions	Yield (%)[a]
1	CDI, DIPEA, CH_2Cl_2, rt, 18 h	0[b]
2	HATU, Et_3N, DMF, rt, 16 h	0[b]
3	EDCI, DMAP, CH_2Cl_2, 0 °C to rt, 16 h	0[b]
4	EDCI, DMAP, Et_3N, CH_2Cl_2, rt, 16 h	0[b]

[a] *After purification by chromatography,* [b] *Trace amide trans*-**247** *detected by ESI-MS*

With yields moderate at best for coupling with *β*-sulfonyl acid **235**, a new strategy was attempted by synthesising *β*-sulfonyl amide *trans*-**247** from an acid chloride. To this end, as a quick test reaction, the plan was to remove the Boc group from cyclopropyl BMIDA *trans*-**38** and react the TFA salt with benzoyl chloride. Thus, cyclopropyl BMIDA *trans*-**38** was deprotected using TFA and reacted with Et_3N and benzoyl chloride to give benzamide *trans*-**250** in 45% yield (Scheme 5.23).

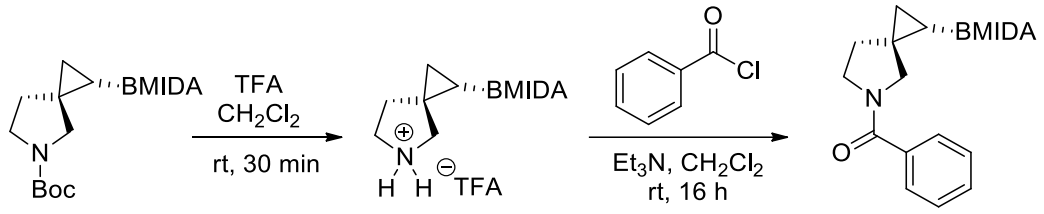

trans-**38** *trans*-**249** *trans*-**250**, 45%

Scheme 5.23

Despite the moderate yield of benzamide *trans*-**250** using benzoyl chloride, we still explored the synthesis and reaction of *β*-sulfonyl acid chloride **251**. Using a literature procedure,[199] reaction of *β*-sulfonyl sulfone acid **235** with $SOCl_2$ at reflux for 2 h gave *β*-sulfonyl acid chloride **251** (together with what is believed to be a small amount of the

corresponding anhydride). Then, reaction of amine•TFA salt *trans*-**249** with Et_3N and slightly impure *β*-sulfonyl acid chloride **251** gave *β*-sulfonyl amide *trans*-**247** in 32% yield (Scheme 5.24).

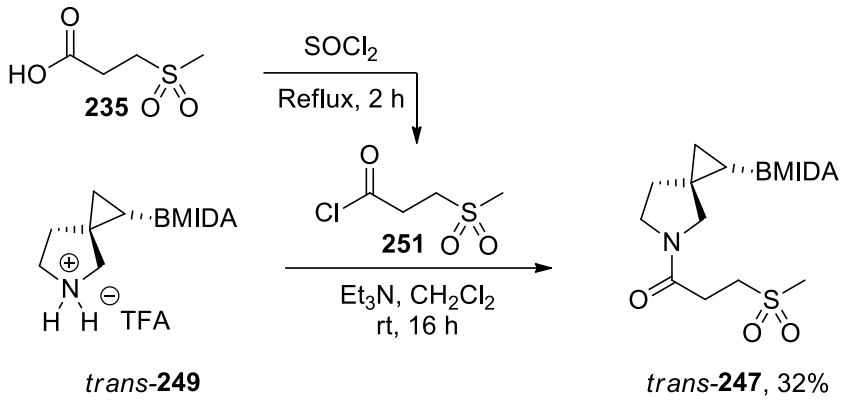

Scheme 5.24

Having explored *N*-functionalisation of Boc-deprotected cyclopropyl BMIDA *trans*-**38** and briefly on *cis*-**38** using *β*-sulfonyl acid **235**, limited success was observed. The highest yield of *β*-sulfonyl amide *trans*-**38** was only 35% (see Table 5.3, entry 2). It appeared that the BMIDA functionality was not fully compatible with the amide forming reaction conditions. In order to explore this idea and to hopefully improve the yield in the amide formation step, the corresponding cyclopropyl Bpin *trans*-**119** was investigated. Therefore, cyclopropyl Bpin *trans*-**119** was first treated with TFA to remove the Boc protecting group. Then, reaction of subsequent amine•TFA salt *trans*-**252** with *β*-sulfonyl acid **235**, T3P and Et_3N in CH_2Cl_2 at rt for 16 h gave *β*-sulfonyl amide *trans*-**253** in 92% yield (Scheme 5.25). This clearly indicated that the BMIDA group was the main problem in the previously studied amide forming reactions.

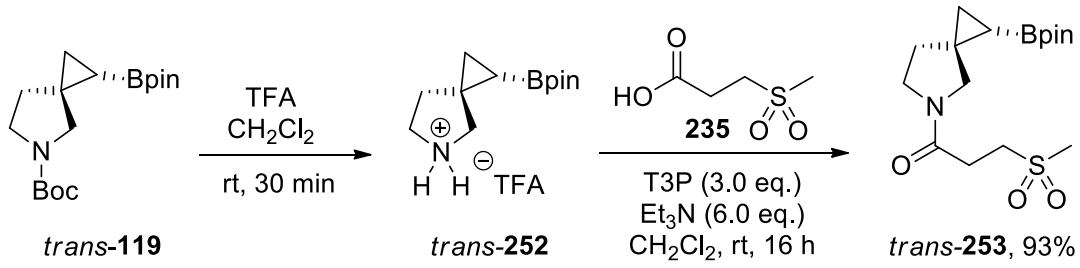

Scheme 5.25

With a high-quality approach to access *β*-sulfonyl amide *trans*-**253** established, attempts to form *β*-sulfonyl amides from other building blocks were explored, for example *β*-sulfonyl amides *exo*-**256** and **257**. Using the same procedure, the corresponding

cyclopropyl Bpins **254** were reacted with TFA before the amine•TFA salts **255** were coupled with *β*-sulfonyl acid **235** to generate *β*-sulfonyl amides *exo*-**256** and **257** in 53% and 92% yields respectively (Scheme 5.26)

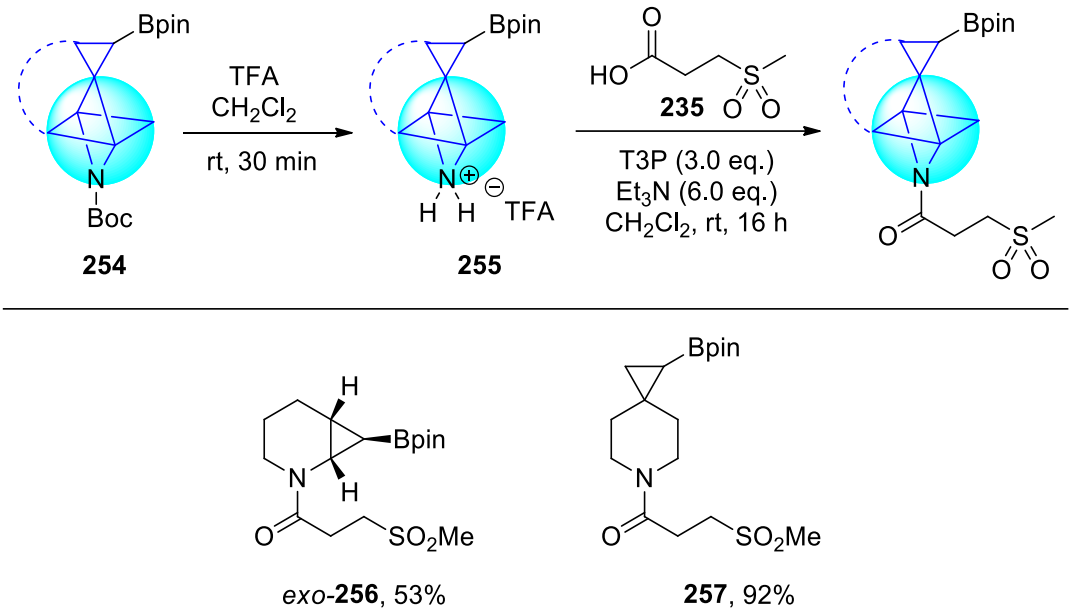

Scheme 5.26

Two other organoboron compounds were considered: a BF_3K salt and a BDEA (where DEA = diethanolamine). As previously discussed in Chapter 3, the use of BF_3K salts in cross-coupling was popularised by Molander *et al.* where they act as precursors to the reactive boronic acid.[200] To this end, conditions adapted from the original work of Molander *et al.* were used in the attempted synthesis of cyclopropyl BF_3K salt **258**.[143] Reaction of cyclopropyl Bpin **257** with KHF_2 in H_2O and MeOH at rt for 3 h provided the crude cyclopropyl BF_3K salt **258**. Unfortunately, attempts to purify cyclopropyl BF_3K salt **258** by recrystallisation and chromatography were unsuccessful (Scheme 5.27). For the attempted synthesis of cyclopropyl BDEA **259**, a procedure was adapted from researchers at AstraZeneca.[201] Cyclopropyl Bpin **257** was mixed with diethanolamine (DEA) in *i*-PrOH and THF at rt. After 16 h, the reaction only showed the presence of cyclopropyl Bpin **257**.

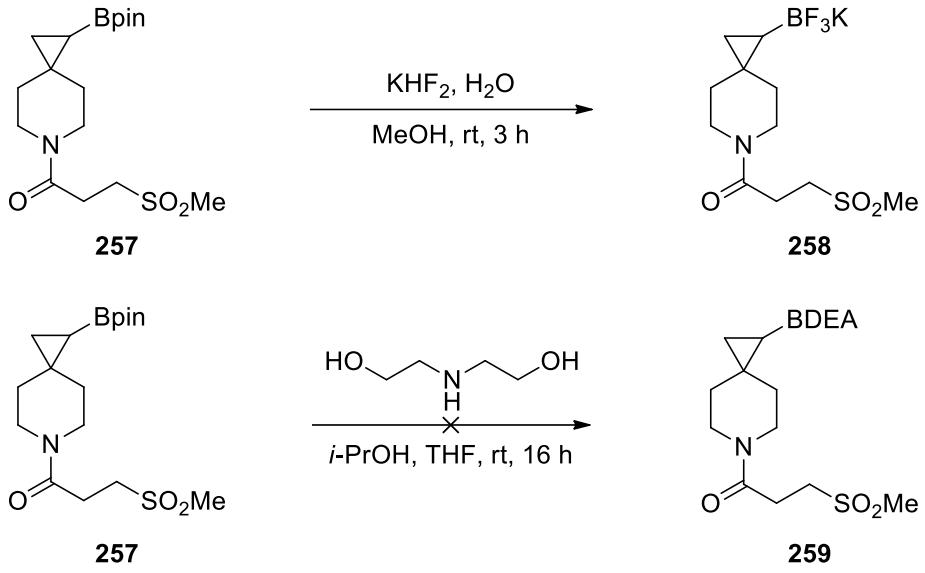

Scheme 5.27

In summary, the attempted *N*-functionalisation of the building blocks with *β*-sulfonyl acid **235** led to limited yields (≤ 35%) with cyclopropyl BMIDA *trans*-**38** and *cis*-**38**. However, when the boronate group was changed to Bpin, our first attempt led to a high yield (92%) of *β*-sulfonyl amide *trans*-**253**. The success of cyclopropyl Bpins to undergo *β*-sulfonyl amide formation was also reflected in the synthesis of *β*-sulfonyl amides *exo*-**256** and **257** in 53% and 92% yields. Unfortunately, attempts to synthesise cyclopropyl BF_3K **258** and cyclopropyl BDEA **259** were unsuccessful.

5.1.4 Investigation into the Tandem Suzuki-Miyaura–Elimination Reaction

Before exploring the tandem Suzuki-Miyaura–elimination reactions, it was decided to prepare an authentic sample of the acrylamide **260** which would be the product of the planned reactions. Obtaining the target compound first could aid in the characterisation of acrylamide **260** in subsequent tandem Suzuki-Miyaura– elimination reactions, where there is greater potential for more by-products to be formed. The removal of the Boc group from cyclopropyl pyrimidine **168** was carried out using HCl, before the amine•HCl salt was reacted with acryloyl chloride, Et_3N, and DMAP in CH_2Cl_2 at rt for 16 h to obtain acrylamide **260** in 33% yield (Scheme 5.28).

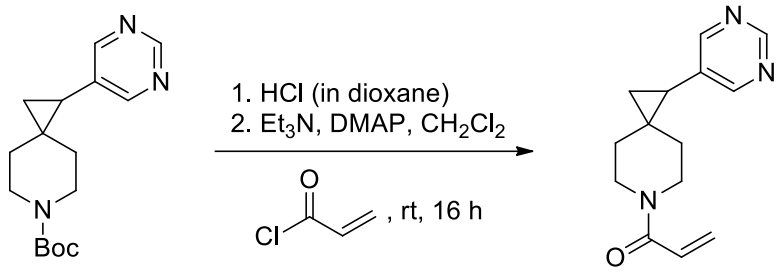

Scheme 5.28

Given the low yield in the synthesis of BMIDA *β*-sulfonyl amides such as *trans*-**247**, it was decided to focus on the Bpin *β*-sulfonyl amides. These were accessible in higher yields allowing the two different aspects of the reaction to be explored, the cross-coupling and the elimination. As a result, an investigation into the cross-coupling of *N*-Boc cyclopropyl Bpin **107** was proposed, as little work on cyclopropyl Bpin cross-coupling reactions had been carried out in the group. Despite this, multiple examples of cyclopropyl Bpin cross-coupling have been reported in the literature (see Chapter 3.1). The reaction conditions explored for the cross-coupling of *N*-Boc cyclopropyl Bpin **107** with 5-bromopyrimidine are summarised in Table 5.5. By subjecting cyclopropyl Bpin **107** to cross-coupling conditions previously used the corresponding BMIDA building block **37** ($Pd(OAc)_2$ (5 mol%), PCy_3 (10 mol%) and Cs_2CO_3 (3.0 eq.) in 10:1 Toluene–H_2O), cyclopropyl pyrimidine **168** was isolated in 31% yield (Table 5.5, entry 1). Conditions reported by Charette and Benoit showed that substituted cyclopropyl Bpins could be cross-coupled to 3-bromopyridine using $Pd(dba)_2$ (5 mol%), PCy_3 (10 mol%) and KOH (6.0 eq.) in 3:1 Toluene–H_2O at 115 °C for 20 h to give the cross-coupled products in up to 99% yield (see Scheme 3.5).[118] Using these conditions, cyclopropyl Bpin **107** was converted into cyclopropyl pyrimidine **168** in 33% yield (Table 5.5, entry 2). At this time, other members of the O'Brien group were exploring sp^3–sp^2 Suzuki-Miyaura cross-coupling of saturated heterocyclic Bpin compounds with aryl halides.[202,203] In particular, reaction conditions used by Matthew Gill, which were based on a procedure reported by Walsh *et al.*[204] were explored. Thus, cyclopropyl Bpin **107** and 5-bromopyrimidine were reacted with $Pd(OAc)_2$ (10 mol%), CataCXium® A (20 mol%) and Cs_2CO_3 (3.0 eq.) in 6:5 toluene and H_2O at 120 °C for 16 h. After chromatography, this gave cyclopropyl pyrimidine **168** in 74% yield (Table 5.5, entry 3). The high yield observed in the cross-coupling of cyclopropyl Bpin **107** with 5-bromopyrimidine (74%,

Table 5.5, entry 3) rivalled that of cyclopropyl BMIDA **37** using standard conditions ($Pd(OAc)_2$, PCy_3) where a yield of 70% was observed.[131]

Table 5.5 – Optimisation of cyclopropyl Bpin cross-coupling

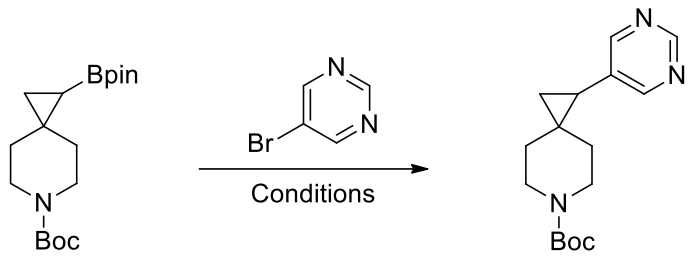

107 **168**

Entry	Conditions	Yield (%)
1	Ar-Br (1.4 eq.), $Pd(OAc)_2$ (5 mol%), PCy_3 (10 mol%) Cs_2CO_3 (3.0 eq.) in 10:1 Toluene–H_2O	31
2	Ar-Br (2.0 eq.), $Pd(dba)_2$ (5 mol%), PCy_3 (10 mol%) KOH (6.0 eq.) in 3:1 Toluene–H_2O	33
3	Ar-Br (1.5 eq.), $Pd(OAc)_2$ (10 mol%), CataCXium® A (20 mol%) Cs_2CO_3 (3.0 eq.) in 6:5 Toluene–H_2O	74

Next, studies on the tandem Suzuki-Miyaura–elimination reaction with Bpin *β*-sulfonyl amide **257** were carried out using the cross-coupling conditions previously established on *N*-Boc cyclopropyl Bpin **107** (see Table 5.5, entry 3). To this end, Bpin *β*-sulfonyl amide **257** was reacted with 5-bromopyrimidine (1.5 eq.) using $Pd(OAc)_2$ (10 mol%), cataCXium® A (20 mol%) and Cs_2CO_3 (3.0 eq.) in 6:5 toluene and H_2O at 100 °C for 16 h. Upon work-up and attempted purification, a 35:65 inseparable mixture of acrylamide **260** and dipyrimidine **261** (from homo-coupling of the aryl bromide) with additional uncharacterised impurities was obtained (Table 5.6, entry 1). From this result, we were delighted to observe product of the tandem Suzuki-Miyaura-elimination reaction, despite the fact that the product could not be isolated in pure form. From our preliminary results, we discovered that the addition of a phase-transfer catalyst increased the generation of acrylamide **246** from 16% to 96% (see Table 5.1). Therefore, the Suzuki-Miyaura cross-coupling and elimination of Bpin *β*-sulfonyl amide **257** was carried out with the addition of benzyltriethylammonium chloride (18 mol%). This time, the product isolated after work-up and attempted purification was discovered to be a 50:50 inseparable mixture of

acrylamide **260** and dipyrimidine **261** with additional uncharacterised impurities (Table 5.6, entry 2). When attempting to change the ligand system from cataCXium® A to PCy_3 (20 mol%) in 10:1 toluene and H_2O at 100 °C, the product isolated after work-up and attempted purification was a 45:55 inseparable mixture of acrylamide **260** and dipyrimidine **261** with additional uncharacterised impurities (Table 5.6, entry 3). When using PCy_3 (20 mol%) in 10:1 dioxane and H_2O at 80 °C, an 85:15 inseparable mixture of acrylamide **260** and dipyrimidine **261** with additional uncharacterised impurities was observed (Table 5.6, entry 4). The results presented in Table 5.6 indicates that the temperature of the reaction could influence formation of byproducts. Presumably, lower temperatures inhibit the elimination of methylsulfinate, which is discussed further below, allowing the cross-coupling to take place first.

Table 5.6 – Tandem Suzuki-Miyaura–elimination reactions (5-bromopyrimidine)

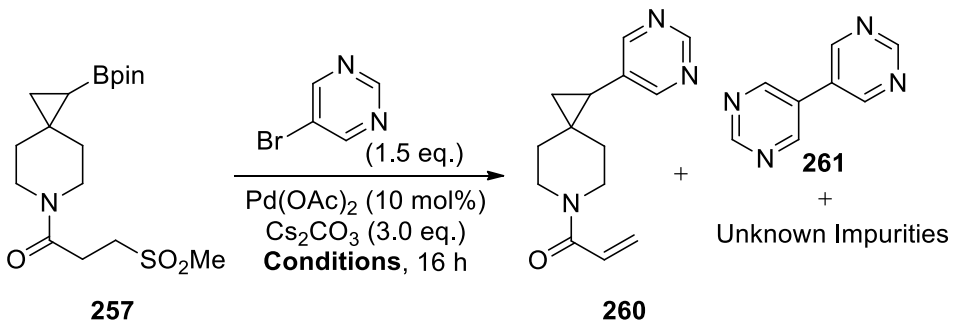

Entry	Conditions	Mixture of 260 and 261[a]
1	cataCXium® A (20 mol%) 6:5 Toluene–H_2O, 120 °C	35:65
2	cataCXium® A (20 mol%), $BnEt_3N^+Cl^-$ (18 mol%) 6:5 Toluene–H_2O, 100 °C	50:50
3	PCy_3 (20 mol%) 10:1 Toluene–H_2O, 100 °C	45:55
4	PCy_3 (20 mol%) 10:1 Dioxane–H_2O, 80 °C	85:15

[a] *Ratio calculated from the ^1H NMR spectrum of the impure product after purification*

Due to the observation of homo-coupling when using 5-bromopyrimidine, investigations were attempted into the tandem Suzuki-Miyaura–elimination reaction with Bpin *β*-sulfonyl amide **257** and 4-bromoanisole. Cross-coupling was carried out using $Pd(OAc)_2$ (10 mol%), cataCXium® A (20 mol%) and Cs_2CO_3 (3.0 eq.) in 6:5 Toluene–H_2O at 120 °C for 16 h. Analysis of the crude product by ^1H NMR spectroscopy indicated that there

was no evidence of the desired product (Table 5.7, entry 1). This result was also observed when the reaction was repeated at a slightly lower temperature of 100 °C (Table 5.7, entry 2). Similarly, when using the cataCXium® A–palladium 3rd generation pre-catalyst (structure shown in Figure 5.2) (10 mol%) in 6:5 Toluene–H_2O at 120 °C for 16 h, the reaction also did not produce acrylamide **262** (Table 5.7, entry 3).

Table 5.7 – Tandem Suzuki-Miyaura–elimination reactions (4-Bromoanisole)

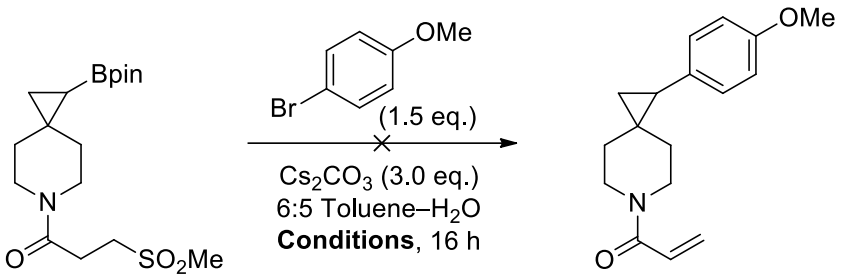

257 **262**

Entry	Catalyst (10 mol%)	Ligand (20 mol%)	Temp (°C)	Observations[a]
1	$Pd(OAc)_2$	cataCXium® A	120	No product
2	$Pd(OAc)_2$	cataCXium® A	100	No product
3	cataCXium® A Pd G3 pre-cat.	-	120	No product

[a] *Characterised by ^1H NMR spectroscopy of the crude product*

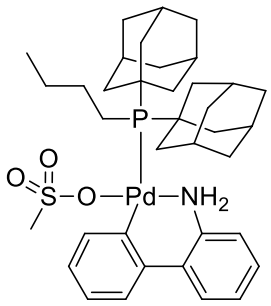

Figure 5.2 – Structure of cataCXium® A Pd G3

Before different strategies were attempted to achieve the tandem Suzuki-Miyaura–elimination reaction, a brief investigation into the use of piperidine Bpin *β*-sulfonyl amide *exo*-**256** was carried out. The fused piperidine system was subjected to 5-bromopiperidine, $Pd(OAc)_2$, cataCXium® A and Cs_2CO_3 in 6:5 toluene and H_2O at 120

°C for 16 h. Analysis of the ^{1}H NMR spectrum of the crude product showed no evidence of acrylamide *exo*-**263**.

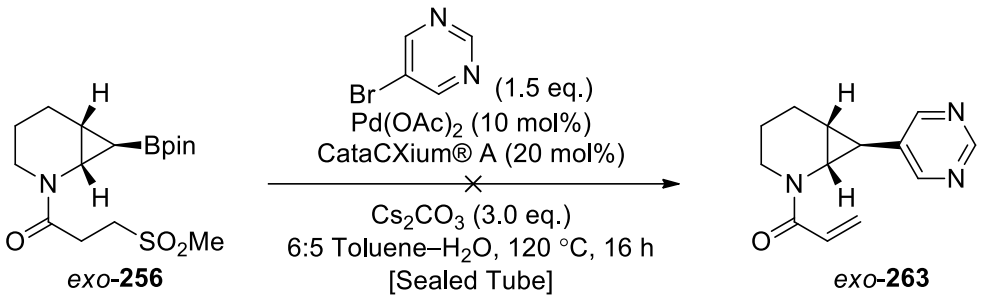

Scheme 5.29

After attempting multiple variations of the tandem Suzuki-Miyaura–elimination reaction without success, a new strategy was proposed based on the presumption that the acrylamide moiety was not compatible with the Suzuki-Miyaura cross-coupling conditions. Although adducts from any potential Heck reactions were not observed, several reports successfully used $Pd(OAc)_2$ systems to catalyse Heck reactions.[205,206] Of note, Beller and Zapf reported on the use of $Pd(OAc)_2$–phosphine systems to achieve cross-coupling between acrylamides and *α*,*β*-unsaturated esters to aryl chlorides.[207] In the next approach to synthesis of acrylamides, we envisaged the cross-coupling of Bpin *β*-sulfonyl amide **257** with preservation of the *β*-sulfonyl amide group (Scheme 5.30). Then in a second reaction (ideally in the same reaction vessel), elimination of the *β*-sulfonyl amide **264** would generate acrylamide **260**.

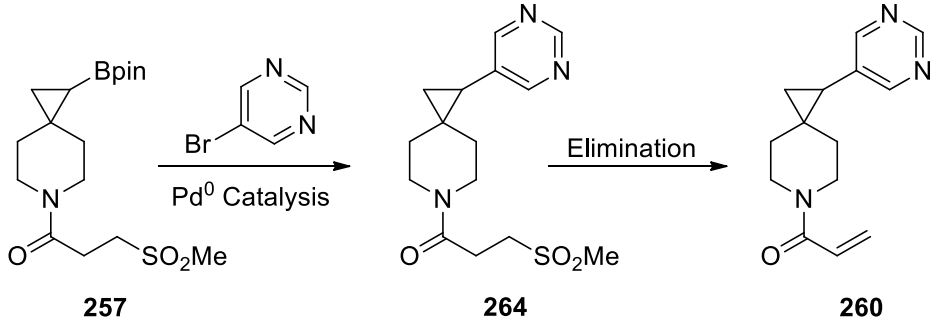

Scheme 5.30

Initial studies began with an investigation of the effects of solvent ratio, concentration, and temperature of the elimination reaction with a summary of the results displayed in Table 5.8. Under the standard cyclopropyl Bpin Suzuki-Miyaura cross-coupling conditions of a 0.23 M 6:5 toluene–H_2O solution at 120 °C for 16 h, the complete

conversion of *β*-sulfonyl amide **245** to acrylamide **246** was observed (Table 5.8, entry 1). By increasing the volume of added toluene to 10:1 toluene–H_2O at a concentration of 0.05 M, a 90:10 mixture of acrylamide **246** and *β*-sulfonyl amide **245** was obtained (Table 5.8, entry 2). Reducing the temperature under the conditions described in Table 5.8, entry 1 and 2, from 120 °C to 100 °C was attempted. When the more concentrated 0.23 M solution of 6:5 toluene–H_2O was adopted, a 15:85 mixture of *β*-sulfonyl amide **245** to acrylamide **246** was observed (Table 5.8, entry 3). For the 0.05 M solution of 10:1 toluene–H_2O, a 35:65 mixture of *β*-sulfonyl amide **245** to acrylamide **246** was observed (Table 5.8, entry 4). From the results at lower reaction temperatures of 100 °C, the formation of the acrylamide was disfavoured. Based on this result, the temptation to further decrease the reaction temperature was ignored by the high temperatures (>100 °C) required for the sp^3–sp^2 Suzuki-Miyaura cross-coupling reactions.[203,204] However, when the biphasic solvent was concentrated to 0.23 M, an impressive 95:5 mixture of *β*-sulfonyl amide **245** to acrylamide **246** was observed (Table 5.8, entry 5).

Table 5.8 – Effects of solvent ratio, concentration, and temperature on elimination

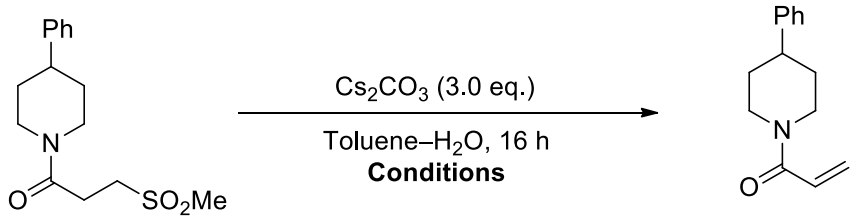

245 **246**

Entry	Toluene:H_2O	Concentration (M)	Temperature (°C)	SM:Prod[a]
1	6:5	0.23	120	0:100
2	10:1	0.05	120	10:90
3	6:5	0.23	100	15:85
4	10:1	0.05	100	35:65
5	10:1	0.23	100	95:5

[a] *Ratio determined by analysis of the ^1H NMR spectrum of the crude product*

Having established conditions that essentially prevented the formation of an acrylamide from a *β*-sulfonyl amide (Table 5.8, entry 5), a test reaction was performed to check the performance of the modified conditions in the Suzuki-Miyaura cross-coupling of

cyclopropyl Bpin **107** with 5-bromopyrimidine. To this end, a reaction of *N*-Boc protected cyclopropyl Bpin **107** with 5-bromopyrimidine, $Pd(OAc)_2$, cataCXium® A and Cs_2CO_3 was carried out in a 0.23 M solution of 10:1 toluene–H_2O at 100 °C for 16 h (Scheme 5.31). Upon work-up and purification, cyclopropyl pyrimidine **168** was obtained in an isolated yield of 83%, clearly indicating the success of the cross-coupling reaction under these modified conditions.

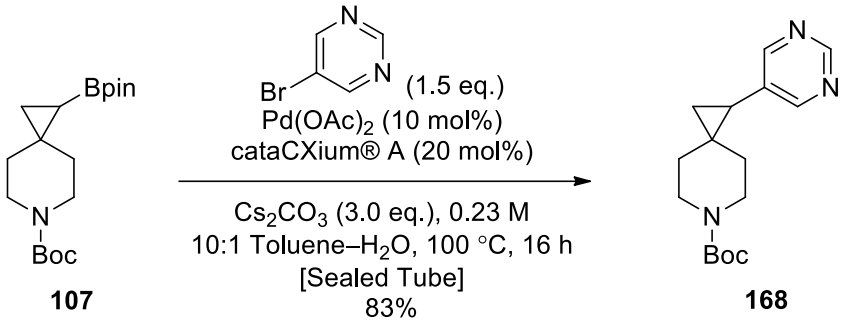

Scheme 5.31

Attempting the new conditions (see Table 5.8, entry 5), *β*-sulfonyl amide **257**, was subjected to cross-coupling conditions in the expectation that only Suzuki-Miyaura cross-coupling would occur initially. However, upon work-up and purification of the crude product, arylated acrylamide **260** was isolated in 15% yield. In addition to this, Bpin acrylamide **265** was also isolated with a yield of 47% (Scheme 5.32). It was perhaps surprising that, despite our model studies, this experiment did not proceed as anticipated. Indeed, the isolation of a significant amount of Bpin acrylamide **265** was a particular surprise. On the other hand, this was the first successful demonstration of the desired Suzuki-Miyaura–elimination reaction (albeit in 15% yield). At this point, there was insufficient time remaining for any further studies but this result does provide a proof-of-principle result that will warrant further reaction optimisation.

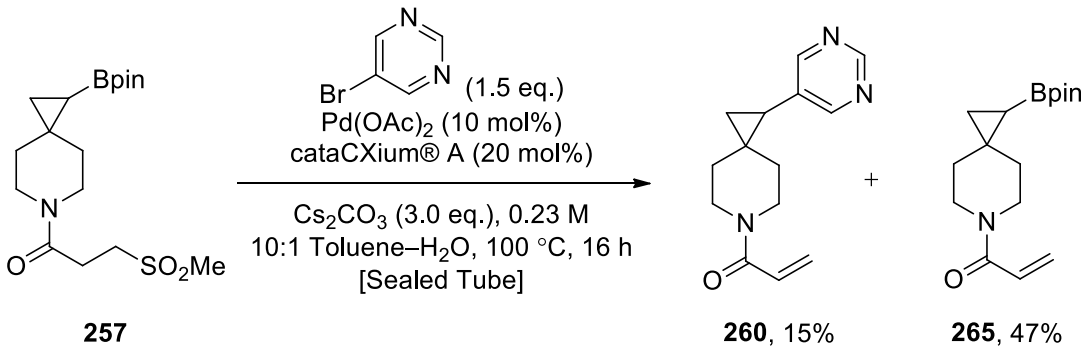

Scheme 5.32

Conclusion and Future Work

In summary, initial studies on the tandem Suzuki-Miyaura–elimination reaction were explored with the ambition to ultimately produce a library of 3-D covalent fragments from cyclopropyl 3-D building blocks. Investigations into a masked acrylamide strategy was successfully demonstrated on a model system proving that acrylamides could be synthesised under the basic conditions used in the Suzuki-Miyaura cross-coupling reactions. When Bpin β-sulfonyl amides were subjected to cross-coupling conditions without any specific modifications, no product or starting material was observed after work-up. Presumably, the electrophilic acrylamide group negatively affects the cross-coupling reaction as the elimination of methylsulfinate occurs. Methods controlling temperature, solvent ratio and concentration were investigated to inhibit the elimination reaction and allow for the cross-coupling to be carried out first *in situ*. By doing so, the tandem Suzuki-Miyaura–elimination was achieved in a low yield of 15%; surprisingly, Bpin acrylamide **265** was isolated as the main product (47%).

Although we have successfully demonstrated the possibility for tandem Suzuki-Miyaura–elimination reactions, further optimisation of this reaction needs to be carried out, where a delicate balance between driving the cross-coupling reaction to completion, and control of the elimination reaction, needs to be struck. During the model studies on the elimination reaction in Table 5.8, a trend was observed where the volume of H_2O and temperature correlated with the inhibition of the elimination reaction. Although, this observation did not directly apply when Bpin β-sulfonyl amide **257** was used, a promising 15% yield reinforces the notion that the cross-coupling should be carried out first prior to elimination. To this end, we propose a reaction optimisation screen at various temperatures and using different solvents to hopefully achieve a tandem reaction in one-pot (Scheme 5.33).

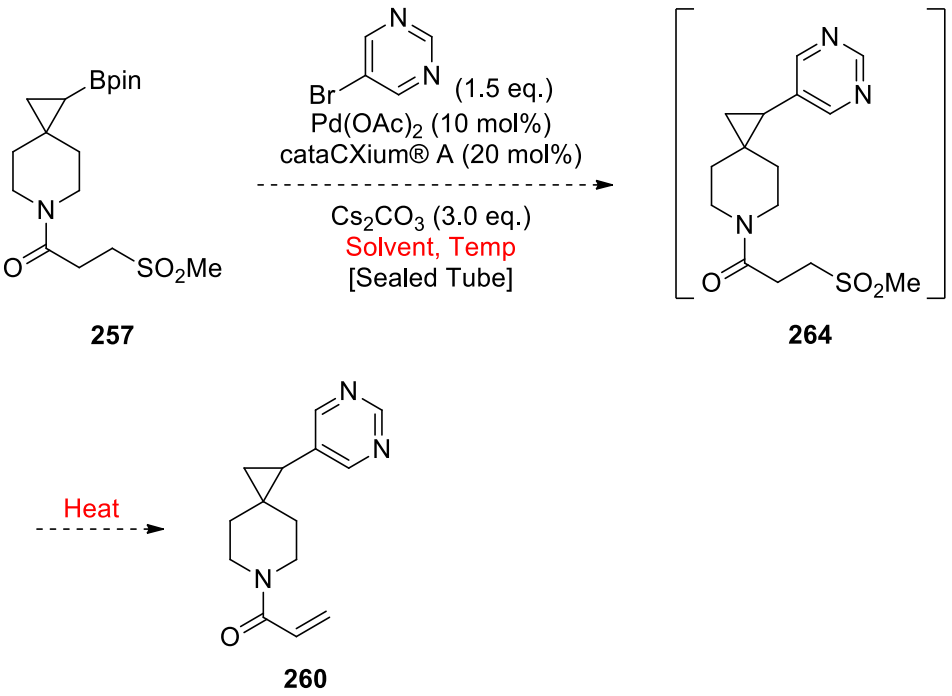
Bpin
N
O
SO2Me
257
N
Br
N
(1.5 eq.)
Pd(OAc)2 (10 mol%)
cataCXium® A (20 mol%)
Cs2CO3 (3.0 eq.)
Solvent, Temp
[Sealed Tube]
N
N
N
O
SO2Me
264
Heat
N
N
N
O
260

Scheme 5.33

Chapter 6: Synthesis of Covalent JAK3 Inhibitor Analogues: Application of York 3-D Building Blocks in Fragment Elaboration

Janus Kinase (JAK) describes a subset of intracellular protein tyrosine kinases (PTKs). Within this family, there are four enzymes: JAK1, JAK2, JAK3, and tyrosine kinase 2 (TYK2).[208] Data from several studies have identified that inhibition of the JAK protein has therapeutic effects in the treatment of cancer, inflammatory and autoimmune diseases.[209,210] As a case study in an application of the nine 3-D cyclopropyl BMIDA building blocks in fragment elaboration, it was decided to target some potential analogues of Pfizer's Litfulo™ (Ritlecitinib), a known JAK3 inhibitor (Figure 6.1).[211] This study was carried out in collaboration with Simon Lucas and Lucia Fusani, medicinal chemists at AstraZeneca.

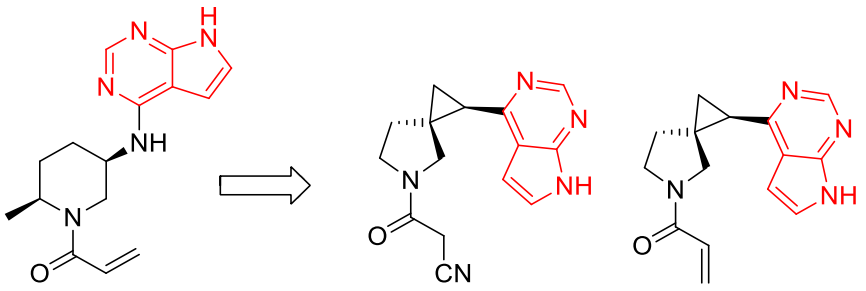

Figure 6.1 – Scaffold hopping analogues generated from Litfulo™

To begin, Chapter 6.1 will introduce the importance of JAK3 as a target for drug design with several covalent drug discovery programmes targeting JAK3 to promote various therapeutic effects. Molecular docking studies conducted by researchers at AstraZeneca proposed two covalent targets derived from our library of cyclopropyl 3-D building blocks. The synthesis and biological evaluation of these targets are presented in Chapter 6.2.

JAK3 as a Target for Drug Design

Of the numerous diseases in which inhibition of the JAK proteins can have therapeutic effects, a considerable amount has explored the specific inhibition of the JAK3 enzyme for the treatment of rheumatoid arthritis.[212,213] As rheumatoid arthritis is a form of autoimmune disease, selective inhibition of JAK3 is beneficial because its functions are restricted to the JAK-STAT signalling pathways (immune regulation) in lymphocytes, a type of white blood cell in the human immune system.[212] Therefore, numerous studies have concluded that the inhibition of JAK3 is an attractive drug design option for the treatment of rheumatoid arthritis.[213,214] However, one problem with this approach is the difficulty in designing a selective inhibitor of JAK3 among the rest of the JAK family due to the structural similarities. However, a unique structural feature of JAK3 is the presence of a cysteine residue (Cys^{909}).[213] Using this fact, in 2011, it was suggested that JAK3 selectivity has been addressed with the "resurgence of covalent drugs", the title of the work of Singh *et al*. This detailed study describes the use of molecules that have the possibility of forming covalent bonds with target protein receptors such as Cys^{909} in the case of JAK3.[157] The mechanism of action begins initially with non-covalent interactions to bind the drug to the target receptor. Then, the formation of a physical covalent bond occurs to cement the drug into the protein pocket.[157] The result of this process has been shown to allow the synthesis of JAK3–selective inhibitors on top of increasing the potency and efficacy of any potential pharmaceutical agent.[213,215]

In 2000, researchers at AstraZeneca were the first to report on the synthesis of a JAK3-selective inhibitor.[216] In an era which pre-dated the idea that irreversible kinase inhibition was a valid strategy for drug design, Brown and co-workers showed that Mannich base **268** could undergo a *retro*-Michael reaction under biological assay conditions to give amine **270** and α, β-unsaturated ketone **269**, leading to therapeutic effects being observed (Scheme 6.1).[216] Unknown to the researchers at the time, α,β-unsaturated ketone **269** probably demonstrated selectivity to JAK3 (IC_{50} = 79 nM) due to the irreversible covalent interactions with Cys^{909} unique to JAK3.[213]

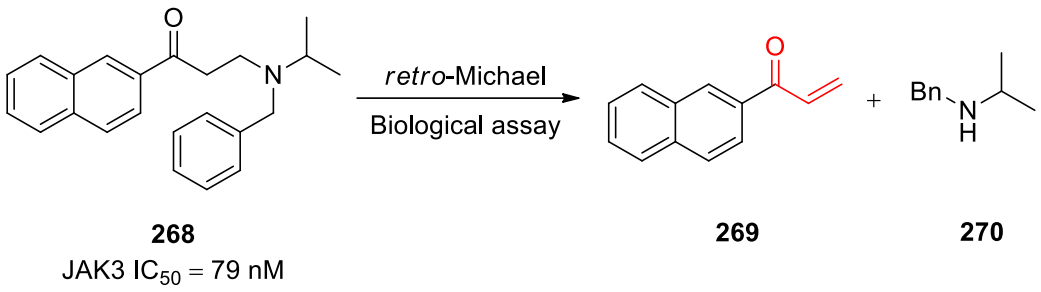

Scheme 6.1

However, researchers at Pfizer were the first to develop a JAK3–selective inhibitor, Xeljantz® (Figure 6.2), that was licensed as a drug by the FDA for the treatment of rheumatoid arthritis.[217] The novel JAK3–selective inhibitor Xeljantz® showed IC_{50} values of 1 nM, 20 nM, and 112 nM against each of JAK3, JAK2, and JAK1, respectively.[217–219] A few years later, Pfizer furthered their initial study and discovered Ritlecitinib (Figure 6.2). This compound demonstrated higher potency and selectivity toward JAK3 with an IC_{50} of 33 nM, compared to 10,000 nM against JAK1, JAK2, and TYK2.[211] Prior to the discovery of Ritlecitinib, the effects on the JAK-STAT signalling pathway were attributed to both JAK1 and JAK3.[220] Since this discovery, researchers are able to investigate the exclusive effects of JAK3 inhibition.[221] In late 2022, Pfizer announced the acceptance for the regulatory submission of Ritlecitinib to the FDA and EMA for adults and adolescents 12 years of age and older with alopecia areata.[222] Less than a year later, both agencies approved Ritlecitinib, thus, the brand name Litfulo™ was given.[223,224]

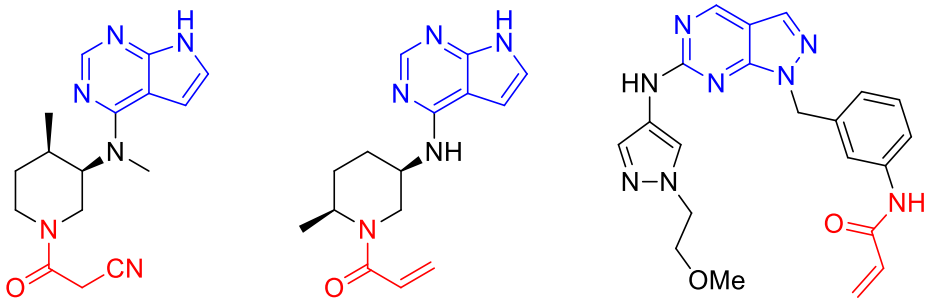

Figure 6.2 – Examples of irreversible covalent JAK3–selective inhibitors

Recent developments by Zhang *et al.* have attracted attention as they reported a novel and highly selective JAK3 inhibitor, Z583 (Figure 6.2). The potency data showed an IC_{50} value of 11 nM against JAK3 and > 10,000 nM against the remaining JAK family.[220] In the chemical structures of Litfulo™, and Z583, the covalent unit responsible for binding

to Cys[909] through the Michael addition reaction is highlighted in red. The amide group also forms an additional hydrogen bond with Leu[956], which accounts for the JAK3–selectivity.[213] Furthermore, it is proposed that the pyrrolo- or pyrazolopyrimidine ring (highlighted in blue) interacts with the ATP binding pocket of JAK3 by hydrogen bond interactions with Glu[903] and Leu[905].[211,215,218–220] The additional methoxyethyl side-chain of Z583 is proposed to account for the greater potency and selectivity observed through added hydrogen bond interactions with Leu[828], Val[836], Ala[853] and Try[904].[220]

Although reversible non-covalent JAK3 selective inhibitors have been reported, these inhibitors appear to not maintain their selectivity for JAK3 at cellular ATP levels.[213] Decernotinib (Figure 6.3) is a non-covalent inhibitor of JAK3 developed by Vertex for treatment of rheumatoid arthritis with good potency *in vitro*. In the end, this pharmaceutical agent failed beyond phase two clinical trials, where its development was unfortunately terminated.[225] Another non-covalent inhibitor for JAK3 WYE-151650 (Figure 6.3) has been shown to exhibit high selectivity for JAK3 (IC_{50} = 0.8 nM) compared to JAK1, JAK2, and TYK2 by 36, 14 and 34 times respectively.[226] Although the IC_{50} of this compound looks promising, no further clinical studies have been carried out to date. WYE-151650 shared potency and effects on natural killer cell count *in vitro* similar to that of Xeljantz®, which is a covalent drug for the treatment of rheumatoid arthritis developed by Pfizer.[213] Ultimately, WYE-151650 was disregarded in favour of Xeljantz®.[212,217,219]

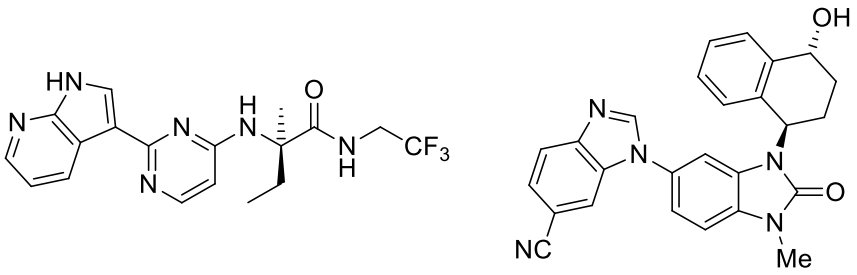

Decernotinib WYE-151650

Figure 6.3 – Examples of reversible non-covalent JAK3–selective inhibitors

Design, Synthesis and Biological Evaluation of York 3-D Building Block–Derived JAK3–Selective Inhibitors

To design and subsequently synthesise a drug-type molecule from our existing library of York 3-D building blocks, inspiration was used from three reference pharmaceuticals (Figure 6.4). The structural components of the blockbuster drug Xeljantz® has a piperidine core together with pyrrolopyrimidine and a cyanoamide covalent warhead incorporated into its structure. Pfizer's most recent clinical candidate Litfulo™ is very similar to that of Xeljantz®. Besides the absence and positioning of methyl groups, the replacement of the cyanoamide with an acrylamide is one of the key structural differences. Although the drug Corectim® is a pan-JAK inhibitor (no selectivity in the JAK family).[227] this drug was considered because of the structural similarities of the pyrrolopyrimidine and cyanoamide, both attached to a bicyclic pyrrolidine-derived core.

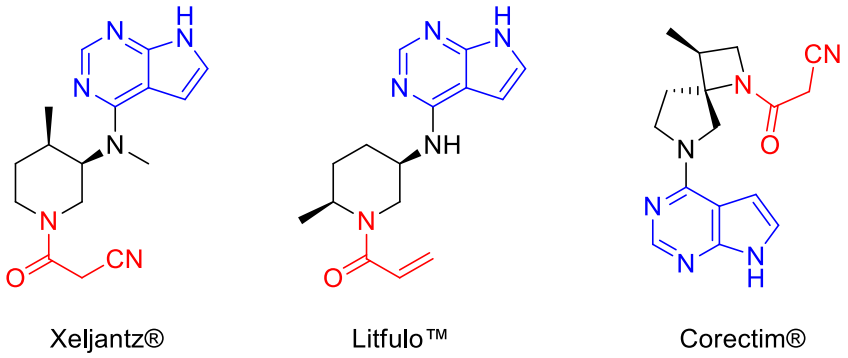

Figure 6.4 – Reference JAK Inhibitors for Docking Studies

The molecular docking studies for designing potential JAK3 inhibitors were conducted by Simon Lucas and Lucia Fusani at AstraZeneca. They started with the X-ray crystal structure of Litfulo™ (Ritlecitinib) bound to JAK3. In the X-ray crystal structure, the acrylamide moiety of Litfulo™ interacts with the Cys^{909} residue of JAK3 *via* a covalent bond (Figure 6.5). In addition, the pyrrolopyrimidine also enables hydrogen bond accepting and donating interactions to Glu^{903} and Leu^{905} residues of JAK3, respectively. The conformation of Litfulo™ is held by two hydrogen bond donating interactions to H_2O.

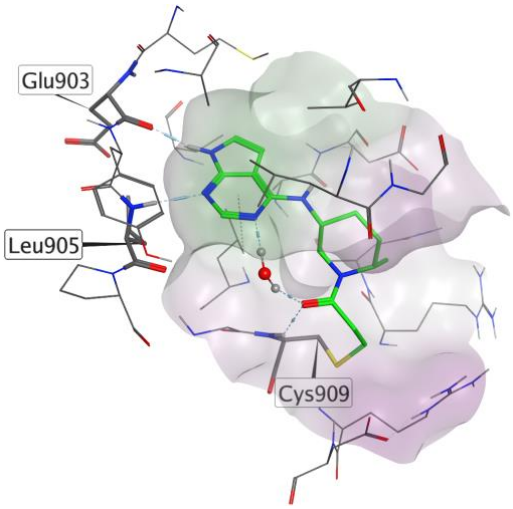

Figure 6.5 – X-ray crystal structure of Litfulo™ bound into JAK3

The computational modelling of each of the nine building blocks was carried out by attaching pyrrolopyrimidine at the point of the cyclopropyl BMIDA, and an acrylamide at the nitrogen. In modelling the resulting building block derived potential JAK inhibitors against the JAK3 protein, a covalent bond was made from the acrylamide to Cys^{909}. The energy of these structures were calculated and acrylamide inhibitors **272** and *cis*-**267** were found to have the best docking scores and binding poses (Figure 6.6). The binding interactions of pyrrolopyrimidine in acrylamide inhibitors **272** ((*S*)-enantiomer) and *cis*-**267** (*S*,*S*-enantiomer) were analogous to that of Litfulo™.

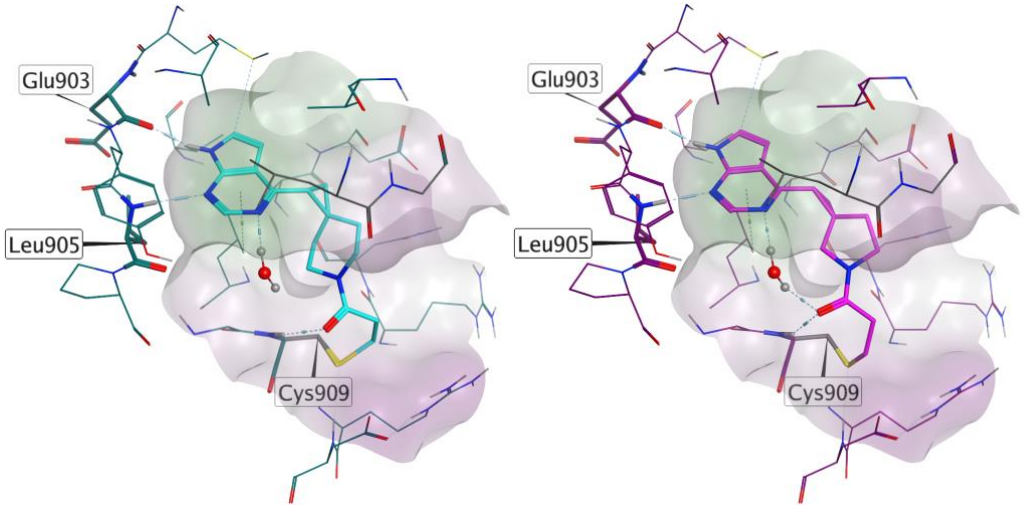

Figure 6.6 – X-ray of **272** *and cis*-**267** *bound to JAK3*

In addition to the modelled acrylamide inhibitors **272** and *cis*-**267**, we also proposed an additional fused piperidine scaffold due to its comparable spatial orientation. Therefore, the three scaffolds were proposed to be each attached to three different covalent warheads

(cyanoamide, acrylamide and chloroamide). Given that the building blocks in each were previously synthesised in racemic form, a racemic mixture of compounds **271**–**273**, *cis*-**266**, *cis*-**267**, *cis*-**274** and *exo*-**275**–**277** were proposed to be synthesised (Figure 6.7). The nine compounds contain the pyrrolopyrimidine and a covalent element, as seen in the structure of the reference drugs in Figure 6.4. The synthesis of the proposed nine pyrrolopyrimidines shown in Figure 6.7 was divided up between myself and another member of the O'Brien group. The synthesis of JAK inhibitors *cis*-**266**, *cis*-**267**, *cis*-**274** and *exo*-**275**–**277** will be described herein.

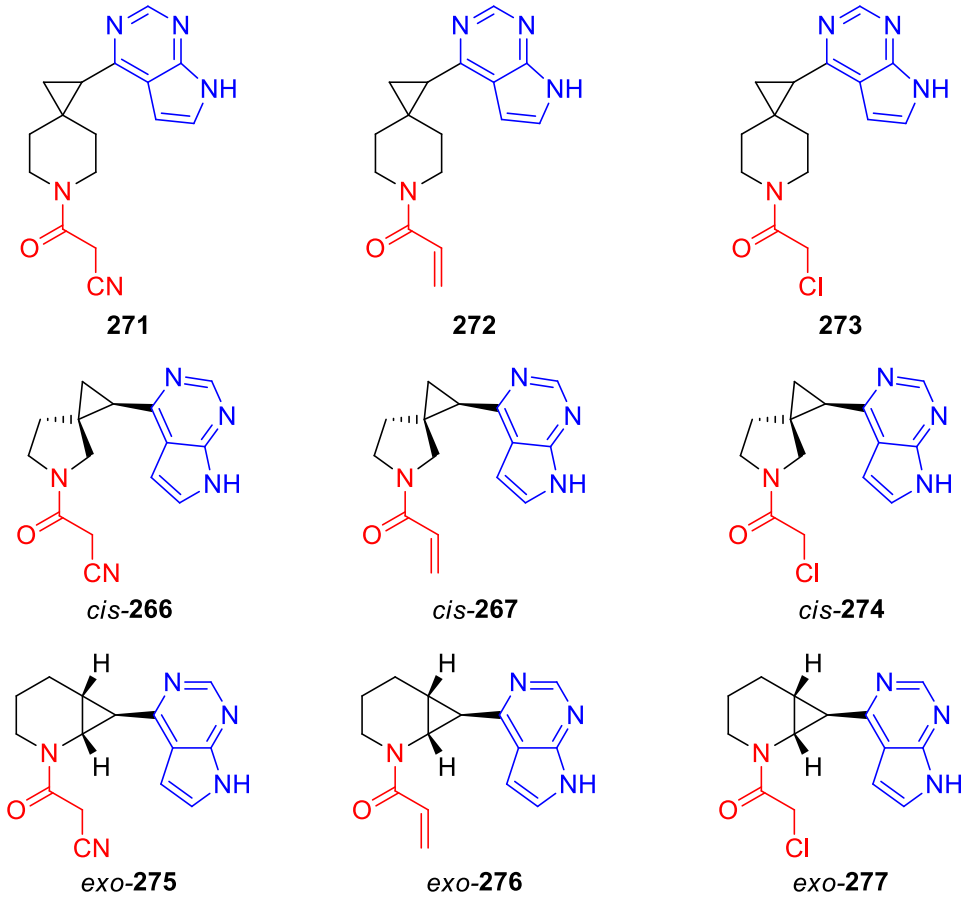

Figure 6.7 – Proposed JAK3–selective Inhibitors

Before our work commenced on spiro pyrrolidines *cis*-**266**, *cis*-**267**, *cis*-**274**, and fused piperidines *exo*-**275**–**277**, Andres Gomez Angel carried out the synthesis of spiro piperidine acrylamide **279** (Scheme 6.2). In the synthesis, cyclopropyl BMIDA **37** was cross-coupled to 5-bromo-tosyl-azaindole *via* the high loading standard Suzuki-Miyaura cross-coupling conditions (15 mol% $Pd(OAc)_2$, 30 mol% PCy_3, 6.0 eq. Cs_2CO_3). Under these conditions, reaction of cyclopropyl BMIDA **37** gave cyclopropyl tosyl-azaindole

277 in 73% yield (Scheme 6.2).[131] In the next step, it was found that it was better to remove the tosyl group prior to carrying out the acylation step. This is because under the reaction conditions for tosyl group removal, Cs_2CO_3 and MeOH in MeCN at rt, if the acrylamide was already in place, a by-product formed whereby addition of methoxide to the acrylamide had occurred.[131] Consequently, reaction of cyclopropyl tosyl-azaindole **277** with Cs_2CO_3 and MeOH in MeCN at rt for 16 h afforded cyclopropyl azaindole **278** in 82% yield.[131] In the last step, removal of the Boc group was carried out by treating cyclopropyl azaindole **278** with 4 M HCl in dioxane at rt for 30 min. Then, addition of Et_3N, DMAP and acryloyl chloride in CH_2Cl_2 at 0 °C to rt for 4 h gave acrylamide **279** in 76% yield. The plan was to apply this standard synthetic approach to the other targeted acrylamides, as well as the chloro amides and the cyano amides.

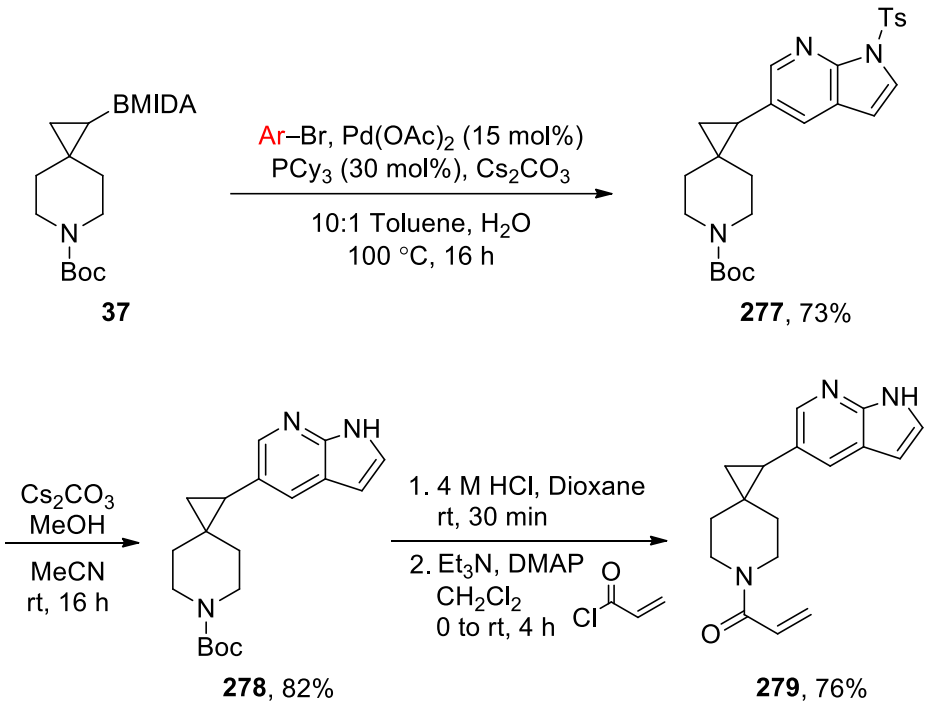

Scheme 6.2

To begin, tosyl protection of bromopyrrolopyrimidine **280** was carried out following a literature procedure.[228] Bromopyrrolopyrimidine **280** was reacted with sodium hydride and tosyl chloride in THF, at 0 °C then, rt for 4 h to yield 79% of bromo-tosyl-pyrrolopyrimidine **281** after chromatography.

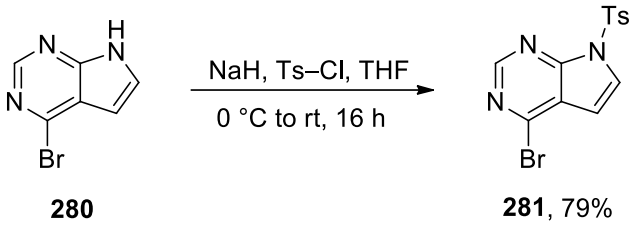

280 **281**, 79%

Scheme 6.3

Suzuki-Miyaura cross-coupling of cyclopropyl BMIDA *cis*-**38** with bromo-tosyl-pyrrolopyrimidine **281** was carried out using 15 mol% $Pd(OAc)_2$, 30 mol% PCy_3, 6.0 eq. Cs_2CO_3. Upon purification by chromatography, cyclopropyl tosyl-pyrrolopyrimidine *cis*-**282** was isolated in 63 – 84% yields (Scheme 6.4). Similarly, cyclopropyl BMIDA *exo*-**36** afforded cyclopropyl tosyl-pyrrolopyrimidine *exo*-**283** in 30 – 51% yields. In this case, the yields were more variable when the reaction was repeated although there was no obvious reason why that should be the case.

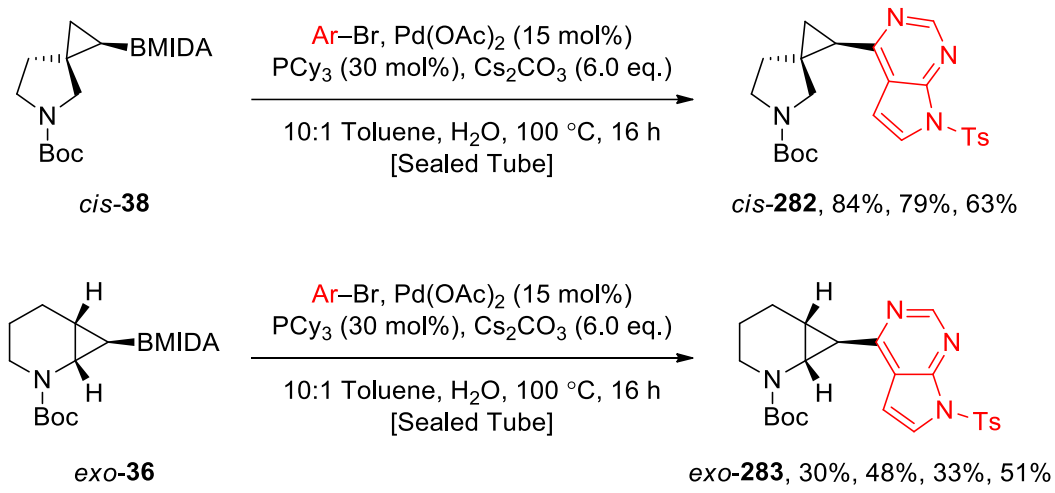

cis-**38** *cis*-**282**, 84%, 79%, 63%

exo-**36** *exo*-**283**, 30%, 48%, 33%, 51%

Scheme 6.4

Removal of the *N*-tosyl protecting group was to be carried out by treating the *N*-tosyl heterocycle with Cs_2CO_3 and MeOH in THF to deliver the unprotected pyrrole group. Thus, cyclopropyl tosyl-pyrrolopyrimidine *cis*-**282** was reacted with Cs_2CO_3 in MeOH and THF at rt for 16 h. Purification by chromatography gave the desired cyclopropyl pyrrolopyrimidine *cis*-**284** in 43% yield and, unexpectedly, cyclopropyl *N*-methyl-pyrrolopyrimidine *cis*-**285** in 29% yield in which *N*-methylation had occurred (Scheme 6.5). The reaction was repeated to confirm that *N*-methylation was reproducible. Indeed, cyclopropyl pyrrolopyrimidine *cis*-**284** and cyclopropyl *N*-methyl-pyrrolopyrimidine *cis*-**285** were isolated in 42% and 33% yields respectively (Scheme 6.5). A similar

N-methylated side-product was also obtained on a different building block scaffold. Thus, treatment of cyclopropyl tosyl-pyrrolopyrimidine *exo*-**283** to the same conditions gave cyclopropyl pyrrolopyrimidine *exo*-**286** and cyclopropyl *N*-methyl-pyrrolopyrimidine *cis*-**287** in 44% and 47% yields respectively (Scheme 6.5).

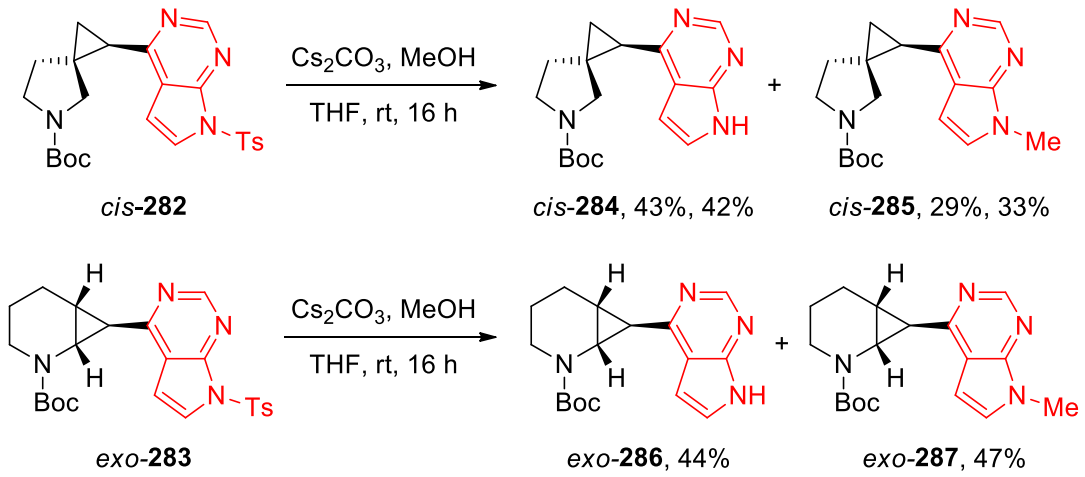

Scheme 6.5

The *N*-methylation side-reaction had not been observed during the previous studies of *N*-tosyl group removal in the group on different *N*-tosyl heterocycles (see Scheme 6.2 for example).[131] A mechanism to account for the formation of *N*-methyl side-products is shown in Scheme 6.6. For the deprotection step, the methoxide will attack sulfonamide **288** to generate pyrrole anion **290** and methyl tosylate **289** (Scheme 6.6). It is proposed that pyrrole anion **290** could partake in nucleophilic attack on the by-product of detosylation, methyl tosylate **289** akin to *N*-methylation using dimethyl sulfate.[229] This would generate *N*-methylated by-product **292** and tosylate **291**.

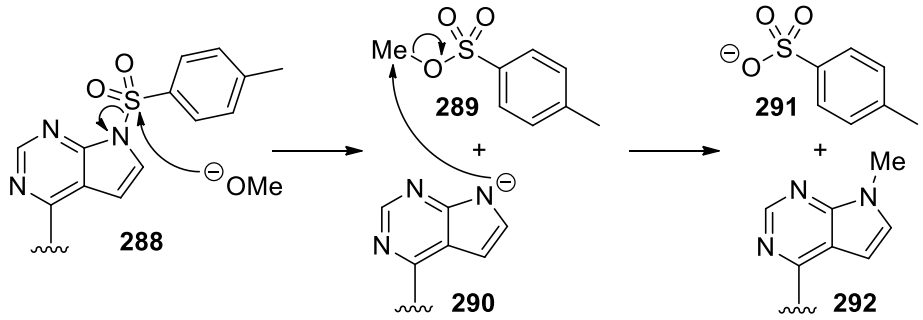

Scheme 6.6

Based on our proposed mechanism for the formation of *N*-methyl pyrrole by-products, we envisaged adding in a sacrificial nucleophile which could preferentially trap methyl

toluenesulfonate **289** *in situ* as it is formed. With this in mind, we decided to explore the use of 5.0 eq. pyrrolidine. Thus, reaction of cyclopropyl tosyl-pyrrolopyrimidines *cis*-**282** and *exo*-**283** with Cs_2CO_3 and MeOH in THF in the presence of 5.0 eq. pyrrolidine was explored. Pleasingly, this gave cyclopropyl pyrrolopyrimidines *cis*-**284** and *exo*-**286** in 82% and 81% yield respectively, without the formation of any methylated products (Scheme 6.7).

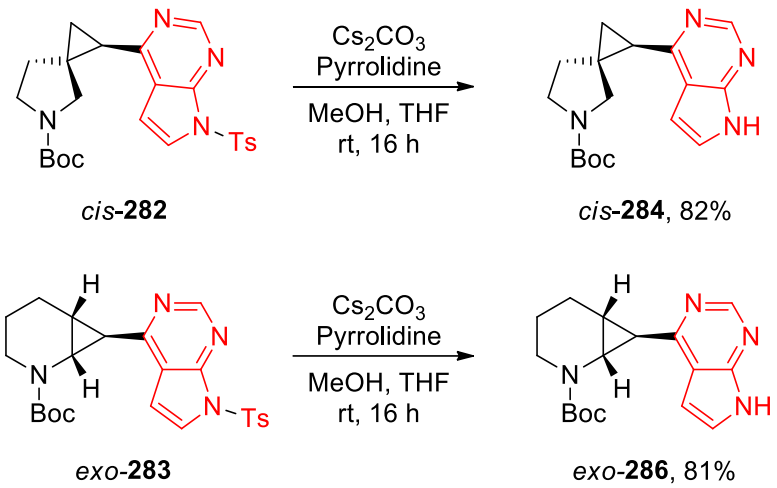

Scheme 6.7

In the final step, the plan was to functionalise the pyrrolidine/piperidine with a cyanoamide, acrylamide and chloroamide. To this end, cyclopropyl pyrrolopyrimidine *cis*-**284** was treated with HCl in dioxane to remove the Boc group and then reaction with 2-cyanoacetic acid and Et_3N in DMF at rt for 16 h. This gave cyanoamide *cis*-**266** in 59% yield after chromatography over the two steps (Scheme 6.8). Similarly, cyclopropyl pyrrolopyrimidine *cis*-**284** was deprotected and reacted with acryloyl chloride and DIPEA in CH_2Cl_2 at rt for 16 h to give acrylamide *cis*-**267** in 26% yield. Unfortunately, the same sequences starting with cyclopropyl pyrrolopyrimidine *exo*-**286** failed to give cyanoamide *exo*-**275** and acrylamide *exo*-**276** (Scheme 6.8). It is not clear why these reactions were unsuccessful.

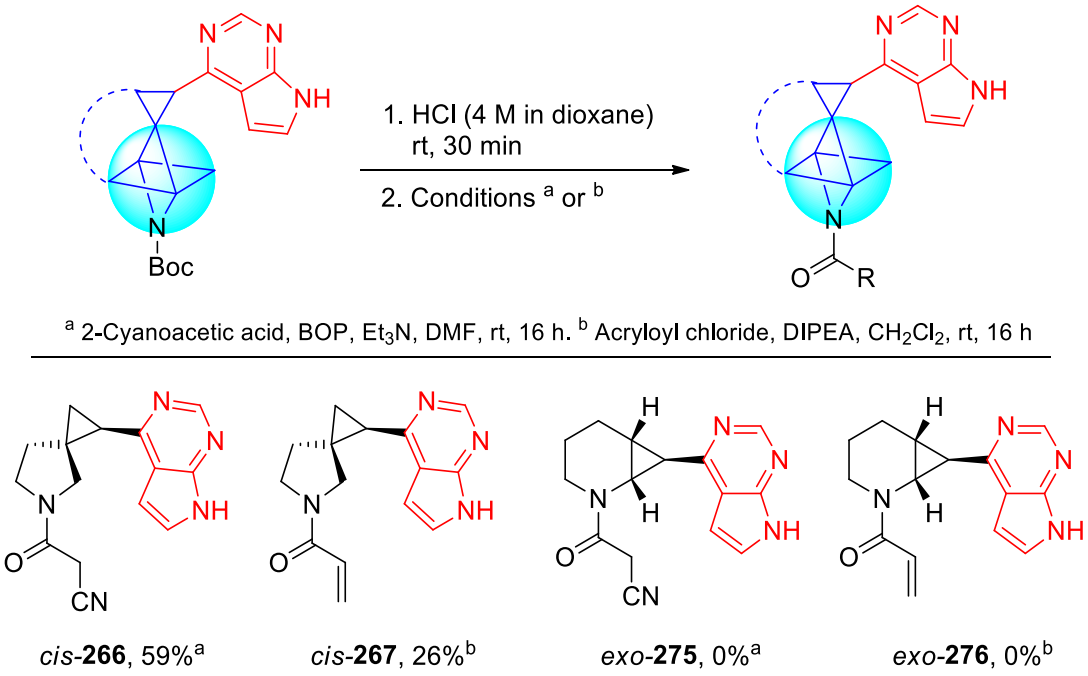

Scheme 6.8

Attempts to obtain pure samples of chloroamides *cis*-**274** and *exo*-**277** were also unsuccessful (Scheme 6.9). Removal of the Boc group from cyclopropyl pyrrolopyrimidine *cis*-**284** with HCl was followed by reaction with 2-chloroacetic acid, BOP and Et_3N. Analysis of the crude product by ^1H NMR spectroscopy and HRMS showed evidence for the formation of chloroamide *cis*-**274**. However, after numerous attempts at chromatography, isolation of pure chloroamide *cis*-**274** was unattainable. Similarly, changing the coupling agent to T3P also did not provide any aid in isolating pure chloroamide *cis*-**274**. Even less success was observed with cyclopropyl pyrrolopyrimidine *exo*-**286**. Using BOP and T3P as coupling agents for amide bond formation with 2-cyanoacetic acid, both conditions failed to give any evidence for chloroamide *exo*-**277**.

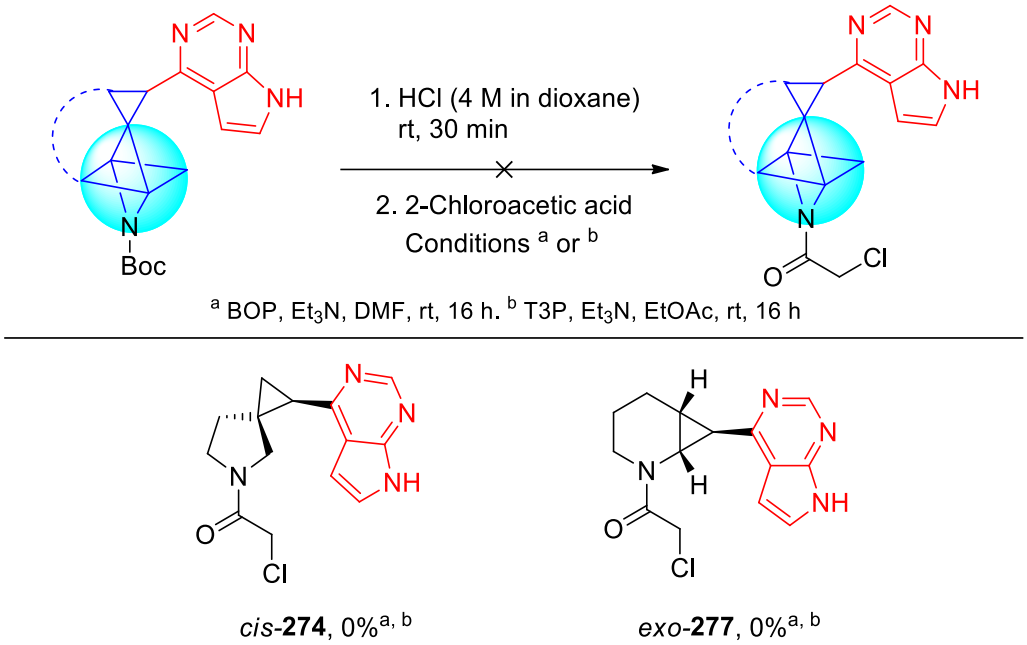

Scheme 6.9

With cyanoamide *cis*-**266** and acrylamide *cis*-**267** in hand, our samples underwent biological evaluation, facilitated by our collaboration with AstraZeneca. Specifically, they were subjected to screening against JAK1, JAK2, JAK3 and TYK2. To our delight, the JAK inhibition data showed that both cyanoamide *cis*-**266** and acrylamide *cis*-**267** were found to be selective for JAK3 with IC_{50} values of 1,420 nM and 69 nM respectively (Table 4.1). A comparison with current drugs is also shown in Table 4.1: Xeljantz® shows moderate JAK3–selectivity (IC_{50} = 1 nM); Corectim® is pan-JAK inhibitor (IC_{50} = 13 nM for JAK3); Litfulo™ (JAK3–selective, IC_{50} = 33 nM); Z583 is JAK3–selective (IC_{50} = 11 nM). All of these four drugs/potential drugs show better IC_{50} values than our compounds although it should also be highlighted that, unlike the drug compounds in Table 4.1, our compounds are racemates. It is notable that acrylamide *cis*-**267** has an IC_{50} value in the same order of magnitude as these compounds. In particular, it shows a similar selectivity profile and inhibition to Litfulo™, which was used as a model for the computational docking studies.

Table 6.1 – JAK IC_{50} inhibition values against JAK1, JAK2, JAK3 and TYK2

Compound	JAK1/nM	JAK2/nM	JAK3/nM	TYK2/nM
Xeljantz®[230]	112	20	1	–
Corectim®[227]	3	3	13	58
Litfulo™ [227]	>10,000	>10,000	33	>10,000
Z583[220]	>10,000	>10,000	11	>10,000
Cyanoamide *cis*-266	>10,000	>10,000	1,420	>10,000
Acrylamide *cis*-267	>10,000	>10,000	69	>10,000

The JAK3–selectivity and IC_{50} value for acrylamide *cis*-**267** is a proof-of-concept case study to show that the nine cyclopropane building blocks can be used in fragment elaboration in 3-D space to develop an interesting and novel lead-like compound. It also demonstrates how our fragment elaboration methodology could be used in practice. Once targets were identified from the docking studies, having the synthetic methodology already developed meant that the compounds could be quickly synthesised and be ready for biological evaluation. We hope the methodology we have developed takes a step towards addressing the synthetic limitations highlighted by researchers at Astex.[2,52]

Conclusion

In summary, of the six targeted pyrrolopyrimidines in this work, only the synthesis of cyanoamide *cis*-**266** and acrylamide *cis*-**267** were successfully carried out. For chloroamide *cis*-**274**, while evidence of its synthesis was supported by ^{1}H NMR spectroscopy and HRMS, unfortunately, the compound could not be isolated pure. There was no evidence that we had generated cyanoamide *exo*-**275**, acrylamide *exo*-**276** or chloroamide *exo*-**277**. From the synthesis of a handful of screening compounds derived from York building blocks, cyanoamide *cis*-**266** and acrylamide *cis*-**267** were the most promising. While cyanoamide *cis*-**266** was able to demonstrate JAK3 selectivity, acrylamide *cis*-**267** additionally showed potency in the same order of magnitude as Pfizer's Litfulo™ which recently received FDA approval for the treatment of alopecia areata.

Overall, we have presented a novel approach to elaborate bromo-tosyl-pyrrolopyrimidine **281** into JAK inhibitors through the use of York 3-D building blocks. In a three-step protocol, synthesis of cyanoamide *cis*-**266** and acrylamide *cis*-**267** were carried out. This showed that the fragment elaboration platform developed by the O'Brien group can allow the rapid generation of screening compounds against JAK3.

Chapter 7: Experimental

General Information

All non-aqueous reactions were carried out under oxygen free Ar or N_2 using flame-dried glassware. Dry solvents (THF, CH_2Cl_2, DMF, toluene, Et_2O, hexane, MeCN and MeOH) were obtained and used without further purification from PureSolv 300-3-MD dry solvent dispenser unless otherwise stated. EtOAc, pyridine, DIPEA and Et_3N were freshly distilled over CaH_2, all other anhydrous solvents were purchased and used without further purification. Alkyllithiums were titrated against *N*-benzylbenzamide before use. *i*-PrO–Bpin was used without further purification. Brine refers to saturated aqueous sodium chloride solution and water is deionised water. Flash column chromatography was carried out according to standard techniques using silica gel (60 Å, 220-440 mesh particle size 40–63 μm) purchased from Sigma-Aldrich or Fluka silica gel, 35–70 µm, 60 Å and the solvent system as stated. Thin layer chromatography was carried out using Merck TLC Silica gel 60G F254 aluminium backed plates (100390 Supelco). Spots were visualised by UV and appropriate stains ($KMnO_4$, Vanillin, Ninhydrin). Melting points were carried out on a Gallenkamp melting point apparatus. Proton (400 MHz) and carbon (100.6 MHz) NMR spectra were recorded on a Jeol ECX-400 or a JEOL ECS400 instrument using an internal deuterium lock. Chemical shifts (δ) are recorded in parts per million (ppm) and referenced to the residual solvent peak of the stated solvent, with tetramethylsilane defined as 0 ppm. NMR spectra were analysed, assigned, and reported using recommended methods and DEPT as well as 2-D NMR techniques such as HH-COSY, HMQC, HMBC and NOESY where required. Coupling constants (*J*) are quoted in Hertz. For samples recorded in $CDCl_3$, chemical shifts are quoted in parts per million relative to $CHCl_3$ (δ_H 7.26 ppm) and $CDCl_3$ (δ_C 77.16 ppm, central line of triplet). For samples recorded in CD_3OD, chemical shifts are quoted in parts per million relative to CD_3OD (δ_H 3.31 ppm, central line of quintet) and CD_3OD (δ_C 49.0 ppm, central line of septet). For samples recorded in DMSO-d_6, chemical shifts are quoted in parts per million relative to d_6-DMSO (δ_H 2.50 ppm, central line of quintet) and DMSO-d_6 (δ_C 39.5 ppm, central line of septet). For samples recorded in acetone-d_6, chemical shifts are quoted in parts per million relative to d_6-acetone (δ_H 2.05 ppm, central line of quintet) and d_6-acetone (δ_C 29.8 ppm, central line of septet). Infrared spectra were recorded on a PerkinElmer UATR 2 FT-IR spectrometer. Electrospray and atmospheric pressure chemical ionisation

techniques (ESI and APCI) have been applied and mass spectra were recorded at room temperature on a Bruker Daltronics microOTOF spectrometer.

Note: Solvent systems for flash column chromatography using acetone and CH_2Cl_2 can be explosive in the presence of trace NaOH.

General Procedures

General Procedure A: Suzuki-Miyaura Cross-Coupling Using Conditions A

Cyclopropyl BMIDA, aryl bromide, PCy_3 (30 mol%) and Cs_2CO_3 (6.0 eq.) were placed in a pressure tube. Toluene and H_2O were added and the resulting mixture was stirred at rt. Then, Ar was bubbled through the mixture for 20 min using a balloon through a septum with an outlet in order to deoxygenate the solvents. $Pd(OAc)_2$ (15 mol%) was added and the resulting mixture was stirred and heated at 100 °C in a sealed pressure tube for 16 h. After being allowed to cool to rt, the solids were removed by filtration through a plug of Celite® and washed with EtOAc and H_2O. The two layers of the filtrate were separated and the aqueous layer was extracted with EtOAc . The combined organic layers were dried (Na_2SO_4), filtered, and evaporated under reduced pressure to give the crude product.

General Procedure B: Suzuki-Miyaura Cross-Coupling Using Conditions B

Toluene and H_2O were added to separate flasks. Then, in each flask, Ar was bubbled through the mixture for 20 min using a balloon through a septum with an outlet in order to deoxygenate the solvents. Cyclopropyl BMIDA, aryl bromide, $Pd(OAc)_2$ (5 mol%), PCy_3 (10 mol%) and Cs_2CO_3 (3.0 eq.) were placed in a pressure tube which was evacuated and refilled with Ar. Then, the deoxygenated toluene and H_2O were added and the resulting mixture was stirred and heated at 100 °C in a sealed pressure tube for 16 h. After being allowed to cool to rt, H_2O was added. The mixture was extracted with EtOAc. The combined organic extracts were washed with H_2O, dried (Na_2SO_4), filtered, and evaporated under reduced pressure to give the crude product.

General Procedure C: Synthesis of Methanesulfonamides

HCl (4 M solution in dioxane) was added dropwise to a stirred solution of cyclopropyl-pyrimidine at rt under Ar. The resulting solution was stirred at rt for 1 h. Then, the solvent was concentrated under reduced pressure to give the crude HCl salt. Et_3N was added to a stirred solution the HCl salt in CH_2Cl_2 at rt under Ar. The resulting solution was stirred at rt for 10 min and MsCl was added. The resulting solution was stirred at rt for 16 h. The mixture was poured into $NaHCO_{3(aq)}$ and extracted with CH_2Cl_2. The combined organics

were dried (Na_2SO_4), filtered, and concentrated under reduced pressure to give the crude product.

General Procedure D: Removal of the Boc Group

HCl (4 M solution in dioxane) was added dropwise to a stirred solution of cyclopropyl aryl at rt under Ar. The resulting solution was stirred at rt for 1 h. Then, the solvent was evaporated under reduced pressure to give the crude HCl salt.

General Procedure E: Suzuki-Miyaura Cross-Coupling of Cyclopropyl Bpin

Toluene and H_2O were added to separate flasks. Then, in each flask, Ar was bubbled through the mixture for 20 min using a balloon through a septum with an outlet in order to deoxygenate the solvents. pinacol boronate, aryl bromide, $Pd(OAc)_2$, cataCXium® A and Cs_2CO_3 were placed in a pressure tube which was evacuated and refilled with Ar. Then, the deoxygenated toluene and H_2O were added, and the resulting mixture was stirred and heated at 120 °C in a sealed pressure tube for 16 h. After being allowed to cool to rt, H_2O was added. The mixture was extracted with EtOAc. The combined organic extracts were washed with H_2O, dried (Na_2SO_4), filtered, and evaporated under reduced pressure to give the crude product.

Experimental Procedures for Chapter 2

tert-Butyl 7,7-dibromo-2-azabicyclo[4.1.0]heptane-2-carboxylate 90

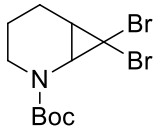

90

DIBAL–H (107.5 mL of a 1.0 M solution in hexane, 107.5 mmol, 1.5 eq.) was added dropwise to a stirred solution of lactam **88** (14.28 g, 71.7 mmol, 1.0 eq.) in THF (200 mL) at –78 °C under Ar. The resulting solution was stirred at –78 °C for 2 h. Then, saturated potassium sodium tartrate$_{(aq)}$ (100 mL) was added. The mixture was allowed to warm to rt and stirred at rt for 16 h. H_2O (100 mL) was added and the mixture was extracted with EtOAc (3 × 150 mL). The combined organic extracts were dried ($MgSO_4$), filtered, and evaporated under reduced pressure to give the crude hydroxy piperidine **93** as a colourless oil. Then, *p*-TsOH•H_2O (177 mg, 105 μmol, 0.13 mol%) was added to a stirred solution of crude hydroxy piperidine **93** in toluene (120 mL). The solution was connected to a Dean-Stark apparatus and stirred and heated at reflux for 30 min. After being allowed to cool to rt, the solvent was evaporated under reduced pressure to give crude enamide **89**. Then, $CHBr_3$ (18.4 mL, 210.0 mmol, 3.0 eq.) and $BnEt_3N^+Cl^-$ (2.87 g, 12.6 mmol, 0.2 eq.) were added to a stirred solution of enamide **89** (12.83 g, 70.0 mmol, 1.0 eq.) in CH_2Cl_2 (200 mL) at rt under Ar. A solution of NaOH (109.2 g, 2.7 mol, 39.0 eq.) in H_2O (110 mL) was added. The resulting mixture was stirred vigorously and heated at 50 °C for 16 h. After being allowed to cool to rt, the mixture was evaporated under reduced pressure to remove CH_2Cl_2. Then, H_2O (100 mL) was added and the mixture was extracted with Et_2O (3 × 150 mL). The combined organic extracts were dried ($MgSO_4$), filtered, and evaporated under reduced pressure to give the crude product. Purification by flash chromatography on silica with 90:10 hexane–Et_2O as eluent gave dibromocyclopropane **90** (20.18 g, 81%) as a yellow solid, mp 48 – 50 °C; R_F (90:10 hexane–Et_2O) 0.19; IR (ATR) 2973, 2938, 2874, 1701 (C=O), 1366, 1352, 1164, 1135, 758 cm^{-1}; ^{1}H NMR (400 MHz, $CDCl_3$) (85:15 mixture of rotamers) δ 3.43 (ddd, J = 12.5, 8.0, 4.0 Hz, 0.85H, NCH), 3.37 (d, J = 9.5 Hz, 0.15H, NCH), 3.29 (d, J = 9.0 Hz, 0.85H, NCH), 3.27 – 3.18 (m, 0.15H, NCH), 3.08 (ddd, J = 12.5, 6.5, 4.0 Hz, 0.15H, NCH), 2.90 (ddd, J = 12.5 8.0, 4.0 Hz, 0.85H, NCH), 2.15 – 2.01 (m, 2H, CH), 1.79 – 1.67 (m, 1H, CH), 1.61 – 1.57 (m, 1H, CH), 1.56 (s, 7.65H, CMe_3), 1.50 (s, 1.35H, CMe_3), 1.49 – 1.36

(m, 1H, CH); ^{13}C NMR (100.6 MHz, $CDCl_3$) δ 156.0 (C=O), 80.6 ($OCMe_3$), 40.8 (NCH), 40.4 (NCH_2), 36.9 (CBr_2), 29.6 (CH), 28.5 (CMe_3), 21.3 (CH_2), 19.2 (CH_2); MS (ESI) *m/z* 376 [(^{79,79}M + Na)$^+$, 100]; HRMS (ESI) *m/z* calcd for $C_{11}H_{17}{}^{79}Br_2NO_2$ [(^{79,79}M + Na)$^+$, 100] 375.9518, found 375.9518 (0.0 ppm error). Spectroscopic data consistent with those previously reported in the group.[47,49]

Lab Book Reference: SY-3-71

tert-Butyl-7-bromo-2-azabicyclo[4.1.0]heptane-2-carboxylate _exo_-91

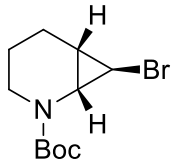

exo-**91**

KO*t*-Bu (37.93 g, 0.338 mol, 6.0 eq.) was added portionwise to a stirred solution of dibromocyclopropane **90** (20.00 g, 0.563 mol, 1.0 eq.) and dimethyl phosphite (31.0 mL, 0.338 mol, 6.0 eq.) in anhydrous DMSO (250 mL) at 0 °C under Ar. The resulting solution was stirred at rt for 1.5 h. Then, Et_2O (120 mL) and saturated $NaHCO_{3(aq)}$ (120 mL) were added. A white precipitate formed and additional H_2O (~100 mL) was added to redissolve the solids. The two layers were separated and the aqueous layer was extracted with Et_2O (3 × 150 mL). The combined organic layers were dried ($MgSO_4$), filtered, and evaporated under reduced pressure to give the crude product. Purification by flash column chromatography on silica with 90:10 hexane–Et_2O as eluent gave monobromocyclopropane *exo*-**91** (13.41 g, 86%) as a colourless oil, R_F (90:10 hexane–EtOAc) 0.38; IR (ATR) 2979, 2934, 2867, 1696 (C=O), 1365, 1159, 1130, 1032, 894, 894, 859, 772 cm^{-1}; ^{1}H NMR (400 MHz, $CDCl_3$) (80:20 mixture of rotamers) δ 3.77 (br d, *J* = 12.5 Hz, 0.8H, NCH), 3.59 (br d, *J* = 12.5 Hz, 0.2H, NCH), 3.21 (br d, *J* = 9.0 Hz, 0.2H, NCH), 3.08 (d, *J* = 9.0 Hz, 0.8H, NCH), 2.61 – 2.57 (m, 0.4H, NCH), 2.56 – 2.52 (m, 0.8H, NCH), 2.49 – 2.38 (m, 0.8H, CHBr), 2.03 – 1.93 (m, 1H, CH), 1.76 – 1.66 (m, 1H, CH), 1.66 – 1.53 (m, 2H, CH), 1.50 (s, 7.2H, CMe_3), 1.46 (s, 1.8H, CMe_3), 1.21 – 1.06 (m, 1H, CH); ^{13}C NMR (100.6 MHz, $CDCl_3$) (rotamers) δ 156.2 (C=O), 80.1 (O*C*Me_3), 41.5 (NCH), 39.8 (NCH), 37.6 (NCH_2), 37.4 (NCH_2), 28.6 (C*Me*$_3$), 23.4 (CH_2), 22.9 (CHBr), 22.3 (CH), 19.6 (CH_2); MS (ESI) *m/z* 298 [(^{79}M + Na)$^+$, 100]; HRMS (ESI)

m/z calcd for $C_{11}H_{18}{}^{79}BrNO_2$ [(^{79}M + Na)$^+$, 100] 298.0413, found 298.0410 (+0.9 ppm error). Spectroscopic data consistent with those previously reported in the group.[47,49]

Lab Book Reference: SY-3-73

tert-Butyl 7-(4,4,5,5-tetramethyl-1,3,2-dioxaborolan-2-yl)-2-azabicyclo[4.1.0] heptane-2-carboxylate _exo_-92

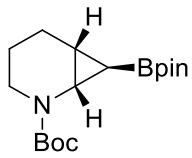

exo-**92**

n-BuLi (47.9 mL of a 1.50 M solution in hexanes, 71.9 mmol, 1.5 eq.) was added dropwise to a stirred solution of monobromocyclopropane *exo*-**91** (13.23 g, 47.9 mmol, 1.0 eq.) in THF (250 mL) at –78 °C under Ar. The resulting solution was stirred at –78 °C for 1 h. Then, *i*-PrO–Bpin (14.7 mL, 71.9 mmol, 1.5 eq.) was added and the solution was stirred at –78 °C for 10 min. After being allowed to warm to rt, saturated $NH_4Cl_{(aq)}$ (200 mL) was added and the two layers were separated. The aqueous layer was extracted with Et_2O (3 × 120 mL). The combined organic layers were washed with brine (120 mL), dried ($MgSO_4$), filtered, and evaporated under reduced pressure to give the crude product. Purification by flash column chromatography on silica with 90:10 to 80:20 to 70:30 hexane–Et_2O as eluent gave cyclopropyl Bpin *exo*-**92** (9.32 g, 60%) as a white solid, mp 59 – 62 °C; R_F (90:10 hexane–EtOAc) 0.41; IR (ATR) 2978, 2934, 2867, 1697 (C=O), 1398, 1366, 1319, 1167, 1143, 962, 893, 857, 778 cm^{-1}; ^{1}H NMR (400 MHz, $CDCl_3$) (90:10 mixture of rotamers) δ 3.77 (ddd, J = 12.5, 3.5, 3.5 Hz, 0.9H, NCH), 3.63 – 3.54 (m, 0.1H, NCH), 3.13 – 3.06 (m, 0.1H, NCH), 2.93 (dd, J = 8.0, 3.5 Hz, 0.9H, NCH), 2.72 – 2.61 (m, 0.1H, NCH), 2.55 (ddd, J = 12.5, 12.5, 2.5 Hz, 0.9H, NCH), 1.91 – 1.76 (m, 2H, CH), 1.59 – 1.52 (m, 1H, CH), 1.46 (s, 9H, CMe_3), 1.43 – 1.35 (m, 1H, CH), 1.35 – 1.26 (m, 1H, CH), 1.212 (s, 6H, CMe), 1.206 (s, 6H, CMe), –0.17 (dd, J = 7.5, 3.5 Hz, 1H, BCH); ^{13}C NMR (100.6 MHz, $CDCl_3$) δ 156.6 (C=O), 83.1 (O*C*Me$_2$), 79.3 (O*C*Me$_3$), 40.8 (NCH_2), 35.0 (NCH), 28.6 (C*Me*$_3$), 25.0 (C*Me*), 24.6 (C*Me*), 21.5 (CH_2), 21.3 (CH_2), 18.0 (CH), (BCH not resolved); MS (ESI) *m/z* 346 [(M + Na)$^+$, 100]; HRMS (ESI) *m/z*

calcd for $C_{17}H_{30}BNO_4$ [(M + Na)$^+$, 100] 346.2160, found 346.2164 (–0.5 ppm error). Spectroscopic data consistent with those previously reported in the group.[47,49]

Lab Book Reference: SY-3-75

tert-Butyl 7-(6-methyl-4,8-dioxo-1,3,6,2-dioxazaborocan-2-yl)-2-azabicyclo [4.1.0]heptane-2-carboxylate *exo*-36

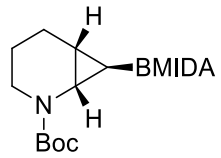

exo-**36**

MIDA (11.82 g, 80.3 mmol, 6.5 eq.) and $HC(OEt)_3$ (9.3 mL, 55.6 mmol, 4.5 eq.) were added to a stirred solution of cyclopropyl Bpin *exo*-**92** (4.00 g, 12.4 mmol, 1.0 eq.) in anhydrous DMSO (80 mL) at rt under Ar. The resulting suspension was stirred and heated at 100 °C for 48 h. After being allowed to cool to rt, saturated $NH_4Cl_{(aq)}$ (50 mL) was added and the mixture was extracted with EtOAc (3 × 50 mL). The combined organic extracts were washed with brine (50 mL), dried ($MgSO_4$), filtered, and evaporated under reduced pressure to give the crude product. Purification by flash column chromatography on silica with 95:5 to 80:20 CH_2Cl_2–acetone as eluent gave cyclopropyl BMIDA *exo*-**36** (3.92 g, 90%) as an off-white solid, mp 189 – 192 °C; R_F (90:10 CH_2Cl_2–acetone) 0.21; IR (ATR) 1758 (C=O, ester), 1675 (C=O, Boc), 1399, 1283, 1168, 1122, 995, 965, 915, 732 cm^{-1}; ^{1}H NMR (400 MHz, $CDCl_3$) δ 4.62 (d, J = 16.0 Hz, 1H, NCHC=O), 3.78 (d, J = 16.0 Hz, 1H, NCHC=O), 3.74 – 3.70 (m, 2H, MeNC*H*), 3.60 (ddd, J = 12.5, 4.0, 4.0 Hz, 1H, NCH), 3.15 (s, 3H, NMe), 2.63 (ddd, J = 12.5, 12.5, 2.5 Hz, 1H, NCH), 2.46 (dd, J = 8.0, 4.0 Hz, 1H, NCH), 1.93 – 1.77 (m, 2H, CH), 1.60 – 1.54 (m, 1H, CH), 1.42 (s, 9H, CMe_3), 1.40 – 1.35 (m, 1H, CH), 1.34 – 1.25 (m, 1H, CH), –0.38 (dd, J = 7.5, 4.0 Hz, 1H, BCH); ^{13}C NMR (100.6 MHz, $CDCl_3$) δ 168.7 (C=O, ester), 167.6 (C=O, ester), 156.6 (C=O, Boc), 79.6 (O*C*Me$_3$), 61.9 (MeN*C*H$_2$), 61.4 (MeN*C*H$_2$), 45.1 (NMe), 42.1 (NCH$_2$), 32.0 (NCH), 28.5 (C*Me*$_3$), 21.7 (CH$_2$), 21.1 (CH$_2$), 14.3 (CH) (BCH not resolved); MS (ESI) *m/z* 375 [(M + Na)$^+$, 100]; HRMS (ESI) *m/z* calcd for $C_{16}H_{25}BN_2O_6$ [(M + Na)$^+$, 100] 375.1698, found 375.1703 (−0.5 ppm error). Spectroscopic data consistent with those previously reported in the group.[47,49]

Lab Book Reference: SY-3-79

***tert*-Butyl 1,1-dichloro-6-azaspiro[2.5]octane-6-carboxylate 109**

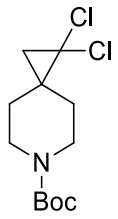

109

A solution of NaOH (20.3 g, 506.8 mmol, 10 eq) in H_2O (21 mL) was added dropwise to a stirred solution of alkene **105** (10.0 g, 50.68 mmol, 1.0 eq) and $BnEt_3N^+Cl^-$ (2.08 g, 9.12 mmol, 0.18 eq.) in $CHCl_3$ (200 mL) at rt under Ar. The resulting mixture was stirred vigorously and heated at 50 °C for 3 h and then at rt for 16 h. The resulting solution was poured into H_2O (100 mL) and extracted with CH_2Cl_2 (3 × 100 mL). The combined organics were dried ($MgSO_4$), filtered, and evaporated under reduced pressure to give the crude product. Purification by recrystallisation from Et_2O gave dichlorocyclopropane **109** (10.67 g, 75%) as a white solid, mp 82 – 84 °C; R_F (80:20 hexane–Et_2O) 0.21; IR (ATR) 2974, 1696 (C=O), 1420, 1366, 1240, 1170, 1127, 1048, 962, 760 cm^{-1}; ^1H NMR (400 MHz, $CDCl_3$) δ 3.61 – 3.50 (m, 2H, NCH), 3.50 – 3.40 (m, 2H, NCH), 1.85 – 1.75 (m, 2H, CH), 1.71 – 1.60 (m, 2H, CH), 1.47 (s, 9H, CMe_3), 1.29 (s, 2H, CH); ^{13}C NMR (100.6 MHz, $CDCl_3$) δ 155.0 (C=O), 79.9 (O*C*Me_3), 66.5 (CCl_2), 43.2 (NCH_2), 32.7 (CH_2), 31.6 (C), 31.4 (CH_2), 28.6 (C*Me*$_3$); MS (ESI) *m/z* 302 [(^{35,35}M + Na)$^+$, 100], HRMS ESI *m/z* calcd for $C_{12}H_{19}{}^{35}Cl_2NO_2$ [(^{35,35}M + Na)$^+$, 100] 302.0685, found 302.0690 (–1.7 ppm error). Spectroscopic data consistent with those previously reported in the group.[47,50]

Lab Book Reference: SY-4-196

***tert*-Butyl 1-(4,4,5,5-tetramethyl-1,3,2-dioxaborolan-2-yl)-6-azaspiro[2.5]octane-6-carboxylate 107**

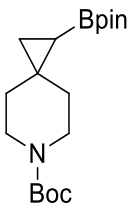

107

s-BuLi (18.7 mL, of a 1.29 M solution in cyclohexane, 1.2 mmol, 1.2 eq) was added drop-wise to a stirred solution of dichlorocyclopropane **109** (5.55 g, 19.81 mmol, 1.0 eq.) and H–Bpin (3.5 mL, 23.78 mmol, 1.2 eq.) in THF (100 mL) at –78 °C under Ar. The resulting mixture was stirred at –78 °C for 30 min. The cooling bath was removed, and the reaction was stirred for 1.5 h, and then cooled to 0 °C and saturated $NH_4Cl_{(aq)}$ (80 mL) was added. The mixture was extracted with EtOAc (3 × 80 mL), and the combined organics dried ($MgSO_4$), filtered, and evaporated under reduced pressure to give the crude product. Purification by flash column chromatography on silica using 80:20 hexane–EtOAc as eluent gave cyclopropyl Bpin **107** (4.25 g, 64%) as a white solid, mp 56 – 58 °C; R_F (80:20 hexane–EtOAc) 0.25; IR (ATR) 2976, 2931, 2868, 1682 (C=O), 1421, 1375, 1322, 1292, 1257, 1205, 1190, 842 cm^{-1}; ^1H NMR (400 MHz, $CDCl_3$) δ 3.52 – 3.27 (m, 4H, NCH), 1.59 – 1.54 (m, 2H, CH), 1.46 (s, 9H, CMe_3), 1.38 – 1.32 (m, 2H, CH), 1.23 (s, 6H, CMe_2), 1.21 (s, 6H, CMe_2), 0.70 – 0.62 (m, 2H, CH), –0.19 (dd, J = 9.0, 7.0 Hz, 1H, BCH); ^{13}C NMR (100.6 MHz, $CDCl_3$) δ 155.3 (C=O), 83.2 (O*C*Me_2), 79.4 (O*C*Me_3), 44.1 (NCH_2), 37.1 (CH_2), 31.6 (CH_2), 28.6 (C*Me*$_3$), 25.3 (C*Me*$_2$), 25.1 (C), 24.6 (C*Me*$_2$), 17.7 (CH2), (BCH resonance not resolved); ^{11}B (128.4 MHz, $CDCl_3$) δ 32.0; MS (ESI) *m/z* 360 [$(M + Na)^+$, 100], HRMS ESI *m/z* calcd for $C_{18}H_{32}BNO_4$ [$(M + Na)^+$, 100] 360.2317, found 360.2325 (–1.4 ppm error). Spectroscopic data consistent with those previously reported in the group.[47,50]

Lab Book Reference: SY-4-210

***tert*-Butyl 1-(6-methyl-4,8-dioxo-1,3,6,2-dioxazaborocan-2-yl)-6-azaspiro[2.5] octane-6-carboxylate 37**

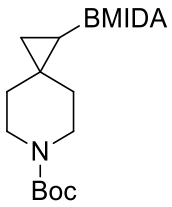

37

MIDA (4.26 g, 4.45 mmol, 6.5 eq.) and triethyl orthoformate (3.3 mL, 20.03 mmol, 4.5 eq.) were added to a stirred solution of cyclopropyl Bpin **107** (1.50 g, 4.45 mmol, 1.0 eq.) in anhydrous DMSO (50 mL) at rt under Ar. The resulting solution was stirred and heated at 100 °C for 72 h. After being allowed to cool to rt, saturated $NH_4Cl_{(aq)}$ (50 mL) was added, and the mixture was extracted with EtOAc (3 × 50 mL). The combined organic extracts were washed with brine (50 mL), dried ($MgSO_4$), filtered, and evaporated under reduced pressure to give the crude product. Purification by flash column chromatography on silica with 80:20 to 40:60 CH_2Cl_2–acetone as eluent gave cyclopropyl BMIDA **37** (0.99 g, 61%) as a white solid, mp 214 – 216 °C; R_F (80:20 CH_2Cl_2–acetone) 0.31; IR (ATR) 2976, 1749 (C=O, ester), 1677 (C=O, Boc), 1453, 1424, 1365, 1275, 1167, 1123, 991, 964, 892, 846 cm^{-1}; ^1H NMR (400 MHz, $CDCl_3$) (50:50 mixture of rotamers) δ 3.87 – 3.79 (m, 2H, $NCH_2C(O)$), 3.72 (d, J = 16.5 Hz, 2H, $NCH_2C(O)$), 3.65 – 3.50 (m, 2H, NCH), 3.41 – 3.25 (m, 2H, NCH), 3.01 (s, 3H, Me), 1.86 – 1.64 (m, 2H, CH), 1.57 – 1.47 (m, 2H, CH), 1.45 (s, 9H, CMe_3), 0.57 (dd, J = 9.5, 3.5 Hz, 1H, CH), 0.37 (dd, J = 7.0, 3.5 Hz, 1H, CH), –0.45 (dd, J = 9.5, 7.0 Hz, 1H, BCH); ^{13}C NMR (100.6 MHz, $CDCl_3$) δ 167.5 (C=O, ester), 166.8 (C=O, ester), 156.8 (C=O, Boc), 79.3 (O*C*Me_3), 61.88 ($NCH_2C(O)$), 61.82 ($NCH_2C(O)$), 46.3 (Me), 38.2 (CH_2), 30.6 (CH_2), 28.6 (C*Me*$_3$), 22.8 (C), 14.6 (CH_2) (BCH resonance not resolved); ^{11}B (128.4 MHz, $CDCl_3$) δ 11.0; MS (ESI) *m/z* 389 [$(M + Na)^+$, 100], HRMS ESI *m/z* calcd for $C_{17}H_{27}BN_2O_6$ [$(M + Na)^+$, 100] 389.1854, found 389.1861 (–0.9 ppm error). Spectroscopic data consistent with those previously reported in the group.[47,50]

Lab Book Reference: SY-4-222

***tert*-Butyl 6,6-dibromo-3-azabicyclo[3.1.0]hexane-3-carboxylate 74**

74

$CHBr_3$ (7.8 mL, 88.7 mmol, 3.0 eq.) was added dropwise over 1 h to a stirred solution of *N*-Boc pyrroline **67** (5.00 g, 29.6 mmol, 1.0 eq.) and NaO*t*-Pent (22.8 g, 0.21 mol, 7.0 eq.) in *n*-heptane (100 mL) at –10 °C under Ar. The resulting solution was stirred vigorously at –10 °C for 5 h. After being allowed to warm to rt, the solids were removed by filtration and washed with Et_2O (50 mL). The filtrate was poured into H_2O (200 mL) and extracted with Et_2O (3 × 150 mL). The combined organics were dried ($MgSO_4$) and evaporated under reduced pressure to give the crude product (9.80 g) as a black viscous oil which contained a 60:40 mixture (by ^{1}H NMR spectroscopy) of dibromocyclopropane **74** and *N*-Boc pyrroline **67**. The crude product was dissolved in DMSO (80 mL) and H_2O (6 mL) and cooled to 0 °C. Then, NBS (5.80 g, 32.8 mmol, 2.4 eq.) was added portionwise at 0 °C. The resulting mixture was stirred at rt for 16 h. Then, H_2O (50 mL) was added, and the mixture was extracted with EtOAc (3 × 100 mL). The combined organics were washed with brine (100 mL), dried ($MgSO_4$), filtered, and evaporated under reduced pressure to give the crude product as a brown oil. Purification by flash column chromatography on silica with 90:10 hexane–EtOAc as eluent gave dibromocyclopropane **74** (5.00 g, 47%) as a pale-yellow solid, mp 74 – 76 °C; R_F (80:20 hexane–EtOAc) 0.32; IR (ATR) 2975, 2932, 2881, 1694 (C=O), 1392, 1366, 1171, 1117, 881, 861, 769, 724, 552 cm^{-1}; ^{1}H NMR (400 MHz, $CDCl_3$) δ 3.66 – 3.51 (m, 4H, NCH), 2.44 – 2.34 (m, 2H, CH), 1.43 (s, 9H, CMe_3); ^{13}C NMR (100.6 MHz, $CDCl_3$) δ 153.7 (C=O), 80.0 (O*C*Me), 48.9 (NCH_2), 48.8 (NCH_2), 35.6 (CH), 34.9 (CBr_2), 34.8 (CH), 28.5 (C*Me*$_3$); MS (ESI) *m/z* 361 [(^{79,79}M + Na)$^+$, 100], HRMS ESI *m/z* calcd for $C_{10}H_{15}{}^{79}Br_2NO_2$ [(^{79,79}M + Na)$^+$, 100] 361.9362, found 361.9363 (–0.3 ppm error) and bromohydrin *trans*-**111** (2.3 g, 30%) as a brown solid, mp 42 – 44 °C; R_F (20:80 EtOAc–hexane) 0.10; IR (ATR) 3380 (br, OH), 2977, 2934, 2886, 1670, 1420, 1367, 1162, 1118, 960, 867, 770, 643, 553 cm^{-1}; ^{1}H NMR (400 MHz, $CDCl_3$) δ 4.50 – 4.45 (m, 1H, HOC*H*), 4.18 – 4.13 (m, 1H, BrCH), 4.07 – 3.98 (m, 1H, NCH), 3.93 – 3.69 (m, 2H, NCH), 3.40 (dd, *J* = 12.0, 6.0 Hz, 1H, NCH), 2.37 (br s, 1H, OH), 1.47 (s, 9H, CMe_3); ^{13}C NMR

(100.6 MHz, $CDCl_3$) (rotamers) δ 154.8 (C=O), 80.4 (O*C*Me_3), 80.3 (O*C*Me_3), 77.1 (HOCH), 76.2 (HOCH), 53.1 (NCH_2), 52.5 (NCH_2), 51.6 (NCH_2), 51.3 (NCH_2), 50.7 (CHBr), 50.2 (CHBr), 28.6 (C*Me*$_3$); MS (ESI) *m/z* 288 [(^{79}M + Na)$^+$, 100], HRMS ESI *m/z* calcd for $C_9H_{16}{}^{79}BrNO_3$ [(^{79}M + Na)$^+$, 100] 288.0206, found 288.0206 (–0.1 ppm error). Spectroscopic data of dibromocyclopropane **74**[231] and bromohydrin *trans*-**111**[103] consistent with those reported in the literature.

Lab Book Reference: SY-1-40

A solution of NaOH (1.6 g, 39.0 mmol, 39 eq.) in H_2O (1.6 mL) was added dropwise to a stirred solution of *N*-Boc pyrroline **67** (170 mg, 1.0 mmol, 1.0 eq.) and $BnEt_3N^+Cl^-$ (82 mg, 0.36 mmol, 0.36 eq.) in CH_2Cl_2 (5 mL) at rt under Ar. The resulting mixture was stirred vigorously and heated at 50 °C for 16 h. After being allowed to cool to rt, the mixture was poured into H_2O (10 mL) and extracted with CH_2Cl_2 (3 × 10 mL). The combined organics were dried ($MgSO_4$), filtered, and evaporated under reduced pressure to give the crude product which contained a 65:45 mixture (by ^{1}H NMR spectroscopy) of *N*-Boc pyrroline **67** and dibromocyclopropane **74**. Purification by flash column chromatography on silica with 90:10 hexane–EtOAc as eluent gave dibromocyclopropane **74** (133 mg, 39%) as a brown solid.

Lab Book Reference: SY-1-1

Bromoform (3.1 mL, 35.5 mmol, 3.0 eq.) was added dropwise over 10 min to a stirred solution of *N*-Boc pyrroline **67** (2.00 g, 11.8 mmol, 1.0 eq.) and NaO*t*-Pent (9.11 g, 82.7 mmol, 7.0 eq.) in *n*-heptane (40 mL) at –10 °C under Ar. The resulting solution was stirred vigorously at – 10 °C for 5 h. After being allowed to warm to rt, the solids were removed by filtration and washed with hexane (50 mL). The filtrate was poured into H_2O (50 mL) and extracted with hexane (3 × 50 mL). The combined organics were dried ($MgSO_4$), filtered, and evaporated under reduced pressure to give the crude product which contained a 60:40 mixture (by ^{1}H NMR spectroscopy) of *N*-Boc pyrroline **67** and dibromocyclopropane **74**. Purification by flash column chromatography on silica with 90:10 hexane–EtOAc as eluent gave dibromocyclopropane **74** (1.16 g, 29%) as a pale-yellow solid.

Lab Book Reference: SY-1-17

A 0 °C solution of NaOH (800 mg, 20.0 mmol, 20 eq.) in H_2O (0.8 mL) was added dropwise to a stirred solution of *N*-Boc pyrroline **67** (170 g, 1.0 mmol, 1.0 eq.), bromoform (0.18 mL, 2.0 mmol, 2.0 eq.), dibenzo-18-crown-6 (3.6 mg, 10.0 μmol, 0.01 eq.) and pinacol (4.3 mg, 36.0 μmol, 0.04 eq.) in CH_2Cl_2 (5 mL) at rt under Ar. The resulting mixture was stirred vigorously and heated at 40 °C for 16 h. After being allowed to cool to rt, the mixture was poured into H_2O (10 mL) and extracted with CH_2Cl_2 (3 × 10 mL). The combined organics were dried ($MgSO_4$), filtered, and evaporated under reduced pressure to give the crude product as a black viscous oil which contained a 45:55 mixture (by ^{1}H NMR spectroscopy) of *N*-Boc pyrroline **67** and dibromocyclopropane **74**. A 26% yield of dibromocyclopropane **74** was determined by ^{1}H NMR spectroscopy using 1,3-benzodioxole as an internal standard.

Lab Book Reference: SY-1-24

tert-Butyl 6-bromo-3-azabicyclo[3.1.0]hexane-3-carboxylate _exo_-110 and _endo_-110

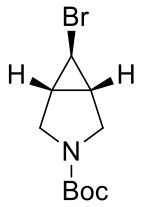

exo-**110**

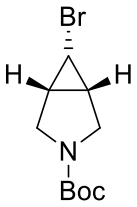

endo-**110**

KO*t*-Bu (13.6 g, 0.12 mol, 6.0 eq.) was added portionwise to a stirred solution of dibromocyclopropane **74** (6.9 g, 20.3 mmol, 1.0 eq.) and dimethyl phosphite (13.4 mL, 0.12 mol, 6.0 eq.) in anhydrous DMSO (120 mL) at 0 °C under Ar. The resulting solution was stirred at rt for 1.5 h. Then, Et_2O (50 mL, chilled to 0 °C) was added. Saturated $Na_2CO_{3(aq)}$ (50 mL) and H_2O (200 mL) were added, and the two layers were separated. The aqueous layer was extracted with Et_2O (3 × 150 mL). The combined organic layers were dried ($MgSO_4$), filtered, and evaporated under reduced pressure to give the crude product which contained a 70:30 mixture (by ^{1}H NMR spectroscopy) of monobromocyclopropanes *exo*-**110** and *endo*-**110**. Purification by flash column chromatography on silica using 90:10 hexane–EtOAc as eluent gave monobromocyclopropane *exo*-**110** (3.1 g, 58%) as a yellow oil, R_F (80:20 hexane–EtOAc) 0.40; IR (ATR) 2975, 2874, 1694 (C=O), 1478, 1376, 1365, 1333, 1223, 1169, 1047, 996, 885, 862, 773, 675, 547 cm^{-1}; ^{1}H NMR (400 MHz, $CDCl_3$) (50:50 mixture of rotamers) δ

3.71 (d, *J* = 11.5 Hz, 1H, NCH), 3.63 (d, *J* = 11.5 Hz, 1H, NCH), 3.39 – 3.30 (m, 2H, NCH), 2.55 (t, *J* = 2.5 Hz, 1H, BrCH), 1.97 – 1.89 (m, 2H, CH), 1.43 (s, 9H, CMe_3); ^{13}C NMR (100.6 MHz, $CDCl_3$) (rotamers) δ 154.7 (C=O), 79.9 ($OCMe_3$), 48.4 (NCH_2), 48.2 (NCH_2), 28.5 (CMe_3), 27.4 (CH), 26.6 (CH), 21.7 (BrCH); HRMS ESI *m/z* calcd for $C_{10}H_{16}{}^{79}BrNO_2$ $(M + Na)^+$ 284.0257, found 284.0258 (+0.4 ppm error) and monobromocyclopropane *endo*-**110** (1.2 g, 23%) as an off-white crystalline solid, mp 71 – 73 °C; R_F (80:20 hexane–EtOAc) 0.19; IR (ATR) 2976, 1676 (C=O), 1474, 1405, 1364, 1346, 1247, 1174, 1115, 933, 871, 778, 640, 543 cm^{-1}; ^1H NMR (400 MHz, $CDCl_3$) (50:50 mixture of rotamers) δ 3.66 – 3.53 (m, 3H, NCH), 3.48 (d, *J* = 11.0 Hz, 1H, NCH), 3.39 (t, *J* = 7.0 Hz, 1H, BrCH), 1.92 – 1.81 (m, 2H, CH), 1.44 (s, 9H, CMe_3); ^{13}C NMR (100.6 MHz, $CDCl_3$) (rotamers) δ 153.8 (C=O), 79.6 ($OCMe_3$), 47.3 (NCH_2), 47.1 (NCH_2), 31.5 (BrCH), 28.6 (CMe_3), 22.0 (CH), 21.3 (CH); HRMS ESI *m/z* calcd for $C_{10}H_{16}{}^{79}BrNO_2$ $(M + Na)^+$ 284.0257, found 284.0257 (+0.0 ppm error).

Lab Book Reference: SY-1-48

K_2CO_3 (150 g, 0.44 mol, 1.0 eq.) was added to a stirred solution of dibromocyclopropane **74** (610 g, 0.44 mmol, 1.0 eq.) and dimethyl phosphite (0.08 mL, 0.88 mol, 2.0 eq.) in anhydrous dioxane (1 mL) at rt under Ar. The resulting solution was stirred and heated at 80 °C for 16 h. After being allowed to cool to rt, saturated $Na_2CO_{3(aq)}$ (5 mL) was added, and the two layers were separated. The aqueous layer was extracted with EtOAc (3 × 5 mL). The combined organic layers were dried ($MgSO_4$), filtered, and evaporated under reduced pressure to give the crude product. Purification by flash column chromatography on silica using 90:10 hexane–EtOAc as eluent gave monobromocyclopropane *exo*-**110** (13.9 mg, 12%) as a yellow oil and monobromocyclopropane *endo*-**110** (11.4 mg, 10%) as an off-white crystalline solid.

Lab Book Reference: SY-1-7

***tert*-Butyl 6-(4,4,5,5-tetramethyl-1,3,2-dioxaborolan-2-yl)-3-azabicyclo[3.1.0] hexane-3-carboxylate *exo*-112**

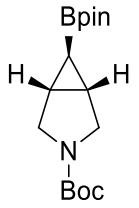

exo-**112**

n-BuLi (0.98 mL of a 2.44 M solution in hexane, 2.4 mmol, 1.5 eq.) was added dropwise to a stirred solution of monobromocyclopropane *exo*-**110** (420 mg, 1.6 mmol, 1.0 eq.) in THF (20 mL) at –78 °C under Ar. The resulting solution was stirred at –78 °C for 1 h. Then, *i*-PrO–Bpin (0.49 mL, 2.4 mmol, 1.5 eq.) was added and the solution was stirred at –78 °C for 10 min. After being allowed to warm to rt, saturated $NH_4Cl_{(aq)}$ (20 mL) was added, and the two layers were separated. The aqueous layer was extracted with Et_2O (3 × 20 mL). The combined organic layers were dried ($MgSO_4$), filtered, and evaporated under reduced pressure to give the crude product. Purification by flash column chromatography on silica using 60:40 hexane–Et_2O as eluent gave cyclopropyl Bpin *exo*-**112** (390 mg, 80%) as an off-white solid, mp 106 – 109 °C; R_F (60:40 hexane–Et_2O) 0.36; IR (ATR) 2977, 2931, 2868, 1699 (C=O), 1394, 1320, 1171, 1144, 1112, 858 cm^{-1}; ^1H NMR (400 MHz, $CDCl_3$) (50:50 mixture of rotamers) δ 3.61 (d, J = 11.0 Hz, 1H, NCH), 3.53 (d, J = 11.0 Hz, 1H, NCH), 3.37 – 3.27 (m, 2H, NCH), 1.68 – 1.59 (m, 2H, CH), 1.41 (s, 9H, CMe_3), 1.22 (s, 12H, CMe_2), –0.28 (t, J = 4.5 Hz, 1H, BCH); ^{13}C NMR (100.6 MHz, $CDCl_3$) (rotamers) δ 155.4 (C=O), 83.3 (O*C*Me_2), 79.3 (O*C*Me_3), 48.7 (NCH_2), 48.4 (NCH_2), 28.6 (C*Me*$_3$), 24.8 (C*Me*$_2$), 22.3 (CH), 21.5 (CH) (BCH resonance not resolved); HRMS ESI *m/z* calcd for $C_{16}H_{29}BNO_4$ $(M + Na)^+$ 332.2004, found 332.2004 (+0.7 ppm error).

Lab Book Reference: SY-1-43

n-BuLi (10.2 mL of a 2.30 M solution in hexane, 23.5 mmol, 1.5 eq.) was added dropwise to a stirred solution of monobromocyclopropane *exo*-**110** (4.10 g, 15.6 mmol, 1.0 eq.) in THF (150 mL) at –78 °C under Ar. The resulting solution was stirred at –78 °C for 1 h. Then, *i*-PrO–Bpin (4.8 mL, 23.5 mmol, 1.5 eq.) was added and the solution was stirred at

–78 °C for 10 min. After being allowed to warm to rt, saturated $NH_4Cl_{(aq)}$ (100 mL) was added, and the two layers were separated. The aqueous layer was extracted with Et_2O (3 × 100 mL). The combined organic layers were dried ($MgSO_4$), filtered, and evaporated under reduced pressure to give the crude product. Purification by flash column chromatography on silica using 40:60 to 60:40 Et_2O–hexane as eluent gave cyclopropyl Bpin *exo*-**112** (3.54 g, 73%) as an off-white solid.

Lab Book Reference: SY-1-49

tert-Butyl 6-(6-methyl-4,8-dioxo-1,3,6,2-dioxazaborocan-2-yl)-3-azabicyclo [3.1.0] hexane-3-carboxylate _exo_-39

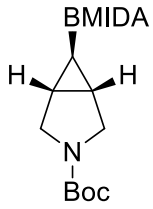

exo-**39**

MIDA (10.6 g, 72.0 mmol, 6.5 eq.) and $HC(OEt)_3$ (8.3 mL, 49.8 mmol, 4.5 eq.) were added to a stirred solution of cyclopropyl Bpin *exo*-**112** (3.4 g, 11.1 mmol, 1.0 eq.) in anhydrous DMSO (80 mL) at rt under Ar. The resulting solution was stirred and heated at 100 °C for 48 h. After being allowed to cool to rt, saturated $NH_4Cl_{(aq)}$ (200 mL) was added, and the mixture was extracted with EtOAc (3 × 300 mL). The combined organic extracts were washed with brine (200 mL), dried ($MgSO_4$), filtered, and evaporated under reduced pressure to give the crude product. Purification by flash column chromatography on silica with 80:20 to 40:60 CH_2Cl_2–acetone as eluent gave cyclopropyl BMIDA *exo*-**39** (2.97 g, 79%) as a white solid, mp 146 – 150 °C; R_F (80:20 CH_2Cl_2–acetone) 0.36; IR (ATR) 2974, 2934, 2871, 1753 (C=O, ester), 1680 (C=O, Boc), 1391, 1295, 1174, 1112, 1028, 988, 963, 868 cm^{-1}; ^1H NMR (400 MHz, $CDCl_3$) (50:50 mixture of rotamers) δ 3.85 (d, J = 16.5 Hz, 2H, NCHC=O), 3.74 (d, J = 16.5 Hz, 1H, NCHC=O), 3.70 (d, J = 16.5 Hz, 1H, NCHC=O), 3.58 (d, J = 11.0 Hz, 1H, NCH), 3.54 (d, J = 11.0 Hz, 1H, NCH), 3.40 – 3.31 (m, 2H, NCH), 3.03 (s, 3H, NMe), 1.59 – 1.53 (m, 1H, CH), 1.43 (s, 9H, CMe_3), 1.41 – 1.35 (m, 1H, CH), –0.45 (t, J = 5.0 Hz, 1H, BCH); ^{13}C NMR (100.6 MHz, $CDCl_3$) (rotamers) δ 166.7 (C=O, ester), 155.6 (C=O, Boc), 79.6 (O*C*Me_3), 62.2 ($NCH_2C(O)$), 62.1 ($NCH_2C(O)$), 48.6 (NCH_2), 48.2 (NCH_2), 46.6 (NMe), 28.6 (C*Me*$_3$),

20.3 (CH), 19.0 (CH) (BCH resonance not resolved); MS (ESI) *m/z* 361 [(M + Na)$^+$, 100], HRMS ESI *m/z* calcd for $C_{15}H_{23}BN_2O_6$ [(M + Na)$^+$, 100] 361.1541, found 338.1545 (–0.4 ppm error).

Lab Book Reference: SY-1-50

tert-Butyl 6,6-dichloro-3-azabicyclo[3.1.0]hexane-3-carboxylate 113

113

A solution of NaOH (2.4 g, 59.1 mmol, 10 eq) in H_2O (2.4 mL) was added dropwise to a stirred solution of *N*-Boc pyrroline **67** (1.0 g, 5.91 mmol, 1.0 eq) and $BnEt_3N^+Cl^-$ (0.24 g, 1.1 mmol, 0.2 eq) in $CHCl_3$ (22 mL) at rt under Ar. The resulting mixture was stirred vigorously and heated at 50 °C for 3 h and then at rt for 16 h. The resulting solution was poured into H_2O (50 mL) and extracted with CH_2Cl_2 (3 × 50 mL). The combined organics were dried ($MgSO_4$), filtered, and evaporated under reduced pressure to give the crude product. Purification by flash column chromatography on silica with 80:20 hexane–EtOAc as eluent gave dichlorocyclopropane **113** (780 mg, 52%) as a pale-yellow solid, mp 56 – 58 °C; R_F (80:20 hexane–EtOAc) 0.45; IR (ATR) 2976, 2934, 2884, 1693 (C=O), 1391, 1366, 1172, 1115, 885, 831, 794, 555 cm^{-1}; ^{1}H NMR (400 MHz, $CDCl_3$) δ 3.75 – 3.68 (m, 1H, NCH), 3.67 – 3.55 (m, 3H, NCH), 2.36 – 2.26 (m, 2H, CH), 1.43 (s, 9H, CMe_3); ^{13}C NMR (100.6 MHz, $CDCl_3$) δ 153.8 (C=O), 80.0 (O*C*Me$_3$), 64.5 (CCl_2), 47.37 (NCH_2), 47.30 (NCH_2), 34.7 (CH_2), 33.9 (CH_2), 28.6 (C*Me*$_3$); MS (ESI) *m/z* 274 [(^{35,35}M + Na)$^+$, 100], HRMS ESI *m/z* calcd for $C_{10}H_{15}{}^{35}Cl_2NO_2$ [(^{35,35}M + Na)$^+$, 100] 274.0372, found 274.0376 (–1.4 ppm error).

Lab Book Reference: SY-1-33

***tert*-Butyl 6-(4,4,5,5-tetramethyl-1,3,2-dioxaborolan-2-yl)-3-azabicyclo[3.1.0] hexane-3-carboxylate *endo*-112**

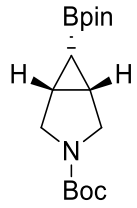

endo-**112**

s-BuLi (0.93 mL, of a 1.29 M solution in cyclohexane, 1.2 mmol, 1.2 eq) was added dropwise to a stirred solution of dichlorocyclopropane **113** (0.25 g, 1.0 mmol, 1.0 eq) and H–Bpin (0.18 mL, 1.2 mmol, 1.2 eq.) in THF (10 mL) at –78 °C under Ar. The resulting mixture was stirred at –78 °C for 30 min. The cooling bath was removed, and the reaction was stirred for 1.5 h, and then cooled to 0 °C and saturated $NH_4Cl_{(aq)}$ (20 mL) was added. The mixture was extracted with EtOAc (3 × 20 mL), and the combined organics dried ($MgSO_4$), filtered, and evaporated under reduced pressure to give the crude product. Purification by flash column chromatography on silica using 90:10 hexane–EtOAc as eluent gave cyclopropyl Bpin *endo*-**112** with impurities (13 mg, 5% yield estimated by ^{1}H NMR spectroscopy) as a viscous colourless oil, ^{1}H NMR (400 MHz, $CDCl_3$) δ 3.65 – 3.49 (m, 4H, NCH), 1.67 (dd, J = 9.0, 3.0 Hz, 2H, CH), 1.41 (s, 9H, CMe_3), 1.21 (s, 12H, CMe_2), 0.10 (dd, J = 9.0, 9.0 Hz, 1H, BCH); HRMS ESI *m/z* calcd for $C_{16}H_{29}BNO_4$ $(M + Na)^+$ 332.2004, found 332.2004 (+0.0 ppm error).

Lab Book Reference: SY-1-37

***tert*-Butyl 3-methylenepyrrolidine-1-carboxylate 114**

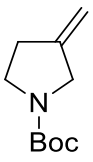

114

KO*t*-Bu (3.96 g, 32.4 mmol, 1.2 eq.) was added to a stirred suspension of methyltriphenylphosphonium bromide (11.3 g, 32.4 mmol, 1.2 eq.) in THF (60 mL) at 0 °C under Ar. The resulting mixture was stirred at 0 °C for 1 h. Then, a solution of *N*-Boc

pyrrolidinone **117** (5.00 g, 27.0 mmol, 1.0 eq.) in THF (30 mL) was added at 0 °C. After being allowed to warm to rt, the mixture was stirred at rt for 16 h. The mixture was poured into H_2O (100 mL) and the two layers were separated. The aqueous layer was extracted with Et_2O (3 × 100 mL). The combined organic layers were dried ($MgSO_4$), filtered, and evaporated under reduced pressure to give the crude product. Purification by flash column chromatography on silica using 80:20 hexane–EtOAc as eluent gave alkene **114** (3.9 g, 79%) as a pale-yellow oil, R_F (80:20 hexane–EtOAc) 0.48; IR (ATR) 2978, 2934, 2897, 1687 (C=O), 1391, 1367, 1253, 1159, 890, 775, 730 cm^{-1}; ^1H NMR (400 MHz, $CDCl_3$) δ 5.00 – 4.91 (m, 2H, C=CH_2), 3.96 – 3.88 (m, 2H, NCH_2), 3.50 – 3.41 (m, 2H, NCH_2), 2.58 – 2.52 (m, 2H, CH_2), 1.46 (s, 9H, CMe_3). ^{13}C NMR (100.6 MHz, $CDCl_3$) δ 154.5 (C=O), 146.1 (*C*=CH_2), 145.2 (*C*=CH_2), 106.7 (C=*C*H_2), 106.6 (C=*C*H_2), 79.3 (O*C*Me_3), 50.4 (NCH), 50.1 (NCH), 45.9 (NCH), 45.4 (NCH), 32.2 (CH), 31.5 (CH), 28.5 (C*Me*3); MS (ESI) *m/z* 206 [$(M + Na)^+$, 100], HRMS ESI *m/z* calcd for $C_{10}H_{17}NO_2$ [$(M + Na)^+$, 100] 206.1151, found 206.1155 (–1.8 ppm error). Spectroscopic data consistent with those reported in the literature.[108]

Lab Book Reference: SY-2-28

KO*t*-Bu (15.8 g, 130 mmol, 1.2 eq.) was added to a stirred suspension of methyltriphenylphosphonium bromide (45.4 g, 130 mmol, 1.2 eq.) in THF (150 mL) at 0 °C under Ar. The resulting mixture was stirred at 0 °C for 1 h. Then, a solution of *N*-Boc pyrrolidinone **117** (20.0 g, 108 mmol, 1.0 eq.) in THF (100 mL) was added at 0 °C. After being allowed to warm to rt, the mixture was stirred at rt for 16 h. The mixture was poured into H_2O (150 mL) and the two layers were separated. The aqueous layer was extracted with Et_2O (3 × 150 mL). The combined organic layers were dried ($MgSO_4$), filtered, and evaporated under reduced pressure to give the crude product. Purification by flash column chromatography on silica using 90:10 hexane–EtOAc as eluent gave alkene **114** (11.1 g, 56%) as a pale-yellow oil.

Lab Book Reference: SY-2-117

***tert*-Butyl 1,1-dibromo-5-azaspiro[2.4]heptane-5-carboxylate 115**

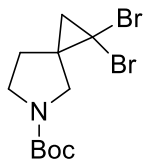

115

A solution of NaOH (93.6 g, 2.34 mol, 39.0 eq.) in H_2O (94 mL) was added to a stirred solution of alkene **114** (11.0 g, 60.0 mmol, 1.0 eq.) and $BnEt_3N^+Cl^-$ (2.46 g, 10.8 mmol, 0.18 eq.) in CH_2Cl_2 (200 mL) at rt under Ar. Then, bromoform (7.4 mL, 84.0 mmol, 1.4 eq.) was added dropwise. The resulting mixture was stirred vigorously and heated at 50 °C for 16 h. After being allowed to cool to rt, the mixture was poured into H_2O (200 mL) and extracted with CH_2Cl_2 (3 × 200 mL). The combined organics were dried ($MgSO_4$), filtered, and evaporated under reduced pressure to give the crude product. Purification by flash column chromatography on silica using 90:10 hexane–EtOAc as eluent gave dibromocyclopropane **115** (14.7 g, 69%) as an off-white solid, mp 64 – 66 °C; R_F (90:10 hexane–EtOAc) 0.26; IR (ATR) 2976, 2930, 2873, 1691, 1397, 1365, 1246, 1167, 1112, 1036, 877, 771, 687 cm^{-1}; ^1H NMR (400 MHz, $CDCl_3$) (50:50 mixture of rotamers) δ 3.85 – 3.46 (m, 3H, NCH), 3.32 (d, J = 11.5 Hz, 0.5H, NCH), 3.24 (d, J = 11.5 Hz, 0.5H, NCH), 2.49 – 2.35 (m, 1H, CH), 1.86 – 1.70 (m, 3H, CH), 1.47 (s, 9H, CMe_3); ^{13}C NMR (100.6 MHz, $CDCl_3$) (rotamers) δ 154.3 (C=O), 79.9 (O*C*Me_3), 53.8 (NCH_2), 53.6 (NCH_2), 46.4 (NCH_2), 46.0 (NCH_2), 36.3 (C), 35.6 (C), 35.0 (CBr_2), 34.4 (CH_2), 34.3 (CBr_2), 31.5 (CH_2), 28.6 (C*Me*$_3$); MS (ESI) *m/z* 376 [(^{79,79}M + Na)$^+$, 100], HRMS (ESI) *m/z* calcd for $C_{11}H_{18}{}^{79}Br_2NO_2$ (^{79,79}M + Na)$^+$ 375.9518, found 375.9515 (+0.8 ppm error).

Lab Book Reference: SY-2-120

***tert*-Butyl 1-bromo-5-azaspiro[2.4]heptane-5-carboxylates *trans*-116 and *cis*-116**

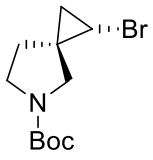

trans-**116**

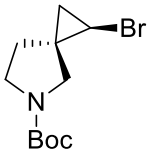

cis-**116**

KO*t*-Bu (29.3 g, 0.261 mol, 6.0 eq.) was added portion wise to a stirred solution of dibromocyclopropane **115** (15.45 g, 43.5 mmol, 1.0 eq.) and dimethyl phosphite (23.9 mL, 0.261 mol, 6.0 eq.) in anhydrous DMSO (200 mL) at 0 °C under Ar. The resulting solution was stirred at rt for 1.5 h. Then, Et_2O (100 mL, chilled to 0 °C) and saturated $NaHCO_{3(aq)}$ (100 mL) were added. A white precipitate formed, and additional H_2O (~100 mL) was added to redissolve the solids. The two layers were separated, and the aqueous layer was extracted with Et_2O (3 × 150 mL). The combined organic layers were dried ($MgSO_4$), filtered, and evaporated under reduced pressure to give the crude product which contained a 55:45 mixture (by ^{1}H NMR spectroscopy) of monobromocyclopropanes *trans*-**116** and *cis*-**116**. Purification by flash column chromatography on silica using 90:10 hexane–EtOAc as eluent gave monobromocyclopropane *trans*-**116** (5.82 g, 48%) as a pale yellow oil, R_F (90:10 hexane–EtOAc) 0.38; IR (ATR) 2977, 2934, 2871, 1696, 1403, 1366, 1171, 1112, 882, 772 cm^{-1}; ^{1}H NMR (400 MHz, $CDCl_3$) δ 3.60 – 3.38 (m, 2H, NCH), 3.34 – 3.18 (m, 2H, NCH), 3.07 – 3.02 (m, 1H, BrCH), 2.13 (ddd, J = 13.0, 7.5, 5.0 Hz, 1H, CH), 1.97 – 1.84 (m, 1H, CH), 1.46 (s, 9H, CMe_3), 1.39 – 1.29 (m, 1H, CH), 0.93 (dd, J = 7.0, 4.5 Hz, 1H, CHBr); ^{13}C NMR (100.6 MHz, $CDCl_3$) (rotamers) δ 154.4 (C=O), 154.2 (C=O), 79.4 (O*C*Me$_3$), 53.0 (NCH_2), 52.5 (NCH_2), 45.8 (NCH_2), 45.4 (NCH_2), 31.9 (CH_2), 31.2 (C), 28.5 (C*Me*$_3$), 26.9 (CH_2), 26.6 (CH_2), 19.8 (CH), 19.5 (CH); MS (ESI) *m/z* 298 [(M + Na)$^+$, 100]; HRMS (ESI) *m/z* calcd for $C_{11}H_{18}{}^{79}BrNO_2$ (^{79}M + Na)$^+$ 298.0413, found 298.0412 (+0.3 ppm error), a 55:45 mixture of monobromocyclopropanes *trans*-**116** and *cis*-**116** (610 mg, 5%) as an oil and monobromocyclopropane *cis*-**116** (4.24 g, 35%) as an off-white crystalline solid, mp 49 – 50 °C; R_F (90:10 hexane–EtOAc) 0.29; IR (ATR) 2975, 2934, 2873, 1693, 1402, 1366, 1170, 1111, 884, 771 cm^{-1}; ^{1}H NMR (400 MHz, $CDCl_3$) δ 3.67 – 3.45 (m, 3H, NCH), 3.41 – 3.27 (m, 1H, NCH), 3.00 (dd, J = 8.0, 4.5 Hz, 1H, BrCH), 1.87 – 1.79 (m, 2H, CH), 1.47 (s, 9H, CMe_3), 1.37 – 1.29 (m, 1H, CH), 1.01 – 0.97 (m, 1H, CH); ^{13}C NMR (100.6 MHz, $CDCl_3$) (rotamers) δ 154.5 (C=O), 79.5 (O*C*Me$_3$), 51.8 (NCH_2), 51.6 (NCH_2), 46.2 (NCH_2), 45.8 (NCH_2), 34.0 (CH_2), 33.3 (C),

28.6 (C*Me*$_3$), 26.0 (CH), 25.7 (CH), 20.7 (CH_2), 20.5 (CH_2); MS (ESI) *m/z* 298 [(^{79}M + Na)$^+$, 100]; HRMS (ESI) *m/z* calcd for $C_{11}H_{18}{}^{79}BrNO_2$ (M + Na)$^+$ 298.0413, found 298.0412 (+0.3 ppm error).

Lab Book Reference: SY-2-127

tert-Butyl 1-(4,4,5,5-tetramethyl-1,3,2-dioxaborolan-2-yl)-5-azaspiro[2.4] heptane-5-carboxylate _trans_-119

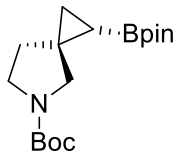

trans-**119**

n-BuLi (0.61 mL of a 2.44 M solution in hexane, 1.5 mmol, 1.5 eq.) was added dropwise to a stirred solution of monobromocyclopropane *trans*-**116** (280 mg, 1.0 mmol, 1.0 eq.) in THF (12 mL) at –78 °C under Ar. The resulting solution was stirred at –78 °C for 1 h. Then, *i*-PrO–Bpin (0.31 mL, 1.5 mmol, 1.5 eq.) was added and the solution was stirred at –78 °C for 10 min. After being allowed to warm to rt, saturated $NH_4Cl_{(aq)}$ (15 mL) was added, and the two layers were separated. The aqueous layer was extracted with Et_2O (3 × 20 mL). The combined organic layers were dried ($MgSO_4$), filtered, and evaporated under reduced pressure to give the crude product. Purification by flash column chromatography on silica using 90:10 hexane–Et_2O as eluent gave cyclopropyl Bpin *trans*-**119** (230 mg, 71%) as a white solid, mp 73 – 75 °C; R_F (90:10 hexane–Et_2O) 0.16; IR (ATR) 2977, 2933, 2870, 1696 (C=O), 1402, 1361, 1322, 1169, 1145, 1108, 858 cm^{-1}; ^{1}H NMR (400 MHz, $CDCl_3$) (50:50 mixture of rotamers) δ 3.54 – 3.37 (m, 2H, NCH), 3.28 (d, *J* = 10.5 Hz, 0.5H NCH), 3.24 (d, *J* = 10.5 Hz, 0.5H, NCH), 3.17 (d, *J* = 10.5 Hz, 0.5H, NCH), 3.11 (d, *J* = 10.5 Hz, 0.5H, NCH), 2.02 – 1.91 (m, 1H, CH), 1.88 – 1.77 (m, 1H, CH), 1.45 (s, 9H, CMe_3), 1.22 (s, 12H, CMe_2), 0.99 – 0.77 (m, 2H, CH), 0.15 – 0.03 (m, 1H, BCH); ^{13}C NMR (100.6 MHz, $CDCl_3$) (rotamers) δ 154.6 (C=O), 83.3 (O*C*Me$_2$), 79.1 (O*C*Me$_3$), 55.0 (NCH_2), 54.6 (NCH_2), 46.5 (NCH_2), 46.1 (NCH_2), 31.8 (CH_2), 31.1 (CH_2), 28.7 (C*Me*$_3$), 28.6 (C), 28.0 (C), 25.2 (C*Me*), 24.7 (C*Me*), 24.6 (C*Me*), 17.2 (CH_2), (BCH not resolved); MS (ESI) *m/z* 346 [(M + Na)$^+$, 100]; HRMS (ESI) *m/z* calcd for $C_{17}H_{30}BNO_4$ (M + Na)$^+$ 346.2160, found 346.2161 (+0.2 ppm error).

Lab Book Reference: SY-2-36

n-BuLi (20.8 mL of a 1.52 M solution in hexane, 31.6 mmol, 1.5 eq.) was added dropwise to a stirred solution of monobromocyclopropane *trans*-**116** (5.82 g, 21.1 mmol, 1.0 eq.) in THF (100 mL) at –78 °C under Ar. The resulting solution was stirred at –78 °C for 1 h. Then, *i*-PrO–Bpin (6.5 mL, 31.6 mmol, 1.5 eq.) was added and the solution was stirred at –78 °C for 10 min. After being allowed to warm to rt, saturated $NH_4Cl_{(aq)}$ (100 mL) was added, and the two layers were separated. The aqueous layer was extracted with Et_2O (3 × 100 mL). The combined organic layers were dried ($MgSO_4$), filtered, and evaporated under reduced pressure to give the crude product. Purification by flash column chromatography on silica using 90:10 hexane–Et_2O as eluent gave cyclopropyl Bpin *trans*-**119** (4.01 g, 59%) as a white solid.

Lab Book Reference: SY-2-132

tert-Butyl 1-(4,4,5,5-tetramethyl-1,3,2-dioxaborolan-2-yl)-5-azaspiro[2.4] heptane-5-carboxylate _cis_-119

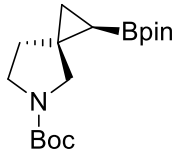

cis-**119**

n-BuLi (13.1 mL of a 1.50 M solution in hexane, 19.7 mmol, 1.5 eq.) was added dropwise to a stirred solution of monobromocyclopropane *cis*-**116** (3.62 g, 13.1 mmol, 1.0 eq.) in THF (200 mL) at –78 °C under Ar. The resulting solution was stirred at – 78 °C for 1 h. Then, *i*-PrO–Bpin (4.0 mL, 19.7 mmol, 1.5 eq.) was added and the solution was stirred at –78 °C for 10 min. After being allowed to warm to rt, saturated $NH_4Cl_{(aq)}$ (100 mL) was added, and the two layers were separated. The aqueous layer was extracted with Et_2O (3 × 100 mL). The combined organic layers were dried ($MgSO_4$), filtered, and evaporated under reduced pressure to give the crude product. Purification by flash column chromatography on silica using 90:10 hexane–Et_2O as eluent gave cyclopropyl Bpin *cis*-**119** (3.01 g, 71%) as a white solid, mp 48 – 50 °C; R_F (90:10 hexane–Et_2O) 0.10; IR (ATR) 2976, 2933, 2869, 1694 (C=O), 1402, 1363, 1322, 1259, 1168, 1144, 1109, 859 cm^{-1}; ^1H NMR (400 MHz, $CDCl_3$) δ 3.52 – 3.44 (m, 1H, NCH), 3.43 – 3.35 (m, 2H, NCH), 3.25 (d, J = 11.0 Hz, 1H, NCH), 2.02 – 1.88 (m, 1H, CH), 1.65 – 1.55 (m, 1H,

CH), 1.45 (s, 9H, CMe_3), 1.21 (s, 6H, CMe), 1.21 (s, 6H, CMe), 0.91 – 0.74 (m, 2H, CH), 0.09 (dd, J = 9.5, 7.0 Hz, 1H, CH); ^{13}C NMR (100.6 MHz, $CDCl_3$) δ 154.7 (C=O), 83.4 ($OCMe_2$), 79.0 ($OCMe_3$), 51.5 (NCH), 45.6 (NCH_2), 35.6 (CH_2), 28.7 (CMe_3), 25.3 (C*Me*), 25.0 (C), 24.9 (C), 24.6 (C*Me*) (BCH not resolved); MS (ESI) *m/z* 346 [(M + Na)$^+$, 100]; HRMS (ESI) *m/z* calcd for $C_{17}H_{30}BNO_4$ (M + Na)$^+$ 346.2160, found 346.2165 (–0.6 ppm error).

Lab Book Reference: SY-2-77

tert-Butyl 1-(6-methyl-4,8-dioxo-1,3,6,2-dioxazaborocan-2-yl)-5-azaspiro[2.4] heptane-5-carboxylate _trans_-38

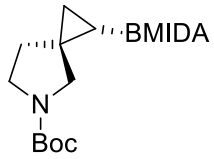

trans-**38**

MIDA (956 mg, 6.5 mmol, 6.5 eq.) and $HC(OEt)_3$ (0.75 mL, 4.5 mmol, 4.5 eq.) were added to a stirred solution of cyclopropyl Bpin *trans*-**119** (323 mg, 1.0 mmol, 1.0 eq.) in anhydrous DMSO (5 mL) at rt under Ar. The resulting mixture was stirred and heated at 100 °C for 48 h. After being allowed to cool to rt, saturated $NH_4Cl_{(aq)}$ (15 mL) was added, and the mixture was extracted with EtOAc (3 × 15 mL). The combined organic extracts were washed with brine (10 mL), dried ($MgSO_4$), filtered, and evaporated under reduced pressure to give the crude product. Purification by flash column chromatography on silica with 70:30 to 60:40 CH_2Cl_2–acetone as eluent gave cyclopropyl BMIDA *trans*-**38** (284 mg, 81%) as an off-white solid, mp 222 – 224 °C; R_F (70:30 CH_2Cl_2–acetone) 0.23; IR (ATR) 2975, 2873, 1759 (C=O, ester), 1682 (C=O, Boc), 1411, 1345, 1298, 1162, 1130, 1024, 996, 893 cm^{-1}; ^{1}H NMR (400 MHz, $CDCl_3$) (60:40 mixture of rotamers) δ 3.92 – 3.84 (m, 2H, NCHC=O), 3.79 – 3.66 (m, 2H, NCHC=O), 3.63 – 3.47 (m, 1H, NCH), 3.43 – 3.33 (m, 2H, NCH), 3.16 – 3.05 (m, 1H, NCH), 3.03 (s, 3H, NMe), 2.11 – 1.99 (m, 1H, CH), 1.85 – 1.75 (m, 1H, CH), 1.46 (s, 5.4H, CMe_3), 1.44 (s, 3.6H, CMe_3), 0.81 – 0.74 (m, 1H, CH), 0.52 – 0.47 (m, 1H, CH), -0.03 – -0.15 (m, 1H, BCH); ^{13}C NMR (100.6 MHz, $CDCl_3$) (rotamers) δ 167.2 (C=O, ester), 167.1 (C=O, ester), 154.7 (C=O, Boc), 154.5 (C=O, Boc), 79.2 ($OCMe_3$), 62.0 ($NCH_2C(O)$), 61.9 ($NCH_2C(O)$), 55.6 (NCH_2),

55.2 (NCH_2), 46.7 (NCH_2), 46.5 (NMe), 31.0 (CH_2), 30.4 (CH_2), 28.7 (C*Me*$_3$), 26.2 (C), 25.5 (C), 16.0 (CH_2), 15.6 (CH_2) (BCH not resolved); MS (ESI) *m/z* 375 [$(M + Na)^+$, 100]; HRMS (ESI) m/z calcd for $C_{16}H_{25}BN_2O_6$ [$(M + Na)^+$, 100] 375.1698, found 375.1699 (+0.4 ppm error).

Lab Book Reference: SY-2-76

MIDA (15.69 g, 106.7 mmol, 6.5 eq.) and $HC(OEt)_3$ (12.3 mL, 73.8 mmol, 4.5 eq.) were added to a stirred solution of cyclopropyl Bpin *trans*-**119** (5.30 g, 16.4 mmol, 1.0 eq.) in anhydrous DMSO (200 mL) at rt under Ar. The resulting mixture was stirred and heated at 100 °C for 48 h. After being allowed to cool to rt, saturated $NH_4Cl_{(aq)}$ (60 mL) was added, and the mixture was extracted with EtOAc (3 × 50 mL). The combined organic extracts were washed with brine (50 mL), dried ($MgSO_4$), filtered, and evaporated under reduced pressure to give the crude product. Purification by flash column chromatography on silica with 90:10 to 60:40 CH_2Cl_2–acetone as eluent gave cyclopropyl BMIDA *trans*-**38** (4.27 g, 74%) as an off-white solid.

Lab Book Reference: SY-2-202

***tert*-Butyl 1-(6-methyl-4,8-dioxo-1,3,6,2-dioxazaborocan-2-yl)-5-azaspiro[2.4] heptane-5-carboxylate *cis*-38**

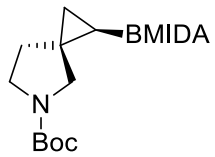

cis-**38**

MIDA (11.82 g, 80.3 mmol, 6.5 eq.) and $HC(OEt)_3$ (9.3 mL, 55.6 mmol, 4.5 eq.) were added to a stirred solution of cyclopropyl Bpin *cis*-**119** (4.0 g, 12.4 mmol, 1.0 eq.) in anhydrous DMSO (80 mL) at rt under Ar. The resulting mixture was stirred and heated at 100 °C for 48 h. After being allowed to cool to rt, saturated $NH_4Cl_{(aq)}$ (60 mL) was added, and the mixture was extracted with EtOAc (3 × 60 mL). The combined organic extracts were washed with brine (60 mL), dried ($MgSO_4$), filtered, and evaporated under reduced pressure to give the crude product. Purification by flash column chromatography

on silica with 95:5 to 80:20 CH_2Cl_2–acetone as eluent gave cyclopropyl BMIDA *cis*-**38** (3.92 g, 90%) as an off-white solid, mp 200 – 203 °C; R_F (70:30 CH_2Cl_2–acetone) 0.26; IR (ATR) 2974, 2938, 2874, 1758 (C=O, ester), 1680 (C=O, Boc), 1410, 1342, 1296, 1167, 1116, 1026, 1002, 885 cm^{-1}; ^1H NMR (400 MHz, $CDCl_3$) (50:50 mixture of rotamers) δ 4.03 (d, J = 16.5 Hz, 1H, MeNC*H*), 3.95 (d, J = 16.5 Hz, 0.5H, MeNC*H*), 3.93 (d, J = 16.5 Hz, 0.5H, MeNC*H*), 3.84 (d, J = 16.5 Hz, 0.5H, MeNC*H*), 3.80 (d, J = 16.5 Hz, 0.5H, MeNC*H*), 3.76 (d, J = 16.5 Hz, 1H, MeNC*H*), 3.56 – 3.43 (m, 1H, NCH), 3.41 (d, J = 11.0 Hz, 1H, NCH), 3.39 – 3.29 (m, 1H NCH), 3.21 (d, J = 11.0, 0.5H, NCH), 3.20 (d, J = 11.0, 0.5H, NCH), 3.05 (s, 3H, NMe), 2.15 – 1.99 (m, 1H, CH), 1.53 – 1.47 (m, 1H, CH), 1.44 (s, 9H, CMe_3), 0.72 (dd, J = 9.5, 3.5 Hz, 1H, CH), 0.53 – 0.46 (m, 1H, CH), –0.01 – –0.10 (m, 1H, BCH); ^{13}C NMR (100.6 MHz, $CDCl_3$) (rotamers) δ 168.3 (C=O, ester), 167.8 (C=O, ester), 154.7 (C=O, Boc), 79.1 (O*C*Me_3), 62.1 ($NCH_2C(O)$), 51.2 (NCH_2), 50.9 (NCH_2), 46.5 (NMe), 45.5 (NCH_2), 36.4 (CH_2), 36.0 (CH_2), 28.7 (C*Me*$_3$), 26.1 (C), 25.3 (C), 16.7 (CH_2), 16.3 (CH_2) (BCH not resolved); MS (ESI) *m/z* 375 [$(M + Na)^+$, 100]; HRMS (ESI) m/z calcd for $C_{16}H_{25}BN_2O_6$ [$(M + Na)^+$, 100] 375.1698, found 375.1701 (+0.1 ppm error).

Lab Book Reference: SY-2-79

MIDA (956 mg, 6.5 mmol, 6.5 eq.) and $HC(OEt)_3$ (0.7 mL, 4.5 mmol, 4.5 eq.) were added to a stirred solution of cyclopropyl Bpin *cis*-**119** (323 mg, 1.0 mmol, 1.0 eq.) in anhydrous DMSO (10 mL) at rt under Ar. The resulting mixture was stirred and heated at 100 °C for 48 h. After being allowed to cool to rt, saturated $NH_4Cl_{(aq)}$ (20 mL) was added, and the mixture was extracted with EtOAc (3 × 20 mL). The combined organic extracts were washed with brine (20 mL), dried ($MgSO_4$), filtered, and evaporated under reduced pressure to give the crude product. Purification by flash column chromatography on silica with 80:20 to 70:30 CH_2Cl_2–acetone as eluent gave cyclopropyl BMIDA *cis*-**38** (300 mg, 85%) as an off-white solid.

Lab Book Reference: SY-2-78

***tert*-Butyl 1,1-dichloro-5-azaspiro[2.4]heptane-5-carboxylate 120**

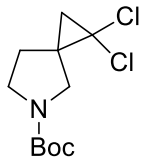

120

A solution of NaOH (2.32 g, 57.9 mmol, 10 eq) in H_2O (2.5 mL) was added dropwise to a stirred solution of alkene **114** (1.06 g, 5.79 mmol, 1.0 eq.) and $BnEt_3N^+Cl^-$ (237 mg, 1.04 mmol, 0.18 eq.) in $CHCl_3$ (20 mL) at rt under Ar. The resulting mixture was stirred vigorously and heated at 50 °C for 3 h and then at rt for 16 h. The resulting solution was poured into H_2O (50 mL) and extracted with CH_2Cl_2 (3 × 50 mL). The combined organics were dried ($NaSO_4$), filtered, and evaporated under reduced pressure to give the crude product. Purification by flash column chromatography on silica using 90:10 hexane–Et_2O as eluent gave dichlorocyclopropane **120** (1.10 g, 72%) as an off-white solid, R_F (80:20 hexane–Et_2O) 0.42; IR (ATR) 2978, 1785, 1694 (C=O), 1392, 1367, 1311, 1251, 1161, 1117, 1051, 878, 765 cm^{-1}; ^1H NMR (400 MHz, $CDCl_3$) δ 3.80 – 3.65 (m, 1H, NCH), 3.64 – 3.45 (m, 2H, NCH), 3.33 – 3.19 (m, 1H, NCH), 2.39 – 2.28 (m, 1H, CH), 1.88 – 1.75 (m, 1H, CH), 1.54 – 1.47 (m, 2H, CH), 1.43 (s, 9H, CMe_3); ^{13}C NMR (100.6 MHz, $CDCl_3$) (rotamers) δ 154.2 (C=O), 79.7 (O*C*Me_3), 63.0 (CCl_2), 51.5 (NCH_2), 51.3 (NCH_2), 46.2 (NCH_2), 45.8 (NCH_2), 36.6 (CH_2), 35.9 (CH_2), 32.5 (C), 31.9 (C), 31.4 (CH_2), 28.5 (C*Me*$_3$); MS (ESI) *m/z* 288 [(^{35,35}M + Na)$^+$, 100], HRMS ESI *m/z* calcd for $C_{11}H_{17}{}^{35}Cl_2NO_2$ [(^{35,35}M + Na)$^+$, 100] 288.0529, found 288.0532 (–1.1 ppm error).

Lab Book Reference: SY-2-171

***tert*-Butyl 1-(4,4,5,5-tetramethyl-1,3,2-dioxaborolan-2-yl)-5-azaspiro[2.4] heptane-5-carboxylate *trans*-119 and *cis*-119**

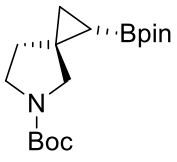

trans-**119**

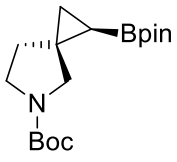

cis-**119**

s-BuLi (4.0 mL, of a 1.16 M solution in cyclohexane, 4.61 mmol, 1.2 eq) was added dropwise to a stirred solution of dichlorocyclopropane **120** (1.02 g, 3.84 mmol, 1.0 eq.) and H–Bpin (0.7 mL, 4.61 mmol, 1.2 eq.) in THF (20 mL) at –78 °C under Ar. The resulting mixture was stirred at –78 °C for 30 min. The cooling bath was removed, and the reaction was stirred for 1.5 h, and then cooled to 0 °C and saturated $NH_4Cl_{(aq)}$ (50 mL) was added. The mixture was extracted with EtOAc (3 × 50 mL), and the combined organics dried ($NaSO_4$), filtered, and evaporated under reduced pressure to give the crude product. Purification by flash column chromatography on silica using 90:10 hexane–EtOAc as eluent gave an inseparable mixture of cyclopropyl Bpin *trans*-**119** and *cis*-**119** (868 mg, 70%) as a viscous colourless oil.

Lab Book Reference: SY-2-176

Experimental Procedures for Chapter 3

tert-Butyl 7-(pyrimidin-5-yl)-2-azabicyclo[4.1.0]heptane-2-carboxylate *exo*-166

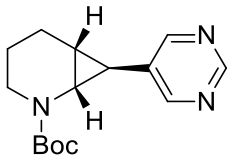

exo-**166**

Using general procedure A, cyclopropyl BMIDA *exo*-**36** (176 mg, 0.5 mmol, 1.0 eq.), 5-bromopyrimidine (111 mg, 0.7 mmol, 1.4 eq.), PCy_3 (42 mg, 0.15 mmol, 0.30 eq.), Cs_2CO_3 (977 mg, 3.0 mmol, 6.0 eq.) and $Pd(OAc)_2$ (17 mg, 75 μmol, 0.15 eq.) in toluene (5.0 mL) and H_2O (0.5 mL) gave the crude product. Purification by flash column chromatography on silica with EtOAc as eluent gave cyclopropyl pyrimidine *exo*-**166** (108 mg, 78%) as an off-white solid, mp 89 – 91 °C; R_F (EtOAc) 0.20; IR (ATR) 2975, 2933, 2863, 1690 (C=O), 1557, 1410, 1386, 1364, 1159, 1132, 1040, 727, 631 cm^{-1}; ^1H NMR (400 MHz, $CDCl_3$) (70:30 mixture of rotamers) δ 9.00 (s, 0.7H, Ar), 8.98 (s, 0.3H, Ar), 8.49 (s, 0.6H, Ar), 8.47 (s, 1.4H, Ar), 3.86 (ddd, J = 12.5, 4.0, 4.0 Hz, 0.7H, NCH), 3.69 (ddd, J = 12.5, 4.0, 4.0 Hz, 0.3H, NCH), 3.17 (dd, J = 8.5, 3.0 Hz, 0.3H, NCH), 3.01 (dd, J = 8.5, 3.0 Hz, 0.7H, NCH), 2.71 (ddd, J = 12.5, 12.5, 2.5 Hz, 0.3H, NCH), 2.59 (ddd, J = 12.5, 12.5 , 2.5 Hz, 0.8H, NCH), 2.06 – 1.98 (m, 1H, CH), 1.97 – 1.84 (m, 1H, CH), 1.75 – 1.62 (m, 3H, CH), 1.44 (s, 2.7H, CMe_3), 1.43 – 1.37 (m, 1H, CH), 1.35 (s, 6.3H, CMe_3); ^{13}C NMR (100.6 MHz, $CDCl_3$) (rotamers) δ 156.5 (C=O), 156.3 (C=O), 156.1 (Ar), 155.8 (Ar), 154.6 (Ar), 154.5 (Ar), 134.8 (*ipso*-Ar), 134.7 (*ipso*-Ar), 80.1 (O*C*Me_3), 40.40 (NCH_2), 40.36 (NCH_2), 38.9 (NCH), 38.8 (NCH), 28.59 (C*Me*$_3$), 28.55 (C*Me*$_3$), 24.8 (CH), 24.1 (CH), 22.2 (CH_2), 22.0 (CH_2), 21.8 (CH), 20.4 (CH_2); MS (ESI) *m/z* 298 [$(M + Na)^+$, 100]; HRMS (ESI) *m/z* calcd for $C_{15}H_{21}N_3O_2$ $(M + Na)^+$ 298.1526, found 298.1529 (–1.0 ppm error).

Lab Book Reference: SY-3-86

Using general procedure B, cyclopropyl BMIDA *exo*-**36** (88 mg, 0.25 mmol, 1.0 eq.), 5-bromopyrimidine (56 mg, 0.35 mmol, 1.4 eq.), PCy_3 (7 mg, 25 μmol, 0.10 eq.), Cs_2CO_3 (490 mg, 1.5 mmol, 3.0 eq.) and $Pd(OAc)_2$ (3 mg, 13 μmol, 0.05 eq.) in toluene (5.0 mL) and H_2O (0.5 mL) gave the crude product. Purification by flash column chromatography

on silica with EtOAc as eluent gave cyclopropyl pyrimidine *exo*-**166** (50 mg, 73%) as an off-white solid.

Lab Book Reference: SY-3-102

Using general procedure B, cyclopropyl BMIDA *exo*-**36** (88 mg, 0.25 mmol, 1.0 eq.), 5-bromopyrimidine (56 mg, 0.35 mmol, 1.4 eq.), PCy_3 (3.5 mg, 12.5 μmol, 0.05 eq.), Cs_2CO_3 (490 mg, 1.5 mmol, 6.0 eq.) and $Pd(OAc)_2$ (1.4 mg, 6.3 μmol, 0.025 eq.) in toluene (5.0 mL) and H_2O (0.5 mL) gave the crude product. Purification by flash column chromatography on silica with EtOAc as eluent gave cyclopropyl pyrimidine *exo*-**166** (60 mg, 87%) as an off-white solid.

Lab Book Reference: SY-3-104

Using general procedure B, cyclopropyl BMIDA *exo*-**36** (88 mg, 0.25 mmol, 1.0 eq.), 5-bromopyrimidine (56 mg, 0.35 mmol, 1.4 eq.), PCy_3 (3.5 mg, 12.5 μmol, 0.05 eq.), Cs_2CO_3 (490 mg, 1.5 mmol, 6.0 eq.) and $Pd(OAc)_2$ (1.4 mg, 6.3 μmol, 0.025 eq.) in toluene (5.0 mL) and H_2O (0.5 mL) gave the crude product. Purification by flash column chromatography on silica with EtOAc as eluent gave cyclopropyl pyrimidine *exo*-**166** (58 mg, 84%) as an off-white solid.

Lab Book Reference: SY-3-177

Using general procedure B, cyclopropyl BMIDA *exo*-**36** (88 mg, 0.25 mmol, 1.0 eq.), 5-bromopyrimidine (56 mg, 0.35 mmol, 1.4 eq.), PCy_3 (1.4 mg, 5 μmol, 0.02 eq.), Cs_2CO_3 (490 mg, 1.5 mmol, 6.0 eq.) and $Pd(OAc)_2$ (0.6 mg, 2.5 μmol, 0.01 eq.) in toluene (5.0 mL) and H_2O (0.5 mL) gave the crude product. Purification by flash column chromatography on silica with EtOAc as eluent gave cyclopropyl pyrimidine *exo*-**166** (40 mg, 58%) as an off-white solid.

Lab Book Reference: SY-3-103

Using general procedure B, cyclopropyl BMIDA *exo*-**36** (88 mg, 0.25 mmol, 1.0 eq.), 5-bromopyrimidine (56 mg, 0.35 mmol, 1.4 eq.), PCy_3 (7 mg, 25 μmol, 0.10 eq.), Cs_2CO_3 (244 mg, 0.75 mmol, 3.0 eq.) and $Pd(OAc)_2$ (3 mg, 13 μmol, 0.05 eq.) in toluene (5.0 mL) and H_2O (0.5 mL) gave the crude product. Purification by flash column chromatography on silica with EtOAc as eluent gave cyclopropyl pyrimidine *exo*-**166** (50 mg, 73%) as an off-white solid.

Lab Book Reference: SY-3-107

Using general procedure B, cyclopropyl BMIDA *exo*-**36** (88 mg, 0.25 mmol, 1.0 eq.), 5-bromopyrimidine (56 mg, 0.35 mmol, 1.4 eq.), PCy_3 (3.5 mg, 12.5 μmol, 0.05 eq.), Cs_2CO_3 (244 mg, 0.75 mmol, 3.0 eq.) and $Pd(OAc)_2$ (1.4 mg, 6.3 μmol, 0.025 eq.) in toluene (5.0 mL) and H_2O (0.5 mL) gave the crude product. Purification by flash column chromatography on silica with EtOAc as eluent gave cyclopropyl pyrimidine *exo*-**166** (36 mg, 52%) as an off-white solid.

Lab Book Reference: SY-3-105

***tert*-Butyl 6-(pyrimidin-5-yl)-3-azabicyclo[3.1.0]hexane-3-carboxylate *exo*-170**

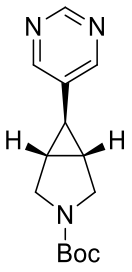

exo-**170**

Using general procedure A, cyclopropyl BMIDA *exo*-**39** (100 mg, 0.3 mmol, 1.0 eq.), 5-bromopyrimidine (66 mg, 0.41 mmol, 1.4 eq.), PCy_3 (25 mg, 0.09 mmol, 0.3 eq.), Cs_2CO_3 (579 mg, 1.8 mmol, 6.0 eq.) and $Pd(OAc)_2$ (10 mg, 0.04 mmol, 0.15 eq.) in toluene (3.1 mL) and H_2O (0.2 mL) gave crude the product. Purification by flash column chromatography on silica with EtOAc as eluent gave cyclopropyl pyrimidine *exo*-**170** (64 mg, 83%) as a colourless oil, R_F (EtOAc) 0.20; IR (ATR) 2975, 2931, 2872, 1690 (C=O), 1555, 1403, 1387, 1169, 1113, 1051, 727, 630, 552 cm^{-1}; ^1H NMR (400 MHz, $CDCl_3$)

(50:50 mixture of rotamers) δ 9.00 (s, 1H, Ar), 8.42 (s, 2H, Ar), 3.78 (d, J = 11.0 Hz, 1H, NCH), 3.70 (d, J = 11.0 Hz, 1H, NCH), 3.52 – 3.43 (m, 2H, NCH), 1.92 – 1.83 (m, 2H, CH), 1.68 (t, J = 3.5 Hz, 1H, CH), 1.43 (s, 9H, CMe_3); ^{13}C NMR (100.6 MHz, $CDCl_3$) (rotamers) δ 156.5 (Ar), 154.9 (C=O), 154.4 (Ar), 134.7 (*ipso*-Ar), 79.9 ($OCMe_3$), 48.5 (NCH_2), 48.3 (NCH_2), 28.5 (CMe_3), 27.2 (CH), 26.5 (CH), 22.1 (*C*HAr); MS (ESI) *m/z* 284 [$(M + Na)^+$, 100]; HRMS (ESI) *m/z* calcd for $C_{14}H_{19}N_3O_2$ $(M + Na)^+$ 284.1369, found 284.1375 (+1.9 ppm error).

Lab Book Reference: SY-1-51

Using general procedure B, cyclopropyl BMIDA *exo*-**39** (169 mg, 0.50 mmol, 1.0 eq.), 5-bromopyrimidine (111 mg, 0.70 mmol, 1.4 eq.), PCy_3 (14 mg, 50 μmol, 0.10 eq.), Cs_2CO_3 (490 mg, 1.50 mmol, 3.0 eq.) and $Pd(OAc)_2$ (6 mg, 25 μmol, 0.05 eq.) in toluene (5.0 mL) and H_2O (0.5 mL) gave the crude product. Purification by flash column chromatography on silica with 90:10 EtOAc–hexane as eluent gave cyclopropyl pyrimidine *exo*-**170** (71 mg, 54%) as a colourless oil.

Lab Book Reference: SY-1-110

tert-Butyl 1-(pyrimidin-5-yl)-5-azaspiro[2.4]heptane-5-carboxylate _trans_-171

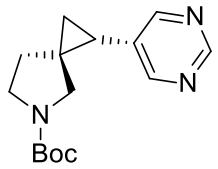

trans-**171**

Using general procedure A, cyclopropyl BMIDA *trans*-**38** (176 mg, 0.50 mmol, 1.0 eq.), 5-bromopyrimidine (111 mg, 0.70 mmol, 1.4 eq.), PCy_3 (42 mg, 0.15 mmol, 0.30 eq.), Cs_2CO_3 (977 mg, 3.0 mmol, 6.0 eq.) and $Pd(OAc)_2$ (17 mg, 75 μmol, 0.15 eq.) in toluene (5.0 mL) and H_2O (0.5 mL) gave the crude product. Purification by flash column chromatography on silica with EtOAc as eluent gave cyclopropyl pyrimidine *trans*-**171** (94 mg, 68%) as a pale-yellow oil, R_F (EtOAc) 0.24; IR (ATR) 2974, 2931, 2869, 1688 (C=O), 1554, 1398, 1166, 1107, 882, 771, 729, 631 cm^{-1}; ^1H NMR (400 MHz, $CDCl_3$) δ 9.05 (s, 1H, Ar), 8.52 (s, 2H, Ar), 3.51 – 3.35 (m, 3H, NCH), 3.34 – 3.21 (m, 1H, NCH),

2.13 – 2.04 (m, 1H, CH), 1.72 – 1.61 (m, 1H, CH), 1.50 – 1.40 (m, 1H, CH), 1.44 (s, 9H, CMe_3), 1.32 – 1.25 (m, 1H, CH), 1.20 (dd, J = 6.0, 6.0 Hz, 1H, CH); ^{13}C NMR (100.6 MHz, $CDCl_3$) (rotamers) δ 156.8 (Ar), 156.6 (Ar), 154.5 (C=O), 132.6 (*ipso*-Ar), 79.6 ($OCMe_3$), 54.5 (NCH_2), 54.0 (NCH_2), 45.9 (NCH_2), 45.5 (NCH_2), 30.1 (C), 29.5 (C), 28.6 (CMe_3), 22.4 (CH), 22.3 (CH), 15.4 (CH_2), 15.1 (CH_2); MS (ESI) *m/z* 298 [$(M + Na)^+$, 100]; HRMS (ESI) *m/z* calcd for $C_{15}H_{21}N_3O_2$ $(M + Na)^+$ 298.1526, found 298.1524 (+0.8 ppm error).

Lab Book Reference: SY-2-89

Using general procedure B, cyclopropyl BMIDA *trans*-**38** (88 mg, 0.25 mmol, 1.0 eq.), 5-bromopyrimidine (56 mg, 0.35 mmol, 1.4 eq.), PCy_3 (7 mg, 25 μmol, 0.10 eq.), Cs_2CO_3 (244 mg, 0.75 mmol, 3.0 eq.) and $Pd(OAc)_2$ (3 mg, 13 μmol, 0.05 eq.) in toluene (5.0 mL) and H_2O (0.5 mL) gave the crude product. Purification by flash column chromatography on silica with EtOAc as eluent gave cyclopropyl pyrimidine *trans*-**171** (39 mg, 57%) as a pale-yellow oil.

Lab Book Reference: SY-2-134

tert-Butyl 1-(pyrimidin-5-yl)-5-azaspiro[2.4]heptane-5-carboxylate _cis_-171

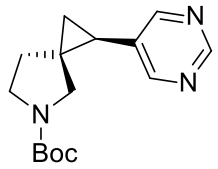

cis-**171**

Using general procedure A, cyclopropyl BMIDA *cis*-**38** (176 mg, 0.50 mmol, 1.0 eq.), 5-bromopyrimidine (111 mg, 0.70 mmol, 1.4 eq.), PCy_3 (42 mg, 0.15 mmol, 0.30 eq.), Cs_2CO_3 (977 mg, 3.00 mmol, 6.0 eq.) and $Pd(OAc)_2$ (17 mg, 75 μmol, 0.15 eq.) in toluene (5.0 mL) and H_2O (0.5 mL) gave the crude product. Purification by flash column chromatography on silica with EtOAc as eluent gave cyclopropyl pyrimidine *cis*-**171** (119 mg, 86%) as a colourless oil, R_F (EtOAc) 0.27; IR (ATR) 2974, 2932, 2870, 1686 (C=O), 1554, 1399, 1166, 1109, 884, 771, 728, 631 cm^{-1}; ^1H NMR (400 MHz, $CDCl_3$) (60:40 mixture of rotamers) δ 9.07 (s, 0.6H, Ar), 9.04 (s, 0.4H, Ar), 8.51 – 8.46 (m, 2H, Ar), 3.58

– 3.45 (m, 2H, NCH), 3.13 (d, *J* = 11.0 Hz, 0.4H, NCH), 3.07 (d, *J* = 11.0 Hz, 0.6H, NCH), 2.92 (d, *J* = 11.0 Hz, 0.4H, NCH), 2.85 (d, *J* = 11.0 Hz, 0.6H, NCH), 2.05 (dd, *J* = 9.0, 6.0 Hz, 1H, CH), 2.01 – 1.90 (m, 2H, CH), 1.42 (s, 3.6H, CMe_3), 1.35 (s, 5.4H, CMe_3), 1.32 – 1.24 (m, 1H, CH), 1.23 – 1.15 (m, 1H, CH); ^{13}C NMR (100.6 MHz, $CDCl_3$) (rotamers) δ 156.9 (Ar), 156.7 (Ar), 156.5 (Ar), 154.4 (C=O), 132.6 (*ipso*-Ar), 79.6 ($OCMe_3$), 48.8 (NCH_2), 46.0 (NCH_2), 45.5 (NCH_2), 35.4 (CH), 34.7 (CH), 30.2 (C), 29.6 (C), 28.5 (CMe_3), 22.6 (CH_2), 22.4 (CH_2), 15.9 (CH_2), 15.3 (CH_2); MS (ESI) *m/z* 298 [(M + Na)$^+$, 100]; HRMS (ESI) *m/z* calcd for $C_{15}H_{21}N_3O_2$ (M + Na)$^+$ 298.1526, found 298.1527 (–0.4 ppm error).

Lab Book Reference: SY-2-92

Using general procedure B, cyclopropyl BMIDA *cis*-**38** (88 mg, 0.25 mmol, 1.0 eq.), 5-bromopyrimidine (56 mg, 0.35 mmol, 1.4 eq.), PCy_3 (7 mg, 25 μmol, 0.10 eq.), Cs_2CO_3 (244 mg, 0.75 mmol, 3.0 eq.) and $Pd(OAc)_2$ (3 mg, 13 μmol, 0.05 eq.) in toluene (5.0 mL) and H_2O (0.5 mL) gave the crude product. Purification by flash column chromatography on silica with EtOAc as eluent gave cyclopropyl pyrimidine *cis*-**171** (61 mg, 88%) as a colourless oil.

Lab Book Reference: SY-2-135

***tert*-Butyl 6-(4-(methylsulfonyl)phenyl)-3-azabicyclo[3.1.0]hexane-3-carboxylate *exo*-173**

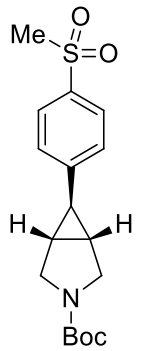

exo-**173**

Using general procedure A, cyclopropyl BMIDA *exo*-**39** (100 mg, 0.3 mmol, 1.0 eq.), 4-bromophenylmethyl sulfone (97 mg, 0.41 mmol, 1.4 eq.), PCy_3 (25 mg, 0.09 mmol, 0.3

eq.), Cs_2CO_3 (579 mg, 1.8 mmol, 6.0 eq.) and $Pd(OAc)_2$ (10 mg, 0.04 mmol, 0.15 eq.) in toluene (3.1 mL) and H_2O (0.2 mL) gave crude the product. Purification by flash column chromatography on silica with 60:40 EtOAc–hexane as eluent gave cyclopropyl sulfone *exo*-**173** (72 mg, 72%) as a white solid, mp 158 – 160 °C; R_F (60:40 EtOAc–hexane) 0.40; IR (ATR) 2976, 2929, 2873, 1689 (C=O), 1402 (SO_2), 1300, 1147, 1116, 957, 865, 762, 535 cm^{-1}; ^1H NMR (400 MHz, $CDCl_3$) (50:50 mixture of rotamers) δ 7.82 (d, J = 8.5 Hz, 2H, Ar), 7.19 (d, J = 8.5 Hz, 2H, Ar), 3.80 (d, J = 11.0 Hz, 1H, NCH), 3.71 (d, J = 11.0 Hz, 1H, NCH), 3.55 – 3.45 (m, 2H, NCH), 3.03 (s, 3H, SO_2Me), 1.91 – 1.86 (m, 2H, CH), 1.80 (t, J = 3.5 Hz, 1H, CH), 1.47 (s, 9H, CMe_3); ^{13}C NMR (100.6 MHz, $CDCl_3$) (rotamers) δ 155.0 (C=O), 148.4 (*ipso*-Ar), 137.8 (*ipso*-Ar), 127.7 (Ar), 126.4 (Ar), 79.9 ($OCMe_3$), 48.8 (NCH_2), 48.5 (NCH_2), 44.8 (SO_2Me), 28.6 (CMe_3), 28.0 (CH), 27.2 (*C*HAr); MS (ESI) *m/z* 360 [$(M + Na)^+$, 100]; HRMS (ESI) *m/z* calcd for $C_{17}H_{23}NO_4S$ $(M + Na)^+$ 360.1240, found 360.1249 (–2.6 ppm error).

Lab Book Reference: SY-1-53

tert-Butyl 6-(2-cyanophenyl)-3-azabicyclo[3.1.0]hexane-3-carboxylate _exo_-174

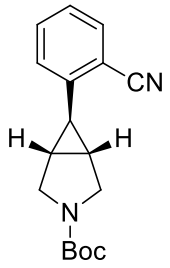

exo-**174**

Using general procedure B, cyclopropyl BMIDA *exo*-**39** (85 mg, 0.25 mmol, 1.0 eq.), 2-bromobenzonitrile (64 mg, 0.35 mmol, 1.4 eq.), PCy_3 (7 mg, 25 μmol, 0.10 eq.), Cs_2CO_3 (244 mg, 0.75 mmol, 3.0 eq.) and $Pd(OAc)_2$ (10 mg, 13 μmol, 0.05 eq.) in toluene (5.0 mL) and H_2O (0.5 mL) gave the crude product. Purification by flash column chromatography on silica with EtOAc as eluent gave cyclopropyl benzonitrile *exo*-**174** (28 mg, 39%) as a colourless oil, R_F (80:20 hexane–EtOAc) 0.17; IR (ATR) 2975, 2931, 2873, 2224 (C≡N), 1691 (C=O), 1418, 1388, 1366, 1171, 1115, 860, 762, 505 cm^{-1}; ^1H NMR (400 MHz, $CDCl_3$) (50:50 mixture of rotamers) δ 7.59 (dd, J = 7.5, 1.5 Hz, 1H, Ar), 7.48 (ddd, J = 7.5, 7.5, 1.5 Hz, 1H, Ar), 7.26 (ddd, J = 7.5, 7.5, 1.0 Hz, 1H, Ar), 6.98 (dd, J = 7.5, 1.0 Hz, 1H, Ar), 3.81 (d, J = 11.0 Hz, 1H, NCH), 3.75 (d, J = 11.0 Hz, 1H,

NCH), 3.53 (dd, *J* = 11.0, 4.0 Hz, 1H, NCH), 3.49 (dd, *J* = 11.0, 4.0 Hz, 1H, NCH), 2.09 (t, *J* = 4.0 Hz, 1H, CH), 1.98 – 1.92 (m, 1H, CH), 1.90 – 1.83 (m, 1H, CH), 1.46 (s, 9H, CMe_3); ^{13}C NMR (100.6 MHz, $CDCl_3$) (rotamers) δ 155.0 (C=O), 145.1 (*ipso*-Ar), 133.0 (Ar), 132.9 (Ar), 126.4 (Ar), 125.4 (Ar), 118.3 (C≡N), 112.8 (*ipso*-Ar), 79.8 ($OCMe_3$), 48.8 (NCH_2), 48.5 (NCH_2), 28.6 (CMe_3), 28.0 (CH), 26.4 (CH), 25.6 (*C*HAr); MS (ESI) *m/z* 307 [$(M + Na)^+$, 100]; HRMS (ESI) *m/z* calcd for $C_{17}H_{20}N_2O_2$ $(M + Na)^+$ 307.1417, found 307.1411 (+2.0 ppm error).

Lab Book Reference: SY-1-119

***tert*-Butyl 6-(thiophen-3-yl)-3-azabicyclo[3.1.0]hexane-3-carboxylate *exo*-175**

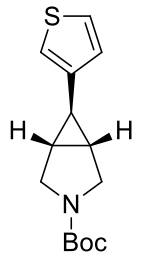

exo-**175**

Using general procedure B, cyclopropyl BMIDA *exo*-**39** (85 mg, 0.25 mmol, 1.0 eq.), 3-bromothiophene (33 μL, 0.35 mmol, 1.4 eq.), PCy_3 (7 mg, 25 μmol, 0.10 eq.), Cs_2CO_3 (244 mg, 0.75 mmol, 3.0 eq.) and $Pd(OAc)_2$ (3 mg, 13 μmol, 0.05 eq.) in toluene (5.0 mL) and H_2O (0.5 mL) gave the crude product. Purification by flash column chromatography on silica with 90:10 hexane–EtOAc as eluent gave cyclopropyl thiophene *exo*-**175** (39 mg, 59%) as a pale-yellow oil, R_F (90:10 hexane–EtOAc) 0.22; IR (ATR) 2974, 2929, 2868, 1690 (C=O), 1392, 1365, 1169, 1111, 861, 767, 631, 546 cm^{-1}; ^1H NMR (400 MHz, $CDCl_3$) (50:50 mixture of rotamers) δ 7.23 (dd, *J* = 5.0, 3.0 Hz, 1H, Ar), 6.85 – 6.83 (m, 1H, Ar), 6.82 – 6.79 (m, 1H, Ar), 3.74 (d, *J* = 11.0 Hz, 1H, NCH), 3.65 (d, *J* = 11.0 Hz, 1H, NCH), 3.49 – 3.39 (m, 2H, NCH), 1.79 – 1.76 (m, 1H, CH), 1.76 – 1.72 (m, 2H, CH), 1.46 (s, 9H, CMe_3); ^{13}C NMR (100.6 MHz, $CDCl_3$) (rotamers) δ 155.1 (C=O), 142.0 (*ipso*-Ar), 126.1 (Ar), 125.8 (Ar), 118.1 (Ar), 79.6 ($OCMe_3$), 48.7 (NCH_2), 48.4 (NCH_2), 28.6 (CMe_3), 26.8 (CH), 26.1 (CH), 23.1 (CH); MS (ESI) *m/z* 288 [$(M + Na)^+$, 100]; HRMS (ESI) *m/z* calcd for $C_{14}H_{19}NO_2S$ $(M + Na)^+$ 288.1029, found 288.1035 (–2.1 ppm error).

Lab Book Reference: SY-1-112

tert-Butyl 6-(1-tosyl-1*H*-benzo[d]imidazol-4-yl)-3-azabicyclo[3.1.0]hexane-3-carboxylate _exo_-176

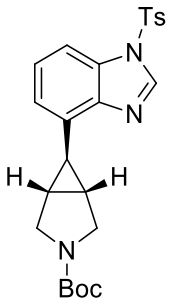

exo-**176**

Using general procedure B, cyclopropyl BMIDA *exo*-**39** (85 mg, 0.25 mmol, 1.0 eq.), tosyl benzimidazole (123 mg, 0.35 mmol, 1.4 eq.), PCy_3 (7 mg, 25 μmol, 0.10 eq.), Cs_2CO_3 (244 mg, 0.75 mmol, 3.0 eq.) and $Pd(OAc)_2$ (10 mg, 13 μmol, 0.05 eq.) in toluene (5.0 mL) and H_2O (0.5 mL) gave the crude product. Purification by flash column chromatography on silica with 60:40 hexane–EtOAc as eluent gave cyclopropyl benzimidazole *exo*-**176** (80 mg, 71%) as an off-white solid, mp 175 – 176 °C; R_F (60:40 hexane–EtOAc) 0.27; IR (ATR) 2975, 2930, 2871, 1688 (C=O), 1597, 1493, 1409, 1382, 1179, 1162, 1145, 1099, 910, 729, 676, 598, 573 cm^{-1}; ^1H NMR (400 MHz, $CDCl_3$) (50:50 mixture of rotamers) δ 8.36 (s, 1H, Ar), 7.90 – 7.85 (m, 2H, Ar), 7.65 (dd, J = 8.5, 1.0 Hz, 1H, Ar), 7.33 – 7.27 (m, 3H, Ar), 6.85 (dd, J = 7.5, 1.0 Hz, 1H, Ar), 3.78 (d, J = 11.0 Hz, 1H, NCH), 3.73 (d, J = 11.0 Hz, 1H, NCH), 3.53 (dd, J = 11.0, 4.0 Hz, 1H, NCH), 3.48 (dd, J = 11.0, 4.0 Hz, 1H, NCH), 2.38 (s, 3H, Me), 2.34 (t, J = 4.0 Hz, 1H, CH), 2.15 – 2.06 (m, 2H, CH), 1.47 (s, 9H, CMe_3); ^{13}C NMR (100.6 MHz, $CDCl_3$) (rotamers) δ 155.0 (C=O), 146.3 (*ipso*-Ar), 142.3 (*ipso*-Ar), 140.5 (Ar), 134.8 (*ipso*-Ar), 134.5 (*ipso*-Ar), 130.7 (*ipso*-Ar), 130.4 (Ar), 127.3 (Ar), 125.7 (Ar), 120.1 (Ar), 109.6 (Ar), 79.5 (O*C*Me_3), 48.8 (NCH_2), 48.6 (NCH_2), 28.6 (C*Me*$_3$), 28.0 (CH), 27.0 (CH), 23.4 (*C*HAr), 21.8 (Me); MS (ESI) *m/z* 476 [$(M + Na)^+$, 100]; HRMS (ESI) *m/z* calcd for $C_{24}H_{27}N_3O_4S$ $(M + Na)^+$ 476.1614, found 476.1620 (–1.1 ppm error).

Lab Book Reference: SY-1-131

***tert*-Butyl 6-(3,5-dimethoxyphenyl)-3-azabicyclo[3.1.0]hexane-3-carboxylate *exo*-177**

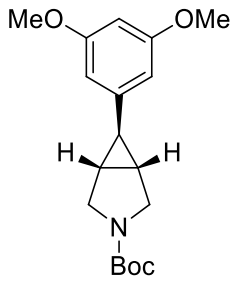

exo-**177**

Using general procedure B, cyclopropyl BMIDA *exo*-**39** (85 mg, 0.25 mmol, 1.0 eq.), 1-bromo-3,5-dimethoxybenzene (76 mg, 0.35 mmol, 1.4 eq.), PCy_3 (7 mg, 25 μmol, 0.10 eq.), Cs_2CO_3 (244 mg, 0.75 mmol, 3.0 eq.) and $Pd(OAc)_2$ (3 mg, 13 μmol, 0.05 eq.) in toluene (5.0 mL) and H_2O (0.5 mL) gave the crude product. Purification by flash column chromatography on silica with 90:10 hexane–Et_2O as eluent gave cyclopropyl dimethoxybenzene *exo*-**177** (45 mg, 56%) as a white solid, mp 76 – 78 °C; R_F (80:20 hexane–EtOAc) 0.29; IR (ATR) 2972, 2931, 2869, 1692 (C=O), 1594, 1459, 1407, 1389, 1204, 1151, 1113, 1061, 867, 825, 772, 692, 544 cm^{-1}; ^1H NMR (400 MHz, $CDCl_3$) (50:50 mixture of rotamers) δ 6.27 (t, J = 2.5 Hz, 1H, Ar), 6.18 (d, J = 2.5 Hz, 2H, Ar), 3.76 (s, 6H, OMe), 3.75 – 3.71 (m, 1H, NCH), 3.66 (d, J = 11.0 Hz, 1H, NCH), 3.50 – 3.41 (m, 2H, NCH), 1.80 – 1.76 (m, 2H, CH), 1.64 (t, J = 3.5 Hz, 1H, CH), 1.46 (s, 9H, CMe_3); ^{13}C NMR (100.6 MHz, $CDCl_3$) (rotamers) δ 160.9 (*ipso*-Ar), 155.1 (C=O), 143.9 (*ipso*-Ar), 103.9 (Ar), 97.7 (Ar), 79.6 ($OCMe_3$), 55.4 (OMe), 48.9 (NCH_2), 48.6 (NCH_2), 28.6 (CMe_3), 27.5 (*C*HAr), 27.4, (CH) 26.8 (CH); MS (ESI) *m/z* 342 $[(M + Na)^+$, 100]; HRMS (ESI) *m/z* calcd for $C_{18}H_{25}NO_4$ $(M + Na)^+$ 342.1676, found 342.1677 (–0.4 ppm error).

Lab Book Reference: SY-1-118

***tert*-Butyl 1-(3,5-bis(trifluoromethyl)phenyl)-5-azaspiro[2.4]heptane-5-carboxylate *trans*-178**

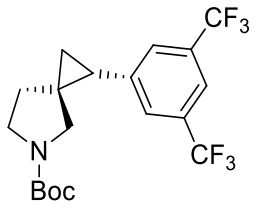

trans-**178**

Using general procedure B, cyclopropyl BMIDA *trans*-**38** (88 mg, 0.25 mmol, 1.0 eq.), 3,6-bis(trifluoromethyl)bromobenzene (60 μL, 0.35 mmol, 1.4 eq.), PCy_3 (7 mg, 25 μmol, 0.10 eq.), Cs_2CO_3 (244 mg, 0.75 mmol, 3.0 eq.) and $Pd(OAc)_2$ (3 mg, 13 μmol, 0.05 eq.) in toluene (5.0 mL) and H_2O (0.5 mL) gave the crude product. Purification by flash column chromatography on silica with 90:10 hexane–EtOAc as eluent gave cyclopropyl phenyltrifluoromethane *trans*-**178** (58 mg, 57%) as a colourless oil, R_F (80:20 hexane–EtOAc) 0.57; IR (ATR) 2978, 2934, 2872, 1692 (C=O), 1478, 1402, 1368, 1276, 1168, 1127, 894, 844, 772, 706, 682 cm^{-1}; ^1H NMR (400 MHz, $CDCl_3$) δ 7.71 (s, 1H, Ar), 7.56 (s, 2H, Ar), 3.52 – 3.36 (m, 3H, NCH), 3.36 – 3.19 (m, 1H, NCH), 2.34 – 2.23 (m, 1H, CH), 1.69 – 1.59 (m, 1H, CH), 1.46 (s, 9H, CMe_3), 1.44 – 1.35 (m, 1H, CH), 1.35 – 1.26 (m, 1H, CH), 1.26 – 1.19 (m, 1H, CH); ^{13}C NMR (100.6 MHz, $CDCl_3$) (rotamers) δ 154.5 (C=O), 141.9 (*ipso*-Ar), 141.7 (*ipso*-Ar), 131.7 (q, J = 33.0 Hz, *ipso*-Ar), 128.3 (q, J = 4.0 Hz, Ar), 123.4 (q, J = 273.0 Hz, CF_3), 120.2 (Ar), 79.6 (O*C*Me_3), 54.7 (NCH_2), 54.2 (NCH_2), 46.0 (NCH_2), 45.6 (NCH_2), 30.6 (C), 30.0 (C), 29.1 (CH), 28.6 (C*Me*$_3$), 28.5 (CH), 27.1 (CH_2), 16.1 (CH_2); MS (ESI) *m/z* 432 [$(M + Na)^+$, 100]; HRMS (ESI) *m/z* calcd for $C_{19}H_{21}F_6NO_2$ $(M + Na)^+$ 432.1369, found 432.1373 (–1.1 ppm error).

Lab Book Reference: SY-2-125

***tert*-Butyl 1-(quinazolin-7-yl)-5-azaspiro[2.4]heptane-5-carboxylate *trans*-179**

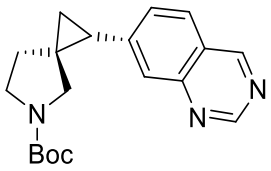

trans-**179**

Using general procedure B, cyclopropyl BMIDA *trans*-**38** (88 mg, 0.25 mmol, 1.0 eq.), 6-bromoquinazoline (73 mg, 0.35 mmol, 1.4 eq.), PCy_3 (7 mg, 25 μmol, 0.10 eq.), Cs_2CO_3 (244 mg, 0.75 mmol, 3.0 eq.) and $Pd(OAc)_2$ (3 mg, 13 μmol, 0.05 eq.) in toluene (5.0 mL) and H_2O (0.5 mL) gave the crude product. Purification by flash column chromatography on silica with 70:30 EtOAc–hexane as eluent gave cyclopropyl quinazoline *trans*-**179** (47 mg, 58%) as a colourless oil, R_F (80:20 EtOAc–hexane) 0.33; IR (ATR) 2972, 2927, 2866, 1689 (C=O), 1621, 1400, 1364, 1167, 1109, 927, 889, 771, 730, 631 cm^{-1}; ^1H NMR (400 MHz, $CDCl_3$) (55:45 mixture of rotamers) δ 9.33 (s, 1H, Ar), 9.26 (s, 1H, Ar), 7.83 (d, J = 8.5 Hz, 1H, Ar), 7.67 (s, 1H, Ar), 7.51 (dd, J = 8.5, 1.5 Hz, 1H, Ar), 3.50 – 3.31 (m, 3H, NCH), 3.28 – 3.12 (m, 1H, NCH), 2.41 – 2.31 (m, 1H, CH), 1.76 – 1.64 (m, 1H, CH), 1.45 (s, 4H, CMe_3), 1.43 (s, 5H, CMe_3), 1.42 – 1.39 (m, 1H, CH), 1.39 – 1.26 (m, 2H, CH); ^{13}C NMR (100.6 MHz, $CDCl_3$) (rotamers) δ 159.7 (Ar), 155.5 (Ar), 154.5 (C=O), 154.5 (C=O) 150.2 (*ipso*-Ar), 146.9 (*ipso*-Ar), 146.7 (*ipso*-Ar), 129.8 (Ar), 127.0 (Ar), 127.0 (Ar), 125.6 (Ar), 125.6 (Ar), 123.8 (Ar), 79.4 (O*C*Me_3), 54.9 (NCH_2), 54.4 (NCH_2), 46.0 (NCH_2), 45.6 (NCH_2), 31.6 (C), 30.9 (C), 28.8 (CH) 28.6 (C*Me*$_3$), 28.1 (CH_2), 15.9 (CH_2); MS (ESI) *m/z* 348 [$(M + Na)^+$, 100]; HRMS (ESI) *m/z* calcd for $C_{19}H_{23}N_3O_2$ $(M + Na)^+$ 348.1682, found 348.1683 (–0.1 ppm error).

Lab Book Reference: SY-2-147

tert-Butyl 1-(2-chloropyridin-4-yl)-5-azaspiro[2.4]heptane-5-carboxylate _trans_-180

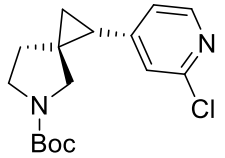

trans-**180**

Using general procedure B, cyclopropyl BMIDA *trans*-**38** (88 mg, 0.25 mmol, 1.0 eq.), 2-chloro-4-bromopyridine (67 mg, 0.35 mmol, 1.4 eq.), PCy_3 (7 mg, 25 μmol, 0.10 eq.), Cs_2CO_3 (244 mg, 0.75 mmol, 3.0 eq.) and $Pd(OAc)_2$ (3 mg, 13 μmol, 0.05 eq.) in toluene (5.0 mL) and H_2O (0.5 mL) gave the crude product. Purification by flash column chromatography on silica with 80:20 hexane–EtOAc as eluent gave cyclopropyl chloropyridine *trans*-**180** (54 mg, 70%) as a pale-yellow oil, R_F (80:20 hexane–EtOAc) 0.20; IR (ATR) 2975, 2925, 2869, 1687 (C=O), 1591, 1400, 1365, 1168, 1109, 1087, 990,

869, 772 cm^{-1}; ^{1}H NMR (400 MHz, $CDCl_3$) δ 8.24 (d, J = 5.0 Hz, 1H, Ar), 7.05 (d, J = 1.5 Hz, 1H, Ar), 6.95 (dd, J = 5.0, 1.5 Hz, 1H, Ar), 3.50 – 3.32 (m, 3H, NCH), 3.31 – 3.15 (m, 1H, NCH), 2.16 – 2.05 (m, 1H, CH), 1.77 – 1.64 (m, 1H, CH), 1.51 – 1.46 (m, 1H, CH), 1.45 (s, 9H, CMe_3), 1.32 – 1.17 (m, 2H, CH); ^{13}C NMR (100.6 MHz, $CDCl_3$) (rotamers) δ 154.4 (C=O), 152.1 (*ipso*-Ar), 151.9 (*ipso*-Ar), 151.8 (Ar), 149.4 (Ar), 123.4 (Ar), 122.1 (Ar), 79.5 (O*C*Me_3), 54.7 (NCH_2), 54.3 (NCH_2), 46.0 (NCH_2), 45.9 (NCH_2), 31.5 (C), 30.9 (C), 28.7 (CH), 28.6 (C*Me*$_3$), 28.1 (CH_2), 26.9 (CH_2), 16.1 (CH_2); MS (ESI) *m/z* 331 [($^{35}M + Na)^+$, 100]; HRMS (ESI) *m/z* calcd for $C_{16}H_{21}{}^{35}ClN_2O_2$ ($^{35}M + Na)^+$ 331.1184, found 331.1187 (–1.0 ppm error).

Lab Book Reference: SY-2-115

tert-Butyl 1-(2-(methoxycarbonyl)phenyl)-5-azaspiro[2.4]heptane-5-carboxylate _trans_-181

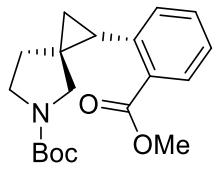

trans-**181**

Using general procedure B, cyclopropyl BMIDA *trans*-**38** (88 mg, 0.25 mmol, 1.0 eq.), methyl 2-bromobenzoate (49 μL, 0.35 mmol, 1.4 eq.), PCy_3 (7 mg, 25 μmol, 0.10 eq.), Cs_2CO_3 (244 mg, 0.75 mmol, 3.0 eq.) and $Pd(OAc)_2$ (3 mg, 13 μmol, 0.05 eq.) in toluene (5.0 mL) and H_2O (0.5 mL) gave the crude product. Purification by flash column chromatography on silica with 80:20 hexane–EtOAc as eluent gave cyclopropyl benzoate *trans*-**181** (53 mg, 64%) as a pale-yellow oil, R_F (80:20 hexane–EtOAc) 0.25; IR (ATR) 2974, 2867, 1722 (C=O, ester), 1689 (C=O, Boc), 1398, 1365, 1293, 1253, 1169, 1131, 1106, 1078, 881, 771, 736, 715 cm^{-1}; ^{1}H NMR (400 MHz, $CDCl_3$) (55:45 mixture of rotamers) δ 7.90 (dd, J = 7.5, 1.5 Hz, 1H, Ar), 7.43 (ddd, J = 7.5, 7.5, 1.5 Hz, 1H, Ar), 7.30 – 7.24 (m, 1H, Ar), 7.16 (d, J = 7.5 Hz, 1H, Ar), 3.86 (s, 3H, OMe), 3.53 (d, J = 10.5 Hz, 1H, NCH), 3.42 – 3.27 (m, 2H, NCH), 3.25 – 3.11 (m, 1H, NCH), 2.73 – 2.62 (m, 1H, CH), 1.47 (s, 4.95H, CMe_3), 1.45 (s, 4.05H, CMe_3), 1.44 – 1.34 (m, 1H, CH), 1.31 – 1.19 (m, 1H, CH), 1.16 – 1.07 (m, 2H, CH); ^{13}C NMR (100.6 MHz, $CDCl_3$) (rotamers) δ 168.4 (C=O, ester), 168.1 (C=O, ester), 154.6 (C=O, Boc), 154.5 (C=O, Boc), 140.1

(*ipso*-Ar), 139.8 (*ipso*-Ar), 132.1 (Ar), 131.8 (*ipso*-Ar), 131.5 (*ipso*-Ar), 130.9 (Ar), 130.8 (Ar), 128.8 (Ar), 126.4 (Ar), 79.1 (O*C*Me$_3$), 54.7 (NCH$_2$), 54.2 (NCH$_2$), 52.1 (OMe), 46.0 (NCH$_2$), 45.6 (NCH$_2$), 29.6 (CH), 29.0 (C), 28.9 (C), 28.7 (C*Me*$_3$), 27.6 (CH$_2$), 27.1 (CH$_2$), 15.5 (CH$_2$), 15.2 (CH$_2$); MS (ESI) *m/z* 354 [(M + Na)$^+$, 100]; HRMS (ESI) *m/z* calcd for $C_{19}H_{25}NO_4$ (M + Na)$^+$ 354.1676, found 354.1676 (+0.0 ppm error).

Lab Book Reference: SY-2-128

3-(5-(*tert*-Butoxycarbonyl)-5-azaspiro[2.4]heptan-1-yl)pyridine 1-oxide *cis*-182

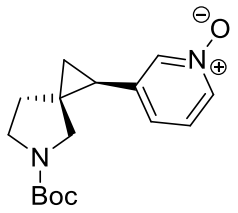

cis-**182**

Using general procedure B, cyclopropyl BMIDA *cis*-**38** (88 mg, 0.25 mmol, 1.0 eq.), 3-bromopyridine *N*-oxide (64 mg, 0.35 mmol, 1.4 eq.), PCy$_3$ (7 mg, 25 μmol, 0.10 eq.), Cs$_2$CO$_3$ (244 mg, 0.75 mmol, 3.0 eq.) and Pd(OAc)$_2$ (3 mg, 13 μmol, 0.05 eq.) in toluene (5.0 mL) and H$_2$O (0.5 mL) gave the crude product. Purification by flash column chromatography on silica with 90:10 acetone–MeOH as eluent gave cyclopropyl *N*-oxide *cis*-**182** (44 mg, 60%) as a colourless oil, R_F (90:10 acetone–MeOH) 0.30; IR (ATR) 2974, 2931, 2870, 2229, 1683 (C=O), 1401, 1365, 1270, 1164, 1111, 1011, 881, 729, 682 cm^{-1}; ^{1}H NMR (400 MHz, CDCl$_3$) (50:50 mixture of rotamers) δ 8.09 – 8.02 (m, 1H, Ar), 8.02 – 7.97 (m, 1H, Ar), 7.22 – 7.10 (m, 1H, Ar), 7.02 (d, J = 7.5 Hz, 0.5H, Ar), 6.89 (d, J = 7.5 Hz, 0.5H, Ar), 3.57 – 3.37 (m, 2H, NCH), 3.12 (d, J = 11.0 Hz, 0.5H, NCH), 3.04 (d, J = 11.0 Hz, 0.5H, NCH), 2.90 (d, J = 11.0 Hz, 0.5H, NCH), 2.80 (d, J = 11.0 Hz, 0.5H, NCH), 2.06 – 1.97 (m, 1H, CH), 1.96 – 1.82 (m, 2H, CH), 1.40 (s, 4.5H, CMe$_3$), 1.34 (s, 4.5H, CMe$_3$), 1.26 – 1.18 (m, 1H, CH), 1.15 – 1.06 (m, 1H, CH); ^{13}C NMR (100.6 MHz, CDCl$_3$) (rotamers) δ 154.4 (C=O), 139.4 (*ipso*-Ar), 138.9 (*ipso*-Ar), 138.8 (Ar), 137.2 (Ar), 137.1 (Ar), 126.7 (Ar), 125.6 (Ar), 125.2 (Ar), 79.6 (O*C*Me$_3$), 48.7 (NCH$_2$), 48.5 (NCH$_2$), 45.9 (NCH$_2$), 45.5 (NCH$_2$), 35.4 (CH), 34.6 (CH), 30.5 (C), 29.9 (C), 28.5 (C*Me*$_3$), 24.7 (CH$_2$), 16.0 (CH$_2$), 15.4 (CH$_2$); MS (ESI) *m/z* 313 [(M + Na)$^+$, 100]; HRMS (ESI) *m/z* calcd for $C_{16}H_{22}N_2O_3$ (M + Na)$^+$ 313.1523, found 313.1527 (–1.5 ppm error).

Lab Book Reference: SY-2-121

***tert*-Butyl 1-(pyridin-3-yl)-5-azaspiro[2.4]heptane-5-carboxylate *cis*-183**

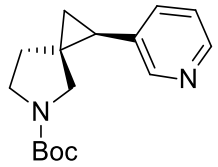

cis-**183**

Using general procedure B, cyclopropyl BMIDA *cis*-**38** (88 mg, 0.25 mmol, 1.0 eq.), 3-bromopyridine (55 mg, 0.35 mmol, 1.4 eq.), PCy_3 (7 mg, 25 μmol, 0.10 eq.), Cs_2CO_3 (244 mg, 0.75 mmol, 3.0 eq.) and $Pd(OAc)_2$ (3 mg, 13 μmol, 0.05 eq.) in toluene (5.0 mL) and H_2O (0.5 mL) gave the crude product. Purification by flash column chromatography on silica with 90:10 EtOAc–hexane as eluent gave cyclopropyl pyridine *cis*-**183** (41 mg, 59%) as a colourless oil, R_F (EtOAc) 0.40; IR (ATR) 2975, 2932, 2869, 1687 (C=O), 1400, 1365, 1167, 1109, 884, 771, 730, 714 cm^{-1}; ^1H NMR (400 MHz, $CDCl_3$) (50:50 mixture of rotamers) δ 8.46 – 8.36 (m, 2H, Ar), 7.36 (d, J = 8.0 Hz, 0.5H, Ar), 7.28 (d, J = 8.0 Hz, 0.5H, Ar), 7.23 – 7.11 (m, 1H, Ar), 3.55 – 3.39 (m, 2H, NCH), 3.08 (d, J = 11.0 Hz, 0.5H, NCH), 3.02 (d, J = 11.0 Hz, 0.5H, NCH), 2.91 (d, J = 11.0 Hz, 0.5H, NCH), 2.80 (d, J = 11.0 Hz, 0.5H, NCH), 2.12 – 2.03 (m, 1H, CH), 1.99 – 1.82 (m, 2H, CH), 1.40 (s, 4.5H, CMe_3), 1.32 (s, 4.5H, CMe_3), 1.24 – 1.08 (m, 1H, CH); ^{13}C NMR (100.6 MHz, $CDCl_3$) (rotamers) δ 154.5 (C=O), 150.3 (Ar), 150.0 (Ar), 147.6 (Ar), 147.6 (Ar), 135.7 (Ar), 134.5 (*ipso*-Ar), 134.5 (Ar), 123.2 (Ar), 79.3 (O*C*Me_3), 48.8 (NCH_2), 46.0 (NCH_2), 45.5 (NCH_2), 35.3 (CH), 34.8 (CH), 29.8 (C), 29.2 (C), 28.53 (C*Me*$_3$), 28.50 (C*Me*$_3$), 25.2 (CH_2), 24.8 (CH_2), 16.1 (CH_2), 15.0 (CH_2); MS (ESI) *m/z* 297 [$(M + Na)^+$, 100]; HRMS (ESI) *m/z* calcd for $C_{16}H_{22}N_2O_2$ $(M + Na)^+$ 297.1573, found 297.1575 (–0.4 ppm error).

Lab Book Reference: SY-2-124

***tert*-Butyl 1-(4-nitrophenyl)-5-azaspiro[2.4]heptane-5-carboxylate *cis*-184**

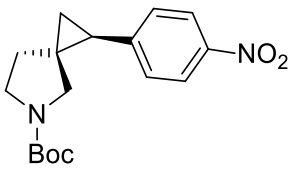

cis-**184**

Using general procedure B, cyclopropyl BMIDA *cis*-**38** (88 mg, 0.25 mmol, 1.0 eq.), 1-bromo-4-nitrobenzene (71 mg, 0.35 mmol, 1.4 eq.), PCy_3 (7 mg, 25 μmol, 0.10 eq.), Cs_2CO_3 (244 mg, 0.75 mmol, 3.0 eq.) and $Pd(OAc)_2$ (3 mg, 13 μmol, 0.05 eq.) in toluene (5.0 mL) and H_2O (0.5 mL) gave the crude product. Purification by flash column chromatography on silica with 80:20 hexane–EtOAc as eluent gave cyclopropyl nitrobenzene *cis*-**184** (72 mg, 90%) as an off-white solid, mp 88 – 89 °C; R_F (80:20 hexane–EtOAc) 0.24; IR (ATR) 2974, 2934, 2869, 1687 (C=O), 1597, 1516 (NO_2), 1400, 1342 (NO_2), 1167, 1108, 856, 771, 739, 700 cm^{-1}; ^1H NMR (400 MHz, $CDCl_3$) (50:50 mixture of rotamers) δ 8.14 (d, J = 8.0 Hz, 1H, Ar), 8.10 (d, J = 8.0 Hz, 1H, Ar), 7.23 (d, J = 8.0 Hz, 1H, Ar), 7.20 (d, J = 8.0 Hz, 1H, Ar), 3.58 – 3.42 (m, 2H, NCH), 3.15 (d, J = 11.0 Hz, 0.5H, NCH), 3.09 (d, J = 11.0 Hz, 0.5H, NCH), 2.91 (d, J = 11.0 Hz, 0.5H, NCH), 2.80 (d, J = 11.0 Hz, 0.5H, NCH), 2.20 (dd, J = 8.5, 6.5 Hz, 1H, C*H*Ar), 2.05 – 1.87 (m, 2H, CH), 1.41 (s, 4.5H, CMe_3), 1.32 (s, 4.5H, CMe_3), 1.30 – 1.24 (m, 2H, CH); ^{13}C NMR (100.6 MHz, $CDCl_3$) (rotamers) δ 154.5 (C=O), 147.2 (*ipso*-Ar), 146.4 (*ipso*-Ar), 128.8 (Ar), 128.5 (Ar), 123.7 (Ar), 79.5 (O*C*Me_3), 48.7 (NCH_2), 46.0 (NCH_2), 45.5 (NCH_2), 35.7 (*C*HAr), 35.0 (*C*HAr), 31.3 (C), 30.7 (C), 28.5 (C*Me*$_3$), 28.1 (CH_2), 27.7 (CH_2), 17.6 (CH_2), 16.5 (CH_2); MS (ESI) *m/z* 341 [$(M + Na)^+$, 100]; HRMS (ESI) *m/z* calcd for $C_{17}H_{22}N_2O_4$ $(M + Na)^+$ 341.1472, found 341.1472 (–0.1 ppm error).

Lab Book Reference: SY-2-116

tert-Butyl 1-(1-methyl-1*H*-pyrazol-4-yl)-5-azaspiro[2.4]heptane-5-carboxylate _cis_-185

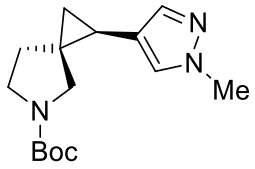

cis-**185**

Using general procedure B, cyclopropyl BMIDA *cis*-**38** (88 mg, 0.25 mmol, 1.0 eq.), 4-bromo-1-methyl-1*H*-pyrazole (36 μL, 0.35 mmol, 1.4 eq.), PCy_3 (7 mg, 25 μmol, 0.10 eq.), Cs_2CO_3 (244 mg, 0.75 mmol, 3.0 eq.) and $Pd(OAc)_2$ (3 mg, 13 μmol, 0.05 eq.) in toluene (5.0 mL) and H_2O (0.5 mL) gave the crude product. Purification by flash column chromatography on silica with 80:20 hexane–EtOAc as eluent gave cyclopropyl pyrazole

cis-**185** (21 mg, 30%) as a colourless oil, R_F (80:20 hexane–EtOAc) 0.25; IR (ATR) 2974, 2930, 2869, 1687 (C=O), 1398, 1364, 1167, 1364, 1167, 1109, 987, 882, 771, 680 cm^{-1}; ^1H NMR (400 MHz, $CDCl_3$) (50:50 mixture of rotamers) δ 7.24 (s, 0.5H, Ar), 7.21 (s, 0.5H, Ar), 7.11 (s, 0.5H, Ar), 7.01 (s, 0.5H, Ar), 3.85 (s, 1.5H, Me), 3.81 (s, 1.5H, Me), 3.56 – 3.39 (m, 2H, NCH), 3.14 – 2.92 (m, 2H, NCH), 1.93 – 1.74 (m, 3H, CH), 1.44 (s, 4.5H, CMe_3), 1.39 (s, 4.5H, CMe_3), 1.11 – 1.04 (m, 1H, CH), 0.79 (dd, J = 5.5, 5.5 Hz, 1H, CH); ^{13}C NMR (100.6 MHz, $CDCl_3$) (rotamers) δ 154.7 (C=O), 139.1 (Ar), 138.9 (Ar), 129.0 (Ar), 128.1 (Ar), 120.0 (*ipso*-Ar), 79.2 (O*C*Me_3), 49.4 (NCH_2), 46.2 (NCH_2), 45.7 (NCH_2), 39.1 (Me), 39.0 (Me), 35.1 (*C*HAr), 34.5 (*C*HAr), 28.6 (C*Me*$_3$), 28.0 (C), 17.44 (CH_2) 17.35 (CH_2), 17.3 (CH_2), 16.3 (CH_2) (C not resolved); MS (ESI) *m/z* 300 [$(M + Na)^+$, 100]; HRMS (ESI) *m/z* calcd for $C_{15}H_{23}N_3O_2$ $(M + Na)^+$ 300.1682, found 300.1681 (+0.5 ppm error).

Lab Book Reference: SY-2-129

tert-Butyl 7-(furan-3-yl)-2-azabicyclo[4.1.0]heptane-2-carboxylate _exo_-186

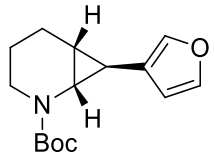

exo-**186**

Using general procedure B, cyclopropyl BMIDA *exo*-**36** (88 mg, 0.25 mmol, 1.0 eq.), 3-bromofuran (51 mg, 0.35 mmol, 1.4 eq.), PCy_3 (7 mg, 25 μmol, 0.10 eq.), Cs_2CO_3 (244 mg, 0.75 mmol, 3.0 eq.) and $Pd(OAc)_2$ (3 mg, 13 μmol, 0.05 eq.) in toluene (5.0 mL) and H_2O (0.5 mL) gave the crude product. Purification by flash column chromatography on silica with 90:10 hexane–EtOAc as eluent gave cyclopropyl furan *exo*-**186** (40 mg, 61%) as a yellow oil, R_F (90:10 hexane–EtOAc) 0.23; IR (ATR) 2972, 2933, 2865, 1691 (C=O), 1391, 1365, 1254, 1153, 1031, 874, 770, 734, 599 cm^{-1}; ^1H NMR (400 MHz, $CDCl_3$) (80:20 mixture of rotamers) δ 7.31 – 7.18 (m, 2H, Ar), 6.22 – 6.17 (m, 1H, Ar), 3.83 (ddd, J = 12.5, 4.0, 4.0 Hz, 0.8H, NCH), 3.65 (ddd, J = 12.5, 4.0, 4.0 Hz, 0.2H, NCH), 2.96 (dd, J = 8.5, 3.0 Hz, 0.2H, NCH), 2.83 (dd, J = 8.5, 3.0 Hz, 0.8H, NCH), 2.66 (ddd, J = 12.5, 12.5, 2.5 Hz, 0.2H, NCH), 2.55 (ddd, J = 12.5, 12.5, 2.5 Hz, 0.8H, NCH), 2.01 – 1.92 (m, 1H, CH), 1.89 – 1.75 (m, 1H, CH), 1.70 – 1.58 (m, 1H, CH), 1.50 (dd, J = 6.0,

3.0 Hz, 1H, CH), 1.46 (s, 1.8H, CMe_3), 1.43 (s, 7.2H, CMe_3), 1.37 – 1.32 (m, 1H, CH), 1.31 – 1.22 (m, 1H, CH); ^{13}C NMR (100.6 MHz, $CDCl_3$) (rotamers) δ 156.7 (C=O), 142.9 (Ar), 142.8 (Ar), 138.6 (Ar), 138.4 (Ar), 125.5 (*ipso*-Ar), 109.9 (Ar), 109.8 (Ar), 79.6 ($OCMe_3$), 42.0 (NCH_2), 40.5 (NCH_2), 37.3 (NCH), 37.0 (NCH), 28.7 (CMe_3), 28.7 (CMe_3), 22.3 (CH_2), 20.7 (CH), 20.5 (CH_2), 20.5 (CH), 20.1 (CH), 19.5 (CH); MS (ESI) *m/z* 286 [$(M + Na)^+$, 100]; HRMS (ESI) *m/z* calcd for $C_{15}H_{21}NO_3$ $(M + Na)^+$ 286.1414, found 286.1415 (–0.6 ppm error).

Lab Book Reference: SY-3-113

tert-Butyl 7-(benzofuran-5-yl)-2-azabicyclo[4.1.0]heptane-2-carboxylate _exo_-187

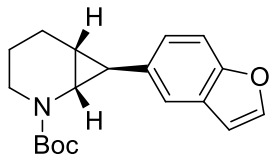

exo-**187**

Using general procedure B, cyclopropyl BMIDA *exo*-**36** (88 mg, 0.25 mmol, 1.0 eq.), 5-bromobenzofuran (69 mg, 0.35 mmol, 1.4 eq.), PCy_3 (7 mg, 25 μmol, 0.10 eq.), Cs_2CO_3 (244 mg, 0.75 mmol, 3.0 eq.) and $Pd(OAc)_2$ (3 mg, 13 μmol, 0.05 eq.) in toluene (5.0 mL) and H_2O (0.5 mL) gave the crude product. Purification by flash column chromatography on silica with 90:10 hexane–Et_2O as eluent gave cyclopropyl benzofuran *exo*-**187** (61 mg, 78%) as a pale-yellow oil, R_F (90:10 hexane–Et_2O) 0.37; IR (ATR) 2979, 2931, 2860, 1691 (C=O), 1470, 1389, 1364, 1164, 1130, 1032, 765, 735 cm^{-1}; ^1H NMR (400 MHz, $CDCl_3$) (80:20 mixture of rotamers) δ 7.59 (d, J = 2.0 Hz, 0.8H, Ar), 7.55 (d, J = 2.0 Hz, 0.2H, Ar), 7.46 – 7.44 (m, 0.2H, Ar), 7.39 (d, J = 8.5 Hz, 0.8H, Ar), 7.37 – 7.36 (m, 0.2H, Ar), 7.33 (d, J = 2.0 Hz, 0.8H, Ar), 7.18 (dd, J = 8.5, 2.0 Hz, 0.2H, Ar), 7.10 (dd, J = 8.5, 2.0 Hz, 0.8H, Ar), 6.72 – 6.67 (m, 1H, Ar), 3.89 (ddd, J = 12.5, 2.5, 2.5 Hz, 0.8H, NCH), 3.71 (ddd, J = 12.5, 2.5, 2.5 Hz, 0.2H, NCH), 3.13 (dd, J = 8.5, 3.0 Hz, 0.2H, NCH), 2.97 (dd, J = 8.5, 3.0 Hz, 0.8H, NCH), 2.71 (ddd, J = 12.5, 12.5, 2.5 Hz, 0.2H, NCH), 2.60 (ddd, J = 12.5, 12.5, 2.5 Hz, 0.8H, NCH), 2.08 – 2.01 (m, 1H, CH), 1.95 – 1.87 (m, 1H, CH), 1.86 (dd, J = 6.5, 3.0 Hz, 1H, CH), 1.74 – 1.65 (m, 1H, CH), 1.65 – 1.54 (m, 2H, CH), 1.49 (s, 1.8H, CMe_3), 1.40 (s, 7.2H, CMe_3); ^{13}C NMR (100.6 MHz, $CDCl_3$) (rotamers) δ 156.7 (C=O), 153.7 (*ipso*-Ar), 145.32 (Ar), 145.30 (Ar), 135.8 (*ipso*-Ar),

127.5 (*ipso*-Ar), 123.6 (Ar), 118.3 (Ar), 111.0 (Ar), 106.5 (Ar), 79.7 (O*C*Me$_3$), 42.1 (NCH$_2$), 40.6 (NCH$_2$), 38.4 (NCH), 37.6 (NCH), 29.3 (CH), 28.7 (C*Me*$_3$), 22.4 (CH$_2$), 21.5 (CH), 21.3 (CH), 20.9 (CH$_2$), 20.8 (CH$_2$); MS (ESI) *m/z* 336 [(M + Na)$^+$, 100]; HRMS (ESI) *m/z* calcd for $C_{19}H_{23}NO_3$ (M + Na)$^+$ 336.1570, found 336.1573 (–0.7 ppm error).

Lab Book Reference: SY-3-111

tert-Butyl 7-(3-acetylphenyl)-2-azabicyclo[4.1.0]heptane-2-carboxylate _exo_-188

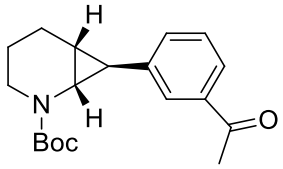

exo-**188**

Using general procedure B, cyclopropyl BMIDA *exo*-**36** (88 mg, 0.25 mmol, 1.0 eq.), 3-bromoacetophenone (70 mg, 0.35 mmol, 1.4 eq.), PCy$_3$ (7 mg, 25 μmol, 0.10 eq.), Cs$_2$CO$_3$ (244 mg, 0.75 mmol, 3.0 eq.) and Pd(OAc)$_2$ (3 mg, 13 μmol, 0.05 eq.) in toluene (5.0 mL) and H$_2$O (0.5 mL) gave the crude product. Purification by flash column chromatography on silica with 90:10 hexane–EtOAc as eluent gave cyclopropyl acetophenone *exo*-**188** (68 mg, 86%) as an off-white solid, mp 90 – 93 °C; R_F (80:20 hexane-EtOAc) 0.38; IR (ATR) 2975, 2933, 2861, 1683 (C=O), 1387, 1363, 1291, 1252, 1161, 1131, 775, 694, 588 cm^{-1}; ^{1}H NMR (400 MHz, CDCl$_3$) (75:25 mixture of rotamers) δ 7.74 – 7.62 (m, 2H, Ar), 7.37 – 7.27 (m, 2H, Ar), 3.86 (ddd, *J* = 13.0, 4.0, 4.0 Hz, 0.75H, NCH), 3.69 (ddd, *J* = 13.0, 3.5, 3.5 Hz, 0.25H), 3.13 (dd, *J* = 8.5, 3.0 Hz, 0.25H, NCH), 2.98 (dd, *J* = 8.5, 3.0 Hz, 0.75H, NCH), 2.75 – 2.60 (m, 1H, NCH), 2.57 (s, 2.3H, Me), 2.55 (s, 0.7H, Me), 2.04 – 1.96 (m, 1H, CH), 1.94 – 1.84 (m, 1H, CH), 1.82 (dd, *J* = 6.5, 3.5, 0.25H, CH), 1.79 (dd, *J* = 6.5, 3.0 Hz, 0.75H, CH), 1.73 – 1.58 (m, 2H, CH), 1.45 (s, 2.25H, CMe$_3$), 1.33 (s, 6.75H, CMe$_3$); ^{13}C NMR (100.6 MHz, CDCl$_3$) (rotamers) δ 198.5 (C=O, ketone), 198.3 (C=O, ketone), 156.4 (C=O, Boc), 155.9 (C=O, Boc), 142.1 (*ipso*-Ar), 137.1 (*ipso*-Ar), 131.2 (Ar), 131.0 (Ar), 128.6 (Ar), 128.5 (Ar), 126.0 (Ar), 125.8 (Ar), 125.3 (Ar), 79.7 (O*C*Me$_3$), 79.6 (O*C*Me$_3$), 42.0 (NCH$_2$), 40.4 (NCH$_2$), 38.9 (NCH), 38.5 (NCH), 29.4 (CH), 28.5 (C*Me*$_3$), 26.8 (Me), 22.3 (CH$_2$), 22.2 (CH$_2$), 22.1

(CH), 22.0 (CH), 20.6 (CH_2), 20.6 (CH_2); MS (ESI) *m/z* 338 [$(M + Na)^+$, 100]; HRMS (ESI) *m/z* calcd for $C_{19}H_{25}NO_3$ $(M + Na)^+$ 338.1727, found 338.1726 (+0.1 ppm error).

Lab Book Reference: SY-3-126

***tert*-Butyl 7-(4-chlorophenyl)-2-azabicyclo[4.1.0]heptane-2-carboxylate *exo*-189**

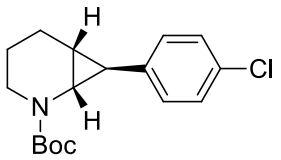

exo-**189**

Using general procedure B, cyclopropyl BMIDA *exo*-**36** (88 mg, 0.25 mmol, 1.0 eq.), 1-bromo-4-chlorobenzene (67 mg, 0.35 mmol, 1.4 eq.), PCy_3 (7 mg, 25 μmol, 0.10 eq.), Cs_2CO_3 (244 mg, 0.75 mmol, 3.0 eq.) and $Pd(OAc)_2$ (3 mg, 13 μmol, 0.05 eq.) in toluene (5.0 mL) and H_2O (0.5 mL) gave the crude product. Purification by flash column chromatography on silica with 90:10 hexane–EtOAc as eluent gave cyclopropyl chlorobenzene *exo*-**189** (64 mg, 83%) as an off-white solid, mp 86 – 88 °C; R_F (80:20 hexane–EtOAc) 0.43; IR (ATR) 2976, 2933, 2861, 1691 (C=O), 1494, 1385, 1364, 1161, 1131, 1090, 894, 849, 731, 511 cm^{-1}; ^1H NMR (400 MHz, $CDCl_3$) (80:20 mixture of rotamers) δ 7.24 – 7.16 (m, 2H, Ar), 7.11 – 7.05 (m, 0.4H, Ar), 7.03 – 6.93 (m, 1.6H, Ar), 3.86 (ddd, *J* = 12.5, 3.5, 3.5 Hz, 0.8H, NCH), 3.68 (ddd, *J* = 12.5, 3.5, 3.5 Hz, 0.2H, NCH), 3.06 (dd, *J* = 8.5, 3.0 Hz, 0.2H, NCH), 2.91 (dd, *J* = 8.5, 3.0 Hz, 0.8H, NCH), 2.69 (ddd, *J* = 12.5, 12.5, 3.5 Hz, 0.2H, NCH), 2.58 (ddd, *J* = 12.5, 12.5, 2.5 Hz, 0.8H, NCH), 2.03 – 1.95 (m, 1H, CH), 1.93 – 1.80 (m, 1H, CH), 1.78 – 1.72 (m, 0.4H, CH), 1.70 (dd, *J* = 6.5, 3.0 Hz, 1H, CH), 1.68 – 1.61 (m, 0.6H, CH), 1.59 – 1.50 (m, 1H, CH), 1.46 (s, 1.8H, CMe_3), 1.45 – 1.38 (m, 1H, CH), 1.36 (s, 7.2H, CMe_3); ^{13}C NMR (100.6 MHz, $CDCl_3$) (rotamers) δ 156.5 (C=O), 140.0 (Ar), 131.3 (*ipso*-Ar), 131.2 (*ipso*-Ar), 128.4 (Ar), 128.4 (Ar), 128.0 (Ar), 127.3 (Ar), 79.7 (O*C*Me_3), 42.0 (NCH_2), 40.4 (NCH_2), 38.8 (NCH), 38.0 (NCH), 29.0 (CH), 28.6 (C*Me*$_3$), 28.2 (CH), 22.2 (CH_2), 21.9 (CH), 21.9 (CH), 20.6 (CH_2), 20.6 (CH_2); MS (ESI) *m/z* 330 [$(^{35}M + Na)^+$, 100]; HRMS (ESI) *m/z* calcd for $C_{17}H_{22}{}^{35}ClNO_2$ $(^{35}M + Na)^+$ 330.1231, found 330.1228 (+1.0 ppm error).

Lab Book Reference: SY-3-122

3-(Methylsulfonyl)-6-(pyrimidin-5-yl)-3-azabicyclo[3.1.0]hexane 190

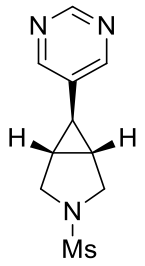

exo-**190**

Using general procedure C, cyclopropyl-pyrimidine *exo*-**170** (69 mg, 0.26 mmol, 1 eq.) and HCl (4.0 M in dioxane) (5 mL) then Et_3N (0.2 mL, 1.3 mmol, 4.8 eq.) and MsCl (45 μL, 0.6 mmol, 2.2 eq.) in CH_2Cl_2 (5 mL) gave the crude product. Purification by flash column chromatography on silica with 80:20 CH_2Cl_2–acetone as eluent gave mesyl cyclopropyl pyrimidine *exo*-**190** (60 mg, 95%) as a crystalline off-white solid, R_F (80:20 CH_2Cl_2–acetone) 0.21; ^{1}H NMR (400 MHz, $CDCl_3$) δ 9.02 (s, 1H, Ar), 8.45 (s, 2H, Ar), 3.77 (d, J = 9.5 Hz, 2H, NCH), 3.47 – 3.42 (m, 2H, NCH), 2.87 (s, 3H, SO_2Me), 2.03 (t, J = 3.5 Hz, 1H, CH), 1.99 – 1.93 (m, 2H, CH); ^{13}C NMR (100.6 MHz, $CDCl_3$) 156.8 (Ar), 154.6 (Ar), 133.8 (*ipso*-Ar), 49.9 (NCH_2), 36.1 (SO_2Me), 26.3 (CH), 20.2 (*C*HAr).

Lab Book Reference: SY-1-114

5-(Methylsulfonyl)-1-(pyrimidin-5-yl)-5-azaspiro[2.4]heptane *trans*-191

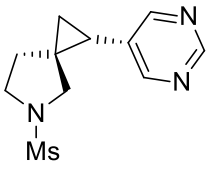

trans-**191**

Using general procedure C, cyclopropyl-pyrimidine *trans*-**171** (149 mg, 0.54 mmol, 1.0 eq.) and HCl (4.0 M in dioxane) (8 mL) then Et_3N (0.4 mL, 2.59 mmol, 4.8 eq.) and MsCl (92 μL, 1.19 mmol, 2.2 eq.) in CH_2Cl_2 (7 mL) gave the crude product. Purification by flash column chromatography on silica with 80:20 to 60:40 CH_2Cl_2–acetone as eluent gave mesyl cyclopropyl-pyrimidine *trans*-**191** (107 mg, 78%) as a crystalline white solid, mp 139 – 140 °C, R_F (80:20 CH_2Cl_2–acetone) 0.12; IR (ATR) 2984, 2931, 2869, 1556, 1416, 1325 (S=O), 1151 (S=O), 1052, 730, 563, 519 cm^{-1}; ^{1}H NMR (400 MHz, $CDCl_3$) δ 9.08 (s, 1H, Ar), 8.54 (s, 2H, Ar), 3.48 – 3.40 (m, 2H, NCH), 3.40 – 3.33 (m, 2H, NCH),

2.87 (s, 3H, SO_2Me), 2.18 (dd, *J* = 9.0, 6.0 Hz, 1H, CH), 1.75 (ddd, *J* = 13.0, 7.5, 6.0 Hz, 1H, CH), 1.59 (ddd, *J* = 13.0, 7.5, 6.0 Hz, 1H, CH), 1.35 (dd, *J* = 9.0, 6.0 Hz, 1H), 1.26 (dd, *J* = 6.0, 6.0 Hz, 1H, CH); ^{13}C NMR (100.6 MHz, $CDCl_3$) 157.1 (Ar), 156.6 (Ar), 132.0 (*ipso*-Ar), 55.9 (NCH_2), 47.8 (NCH_2), 35.4 (SO_2Me), 30.0 (C), 29.5 (CH_2), 22.5 (CH), 15.7 (CH_2); MS (ESI) *m/z* 276 [$(M + Na)^+$, 100]; HRMS (ESI) *m/z* calcd for $C_{11}H_{15}N_3O_2S$ $(M + Na)^+$ 276.0777, found 276.0776 (+0.4 ppm error).

Lab Book Reference: SY-2-93

5-(Methylsulfonyl)-1-(pyrimidin-5-yl)-5-azaspiro[2.4]heptane *cis*-191

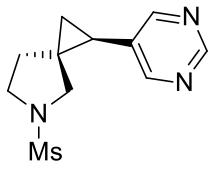

cis-**191**

Using general procedure C, cyclopropyl-pyrimidine *cis*-**171** (109 mg, 0.40 mmol, 1.0 eq.) and HCl (4.0 M in dioxane) (7 mL) then Et_3N (0.3 mL, 1.90 mmol, 4.8 eq.) and MsCl (69 μL, 0.6 mmol, 2.2 eq.) in CH_2Cl_2 (6 mL) gave the crude product. Purification by flash column chromatography on silica with 80:20 CH_2Cl_2–acetone as eluent gave mesyl cyclopropyl-pyrimidine *cis*-**191** (86 mg, 86%) as a crystalline off-white solid, mp 120 – 121 °C, R_F (80:20 CH_2Cl_2–acetone) 0.19; IR (ATR) 2988, 2930, 2875, 1556, 1417, 1327 (S=O), 1151 (S=O), 1055, 754, 729, 518 cm^{-1}; ^1H NMR (400 MHz, $CDCl_3$) δ 9.09 (s, 1H, Ar), 8.52 (s, 2H, Ar), 3.63 – 3.43 (m, 2H, NCH), 3.14 (d, *J* = 10.5 Hz, 1H, NCH), 2.89 (d, *J* = 10.5 Hz, 1H, NCH), 2.73 (s, 3H, SO_2Me), 2.15 (dd, *J* = 9.0, 6.0 Hz, 1H, CH), 2.11 – 2.06 (m, 2H, CH), 1.36 (dd, *J* = 9.0, 6.0 Hz, 1H, CH), 1.28 (dd, *J* = 6.0, 6.0 Hz, 1H, CH); ^{13}C NMR (100.6 MHz, $CDCl_3$) δ 157.2 (Ar), 156.6 (Ar), 131.9 (*ipso*-Ar), 50.6 (NCH_2), 47.9 (NCH_2), 35.5 (CH_2), 35.3 (SO_2Me), 30.2 (C), 22.8 (CH), 15.7 (CH_2); MS (ESI) *m/z* 276 [$(M + Na)^+$, 100]; HRMS (ESI) *m/z* calcd for $C_{11}H_{15}N_3O_2S$ $(M + Na)^+$ 276.0777, found 276.0780 (–0.9 ppm error).

Lab Book Reference: SY-2-94

2-(Methylsulfonyl)-7-(pyrimidin-5-yl)-2-azabicyclo[4.1.0]heptane *exo*-192

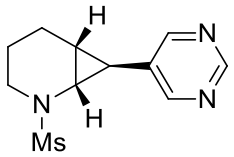

exo-**192**

Using general procedure C, cyclopropyl-pyrimidine *exo*-**166** (108 mg, 0.39 mmol, 1.0 eq.) and HCl (4.0 M in dioxane) (5 mL) then Et_3N (0.3 mL, 1.9 mmol, 4.8 eq.) and MsCl (67 μL, 0.9 mmol, 2.2 eq.) in CH_2Cl_2 (6 mL) gave the crude product. Purification by flash column chromatography on silica with 80:20 CH_2Cl_2–acetone as eluent gave mesyl cyclopropyl-pyrimidine *exo*-**192** (99 mg, 72%) as a crystalline white solid, mp 191 – 193 °C, R_F (80:20 CH_2Cl_2–acetone) 0.24; IR (ATR) 3006, 2928, 2872, 1558, 1424, 1333 (S=O), 1323, 1142 (S=O), 1042, 972, 941, 773, 524, 504 cm^{-1}; ^1H NMR (400 MHz, $CDCl_3$) δ 9.05 (s, 1H, Ar), 8.52 (s, 2H, Ar), 3.54 (ddd, J = 12.5, 4.0, 4.0 Hz, 1H, NCH), 3.09 (dd, J = 9.0, 3.0 Hz, 1H, NCH), 2.89 (s, 3H, SO_2Me), 2.89 – 2.82 (m, 1H, NCH), 2.12 – 2.03 (m, 1H, CH), 2.03 – 1.92 (m, 2H, CH), 1.86 – 1.74 (m, 2H, CH), 1.62 – 1.46 (m, 1H, CH); ^{13}C NMR (100.6 MHz, $CDCl_3$) δ 156.9 (Ar), 155.1 (Ar), 133.5 (*ipso*-Ar), 42.8 (NCH_2), 38.1 (NCH), 37.9 (SO_2Me), 24.5 (CH), 22.3 (CH_2), 20.7 (CH), 19.9 (CH_2); MS (ESI) *m/z* 276 [$(M + Na)^+$, 100]; HRMS (ESI) *m/z* calcd for $C_{11}H_{15}N_3O_2S$ $(M + Na)^+$ 276.0777, found 276.0779 (–0.6 ppm error).

Lab Book Reference: SY-3-87

Experimental Procedures for Chapter 4

2-Bromo-1-(pyrrolidin-1-yl)ethanone 209

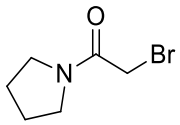

209

Pyrrolidine (1.2 mL, 14.4 mmol, 2.0 eq.) was added dropwise to a stirred solution of bromoacetal bromide (0.5 mL, 7.2 mmol, 1.0 eq.) in anhydrous CH_2Cl_2 (10 mL) at 0 °C under Ar. The resulting solution was allowed to warm to rt and stirred at rt for 4 h. Saturated $NH_4Cl_{(aq)}$ (10 mL) and CH_2Cl_2 (10 mL) were added, and the two layers were separated. The aqueous layer was extracted with CH_2Cl_2 (3 × 10 mL). The combined organic layers were dried (Na_2SO_4), filtered, and evaporated under reduced pressure to give the crude product. Purification by flash column chromatography on silica using 80:20 EtOAc–hexane as eluent gave bromopyrroloamide **209** (965 mg, 70%) as a white solid, mp 32 – 35 °C; R_F (80:20 EtOAc–hexane) 0.32; IR (ATR) 2973, 2876, 1634 (C=O), 1446, 1421, 1421, 1341, 635, 517 cm^{-1}; ^1H NMR (400 MHz, $CDCl_3$) (50:50 mixture of rotamers) δ 3.78 (s, 2H, CH_2Br), 3.48 (dt, J = 18.0, 7.0, 7.0 Hz, 4H, NCH), 2.04 – 1.92 (m, 2H, CH_2), 1.92 – 1.81 (m, 2H, CH_2); ^{13}C NMR (100.6 MHz, $CDCl_3$) (rotamers) δ 165.1 (C=O), 47.1 (NCH_2), 46.5 (NCH_2), 27.5 (CH_2Br), 26.2 (CH_2), 24.4 (CH_2); MS (ESI) *m/z* 214 [($^{79}M + Na)^+$, 100]; HRMS ESI *m/z* calcd for $C_6H_{10}{}^{79}BrNO$ [($^{79}M + Na)^+$, 100] 213.9838, found 213.9844 (–2.6 ppm error). Spectroscopic data consistent with those reported in the literature.[152]

Lab Book Reference: SY-7-340

tert-Butyl but-3-en-1-yl(2-oxo-2-(pyrrolidin-1-yl)ethyl)carbamate 211

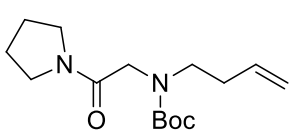

211

Amino alkene **210** (3.4 mL, 37.26 mmol, 1.0 eq.), $NaHCO_3$ (9.39 g, 111.78 mmol, 3.0 eq.) and Boc_2O (9.76 g, 44.71 mmol, 1.2 eq.) were added to a stirred solution of THF (50 mL) and H_2O (50 mL) at rt. The resulting solution was stirred at rt for 16 h. The two

layers were separated, and the aqueous layer was extracted with EtOAc (3 x 50 mL). The combined organic layers were dried ($NaSO_4$) and evaporated under reduced pressure to give the crude Boc-amine intermediate. Then, NaH (350 mg of a 60% dispersion in mineral oil, 8.76 mmol, 1.5 eq.) was added portionwise to a stirred solution of crude Boc-amine intermediate (1.00 g, 5.84 mmol, 1.0 eq.) in DMF (20 mL) at 0 °C under Ar. The resulting solution was stirred at rt for 2 h. Bromopyrroloamide **209** (1.46 g, 7.59 mmol, 1.3 eq.) was then added to the reaction mixture at 0 °C under Ar. The resulting solution was further stirred at rt for 16 h. Brine (20 mL) and EtOAc (20 mL) were added, and the two layers were separated. The aqueous layer was extracted with EtOAc (3 × 20 mL). The combined organic layers were washed with brine (3 × 20 mL), dried (Na_2SO_4), filtered, and evaporated under reduced pressure to give the crude product. Purification by flash column chromatography on silica using 50:50 EtOAc–hexane as eluent gave dialkylcarbamate **211** (968 mg, 59%) as a colourless oil, R_F (EtOAc) 0.29; IR (ATR) 2974, 2876, 1692 (C=O), 1651 (C=O), 1439, 1404, 1364, 1231, 1167, 1147, 913, 889 cm^{-1}; ^1H NMR (400 MHz, $CDCl_3$) (65:35 mixture of rotamers) δ 5.71 – 5.52 (m, 1H, C*H*=CH_2), 4.97 – 4.77 (m, 2H, CH=C*H*$_2$), 3.81 (s, 1.3H, NCH_2), 3.72 (s, 0.7H, NCH_2), 3.35 – 3.17 (m, 6H, NCH_2), 2.21 – 2.10 (m, 2H, CH_2), 1.89 – 1.77 (m, 2H, CH_2), 1.77 – 1.62 (m, 2H, CH_2), 1.32 (s, 5.9H, CMe_3), 1.26 (s, 3.1H, CMe_3); ^{13}C NMR (100.6 MHz, $CDCl_3$) (rotamers) δ 167.3 (C=O), 167.1 (C=O), 155.9 (C=O), 155.3 (C=O), 135.7 (*C*H=CH_2), 116.4 (CH=*C*H$_2$), 116.3 (CH=*C*H$_2$), 79.8 (O*C*Me$_3$), 79.6 (O*C*Me$_3$), 49.8 (NCH_2), 49.3 (NCH_2), 47.9 (NCH_2), 46.6 (NCH_2), 46.3 (NCH_2), 45.9 (NCH_2), 45.5 (NCH_2), 32.9 (CH_2), 32.5 (CH_2), 28.3 (C*Me*$_3$), 28.2 (C*Me*$_3$), 26.2 (CH_2), 26.1 (CH_2), 24.2 (CH_2), 24.0 (CH_2); MS (ESI) *m/z* 305 [(M + Na)$^+$, 100], HRMS ESI *m/z* calcd for $C_{15}H_{26}N_2O_3$ [(M + Na)$^+$, 100] 305.1836, found 305.1834 (0.6 ppm error).

Lab Book Reference: SY-7-317

N-(But-3-en-1-yl)-4-methylbenzenesulfonamide 214

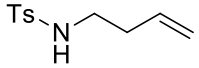

214

Bromo alkene **213** (5.0 mL, 49.26 mmol, 1.1 eq.) was added to a stirred solution of 4-methylbenzenesulfonamide (7.67 g, 44.78 mmol, 1.0 eq.) and K_2CO_3 (12.38 g, 89.56

mmol, 2.0 eq.) in MeCN (100 mL) at rt. The resulting solution was stirred and heated at 80 °C for 16 h. H_2O (50 mL) and EtOAc (50 mL) were added, and the two layers were separated. The aqueous layer was extracted with EtOAc (3 × 50 mL). The combined organic layers were dried (Na_2SO_4), filtered, and evaporated under reduced pressure to give the crude product. Purification by flash column chromatography on silica using 50:50 EtOAc–hexane as eluent gave alkylsulfonamide **214** (9.70 g, 96%) as a crystalline white solid, mp 98 – 101 °C; R_F (40:60 EtOAc–hexane) 0.39; IR (ATR) 3272 (NH), 3078, 2980, 2926, 1321 (SO_2), 1306, 1290, 1154, 1093, 916, 813, 660, 548 cm^{-1}; ^1H NMR (400 MHz, $CDCl_3$) δ 7.78 – 7.71 (m, 2H, Ar), 7.34 – 7.27 (m, 2H, Ar), 5.62 (ddt, J = 17.0, 10.5, 7.0 Hz, 1H, C*H*=CH_2), 5.10 – 4.97 (m, 2H, CH=C*H*$_2$), 4.74 – 4.48 (m, 1H, NH), 3.05 – 2.95 (m, 2H, NCH_2), 2.42 (s, 3H, Me), 2.24 – 2.14 (m, 2H, CH_2); ^{13}C NMR (100.6 MHz, $CDCl_3$) δ 143.5 (*ipso*-Ar), 137.0 (*ipso*-Ar), 134.3 (*C*H=CH_2), 129.8 (Ar), 127.2 (Ar), 118.2 (CH=*C*H$_2$), 42.2 (NCH_2), 33.7 (CH_2), 21.6 (Me); MS (ESI) *m/z* 248 [(M + $Na)^+$, 100]; HRMS ESI *m/z* calcd for $C_{11}H_{15}NO_2S$ [(M + $Na)^+$, 100] 248.0716, found 248.0708 (+3.0 ppm error).

Lab Book Reference: SY-7-330

N-(But-3-en-1-yl)-4-methyl-*N*-(2-oxo-2-(pyrrolidine-1-yl)ethyl) benzenesulfonamide 203

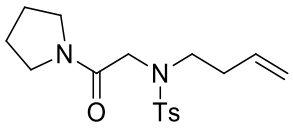

203

Bromopyrroloamide **209** (8.27 g, 43.04 mmol, 1.0 eq.) was added to a stirred solution of alkylsulfonamide **214** (9.70 g, 43.04 mmol, 1.0 eq.) and K_2CO_3 (29.74 g, 215.19 mmol, 5.0 eq.) in MeCN (200 mL) at rt. The resulting solution was stirred and heated at 80 °C for 16 h. H_2O (80 mL) and EtOAc (80 mL) were added, and the two layers were separated. The aqueous layer was extracted with EtOAc (3 × 80 mL). The combined organic layers were dried (Na_2SO_4), filtered, and evaporated under reduced pressure to give the crude product. Purification by flash column chromatography on silica using 50:50 EtOAc–hexane as eluent gave dialkylsulfonamide **203** (7.35 g, 51%) as a crystalline white solid, mp 80 – 82 °C; R_F (EtOAc) 0.50; IR (ATR) 2978, 2879, 2246, 1651 (C=O), 1447, 1335 (SO_2), 1156, 1091, 908, 725, 646, 547 cm^{-1}; ^1H NMR (400 MHz, $CDCl_3$) (50:50 mixture

of rotamers) δ 7.75 – 7.67 (m, 2H, Ar), 7.30 – 7.23 (m, 2H, Ar), 5.68 (ddt, J = 17.0, 10.0, 7.0 Hz, 1H, C*H*=CH_2), 5.07 – 4.94 (m, 2H, CH=C*H*$_2$), 3.98 (s, 2H, NCH_2), 3.49 (t, J = 7.0 Hz, 2H, NCH_2), 3.38 (t, J = 7.0 Hz, 2H, NCH_2), 3.32 – 3.24 (m, 2H, NCH_2), 2.39 (s, 3H, Me), 2.28 (q, J = 7.0 Hz, 2H, CH_2), 2.00 – 1.89 (m, 2H, CH), 1.87 – 1.76 (m, 2H, CH); ^{13}C NMR (100.6 MHz, $CDCl_3$) (rotamers) δ 165.9 (C=O), 143.4 (*ipso*-Ar), 136.3 (*ipso*-Ar), 134.9 (C*H*=CH_2), 129.6 (Ar), 127.6 (Ar), 117.0 (CH=C*H*$_2$), 50.0 (NCH_2), 48.0 (NCH_2), 46.24 (NCH_2), 46.18 (NCH_2), 32.6 (CH_2), 26.3 (CH_2), 24.1 (CH_2), 21.6 (Me); MS (ESI) *m/z* 359 [$(M + Na)^+$, 100;, HRMS ESI *m/z* calcd for $C_{17}H_{24}N_2O_3S$ [$(M + Na)^+$, 100] 359.1400, found 359.1398 (–0.5 ppm error).

Lab Book Reference: SY-7-331

2-Tosyl-2-azabicyclo[3.2.0]heptan-7-one 205

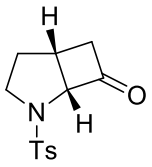

205

A solution of dialkylsulfonamide **203** (7.35 g, 21.86 mmol, 1.0 eq.) in 1,2-dichloroethane (60 mL) was added dropwise to a stirred solution of triflic anhydride (5.5 mL, 32.78 mmol, 1.5 eq.) in 1,2-dichloroethane (60 mL) at rt under Ar. Then, a solution of 2,4,6-trimethylpyridine (3.2 mL, 24.04 mmol, 1.1 eq.) in 1,2-dichloroethane (60 mL) was added at rt under Ar. The resulting solution was stirred and heated at 80 °C for 2 h under Ar. The solvent was evaporated under reduced pressure and then H_2O (90 mL) and CH_2Cl_2 (90 mL) were added. The resulting mixture was stirred and heated at 60 °C for 2 h. After being allowed to cool to rt, the two layers were separated, and the aqueous layer was extracted with CH_2Cl_2 (3 × 60 mL). The combined organic layers were dried (Na_2SO_4), filtered, and evaporated under reduced pressure to give the crude product. Purification by flash column chromatography on silica using 60:40 hexane–EtOAc as eluent gave tosyl cyclobutanone **205** (3.74 g, 65%) as a white solid, mp 99 – 100 °C; R_F (60:40 hexane–EtOAc) 0.24; IR (ATR) 2980, 2873, 1786 (C=O), 1597, 1342 (S=O), 1159, 1090, 1014, 982, 817, 771, 658, 577, 549 cm^{-1}; ^{1}H NMR (400 MHz, $CDCl_3$) δ 7.79 – 7.71 (m, 2H, Ar), 7.36 – 7.27 (m, 2H, Ar), 5.07 (ddd, J = 7.0, 3.5, 3.5 Hz, 1H, NCH), 3.86 (ddd, J =

10.5, 8.0, 2.0 Hz, 1H, NCH), 3.22 – 3.10 (m, 2H, NCH, CH), 3.10 – 3.00 (m, 1H, CH), 2.53 (ddd, *J* = 18.5, 5.0, 3.5 Hz, 1H, CH), 2.42 (s, 3H, Me), 1.96 – 1.82 (m, 1H, CH), 1.82 – 1.73 (m, 1H, CH); ^{13}C NMR (100.6 MHz, $CDCl_3$) δ 205.2 (C=O), 143.9 (*ipso*-Ar), 135.9 (*ipso*-Ar), 129.8 (Ar), 127.8 (Ar), 77.2 (NCH), 50.4 (NCH_2), 48.1 (CH_2), 30.8 (CH), 30.6 (CH_2), 21.7 (Me); MS (ESI) *m/z* 288 [$(M + Na)^+$, 100]; HRMS ESI *m/z* calcd for $C_{13}H_{15}NO_3S$ [$(M + Na)^+$, 100] 288.0665, found 288.0665 (+0.1 ppm error).

Lab Book Reference: SY-7-333

2-Tosyl-2-azabicyclo[3.2.0]heptan-7-ol 215

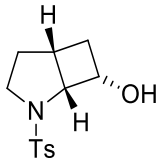

215

$NaBH_4$ (1.07, 28.22 mmol, 2.0 eq.) was added portionwise to a stirred solution of tosyl cyclobutanone **205** (3.74 g, 14.11 mmol, 1.0 eq.) in MeOH (250 mL) at rt. The resulting solution was stirred at rt for 4 h. Brine (100 mL) and EtOAc (80 mL) were added, and the two layers were separated. The aqueous layer was extracted with EtOAc (3 × 80 mL). The combined organic layers were washed with brine (3 × 50 mL), dried (Na_2SO_4), filtered, and evaporated under reduced pressure to give tosyl cyclobutanol **215** (3.93 g, 80%) as a white solid, mp 80 – 82 °C; R_F (EtOAc) 0.22; IR (ATR) 3499 (OH), 2971, 2927, 1709, 1597, 1329 (S=O), 1152, 1091, 1051, 957, 816, 678, 656, 596, 560 cm^{-1}; ^{1}H NMR (400 MHz, $CDCl_3$) δ 7.76 – 7.67 (m, 2H, Ar), 7.33 – 7.27 (m, 2H, Ar), 4.31 – 4.23 (m, 1H, HOC*H*), 4.23 – 4.18 (m, 1H, NCH), 3.78 – 3.62 (m, 2H, NCH), 2.91 (br s, 1H, OH), 2.69 – 2.58 (m, 1H, CH), 2.53 – 2.43 (m, 1H, CH), 2.42 (s, 3H, Me), 1.69 – 1.63 (m, 1H, CH), 1.63 – 1.56 (m, 1H, CH), 1.55 – 1.40 (m, 1H, CH); ^{13}C NMR (100.6 MHz, $CDCl_3$) δ 143.8 (*ipso*-Ar), 135.9 (*ipso*-Ar), 129.9 (Ar), 127.3 (Ar), 64.34 (NCH), 64.32 (HOCH), 50.1 (NCH_2), 34.7 (CH_2), 33.1 (CH), 30.0 (CH_2), 21.6 (Me); MS (ESI) *m/z* 290 [$(M + Na)^+$, 100]; HRMS ESI *m/z* calcd for $C_{13}H_{17}NO_3S$ [$(M + Na)^+$, 100] 290.0821, found 290.0824 (–0.8 ppm error).

Lab Book Reference: SY-7-334

***N*-(But-3-en-1-yl)-4-nitrobenzenesulfonamide 216 and *N*,*N*-di(But-3-en-1-yl)-4-nitrobenzenesulfonamide 217**

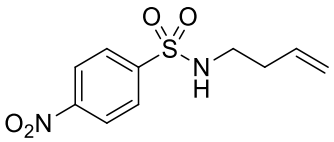

216

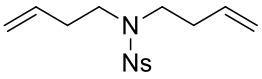

217

Bromo alkene **213** (18 mL, 177.3 mmol, 1.0 eq.) was added to a stirred suspension of 4-nitrobenzenesulfonamide (30.36 g, 177.3 mmol, 1.0 eq.) and K_2CO_3 (29.41 g, 212.8 mmol, 1.2 eq.) in MeCN (300 mL) at rt under Ar. The resulting solution was stirred and heated at 60 °C for 168 h under Ar. Saturated $NH_4Cl_{(aq.)}$ (80 mL) and EtOAc (80 mL) were added, and the two layers were separated. The aqueous layer was extracted with EtOAc (3 × 80 mL). The combined organic layers were dried ($NaSO_4$), filtered, and evaporated under reduced pressure to give the crude product. Purification by flash column chromatography on silica using hexane to 70:30 hexane–EtOAc as eluent gave alkylsulfonamide **216** (11.27 g, 25%) as a crystalline white solid, mp 140 – 142 °C; R_F (60:40 hexane–EtOAc) 0.26; IR (ATR) 3274 (NH), 3107, 1607, 1525 (NO_2), 1347 (S=O), 1309, 1159, 1093, 853, 736, 611 cm^{-1}; ^1H NMR (400 MHz, DMSO-d_6) δ 8.45 – 8.37 (m, 2H, Ar), 8.10 – 8.00 (m, 2H, Ar), 5.77 – 5.63 (m, 1H, C*H*=CH_2), 5.06 – 4.92 (m, 2H, CH=C*H*$_2$), 3.32 (s, 1H, NH), 2.87 (t, J = 7.0 Hz, 2H, NCH_2), 2.19 – 2.09 (m, 2H, CH_2); ^{13}C NMR (100.6 MHz, DMSO-d_6) δ 149.5 (*ipso*-Ar), 146.2 (*ipso*-Ar), 135.1 (*C*H=CH_2), 128.1 (Ar), 124.6 (Ar), 116.9 (CH=*C*H_2), 42.1 (NCH_2), 33.4 (CH_2); MS (ESI) *m/z* 279 [(M + Na)$^+$, 100]; HRMS ESI *m/z* calcd for $C_{10}H_{12}N_2O_4S$ [(M + Na)$^+$, 100] 279.0410, found 279.0407 (+1.2 ppm error) and dialkylsulfonamide **217** (5.65 g, 21%) as a yellow oil, R_F (40:60 EtOAc-hexane) 0.44; IR (ATR) 3106, 3079, 2980, 2936, 2870, 1527 (NO_2), 1347 (S=O), 1310, 1256, 1088, 918, 855, 755, 741, 599, 551, 463 cm^{-1}; ^1H NMR (400 MHz, $CDCl_3$) δ 8.39 – 8.31 (m, 2H, Ar), 8.04 – 7.96 (m, 2H, Ar), 5.69 (ddt, J = 17.0, 10.5, 7.0 Hz, 2H, C*H*=CH_2), 5.12 – 5.01 (m, 4H, CH=C*H*$_2$), 3.31 – 3.22 (m, 4H, NCH_2), 2.36 – 2.26 (m, 4H, CH_2); ^{13}C NMR (100.6 MHz, $CDCl_3$) δ 150.0 (*ipso*-Ar), 146.2 (*ipso*-Ar), 134.2 (*C*H=CH_2), 128.4 (Ar), 124.5 (Ar), 117.8 (CH=C*H*$_2$), 47.8 (NCH_2), 33.2 (CH_2); MS (ESI) *m/z* 333 [(M + Na)$^+$, 100], HRMS ESI *m/z* calcd for $C_{14}H_{18}N_2O_4S$ [(M + Na)$^+$, 100] 333.0879, found 333.0881 (–0.6 ppm error).

Lab Book Reference: SY-7-343

***N*-(But-3-en-1-yl)-4-nitro-N-(2-oxo-2-(pyrrolidin-1-yl)ethyl)benzenesulfonamide 218**

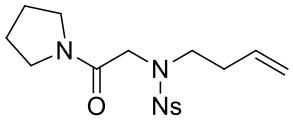

218

Bromopyrroloamide **209** (2.88 g, 15.00 mmol, 1.2 eq.) was added to a stirred solution of alkylsulfonamide **216** (3.20 g, 12.50 mmol, 1.0 eq.) and K_2CO_3 (2.59 g, 18.75 mmol, 1.5 eq.) in MeCN (40 mL) at rt under Ar. The resulting solution was stirred and heated at 60 °C for 96 h. H_2O (40 mL) and EtOAc (40 mL) were added, and the two layers were separated. The aqueous layer was extracted with EtOAc (3 × 40 mL). The combined organic layers were dried (Na_2SO_4), filtered, and evaporated under reduced pressure to give the crude product. Purification by flash column chromatography on silica using 50:50 EtOAc–hexane as eluent gave dialkylsulfonamide **218** (3.52 g, 77%) as a crystalline white solid, mp 116 – 118 °C; IR (ATR) 2976, 2878, 1656 (C=O), 1529 (NO_2), 1449, 1349 (S=O), 1160, 1091, 932, 547 cm^{-1}; ^1H NMR (400 MHz, $CDCl_3$) δ 8.38 – 8.27 (m, 2H, Ar), 8.12 – 8.03 (m, 2H, Ar), 5.74 (ddt, J = 17.0, 10.0, 6.5 Hz, 1H, C*H*=CH_2), 5.15 – 5.02 (m, 2H, CH=C*H*$_2$), 4.16 (s, 2H, NCH_2), 3.45 – 3.33 (m, 6H, NCH_2), 2.41 – 2.31 (m, 2H, CH_2), 2.06 – 1.94 (m, 2H, CH_2), 1.91 – 1.80 (m, 2H, CH_2); ^{13}C NMR (100.6 MHz, $CDCl_3$) (rotamers) δ 165.3 (C=O), 150.0 (*ipso*-Ar), 145.8 (*ipso*-Ar), 134.5 (CH=CH_2), 129.0 (Ar), 124.1 (Ar), 117.6 (CH=CH_2), 48.7 (NCH_2), 47.7 (NCH_2), 46.2 (NCH_2), 46.0 (NCH_2), 32.7 (CH_2), 26.4 (CH_2), 24.1 (CH_2); MS (ESI) *m/z* 390 [$(M + Na)^+$, 100]; HRMS ESI *m/z* calcd for $C_{16}H_{21}N_3O_5S$ [$(M + Na)^+$, 100] 390.1094, found 390.1100 (–1.6 ppm error).

Lab Book Reference: SY-7-351

2-((4-Nitrophenyl)sulfonyl)-2-azabicyclo[3.2.0]heptan-7-one 219

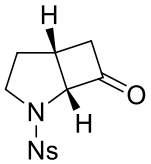

219

A solution of dialkylsulfonamide **218** (1.00 g, 2.72 mmol, 1.0 eq.) in 1,2-dichloroethane (10 mL) was added dropwise to a stirred solution of triflic anhydride (0.7 mL, 4.08 mmol, 1.5 eq.) in 1,2-dichloroethane (20 mL) at rt under Ar. Then, a solution of 2,4,6-trimethylpyridine (0.4 mL, 2.99 mmol, 1.1 eq.) in 1,2-dichloroethane (10 mL) was added at rt under Ar. The resulting solution was stirred and heated at 80 °C for 2 h under Ar. The solvent was evaporated under reduced pressure and then H_2O (20 mL) and CH_2Cl_2 (20 mL) were added. The resulting mixture was stirred and heated at 60 °C for 2 h. After being allowed to cool to rt, the two layers were separated, and the aqueous layer was extracted with CH_2Cl_2 (3 × 20 mL). The combined organic layers were dried (Na_2SO_4), filtered, and evaporated under reduced pressure to give the crude product. Purification by flash column chromatography on silica using 50:50 EtOAc–hexane as eluent gave nosyl cyclobutanone **219** (660 mg, 82%) as a white solid, mp 121 – 123 °C; R_F (50:50 EtOAc–hexane) 0.21; IR (ATR) 3069, 2132, 1651 (C=O), 1531 (NO_2), 1351 (S=O), 1167, 1047, 1024, 990, 826, 764 cm^{-1}; ^1H NMR (400 MHz, DMSO-d_6) δ 8.45 – 8.38 (m, 2H, Ar), 8.15 – 8.06 (m, 2H, Ar), 5.15 (ddd, J = 7.0, 3.5, 3.5 Hz, 1H, NCH), 3.85 – 3.77 (m, 1H, NCH), 3.27 (ddd, J = 11.5, 11.5, 6.5 Hz, 1H, NCH), 3.17 (ddd, J = 18.5, 9.5, 3.0 Hz, 1H, CH), 2.98 – 2.88 (m, 1H, CH), 2.71 – 2.62 (m, 1H, CH), 1.78 – 1.68 (m, 1H, CH), 1.56 – 1.43 (m, 1H, CH); ^{13}C NMR (101 MHz, DMSO-d_6) δ 206.2 (C=O), 150.1 (*ipso*-Ar), 143.7 (*ipso*-Ar), 128.8 (Ar), 124.7 (Ar), 76.8 (NCH), 50.0 (CH_2), 48.6 (NCH_2), 29.9 (CH), 29.6 (CH_2); MS (ESI) *m/z* 319 [$(M + Na)^+$, 100], HRMS ESI *m/z* calcd for $C_{12}H_{12}N_2O_5S$ [$(M + Na)^+$, 100] 319.0359, found 319.0370 (–3.5 ppm error).

Lab Book Reference: SY-7-355

2-((4-Nitrophenyl)sulfonyl)-2-azabicyclo[3.2.0]heptan-7-ol *endo*-220

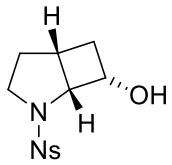

endo-**220**

$NaBH_4$ (39 mg, 1.02 mmol, 2.0 eq.) was added portionwise to a stirred solution of nosyl cyclobutanone **219** (151 mg, 0.51 mmol, 1.0 eq.) in MeOH (10 mL) at rt. The resulting solution was stirred at rt for 4 h. Brine (10 mL) and EtOAc (20 mL) were added, and the two layers were separated. The aqueous layer was extracted with EtOAc (3 × 20 mL).

The combined organic layers were washed with brine (3 × 10 mL), dried (Na_2SO_4), filtered, and evaporated under reduced pressure to give nosyl cyclobutanol *endo*-**220** (138 mg, 91%) as a white solid, mp 115 – 117 °C; R_F (EtOAc) 0.29; IR (ATR) 3521 (OH), 3106, 2979, 1528 (NO_2), 1349 (S=O), 1308, 1159, 1095, 856, 733, 688, 620 cm^{-1}; ^1H NMR (400 MHz, DMSO-d_6) δ 8.39 – 8.33 (m, 2H, Ar), 8.10 – 8.05 (m, 2H, Ar), 5.04 (d, J = 7.0 Hz, 1H, OH), 4.38 (ddd, J = 6.0, 6.0, 3.0 Hz, 1H, NCH), 4.19 – 4.07 (m, 1H, HOC*H*), 3.78 (dd, J = 11.5, 8.0 Hz, 1H, NCH), 3.53 (ddd, J = 11.5, 11.5, 6.0 Hz, 1H, NCH), 2.62 – 2.53 (m, 1H, CH), 2.36 – 2.25 (m, 1H, CH), 1.49 (dd, J = 12.5, 6.0 Hz, 1H, CH), 1.42 (ddd, J = 12.5, 7.5, 7.5 Hz, 1H, CH), 1.25 – 1.14 (m, 1H, CH); ^{13}C NMR (101 MHz, DMSO-d_6) δ 149.6 (*ipso*-Ar), 145.4 (*ipso*-Ar), 128.4 (Ar), 124.5 (Ar), 65.1 (NCH), 64.2 (HOCH), 48.8 (NCH_2), 34.1 (CH_2), 32.3 (CH), 29.8 (CH_2); MS (ESI) *m/z* 321 [(M + Na)$^+$, 100]; HRMS ESI *m/z* calcd for $C_{12}H_{14}N_2O_5S$ [(M + Na)$^+$, 100] 321.0516, found 321.0518 (–0.7 ppm error).

Lab Book Reference: SY-7-354

Experimental Procedures for Chapter 5

3-(Methylsulfonyl)propanoic acid 235

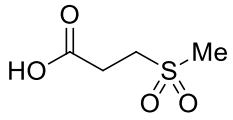

235

β-Sulfido acid **247** (7.54 g, 62.7 mmol, 1.0 eq.) was added to a stirred mixture of acetic acid (30.5 mL, 0.53 mol, 8.5 eq.) and acetic anhydride (29.7 mL, 0.31 mol, 5.0 eq.) at 0 °C. The resulting mixture was stirred at 0 °C for 30 min. Then, H_2O_2 (32.0 mL of a 30% w/v aqueous solution, 0.28 mol, 4.5 eq.) was added portion wise over 30 min at 0 °C. After being allowed to warm to rt, the resulting solution was stirred at rt for 16 h. A spatula tip of MnO_2 was added and the mixture was stirred at rt for 2 h. The reaction mixture was evaporated under reduced pressure to give the crude product. The solids were removed by purification by hot filtration using boiling EtOAc and the filtrate was evaporated under reduced pressure to give *β*-sulfonyl acid **235** (9.46 g, 99%) as a white solid, ^{1}H NMR (400 MHz, DMSO-d_6) δ 12.59 (br s, 1H, OH), 3.33 (t, J = 7.5 Hz, 2H, CH_2), 2.99 (s, 3H, SO_2Me), 2.67 (t, J = 7.5 Hz, 2H, CH_2). Spectroscopic data consistent with those reported in the literature.[194]

Lab Book Reference: SY-4-142

3-(Methylsulfonyl)-1-(4-phenylpiperidin-1-yl)propan-1-one 245

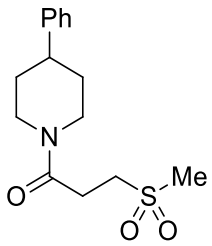

245

4-Phenylpiperidine **244** (320 mg, 2.0 mmol, 1.0 eq.) was added to a stirred solution of *β*-sulfonyl acid **235** (610 mg, 4.0 mmol, 2.0 eq.) and pyridine (1.0 mL, 12.0 mmol, 6.0 eq.) in anhydrous EtOAc (20 mL) at rt under Ar. Then, T3P (3.8 mL of a 50% wt solution in toluene, 6.0 mmol, 3.0 eq.) was added and the resulting solution was stirred at

rt for 16 h. 1.0 M $HCl_{(aq)}$ (10 mL) and EtOAc (10 mL) were added. The two layers were separated, and the aqueous layer was extracted with EtOAc (3 × 10 mL). The combined organic extracts were dried ($NaSO_4$), filtered, and evaporated under reduced pressure to give the crude product. Purification by flash column chromatography on silica with 90:10 to 80:20 CH_2Cl_2–acetone as eluent gave *β*-sulfonyl amide **245** (370 mg, 62%) as a white solid, mp 138 – 140 °C; R_F (80:20 hexane–EtOAc) 0.29; IR (ATR) 3008, 2931, 2862, 1730, 1633 (C=O), 1454, 1302 (SO_2), 1278, 1121, 1007, 761, 701, 509, 464 cm^{-1}; ^1H NMR (400 MHz, $CDCl_3$) δ 7.35 – 7.29 (m, 2H, Ar), 7.25 – 7.17 (m, 3H, Ar), 4.80 – 4.70 (m, 1H, NCH), 4.03 – 3.93 (m, 1H, NCH), 3.46 (t, J = 7.5 Hz, 2H, CH), 3.18 (ddd, J = 13.0, 13.0, 2.5 Hz, 1H, NCH), 3.00 (s, 3H, SO_2Me), 2.98 – 2.92 (m, 2H, CH), 2.81 – 2.73 (m, 1H, C*H*Ar), 2.73 – 2.65 (m, 1H, NCH), 2.00 – 1.87 (m, 2H, CH), 1.72 – 1.56 (m, 2H, CH); ^{13}C NMR (100.6 MHz, $CDCl_3$) (rotamers) δ 167.2 (C=O), 144.9 (*ipso*-Ar), 135.9 (*ipso*-Ar), 128.8 (Ar), 126.8 (Ar), 50.7 (CH_2), 46.2 (NCH_2), 43.1 (CH), 42.7 (NCH_2), 42.0 (SO_2Me), 41.9 (SO_2Me), 33.8 (CH_2), 32.9 (CH_2), 26.1 (CH_2); MS (EI) *m/z* 318 [(M + $Na)^+$, 100]; HRMS (ESI) *m/z* calcd for $C_{15}H_{21}NO_3S$ [(M + $Na)^+$, 100] 318.1134, found 318.1134 (+0.1 ppm error).

Lab Book Reference: SY-4-141

1-(4-Phenylpiperidin-1-yl)prop-2-en-1-one 246

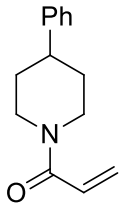

246

β-Sulfonyl amide **245** (150 mg, 0.5 mmol, 1.0 eq.), Cs_2CO_3 (500 mg, 1.5 mmol, 3.0 eq.), toluene (5 mL) and H_2O (0.5 mL) were added to a pressure tube. The resulting mixture was stirred and heated at 100 °C in a sealed pressure tube for 16 h. After being allowed to cool to rt, the mixture was added to EtOAc (10 mL) and H_2O (10 mL). The two layers were separated, and the aqueous layer was extracted with EtOAc (3 × 10 mL). The combined organic extracts were dried ($NaSO_4$), filtered, and evaporated under reduced pressure to give the crude product. Purification by flash column chromatography on silica

with 50:50 EtOAc–hexane as eluent gave *β*-sulfonyl amide **245** (130 mg, 84% recovery) as a white solid and acrylamide **246** (18 mg, 16%) as a colourless oil, R_F (50:50 hexane–EtOAc) 0.20; IR (ATR) 2936, 1644 (C=O), 1608, 1452, 1263, 1215, 1008, 759, 700 cm^{-1}; ^1H NMR (400 MHz, $CDCl_3$) δ 7.35 – 7.29 (m, 2H, Ar), 7.25 – 7.17 (m, 3H, Ar), 6.63 (dd, *J* = 17.0, 10.5 Hz, 1H, C*H*=CH_2), 6.30 (dd, *J* = 17.0, 2.0 Hz, 1H, CH=C*H*$_2$), 5.70 (dd, *J* = 10.5, 2.0 Hz, 1H, CH=C*H*$_2$), 4.89 – 4.79 (m, 1H, NCH), 4.18 – 4.08 (m, 1H, NCH), 3.24 – 3.11 (m, 1H, NCH), 2.83 – 2.65 (m, 2H, NCH, C*H*Ar), 1.97 – 1.88 (m, 2H, CH), 1.75 – 1.58 (m, 2H, CH); ^{13}C NMR (100.6 MHz, $CDCl_3$) δ 165.5 (C=O), 145.2 (*ipso*-Ar), 128.7 (Ar), 128.0 (*C*H=CH_2), 127.6 (CH=*C*H_2), 126.8 (Ar), 126.6 (*ipso*-Ar), 46.5 (br, NCH) 42.8 (*C*HAr), 33.5 (br, CH_2); MS (EI) *m/z* 238 [$(M + Na)^+$, 100]; HRMS (ESI) *m/z* calcd for $C_{14}H_{17}NO$ [$(M + Na)^+$, 100] 238.1202, found 238.1202 (+0.1 ppm error).

Lab Book Reference: SY-4-144

β-Sulfonyl amide **245** (150 mg, 0.5 mmol, 1.0 eq.), NaOH (0.8 mL of a 2.0 M aqueous solution, 1.5 mmol, 3 eq.) and DMF (10 mL) was added to a pressure tube. The resulting mixture was stirred and heated at 100 °C in a sealed pressure tube for 16 h. After being allowed to cool to rt, the mixture was added to EtOAc (10 mL) and brine (10 mL). The two layers were separated, and the aqueous layer was extracted with EtOAc (3 × 10 mL). The combined organic extracts were washed with brine (3 × 10 mL), dried ($NaSO_4$), filtered, and evaporated under reduced pressure to give the crude product. Purification by flash column chromatography on silica with 50:50 EtOAc–hexane as eluent gave acrylamide **246** (18 mg, 16%) as a colourless oil.

Lab Book Reference: SY-4-143

β-Sulfonyl amide **245** (150 mg, 0.5 mmol, 1.0 eq.), Cs_2CO_3 (500 mg, 1.5 mmol, 3 eq.), $BnEt_3N^+Cl^-$ (14 mg, 61 μmol, 0.18 eq.), toluene (5 mL) and H_2O (0.5 mL) were added to a pressured tube. The resulting mixture was stirred and heated at 100 °C in a sealed pressure tube for 16 h. After being allowed to cool to rt, the mixture was added to EtOAc (10 mL) and H_2O (10 mL). The two layers were separated, and the aqueous layer was extracted with EtOAc (3 × 10 mL). The combined organic extracts were dried ($NaSO_4$), filtered, and evaporated under reduced pressure to give the crude product. Purification by

flash column chromatography on silica with 50:50 EtOAc–hexane as eluent gave acrylamide **246** (70 mg, 96%) as a colourless oil.

Lab Book Reference: SY-4-145

6-Methyl-2-(5-(3-(methylsulfonyl)propanoyl)-5-azaspiro[2.4]heptan-1-yl)-1,3,6,2-dioxazaborocane-4,8-dione *trans*-247

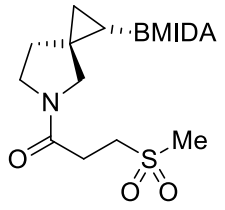

trans-**247**

TFA (2.0 mL) was added to a stirred solution of MIDA building block *trans*-**38** (100 mg, 0.28 mmol, 1.0 eq.) in CH_2Cl_2 (10 mL) at rt under Ar. The resulting solution was stirred at rt for 30 min. Then, the solvent was evaporated under reduced pressure to give a residue. Toluene (5 × 10 mL) was added, and the solvent was evaporated under reduced pressure to give the crude amine•TFA salt *trans*-**249**. To a stirred mixture of the crude amine•TFA salt *trans*-**249** in CH_2Cl_2 (10 mL) under Ar was added *β*-sulfonyl acid **235** (87 mg, 0.57 mmol, 2.0 eq.), DIPEA (0.1 mL, 0.57 mmol, 2.0 eq.) and pyridine (0.3 mL, 3.41 mmol, 12.0 eq.). Then, T3P (0.6 mL of a 50% wt solution in toluene, 0.85 mmol, 3.0 eq.) was added and the resulting solution was stirred at rt for 16 h. H_2O (10 mL) and CH_2Cl_2 (10 mL) were added. The two layers were separated and the aqueous layer was extracted with CH_2Cl_2 (3 × 10 mL). The combined organic extracts were dried (Na_2SO_4), filtered, and evaporated under reduced pressure to give the crude product. Purification by flash column chromatography on silica with acetone as eluent gave *β*-sulfonyl amide *trans*-**247** (11 mg, 10%) as a white solid, R_F (80:20 acetone–CH_2Cl_2) 0.25; IR (ATR) 2931, 1746 (C=O), 1706 (C=O), 1627 (C=O), 1452, 1417, 1359, 1299 (SO_2), 1225, 1200, 1122, 1024, 507 cm^{-1}; ^1H NMR (400 MHz, Acetone-d_6) (50:50 mixture of rotamers) δ 4.26 – 4.20 (m, 2H, MeNC*H*), 4.12 – 4.03 (m, 2H, MeNC*H*), 3.76 – 3.57 (m, 2H, NCH), 3.46 – 3.37 (m, 1H, NCH), 3.37 – 3.33 (m, 2H, CH), 3.33 – 3.29 (m, 2H, CH), 3.22 (s, 1.5H, NMe), 3.22 (s, 1.5H, NMe), 3.21 – 3.11 (m, 1H, NCH), 2.96 (s, 1.5H, SO_2Me), 2.95 (s, 1.5H, SO_2Me), 2.76 – 2.68 (m, 1H, CH), 1.87 (ddd, *J* = 12.5, 7.0, 4.0 Hz, 0.5H, CH), 1.76 (ddd, *J* = 12.5, 7.0, 4.0 Hz, 0.5H, CH), 0.82 (dd, *J* = 10.0, 3.5 Hz, 0.5H, CH),

0.75 (dd, J = 10.0, 3.5 Hz, 0.5H, CH), 0.53 – 0.46 (m, 1H, CH), 0.20 – 0.10 (m, 1H, BCH); ^{13}C NMR (100.6 MHz, Acetone-d_6) (rotamers) δ 169.0 (C=O, ester), 168.9 (C=O, ester), 167.8 (C=O, Boc), 167.7 (C=O, Boc), 62.7 (MeN*C*H), 62.7 (MeN*C*H), 62.6 (MeN*C*H), 56.3 (CH_2), 55.9 (CH_2), 50.8 (NMe), 50.8 (NMe), 47.5 (CH_2), 47.1 (CH_2), 41.1 (SO_2Me), 41.0 (SO_2Me), 32.0 (CH_2), 31.8 (CH_2), 28.1 (CH_2), 28.0 (CH_2), 26.8 (C), 25.3 (C), 16.2 (CH_2), 16.0 (CH_2) (BCH not resolved); MS (EI) *m/z* 409 [(M + Na)$^+$, 100]; HRMS (ESI) *m/z* calcd for $C_{15}H_{23}BN_2O_7S$ [(M + Na)$^+$, 100] 409.1211, found 409.1217 (–0.7 ppm error).

Lab Book Reference: SY-2-155

TFA (2.0 mL) was added to a stirred solution of MIDA building block *trans*-**38** (100 mg, 0.28 mmol, 1.0 eq.) in CH_2Cl_2 (10 mL) at rt under Ar. The resulting solution was stirred at rt for 30 min. Then, the solvent was evaporated under reduced pressure to give a residue. Toluene (5 × 10 mL) was added, and the solvent was evaporated under reduced pressure to give the crude amine•TFA salt *trans*-**249**. To a stirred mixture of the crude amine•TFA salt *trans*-**249** in EtOAc (3 mL) under Ar was added *β*-sulfonyl acid **235** (47 mg, 0.31 mmol, 1.1 eq.) and Et_3N (0.2 mL, 1.16 mmol, 4.0 eq.). Then, T3P (0.4 mL of a 50% wt solution in toluene, 0.56 mmol, 2.0 eq.) was added and the resulting solution was stirred at rt for 16 h. H_2O (10 mL) and EtOAc (10 mL) were added. The two layers were separated, and the aqueous layer was extracted with EtOAc (3 × 10 mL). The combined organic extracts were dried (Na_2SO_4), filtered, and evaporated under reduced pressure to give the crude product. Purification by flash column chromatography on silica with acetone as eluent gave *β*-sulfonyl amide *trans*-**247** (20 mg, 19%) as a white solid.

Lab Book Reference: SY-2-161

TFA (2.0 mL) was added to a stirred solution of MIDA building block *trans*-**38** (100 mg, 0.28 mmol, 1.0 eq.) in CH_2Cl_2 (10 mL) at rt under Ar. The resulting solution was stirred at rt for 30 min. Then, the solvent was evaporated under reduced pressure to give a residue. Toluene (5 × 10 mL) was added, and the solvent was evaporated under reduced pressure to give the crude amine•TFA salt *trans*-**249**. To a stirred mixture of the crude amine•TFA salt *trans*-**249** in EtOAc (10 mL) under Ar was added *β*-sulfonyl acid **235**

(64 mg, 0.42 mmol, 1.5 eq.) and Et_3N (0.2 mL, 1.40 mmol, 5.0 eq.). Then, T3P (0.6 mL of a 50% wt solution in toluene, 0.85 mmol, 3.0 eq.) was added and the resulting solution was stirred at rt for 16 h. H_2O (10 mL) and EtOAc (10 mL) were added. The two layers were separated, and the aqueous layer was extracted with EtOAc (3 × 10 mL). The combined organic extracts were dried (Na_2SO_4), filtered, and evaporated under reduced pressure to give the crude product. Purification by flash column chromatography on silica with acetone as eluent gave *β*-sulfonyl amide *trans*-**247** (38 mg, 35%) as a white solid.

Lab Book Reference: SY-2-162

TFA (2.0 mL) was added to a stirred solution of MIDA building block *trans*-**38** (100 mg, 0.28 mmol, 1.0 eq.) in CH_2Cl_2 (10 mL) at rt under Ar. The resulting solution was stirred at rt for 30 min. Then, the solvent was evaporated under reduced pressure to give a residue. Toluene (5 × 10 mL) was added, and the solvent was evaporated under reduced pressure to give the crude amine•TFA salt *trans*-**249**. To a stirred mixture of the crude amine•TFA salt *trans*-**249** in EtOAc (10 mL) under Ar was added *β*-sulfonyl acid **235** (85 mg, 0.56 mmol, 2.0 eq.) and Et_3N (0.3 mL, 1.68 mmol, 6.0 eq.). Then, T3P (0.7 mL of a 50% wt solution in toluene, 0.85 mmol, 3.0 eq.) was added and the resulting solution was stirred at rt for 16 h. H_2O (10 mL) and EtOAc (10 mL) were added. The two layers were separated, and the aqueous layer was extracted with EtOAc (3 × 10 mL). The combined organic extracts were dried (Na_2SO_4), filtered, and evaporated under reduced pressure to give the crude product. Purification by flash column chromatography on silica with acetone as eluent gave *β*-sulfonyl amide *trans*-**247** (33 mg, 31%) as a white solid.

Lab Book Reference: SY-2-164

β-Sulfonyl acid **235** (100 mg, 0.66 mmol, 1.0 eq.) was added to a stirred solution of CDI (117 mg, 0.72, 1.1 eq.) and DIPEA (0.23 mL, 1.32 mmol, 2.0 eq.) in CH_2Cl_2 (10 mL) at rt under Ar. The resulting solution was stirred at rt for 2 h. TFA (2.0 mL) was added to a stirred solution of MIDA building block *trans*-**38** (254 mg, 0.72 mmol, 1.1 eq.) in CH_2Cl_2 (10 mL) at rt for 30 min under Ar. Then, the solvent was evaporated under reduced pressure before toluene (5 × 10 mL) was added and evaporated under reduced pressure to give the crude amine•TFA salt *trans*-**249**. The CDI solution was transferred into the flask

containing crude amine•TFA salt *trans*-**249** before DIPEA (0.12 mL, 0.66 mmol, 1.0 eq.) was added at rt under Ar. The resulting solution was stirred at rt for 16 h. Saturated $NaHCO_{3(aq.)}$ (20 mL) and CH_2Cl_2 (10 mL) were added. The two layers were separated, and the aqueous layer was extracted with CH_2Cl_2 (3 × 20 mL). The combined organic extracts were dried (Na_2SO_4), filtered, and evaporated under reduced pressure to give the crude product. Purification by flash column chromatography on silica with acetone as eluent gave none of *β*-sulfonyl amide *trans*-**247**.

Lab Book Reference: SY-2-166

TFA (2.0 mL) was added to a stirred solution of MIDA Building Block *trans*-**38** (100 mg, 0.28 mmol, 1.0 eq.) in CH_2Cl_2 (5 mL) at rt under Ar. The resulting solution was stirred at rt for 30 min. Then, the solvent was evaporated under reduced pressure to give a residue. Toluene (5 × 10 mL) was added, and the solvent was evaporated under reduced pressure to give the crude amine•TFA salt *trans*-**249**. To a stirred mixture of crude amine•TFA salt *trans*-**249** in DMF (10 mL) was added *β*-sulfonyl acid **235** (47 mg, 0.31 mmol, 1.1 eq.), Et_3N (0.12 mL, 0.73 mmol, 3.0 eq.) and HATU (2.13 g, 5.60 mmol, 20.0 eq.) under Ar. Then, the resulting solution was stirred at rt for 16 h. H_2O (10 mL) and CH_2Cl_2 (10 mL) were added. The two layers were separated. The aqueous layer was extracted with CH_2Cl_2 (3 × 10 mL). The combined organic extracts were washed with brine (3 × 10 mL), dried (Na_2SO_4), filtered, and evaporated under reduced pressure to give the crude product. Purification by flash column chromatography on silica with acetone as eluent gave none of *β*-sulfonyl amide *trans*-**247**.

Lab Book Reference: SY-2-170

TFA (2.0 mL) was added to a stirred solution of MIDA Building Block *trans*-**38** (100 mg, 0.28 mmol, 1.0 eq.) in CH_2Cl_2 (10 mL) at rt under Ar. The resulting solution was stirred at rt for 30 min. Then, the solvent was evaporated under reduced pressure to give a residue. Toluene (5 × 10 mL) was added, and the solvent was evaporated under reduced pressure to give the crude amine•TFA salt *trans*-**249**. To a stirred mixture of crude amine•TFA salt *trans*-**249** in CH_2Cl_2 (10 mL) at 0 °C was added *β*-sulfonyl acid **235** (85 mg, 0.56 mmol, 2.0 eq.), DMAP (68 mg, 0.56 mmol, 2.0 eq.) and EDCI (87 mg, 0.56

mmol, 2.0 eq.) under Ar. Then, the resulting solution was stirred at rt for 16 h. H_2O (10 mL) and CH_2Cl_2 (10 mL) were added. The two layers were separated. The aqueous layer was extracted with CH_2Cl_2 (3 × 10 mL). The combined organic extracts were washed with brine (3 × 10 mL), dried (Na_2SO_4), filtered, and evaporated under reduced pressure to give the crude product. Purification by flash column chromatography on silica with acetone as eluent gave none of *β*-sulfonyl amide *trans*-**247**.

Lab Book Reference: SY-2-178

TFA (2.0 mL) was added to a stirred solution of MIDA Building Block *trans*-**38** (100 mg, 0.28 mmol, 1.0 eq.) in CH_2Cl_2 (5 mL) at rt under Ar. The resulting solution was stirred at rt for 30 min. Then, the solvent was evaporated under reduced pressure to give a residue. Toluene (5 × 10 mL) was added, and the solvent was evaporated under reduced pressure to give the crude amine•TFA salt *trans*-**249**. To a stirred mixture of crude amine•TFA salt *trans*-**249** in DMF (1.0 mL) was added *β*-sulfonyl acid **235** (52 mg, 0.34 mmol, 1.2 eq.), Et_3N (0.12 mL, 0.73 mmol, 3.0 eq.), DMAP (4 mg, 30 *μ*mol, 0.1 eq.) and EDCI (130 mg, 0.84 mmol, 3.0 eq.) under Ar. Then, the resulting solution was stirred at rt for 16 h. H_2O (10 mL) and CH_2Cl_2 (10 mL) were added. The two layers were separated. The aqueous layer was extracted with CH_2Cl_2 (3 × 10 mL). The combined organic extracts were washed with brine (3 × 10 mL), dried (Na_2SO_4), filtered, and evaporated under reduced pressure to give the crude product. Purification by flash column chromatography on silica with acetone as eluent gave none of *β*-sulfonyl amide *trans* **247**.

Lab Book Reference: SY-2-179

TFA (2.0 mL) was added to a stirred solution of MIDA building block *trans*-**38** (100 mg, 0.28 mmol, 1 eq.) in CH_2Cl_2 (10 mL) at rt under Ar. The resulting solution was stirred at rt for 30 min. Then, the solvent was evaporated under reduced pressure to give a residue. Toluene (5 × 10 mL) was added, and the solvent was evaporated under reduced pressure to give the crude amine•TFA salt *trans*-**249**. To a stirred mixture of the crude amine•TFA salt *trans*-**249** in CH_2Cl_2 (10 mL) under Ar was added *β*-sulfonyl acid chloride **251** (128 mg, 0.84 mmol, 3.0 eq.) and Et_3N (0.2 mL, 1.40 mmol, 5.0 eq.) and the resulting solution was stirred at rt for 16 h. Saturated $NaHCO_{3(aq.)}$ (10 mL) and CH_2Cl_2 (10 mL) were added.

The two layers were separated, and the aqueous layer was extracted with CH_2Cl_2 (3 × 10 mL). The combined organic extracts were dried (Na_2SO_4), filtered, and evaporated under reduced pressure to give the crude product. Purification by flash column chromatography on silica with acetone as eluent gave *β*-sulfonyl amide *trans*-**247** (35 mg, 32%) as a white solid.

Lab Book Reference: SY-2-159

6-Methyl-2-(5-(3-(methylsulfonyl)propanoyl)-5-azaspiro[2.4]heptan-1-yl)-1,3,6,2-dioxazaborocane-4,8-dione *cis*-247

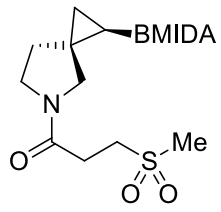

cis-**247**

TFA (2.0 mL) was added to a stirred solution of MIDA building block *cis*-**38** (100 mg, 0.28 mmol, 1.0 eq.) in CH_2Cl_2 (10 mL) at rt under Ar. The resulting solution was stirred at rt for 30 min. Then, the solvent was evaporated under reduced pressure to give a residue. Toluene (5 × 10 mL) was added, and the solvent was evaporated under reduced pressure to give the crude amine•TFA salt *cis*-**249**. To a stirred mixture of the crude amine•TFA salt *cis*-**249** in CH_2Cl_2 (10 mL) under Ar was added *β*-sulfonyl acid **235** (64 mg, 0.42 mmol, 1.5 eq.) and Et_3N (0.2 mL, 1.40 mmol, 5.0 eq.). Then, T3P (0.5 mL of a 50% wt solution in toluene, 0.85 mmol, 3.0 eq.) was added and the resulting solution was stirred at rt for 16 h. H_2O (10 mL) and CH_2Cl_2 (10 mL) were added. The two layers were separated, and the aqueous layer was extracted with CH_2Cl_2 (3 × 10 mL). The combined organic extracts were dried (Na_2SO_4), filtered, and evaporated under reduced pressure to give the crude product. Purification by flash column chromatography on silica with acetone as eluent gave amide *cis*-**247** (26 mg, 24%) as an off-white solid, mp 246 – 248 °C; R_F (Acetone) 0.25; IR (ATR) 2927, 1745 (C=O), 1636 (C=O), 1463, 1387, 1323, 1302 (SO_2), 1228, 1022, 1005, 923, 527 cm^{-1}; ^1H NMR (400 MHz, $CDCl_3$) δ 4.09 – 3.99 (m, 2H, MeNC*H*), 3.86 – 3.80 (m, 1H, MeNC*H*), 3.77 – 3.71 (m, 1H, MeNC*H*), 3.65 – 3.32 (m, 6H, NCH, CH), 3.05 (s, 1.7H, NMe), 3.04 (s, 1.3H, NMe), 2.97 (s, 3H, SO_2Me), 2.85 – 2.75 (m, 2H, CH), 1.69 (ddd, *J* = 12.5, 7.0, 3.5 Hz, 1H, CH), 1.59 (ddd, *J* = 12.5,

7.0, 3.5 Hz, 1H, CH), 0.82 – 0.74 (m, 1H, CH), 0.57 – 0.48 (m, 1H, CH), 0.07 – −0.05 (m, 1H, BCH); MS (EI) *m/z* 409 [(M + Na)$^+$, 100]; HRMS (ESI) *m/z* calcd for $C_{15}H_{23}BN_2O_7S$ [(M + Na)$^+$, 100] 409.1216, found 409.1215 (+0.1 ppm error).

Lab Book Reference: SY-2-163

2-(5-Benzoyl-5-azaspiro[2.4]heptan-1-yl)-6-methyl-1,3,6,2-dioxazaborocane-4,8-dione *trans*-250

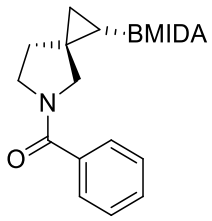

trans-**250**

TFA (1.0 mL) was added to a stirred solution of MIDA building block *trans*-**38** (100 mg, 0.28 mmol, 1.0 eq.) in CH_2Cl_2 (5 mL) at rt under Ar. The resulting solution was stirred at rt for 30 min. Then, the solvent was evaporated under reduced pressure to give a residue. Toluene (5 × 10 mL) was added, and the solvent was evaporated under reduced pressure to give the crude amine•TFA salt *cis*-**249**. To a stirred mixture of the crude amine•TFA salt *cis*-**249** in CH_2Cl_2 (5 mL) under Ar was added benzoyl chloride (50 mg, 0.36 mmol, 2.5 eq.) and NEt_3 (0.1 mL, 0.71 mmol, 5.0 eq.) and the resulting solution was stirred at rt for 16 h. Saturated $NaHCO_{3(aq.)}$ (10 mL) and CH_2Cl_2 (10 mL) were added. The two layers were separated, and the aqueous layer was extracted with CH_2Cl_2 (3 × 10 mL). The combined organic extracts were dried (Na_2SO_4), filtered, and evaporated under reduced pressure to give the crude product. Purification by flash column chromatography on silica with 40:60 to 80:20 acetone–CH_2Cl_2 as eluent gave benzamide *trans*-**250** (23 mg, 45%) as an colourless oil, R_F (60:40 CH_2Cl_2–acetone) 0.15; IR (ATR) 2956, 1759 (C=O), 1613 (C=O) 1450, 1431, 1343, 1295, 1129, 1025, 992, 718 cm^{-1}; ^{1}H NMR (400 MHz, $CDCl_3$) (60:40 mixture of rotamers) δ 7.54 – 7.49 (m, 1.2H, Ar), 7.49 – 7.44 (m, 0.8H, Ar), 7.42 – 7.34 (m, 3H, Ar), 3.98 – 3.93 (m, 0.8H, NCH), 3.93 – 3.87 (m, 1.2H, NCH), 3.84 – 3.53 (m, 5H, NCH, CH), 3.41 (d, *J* = 11.0 Hz, 0.6H, CH), 3.07 (d, *J* = 11.0 Hz, 0.4H, CH), 3.03 (s, 1.8H, NMe), 2.96 (s, 1.2H, NMe), 2.14 – 1.99 (m, 1H, CH), 1.94 – 1.86 (m, 0.4H, CH), 1.86 – 1.77 (m, 0.6H, CH), 0.84 (dd, *J* = 9.5, 3.5 Hz, 0.6H, CH), 0.65 (dd, *J* = 9.5,

3.5 Hz, 0.4H, CH), 0.54 (dd, *J* = 7.5, 3.5 Hz, 0.6H, CH), 0.48 (dd, *J* = 7.5, 3.5 Hz, 0.4H, CH), 0.01 (dd, *J* = 9.5, 7.5 Hz, 0.6H, BCH), −0.17 (dd, *J* = 9.5, 7.5 Hz, 0.4H, BCH); ^{13}C NMR (100.6 MHz, $CDCl_3$) (rotamers) δ 169.8 (C=O, amide), 169.7 (C=O, amide), 167.4 (C=O, ester), 167.2 (C=O, ester), 167.2 (C=O, ester), 137.1 (*ipso*-Ar), 136.7 (*ipso*-Ar), 130.1 (Ar), 130.0 (Ar), 128.5 (Ar), 128.5 (Ar), 127.3 (Ar), 127.2 (Ar), 62.0 (N*C*H$_2$C(O)), 61.9 (N*C*H2C(O)), 58.8 (NCH$_2$), 55.7 (NCH$_2$), 50.3 (NCH$_2$), 47.0 (NCH$_2$), 46.5 (NMe), 46.4 (NMe), 31.5 (CH), 29.7 (CH), 29.4 (CH), 26.7 (C), 24.9 (C), 15.5 (BCH), 15.2 (BCH); MS (EI) *m/z* 379 [(^{79}M + Na)$^+$, 100]; HRMS (ESI) *m/z* calcd for $C_{18}H_{21}BN_2O_5$ [(M + Na)$^+$, 100] 379.1436, found 379.1444 (–1.3 ppm error).

Lab Book Reference: SY-2-156

3-(Methylsulfonyl)-1-(1-(4,4,5,5-tetramethyl-1,3,2-dioxaborolan-2-yl)-5-azaspiro [2.4]heptan-5-yl)propan-1-one *trans*-253

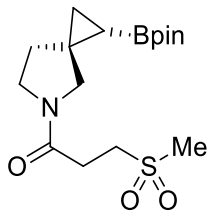

trans-**253**

TFA (1.0 mL) was added to a stirred solution of cyclopropyl Bpin *trans*-**119** (100 mg, 0.28 mmol, 1.0 eq.) in CH_2Cl_2 (5 mL) at rt under Ar. The resulting solution was stirred at rt for 30 min. Then, the solvent was evaporated under reduced pressure to give a residue. Toluene (5 × 10 mL) was added, and the solvent was evaporated under reduced pressure to give the crude amine•TFA salt *trans*-**252**. To a stirred mixture of the crude amine•TFA salt *trans*-**252** in EtOAc (10 mL) under Ar was added *β*-sulfonyl acid **235** (94 mg, 0.62 mmol, 2.0 eq.) and Et_3N (0.3 mL, 1.85 mmol, 6.0 eq.). Then, T3P (0.6 mL of a 50% wt solution in toluene, 0.93 mmol, 3.0 eq.) was added and the resulting solution was stirred at rt for 16 h. H_2O (10 mL) and CH_2Cl_2 (10 mL) were added. The two layers were separated, and the aqueous layer was extracted with CH_2Cl_2 (3 × 10 mL). The combined organic extracts were dried (Na_2SO_4), filtered, and evaporated under reduced pressure to give the crude product. Purification by flash column chromatography on silica with 80:20 CH_2Cl_2–acetone as eluent gave *β*-sulfonyl amide *trans*-**253** (102 mg, 93%) as an

colourless oil, R_F (80:20 CH_2Cl_2–acetone) 0.22; IR (ATR) 2979, 2933, 2871, 1636 (C=O), 1448, 1417, 1264, 1307 (S=O), 1141, 1123, 856, 730, 506 cm^{-1}; ^1H NMR (400 MHz, $CDCl_3$) (55:45 mixture of rotamers) δ 3.65 – 3.48 (m, 2H, NCH), 3.44 – 3.34 (m, 3H, NCH, CH), 3.32 – 3.20 (m, 1H, NCH), 2.94 (s, 1.6H, SO_2Me), 2.93 (s, 1.4H, SO_2Me), 2.81 (t, J = 7.0 Hz, 1H, CH), 2.74 – 2.67 (m, 1H, CH), 2.16 – 1.80 (m, 2H, CH), 1.22 – 1.18 (m, 12H, CMe_2), 0.90 – 0.80 (m, 2H, CH), 0.14 – 0.07 (m, 1H, BCH); ^{13}C NMR (100.6 MHz, $CDCl_3$) (rotamers) δ 167.2 (C=O), 83.4 (O*C*Me_2), 55.6 (NCH_2), 54.7 (NCH_2), 50.2 (CH_2), 47.0 (NCH_2), 46.4 (NCH_2), 41.7 (SO_2Me), 31.8 (CH_2), 30.3 (CH_2), 28.5 (C), 27.4 (CH_2), 27.1 (CH_2), 27.0 (CH_2), 25.1 (C*Me*), 24.6 (C*Me*), 17.21 (CH_2), 17.05 (CH_2) (BCH not resolved); MS (EI) *m/z* 380 [$(M + Na)^+$, 100]; HRMS (ESI) *m/z* calcd for $C_{16}H_{28}BNO_5S$ [$(M + Na)^+$, 100] 380.1673, found 380.1671 (+1.4 ppm error).

Lab Book Reference: SY-2-180

3-(Methylsulfonyl)-1-(7-(4,4,5,5-tetramethyl-1,3,2-dioxaborolan-2-yl)-2-azabicyclo[4.1.0]heptan-2-yl)propan-1-one *exo*-256

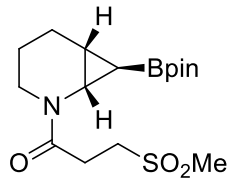

exo-**256**

TFA (5.0 mL) was added to a stirred solution of cyclopropyl Bpin *exo*-**92** (500 mg, 1.55 mmol, 1.0 eq.) in CH_2Cl_2 (10 mL) at rt for 45 min. Then, the solvent was evaporated under reduced pressure to give the crude residue. Toluene (3 × 10 mL) was added, and the solvent was evaporated under reduced pressure to give the crude amine•TFA salt. To a stirred mixture of the crude amine•TFA salt in EtOAc (20 mL) under Ar was added β-sulfone acid **235** (472 mg, 3.1 mmol, 2.0 eq.) and Et_3N (1.3 mL, 9.3 mmol, 6.0 eq.). Then, T3P (3.0 mL of a 50% wt solution in EtOAc, 4.7 mmol, 3.0 eq.) was added and the resulting solution was stirred at rt for 16 h. H_2O (60 mL) and EtOAc (60 mL) were added. The two layers were separated, and the aqueous layer was extracted with EtOAc (3 × 60 mL). The combined organic extracts were dried (Na_2SO_4), filtered, and evaporated under reduced pressure to give the crude product. Purification by flash column chromatography on silica with 90:10 CH_2Cl_2–acetone as eluent gave β-sulfonyl amide **256** (294 mg, 53%) as a white solid, mp 92 – 95 °C; R_F (90:10 CH_2Cl_2–acetone) 0.33; IR (ATR) 2979, 2930,

1637 (C=O), 1414, 1373, 1310 (S=O), 1283, 1211, 1142, 1124, 951, 858, 509 cm^{-1}; ^{1}H NMR (400 MHz, $CDCl_3$) (50:50 mixture of rotamers) δ 3.69 – 3.39 (m, 6H, NCH, CH), 2.96 (s, 3H, SO_2Me), 2.92 – 2.86 (m, 2H, CH), 1.67 – 1.62 (m, 1H, CH), 1.62 – 1.57 (m, 1H, CH), 1.46 – 1.41 (m, 1H, CH), 1.41 – 1.35 (m, 1H, CH), 1.23 (s, 3H, C*Me*$_2$), 1.22 (s, 3H, C*Me*$_2$), 1.20 (s, 3H, C*Me*$_2$), 1.19 (s, 3H, C*Me*$_2$), 0.73 – 0.71 (m, 1H, CH), 0.71 – 0.68 (m, 1H, CH), –0.10 – –0.14 (m, 0.5H, BCH) –0.14 – 0.19 (m, 0.5H, BCH); ^{13}C NMR (100.6 MHz, $CDCl_3$) (rotamers) δ 167.3 (C=O), 167.2 (C=O), 83.3 (O*C*Me$_2$), 50.7 (CH_2), 46.0 (NCH_2), 45.9 (NCH_2), 42.8 (NCH_2), 42.7 (NCH_2), 41.8 (SO_2Me), 37.8 (CH_2), 37.0 (CH_2), 32.4 (CH_2), 31.5 (CH_2), 26.2 (CH_2), 26.1 (CH_2), 25.2 (C*Me*$_2$), 25.0 (C), 24.6 (C*Me*$_2$), 24.5 (C*Me*$_2$), 17.70 (CH_2), 17.65 (CH_2) (BCH not resolved, HSQC cross peak for BCH at δ 6.4); MS (EI) *m/z* 394 [$(M + Na)^+$, 100]; HRMS (ESI) *m/z* calcd for $C_{17}H_{30}BNO_5S$ [$(M + Na)^+$, 100] 394.1830, found 394.1834 (–0.2 ppm error).

Lab Book Reference: SY-3-220

3-(Methylsulfonyl)-1-(1-(4,4,5,5-tetramethyl-1,3,2-dioxaborolan-2-yl)-6-azaspiro[2.5] octan-6-yl)propan-1-one 257

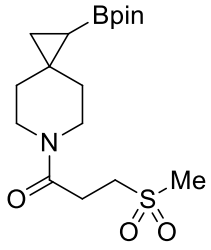

257

TFA (20 mL) was added to a stirred solution of cyclopropyl Bpin **107** (2.38 g, 7.06 mmol, 1.0 eq.) in CH_2Cl_2 (60 mL) at rt for 45 min. Then, the solvent was evaporated under reduced pressure to give the crude residue. Toluene (3 × 10 mL) was added, and the solvent was evaporated under reduced pressure to give the crude amine•TFA salt. To a stirred mixture of the crude amine•TFA salt in EtOAc (20 mL) under Ar was added *β*-sulfone acid **235** (2.15 g, 14.12 mmol, 2.0 eq.) and Et_3N (5.9 mL, 42.37 mmol, 6.0 eq.). Then, T3P (13.5 mL of a 50% wt solution in EtOAc, 21.19 mmol, 3.0 eq.) was added and the resulting solution was stirred at rt for 16 h. H_2O (100 mL) and EtOAc (100 mL) were added. The two layers were separated, and the aqueous layer was extracted with EtOAc (3 × 100 mL). The combined organic extracts were dried (Na_2SO_4), filtered, and

evaporated under reduced pressure to give the crude product. Purification by flash column chromatography on silica with 90:10 CH_2Cl_2–acetone as eluent gave *β*-sulfonyl amide **257** (2.40 mg, 92%) as a white solid, mp 92 – 95 °C; R_F (90:10 CH_2Cl_2–acetone) 0.33; IR (ATR) 2979, 2930, 1637 (C=O), 1414, 1373, 1310 (S=O), 1283, 1211, 1142, 1124, 951, 858, 509 cm^{-1}; ^1H NMR (400 MHz, $CDCl_3$) (50:50 mixture of rotamers) δ 3.69 – 3.39 (m, 6H, NCH, CH), 2.96 (s, 3H, SO_2Me), 2.92 – 2.86 (m, 2H, CH), 1.67 – 1.62 (m, 1H, CH), 1.62 – 1.57 (m, 1H, CH), 1.46 – 1.41 (m, 1H, CH), 1.41 – 1.35 (m, 1H, CH), 1.23 (s, 3H, C*Me*$_2$), 1.22 (s, 3H, C*Me*$_2$), 1.20 (s, 3H, C*Me*$_2$), 1.19 (s, 3H, C*Me*$_2$), 0.73 – 0.71 (m, 1H, CH), 0.71 – 0.68 (m, 1H, CH), –0.10 – –0.14 (m, 0.5H, BCH) –0.14 – 0.19 (m, 0.5H, BCH); ^{13}C NMR (100.6 MHz, $CDCl_3$) (rotamers) δ 167.3 (C=O), 167.2 (C=O), 83.3 (O*C*Me$_2$), 50.7 (CH_2), 46.0 (NCH_2), 45.9 (NCH_2), 42.8 (NCH_2), 42.7 (NCH_2), 41.8 (SO_2Me), 37.8 (CH_2), 37.0 (CH_2), 32.4 (CH_2), 31.5 (CH_2), 26.2 (CH_2), 26.1 (CH_2), 25.2 (C*Me*$_2$), 25.0 (C), 24.6 (C*Me*$_2$), 24.5 (C*Me*$_2$), 17.70 (CH_2), 17.65 (CH_2) (BCH not resolved, HSQC cross peak for BCH at δ 6.4); MS (EI) *m/z* 394 [$(M + Na)^+$, 100]; HRMS (ESI) *m/z* calcd for $C_{17}H_{30}BNO_5S$ [$(M + Na)^+$, 100] 394.1830, found 394.1834 (–0.2 ppm error).

Lab Book Reference: SY-4-209

1-(1-(Pyrimidin-5-yl)-6-azaspiro[2.5]octan-6-yl)prop-2-en-1-one 260

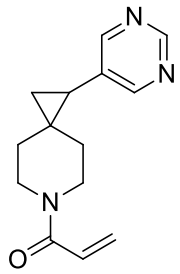

260

HCl (5.0 mL of a 4.0 M solution in dioxane, 20 mmol) was added to a flask containing cyclopropyl pyrimidine **168** (71 mg, 0.25 mmol, 1.0 eq.) at rt under Ar. The resulting solution was stirred at rt for 1 h. Then, the solvent was evaporated under reduced pressure to give a residue. Toluene (3 × 5 mL) was added, and the solvent was evaporated under reduced pressure to give the crude amine•HCl salt. To a stirred mixture of the crude amine•HCl salt in CH_2Cl_2 (5 mL) under Ar was added DMAP (3 mg, 25 μmol, 0.1 eq.) and Et_3N (0.2 mL, 1.13 mmol, 4.5 eq.). Then acryloyl chloride (71 μL, 875 μmol, 3.5 eq.)

was added and the resulting solution was stirred at rt for 16 h. 1 M $HCl_{(aq)}$ (10 mL) and CH_2Cl_2 (10 mL) were added. The two layers were separated, and the aqueous layer was extracted with CH_2Cl_2 (3 × 10 mL). The combined organic extracts were dried (Na_2SO_4), filtered, and evaporated under reduced pressure to give the crude product. Purification by flash column chromatography on silica with 50:50 acetone–CH_2Cl_2 as eluent gave pyrimidine acrylamide **260** (20 mg, 33%) as a colourless oil, R_F (50:50 acetone–CH_2Cl_2) 0.33; IR (ATR) 2907, 2852, 1710, 1639 (C=O), 1610, 1553, 1445, 1404, 1221, 1005, 729, 631, 532 cm^{-1}; ^1H NMR (400 MHz, $CDCl_3$) (50:50 mixture of rotamers) δ 9.05 (s, 1H, Ar), 8.57 (s, 2H, Ar), 6.64 – 6.44 (m, 1H, C*H*=CH_2), 6.29 – 6.19 (m, 1H, CH=C*H*$_2$), 5.71 – 5.60 (m, 1H, CH=C*H*$_2$), 4.01 – 3.91 (m, 0.5H, NCH), 3.77 – 3.64 (m, 1H, NCH), 3.61 – 3.49 (m, 1H, NCH), 3.48 – 3.38 (m, 0.5H, NCH), 3.34 (ddd, *J* = 13.0, 8.5, 3.5 Hz, 1H, NCH), 2.00 – 1.91 (m, 1H, C*H*Ar), 1.73 (ddd, *J* = 13.0, 8.5, 3.5 Hz, 1H, CH), 1.55 – 1.44 (m, 1H, CH), 1.34 – 1.25 (m, 1H, CH), 1.18 – 1.08 (m, 1H, CH), 1.09 – 1.02 (m, 2H, CH); ^{13}C NMR (100.6 MHz, $CDCl_3$) (rotamers) δ 165.7 (C=O), 157.1 (Ar), 156.8 (Ar), 132.3 (*ipso*-Ar) 127.9 (*C*H=CH_2), 127.8 (CH=*C*H$_2$), 55.5 (NCH_2), 45.4 (NCH_2), 42.1 (NCH_2), 36.1 (CH_2), 31.0 (CH_2), 29.8 (CH_2), 25.6 (C), 23.6 (*C*HAr), 16.0 (CH_2); MS (EI) *m/z* 266 [$(M + Na)^+$, 100]; HRMS (ESI) *m/z* calcd for $C_{14}H_{17}N_3O$ [$(M + Na)^+$, 100] 266.1264, found 266.1269 (–2.1 ppm error).

Lab Book Reference: SY-4-194

Using general procedure E, *β*-sulfonyl amide **257** (93 mg, 0.25 mmol, 1.0 eq.), 5-bromopyrimidine (60 mg, 0.38 mmol, 1.5 eq.), cataCXium® A (18 mg, 50 *μ*mol, 0.20 eq.), Cs_2CO_3 (244 mg, 0.75 mmol, 3.0 eq.) and $Pd(OAc)_2$ (6 mg, 25 *μ*mol, 0.10 eq.) in toluene (1.0 mL) and H_2O (0.1 mL) gave the crude product. Purification by flash column chromatography on silica with EtOAc as eluent gave pyrimidine acrylamide **260** (9 mg, 15%) as a colourless oil and Bpin acrylamide **265** (34 mg, 47%) as a colourless oil.

Lab Book Reference: SY-4-323

***tert*-Butyl 1-(pyrimidin-5-yl)-6-azaspiro[2.5]octane-6-carboxylate 168**

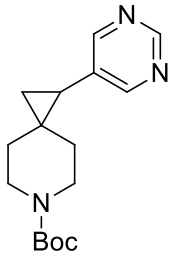

168

Using general procedure E, cyclopropyl Bpin **107** (84 mg, 0.25 mmol, 1.0 eq.), 5-bromopyrimidine (60 mg, 0.38 mmol, 1.5 eq.), cataXCium A (18 mg, 50 μmol, 0.20 eq.), Cs_2CO_3 (244 mg, 0.75 mmol, 3.0 eq.) and $Pd(OAc)_2$ (6 mg, 25 μmol, 0.10 eq.) in toluene (0.6 mL) and H_2O (0.5 mL) gave the crude product. Purification by flash column chromatography on silica with 80:20 EtOAc–hexane as eluent gave cyclopropyl pyrimidine **168** (53 mg, 74%) as an off-white solid, mp 98 – 100 °C; R_F (EtOAc) 0.43; IR (ATR) 2932, 1687 (C=O), 1556, 1416, 1365, 1239, 1168, 1124, 1008, 730 cm^{-1}; ^1H NMR (400 MHz, $CDCl_3$) δ 9.04 (s, 1H, Ar), 8.56 (s, 2H, Ar), 3.68 – 3.56 (m, 1H, NCH), 3.38 (ddd, J = 13.0, 8.0, 3.5 Hz, 1H, NCH), 3.34 – 3.27 (m, 1H, NCH), 3.17 (ddd, J = 13.0, 8.0, 3.5 Hz, 1H, NCH), 1.91 (dd, J = 8.0, 6.5 Hz, 1H, C*H*Ar), 1.65 (ddd, J = 13.0, 8.5, 3.5 Hz, 1H, CH), 1.49 – 1.45 (m, 1H, CH), 1.43 (s, 9H, CMe_3), 1.29 – 1.16 (m, 1H, CH), 1.13 – 1.04 (m, 1H, CH), 1.04 – 0.97 (m, 2H, CH); ^{13}C NMR (100.6 MHz, $CDCl_3$) δ 157.1 (Ar), 156.7 (Ar), 155.0 (*C*=O), 132.6 (*ipso*-Ar), 79.7 (O*C*Me$_3$), 43.3 (br s, NCH_2), 36.5 (CH_2), 30.1 (CH_2), 28.5 (C*Me*$_3$), 25.6 (C), 23.6 (*C*HAr), 15.9 (CH_2); MS (ESI) *m/z* 312 [$(M + Na)^+$, 100]; HRMS (ESI) *m/z* calcd for $C_{16}H_{23}N_3O_2$ $(M + Na)^+$ 312.1682, found 312.1686 (–1.1 ppm error).

Lab Book Reference: SY-4-185

Using general procedure E, cyclopropyl Bpin **107** (84 mg, 0.25 mmol, 1.0 eq.), 5-bromopyrimidine (56 mg, 0.35 mmol, 1.4 eq.), PCy_3 (7 mg, 25 μmol, 0.10 eq.), Cs_2CO_3 (244 mg, 0.75 mmol, 3.0 eq.) and $Pd(OAc)_2$ (3 mg, 12.5 μmol, 0.05 eq.) in toluene (5 mL) and H_2O (0.5 mL) gave the crude product. Purification by flash column chromatography on silica with 80:20 EtOAc–hexane as eluent gave cyclopropyl pyrimidine **168** (22 mg, 31%) as an off-white solid.

Lab Book Reference: SY-4-186

Using general procedure E, cyclopropyl Bpin **107** (84 mg, 0.25 mmol, 1.0 eq.), 5-bromopyrimidine (79 mg, 0.50 mmol, 2.0 eq.), PCy_3 (7 mg, 25 μmol, 0.10 eq.), KOH (84 mg, 1.5 mmol, 6.0 eq.) and $Pd(dba)_2$ (11 mg, 12.5 μmol, 0.05 eq.) in toluene (1.0 mL) and H_2O (0.5 mL) gave the crude product. Purification by flash column chromatography on silica with 80:20 EtOAc–hexane as eluent gave cyclopropyl pyrimidine **168** (24 mg, 33%) as an off-white solid.

Lab Book Reference: SY-4-187

Using general procedure E, cyclopropyl Bpin **107** (84 mg, 0.25 mmol, 1.0 eq.), 5-bromopyrimidine (60 mg, 0.38 mmol, 1.5 eq.), cataXCium A (18 mg, 50 μmol, 0.20 eq.), Cs_2CO_3 (244 mg, 0.75 mmol, 3.0 eq.) and $Pd(OAc)_2$ (6 mg, 25 μmol, 0.10 eq.) in toluene (1.0 mL) and H_2O (0.1 mL) gave the crude product. Purification by flash column chromatography on silica with EtOAc as eluent gave cyclopropyl pyrimidine **168** (60 mg, 83%) as an off-white solid.

Lab Book Reference: SY-4-321

3-(Methylsulfonyl)-1-(1-(pyrimidin-5-yl)-6-azaspiro[2.5]octan-6-yl)propan-1-one 262

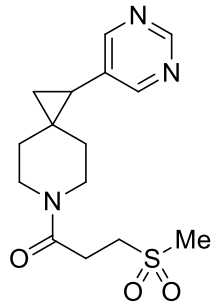

262

TFA (2.0 mL) was added to a stirred solution of cyclopropyl pyrimidine **168** (90 mg, 0.31 mmol, 1.0 eq.) in CH_2Cl_2 (5 mL) at rt. The resulting solution was stirred at rt for 45 min. Then, the solvent was evaporated under reduced pressure to give a residue. Toluene (3 × 5 mL) was added, and the solvent was evaporated under reduced pressure to give the crude TFA salt. To a stirred mixture of the crude amine•TFA salt in EtOAc (5 mL) under Ar was added β-sulfonyl acid **235** (95 mg, 0.62 mmol, 2.0 eq.) and Et_3N (0.3 mL, 1.87

mmol, 6.0 eq.). Then, T3P (0.6 mL of a 50% wt solution in toluene, 0.93 mmol, 3.0 eq.) was added and the resulting solution was stirred at rt for 16 h. H_2O (10 mL) and EtOAc (10 mL) were added. The two layers were separated and the aqueous layer was extracted with EtOAc (3 × 10 mL). The combined organic extracts were dried (Na_2SO_4), filtered, and evaporated under reduced pressure to give the crude product. Purification by flash column chromatography on silica with 50:50 acetone–CH_2Cl_2 as eluent gave *β*-sulfonyl amide **262** (45 mg, 45%) as a colourless oil, R_F (50:50 acetone–CH_2Cl_2) 0.22; IR (ATR) 3005, 2928, 2853, 1634 (C=O), 1557, 1455, 1416, 1304, 1280, 1242, 1212, 1123, 1005, 955, 921, 774, 730, 632, 509, 462 cm^{-1}; ^1H NMR (400 MHz, $CDCl_3$) (50:50 mixture of rotamers) δ 9.03 (s, 1H, Ar), 8.55 (s, 2H, Ar), 3.88 (ddd, J = 13.0, 6.5, 4.0 Hz, 0.5H, CH), 3.62 (ddd, J = 13.0, 6.5, 4.0 Hz, 1H, CH), 3.52 – 3.42 (m, 1H, NCH), 3.42 – 3.35 (m, 2H, NCH), 3.34 – 3.29 (m, 0.5H, CH), 3.92 – 3.22 (m, 1H, NCH), 2.94 (s, 1.5H, SO_2Me), 2.93 (s, 1.5H, SO_2Me), 2.91 – 2.85 (m, 1H, CH), 2.85 – 2.73 (m, 1H, CH), 1.95 (dd, J = 7.0, 7.0 Hz, 1H, CHAr), 1.78 – 1.63 (m, 1H, CH), 1.53 – 1.41 (m, 1H, CH), 1.33 – 1.22 (m, 1H, CH), 1.18 – 1.07 (m, 1H, CH), 1.07 – 1.02 (m, 2H, CH); ^{13}C NMR (100.6 MHz, $CDCl_3$) (rotamers) δ 167.3 (C=O), 167.3 (Ar), 157.1 (Ar), 156.7 (Ar), 132.2 (*ipso*-Ar), 50.5 (NCH_2), 45.3 (CH_2), 44.9 (NCH_2), 42.1 (CH_2), 41.80 (SO_2Me), 41.7 (SO_2Me), 41.6 (CH_2), 36.8 (CH_2), 36.0 (CH_2), 30.6 (CH_2), 29.7 (CH_2), 29.3 (CH_2), 26.1 (CH_2), 26.0 (CH_2), 25.4 (C), 25.3 (C), 23.6 (*C*HAr), 23.5 (*C*HAr), 15.83 (CH_2); MS (EI) *m/z* 346 [(M + Na)$^+$, 100]; HRMS (ESI) *m/z* calcd for $C_{15}H_{21}N_3O_3S$ [(M + Na)$^+$, 100] 346.1196, found 346.1202 (–1.4 ppm error).

Lab Book Reference: SY-4-211

1-(1-(4,4,5,5-Tetramethyl-1,3,2-dioxaborolan-2-yl)-6-azaspiro[2.5]octan-6-yl)prop-2-en-1-one 265

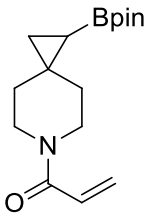

265

β-Sulfonyl amide **257** (100 mg, 0.27 mmol, 1.0 eq.) and Cs_2CO_3 (326 mg, 1.08 mmol, 3.0 eq.) were placed in a pressure tube. Then, toluene (0.6 mL) and H_2O (0.5 mL) were added, and the resulting mixture was stirred and heated at 120 °C in a sealed pressure tube for 16 h. After being allowed to cool to rt, H_2O (10 mL) was added. The mixture was extracted with EtOAc (3 × 10 mL). The combined organic extracts were washed with H_2O (10 mL), dried (Na_2SO_4), filtered, and evaporated under reduced pressure to give acrylamide **265** (55 mg, 71%) as a colourless oil, IR (ATR) 2979, 2932, 2852, 1723, 1706, 1463, 1440, 1422, 1405, 1245, 1218, 889 cm^{-1}; ^1H NMR (400 MHz, $CDCl_3$) (85:15 mixture of rotamers) δ 6.58 – 6.48 (m, 1H, C*H*=CH_2), 6.22 (dd, *J* = 17.0, 2.0 Hz, 0.15H, CH=C*H*$_2$), 6.17 (dd, *J* = 17.0, 2.0 Hz, 0.85H, CH=C*H*$_2$), 5.62 (dd, *J* = 10.5, 2.0 Hz, 0.15H, CH=C*H*$_2$), 5.58 (dd, *J* = 10.5, 2.0 Hz, 0.85H, CH=C*H*$_2$), 3.70 – 3.39 (m, 4H, NCH), 1.64 – 1.49 (m, 2H, CH), 1.41 – 1.26 (m, 2H, CH), 1.16 (s, 6H, CMe_2), 1.14 (s, 6H, CMe_2), 0.67 – 0.60 (m, 2H, CH), –0.21 (dd, *J* = 9.0, 2.0 Hz, 1H, BCH); ^{13}C NMR (100.6 MHz, $CDCl_3$) (rotamers) δ 165.5 (C=O), 165.4 (C=O), 128.1 (*C*H=CH_2), 127.72 (*C*H=CH_2), 127.68 (CH=*C*H_2), 127.1 (CH=*C*H_2), 83.13 (O*C*Me_2), 83.08 (O*C*Me_2), 46.22 (NCH_2), 46.16 (NCH_2), 42.5 (NCH_2), 42.4 (NCH_2), 38.0 (CH_2), 37.0 (CH_2), 32.6 (CH_2), 31.5 (CH_2), 25.1 (C*Me*$_2$), 24.4 (C), 17.6 (CH_2), 6.5 (br s, BCH); MS (EI) *m/z* 314 [$(M + Na)^+$, 100]; HRMS (ESI) *m/z* calcd for $C_{16}H_{26}BNO_3$ [$(M + Na)^+$, 100] 314.1898, found 314.1905 (–1.4 ppm error).

Lab Book Reference: SY-4-221

Experimental Procedures for Chapter 6

4-Bromo-7-tosyl-7*H*-pyrrolo[2,3-d]pyrimidine 281

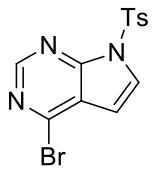

281

A solution of bromopyrrolopyrimidine **280** (1.0 g, 5.05 mmol, 1.0 eq.) in THF (20 mL) was added dropwise to a stirred mixture of NaH (263 mg of a 60% dispersion in paraffin liquid, 6.57 mmol, 1.3 eq.) in THF (10 mL) at 0 °C under Ar. Then, a solution of Ts–Cl (1.25 g, 6.57 mmol, 1.3 eq.) in THF (20 mL) was added dropwise to the stirred mixture at 0 °C under Ar. The reaction was allowed to warm to rt and stirred at rt for 16 h. H_2O (30 mL) was added and the mixture was extracted with EtOAc (3 × 50 mL). The combined organic layers were dried (Na_2SO_4), filtered, and evaporated under reduced pressure to give the crude product. Purification by flash column chromatography on silica with 70:30 to 50:50 EtOAc–hexane as eluent gave bromo-tosyl-pyrrolopyrimidine **281** (1.41 g, 79%) as a white solid, mp 148 – 151 °C, R_F (50:50 EtOAc–hexane) 0.60; IR (ATR) 1595, 1578, 1541, 1508, 1429, 1373, 1349, 1190, 1175, 1152, 1100, 1188, 1008, 905, 830, 813, 728, 702, 682, 658, 627, 534, 516 cm^{-1}; ^1H NMR (400 MHz, $CDCl_3$) δ 8.70 (s, 1H, Ar), 8.11 – 8.03 (m, 2H, Ar), 7.78 (d, J = 4.0 Hz, 1H, Ar), 7.35 – 7.28 (m, 2H, Ar), 6.63 (d, J = 4.0 Hz, 1H, Ar), 2.39 (s, 3H, Me); ^{13}C NMR (100.6 MHz, $CDCl_3$) 152.5 (Ar), 149.9 (*ipso*–Ar), 146.5 (*ipso*–Ar), 145.0 (*ipso*–Ar), 134.4 (*ipso*–Ar), 130.1 (Ar), 128.3 (Ar), 127.2 (Ar), 123.1 (*ipso*–Ar), 104.4 (Ar), 21.8 (Me); MS (ESI) *m/z* 374 [($^{79}M + Na)^+$, 100]; HRMS (ESI) *m/z* calcd for $C_{13}H_{10}{}^{79}BrN_3O_2S$ ($^{79}M + Na)^+$ 373.9569, found 373.9575 (–1.6 ppm error). All spectroscopic data are consistent with those reported in the literature.[228]

Lab Book Reference: SY-2-240

***tert*-Butyl 1-(7-tosyl-7*H*-pyrrolo[2,3-d]pyrimidin-4-yl)-5-azaspiro[2.4]heptane-5-carboxylate *cis*-282**

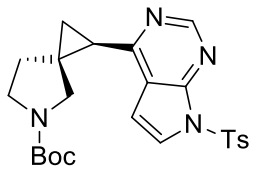

cis-**282**

Using general procedure A, cyclopropyl BMIDA *cis*-**38** (247 mg, 0.70 mmol, 1.0 eq.), bromo-tosyl-pyrrolopyrimidine **281** (344 mg, 0.98 mmol, 1.4 eq.), PCy_3 (59 mg, 0.21 mmol, 0.30 eq.), Cs_2CO_3 (1.37 g, 4.19 mmol, 6.0 eq.) and $Pd(OAc)_2$ (24 mg, 0.11 mmol, 0.15 eq.) in toluene (10 mL) and H_2O (1 mL) gave the crude product. Purification by flash column chromatography on silica with 98:2 CH_2Cl_2–Acetone as eluent gave cyclopropyl tosyl-pyrrolopyrimidine *cis*-**282** (276 mg, 84%) as an off-white solid, mp 86 – 88 °C, R_F (90:10 CH_2Cl_2–Acetone) 0.52; IR (ATR) 2982, 2930, 2874, 1692 (C=O), 1576, 1449, 1403 (S=O), 1382, 1364, 1179, 1159, 1129, 1092, 1043, 683, 580 cm^{-1}; ^1H NMR (400 MHz, $CDCl_3$) (55:45 mixture of rotamers) δ 8.87 – 8.75 (m, 1H, Ar), 8.14 – 8.03 (m, 2H, Ar), 7.70 – 7.63 (m, 1H, Ar), 7.34 – 7.27 (m, 2H, Ar), 6.71 – 6.66 (m, 1H, Ar), 3.57 – 3.34 (m, 3H, NCH), 3.14 – 3.05 (m, 1H, NCH), 2.43 – 2.39 (m, 1H, C*H*Ar), 2.38 (s, 3H, Me), 2.09 – 1.81 (m, 3H, CH), 1.79 – 1.73 (m, 0.45H, CH), 1.38 (s, 4H, CMe_3), 1.35 – 1.33 (m, 0.55H, CH), 1.29 (s, 5H, CMe_3); ^{13}C NMR (100.6 MHz, $CDCl_3$) (rotamers) δ 162.0 (*ipso*-Ar), 154.5 (C=O), 153.0 (Ar), 152.8 (Ar), 150.4 (*ipso*-Ar), 145.9 (*ipso*-Ar), 135.0 (*ipso*-Ar), 130.0 (Ar), 128.3 (Ar), 125.9 (Ar), 120.4 (*ipso*-Ar), 102.9 (Ar), 79.3 (O*C*Me_3), 48.4 (NCH_2), 45.7 (NCH_2), 45.1 (NCH_2), 36.0 (CH_2), 35.3 (CH_2), 34.6 (CH_2), 33.4 (C), 28.5 (C*Me*$_3$), 26.2 (*C*HAr), 26.0 (*C*HAr), 21.8 (Me), 20.2 (CH_2), 19.4 (CH_2); MS (ESI) *m/z* 491 [$(M + Na)^+$, 100]; HRMS (ESI) *m/z* calcd for $C_{24}H_{28}N_4O_4S$ $(M + Na)^+$ 491.1723, found 491.1723 (+0.1 ppm error).

Lab Book Reference: SY-3-238

***tert*-Butyl 7-(7-tosyl-7*H*-pyrrolo[2,3-d]pyrimidin-4-yl)-2-azabicyclo[4.1.0] heptane-2-carboxylate *exo*-283**

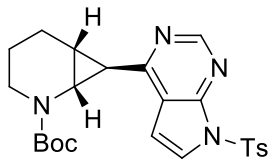

exo-**283**

Using general procedure A, cyclopropyl BMIDA *exo*-**36** (358 mg, 1.02 mmol, 1.0 eq.), bromo-tosyl-pyrrolopyrimidine **281** (500 mg, 1.42 mmol, 1.4 eq.), PCy_3 (86 mg, 0.31 mmol, 0.30 eq.), Cs_2CO_3 (1.99 g, 6.10 mmol, 6.0 eq.) and $Pd(OAc)_2$ (34 mg, 0.15 mmol, 0.15 eq.) in toluene (14 mL) and H_2O (1.4 mL) gave the crude product. Purification by flash column chromatography on silica with 99:1 to 96:4 CH_2Cl_2–Acetone as eluent gave cyclopropyl tosyl-pyrrolopyrimidine *exo*-**283** (228 mg, 48%) as a pale-yellow oil, R_F (96:4 CH_2Cl_2–Acetone) 0.26; IR (ATR) 2975, 2933, 2867, 1692 (C=O), 1570, 1445, 1365, 1177, 1149, 1127, 1090, 1086, 910, 889, 729, 683, 618, 579, 532 cm^{-1}; ^1H NMR (400 MHz, $CDCl_3$) (70:30 mixture of rotamers) δ 8.76 (s, 0.7H, Ar), 8.74 (s, 0.3H, Ar), 8.06 – 7.99 (m, 2H, Ar), 7.67 (d, J = 4.0 Hz, 0.7H, Ar), 7.61 (d, J = 4.0 Hz, 0.2H, Ar), 7.30 – 7.23 (m, 2H, Ar), 6.70 (d, J = 4.0 Hz, 0.7H, Ar), 3.87 (ddd, J = 12.5, 3.5, 3.5 Hz, 0.7H, NCH), 3.70 (ddd, J = 12.5, 3.5, 3.5 Hz, 0.3H, NCH), 3.58 (dd, J = 8.5, 2.5 Hz, 0.3H, NCH), 3.35 (dd, J = 8.5, 2.5 Hz, 0.7H, NCH), 2.77 (ddd, J = 12.5, 12.5, 2.5 Hz, 0.3H, NCH), 2.65 (ddd, J = 12.5, 12.5, 2.5 Hz, 0.7H, NCH), 2.41 – 2.28 (m, 4H, Me, C*H*Ar), 2.10 – 2.01 (m, 1H, CH), 1.99 – 1.86 (m, 2H, CH), 1.79 – 1.65 (m, 1H, CH), 1.51 – 1.44 (m, 1H, CH), 1.41 (s, 2.7H, CMe_3), 1.10 (s, 6.3H, CMe_3); ^{13}C NMR (100.6 MHz, $CDCl_3$) (rotamers) δ 162.9 (*ipso*-Ar), 156.1 (C=O), 155.6 (C=O), 153.4 (Ar), 150.6 (*ipso*-Ar), 150.3 (*ipso*-Ar), 145.8 (*ipso*-Ar), 135.1 (*ipso*-Ar), 130.0 (Ar), 129.9 (Ar), 128.2 (Ar), 128.1 (Ar), 125.7 (Ar), 125.3 (Ar), 118.6 (*ipso*-Ar), 103.5 (Ar), 103.2 (Ar), 79.7 (O*C*Me_3), 42.7 (NCH_2), 42.1 (NCH), 41.6 (NCH), 40.4 (NCH_2), 29.1 (CH), 28.5 (C*Me*$_3$), 28.2 (C*Me*$_3$), 24.4 (*C*HAr), 22.2 (CH_2), 22.1 (CH_2), 21.8 (Me), 20.5 (CH_2); MS (ESI) *m/z* 491 [$(M + Na)^+$, 100]; HRMS (ESI) *m/z* calcd for $C_{24}H_{28}N_4O_4S$ $(M + Na)^+$ 491.1723, found 491.1740 (–3.4 ppm error).

Lab Book Reference: SY-3-242

***tert*-Butyl 1-(7*H*-pyrrolo[2,3-d]pyrimidin-4-yl)-5-azaspiro[2.4] heptane-5-carboxylate *cis*-284 and *tert*-Butyl 1-(7-methyl-7H-pyrrolo[2,3-d]pyrimidin-4-yl)-5-azaspiro[2.4] heptane-5-carboxylate *cis*-285**

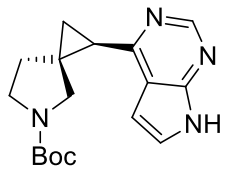

cis-**284**

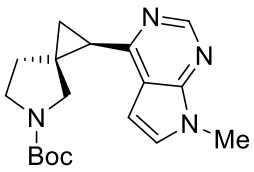

cis-**285**

Cs_2CO_3 (515 mg, 1.58 mmol, 3.0 eq.) was added to a stirred solution of cyclopropyl tosyl-pyrrolopyrimidine *cis*-**282** (247 mg, 0.53 mmol, 1.0 eq.) in MeOH (1.8 mL, 0.3 M) and THF (5.3 mL, 0.1 M). The resulting mixture was stirred at rt for 16 h. H_2O (10 mL) was added and the product was extracted with EtOAc (3 × 10 mL). The combined organic layers were dried (Na_2SO_4), filtered, and evaporated under reduced pressure to give the crude product. Purification by flash column chromatography on silica with 80:20 to 60:40 CH_2Cl_2–acetone as eluent gave cyclopropyl pyrrolopyrimidine *cis*-**284** (71 mg, 43%) as a white solid, mp 181 – 184 °C; R_F (60:40 CH_2Cl_2–acetone) 0.36; IR (ATR) 3201 (NH), 3145 (NH), 2976, 2870, 1678 (C=O), 1578, 1404, 1364, 1254, 1166, 1112, 900, 870, 770, 728, 646, 606 cm^{-1}; ^1H NMR (400 MHz, $CDCl_3$) δ 11.98 – 11.67 (m, 1H, NH), 8.85 – 8.59 (m, 1H, Ar), 7.33 (s, 1H, Ar), 6.70 – 6.56 (m, 1H, Ar), 3.58 – 3.41 (m, 3H, NCH), 3.24 – 3.11 (m, 1H, NCH), 2.53 (dd, J = 8.5, 5.5 Hz, 1H, C*H*Ar), 2.14 – 1.86 (m, 3H, CH), 1.39 (s, 4H, CMe_3), 1.37 – 1.33 (m, 1H, CH), 1.31 (s, 5H, CMe_3); ^{13}C NMR (100.6 MHz, $CDCl_3$) (rotamers) δ 160.8 (*ipso*-Ar), 154.7 (C=O), 154.5 (C=O), 151.0 (Ar), 150.7 (*ipso*-Ar), 125.1 (Ar), 125.0 (Ar), 118.7 (*ipso*-Ar), 118.5 (*ipso*-Ar), 99.5 (Ar), 99.3 (Ar), 79.2 (O*C*Me_3), 48.6 (NCH_2), 45.8 (NCH_2), 45.2 (NCH_2), 36.0 (CH_2), 35.3 (CH_2), 33.6 (C), 32.6 (C), 28.5 (C*Me*$_3$), 26.4 (*C*HAr), 26.3 (*C*HAr), 19.2 (CH_2), 18.5 (CH_2); MS (ESI) *m/z* 337 [$(M + Na)^+$, 100]; HRMS (ESI) *m/z* calcd for $C_{17}H_{22}N_4O_2$ $(M + Na)^+$ 337.1635, found 337.1646 (–3.3 ppm error) and cyclopropyl methyl pyrrolopyrimidine *cis*-**285** (50 mg, 29%) as an off-white solid, mp 120 – 122 °C; R_F (60:40 CH_2Cl_2–acetone) 0.36; IR (ATR) 2975, 2934, 2870, 1684 (C=O), 1576, 1401, 1365, 1241, 1167, 1107, 911, 884, 771, 727, 579 cm^{-1}; ^1H NMR (400 MHz, $CDCl_3$) δ 8.76 – 8.64 (m, 1H, Ar), 7.16 – 7.03 (m, 1H, Ar), 6.60 – 6.48 (m, 1H, Ar), 3.82 (s, 3H, NMe), 3.54 – 3.32 (m, 3H, NCH), 3.13 – 3.05 (m, 1H, NCH), 2.46 (dd, J = 8.5, 5.5 Hz, 1H, C*H*Ar), 2.11 – 1.82 (m, 3H, CH), 1.37 (s, 3.5H, CMe_3), 1.34 – 1.30 (m, 1H, CH), 1.28 (s, 5.5H, CMe_3); ^{13}C NMR (100.6

MHz, $CDCl_3$) (rotamers) δ 160.3 (*ipso*-Ar), 154.6 (C=O), 154.4 (C=O), 151.2 (Ar), 151.0 (Ar), 150.1 (*ipso*-Ar), 128.8 (Ar), 128.6 (Ar), 118.6 (*ipso*-Ar), 118.4 (*ipso*-Ar), 98.6 (Ar), 79.1 (O*C*Me$_3$), 48.5 (NCH_2), 45.7 (NCH_2), 45.2 (NCH_2), 36.0 (CH_2), 35.3 (CH_2), 33.5 (C), 32.3 (C), 31.2 (NMe), 28.6 (C*Me*$_3$), 28.4 (C*Me*$_3$), 26.3 (*C*HAr), 26.2 (*C*HAr), 18.8 (CH_2), 17.9 (CH_2); MS (ESI) *m/z* 351 [$(M + Na)^+$, 100]; HRMS (ESI) *m/z* calcd for $C_{18}H_{24}N_4O_2$ $(M + Na)^+$ 351.1791, found 351.1801 (–2.7 ppm error).

Lab Book Reference: SY-2-239

tert-Butyl 7-(7H-pyrrolo[2,3-d]pyrimidin-4-yl)-2-azabicyclo[4.1.0]heptane-2-carboxylate _exo_-286 and _tert_-Butyl 7-(7-methyl-7H-pyrrolo[2,3-d]pyrimidin-4-yl)-2-azabicyclo[4.1.0] heptane-2-carboxylate _exo_-287

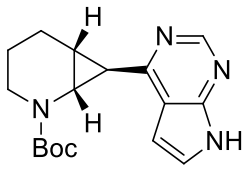

exo-**286**

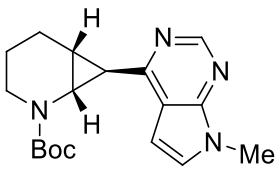

exo-**287**

Cs_2CO_3 (436 mg, 1.34 mmol, 3.0 eq.) was added to a stirred solution of cyclopropyl tosyl-pyrrolopyrimidine *exo*-**283** (209 mg, 0.45 mmol, 1.0 eq.) in MeOH (1.6 mL, 0.3 M) and THF (4.6 mL, 0.1 M). The resulting mixture was stirred at rt for 16 h. H_2O (10 mL) was added and the product was extracted with EtOAc (3 × 10 mL). The combined organic layers were dried (Na_2SO_4), filtered, and evaporated under reduced pressure to give the crude product. Purification by flash column chromatography on silica with 80:20 to 60:40 CH_2Cl_2–acetone as eluent gave cyclopropyl pyrrolopyrimidine *exo*-**286** (62 mg, 44%) as an off-white solid, mp 84 – 86 °C; R_F (60:40 CH_2Cl_2–acetone) 0.33; IR (ATR) 3213 (NH), 3136 (NH), 2975, 2934, 2863, 1696 (C=O), 1582, 1449, 1414, 1391, 1365, 1255, 1165, 901, 734 cm^{-1}; ^1H NMR (400 MHz, $CDCl_3$) (80:20 mixture of rotamers) δ 11.42 (s, 0.8H, NH), 11.13 (s, 0.2H, NH), 8.70 (s, 0.8H, Ar), 8.62 (s, 0.2H, Ar), 7.39 – 7.31 (m, 0.8H, Ar), 7.13 – 7.07 (m, 0.2H, Ar), 6.67 – 6.60 (m, 0.8H, Ar), 6.52 – 6.42 (m, 0.2H, Ar), 3.92 (ddd, *J* = 12.5, 3.5, 3.5 Hz, 0.8H, NCH), 3.79 – 3.76 (m, 0.2H, NCH), 3.76 – 3.70 (m, 0.2H, NCH), 3.44 (dd, *J* = 8.5, 2.5 Hz, 0.8H, NCH), 2.81 (ddd, *J* = 12.5, 12.5, 2.5 Hz, 0.2H, NCH), 2.69 (ddd, *J* = 12.5, 12.5, 2.5 Hz, 0.8H, NCH), 2.49 – 2.40 (m, 0.8H, CH), 2.38 – 2.30 (m, 0.2H, CH), 2.20 (dd, *J* = 6.0, 2.5 Hz, 1H, C*H*Ar), 2.10 – 1.89 (m, 2H,

CH), 1.80 – 1.68 (m, 1H, CH), 1.58 – 1.49 (m, 1H, CH), 1.46 (s, 1.8H, CMe_3), 1.17 (s, 7.2H, CMe_3); ^{13}C NMR (100.6 MHz, $CDCl_3$) (rotamers) δ 160.8 162.0 (*ipso*-Ar), 156.4 (C=O), 151.2 (Ar), 150.7 (*ipso*-Ar), 124.5 (Ar), 116.8 (*ipso*-Ar), 99.6 (Ar), 79.6 (O*C*Me_3), 41.9 (NCH), 40.5 (NCH_2), 29.2 (*C*HAr), 28.6 (CH_2), 28.3 (C*Me*$_3$), 23.8 (CH), 22.3 (CH_2), 20.6 (CH_2); MS (ESI) *m/z* 337 [$(M + Na)^+$, 100]; HRMS (ESI) *m/z* calcd for $C_{17}H_{22}N_4O_2$ $(M + Na)^+$ 337.1635, found 337.1630 (+1.4 ppm error) and cyclopropyl methyl-pyrrolopyrimidine *exo*-**287** (69 mg, 47%) as an colourless oil, R_F (60:40 CH_2Cl_2–acetone) 0.52; IR (ATR) 2974, 2933, 2864, 1690 (C=O), 1567, 1579, 1445, 1388, 1364, 1242, 1162, 1132, 994, 891, 724, 606 cm^{-1}; ^1H NMR (400 MHz, $CDCl_3$) (80:20 mixture of rotamers) δ 8.65 (s, 0.8H, Ar), 8.64 (s, 0.2H, Ar), 7.10 (d, *J* = 3.5 Hz, 0.8H, Ar), 7.05 (d, *J* = 3.5 Hz, 0.2H, Ar), 6.58 – 6.57 (m, 1H, 0.2H, Ar), 6.56 (d, *J* = 3.5 Hz, 0.8H, Ar), 3.89 (ddd, *J* = 13.0, 3.5, 3.5 Hz, 0.8H, NCH), 3.84 (s, 2.4H, NMe), 3.79 (s, 0.6H, NMe), 3.72 (ddd, *J* = 13.0, 3.5, 3.5 Hz, 0.2H, NCH), 3.63 (dd, *J* = 8.5, 2.5, 0.2H, NCH), 3.41 (dd, *J* = 8.5, 2.5 Hz, 0.8H, NCH), 2.77 (ddd, *J* = 12.5, 12.5, 2.5 Hz, 0.2H, NCH), 2.66 (ddd, *J* = 12.5, 12.5, 2.5 Hz, 0.8H, NCH), 2.42 – 2.35 (m, 0.8H, CH), 2.34 – 2.29 (m, 0.2H, CH), 2.16 – 2.08 (m, 1H, C*H*Ar), 2.06 – 2.02 (m, 0.2H, CH), 2.02 – 1.98 (m, 0.8H, CH), 1.98 – 1.87 (m, 1H, CH), 1.77 – 1.65 (m, 1H, CH), 1.54 – 1.44 (m, 1H, CH), 1.42 (s, 1.8H, CMe_3), 1.15 (s, 7.2H, CMe_3); ^{13}C NMR (100.6 MHz, $CDCl_3$) δ 161.4 (*ipso*-Ar), 156.3 (C=O), 151.5 (Ar), 149.8 (*ipso*-Ar), 128.4 (Ar), 116.8 (*ipso*-Ar), 98.7 (Ar), 79.5 (O*C*Me_3), 41.6 (NCH), 40.4 (NCH_2), 31.2 (NMe), 28.9 (*C*HAr), 28.2 (C*Me*$_3$), 23.6 (CH), 22.2 (CH_2), 20.5 (CH_2); MS (ESI) *m/z* 351 [$(M + Na)^+$, 100]; HRMS (ESI) *m/z* calcd for $C_{18}H_{24}N_4O_2$ $(M + Na)^+$ 351.1791, found 351.1788 (+1.1 ppm error).

Lab Book Reference: SY-3-245

tert-Butyl 1-(7*H*-pyrrolo[2,3-d]pyrimidin-4-yl)-5-azaspiro[2.4] heptane-5-carboxylate _cis_-284

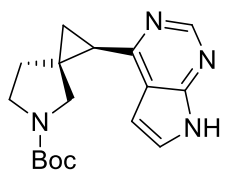

cis-**284**

Pyrrolidine (0.27 mL, 3.21 mmol, 5 eq.) and Cs_2CO_3 (627 mg, 1.93 mmol, 3.0 eq.) were added to a stirred solution of cyclopropyl tosyl pyrrolopyrimidine *cis*-**282** (301 mg, 0.64 mmol, 1.0 eq.) in MeOH (2.2 mL) and THF (6.5 mL) at rt. The resulting mixture was stirred at rt for 16 h. H_2O (10 mL) was added and the mixture was extracted with EtOAc (3 × 10 mL). The combined organic layers were dried (Na_2SO_4), filtered, and evaporated under reduced pressure to give the crude product. Purification by flash column chromatography on silica with 80:20 to 60:40 CH_2Cl_2–acetone as eluent gave cyclopropyl pyrrolopyrimidine *cis*-**284** (166 mg, 82%) as a white solid.

Lab Book Reference: SY-2-249

***tert*-Butyl 7-(7H-pyrrolo[2,3-d]pyrimidin-4-yl)-2-azabicyclo[4.1.0]heptane-2-carboxylate *exo*-286**

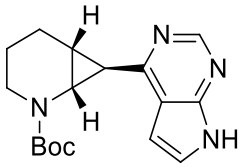

exo-**286**

Pyrrolidine (0.36 mL, 4.32 mmol, 5 eq.) and Cs_2CO_3 (844 mg, 2.59 mmol, 3.0 eq.) were added to a stirred solution of cyclopropyl tosyl pyrrolopyrimidine *exo*-**283** (405 mg, 0.86 mmol, 1.0 eq.) in MeOH (3.0 mL) and THF (9.1 mL) at rt. The resulting mixture was stirred at rt for 16 h. H_2O (10 mL) was added and the mixture was extracted with EtOAc (3 × 10 mL). The combined organic layers were dried (Na_2SO_4) and evaporated under reduced pressure to give the crude product. Purification by flash column chromatography on silica with 80:20 to 60:40 CH_2Cl_2–acetone as eluent gave cyclopropyl pyrrolopyrimidine *exo*-**286** (221 mg, 81%) as a white solid.

Lab Book Reference: SY-3-258

3-(1-(7H-Pyrrolo[2,3-d]pyrimidin-4-yl)-5-azaspiro[2.4]heptan-5-yl)-3-oxopropanenitrile *cis*-266

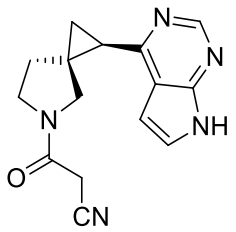

cis-**266**

Using general procedure D, cyclopropyl pyrrolopyrimidine *cis*-**284** (70 mg, 0.22 mmol, 1.0 eq.) and HCl (4 M in dioxane) (5 mL) gave the crude amine•HCl salt. Then, Et_3N (0.1 mL, 0.89 mmol, 4.0 eq.), BOP (148 mg, 0.34 mmol, 1.5 eq.) and 2-cyanoacetic acid (21 mg, 0.25 mmol, 1.1 eq.) were added to a stirred solution of the crude amine·HCl salt in DMF (5 mL) at rt under Ar. The resulting solution was stirred at rt for 16 h. H_2O (10 mL) was added the mixture was extracted with EtOAc (3 × 10 mL). The combined organics were washed with brine (3 × 10 mL), dried (Na_2SO_4), filtered, and evaporated under reduced pressure to give the crude product. Purification by flash column chromatography on silica with 50:50 acetone–CH_2Cl_2 as eluent gave cyanoamide *cis*-**266** (37 mg, 59%) as a white solid, mp 188 – 190 °C, R_F (50:50 acetone–CH_2Cl_2) 0.18; IR (ATR) 3200 (NH), 3139 (NH), 2921, 2874, 2268 (CN), 1645 (C=O), 1579, 1443, 1359, 1299, 1255, 1157, 1025, 1006, 900, 850, 744, 607 cm^{-1}; ^1H NMR (400 MHz, DMSO-d_6) (60:40 mixture of rotamers) δ 12.03 (s, 1H, NH), 8.64 – 8.55 (m, 1H, Ar), 7.51 – 7.45 (m, 1H, Ar), 6.80 – 6.74 (m, 1H, Ar), 3.97 – 3.88 (m, 1H, CH), 3.87 – 3.63 (m, 1H, CH), 3.62 – 3.53 (m, 1H, NCH), 3.53 – 3.40 (m, 2H, NCH), 3.30 – 3.16 (m, 1H, NCH), 2.78 – 2.70 (m, 1H, C*H*Ar), 2.20 – 1.99 (m, 1.6H, CH), 1.97 – 1.87 (m, 0.4H, CH), 1.73 – 1.65 (m, 1H, CH), 1.42 – 1.34 (m, 1H, CH); ^{13}C NMR (100.6 MHz, DMSO-d_6) (rotamers) δ 161.0 (*ipso*-Ar), 160.9 (*ipso*-Ar), 159.6 (C=O), 159.4 (C=O), 150.6 (Ar), 150.5 (*ipso*-Ar), 125.9 (Ar), 117.8 (CN), 116.0 (*ipso*-Ar), 98.9 (Ar), 48.7 (NCH_2), 48.4 (NCH_2), 45.8 (NCH_2), 45.3 (NCH_2), 34.8 (CH_2), 33.6 (CH_2), 32.9 (C), 31.8 (C), 25.3 (*C*HAr), 25.2 (*C*HAr), 25.2 (*C*H_2CN), 24.9 (*C*H_2CN), 18.8 (CH_2), 18.3 (CH_2); MS (ESI) *m/z* 304 [$(M + Na)^+$, 100]; HRMS (ESI) *m/z* calcd for $C_{15}H_{15}N_5O$ $(M + Na)^+$ 304.1169, found 304.1171 (–0.6 ppm error).

Lab Book Reference: SY-2-241

1-(1-(7H-Pyrrolo[2,3-d]pyrimidin-4-yl)-5-azaspiro[2.4]heptan-5-yl) prop-2-en-1-one *cis*-267

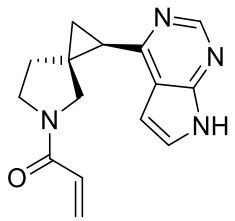

cis-**267**

Using general procedure D, cyclopropyl pyrrolopyrimidine *cis*-**284** (165 mg, 0.53 mmol, 1.0 eq.) and HCl (4 M in dioxane) (5 mL) gave the crude amine•HCl salt. Then, DIPEA (0.4 mL, 2.10 mmol, 4.0 eq.) and acryloyl chloride (52 mg, 0.58 mmol, 1.1 eq.) were added to a stirred solution of the crude amine•HCl salt in DMF (5 mL) at rt under Ar. The resulting solution was stirred at rt for 16 h. H_2O (10 mL) was added the mixture was extracted with EtOAc (3 × 10 mL). The combined organics were dried (Na_2SO_4), filtered, and evaporated under reduced pressure to give the crude product. Purification by flash column chromatography on silica with 50:50 acetone–CH_2Cl_2 as eluent gave acrylamide *cis*-**267** (36 mg, 26%) as a white solid, mp 142 – 145 °C, R_F (50:50 acetone–CH_2Cl_2) 0.16; ^{1}H NMR (400 MHz, DMSO-d_6) (55:45 mixture of rotamers) δ 12.02 (s, 1H, NH), 8.64 – 8.56 (m, 1H, Ar), 7.50 – 7.42 (m, 1H, Ar), 6.81 – 6.72 (m, 1H, Ar), 6.54 (dd, J = 16.5, 10.0 Hz, 0.55H, C*H*=CH$_2$), 6.27 (dd, J = 16.5, 10.0 Hz, 0.45H, C*H*=CH$_2$), 6.04 (dd, J = 16.5, 2.5 Hz, 0.55H, CH=C*H*$_2$), 5.98 (dd, J = 16.5, 2.5 Hz, 0.45H, CH=C*H*$_2$), 5.60 (dd, J = 10.0, 2.5 Hz, 0.55H, CH=C*H*$_2$), 5.54 (dd, J = 10.0, 2.5 Hz, 0.45H, CH=C*H*$_2$), 3.80 – 3.16 (m, 4H, NCH), 2.78 – 2.69 (m, 1H, C*H*Ar), 2.21 – 2.08 (m, 1H, CH), 2.08 – 1.95 (m, 1H, CH), 1.78 – 1.67 (m, 1H, CH), 1.41 (dd, J = 8.0, 4.0 Hz, 0.45H, CH), 1.37 (dd, J = 8.0, 4.0 Hz, 0.55H, CH); ^{13}C NMR (100.6 MHz, DMSO-d_6) (rotamers) δ 163.1 (*ipso*-Ar), 159.6 (C=O), 159.5 (C=O), 150.5 (Ar), 150.4 (*ipso*-Ar), 129.3 (*C*H=CH$_2$), 129.2 (*C*H=CH$_2$), 126.7 (CH=*C*H$_2$), 125.9 (Ar), 125.8 (Ar), 117.8 (*ipso*-Ar), 98.9 (Ar), 48.4 (NCH$_2$), 48.1 (NCH$_2$), 45.6 (NCH$_2$), 44.9 (NCH$_2$), 35.0 (CH$_2$), 33.4 (CH$_2$), 31.7 (C), 25.3 (*C*HAr), 25.2 (*C*HAr), 17.9 (CH$_2$); MS (ESI) *m/z* 291 [(M + Na)$^+$, 100]; HRMS (ESI) *m/z* calcd for $C_{15}H_{16}N_4O$ (M + Na)$^+$ 291.1216, found 291.1218 (–0.6 ppm error).

Lab Book Reference: SY-2-251

Chapter 8: References

1 C. A. Lipinski, *Drug. Discov. Today Technol.*, 2004, **1**, 337–341.

2 C. W. Murray and D. C. Rees, *Angew. Chem. Int. Ed.*, 2016, **55**, 488–492.

3 D. A. Erlanson, S. W. Fesik, R. E. Hubbard, W. Jahnke and H. Jhoti, *Nat. Rev. Drug Discov.*, 2016, **15**, 605–619.

4 R. Macarron, M. N. Banks, D. Bojanic, D. J. Burns, D. A. Cirovic, T. Garyantes, D. V. S. Green, R. P. Hertzberg, W. P. Janzen, J. W. Paslay, U. Schopfer and G. S. Sittampalam, *Nat. Rev. Drug Discov.*, 2011, **10**, 188–195.

5 L. Ruddigkeit, R. van Deursen, L. C. Blum and J.-L. Reymond, *J. Chem. Inf. Model.*, 2012, **52**, 2864–2875.

6 R. S. Bohacek, C. McMartin and W. C. Guida, *Med. Res. Rev.*, 1996, **16**, 3–50.

7 R. Lahana, *Drug. Discov. Today.*, 2003, **8**, 655–656.

8 S. L. McGovern, E. Caselli, N. Grigorieff and B. K. Shoichet, *J. Med. Chem.*, 2002, **45**, 1712–1722.

9 S. B. Shuker, P. J. Hajduk, R. P. Meadows and S. W. Fesik, *Science*, 1996, **274**, 1531–1534.

10 M. J. Harner, A. O. Frank and S. W. Fesik, *J. Biomol. NMR*, 2013, **56**, 65–75.

11 M. Congreve, R. Carr, C. Murray and H. Jhoti, *Drug Discov. Today*, 2003, **8**, 876–877.

12 H. Jhoti, G. Williams, D. C. Rees and C. W. Murray, *Nat. Rev. Drug. Discov.*, 2013, **12**, 644.

13 H. Köster, T. Craan, S. Brass, C. Herhaus, M. Zentgraf, L. Neumann, A. Heine and G. Klebe, *J. Med. Chem.*, 2011, **54**, 7784–7796.

14 M. M. Hann, A. R. Leach and G. Harper, *J. Chem. Inf. Comput. Sci.*, 2001, **41**, 856–864.

15 A. R. Leach and M. M. Hann, *Curr. Opin. Chem. Biol.*, 2011, **15**, 489–496.

16 Q. Li, *Front. Mol. Biosci.*, , **7**, 1–13

17 P. D. Leeson and S. A. St-Gallay, *Nat. Rev. Drug. Discov.*, 2011, **10**, 749–765.

18 A. Douangamath, D. Fearon, P. Gehrtz, T. Krojer, P. Lukacik, C. D. Owen, E. Resnick, C. Strain-Damerell, A. Aimon, P. Ábrányi-Balogh, J. Brandaõ-Neto, A. Carbery, G. Davison, A. Dias, T. D. Downes, L. Dunnett, M. Fairhead, J. D. Firth, S. P. Jones, A. Keely, G. M. Keserü, H. F. Klein, M. P. Martin, M. E. M. Noble, P. O'Brien, A. Powell, R. Reddi, R. Skyner, M. Snee, M. J. Waring, C. Wild, N. London, F. von Delft and M. A. Walsh, *bioRxiv*, , DOI:10.1101/2020.05.27.118117.

19 P. Kirsch, A. M. Hartman, A. K. H. Hirsch and M. Empting, *Molecules*, 2019, **24**, 4309.

20 D. J. Wood, J. D. Lopez-Fernandez, L. E. Knight, I. Al-Khawaldeh, C. Gai, S. Lin, M. P. Martin, D. C. Miller, C. Cano, J. A. Endicott, I. R. Hardcastle, M. E. M. Noble and M. J. Waring, *J. Med. Chem.*, 2019, **62**, 3741–3752.

21 T. Tiefenbrunn, S. Forli, M. Happer, A. Gonzalez, Y. Tsai, M. Soltis, J. H. Elder, A. J. Olson and C. D. Stout, *Chem. Biol. Drug. Des.*, 2014, **83**, 141–148.

22 G. Davison, M. P. Martin, S. Turberville, S. Dormen, R. Heath, A. B. Heptinstall, M. Lawson, D. C. Miller, Y. M. Ng, J. N. Sanderson, I. Hope, D. J. Wood, C. Cano, J. A. Endicott, I. R. Hardcastle, M. E. M. Noble and M. J. Waring, *J. Med. Chem.*, 2022, **65**, 15416–15432.

23 O. B. Cox, T. Krojer, P. Collins, O. Monteiro, R. Talon, A. Bradley, O. Fedorov, J. Amin, B. D. Marsden, J. Spencer, F. von Delft and P. E. Brennan, *Chem. Sci.*, 2016, **7**, 2322–2330.

24 J. D. St. Denis, R. J. Hall, C. W. Murray, T. D. Heightman and D. C. Rees, *RSC Med. Chem.*, 2021, **12**, 321–329.

25 I. J. P. de Esch, D. A. Erlanson, W. Jahnke, C. N. Johnson and L. Walsh, *J. Med. Chem*, 2022, **65**, 84–99.

26 B. C. Doak, R. S. Norton and M. J. Scanlon, *Pharmacol. Ther.*, 2016, **167**, 28–37.

27 T. Wang, M.-B. Wu, Z.-J. Chen, H. Chen, J.-P. Lin and L.-R. Yang, *Curr. Pharm. Biotechnol.*, 2015, **16**, 11–25.

28 B. Lamoree and R. E. Hubbard, *Essays Biochem.*, 2017, **61**, 453–464.

29 D. A. Erlanson, B. J. Davis and W. Jahnke, *Cell. Chem. Biol.*, 2019, **26**, 9–15.

30 M. Sándor, R. Kiss and G. M. Keserű, *J. Chem. Inf. Model.*, 2010, **50**, 1165–1172.

31 P. Kirsch, V. Jakob, K. Oberhausen, S. C. Stein, I. Cucarro, T. F. Schulz and M. Empting, *J. Med. Chem.*, 2019, **62**, 3924–3939.

32 M. P. Storz, C. Brengel, E. Weidel, M. Hoffmann, K. Hollemeyer, A. Steinbach, R. Müller, M. Empting and R. W. Hartmann, *ACS Chem. Biol.*, 2013, **8**, 2794–2801.

33 J. H. Sahner, C. Brengel, M. P. Storz, M. Groh, A. Plaza, R. Müller and R. W. Hartmann, *J. Med. Chem.*, 2013, **56**, 8656–8664.

34 J. H. Sahner, M. Empting, A. Kamal, E. Weidel, M. Groh, C. Börger and R. W. Hartmann, *Eur. J. Med. Chem.*, 2015, **96**, 14–21.

35 M. Mondal, N. Radeva, H. Fanlo-Virgós, S. Otto, G. Klebe and A. K. H. Hirsch, *Angew. Chem. Int. Ed.*, 2016, **55**, 9422–9426.

36 O. Ichihara, J. Barker, R. J. Law and M. Whittaker, *Mol. Inform.*, 2011, **30**, 298–306.

37 A. W. Hung, H. L. Silvestre, S. Wen, A. Ciulli, T. L. Blundell and C. Abell, *Angew. Chem. Int. Ed.*, 2009, **48**, 8452–8456.

38 Y. Y. Ku, V. S. Chan, A. Christesen, T. Grieme, M. Mulhern, Y. M. Pu and M. D. Wendt, *J. Org. Chem.*, 2019, **84**, 4814–4829.

39 C. W. Murray, D. R. Newell and P. Angibaud, *Med. Chem. Comm.*, 2019, 10, 1509–1511.

40 G. Bollag, P. Hirth, J. Tsai, J. Zhang, P. N. Ibrahim, H. Cho, W. Spevak, C. Zhang, Y. Zhang, G. Habets, E. A. Burton, B. Wong, G. Tsang, B. L. West, B. Powell, R. Shellooe, A. Marimuthu, H. Nguyen, K. Y. J. Zhang, D. R. Artis, J. Schlessinger, F. Su, B. Higgins, R. Iyer, K. Dandrea, A. Koehler, M. Stumm, P. S. Lin, R. J. Lee, J. Grippo, I. Puzanov, K. B. Kim, A. Ribas, G. A. McArthur, J. A. Sosman, P. B. Chapman, K. T. Flaherty, X. Xu, K. L. Nathanson and K. Nolop, *Nature*, 2010, **467**, 596–599.

41 W. D. Tap, Z. A. Wainberg, S. P. Anthony, P. N. Ibrahim, C. Zhang, J. H. Healey, B. Chmielowski, A. P. Staddon, A. Lee Cohn, G. I. Shapiro, V. L. Keedy, A. S. Singh, I. Puzanov, E. L. Kwak, A. J. Wagner, D. D. Von Hoff, G. J. Weiss, R. K. Ramanathan, J. Zhang, G. Habets, Y. Zhang, E. A. Burton, G. Visor, L. Sanftner, P. Severson, H. Nguyen, M. J. Kim, A. Marimuthu, G. Tsang, R. Shellooe, C. Gee, B. L. West, P. Hirth, K. Nolop, M. Van De Rijn, H. H. Hsu, C. Peterfy, P. S. Lin, S. Tong-Starksen and G. Bollag, *N. Engl. J. Med.*, 2015, **373**, 428–437.

42 J. Canon, K. Rex, A. Y. Saiki, C. Mohr, K. Cooke, D. Bagal, K. Gaida, T. Holt, C. G. Knutson, N. Koppada, B. A. Lanman, J. Werner, A. S. Rapaport, T. San Miguel, R. Ortiz, T. Osgood, J.-R. Sun, X. Zhu, J. D. McCarter, L. P. Volak, B. E. Houk, M. G. Fakih, B. H. O'Neil, T. J. Price, G. S. Falchook, J. Desai, J. Kuo, R. Govindan, D. S. Hong, W. Ouyang, H. Henary, T. Arvedson, V. J. Cee and J. R. Lipford, *Nature*, 2019, **575**, 217–223.

43 J. M. Ostrem, U. Peters, M. L. Sos, J. A. Wells and K. M. Shokat, *Nature*, 2013, **503**, 548–551.

44 J. Schoepfer, W. Jahnke, G. Berellini, S. Buonamici, S. Cotesta, S. W. Cowan-Jacob, S. Dodd, P. Drueckes, D. Fabbro, T. Gabriel, J.-M. Groell, R. M. Grotzfeld, A. Q. Hassan, C. Henry, V. Iyer, D. Jones, F. Lombardo, A. Loo, P. W. Manley, X. Pellé, G. Rummel, B. Salem, M. Warmuth, A. A. Wylie, T. Zoller, A. L. Marzinzik and P. Furet, *J. Med. Chem.*, 2018, **61**, 8120–8135.

45 S. W. Muchmore, M. Sattler, H. Liang, R. P. Meadows, J. E. Harlan, H. S. Yoon, D. Nettesheim, B. S. Chang, C. B. Thompson, S.-L. Wong, S.-C. Ng and S. W. Fesik, *Nature*, 1996, **381**, 335–341.

46 A. Bancet, C. Raingeval, T. Lomberget, M. Le Borgne, J.-F. Guichou and I. Krimm, *J. Med. Chem.*, 2020, **63**, 11420–11435.

47 H. F. Klein, PhD Thesis, University of York, 2020.

48 J. Donald, *Unpublished Results*.

49 C. Palmer, MChem Thesis, University of York, 2020.

50 J. Lincoln, MChem Thesis, University of York, 2020.

51 P. Brear, C. de Fusco, E. L. Atkinson, J. Iegre, N. J. Francis-Newton, A. R. Venkitaraman, M. Hyvönen and D. R. Spring, *RSC Med. Chem.*, , DOI:10.1039/D2MD00161F.

52 C. W. Murray and D. C. Rees, *Nat. Chem.*, 2009, **1**, 187–192.

53 S. M. Strittmatter, *Nat. Med.*, 2014, **20**, 590–591.

54 S. Ekins, C. L. Waller, M. P. Bradley, A. M. Clark and A. J. Williams, *Drug Discov. Today*, 2013, **18**, 265–271.

55 M. R. Bentley, O. v Ilyichova, G. Wang, M. L. Williams, G. Sharma, W. S. Alwan, R. L. Whitehouse, B. Mohanty, P. J. Scammells, J. L. Martin, M. Totsika, B. Capuano, B. C. Doak and M. J. Scanlon, *J. Med. Chem.*, 2020, **63**, 6875.

56 F. Lovering, J. Bikker and C. Humblet, *J. Med. Chem.*, 2009, **52**, 6752–6756.

57 C. J. Helal, A. Bartolozzi, S. D. Goble, N. S. Mani, A. Guzman-Perez, A. K. Ohri, Z. C. Shi and C. Subramanyam, *Drug Discov. Today*, 2018, **23**, 1458–1462.

58 A. de Meijere, *Angew. Chem. Int. Ed.*, 1979, **18**, 809–826.

59 Z. Časar, *Synthesis Stuttg*, 2020, **52**, 1315–1345.

60 N. A. Meanwell, *J. Med. Chem.*, 2011, **54**, 2529–2591.

61 T. T. Talele, *J. Med. Chem.*, 2016, **59**, 8712–8756.

62 E. Vitaku, D. T. Smith and J. T. Njardarson, *J. Med. Chem.*, 2014, **57**, 10257–10274.

63 A. Millet, A. R. Martin, C. Ronco, S. Rocchi and R. Benhida, *Med. Res. Rev.*, 2017, **37**, 98–148.

64 D. S. Bhalerao, A. K. R. Arkala, Y. V. Madhavi, M. Nagaraju, S. R. Gade, U. K. S. Kumar, R. Bandichhor and V. H. Dahanukar, *Org. Process Res. Dev.*, 2015, **19**, 1559–1567.

65 M. A. Abu-Zaied and G. H. Elgemeie, *Nucleosides Nucleotides Nucleic Acids*, 2017, **36**, 713–725.

66 S. A. Savage, G. S. Jones, S. Kolotuchin, S. A. Ramrattan, T. Vu and R. E. Waltermire, *Org. Process Res. Dev.*, 2009, **13**, 1169–1176.

67 B. Santhamma, K. Acosta, A. Chavez-Riveros and K. Nickisch, *Steroids*, 2015, **102**, 60–64.

68 J. Alliot, E. Gravel, F. Pillon, D. A. Buisson, M. Nicolas and E. Doris, *Chem. Comm.*, 2012, **48**, 8111–8113.

69 F. W. Goldberg, J. G. Kettle, T. Kogej, M. W. D. Perry and N. P. Tomkinson, *Drug. Discov. Today.*, 2015, **20**, 11–17.

70 D. M. Knapp, E. P. Gillis and M. D. Burke, *J. Am. Chem. Soc.*, 2009, **131**, 6961–6963.

71 E. P. Gillis and M. D. Burke, *J. Am. Chem. Soc.*, 2008, **130**, 14084–14085.

72 T. A. Ban, *Dialogues Clin. Neurosci.*, 2006, **8**, 335–344.

73 M. R. Harris, Q. Li, Y. Lian, J. Xiao and A. T. Londregan, *Org. Lett.*, 2017, **19**, 2450–2453.

74 Á. Gutiérrez-Bonet, S. Popov, M. H. Emmert, J. M. E. Hughes, A. F. Nolting, S. Ruccolo and Y. Wang, *Org. Lett.*, 2022, **24**, 3455–3460.

75 I. Kleban, Y. Krokhmaliuk, S. Reut, S. Shuvakin, V. V. Pendyukh, O. I. Khyzhan, D. S. Yarmoliuk, A. V. Tymtsunik, Y. V. Rassukana and O. O. Grygorenko, *European J. Org. Chem.*, 2021, **2021**, 6551–6560.

76 O. v. Hryshchuk, A. O. Varenyk, Y. Yurov, Y. O. Kuchkovska, A. v. Tymtsunik and O. O. Grygorenko, *European J. Org. Chem.*, 2020, **2020**, 2217–2224.

77 A. R. Renslo, P. Jaishankar, R. Venkatachalam, C. Hackbarth, S. Lopez, D. V. Patel and M. F. Gordeev, *J. Med. Chem.*, 2005, **48**, 5009–5024.

78 R. L. Danheiser and A. C. Savoca, *J. Org. Chem.*, 1985, **50**, 2401–2403.

79 World Intellectual Property Organisation, WO 2022/081925, 2022.

80 A. B. Charette, S. Mathieu and J. F. Fournier, *Syn. Lett.*, 2005, **2005**, 1779–1782.

81 N. Kumar, R. R. Reddy and A. Masarwa, *Chem. Eur. J.*, 2019, **25**, 8008–8012.

82 M. R. Harris, H. M. Wisniewska, W. Jiao, X. Wang and J. N. Bradow, *Org. Lett*, 2018, **20**, 2867–2871.

83 C. Chen, P. Kattanguru, O. A. Tomashenko, R. Karpowicz, G. Siemiaszko, A. Bhattacharya, V. Calasans and Y. Six, *Org. Biomol. Chem.*, 2017, **15**, 5364–5372.

84 S. Yamazaki, Y. Yamamoto, Y. Fukushima, M. Takebayashi, T. Ukai and Y. Mikata, *J. Org. Chem.*, 2010, **75**, 5216–5222.

85 G. F. Meijs and I. R. Doyle, *J. Org. Chem.*, 1985, **50**, 3713–3716.

86 M. Mato, I. Martín-Torres, B. Herlé and A. M. Echavarren, *Org. Biomol. Chem.*, 2019, **17**, 4216–4219.

87 W.-X. Lv, Q. Li, J.-L. Li, Z. Li, E. Lin, D.-H. Tan, Y.-H. Cai, W.-X. Fan and H. Wang, *Angew. Chem. Int. Ed.*, 2018, **57**, 16544–16548.

88 C. Chen, P. Kattanguru, O. A. Tomashenko, R. Karpowicz, G. Siemiaszko, A. Bhattacharya, V. Calasans and Y. Six, *Org. Biomol. Chem.*, 2017, **15**, 5364–5372.

89 D. Seyferth, H. Yamazaki and D. L. Alleston, *J. Org. Chem.*, 1963, **28**, 703–706.

90 N. Shimizu, K. Watanabe and Y. Tsuno, *Chem. Lett.*, 1983, **12**, 1877–1878.

91 C. W. Jefford, D. Kirkpatrick and F. Delay, *J. Am. Chem. Soc.*, 1972, **94**, 8905–8907.

92 D. Seyferth and B. Prokai, *J. Org. Chem.*, 1966, **31**, 1702–1704.

93 J. R. A. Dulayymi, M. S. Baird, I. G. Bolesov, V. Tveresovsky and M. Rubin, *Tetrahedron Lett*, 1996, **37**, 8933–8936.

94 J. R. al Dulayymi, M. S. Baird, I. G. Bolesov, A. v. Nizovtsev and V. v. Tverezovsky, *J. Chem. Soc. Perkin Trans.*, 2000, 1603–1618.

95 O. G. Kulinkovich, S. v. Sviridov and D. A. Vasilevski, *Synthesis Stuttg.*, 1991, **1991**, 234–234.

96 T. Harada, T. Katsuhira, K. Hattori and A. Oku, *Tetrahedron*, 1994, **50**, 7987–8002.

97 T. Hirao, T. Masunaga, Y. Ohshiro and T. Agawa, *J. Org. Chem.*, 1981, **46**, 3745–3747.

98 T. Hirao and Y. Ohshiro, *J. Syn. Org. Chem. Jpn.*, 1987, **45**, 784–791.

99 S. Abbas, C. J. Hayes and S. Worden, *Tetrahedron Lett.*, 2000, **41**, 3215–3219.

100 D. Seyferth and R. L. Lambert, *J. Organomet. Chem.*, 1973, **55**, c53–c57.

101 H. M. Hutton and T. Schaefer, *Can. J. Chem.*, 1963, **41**, 684–689.

102 CN108341766, 2018, 1–12.

103 O. A. Davis, R. A. Croft and J. A. Bull, *Chem. Comm.*, 2015, **51**, 15446–15449.

104 K. M. Lynch and W. P. Dailey, *J. Org. Chem.*, 1995, **60**, 4666–4668.

105 E. v. Dehmlow and U. Fastabend, *J. Chem. Soc. Chem. Commun.*, 1993, **16**, 1241–1242.

106 E. v. Dehmlow, *Russian Chem. Bull.*, 1995, **44**, 1998–2005.

107 Y. Zhao, T. Chen, X. B. Wang and L. B. Han, *Phosphorus Sulfur Silicon Relat. Elem.*, 2015, **190**, 1820–1827.

108 G. Verniest, K. Piron, E. Van Hende, J. W. Thuring, G. MacDonald, F. Deroose and N. De Kimpe, *Org. Biomol. Chem.*, 2010, **8**, 2509–2512.

109 S. E. Hooshmand, B. Heidari, R. Sedghi and R. S. Varma, *Green Chemistry*, 2019, 21, 381–405.

110 N. Miyaura, K. Yamada and A. Suzuki, *Tetrahedron Lett.*, 1979, **20**, 3437–3440.

111 P. Maity, V. V. R. Reddy, J. Mohan, S. Korapati, H. Narayana, N. Cherupally, S. Chandrasekaran, R. Ramachandran, C. Sfouggatakis, M. D. Eastgate, E. M. Simmons and R. Vaidyanathan, *Org. Process Res. Dev.*, 2018, **22**, 888–897.

112 I. W. Ashworth, A. D. Campbell, J. H. Cherryman, J. Clark, A. Crampton, E. G. B. Eden-Rump, M. Evans, M. F. Jones, S. McKeever-Abbas, R. E. Meadows, K.

Skilling, D. T. E. Whittaker, R. L. Woodward and P. A. Inglesby, *Org. Process Res. Dev.*, 2018, **22**, 1801–1808.

113 R. N. Bream, H. Clark, D. Edney, A. Harsanyi, J. Hayler, A. Ironmonger, N. Mc Cleary, N. Phillips, C. Priestley, A. Roberts, P. Rushworth, P. Szeto, M. R. Webb and K. Wheelhouse, *Org. Process Res. Dev.*, 2021, **25**, 540.

114 M. A. Graham, H. Askey, A. D. Campbell, L. Chan, K. G. Cooper, Z. Cui, A. Dalgleish, D. Dave, G. Ensor, M. R. Galan Espinosa, P. Hamilton, C. Heffernan, L. V Jackson, D. Jing, M. F. Jones, P. Liu, K. R. Mulholland, M. Pervez, M. Popadynec, E. Randles, S. Tomasi and S. Wang, *Org. Process Res. Dev.*, 2021, **25**, 43–56.

115 J. P. Hildebrand and S. P. Marsden, *Syn. Lett.*, 1996, **1996**, 893–894.

116 M. Rubina, M. Rubin and V. Gevorgyan, *J. Am. Chem. Soc.*, 2003, **125**, 7198–7199.

117 D. J. Wallace and C. Chen, *Tetrahedron Lett.*, 2002, **43**, 6987–6990.

118 G. Benoit and A. B. Charette, *J. Am. Chem. Soc.*, 2017, **139**, 1364–1367.

119 M. Murai, C. Mizuta, R. Taniguchi and K. Takai, *Org. Lett.*, 2017, **19**, 6104–6107.

120 J. Carreras, A. Caballero and P. J. Pérez, *Angew. Chem. Int. Ed.*, 2018, **57**, 2334–2338.

121 G. A. Molander and T. Ito, *Org. Lett.*, 2001, **3**, 393–396.

122 G. H. Fang, Z. J. Yan and M. Z. Deng, *Org. Lett.*, 2004, **6**, 357–360.

123 I. Kleban, D. S. Radchenko, A. V. Tymtsunik, S. Shuvakin, A. I. Konovets, Y. Rassukana and O. O. Grygorenko, *Monatsh. Chem.*, 2020, **151**, 953–962.

124 P. A. Cox, A. G. Leach, A. D. Campbell and G. C. Lloyd-Jones, *J. Am. Chem. Soc.*, 2016, **138**, 9145–9157.

125 J. A. Gonzalez, O. M. Ogba, G. F. Morehouse, N. Rosson, K. N. Houk, A. G. Leach, P. H. Y. Cheong, M. D. Burke and G. C. Lloyd-Jones, *Nat. Chem.*, 2016, **8**, 1067–1075.

126 D. M. Knapp, E. P. Gillis and M. D. Burke, *J. Am. Chem. Soc.*, 2009, **131**, 6961–6963.

127 M. A. J. Duncton and R. Singh, *Org. Lett.*, 2013, **15**, 4284–4287.

128 World Intellectual Property Organization, WO 2017/153459 Al, 2017, 4–84.

129 US 2011/0130415 A1, 2011, 1–112.

130 WO 2012/012619, 2012, 1–125.

131 Andres R. Gomez-Angel, PhD Thesis, University of York, 2024, *Manuscript in preparation.*

132 R. Appiani, MSc. Thesis, University of York, 2019.

133 W. H. B. Sauer and M. K. Schwarz, *J. Chem. Inf. Comput. Sci.*, 2003, **43**, 987–1003.

134 O. O. Grygorenko, P. Babenko, D. M. Volochnyuk, O. Raievskyi and I. V. Komarov, *RSC Adv.*, 2016, **6**, 17595–17605.

135 G. Lauri and P. A. Bartlett, *J. Comput. Aided. Mol. Des.*, 1994, **8**, 51–66.

136 O. O. Grygorenko, R. Prytulyak, D. M. Volochnyuk, V. Kudrya, O. V. Khavryuchenko and I. V. Komarov, *Mol. Divers.*, 2012, **16**, 477–487.

137 O. O. Grygorenko, D. Demenko, D. M. Volochnyuk and I. V. Komarov, *New J. Chem.*, 2018, **42**, 8355–8365.

138 D. J. Hamilton, M. Beemsterboer, C. M. Carter, J. Elsayed, R. E. M. Huiberts, H. F. Klein, P. O'Brien, I. J. P. Esch and M. Wijtmans, *Chem. Med. Chem.*, , DOI:10.1002/cmdc.202200113.

139 M. R. Kolk, M. A. C. H. Janssen, F. P. J. T. Rutjes and D. Blanco-Ania, *Chem. Med. Chem.*, , DOI:10.1002/cmdc.202200020.

140 T. T. Wager, B. A. Pettersen, A. W. Schmidt, D. K. Spracklin, S. Mente, T. W. Butler, H. Howard, D. J. Lettiere, D. M. Rubitski, D. F. Wong, F. M. Nedza, F. R. Nelson, H. Rollema, J. W. Raggon, J. Aubrecht, J. K. Freeman, J. M. Marcek, J. Cianfrogna, K. W. Cook, L. C. James, L. A. Chatman, P. A. Iredale, M. J. Banker, M. L. Homiski, J. B. Munzner and R. Y. Chandrasekaran, *J. Med. Chem.*, 2011, **54**, 7602–7620.

141 S. Ahmad, W. N. Washburn, A. S. Hernandez, S. Bisaha, K. Ngu, W. Wang, M. A. Pelleymounter, D. Longhi, N. Flynn, A. V. Azzara, K. Rohrbach, J. Devenny, S. Rooney, M. Thomas, S. Glick, H. Godonis, S. Harvey, H. Zhang, B. Gemzik, E. B. Janovitz, C. Huang, L. Zhang, J. A. Robl and B. J. Murphy, *J. Med. Chem.*, 2016, **59**, 8848–8858.

142 Z. Dong and D. W. C. MacMillan, *Nature*, 2021, **598**, 451–456.

143 G. A. Molander and P. E. Gormisky, *J. Org. Chem.*, 2008, **73**, 7481–7485.

144 L. Li, S. Zhao, A. Joshi-Pangu, M. Diane and M. R. Biscoe, *J. Am. Chem. Soc.*, 2014, **136**, 14027–14030.

145 M. M. Elsebaie, H. T. Nour El-Din, N. S. Abutaleb, A. A. Abuelkhir, H.-W. Liang, A. S. Attia, M. N. Seleem and A. S. Mayhoub, *Eur. J. Med. Chem.*, 2022, **234**, 114204.

146 O. Gutierrez, J. C. Tellis, D. N. Primer, G. A. Molander and M. C. Kozlowski, *J. Am. Chem. Soc.*, 2015, **137**, 4896–4899.

147 H. Kemp, University of York, 2022.

148 M. T. Crimmins and T. L. Reinhold, in *Org. React.*, John Wiley & Sons, Inc., Hoboken, NJ, USA, 1993, pp. 297–588.

149 S. Poplata, A. Tröster, Y.-Q. Zou and T. Bach, *Chem. Rev.*, 2016, **116**, 9748–9815.

150 L. Ghosez and B. Gobeaux, *Heterocycles*, 1989, **28**, 29.

151 M. A. Maskeri, A. J. Fernandes, G. Di Mauro, N. Maulide and K. N. Houk, *J. Am. Chem. Soc.*, 2022, **144**, 23358–23367.

152 H. Il Kong, J. E. Crichton and J. M. Manthorpe, *Tetrahedron Lett.*, 2011, **52**, 3714–3717.

153 US Patent Application Publication, 2004/0044029 A1, 2004.

154 K. Hirotaki, A. Irie, Y. Nakamura and T. Hanamoto, *Synthesis Stuttg.*, 2017, **49**, 2488–2494.

155 S. K. Kariofillis, S. Jiang, A. M. Żurański, S. S. Gandhi, J. I. Martinez Alvarado and A. G. Doyle, *J. Am. Chem. Soc.*, 2022, **144**, 1045–1055.

156 V. K. Aggarwal, N. Barbero, E. M. McGarrigle, G. Mickle, R. Navas, J. R. Suárez, M. G. Unthank and M. Yar, *Tetrahedron Lett.*, 2009, **50**, 3482–3484.

157 J. Singh, R. C. Petter, T. A. Baillie and A. Whitty, *Nature Rev. Drug Discov.*, 2011, **10**, 307–317.

158 R. Lagoutte, R. Patouret and N. Winssinger, *Curr. Opin. Chem. Biol.*, 2017, **39**, 54–63.

159 P. A. Jackson, J. C. Widen, D. A. Harki and K. M. Brummond, *J. Med. Chem.*, 2017, **60**, 839–885.

160 N. Shindo and A. Ojida, *Bioorg. Med. Chem.*, 2021, **47**, 116386.

161 E. Mons, R. Q. Kim, B. R. van Doodewaerd, P. A. van Veelen, M. P. C. Mulder and H. Ovaa, *J. Am. Chem. Soc.*, 2021, **143**, 6423–6433.

162 A. M. Roberts, D. K. Miyamoto, T. R. Huffman, L. A. Bateman, A. N. Ives, D. Akopian, M. J. Heslin, C. M. Contreras, M. Rape, C. F. Skibola and D. K. Nomura, *ACS Chem. Biol.*, 2017, **12**, 899–904.

163 A. Douangamath, D. Fearon, P. Gehrtz, T. Krojer, P. Lukacik, C. D. Owen, E. Resnick, C. Strain-Damerell, A. Aimon, P. Ábrányi-Balogh, J. Brandão-Neto, A. Carbery, G. Davison, A. Dias, T. D. Downes, L. Dunnett, M. Fairhead, J. D. Firth, S. P. Jones, A. Keeley, G. M. Keserü, H. F. Klein, M. P. Martin, M. E. M. Noble, P. O'Brien, A. Powell, R. N. Reddi, R. Skyner, M. Snee, M. J. Waring, C. Wild, N. London, F. von Delft and M. A. Walsh, *Nat. Commun*, 2020, **11**, 5047.

164 J. Dong, L. Krasnova, M. G. Finn and K. B. Sharpless, *Angew. Chem. Int. Ed.*, 2014, **53**, 9430–9448.

165 A. Narayanan and L. H. Jones, *Chem. Sci.*, 2015, **6**, 2650–2659.

166 X. Yang, J. P. D. van Veldhoven, J. Offringa, B. J. Kuiper, E. B. Lenselink, L. H. Heitman, D. van der Es and A. P. IJzerman, *J. Med. Chem.*, 2019, **62**, 3539–3552.

167 J. Pettinger, M. Carter, K. Jones and M. D. Cheeseman, *J. Med. Chem.*, 2019, **62**, 11383–11398.

168 Q. Zhao, X. Ouyang, X. Wan, K. S. Gajiwala, J. C. Kath, L. H. Jones, A. L. Burlingame and J. Taunton, *J. Am. Chem. Soc.*, 2017, **139**, 680–685.

169 D. A. Shannon, R. Banerjee, E. R. Webster, D. W. Bak, C. Wang and E. Weerapana, *J. Am. Chem. Soc.*, 2014, **136**, 3330–3333.

170 A. R. Gomes, C. L. Varela, E. J. Tavares-da-Silva and F. M. F. Roleira, *Eur. J. Med. Chem.*, 2020, **201**, 112327.

171 A. Fawcett, *Pure Appl. Chem.*, 2020, **92**, 751–765.

172 S. Liu, J. Widom, C. W. Kemp, C. M. Crews and J. Clardy, *Science*, 1998, **282**, 1324–1327.

173 R. Gianatassio, J. M. Lopchuk, J. Wang, C.-M. Pan, L. R. Malins, L. Prieto, T. A. Brandt, M. R. Collins, G. M. Gallego, N. W. Sach, J. E. Spangler, H. Zhu, J. Zhu and P. S. Baran, *Science*, 2016, **351**, 241–246.

174 D. Quach, G. Tang, J. Anantharajan, N. Baburajendran, A. Poulsen, J. L. K. Wee, P. Retna, R. Li, B. Liu, D. H. Y. Tee, P. Z. Kwek, J. K. Joy, W. Yang, C. Zhang, K. Foo, T. H. Keller and S. Q. Yao, *Angew. Chem. Int. Ed.*, 2021, **60**, 17131–17137.

175 S. Cambray and J. Gao, *Acc. Chem. Res.*, 2018, **51**, 2198–2206.

176 G. Akçay, M. A. Belmonte, B. Aquila, C. Chuaqui, A. W. Hird, M. L. Lamb, P. B. Rawlins, N. Su, S. Tentarelli, N. P. Grimster and Q. Su, *Nat. Chem. Biol.*, 2016, **12**, 931–936.

177 J. Schrader, F. Henneberg, R. A. Mata, K. Tittmann, T. R. Schneider, H. Stark, G. Bourenkov and A. Chari, *Science*, 2016, **353**, 594–598.

178 L. Boike, N. J. Henning and D. K. Nomura, *Nat. Rev. Drug Discov.*, 2022, **21**, 881–898.

179 A. J. Streeter, D. C. Dahlin, S. D. Nelson and T. A. Baillie, *Chem. Biol. Interact.*, 1984, **48**, 349–366.

180 E. Albano, M. Rundgren, P. J. Harvison, S. D. Nelson and P. Moldéus, *Mol. Pharmacol.*, 1985, **28**, 306–11.

181 T. Geib, G. Moghaddam, A. Supinski, M. Golizeh and L. Sleno, *Front. Chem.*, DOI:10.3389/fchem.2021.736788.

182 J. A. Hinson, D. W. Roberts and L. P. James, in *Adverse Drug React.*, 2010, vol. 196, pp. 369–405.

183 M. H. Potashman and M. E. Duggan, *J. Med. Chem.*, 2009, **52**, 1231–1246.

184 M. Gehringer and S. A. Laufer, *J. Med. Chem.*, 2019, **62**, 5673–5724.

185 D. G. Silva, J. F. R. Ribeiro, D. de Vita, L. Cianni, C. H. Franco, L. H. Freitas-Junior, C. B. Moraes, J. R. Rocha, A. C. B. Burtoloso, P. W. Kenny, A. Leitão and C. A. Montanari, *Bioorg. Med. Chem. Lett.*, 2017, **27**, 5031–5035.

186 U.S. Food and Drug Administration, *FDA News Release*.

187 J. Canon, K. Rex, A. Y. Saiki, C. Mohr, K. Cooke, D. Bagal, K. Gaida, T. Holt, C. G. Knutson, N. Koppada, B. A. Lanman, J. Werner, A. S. Rapaport, T. San Miguel, R. Ortiz, T. Osgood, J. R. Sun, X. Zhu, J. D. McCarter, L. P. Volak, B. E. Houk, M. G. Fakih, B. H. O'Neil, T. J. Price, G. S. Falchook, J. Desai, J. Kuo, R. Govindan, D. S. Hong, W. Ouyang, H. Henary, T. Arvedson, V. J. Cee and J. R. Lipford, *Nature*, 2019, **575**, 217–223.

188 S. Wu, X. Chen, D.-Y. Jin, D. W. Stafford, L. G. Pedersen and J.-K. Tie, *Blood*, 2018, **132**, 647–657.

189 R. B. Silverman, *J. Am. Chem. Soc.*, 1981, **103**, 3910–3915.

190 G. M. Keating, *Drugs*, 2014, **74**, 587–610.

191 B. Ahrén, A. Schweizer, S. Dejager, E. B. Villhauer, B. E. Dunning and J. E. Foley, *Diabetes Obes. Metab.*, 2011, **13**, 775–783.

192 World Intellectual Property Organization, WO2022136174A1, 2022.

193 World Intellectual Property Organization, WO2018206539A1, 2018.

194 R. J. Kishton, S. E. Miller, H. Perry, T. Lynch, M. Patel, V. K. Gore, G. R. Akkaraju and S. Varadarajan, *Bioorg. Med. Chem.*, 2011, **19**, 5093–5102.

195 R. M. De Figueiredo, J. S. Suppo and J. M. Campagne, *Chem. Rev.*, 2016, 116, 12029–12122.

196 J. R. Dunetz, Y. Xiang, A. Baldwin and J. Ringling, *Org. Lett.*, 2011, **13**, 5048–5051.

197 N. George, S. Ofori, S. Parkin and S. G. Awuah, *RSC Adv.*, 2020, **10**, 24017–24026.

198 World Intellectual Property Organisation, WO 2018/103058 A1, 2018, 1–999.

199 WO 2015/180612 A1, 2015, 1–204.

200 G. A. Molander and D. L. Sandrock, *Curr. Opin. Drug Discov. Devel.*, 2009, **12**, 811–23.

201 P. A. Inglesby, L. R. Agnew, H. L. Carter and O. T. Ring, *Org. Process Res. Dev.*, 2020, **24**, 1683–1689.

202 C. Howman, University of York, 2021.

203 M. Gill, University of York, 2022.

204 R. A. Shelp, A. Ciro, Y. Pu, R. R. Merchant, J. M. E. Hughes and P. J. Walsh, *Chem. Sci.*, 2021, **12**, 7066–7072.

205 P. Cyr, S. T. Deng, J. M. Hawkins and K. E. Price, *Org. Lett.*, 2013, **15**, 4342–4345.

206 X. Cui, Y. Zhou, N. Wang, L. Liu and Q.-X. Guo, *Tetrahedron Lett.*, 2007, **48**, 163–167.

207 A. Zapf and M. Beller, *Chem. Eur. J.*, 2001, **7**, 2908–2915.

208 A. F. Wilks, *Proc. Natl. Acad. Sci.*, 1989, **86**, 1603–1607.

209 A. Kontzias, A. Kotlyar, A. Laurence, P. Changelian and J. J. O'Shea, *Curr. Opin. Pharmacol.*, 2012, **12**, 464–470.

210 M. Pesu, A. Laurence, N. Kishore, S. H. Zwillich, G. Chan and J. J. O'Shea, *Immunol. Rev.*, 2008, **223**, 132–142.

211 E. Guttman-Yassky, A. B. Pavel, A. Diaz, N. Zhang, E. del Duca, Y. Estrada, B. King, A. Banerjee, C. Banfield, L. A. Cox, M. E. Dowty, K. Page, M. S. Vincent, W. Zhang, L. Zhu and E. Peeva, *J. Allergy Clin. Immunol.*, 2022, **149**, 1318–1328.

212 R. Harrington, S. A. al Nokhatha and R. Conway, *J. Inflamm. Res.*, 2020, **13**, 519–531.

213 M. Forster, M. Gehringer and S. A. Laufer, *Bioorg. Med. Chem. Lett.*, 2017, **27**, 4229–4237.

214 K. Yamaoka, P. Saharinen, M. Pesu, V. E. T. Holt, O. Silvennoinen and J. J. O'Shea, *Genome Biol.*, 2004, **5**, 1–6.

215 M. Forster, A. Chaikuad, S. M. Bauer, J. Holstein, M. B. Robers, C. R. Corona, M. Gehringer, E. Pfaffenrot, K. Ghoreschi, S. Knapp and S. A. Laufer, *Cell Chem. Biol.*, 2016, **23**, 1335–1340.

216 G. R. Brown, A. M. Bamford, J. Bowyer, D. S. James, N. Rankine, E. Tang, V. Torr and E. J. Culbert, *Bioorg. Med. Chem. Lett.*, 2000, **10**, 575–579.

217 S. Dhillon, *Drugs*, 2017, **77**, 1987–2001.

218 M. E. Flanagan, T. A. Blumenkopf, W. H. Brissette, M. F. Brown, J. M. Casavant, C. Shang-Poa, J. L. Doty, E. A. Elliott, M. B. Fisher, M. Hines, C. Kent, E. M. Kudlacz, B. M. Lillie, K. S. Magnuson, S. P. McCurdy, M. J. Munchhof, B. D. Perry, P. S. Sawyer, T. J. Strelevitz, C. Subramanyam, J. Sun, D. A. Whipple and P. S. Changelian, *J. Med. Chem.*, 2010, **53**, 8468–8484.

219 A. Editorial, *Drugs R&D*, 2010, **10**, 271–284.

220 C. Chen, Y. Yin, G. Shi, Y. Zhou, S. Shao, Y. Wei, L. Wu, D. Zhang, L. Sun and T. Zhang, *Sci. Adv.*, , DOI:10.1126/sciadv.abo4363.

221 J. B. Telliez, M. E. Dowty, L. Wang, J. Jussif, T. Lin, L. Li, E. Moy, P. Balbo, W. Li, Y. Zhao, K. Crouse, C. Dickinson, P. Symanowicz, M. Hegen, M. E. Banker, F. Vincent, R. Unwalla, S. Liang, A. M. Gilbert, M. F. Brown, M. Hayward, J. Montgomery, X. Yang, J. Bauman, J. I. Trujillo, A. Casimiro-Garcia, F. F. Vajdos, L. Leung, K. F. Geoghegan, A. Quazi, D. Xuan, L. Jones, E. Hett, K. Wright, J. D. Clark and A. Thorarensen, *ACS Chem. Biol.*, 2016, **11**, 3442–3451.

222 Pfizer, FDA and EMA Accept Regulatory Submission for Pfizer's Ritlecitinib for Individuals 12 Years and Older with Alopecia Areata | Pfizer, https://www.pfizer.com/news/press-release/press-release-detail/fda-and-ema-accept-regulatory-submission-pfizers, (accessed 21 November 2022).

223 Pfizer, *FDA Approves Pfizer's Litfulo™ (Ritlecitinib) for Adults and Adolescents with Severe Alopecia Areata*, 2023.

224 European Medicines Agency, *Summary of opinion: Litfulo™ (Ritlecitinib)*, 2023.

225 S. Mahajan, J. K. Hogan, D. Shlyakhter, L. Oh, F. G. Salituro, L. Farmer and T. C. Hoock, *J. Pharmacol. Exp. Ther.*, 2015, **353**, 405–414.

226 A. v Mezentsev, S. A. Bruskin, A. G. Soboleva, V. v Sobolev and E. S. Piruzian, *Int. J. Biomed. Sci.*, 2013, **9**, 112–22.

227 K. Meier, J. Arús-Pous and J. Reymond, *Angew. Chem. Int. Ed.*, 2021, **60**, 2074–2077.

228 United States Patent Application Publication, US 20180215758 A1, 2018.

229 M. Prashad, D. Har, B. Hu, H. Y. Kim, O. Repic and T. J. Blacklock, *Org. Lett.*, 2003, **5**, 125–128.

230 I. B. McInnes, N. L. Byers, R. E. Higgs, J. Lee, W. L. Macias, S. Na, R. A. Ortmann, G. Rocha, T. P. Rooney, T. Wehrman, X. Zhang, S. H. Zuckerman and P. C. Taylor, *Arthritis Res. Ther.*, 2019, **21**, 183.

231 Preparation method of 3-azabicyclo[3.1.0]hexane hydrochloride, CN108341766, 2018, 1–12.

Appendix

I. Crystallographic Data and Refinement Statistics

exo-**36**

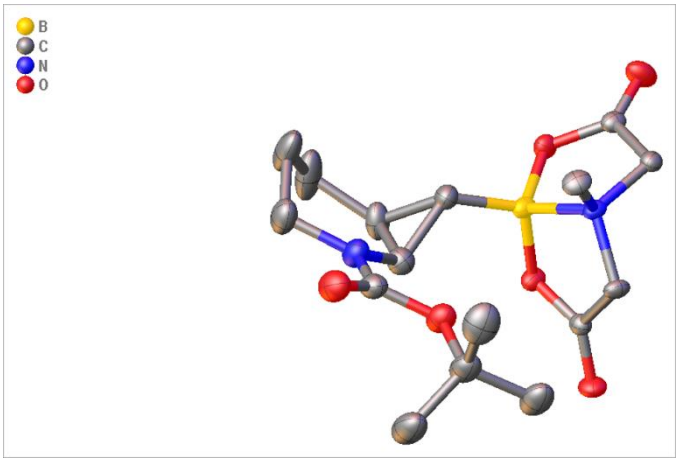

Table 1: Crystal data and structure refinement for *exo*-36.

Identification code	*exo*-**36**
Empirical formula	$C_{16}H_{25}BN_2O_6$
Formula weight	352.19
Temperature/K	110.05(10)
Crystal system	monoclinic
Space group	$P2_1/c$
a/Å	16.1631(10)
b/Å	10.1392(5)
c/Å	10.9560(5)
α/°	90
β/°	97.875(5)
γ/°	90
Volume/Å^3	1778.55(17)
Z	4
ρ_{calc}g/cm^3	1.315
μ/mm^{-1}	0.825
F(000)	752.0
Crystal size/mm^3	0.163 × 0.147 × 0.025

Radiation	Cu Kα (λ = 1.54184)
2Θ range for data collection/°	10.326 to 134.09
Index ranges	$-13 \leq h \leq 19$, $-8 \leq k \leq 12$, $-13 \leq l \leq 12$
Reflections collected	6185
Independent reflections	3160 [R_{int} = 0.0225, R_{sigma} = 0.0322]
Data/restraints/parameters	3160/0/230
Goodness-of-fit on F^2	1.088
Final R indexes [I>=2σ (I)]	R_1 = 0.0515, wR_2 = 0.1433
Final R indexes [all data]	R_1 = 0.0640, wR_2 = 0.1535
Largest diff. peak/hole / e $Å^{-3}$	0.37/-0.28

Data collected, solved, and refined by Adrian C Whitwood

Table 2: Fractional Atomic Coordinates (×10^4) and Equivalent Isotropic Displacement Parameters (Å^2×10^3) for *exo*-36. U_{eq} is defined as 1/3 of the trace of the orthogonalised U_{IJ} tensor.

Atom	*x*	*y*	*z*	U(eq)
O1	1659.5(10)	3730.6(18)	6270.8(16)	31.9(4)
B1	4005.2(16)	5539(2)	7447(2)	18.5(5)
N1	1571.4(13)	5547(2)	7396.5(19)	30.9(5)
C1	1129.0(17)	6422(3)	8156(3)	40.7(7)
O2	494.8(11)	4091(2)	7184.1(17)	37.6(5)
C2	1737.0(19)	7133(4)	9106(3)	53.7(9)
N3	4220.4(11)	3945.4(17)	7380.7(15)	16.3(4)
C3	2324(2)	7978(3)	8478(4)	59.2(10)
O3	4065.4(10)	5950.6(14)	6158.6(13)	20.3(4)
C4	2744.2(15)	7217(3)	7560(3)	34.9(6)
O4	4087.2(10)	5079.1(16)	4287.8(13)	24.7(4)
C5	3153.2(14)	5894(2)	7884(2)	24.4(5)

Table 2: Fractional Atomic Coordinates ($\times 10^4$) and Equivalent Isotropic Displacement Parameters ($Å^2 \times 10^3$) for *exo*-36. U_{eq} is defined as 1/3 of the trace of the orthogonalised U_{IJ} tensor.

Atom	*x*	*y*	*z*	U(eq)
O5	4737.5(10)	6036.4(14)	8281.2(14)	21.3(4)
O6	5999.5(10)	5402.4(16)	9178.1(15)	29.7(4)
C6	2347.8(15)	5974(2)	7008(2)	28.8(5)
C7	1181.1(15)	4433(3)	6963(2)	29.1(6)
C8	1288.6(16)	2592(3)	5535(2)	37.3(6)
C9	1146(2)	1473(3)	6386(3)	50.9(8)
C10	509.0(18)	3009(4)	4712(3)	50.8(8)
C11	1977.2(18)	2227(3)	4787(3)	44.6(7)
C12	4091.3(13)	4962(2)	5385.0(19)	18.3(5)
C13	4102.3(14)	3651(2)	6032.2(18)	19.9(5)
C14	5345.9(14)	5164(2)	8547.3(19)	19.3(5)
C15	5113.7(13)	3850(2)	7956.4(19)	18.1(5)
C16	3678.2(15)	3088(2)	8043(2)	24.0(5)

Table 3: Anisotropic Displacement Parameters ($Å^2 \times 10^3$) for *exo*-36. The Anisotropic displacement factor exponent takes the form: $-2\pi^2[h^2a^{*2}U_{11}+2hka^*b^*U_{12}+\ldots]$.

Atom	U_{11}	U_{22}	U_{33}	U_{23}	U_{13}	U_{12}
O1	26.6(9)	38.1(10)	31.1(9)	-7.6(8)	3.7(7)	-3.6(8)
B1	26.2(13)	13.5(11)	16.1(11)	0.0(9)	4.0(9)	0.8(10)
N1	26.0(11)	37.9(12)	29.2(11)	-5.9(9)	5.1(8)	1.7(9)
C1	28.2(14)	47.7(16)	46.8(16)	-13.1(14)	7.7(12)	5.2(12)
O2	27.9(10)	49.8(11)	35.8(10)	-2.4(9)	6.8(8)	-3.6(8)
C2	31.9(15)	69(2)	62(2)	-36.0(18)	11.9(14)	3.2(15)
N3	22.0(9)	15.1(8)	12.4(8)	0.9(7)	4.5(7)	-2.0(7)
C3	37.6(17)	46.0(18)	95(3)	-33.7(19)	14.0(17)	4.2(14)

Table 3: Anisotropic Displacement Parameters ($Å^2×10^3$) for *exo*-36. The Anisotropic displacement factor exponent takes the form: $-2\pi^2[h^2a^{*2}U_{11}+2hka^*b^*U_{12}+\ldots]$.

Atom	U_{11}	U_{22}	U_{33}	U_{23}	U_{13}	U_{12}
O3	28.1(8)	15.8(7)	17.8(7)	2.1(6)	5.6(6)	1.3(6)
C4	25.9(13)	25.0(13)	53.8(16)	-6.4(12)	6.2(12)	3.2(10)
O4	30.1(9)	29.3(9)	15.1(8)	4.6(6)	4.1(6)	1.0(7)
C5	24.8(12)	26.7(12)	22.2(11)	-1.3(10)	4.6(9)	4.0(10)
O5	24.6(8)	17.0(7)	22.0(8)	-3.0(6)	1.9(6)	1.6(6)
O6	31.0(9)	25.0(8)	29.6(9)	-2.3(7)	-8.5(7)	-2.0(7)
C6	27.4(13)	30.5(13)	28.4(12)	-0.2(10)	3.1(10)	0.9(10)
C7	25.9(13)	38.6(14)	22.8(11)	-1.1(10)	2.8(9)	1.3(11)
C8	28.8(13)	49.3(16)	32.6(13)	-14.4(13)	-0.2(11)	-3.4(12)
C9	46.4(18)	43.9(17)	64(2)	-13.3(16)	11.9(15)	-11.7(14)
C10	34.3(15)	77(2)	39.9(16)	-20.3(16)	1.3(12)	-0.4(15)
C11	33.5(14)	59.0(19)	40.5(15)	-21.4(14)	2.1(12)	-4.7(14)
C12	15.8(10)	21.5(11)	17.7(11)	1.7(9)	2.5(8)	0.2(8)
C13	28.3(12)	17.7(10)	13.2(10)	-2.0(8)	1.3(8)	-1.7(9)
C14	26.1(12)	16.6(10)	15.6(10)	2.3(8)	3.9(9)	-0.6(9)
C15	20.7(11)	17.9(10)	15.7(10)	1.8(8)	2.0(8)	2.1(9)
C16	29.8(12)	22.5(11)	21.0(11)	3.8(9)	8.5(9)	-6.0(10)

Table 4: Bond Lengths for *exo*-36.

Atom	Atom	Length/Å	Atom	Atom	Length/Å
O1	C7	1.357(3)	N3	C16	1.492(3)
O1	C8	1.487(3)	C3	C4	1.501(4)
B1	N3	1.657(3)	O3	C12	1.317(3)
B1	O3	1.488(3)	C4	C5	1.516(3)
B1	C5	1.560(3)	C4	C6	1.502(4)

Table 4: Bond Lengths for *exo*-36.

Atom	Atom	Length/Å	Atom	Atom	Length/Å
B1	O5	1.481(3)	O4	C12	1.207(3)
N1	C1	1.468(3)	C5	C6	1.510(3)
N1	C6	1.446(3)	O5	C14	1.325(3)
N1	C7	1.348(3)	O6	C14	1.205(3)
C1	C2	1.512(4)	C8	C9	1.507(4)
O2	C7	1.218(3)	C8	C10	1.506(4)
C2	C3	1.512(5)	C8	C11	1.516(4)
N3	C13	1.494(3)	C12	C13	1.506(3)
N3	C15	1.497(3)	C14	C15	1.505(3)

Table 5: Bond Angles for *exo*-36.

Atom	Atom	Atom	Angle/°	Atom	Atom	Atom	Angle/°
C7	O1	C8	119.49(19)	C6	C5	B1	122.51(19)
O3	B1	N3	100.95(15)	C6	C5	C4	59.54(16)
O3	B1	C5	113.68(19)	C14	O5	B1	114.50(17)
C5	B1	N3	115.97(18)	N1	C6	C4	118.2(2)
O5	B1	N3	101.78(16)	N1	C6	C5	120.3(2)
O5	B1	O3	109.84(18)	C4	C6	C5	60.40(16)
O5	B1	C5	113.37(18)	N1	C7	O1	111.2(2)
C6	N1	C1	119.7(2)	O2	C7	O1	124.5(2)
C7	N1	C1	117.7(2)	O2	C7	N1	124.3(2)
C7	N1	C6	122.1(2)	O1	C8	C9	109.5(2)
N1	C1	C2	110.9(2)	O1	C8	C10	110.4(2)
C1	C2	C3	110.3(3)	O1	C8	C11	102.2(2)
C13	N3	B1	103.86(15)	C9	C8	C11	109.7(3)

Table 5: Bond Angles for *exo*-36.

Atom	Atom	Atom	Angle/°	Atom	Atom	Atom	Angle/°
C13	N3	C15	112.89(16)	C10	C8	C9	113.3(3)
C15	N3	B1	103.91(15)	C10	C8	C11	111.2(2)
C16	N3	B1	113.98(16)	O3	C12	C13	111.61(17)
C16	N3	C13	111.13(16)	O4	C12	O3	124.7(2)
C16	N3	C15	110.76(16)	O4	C12	C13	123.7(2)
C4	C3	C2	112.5(3)	N3	C13	C12	106.31(17)
C12	O3	B1	114.16(16)	O5	C14	C15	111.23(18)
C3	C4	C5	121.4(3)	O6	C14	O5	123.9(2)
C3	C4	C6	119.6(2)	O6	C14	C15	124.9(2)
C6	C4	C5	60.05(16)	N3	C15	C14	107.07(17)
C4	C5	B1	120.5(2)				

Table 6: Torsion Angles for *exo*-36.

A	B	C	D	Angle/°	A	B	C	D	Angle/°
B1	N3	C13	C12	15.8(2)	O4	C12	C13	N3	172.5(2)
B1	N3	C15	C14	11.1(2)	C5	B1	N3	C13	106.4(2)
B1	O3	C12	O4	175.1(2)	C5	B1	N3	C15	−135.35(19)
B1	O3	C12	C13	−3.3(2)	C5	B1	N3	C16	−14.7(3)
B1	C5	C6	N1	143.9(2)	C5	B1	O3	C12	−112.2(2)
B1	C5	C6	C4	−108.8(3)	C5	B1	O5	C14	134.1(2)
B1	O5	C14	O6	177.6(2)	C5	C4	C6	N1	110.7(2)
B1	O5	C14	C15	−2.2(2)	O5	B1	N3	C13	−130.11(17)
N1	C1	C2	C3	61.0(4)	O5	B1	N3	C15	−11.83(19)
C1	N1	C6	C4	9.4(3)	O5	B1	N3	C16	108.82(18)

Table 6: Torsion Angles for *exo*-36.

A	B	C	D	Angle/°	A	B	C	D	Angle/°
C1	N1	C6	C5	79.8(3)	O5	B1	O3	C12	119.60(19)
C1	N1	C7	O1	179.5(2)	O5	B1	C5	C4	84.8(3)
C1	N1	C7	O2	-1.8(4)	O5	B1	C5	C6	156.0(2)
C1	C2	C3	C4	-52.5(4)	O5	C14	C15	N3	-6.4(2)
C2	C3	C4	C5	-48.2(4)	O6	C14	C15	N3	173.8(2)
C2	C3	C4	C6	22.8(4)	C6	N1	C1	C2	-39.5(4)
N3	B1	O3	C12	12.7(2)	C6	N1	C7	O1	7.6(3)
N3	B1	C5	C4	-157.9(2)	C6	N1	C7	O2	-173.6(2)
N3	B1	C5	C6	-86.7(3)	C6	C4	C5	B1	112.2(2)
N3	B1	O5	C14	8.8(2)	C7	O1	C8	C9	-71.3(3)
C3	C4	C5	B1	-139.4(3)	C7	O1	C8	C10	54.1(3)
C3	C4	C5	C6	108.4(3)	C7	O1	C8	C11	172.4(2)
C3	C4	C6	N1	-0.6(4)	C7	N1	C1	C2	148.4(3)
C3	C4	C6	C5	-111.3(3)	C7	N1	C6	C4	-178.9(2)
O3	B1	N3	C13	-16.9(2)	C7	N1	C6	C5	-108.5(3)
O3	B1	N3	C15	101.34(17)	C8	O1	C7	N1	-169.6(2)
O3	B1	N3	C16	−138.02(17)	C8	O1	C7	O2	11.6(4)
O3	B1	C5	C4	-41.6(3)	C13	N3	C15	C14	122.93(18)
O3	B1	C5	C6	29.6(3)	C15	N3	C13	C12	-96.13(19)
O3	B1	O5	C14	-97.5(2)	C16	N3	C13	C12	138.73(18)
O3	C12	C13	N3	-9.1(2)	C16	N3	C15	C14	−111.73(18)
C4	C5	C6	N1	-107.3(3)					

Table 7: Hydrogen Atom Coordinates (Å×10^4) and Isotropic Displacement Parameters (Å^2×10^3) for *exo*-36.

Atom	*x*	*y*	*z*	U(eq)
H1A	744.11	5908.03	8569.72	49
H1B	806.91	7063.16	7632.61	49
H2A	2055.84	6494.06	9635.96	64
H2B	1431.67	7684.05	9613.82	64
H3A	2013.38	8703.73	8060.24	71
H3B	2747.41	8347.41	9096.6	71
H4	3020.7	7758.66	6994.99	42
H5	3089.7	5571.47	8709.18	29
H6	2397.78	5827.59	6136.76	35
H9A	1660.34	1261.6	6895.13	76
H9B	949.15	713.78	5908.61	76
H9C	736.32	1730.2	6898	76
H10A	76.23	3196.86	5205.77	76
H10B	330.38	2311.13	4144.69	76
H10C	623.52	3785.02	4262.13	76
H11A	2141.06	2994.75	4365.87	67
H11B	1777.82	1562.87	4194.18	67
H11C	2448.93	1893.31	5325.85	67
H13A	3580.43	3185.82	5796.08	24
H13B	4556.54	3108.03	5822.33	24
H15A	5469.14	3653.91	7334.69	22
H15B	5179.83	3155.46	8570.44	22
H16A	3833.89	2181.49	7960.87	36
H16B	3104.92	3205.72	7694.83	36

endo-**110**

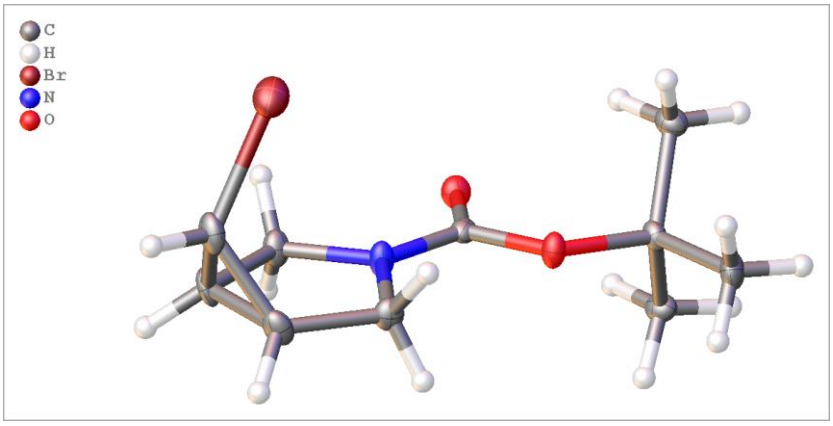

Table 1: Crystal data and structure refinement for *endo*-110.

Identification code	***endo*-110**
Empirical formula	$C_{10}H_{16}BrNO_2$
Formula weight	262.15
Temperature/K	110.00(10)
Crystal system	monoclinic
Space group	Pc
a/Å	8.14698(16)
b/Å	5.94248(17)
c/Å	11.1997(3)
α/°	90
β/°	90.5736(19)
γ/°	90
Volume/Å^3	542.19(2)
Z	2
c_{alcd}/cm^3	1.606
μ/mm^{-1}	4.976
F(000)	268.0
Crystal size/mm^3	0.168 × 0.145 × 0.123
Radiation	CuKα (λ = 1.54184)

2Θ range for data collection/°	10.86 to 141.894
Index ranges	$-9 \leq h \leq 9$, $-6 \leq k \leq 7$, $-13 \leq l \leq 13$
Reflections collected	4956
Independent reflections	1982 [R_{int} = 0.0221, R_{sigma} = 0.0218]
Data/restraints/parameters	1982/2/130
Goodness-of-fit on F^2	1.075
Final R indexes [I>=2σ (I)]	R_1 = 0.0210, wR_2 = 0.0571
Final R indexes [all data]	R_1 = 0.0212, wR_2 = 0.0574
Largest diff. peak/hole / e $Å^{-3}$	0.47/-0.32
Flack parameter	-0.015(12)

Data collected by Adrian C Whitwood, solved, and refined by Theo Tanner.

Table 2: Fractional Atomic Coordinates (×10^4) and Equivalent Isotropic Displacement Parameters ($Å^2$×10^3) for *endo*-110. U_{eq} is defined as 1/3 of the trace of the orthogonalised U_{IJ} tensor.

Atom	*x*	*y*	*z*	U(eq)
Br1	2421.0(3)	6978.7(6)	7275.4(3)	26.26(13)
C1	2337(4)	11142(6)	5786(3)	17.7(7)
C2	1609(4)	9334(7)	4988(3)	18.9(8)
C3	2986(5)	8044(6)	4437(3)	16.5(8)
C4	4180(4)	10957(6)	5727(3)	17.3(7)
C5	1383(4)	9239(7)	6307(3)	20.4(8)
C6	6014(4)	8318(6)	4750(3)	12.5(7)
C7	7525(4)	5590(6)	3534(3)	13.3(7)
C8	6920(5)	3665(7)	2746(3)	19.8(8)
C9	8350(5)	7382(7)	2772(3)	16.6(7)
C10	8625(4)	4704(7)	4534(3)	18.1(7)
N1	4470(3)	8984(6)	4988(3)	15.2(6)

O1	7240(3)	9236(5)	5149(2)	15.8(5)
O2	5979(3)	6492(5)	4024(2)	15.4(5)

Table 3: Anisotropic Displacement Parameters ($Å^2×10^3$) for *endo*-110. The Anisotropic displacement factor exponent takes the form: $-2π^2[h^2a^{*2}U_{11}+2hka^*b^*U_{12}+…]$.

Atom	U_{11}	U_{22}	U_{33}	U_{23}	U_{13}	U_{12}
Br1	30.7(2)	21.4(2)	26.80(19)	0.2(2)	6.55(13)	-2.7(2)
C1	16.6(17)	8.2(18)	28.3(19)	-4.6(15)	1.9(14)	2.6(14)
C2	12.0(16)	18(2)	26.7(18)	-3.5(15)	-5.0(13)	1.3(14)
C3	13.6(17)	17(2)	18.6(18)	-3.5(14)	-1.3(14)	-2.2(14)
C4	14.4(16)	14.4(18)	23.3(16)	-5.8(15)	1.9(12)	-1.6(14)
C5	11.2(16)	18(2)	32(2)	-6.0(15)	4.2(14)	1.0(14)
C6	15.5(17)	9.9(18)	12.0(15)	1.2(12)	1.0(12)	-0.2(13)
C7	9.3(15)	12.8(18)	17.9(15)	-0.3(13)	2.3(12)	1.0(14)
C8	20.2(18)	15.5(19)	23.9(17)	-5.4(15)	4.1(14)	3.0(16)
C9	14.4(16)	19.9(18)	15.6(16)	3.4(15)	2.0(12)	0.3(15)
C10	16.3(16)	18(2)	20.0(16)	4.1(14)	1.3(13)	0.7(14)
N1	10.6(14)	14.7(16)	20.2(15)	-6.1(12)	1.3(11)	-1.8(12)
O1	14.0(12)	14.5(14)	18.8(12)	-2.3(9)	0.1(9)	-2.6(10)
O2	10.9(11)	15.9(13)	19.4(12)	-6.0(10)	2.9(9)	-1.4(10)

Table 4: Bond Lengths for *endo*-110.

Atom	Atom	Length/Å	Atom	Atom	Length/Å
Br1	C5	1.918(4)	C6	N1	1.348(5)
C1	C2	1.515(5)	C6	O1	1.219(4)
C1	C4	1.507(5)	C6	O2	1.356(4)

C1	C5	1.494(6)	C7	C8	1.523(5)
C2	C3	1.497(5)	C7	C9	1.525(5)
C2	C5	1.491(5)	C7	C10	1.522(5)
C3	N1	1.463(4)	C7	O2	1.480(4)
C4	N1	1.455(4)			

Table 5: Bond Angles for *endo*-110.

Atom	Atom	Atom	Angle/°	Atom	Atom	Atom	Angle/°
C4	C1	C2	107.8(3)	O1	C6	N1	123.9(3)
C5	C1	C2	59.4(2)	O1	C6	O2	126.2(3)
C5	C1	C4	119.0(3)	C8	C7	C9	110.0(3)
C3	C2	C1	108.4(3)	C10	C7	C8	110.6(3)
C5	C2	C1	59.6(3)	C10	C7	C9	113.2(3)
C5	C2	C3	119.3(3)	O2	C7	C8	102.4(3)
N1	C3	C2	104.5(3)	O2	C7	C9	109.7(3)
N1	C4	C1	104.6(3)	O2	C7	C10	110.4(3)
C1	C5	Br1	121.5(3)	C4	N1	C3	114.1(3)
C2	C5	Br1	121.9(3)	C6	N1	C3	125.0(3)
C2	C5	C1	61.0(3)	C6	N1	C4	120.4(3)
N1	C6	O2	109.9(3)	C6	O2	C7	120.0(3)

Table 6: Torsion Angles for *endo*-110.

A	B	C	D	Angle/°	A	B	C	D	Angle/°
C1	C2	C3	N1	4.4(4)	C4	C1	C5	C2	-94.5(4)
C1	C2	C5	Br1	-111.0(3)	C5	C1	C2	C3	-113.8(4)
C1	C4	N1	C3	7.5(4)	C5	C1	C4	N1	60.1(4)
C1	C4	N1	C6	-179.8(3)	C5	C2	C3	N1	-60.5(4)

C2	C1	C4	N1	-4.2(4)	
C2	C1	C5	Br1	111.7(3)	
C2	C3	N1	C4	-7.6(4)	
C2	C3	N1	C6	-179.9(3)	
C3	C2	C5	Br1	-15.8(5)	
C3	C2	C5	C1	95.2(4)	
C4	C1	C2	C3	-0.1(4)	
C4	C1	C2	C5	113.6(4)	
C4	C1	C5	Br1	17.1(5)	
C8	C7	O2	C6	-177.5(3)	
C9	C7	O2	C6	-60.7(4)	
C10	C7	O2	C6	64.7(4)	
N1	C6	O2	C7	173.6(3)	
O1	C6	N1	C3	174.2(3)	
O1	C6	N1	C4	2.3(5)	
O1	C6	O2	C7	-7.1(5)	
O2	C6	N1	C3	-6.6(5)	
O2	C6	N1	C4	-178.4(3)	

Table 7: Hydrogen Atom Coordinates (Å×10^4) and Isotropic Displacement Parameters (Å^2×10^3) for *endo*-110.

Atom	*x*	*y*	*z*	U(eq)
H1	1839.67	12643.01	5774.08	21
H2	660.01	9723.27	4484.81	23
H3A	2890.83	6450.28	4609.15	20
H3B	2993.55	8253.21	3577.66	20
H4A	4649.34	12291.96	5367.07	21
H4B	4653.89	10758.13	6517.59	21
H5	278.9	9653.61	6567.29	24
H8A	6366.52	2572	3228.44	30
H8B	7838.12	2969.84	2362.28	30
H8C	6173.77	4240.15	2151.76	30
H9A	7571.82	7971.58	2204.4	25
H9B	9257.05	6725.48	2356.28	25
H9C	8742.13	8576.97	3276.61	25
H10A	8935.1	5923.04	5052.15	27
H10B	9591.74	4042.13	4199.52	27

H10C 8042.46 3588.95 4982.89 27

Experimental

Single crystals of $C_{10}H_{16}BrNO_2$ **[*endo*-110]** were **[Et_2O/Hexane]**. A suitable crystal was selected and **[Oil on 0.2mm mount]** on a **SuperNova, Dual, Cu at home/near, Eos** diffractometer. The crystal was kept at 110.00(10) K during data collection. Using Olex2 [1], the structure was solved with the ShelXT [2] structure solution program using Intrinsic Phasing and refined with the ShelXL [3] refinement package using Least Squares minimisation.

1. Dolomanov, O.V., Bourhis, L.J., Gildea, R.J, Howard, J.A.K. & Puschmann, H. (2009), J. Appl. Cryst. 42, 339-341.
2. Sheldrick, G.M. (2015). Acta Cryst. A71, 3-8.
3. Sheldrick, G.M. (2015). Acta Cryst. C71, 3-8.

Crystal structure determination of [*endo*-**110**]

Crystal Data for $C_{10}H_{16}BrNO_2$ (M =262.15 g/mol): monoclinic, space group Pc (no. 7), a = 8.14698(16) Å, b = 5.94248(17) Å, c = 11.1997(3) Å, β = 90.5736(19)°, V = 542.19(2) Å^3, Z = 2, T = 110.00(10) K, μ(CuKα) = 4.976 mm^{-1}, *Dcalc* = 1.606 g/cm^3, 4956 reflections measured (10.86° ≤ 2Θ ≤ 141.894°), 1982 unique (R_{int} = 0.0221, R_{sigma} = 0.0218) which were used in all calculations. The final R_1 was 0.0210 (I > 2σ(I)) and wR_2 was 0.0574 (all data).

Refinement model description

Number of restraints - 2, number of constraints - unknown.
Details:

```
1. Fixed Uiso
 At 1.2 times of:
  All C(H) groups, All C(H,H) groups
 At 1.5 times of:
  All C(H,H,H) groups
2.a Ternary CH refined with riding coordinates:
 C1(H1), C2(H2), C5(H5)
2.b Secondary CH2 refined with riding coordinates:
 C3(H3A,H3B), C4(H4A,H4B)
2.c Idealised Me refined as rotating group:
 C8(H8A,H8B,H8C), C9(H9A,H9B,H9C), C10(H10A,H10B,H10C)
```

exo-**39**

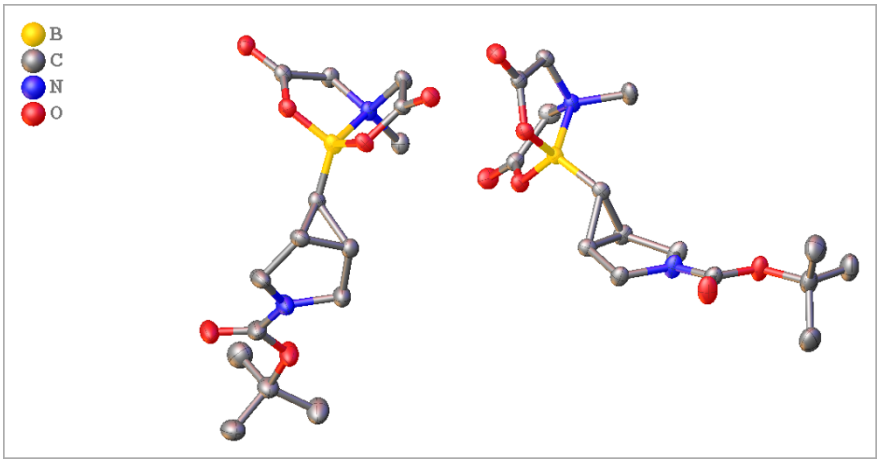

Table 1: Crystal data and structure refinement for *exo*-39.

Identification code	*exo*-**39**
Empirical formula	$C_{15}H_{23}BN_2O_6$
Formula weight	338.16
Temperature/K	109.95(10)
Crystal system	monoclinic
Space group	Cc
a/Å	6.42393(14)
b/Å	32.9595(8)
c/Å	16.3523(4)
α/°	90
β/°	92.289(2)
γ/°	90
Volume/Å^3	3459.50(14)
Z	8
ρ_{calc}g/cm^3	1.299
μ/mm^{-1}	0.827
F(000)	1440.0
Crystal size/mm^3	0.256 × 0.129 × 0.014
Radiation	Cu Kα (λ = 1.54184)

2Θ range for data collection/°	7.62 to 134.158
Index ranges	$-7 \leq h \leq 7, -39 \leq k \leq 38, -19 \leq l \leq 14$
Reflections collected	10941
Independent reflections	4061 [R_{int} = 0.0259, R_{sigma} = 0.0258]
Data/restraints/parameters	4061/2/442
Goodness-of-fit on F^2	1.034
Final R indexes [I>=2σ (I)]	R_1 = 0.0281, wR_2 = 0.0712
Final R indexes [all data]	R_1 = 0.0297, wR_2 = 0.0729
Largest diff. peak/hole / e $Å^{-3}$	0.15/-0.14
Flack parameter	0.14(14)

Data collected, solved, and refined by Adrian C Whitwood.

Table 2: Fractional Atomic Coordinates (×10^4) and Equivalent Isotropic Displacement Parameters (Å^2×10^3) for *exo*-39. U_{eq} is defined as 1/3 of the trace of the orthogonalised U_{IJ} tensor.

Atom	*x*	*y*	*z*	U(eq)
B1	8289(4)	4809.9(8)	4263.0(17)	21.5(5)
C1	7977(5)	3805.3(8)	2880.0(17)	33.3(6)
C2	7253(4)	4108.3(7)	3501.1(15)	26.1(5)
C3	6226(4)	4453.3(7)	3035.7(16)	26.2(5)
C4	6377(5)	4374.0(8)	2133.7(16)	36.2(6)
C5	8285(4)	4521.4(7)	3501.9(15)	23.1(5)
C6	8920(5)	3949.4(8)	1438.6(17)	37.2(7)
C7	11224(5)	3429.5(8)	883.9(17)	36.1(6)
C8	11841(6)	3019.0(9)	1237(2)	48.5(8)
C9	13114(5)	3688.5(10)	752(2)	49.7(8)
C10	9881(5)	3382.1(9)	98.9(19)	43.3(7)
C11	9241(4)	4845.6(7)	5725.8(14)	22.6(5)

Table 2: Fractional Atomic Coordinates ($\times 10^4$) and Equivalent Isotropic Displacement Parameters ($Å^2 \times 10^3$) for *exo*-39. U_{eq} is defined as 1/3 of the trace of the orthogonalised U_{IJ} tensor.

Atom	*x*	*y*	*z*	U(eq)
C12	6928(4)	4781.3(6)	5568.4(14)	20.2(5)
C13	11686(3)	5100.8(7)	4707.5(15)	23.9(5)
C14	10340(4)	5405.4(7)	4230.1(14)	21.7(5)
C15	11324(4)	4362.6(7)	4942.4(16)	25.5(5)
N1	7804(4)	4028.0(6)	2102.4(13)	34.5(5)
N2	10255(3)	4766.7(6)	4930.3(12)	20.8(4)
O1	9984(4)	3600.6(6)	1542.7(12)	42.7(5)
O2	8905(4)	4163.9(6)	832.5(12)	42.9(5)
O3	6465(2)	4750.5(5)	4770.3(10)	23.1(4)
O4	5656(2)	4765.3(5)	6088.1(10)	24.8(4)
O5	8484(2)	5247.2(5)	4045.8(10)	22.4(3)
O6	10897(3)	5735.6(5)	4023.4(10)	26.1(4)
B2	3414(4)	3900.1(8)	7180.4(16)	19.3(5)
C16	2381(3)	2740.9(8)	7778.1(18)	29.1(6)
C17	3076(4)	3088.4(7)	7249.2(16)	24.1(5)
C18	1199(3)	3254.1(7)	6787.1(14)	22.0(5)
C19	-657(4)	2999.5(7)	7003.1(16)	24.5(5)
C20	2258(3)	3505.8(7)	7462.3(14)	20.4(5)
C21	-1251(4)	2581.3(7)	8197.5(16)	25.4(5)
C22	-1391(4)	2102.1(8)	9341.6(17)	32.5(6)
C23	336(5)	1926.8(10)	9889(2)	43.5(7)
C24	-2913(5)	2348.4(10)	9833(2)	45.2(7)
C25	-2483(5)	1773.9(9)	8843(2)	44.1(7)
C26	7252(4)	4025.9(8)	7314.9(15)	25.5(5)
C27	6518(3)	3914.7(7)	6454.3(15)	21.8(5)

Table 2: Fractional Atomic Coordinates ($\times 10^4$) and Equivalent Isotropic Displacement Parameters ($Å^2 \times 10^3$) for *exo*-39. U_{eq} is defined as 1/3 of the trace of the orthogonalised U_{IJ} tensor.

Atom	*x*	*y*	*z*	U(eq)
C28	4811(3)	4506.7(7)	7941.4(14)	21.7(5)
C29	2706(3)	4582.7(7)	7518.5(14)	21.1(5)
C30	5572(4)	3848.8(8)	8597.1(16)	29.2(5)
N3	99(3)	2775.5(6)	7724.6(13)	26.9(5)
N4	5342(3)	4070.4(6)	7801.7(12)	20.5(4)
O7	-225(3)	2369.0(5)	8794.8(11)	30.9(4)
O8	-3131(3)	2602.4(6)	8093.2(12)	35.8(4)
O9	4490(2)	3843.4(5)	6408.4(10)	21.7(3)
O10	7649(3)	3884.4(5)	5886.2(11)	28.6(4)
O11	2024(2)	4258.0(5)	7117.6(10)	21.3(3)
O12	1787(3)	4898.8(5)	7546.0(11)	26.8(4)

Table 3: Anisotropic Displacement Parameters ($Å^2 \times 10^3$) for *exo*-39. The Anisotropic displacement factor exponent takes the form: $-2\pi^2[h^2a^{*2}U_{11}+2hka^*b^*U_{12}+\ldots]$.

Atom	U_{11}	U_{22}	U_{33}	U_{23}	U_{13}	U_{12}
B1	11.7(11)	31.4(14)	21.2(13)	1.9(11)	-0.6(9)	0.4(9)
C1	45.9(16)	28.0(13)	26.1(13)	2.9(11)	2.0(12)	2.6(11)
C2	27.7(12)	26.7(12)	24.1(12)	2.3(10)	3.3(10)	-1.6(10)
C3	26.4(12)	28.2(12)	23.8(12)	-2.6(10)	-2.4(10)	0.1(10)
C4	51.9(18)	30.9(14)	25.1(14)	-3.4(11)	-6.8(12)	8.6(12)
C5	20.6(11)	26.8(12)	22.1(12)	1.9(9)	2.8(9)	-0.7(9)
C6	58.8(19)	24.6(13)	28.3(14)	-1.3(11)	1.7(13)	3.9(12)
C7	47.0(17)	32.1(14)	29.6(14)	-3.1(11)	6.2(12)	6.2(12)
C8	70(2)	37.1(16)	39.0(17)	2.1(13)	14.4(15)	16.3(15)
C9	49.4(19)	49.8(19)	49.3(19)	3.0(15)	-4.9(15)	0.2(15)

Table 3: Anisotropic Displacement Parameters ($Å^2 \times 10^3$) for *exo*-39. The Anisotropic displacement factor exponent takes the form: $-2\pi^2[h^2a^{*2}U_{11}+2hka^*b^*U_{12}+\ldots]$.

Atom	U_{11}	U_{22}	U_{33}	U_{23}	U_{13}	U_{12}
C10	54.3(18)	37.5(15)	38.0(16)	-7.4(13)	-0.3(14)	0.9(14)
C11	17.6(10)	31.0(12)	19.1(11)	1.5(10)	0.3(9)	-1.4(9)
C12	18.4(11)	21.8(11)	20.4(12)	-0.7(9)	-0.3(9)	0.3(9)
C13	15.4(11)	28.9(12)	27.4(12)	3.8(10)	1.6(9)	-2.4(9)
C14	17.2(11)	28.3(12)	19.9(11)	-0.1(9)	2.7(9)	0.8(9)
C15	18.6(11)	30.5(12)	27.6(13)	4.9(10)	1.5(9)	3.2(9)
N1	51.5(15)	27.9(11)	23.8(11)	0.1(9)	-0.6(10)	8.2(10)
N2	14.3(9)	26.8(10)	21.4(10)	3.7(8)	2.3(7)	-0.7(7)
O1	68.5(15)	32.4(10)	27.9(10)	2.8(8)	12.0(9)	14.4(9)
O2	70.2(15)	33.6(10)	25.0(10)	1.7(8)	6.1(9)	8.9(10)
O3	14.2(8)	34.7(9)	20.4(8)	-1.1(7)	1.3(6)	-0.8(6)
O4	20.0(8)	30.8(9)	24.3(9)	0.3(7)	6.7(7)	-0.6(6)
O5	17.4(8)	27.1(8)	22.6(8)	1.2(7)	-2.3(6)	1.2(6)
O6	26.6(9)	27.9(9)	24.3(8)	2.2(7)	5.3(7)	-0.3(7)
B2	14.1(12)	25.2(13)	18.4(12)	0.3(10)	0.1(10)	-0.7(10)
C16	13.5(11)	28.9(13)	44.9(15)	9.5(12)	0.7(10)	1.0(9)
C17	15.2(10)	25.2(11)	32.1(13)	1.7(10)	3.6(9)	-0.5(9)
C18	16.4(10)	25.9(12)	23.9(12)	-1.6(10)	2.5(9)	-0.3(9)
C19	17.7(11)	25.6(11)	29.9(12)	3.8(10)	-1.9(9)	-1.9(9)
C20	12.5(9)	27.4(12)	21.3(11)	0.0(9)	1.6(8)	-0.7(9)
C21	19.1(12)	25.8(12)	31.0(13)	3.6(10)	-1.5(10)	-2.9(9)
C22	32.4(13)	33.1(14)	31.9(14)	9.3(11)	1.9(11)	-5.7(11)
C23	44.5(17)	43.5(16)	41.9(16)	15.8(14)	-5.4(13)	-2.3(13)
C24	50.5(19)	46.9(17)	39.2(17)	7.6(13)	15.1(14)	1.6(14)
C25	47.0(18)	40.2(16)	45.0(18)	8.0(14)	-0.1(14)	-14.0(13)
C26	12.2(10)	32.7(13)	31.8(13)	-3.7(11)	3.7(9)	3.2(9)

Table 3: Anisotropic Displacement Parameters ($Å^2×10^3$) for *exo*-39. The Anisotropic displacement factor exponent takes the form: $-2\pi^2[h^2a^{*2}U_{11}+2hka^*b^*U_{12}+\ldots]$.

Atom	U_{11}	U_{22}	U_{33}	U_{23}	U_{13}	U_{12}
C27	16.6(11)	21.2(11)	27.9(13)	0.7(9)	4.5(9)	-0.4(8)
C28	16.8(11)	28.4(12)	19.9(11)	-2.3(9)	0.9(9)	-0.5(9)
C29	18.5(11)	26.6(12)	18.4(11)	1.0(9)	5.4(9)	-0.7(9)
C30	25.5(12)	35.4(14)	26.2(13)	8.9(11)	-6.5(10)	-3.6(10)
N3	12.9(9)	31.3(11)	36.2(12)	10.3(9)	-1.4(8)	-1.3(8)
N4	14.4(9)	26.9(10)	20.1(10)	1.9(8)	2.1(7)	-0.6(7)
O7	20.9(8)	35.9(10)	35.8(10)	13.6(8)	-1.9(7)	-4.9(7)
O8	16.5(9)	49.2(11)	41.5(11)	15.8(9)	0.3(8)	-3.8(8)
O9	15.7(7)	27.6(8)	22.1(8)	0.7(7)	3.3(6)	-2.6(6)
O10	22.1(8)	33.6(9)	30.8(9)	-1.5(8)	11.1(7)	-1.2(7)
O11	14.7(7)	26.5(8)	22.5(8)	0.6(7)	-1.3(6)	0.1(6)
O12	24.7(9)	28.9(9)	26.8(9)	-0.6(7)	0.2(7)	6.1(7)

Table 4: Bond Lengths for *exo*-39.

Atom	Atom	Length/Å	Atom	Atom	Length/Å
B1	C5	1.566(4)	B2	C20	1.575(3)
B1	N2	1.642(3)	B2	N4	1.668(3)
B1	O3	1.475(3)	B2	O9	1.475(3)
B1	O5	1.491(3)	B2	O11	1.481(3)
C1	C2	1.511(4)	C16	C17	1.513(3)
C1	N1	1.469(3)	C16	N3	1.470(3)
C2	C3	1.506(3)	C17	C18	1.500(3)
C2	C5	1.514(3)	C17	C20	1.518(3)
C3	C4	1.505(4)	C18	C19	1.511(3)
C3	C5	1.516(3)	C18	C20	1.520(3)

Table 4: Bond Lengths for *exo*-39.

Atom	Atom	Length/Å	Atom	Atom	Length/Å
C4	N1	1.466(3)	C19	N3	1.458(3)
C6	N1	1.350(4)	C21	N3	1.347(3)
C6	O1	1.345(3)	C21	O7	1.352(3)
C6	O2	1.217(3)	C21	O8	1.215(3)
C7	C8	1.518(4)	C22	C23	1.512(4)
C7	C9	1.507(5)	C22	C24	1.524(4)
C7	C10	1.526(4)	C22	C25	1.511(4)
C7	O1	1.477(3)	C22	O7	1.479(3)
C11	C12	1.512(3)	C26	C27	1.511(3)
C11	N2	1.501(3)	C26	N4	1.496(3)
C12	O3	1.331(3)	C27	O9	1.323(3)
C12	O4	1.204(3)	C27	O10	1.206(3)
C13	C14	1.520(3)	C28	C29	1.515(3)
C13	N2	1.489(3)	C28	N4	1.497(3)
C14	O5	1.325(3)	C29	O11	1.320(3)
C14	O6	1.198(3)	C29	O12	1.199(3)
C15	N2	1.498(3)	C30	N4	1.494(3)

Table 5: Bond Angles for *exo*-39.

Atom	Atom	Atom	Angle/°	Atom	Atom	Atom	Angle/°
C5	B1	N2	116.89(19)	C20	B2	N4	116.54(18)
O3	B1	C5	113.0(2)	O9	B2	C20	112.85(19)
O3	B1	N2	102.82(18)	O9	B2	N4	101.65(17)
O3	B1	O5	109.77(19)	O9	B2	O11	110.10(18)
O5	B1	C5	113.3(2)	O11	B2	C20	112.81(18)

Table 5: Bond Angles for *exo*-39.

Atom	Atom	Atom	Angle/°	Atom	Atom	Atom	Angle/°
O5	B1	N2	99.94(17)	O11	B2	N4	101.85(17)
N1	C1	C2	103.7(2)	N3	C16	C17	102.90(19)
C1	C2	C5	116.7(2)	C16	C17	C20	116.2(2)
C3	C2	C1	107.4(2)	C18	C17	C16	108.31(19)
C3	C2	C5	60.28(15)	C18	C17	C20	60.48(15)
C2	C3	C5	60.14(16)	C17	C18	C19	107.80(19)
C4	C3	C2	108.7(2)	C17	C18	C20	60.35(15)
C4	C3	C5	115.4(2)	C19	C18	C20	117.9(2)
N1	C4	C3	103.5(2)	N3	C19	C18	103.30(18)
C2	C5	B1	122.2(2)	C17	C20	B2	120.61(19)
C2	C5	C3	59.58(16)	C17	C20	C18	59.17(15)
C3	C5	B1	117.6(2)	C18	C20	B2	116.13(19)
O1	C6	N1	110.2(2)	N3	C21	O7	110.8(2)
O2	C6	N1	123.8(3)	O8	C21	N3	123.5(2)
O2	C6	O1	126.0(3)	O8	C21	O7	125.7(2)
C8	C7	C10	111.1(3)	C23	C22	C24	111.3(3)
C9	C7	C8	111.1(3)	C25	C22	C23	111.1(2)
C9	C7	C10	111.7(3)	C25	C22	C24	111.8(3)
O1	C7	C8	101.7(2)	O7	C22	C23	102.0(2)
O1	C7	C9	110.4(2)	O7	C22	C24	110.6(2)
O1	C7	C10	110.5(2)	O7	C22	C25	109.6(2)
N2	C11	C12	106.60(18)	N4	C26	C27	106.68(19)
O3	C12	C11	110.94(19)	O9	C27	C26	111.5(2)
O4	C12	C11	125.2(2)	O10	C27	C26	124.2(2)
O4	C12	O3	123.9(2)	O10	C27	O9	124.3(2)
N2	C13	C14	105.64(18)	N4	C28	C29	107.09(18)

Table 5: Bond Angles for *exo*-39.

Atom	Atom	Atom	Angle/°	Atom	Atom	Atom	Angle/°
O5	C14	C13	110.20(19)	O11	C29	C28	111.41(19)
O6	C14	C13	125.0(2)	O12	C29	C28	123.9(2)
O6	C14	O5	124.7(2)	O12	C29	O11	124.7(2)
C4	N1	C1	112.6(2)	C19	N3	C16	112.7(2)
C6	N1	C1	125.2(2)	C21	N3	C16	126.3(2)
C6	N1	C4	122.1(2)	C21	N3	C19	120.26(19)
C11	N2	B1	102.24(17)	C26	N4	B2	104.35(17)
C13	N2	B1	103.85(17)	C26	N4	C28	111.84(18)
C13	N2	C11	112.18(19)	C28	N4	B2	104.35(16)
C13	N2	C15	111.92(18)	C30	N4	B2	114.26(17)
C15	N2	B1	115.22(18)	C30	N4	C26	111.14(19)
C15	N2	C11	110.93(18)	C30	N4	C28	110.60(18)
C6	O1	C7	121.3(2)	C21	O7	C22	120.08(19)
C12	O3	B1	112.93(18)	C27	O9	B2	115.03(18)
C14	O5	B1	114.18(18)	C29	O11	B2	115.08(17)

Table 6: Torsion Angles for *exo*-39.

A	B	C	D	Angle/°	A	B	C	D	Angle/°
C1	C2	C3	C4	-2.0(3)	C16	C17	C18	C19	-2.1(3)
C1	C2	C3	C5	-111.2(2)	C16	C17	C18	C20	110.4(2)
C1	C2	C5	B1	-158.9(2)	C16	C17	C20	B2	158.9(2)
C1	C2	C5	C3	95.7(2)	C16	C17	C20	C18	-97.1(2)
C2	C1	N1	C4	-20.7(3)	C17	C16	N3	C19	21.6(3)
C2	C1	N1	C6	154.8(3)	C17	C16	N3	C21	-167.7(2)
C2	C3	C4	N1	-10.0(3)	C17	C18	C19	N3	14.5(3)

Table 6: Torsion Angles for *exo*-39.

A	B	C	D	Angle/°	A	B	C	D	Angle/°
C2	C3	C5	B1	-113.0(2)	C17	C18	C20	B2	111.6(2)
C3	C2	C5	B1	105.3(2)	C18	C17	C20	B2	-104.1(2)
C3	C4	N1	C1	19.4(3)	C18	C19	N3	C16	-23.0(3)
C3	C4	N1	C6	-156.3(3)	C18	C19	N3	C21	165.7(2)
C4	C3	C5	B1	149.2(2)	C19	C18	C20	B2	-152.9(2)
C4	C3	C5	C2	-97.8(2)	C19	C18	C20	C17	95.5(2)
C5	B1	N2	C11	-144.7(2)	C20	B2	N4	C26	115.3(2)
C5	B1	N2	C13	98.5(2)	C20	B2	N4	C28	-127.2(2)
C5	B1	N2	C15	-24.3(3)	C20	B2	N4	C30	-6.3(3)
C5	B1	O3	C12	141.8(2)	C20	B2	O9	C27	-121.8(2)
C5	B1	O5	C14	-106.0(2)	C20	B2	O11	C29	127.6(2)
C5	C2	C3	C4	109.2(2)	C20	C17	C18	C19	-112.5(2)
C5	C3	C4	N1	55.1(3)	C20	C18	C19	N3	-50.8(3)
C8	C7	O1	C6	-172.2(3)	C23	C22	O7	C21	179.2(2)
C9	C7	O1	C6	69.8(3)	C24	C22	O7	C21	-62.3(3)
C10	C7	O1	C6	-54.2(3)	C25	C22	O7	C21	61.4(3)
C11	C12	O3	B1	-3.2(3)	C26	C27	O9	B2	1.9(3)
C12	C11	N2	B1	19.0(2)	C27	C26	N4	B2	9.0(2)
C12	C11	N2	C13	129.63(19)	C27	C26	N4	C28	-103.2(2)
C12	C11	N2	C15	-104.4(2)	C27	C26	N4	C30	132.6(2)
C13	C14	O5	B1	-6.5(3)	C28	C29	O11	B2	1.0(3)
C14	C13	N2	B1	21.5(2)	C29	C28	N4	B2	4.6(2)
C14	C13	N2	C11	-88.1(2)	C29	C28	N4	C26	116.8(2)
C14	C13	N2	C15	146.42(19)	C29	C28	N4	C30	-118.73(19)
N1	C1	C2	C3	13.1(3)	N3	C16	C17	C18	-11.0(3)
N1	C1	C2	C5	-51.8(3)	N3	C16	C17	C20	54.4(3)

Table 6: Torsion Angles for *exo*-39.

A	B	C	D	Angle/°	A	B	C	D	Angle/°
N1	C6	O1	C7	175.9(2)	N3	C21	O7	C22	-174.5(2)
N2	B1	C5	C2	90.5(3)	N4	B2	C20	C17	-87.2(3)
N2	B1	C5	C3	160.2(2)	N4	B2	C20	C18	−155.27(19)
N2	B1	O3	C12	15.0(2)	N4	B2	O9	C27	3.7(2)
N2	B1	O5	C14	19.1(2)	N4	B2	O11	C29	1.9(2)
N2	C11	C12	O3	-11.4(2)	N4	C26	C27	O9	-7.4(3)
N2	C11	C12	O4	169.6(2)	N4	C26	C27	O10	174.4(2)
N2	C13	C14	O5	-10.9(3)	N4	C28	C29	O11	-3.8(2)
N2	C13	C14	O6	171.6(2)	N4	C28	C29	O12	176.4(2)
O1	C6	N1	C1	9.3(4)	O7	C21	N3	C16	5.4(4)
O1	C6	N1	C4	-175.5(2)	O7	C21	N3	C19	175.4(2)
O2	C6	N1	C1	-172.1(3)	O8	C21	N3	C16	-175.3(3)
O2	C6	N1	C4	3.1(5)	O8	C21	N3	C19	-5.3(4)
O2	C6	O1	C7	-2.7(5)	O8	C21	O7	C22	6.2(4)
O3	B1	C5	C2	-28.5(3)	O9	B2	C20	C17	29.9(3)
O3	B1	C5	C3	41.2(3)	O9	B2	C20	C18	-38.2(3)
O3	B1	N2	C11	-20.4(2)	O9	B2	N4	C26	-7.8(2)
O3	B1	N2	C13	−137.19(19)	O9	B2	N4	C28	109.69(18)
O3	B1	N2	C15	100.1(2)	O9	B2	N4	C30	-129.4(2)
O3	B1	O5	C14	126.7(2)	O9	B2	O11	C29	-105.3(2)
O4	C12	O3	B1	175.8(2)	O10	C27	O9	B2	-179.9(2)
O5	B1	C5	C2	-154.1(2)	O11	B2	C20	C17	155.50(19)
O5	B1	C5	C3	-84.4(3)	O11	B2	C20	C18	87.4(2)
O5	B1	N2	C11	92.73(19)	O11	B2	N4	C26	−121.50(19)
O5	B1	N2	C13	-24.1(2)	O11	B2	N4	C28	-4.0(2)

Table 6: Torsion Angles for *exo*-39.

A	B	C	D	Angle/°	A	B	C	D	Angle/°
O5	B1	N2	C15	146.86(18)	O11	B2	N4	C30	116.9(2)
O5	B1	O3	C12	-90.7(2)	O11	B2	O9	C27	111.1(2)
O6	C14	O5	B1	171.0(2)	O12	C29	O11	B2	-179.2(2)

Table 7: Hydrogen Atom Coordinates (Å×10^4) and Isotropic Displacement Parameters (Å^2×10^3) for *exo*-39.

Atom	*x*	*y*	*z*	U(eq)
H1A	9404.62	3722.93	3003.69	40
H1B	7093.56	3566.57	2864.32	40
H2	6635.9	4009.73	4002.22	31
H3	4954.21	4574.62	3239.43	31
H4A	5024.16	4306.98	1884.89	43
H4B	6933.55	4607.98	1856.58	43
H5	9503.6	4544.04	3162.92	28
H8A	10609.78	2866.57	1347.16	73
H8B	12654.45	3056.85	1736.77	73
H8C	12648.69	2874.08	851.6	73
H9A	13967.1	3561.03	357.42	75
H9B	13898.09	3719	1260.2	75
H9C	12679.42	3950.63	553.85	75
H10A	8550.48	3271.71	227.27	65
H10B	10560	3202.3	-267.79	65
H10C	9688.85	3642.31	-156.65	65
H11A	9514.89	5121.19	5907.96	27
H11B	9774.04	4659.98	6144.12	27

Table 7: Hydrogen Atom Coordinates (Å×10^4) and Isotropic Displacement Parameters (Å^2×10^3) for *exo*-39.

Atom	*x*	*y*	*z*	U(eq)
H13A	12785.9	4998.84	4373.59	29
H13B	12313.69	5225.33	5195.12	29
H15A	10353.49	4155.56	5086.5	38
H15B	12468.62	4367.24	5338.1	38
H15C	11834.65	4306.19	4410.54	38
H16A	2836.76	2482.16	7566.34	35
H16B	2913.56	2771.12	8338.32	35
H17	4395.8	3066.07	6972.28	29
H18	1335.49	3338.42	6217.1	26
H19A	-1837.78	3168.93	7127.16	29
H19B	-1059.6	2816.55	6559.88	29
H20	1523.63	3526.44	7974.57	24
H23A	1332.81	1793.18	9559.48	65
H23B	-239.39	1734.71	10258.92	65
H23C	1010.88	2141.21	10195.55	65
H24A	-3924.48	2473.98	9466.29	68
H24B	-2165.97	2554.01	10139.31	68
H24C	-3607.11	2172.35	10201.97	68
H25A	-1489.82	1634.56	8521.44	66
H25B	-3537.44	1893.82	8487.46	66
H25C	-3117.34	1584.6	9203.59	66
H26A	8147.77	3814.94	7546.78	31
H26B	8027.67	4278.46	7314.29	31
H28A	5857.17	4681.6	7714.95	26
H28B	4751.59	4561.62	8522.74	26
H30A	5765.59	3564.83	8494.3	44

Table 7: Hydrogen Atom Coordinates (Å×10^4) and Isotropic Displacement Parameters (Å^2×10^3) for *exo*-39.

Atom	*x*	*y*	*z*	U(eq)
H30B	4339.93	3886.81	8901.74	44
H30C	6757.39	3952.44	8906.29	44

Experimental

Single crystals of $C_{15}H_{23}BN_2O_6$ **[*exo*-39]** were **[crystallisation from acetone, Et_2O, and hexane]**. A suitable crystal was selected and **[Oil on 200 micrometre micromount]** on a **SuperNova, Dual, Cu at home/near, Eos** diffractometer. The crystal was kept at 109.95(10) K during data collection. Using Olex2 [1], the structure was solved with the SHELXT [2] structure solution program using Intrinsic Phasing and refined with the SHELXL [3] refinement package using Least Squares minimisation.

1. Dolomanov, O.V., Bourhis, L.J., Gildea, R.J, Howard, J.A.K. & Puschmann, H. (2009), J. Appl. Cryst. 42, 339-341.
2. Sheldrick, G.M. (2015). Acta Cryst. A71, 3-8.
3. Sheldrick, G.M. (2015). Acta Cryst. C71, 3-8.

Crystal structure determination of [***exo*-39]**

Crystal Data for $C_{15}H_{23}BN_2O_6$ (M =338.16 g/mol): monoclinic, space group Cc (no. 9), a = 6.42393(14) Å, b = 32.9595(8) Å, c = 16.3523(4) Å, β = 92.289(2)°, V = 3459.50(14) Å^3, Z = 8, T = 109.95(10) K, μ(Cu Kα) = 0.827 mm^{-1}, *Dcalc* = 1.299 g/cm^3, 10941 reflections measured (7.62° ≤ 2Θ ≤ 134.158°), 4061 unique (R_{int} = 0.0259, R_{sigma} = 0.0258) which were used in all calculations. The final R_1 was 0.0281 (I > 2σ(I)) and wR_2 was 0.0729 (all data).

Refinement model description

Number of restraints - 2, number of constraints - unknown.

Details:

```
1. Fixed Uiso
 At 1.2 times of:
  All C(H) groups, All C(H,H) groups
 At 1.5 times of:
  All C(H,H,H) groups
2.a Ternary CH refined with riding coordinates:
 C2(H2), C3(H3), C5(H5), C17(H17), C18(H18), C20(H20)
2.b Secondary CH2 refined with riding coordinates:
 C1(H1A,H1B), C4(H4A,H4B), C11(H11A,H11B), C13(H13A,H13B), C16(H16A,H16B),
 C19(H19A,H19B), C26(H26A,H26B), C28(H28A,H28B)
2.c Idealised Me refined as rotating group:
 C8(H8A,H8B,H8C), C9(H9A,H9B,H9C), C10(H10A,H10B,H10C), C15(H15A,H15B,H15C),
 C23(H23A,H23B,H23C), C24(H24A,H24B,H24C), C25(H25A,H25B,H25C), C30(H30A,H30B,
 H30C)
```

cis-**116**

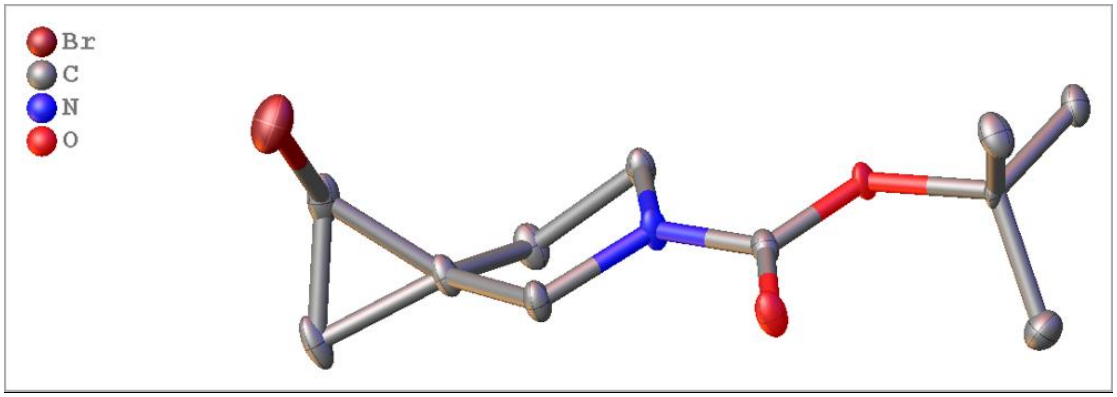

Table 1: Crystal data and structure refinement for *cis*-116.

Identification code	*cis*-**116**
Empirical formula	$C_{11}H_{18}NO_2Br$
Formula weight	276.17
Temperature/K	110.00(10)
Crystal system	triclinic
Space group	P-1
a/Å	5.7890(5)
b/Å	10.6776(10)
c/Å	11.4043(6)
α/°	116.700(7)
β/°	90.215(6)
γ/°	103.568(7)
Volume/Å^3	607.34(9)
Z	2
ρ_{calc}g/cm^3	1.510
μ/mm^{-1}	4.473
F(000)	284.0
Crystal size/mm^3	0.286 × 0.16 × 0.059
Radiation	Cu Kα (λ = 1.54184)
2Θ range for data collection/°	8.748 to 134.104

Index ranges	$-6 \leq h \leq 6, -12 \leq k \leq 12, -8 \leq l \leq 13$
Reflections collected	3660
Independent reflections	2154 [R_{int} = 0.0240, R_{sigma} = 0.0356]
Data/restraints/parameters	2154/0/208
Goodness-of-fit on F^2	1.057
Final R indexes [I>=2σ (I)]	R_1 = 0.0319, wR_2 = 0.0825
Final R indexes [all data]	R_1 = 0.0344, wR_2 = 0.0847
Largest diff. peak/hole / e $Å^{-3}$	0.41/-0.52

Data collected, solved, and refined by Adrian C Whitwood

Table 2: Fractional Atomic Coordinates (×10^4) and Equivalent Isotropic Displacement Parameters (Å^2×10^3) for *cis*-116. U_{eq} is defined as 1/3 of the trace of the orthogonalised U_{IJ} tensor.

Atom	*x*	*y*	*z*	U(eq)
Br1	6278.2(5)	9470.4(3)	6443.5(3)	28.03(13)
C1	3715(4)	4319(3)	2288(2)	12.5(5)
C2	3238(5)	5991(3)	4524(2)	14.4(5)
C3	1795(5)	7096(3)	5028(2)	14.3(5)
C4	2896(5)	8680(3)	5898(3)	18.6(6)
C5	1402(5)	7787(3)	6461(3)	20.1(6)
C6	-58(5)	6661(3)	3873(3)	17.0(6)
C7	1382(5)	6161(3)	2704(3)	13.8(5)
C8	3776(5)	2670(3)	-45(2)	12.6(5)
C9	2463(6)	1303(3)	33(3)	20.3(6)
C10	6472(5)	2894(3)	45(3)	18.4(6)
C11	2816(5)	2642(3)	-1302(3)	16.2(5)
N1	2973(4)	5495(2)	3094(2)	13.7(4)
O1	3168(3)	3953.5(19)	1002.8(16)	12.1(4)

Table 2: Fractional Atomic Coordinates ($\times 10^4$) and Equivalent Isotropic Displacement Parameters ($Å^2 \times 10^3$) for *cis*-116. U_{eq} is defined as 1/3 of the trace of the orthogonalised U_{IJ} tensor.

Atom	*x*	*y*	*z*	U(eq)
O2	4784(3)	3705(2)	2696.3(17)	17.4(4)

Table 3: Anisotropic Displacement Parameters ($Å^2 \times 10^3$) for *cis*-116. The Anisotropic displacement factor exponent takes the form: $-2\pi^2[h^2a^{*2}U_{11}+2hka^*b^*U_{12}+\ldots]$.

Atom	U_{11}	U_{22}	U_{33}	U_{23}	U_{13}	U_{12}
Br1	26.5(2)	21.16(19)	27.8(2)	3.52(14)	-2.97(13)	7.33(13)
C1	11.6(12)	13.8(12)	9.7(12)	3.1(10)	2.4(9)	3.9(10)
C2	18.2(14)	16.1(13)	9.4(12)	3.7(10)	2.9(10)	10.0(11)
C3	14.4(13)	20.1(13)	9.4(12)	4.8(11)	3.8(10)	9.9(11)
C4	22.3(14)	18.0(14)	14.9(13)	3.0(11)	0.6(11)	13.9(12)
C5	22.5(15)	30.6(16)	10.0(13)	6.1(12)	6.2(11)	18.9(13)
C6	14.8(13)	23.4(15)	13.8(13)	6.6(12)	3.4(10)	11.0(12)
C7	17.0(13)	14.7(13)	10.4(12)	4.0(11)	1.7(10)	9.4(11)
C8	15.8(13)	8.8(12)	9.8(12)	0.2(10)	4.8(10)	5.9(10)
C9	23.9(16)	14.1(14)	20.8(15)	6.9(12)	3.5(12)	4.0(11)
C10	14.7(14)	25.0(16)	14.3(14)	6.1(13)	4.4(10)	9.2(12)
C11	16.9(14)	16.8(14)	11.0(13)	2.3(11)	3.2(10)	6.2(11)
N1	19.0(11)	15.0(11)	9.0(10)	3.4(9)	2.3(8)	12.2(9)
O1	17.0(9)	12.4(9)	7.9(8)	2.8(7)	4.9(7)	9.6(7)
O2	23.0(10)	20.0(10)	11.9(9)	5.6(8)	3.8(7)	14.3(8)

Table 4: Bond Lengths for *cis*-116.

Atom	Atom	Length/Å	Atom	Atom	Length/Å
Br1	C4	1.917(3)	C3	C6	1.519(4)
C1	N1	1.350(3)	C4	C5	1.495(4)
C1	O1	1.351(3)	C6	C7	1.528(4)
C1	O2	1.222(3)	C7	N1	1.463(3)
C2	C3	1.509(4)	C8	C9	1.521(4)
C2	N1	1.466(3)	C8	C10	1.518(4)
C3	C4	1.494(4)	C8	C11	1.521(3)
C3	C5	1.504(3)	C8	O1	1.479(3)

Table 5: Bond Angles for *cis*-116.

Atom	Atom	Atom	Angle/°	Atom	Atom	Atom	Angle/°
N1	C1	O1	111.3(2)	C4	C5	C3	59.76(18)
O2	C1	N1	123.1(2)	C3	C6	C7	101.7(2)
O2	C1	O1	125.6(2)	N1	C7	C6	102.8(2)
N1	C2	C3	103.0(2)	C9	C8	C11	110.2(2)
C2	C3	C6	105.5(2)	C10	C8	C9	112.7(2)
C4	C3	C2	123.0(2)	C10	C8	C11	110.7(2)
C4	C3	C5	59.80(19)	O1	C8	C9	110.0(2)
C4	C3	C6	118.0(2)	O1	C8	C10	110.3(2)
C5	C3	C2	120.6(2)	O1	C8	C11	102.37(19)
C5	C3	C6	124.9(2)	C1	N1	C2	119.4(2)
C3	C4	Br1	122.32(19)	C1	N1	C7	126.7(2)
C3	C4	C5	60.44(18)	C7	N1	C2	112.22(19)
C5	C4	Br1	120.84(19)	C1	O1	C8	119.82(19)

Table 6: Torsion Angles for *cis*-116.

A	B	C	D	Angle/°	A	B	C	D	Angle/°
Br1	C4	C5	C3	-112.2(2)	C6	C7	N1	C1	144.5(3)
C2	C3	C4	Br1	0.9(4)	C6	C7	N1	C2	-20.3(3)
C2	C3	C4	C5	-108.9(3)	C9	C8	O1	C1	61.6(3)
C2	C3	C5	C4	112.8(3)	C10	C8	O1	C1	-63.4(3)
C2	C3	C6	C7	-38.0(3)	C11	C8	O1	C1	178.8(2)
C3	C2	N1	C1	-169.2(2)	N1	C1	O1	C8	-178.5(2)
C3	C2	N1	C7	-3.1(3)	N1	C2	C3	C4	-113.8(3)
C3	C6	C7	N1	34.8(3)	N1	C2	C3	C5	174.4(2)
C4	C3	C6	C7	104.0(3)	N1	C2	C3	C6	25.8(3)
C5	C3	C4	Br1	109.8(2)	O1	C1	N1	C2	175.3(2)
C5	C3	C6	C7	175.1(3)	O1	C1	N1	C7	11.4(4)
C6	C3	C4	Br1	-134.1(2)	O2	C1	N1	C2	-6.1(4)
C6	C3	C4	C5	116.1(3)	O2	C1	N1	C7	-170.0(2)
C6	C3	C5	C4	-104.9(3)	O2	C1	O1	C8	2.9(4)

Table 7: Hydrogen Atom Coordinates (Å×10^4) and Isotropic Displacement Parameters (Å^2×10^3) for *cis*-116.

Atom	*x*	*y*	*z*	U(eq)
H2A	2530(50)	5170(30)	4670(30)	15(7)
H2B	4990(50)	6450(30)	4920(30)	11(7)
H4	2340(50)	9300(30)	5750(30)	15(7)
H5A	2130(60)	7520(40)	6960(30)	25(9)
H5B	-90(60)	7960(40)	6710(30)	20(8)
H6A	-760(60)	7430(40)	3960(30)	24(8)
H6B	-1320(60)	5860(40)	3790(30)	24(9)
H7A	2250(50)	7000(30)	2620(30)	4(6)

Table 7: Hydrogen Atom Coordinates (Å×10^4) and Isotropic Displacement Parameters (Å^2×10^3) for *cis*-116.

Atom	*x*	*y*	*z*	U(eq)
H7B	530(60)	5520(40)	1930(40)	22(8)
H9A	3020(60)	1290(40)	740(40)	21(8)
H9B	2630(60)	420(40)	-790(40)	30(9)
H9C	830(60)	1280(30)	90(30)	21(8)
H10A	7280(60)	3680(40)	-20(30)	16(8)
H10B	6750(60)	2130(40)	-650(40)	26(9)
H10C	7160(60)	3000(40)	830(30)	22(8)
H11A	3150(60)	1810(30)	-2050(30)	17(7)
H11B	3490(60)	3430(40)	-1340(30)	28(9)
H11C	1150(70)	2470(40)	-1350(30)	27(9)

exo-**190**

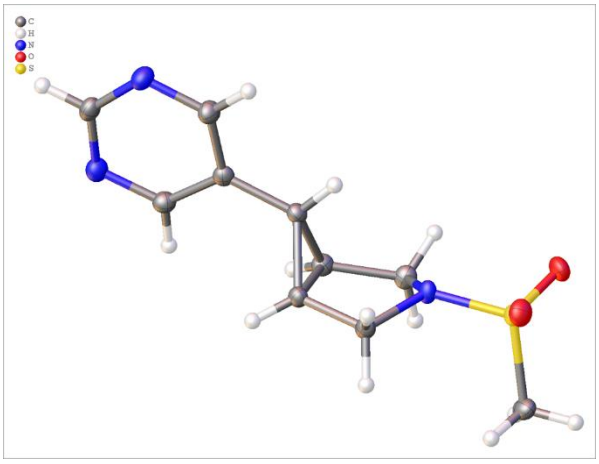

Table 1 Crystal data and structure refinement for *exo*-190.

Identification code	*exo*-**190**
Empirical formula	$C_{10}H_{13}N_3O_2S$
Formula weight	239.29
Temperature/K	110.00(10)
Crystal system	monoclinic
Space group	$P2_1/c$
a/Å	8.7228(4)
b/Å	11.6020(6)
c/Å	11.2672(5)
α/°	90
β/°	105.862(5)
γ/°	90
Volume/Å^3	1096.84(10)
Z	4
ρ_{calc}g/cm^3	1.449
μ/mm^{-1}	2.554
F(000)	504.0
Crystal size/mm^3	0.292 × 0.198 × 0.144
Radiation	Cu Kα (λ = 1.54184)

2Θ range for data collection/°	10.544 to 142.142
Index ranges	$-10 \leq h \leq 7$, $-13 \leq k \leq 14$, $-13 \leq l \leq 13$
Reflections collected	3946
Independent reflections	2069 [R_{int} = 0.0226, R_{sigma} = 0.0312]
Data/restraints/parameters	2069/0/198
Goodness-of-fit on F^2	1.061
Final R indexes [I>=2σ (I)]	R_1 = 0.0316, wR_2 = 0.0771
Final R indexes [all data]	R_1 = 0.0373, wR_2 = 0.0808
Largest diff. peak/hole / e $Å^{-3}$	0.33/-0.37

Data collected by Adrian C. Whitwood, refined by Theo Tanner

Table 2: Fractional Atomic Coordinates (×10^4) and Equivalent Isotropic Displacement Parameters ($Å^2$×10^3) for *exo*-190. U_{eq} is defined as 1/3 of the trace of the orthogonalised U_{IJ} tensor.

Atom	*x*	*y*	*z*	U(eq)
S1	4988.4(5)	3634.7(4)	8351.5(3)	15.92(14)
O1	3936.3(14)	3853.5(11)	9107.5(11)	21.8(3)
O2	5837.9(15)	2557.7(11)	8475.7(11)	22.0(3)
N3	3911.5(16)	3713.9(12)	6929.6(12)	15.1(3)
N1	-648.7(17)	3552.2(13)	1407.7(13)	19.7(3)
N2	-1104.2(17)	1679.9(13)	2123.1(13)	20.2(3)
C3	610.9(19)	3001.3(15)	3506.8(15)	15.3(3)
C5	1711.8(19)	3237.0(15)	4737.5(15)	15.0(3)
C8	4653.2(19)	3476.8(15)	5916.2(15)	16.0(3)
C2	303(2)	3784.9(15)	2536.6(16)	17.9(4)
C7	3317.5(19)	3757.9(15)	4788.7(15)	15.3(3)
C9	2695(2)	4635.2(15)	6563.0(15)	17.5(4)
C6	2098(2)	4466.3(15)	5186.0(15)	16.2(3)

Table 2: Fractional Atomic Coordinates ($\times 10^4$) and Equivalent Isotropic Displacement Parameters ($Å^2 \times 10^3$) for *exo*-190. U_{eq} is defined as 1/3 of the trace of the orthogonalised U_{IJ} tensor.

Atom	*x*	*y*	*z*	U(eq)
C4	−145(2)	1941.8(15)	3239.5(16)	19.0(4)
C1	−1303(2)	2507.0(16)	1267.3(15)	18.8(4)
C10	6408(2)	4753.2(17)	8582.1(17)	21.3(4)

Table 3: Anisotropic Displacement Parameters ($Å^2 \times 10^3$) for *exo*-190. The Anisotropic displacement factor exponent takes the form: $-2\pi^2[h^2a^{*2}U_{11}+2hka^*b^*U_{12}+\ldots]$.

Atom	U_{11}	U_{22}	U_{33}	U_{23}	U_{13}	U_{12}
S1	18.1(2)	17.7(2)	12.0(2)	0.03(15)	4.09(15)	−1.75(16)
O1	25.2(6)	27.3(7)	15.8(6)	−0.7(5)	10.3(5)	−2.8(5)
O2	24.3(7)	20.9(7)	18.6(6)	3.4(5)	2.4(5)	3.4(5)
N3	15.6(7)	18.1(7)	11.7(7)	−1.4(5)	3.8(5)	3.0(6)
N1	18.2(7)	22.2(8)	17.5(7)	1.9(6)	3.0(6)	1.4(6)
N2	20.0(7)	19.4(7)	18.8(7)	−1.6(6)	1.4(6)	−2.0(6)
C3	12.1(7)	17.8(8)	16.4(8)	0.1(7)	4.9(6)	1.9(6)
C5	15.1(8)	15.2(8)	14.9(8)	1.7(7)	4.7(6)	0.3(6)
C8	14.1(8)	19.5(9)	15.0(8)	−2.2(7)	4.9(6)	1.1(7)
C2	17.0(8)	16.8(9)	19.6(8)	0.4(7)	4.6(7)	−0.2(7)
C7	14.8(8)	17.8(8)	13.8(8)	−0.5(6)	5.0(6)	0.0(7)
C9	17.0(8)	17.2(8)	18.5(8)	−1.6(7)	5.0(6)	3.2(7)
C6	16.0(8)	14.4(8)	17.6(8)	1.1(7)	3.8(6)	2.5(7)
C4	19.8(8)	18.0(9)	17.8(8)	1.7(7)	2.9(7)	0.0(7)
C1	15.1(8)	23.8(9)	16.0(8)	−1.9(7)	1.6(7)	1.3(7)
C10	21.5(9)	23.9(10)	19.3(9)	−5.7(7)	6.8(7)	−6.6(7)

Table 4: Bond Lengths for *exo*-190.

Atom	Atom	Length/Å	Atom	Atom	Length/Å
S1	O1	1.4352(12)	N2	C1	1.338(2)
S1	O2	1.4398(13)	C3	C5	1.480(2)
S1	N3	1.6232(13)	C3	C2	1.390(2)
S1	C10	1.7635(18)	C3	C4	1.389(2)
N3	C8	1.484(2)	C5	C7	1.512(2)
N3	C9	1.483(2)	C5	C6	1.520(2)
N1	C2	1.343(2)	C8	C7	1.506(2)
N1	C1	1.331(2)	C7	C6	1.506(2)
N2	C4	1.341(2)	C9	C6	1.508(2)

Table 5: Bond Angles for *exo*-190.

Atom	Atom	Atom	Angle/°	Atom	Atom	Atom	Angle/°
O1	S1	O2	119.43(8)	C3	C5	C7	117.81(14)
O1	S1	N3	106.52(7)	C3	C5	C6	120.86(14)
O1	S1	C10	108.65(8)	C7	C5	C6	59.55(11)
O2	S1	N3	106.78(7)	N3	C8	C7	102.09(13)
O2	S1	C10	107.59(9)	N1	C2	C3	123.37(16)
N3	S1	C10	107.31(8)	C8	C7	C5	116.14(14)
C8	N3	S1	119.51(11)	C6	C7	C5	60.49(11)
C9	N3	S1	119.51(11)	C6	C7	C8	108.29(13)
C9	N3	C8	110.41(13)	N3	C9	C6	102.25(13)
C1	N1	C2	115.45(15)	C7	C6	C5	59.96(10)
C1	N2	C4	116.00(15)	C7	C6	C9	107.68(13)
C2	C3	C5	123.51(15)	C9	C6	C5	116.54(14)
C4	C3	C5	120.98(15)	N2	C4	C3	122.78(16)

Table 5: Bond Angles for *exo*-190.

Atom	Atom	Atom	Angle/°	Atom	Atom	Atom	Angle/°
C4	C3	C2	115.47(15)	N1	C1	N2	126.94(15)

Table 6: Torsion Angles for *exo*-190.

A	B	C	D	Angle/°	A	B	C	D	Angle/°
S1	N3	C8	C7	−174.55(11)	C8	C7	C6	C5	−110.25(15)
S1	N3	C9	C6	175.03(11)	C8	C7	C6	C9	0.69(18)
O1	S1	N3	C8	−177.43(12)	C2	N1	C1	N2	-0.3(3)
O1	S1	N3	C9	41.24(14)	C2	C3	C5	C7	-46.1(2)
O2	S1	N3	C8	-48.76(14)	C2	C3	C5	C6	23.2(2)
O2	S1	N3	C9	169.91(12)	C2	C3	C4	N2	0.3(3)
N3	C8	C7	C5	-48.38(18)	C7	C5	C6	C9	-95.93(16)
N3	C8	C7	C6	17.05(17)	C9	N3	C8	C7	-30.01(17)
N3	C9	C6	C5	46.52(18)	C6	C5	C7	C8	97.12(16)
N3	C9	C6	C7	-18.14(17)	C4	N2	C1	N1	0.2(3)
C3	C5	C7	C8	−151.63(15)	C4	C3	C5	C7	131.47(17)
C3	C5	C7	C6	111.26(17)	C4	C3	C5	C6	−159.16(16)
C3	C5	C6	C7	−106.21(17)	C4	C3	C2	N1	-0.4(3)
C3	C5	C6	C9	157.85(15)	C1	N1	C2	C3	0.3(3)
C5	C3	C2	N1	177.36(15)	C1	N2	C4	C3	-0.3(3)
C5	C3	C4	N2	−177.46(15)	C10	S1	N3	C8	66.36(14)
C5	C7	C6	C9	110.94(15)	C10	S1	N3	C9	-74.97(14)
C8	N3	C9	C6	30.49(17)					

Table 7: Hydrogen Atom Coordinates (Å×10^4) and Isotropic Displacement Parameters (Å^2×10^3) for *exo*-190.

Atom	*x*	*y*	*z*	U(eq)
H8A	4990(20)	2698(17)	5939(17)	16(5)
H5	1680(20)	2680(17)	5346(17)	15(5)
H9A	1880(20)	4506(17)	7025(18)	23(5)
H8B	5630(20)	3976(17)	5950(16)	17(5)
H4	30(20)	1347(17)	3877(18)	23(5)
H1	-1990(20)	2342(17)	469(18)	18(5)
H9B	3170(20)	5395(18)	6740(17)	21(5)
H7	3560(20)	3870(17)	4043(18)	20(5)
H6	1560(20)	5078(18)	4693(18)	24(5)
H2	740(20)	4559(18)	2632(17)	19(5)
H10A	7070(20)	4595(19)	8042(19)	28(6)
H10B	5890(30)	5490(20)	8437(19)	29(6)
H10C	7040(30)	4710(20)	9430(20)	37(6)

Experimental

Single crystals of $C_{10}H_{13}N_3O_2S$ **[*exo*-190]** were **[Acetone and Hexane]**. A suitable crystal was selected and **[oil on micromount]** on a **SuperNova, Dual, Cu at home/near, Eos** diffractometer. The crystal was kept at 110.00(10) K during data collection. Using Olex2 [1], the structure was solved with the SHELXT [2] structure solution program using Intrinsic Phasing and refined with the SHELXL [3] refinement package using Least Squares minimisation.

1. Dolomanov, O.V., Bourhis, L.J., Gildea, R.J, Howard, J.A.K. & Puschmann, H. (2009), J. Appl. Cryst. 42, 339-341.
2. Sheldrick, G.M. (2015). Acta Cryst. A71, 3-8.
3. Sheldrick, G.M. (2015). Acta Cryst. C71, 3-8.

Crystal structure determination of [***exo***-190]

Crystal Data for $C_{10}H_{13}N_3O_2S$ (M =239.29 g/mol): monoclinic, space group $P2_1/c$ (no. 14), a = 8.7228(4) Å, b = 11.6020(6) Å, c = 11.2672(5) Å, β = 105.862(5)°, V = 1096.84(10) Å^3, Z = 4, T = 110.00(10) K, μ(Cu Kα) = 2.554 mm^{-1}, *Dcalc* = 1.449 g/cm^3, 3946 reflections measured (10.544° ≤ 2Θ ≤ 142.142°), 2069 unique (R_{int} = 0.0226, R_{sigma} = 0.0312) which were used in all calculations. The final R_1 was 0.0316 (I > 2σ(I)) and wR_2 was 0.0808 (all data).

Refinement model description

Number of restraints - 0, number of constraints - unknown.

Details:

N/A

trans-**191**

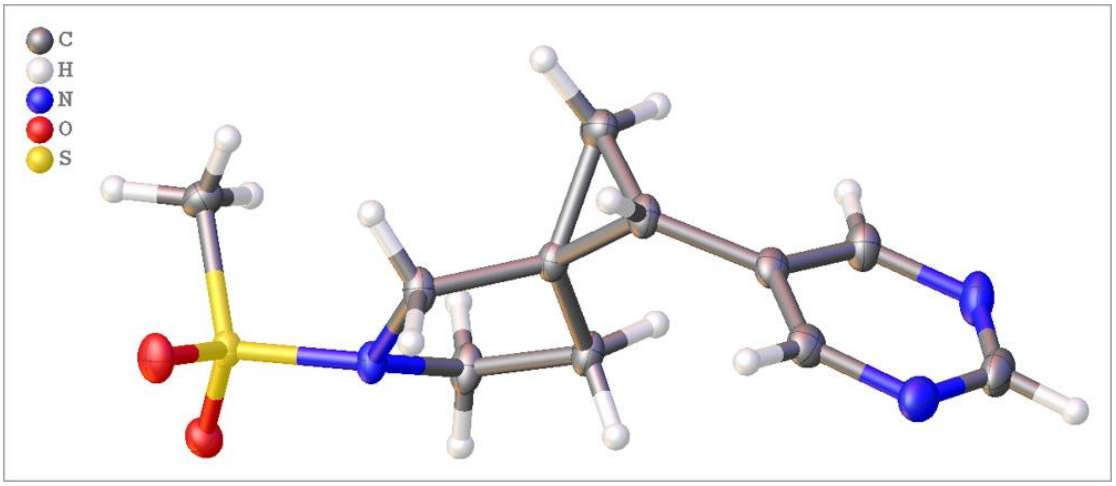

Table 1: Crystal data and structure refinement for *trans*-191.

Identification code	*trans*-**191**
Empirical formula	$C_{11}H_{15}N_3O_2S$
Formula weight	253.32
Temperature/K	110.00(10)
Crystal system	monoclinic
Space group	$P2_1/c$
a/Å	5.3765(2)
b/Å	22.8875(6)
c/Å	9.6680(3)
α/°	90
β/°	97.960(4)
γ/°	90
Volume/Å^3	1178.22(7)
Z	4
ρ_{calc}g/cm^3	1.428
μ/mm^{-1}	0.269
F(000)	536.0
Crystal size/mm^3	0.187 × 0.133 × 0.064

Radiation	Mo Kα (λ = 0.71073)
2Θ range for data collection/°	6.828 to 64.368
Index ranges	-8 ≤ h ≤ 8, -33 ≤ k ≤ 29, -14 ≤ l ≤ 11
Reflections collected	6646
Independent reflections	3736 [R_{int} = 0.0371, R_{sigma} = 0.0585]
Data/restraints/parameters	3736/0/214
Goodness-of-fit on F^2	1.085
Final R indexes [I>=2σ (I)]	R_1 = 0.0453, wR_2 = 0.1109
Final R indexes [all data]	R_1 = 0.0573, wR_2 = 0.1199
Largest diff. peak/hole / e $Å^{-3}$	0.46/-0.46

Data collected, solved, and refined by Adrian C Whitwood

Table 2: Fractional Atomic Coordinates (×10^4) and Equivalent Isotropic Displacement Parameters (Å²×10^3) for *trans*-191. U_{eq} is defined as 1/3 of the trace of the orthogonalised U_{IJ} tensor.

Atom	*x*	*y*	*z*	U(eq)
C1	7787(4)	5807.3(7)	8395.4(16)	20.6(3)
C2	7161(3)	6366.8(7)	7569.0(16)	18.5(3)
C3	8211(3)	6248.7(7)	6220.4(15)	15.5(3)
C4	7816(3)	5603.6(7)	5911.9(16)	17.8(3)
C5	10532(3)	6556.5(8)	5907.0(18)	21.3(3)
C6	8038(3)	6682.8(7)	5031.6(16)	18.4(3)
C7	6656(3)	7237.4(7)	5117.4(16)	18.6(3)
C8	7425(4)	7692.5(8)	6024.0(18)	23.5(4)
C9	3927(4)	8209.0(8)	5233(2)	26.8(4)
C10	4387(3)	7325.6(8)	4261.2(18)	21.6(3)
C11	11720(3)	4703.2(8)	7935.4(18)	20.0(3)
N1	7447(3)	5353.6(6)	7289.8(13)	15.8(3)

Table 2: Fractional Atomic Coordinates ($\times 10^4$) and Equivalent Isotropic Displacement Parameters ($Å^2 \times 10^3$) for *trans*-191. U_{eq} is defined as 1/3 of the trace of the orthogonalised U_{IJ} tensor.

Atom	*x*	*y*	*z*	U(eq)
N2	6080(3)	8182.0(7)	6096.0(16)	27.5(3)
N3	2994(3)	7806.5(7)	4307.0(16)	26.0(3)
O1	7583(2)	4552.1(5)	8974.7(11)	19.2(2)
O2	7619(2)	4342.8(5)	6462.7(12)	21.5(3)
S1	8419.8(7)	4697.8(2)	7670.6(4)	14.46(11)

Table 3: Anisotropic Displacement Parameters ($Å^2 \times 10^3$) for *trans*-191. The Anisotropic displacement factor exponent takes the form: $-2\pi^2[h^2a^{*2}U_{11}+2hka^*b^*U_{12}+\ldots]$.

Atom	U_{11}	U_{22}	U_{33}	U_{23}	U_{13}	U_{12}
C1	33.0(9)	15.1(7)	13.1(7)	-1.3(6)	1.7(7)	4.7(7)
C2	25.2(8)	15.1(7)	15.1(7)	-0.1(5)	2.4(6)	5.0(7)
C3	18.8(7)	13.7(7)	13.3(6)	-0.8(5)	-0.2(5)	2.4(6)
C4	27.1(8)	13.7(7)	12.0(6)	0.2(5)	0.0(6)	1.8(7)
C5	21.2(8)	18.5(7)	24.4(8)	-3.0(6)	4.1(7)	0.5(7)
C6	26.0(8)	14.6(7)	14.8(7)	-0.1(6)	3.2(6)	2.7(6)
C7	24.9(8)	15.6(7)	16.2(7)	3.7(6)	6.1(6)	1.8(6)
C8	29.9(9)	16.9(8)	23.6(8)	-0.4(6)	3.4(7)	2.2(7)
C9	35.0(10)	17.9(8)	29.9(9)	7.9(7)	12.5(8)	8.7(8)
C10	26.8(8)	19.1(7)	19.5(7)	5.4(6)	4.9(7)	1.5(7)
C11	16.4(7)	22.8(8)	20.4(8)	-0.1(6)	1.6(6)	2.0(7)
N1	21.9(7)	12.4(6)	12.7(6)	0.1(5)	0.4(5)	2.3(5)
N2	40.6(9)	16.0(7)	26.9(7)	0.6(6)	8.6(7)	5.4(7)
N3	28.9(8)	22.2(7)	28.1(8)	9.0(6)	7.7(6)	5.4(6)
O1	21.2(6)	17.6(5)	18.8(5)	3.2(4)	2.7(4)	-0.4(5)

Table 3: Anisotropic Displacement Parameters ($Å^2×10^3$) for *trans*-191. The Anisotropic displacement factor exponent takes the form: $-2\pi^2[h^2a^{*2}U_{11}+2hka^*b^*U_{12}+\ldots]$.

Atom	U_{11}	U_{22}	U_{33}	U_{23}	U_{13}	U_{12}
O2	27.5(6)	16.5(5)	18.8(5)	-4.2(4)	-3.0(5)	-0.3(5)
S1	16.04(18)	12.28(18)	14.34(18)	-0.19(12)	-0.51(13)	0.85(14)

Table 4: Bond Lengths for *trans*-191.

Atom	Atom	Length/Å	Atom	Atom	Length/Å
C1	C2	1.522(2)	C7	C10	1.391(2)
C1	N1	1.483(2)	C8	N2	1.341(2)
C2	C3	1.515(2)	C9	N2	1.332(3)
C3	C4	1.515(2)	C9	N3	1.333(3)
C3	C5	1.500(2)	C10	N3	1.336(2)
C3	C6	1.512(2)	C11	S1	1.7572(17)
C4	N1	1.4882(19)	N1	S1	1.6151(14)
C5	C6	1.511(2)	O1	S1	1.4353(11)
C6	C7	1.479(2)	O2	S1	1.4388(12)
C7	C8	1.387(2)			

Table 5: Bond Angles for *trans*-191.

Atom	Atom	Atom	Angle/°	Atom	Atom	Atom	Angle/°
N1	C1	C2	102.38(12)	C10	C7	C6	119.81(15)
C3	C2	C1	102.72(13)	N2	C8	C7	123.01(18)
C2	C3	C4	106.52(13)	N2	C9	N3	127.05(17)
C5	C3	C2	120.63(14)	N3	C10	C7	123.33(17)
C5	C3	C4	121.05(14)	C1	N1	C4	110.94(12)

Table 5: Bond Angles for *trans*-191.

Atom	Atom	Atom	Angle/°	Atom	Atom	Atom	Angle/°
C5	C3	C6	60.23(11)	C1	N1	S1	118.86(11)
C6	C3	C2	123.08(13)	C4	N1	S1	118.83(10)
C6	C3	C4	119.89(13)	C9	N2	C8	115.75(17)
N1	C4	C3	103.35(12)	C9	N3	C10	115.55(17)
C3	C5	C6	60.29(11)	N1	S1	C11	108.38(8)
C5	C6	C3	59.48(11)	O1	S1	C11	107.85(8)
C7	C6	C3	120.00(13)	O1	S1	N1	106.57(7)
C7	C6	C5	123.11(15)	O1	S1	O2	119.14(7)
C8	C7	C6	124.89(16)	O2	S1	C11	107.74(8)
C8	C7	C10	115.29(16)	O2	S1	N1	106.78(7)

Table 6: Torsion Angles for *trans*-191.

A	B	C	D	Angle/°	A	B	C	D	Angle/°
C1	C2	C3	C4	35.20(17)	C4	C3	C6	C7	136.04(16)
C1	C2	C3	C5	−108.01(17)	C4	N1	S1	C11	70.21(14)
C1	C2	C3	C6	179.63(15)	C4	N1	S1	O1	−173.96(12)
C1	N1	S1	C11	-70.07(14)	C4	N1	S1	O2	-45.62(14)
C1	N1	S1	O1	45.77(14)	C5	C3	C4	N1	123.51(15)
C1	N1	S1	O2	174.11(12)	C5	C3	C6	C7	−113.08(18)
C2	C1	N1	C4	25.58(18)	C5	C6	C7	C8	-2.1(2)
C2	C1	N1	S1	168.75(11)	C5	C6	C7	C10	178.98(15)
C2	C3	C4	N1	-19.51(17)	C6	C3	C4	N1	−165.31(14)
C2	C3	C5	C6	−113.08(16)	C6	C7	C8	N2	−178.06(15)

Table 6: Torsion Angles for *trans*-191.

A	B	C	D	Angle/°	A	B	C	D	Angle/°
C2	C3	C6	C5	109.15(18)	C6	C7	C10	N3	177.91(15)
C2	C3	C6	C7	-3.9(2)	C7	C8	N2	C9	-0.1(3)
C3	C4	N1	C1	-4.10(18)	C7	C10	N3	C9	0.5(2)
C3	C4	N1	S1	147.28(12)	C8	C7	C10	N3	-1.1(2)
C3	C5	C6	C7	107.96(16)	C10	C7	C8	N2	0.9(2)
C3	C6	C7	C8	69.0(2)	N1	C1	C2	C3	-36.21(17)
C3	C6	C7	C10	109.90(18)	N2	C9	N3	C10	0.5(3)
C4	C3	C5	C6	109.01(16)	N3	C9	N2	C8	-0.6(3)
C4	C3	C6	C5	110.89(17)					

Table 7: Hydrogen Atom Coordinates (Å×10^4) and Isotropic Displacement Parameters (Å^2×10^3) for *trans*-191.

Atom	*x*	*y*	*z*	U(eq)
H1A	9490(40)	5828(9)	8880(20)	26(5)
H1B	6700(40)	5734(9)	9060(20)	27(5)
H2A	5290(40)	6433(9)	7410(20)	25(5)
H2B	7880(40)	6710(9)	8044(19)	19(5)
H4A	9270(40)	5431(9)	5550(20)	21(5)
H4B	6310(40)	5513(8)	5209(18)	13(4)
H5A	11800(40)	6341(8)	5435(18)	15(5)
H5B	11320(40)	6853(10)	6620(20)	32(6)
H6	7850(30)	6521(8)	4139(18)	15(5)
H8	8990(40)	7674(9)	6640(20)	21(5)
H9	2930(50)	8540(11)	5270(20)	48(7)

Table 7: Hydrogen Atom Coordinates (Å×10^4) and Isotropic Displacement Parameters (Å^2×10^3) for *trans*-191.

Atom	*x*	*y*	*z*	U(eq)
H10	3790(40)	7026(9)	3600(20)	23(5)
H11A	12210(40)	4939(9)	8740(20)	25(5)
H11B	12330(40)	4849(9)	7160(20)	25(5)
H11C	12280(40)	4303(10)	8070(20)	30(6)

Experimental

Single crystals of $C_{11}H_{15}N_3O_2S$ **[*trans*-191]** were **[Crystallisation from acetone and hexane]**. A suitable crystal was selected and **[oil on 200 micrometre micromount]** on a **SuperNova, Dual, Cu at home/near, Eos** diffractometer. The crystal was kept at 110.00(10) K during data collection. Using Olex2 [1], the structure was solved with the SHELXT [2] structure solution program using Intrinsic Phasing and refined with the SHELXL [3] refinement package using Least Squares minimisation.

1. Dolomanov, O.V., Bourhis, L.J., Gildea, R.J, Howard, J.A.K. & Puschmann, H. (2009), J. Appl. Cryst. 42, 339-341.
2. Sheldrick, G.M. (2015). Acta Cryst. A71, 3-8.
3. Sheldrick, G.M. (2015). Acta Cryst. C71, 3-8.

Crystal structure determination of [*trans*-**191**]

Crystal Data for $C_{11}H_{15}N_3O_2S$ (M =253.32 g/mol): monoclinic, space group $P2_1/c$ (no. 14), a = 5.3765(2) Å, b = 22.8875(6) Å, c = 9.6680(3) Å, β = 97.960(4)°, V = 1178.22(7) Å^3, Z = 4, T = 110.00(10) K, μ(Mo Kα) = 0.269 mm^{-1}, *Dcalc* = 1.428 g/cm^3, 6646 reflections measured (6.828° ≤ 2Θ ≤ 64.368°), 3736 unique (R_{int} = 0.0371, R_{sigma} = 0.0585) which were used in all calculations. The final R_1 was 0.0453 (I > 2σ(I)) and wR_2 was 0.1199 (all data).

Refinement model description

Number of restraints - 0, number of constraints - unknown.
Details:
N/A

cis-**191**

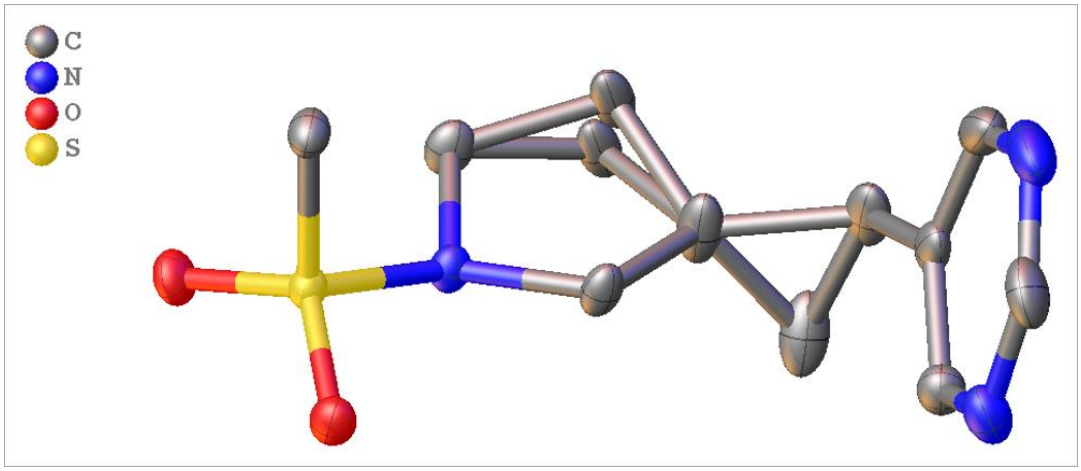

Table 1: Crystal data and structure refinement for *cis*-191.

Identification code	*cis*-**191**
Empirical formula	$C_{11}H_{15}N_3O_2S$
Formula weight	253.32
Temperature/K	110.00(10)
Crystal system	monoclinic
Space group	$P2_1$
a/Å	5.5821(2)
b/Å	9.2130(4)
c/Å	11.4922(5)
α/°	90
β/°	95.183(4)
γ/°	90
Volume/Å^3	588.60(4)
Z	2
ρ_{calc}g/cm^3	1.429
μ/mm^{-1}	0.269
F(000)	268.0
Crystal size/mm^3	0.28 × 0.198 × 0.037
Radiation	Mo Kα (λ = 0.71073)

2Θ range for data collection/°	7.12 to 60.16
Index ranges	$-7 \leq h \leq 7, -8 \leq k \leq 12, -16 \leq l \leq 10$
Reflections collected	3229
Independent reflections	2312 [R_{int} = 0.0274, R_{sigma} = 0.0508]
Data/restraints/parameters	2312/1/160
Goodness-of-fit on F^2	1.117
Final R indexes [I>=2σ (I)]	R_1 = 0.0421, wR_2 = 0.0961
Final R indexes [all data]	R_1 = 0.0485, wR_2 = 0.1018
Largest diff. peak/hole / e $Å^{-3}$	0.43/-0.36
Flack parameter	0.16(15)

Data collected, solved, and refine by Adrian C Whitwood

Refinement Special Details

One carbon (C2) in the 5-membered pyrrolidine ring was disordered and modelled in two positions with refined occupancies of 0.741:0.259(15). The ADPs of the disordered carbons were constrained to be equal.

Table 2: Fractional Atomic Coordinates (×10^4) and Equivalent Isotropic Displacement Parameters (Å^2×10^3) for *cis*-191. U_{eq} is defined as 1/3 of the trace of the orthogonalised U_{IJ} tensor.

Atom	*x*	*y*	*z*	U(eq)
C1	6797(7)	8510(4)	3400(3)	22.8(8)
C2	6481(15)	7970(7)	2139(5)	28.5(14)
C2A	5410(50)	8130(20)	2301(16)	28.5(14)
C3	5585(8)	6418(5)	2244(3)	32.7(9)
C4	6797(7)	5849(4)	3393(3)	20.5(7)
C5	3130(7)	5840(4)	1813(3)	35.7(9)
C6	5306(7)	5451(4)	1173(3)	32.3(8)
C007	11573(4)	7133(6)	5024(2)	20.3(5)
C7	6440(6)	3998(4)	1228(2)	24.1(7)
C8	5671(6)	2834(4)	1873(3)	23.4(7)

Table 2: Fractional Atomic Coordinates ($\times 10^4$) and Equivalent Isotropic Displacement Parameters ($Å^2 \times 10^3$) for *cis*-191. U_{eq} is defined as 1/3 of the trace of the orthogonalised U_{IJ} tensor.

Atom	*x*	*y*	*z*	U(eq)
C9	8854(6)	1486(5)	1436(3)	32.3(8)
C10	8505(7)	3731(5)	660(3)	35.8(9)
N1	6874(3)	7177(4)	4129.4(17)	16.9(4)
N2	6858(5)	1580(4)	1991(2)	27.3(6)
N3	9729(5)	2465(5)	754(2)	39.5(11)
O1	8126(4)	8481(3)	5963(2)	23.0(6)
O2	8077(4)	5788(3)	5920(2)	21.0(6)
S1	8548.9(10)	7140.4(11)	5360.2(5)	15.59(15)

Table 3: Anisotropic Displacement Parameters ($Å^2 \times 10^3$) for *cis*-191. The Anisotropic displacement factor exponent takes the form: $-2\pi^2[h^2a^{*2}U_{11}+2hka^*b^*U_{12}+\ldots]$.

Atom	U_{11}	U_{22}	U_{33}	U_{23}	U_{13}	U_{12}
C1	30.0(19)	14.0(18)	23.3(17)	4.0(15)	-4.1(14)	0.5(15)
C2	58(4)	12(2)	16(2)	1.5(17)	6(2)	-2(3)
C2A	58(4)	12(2)	16(2)	1.5(17)	6(2)	-2(3)
C3	59(2)	16.9(19)	19.7(17)	3.9(15)	-10.5(16)	-5(2)
C4	28.9(18)	11.7(17)	19.5(16)	1.9(15)	-5.1(13)	-2.6(15)
C5	49(2)	22.1(19)	32.5(18)	-5.0(17)	-16.8(16)	11.0(17)
C6	60(2)	20.6(17)	14.5(14)	5.5(14)	-6.1(14)	-8.8(17)
C007	18.6(10)	21.6(14)	20.6(11)	-5(2)	1.4(8)	-1.5(18)
C7	36.9(16)	23.0(18)	11.4(12)	-1.1(13)	-2.9(11)	-10.2(15)
C8	30.2(15)	20.0(18)	20.0(14)	1.2(14)	1.7(12)	-2.7(15)
C9	38.2(17)	35(2)	23.5(15)	-12.4(16)	1.3(13)	4.5(17)
C10	48(2)	40(2)	19.6(15)	-2.2(17)	3.7(14)	-25(2)

Table 3: Anisotropic Displacement Parameters ($Å^2×10^3$) for *cis*-191. The Anisotropic displacement factor exponent takes the form: $-2\pi^2[h^2a^{*2}U_{11}+2hka^*b^*U_{12}+\ldots]$.

Atom	U_{11}	U_{22}	U_{33}	U_{23}	U_{13}	U_{12}
N1	21.1(9)	12.2(10)	16.9(9)	0.1(15)	-1.3(7)	1.0(15)
N2	39.9(15)	23.1(15)	19.3(12)	-1.3(12)	4.5(11)	1.9(14)
N3	36.0(14)	58(3)	25.3(13)	-16.3(17)	7.9(11)	-8.8(16)
O1	28.8(14)	20.1(15)	20.5(12)	-6.1(11)	4.5(10)	2.3(11)
O2	27.3(13)	18.2(15)	17.2(11)	2.6(11)	-0.4(10)	-2.0(11)
S1	18.1(3)	13.6(3)	14.9(3)	-1.1(4)	0.70(19)	-1.1(4)

Table 4: Bond Lengths for *cis*-191.

Atom	Atom	Length/Å	Atom	Atom	Length/Å
C1	C2	1.527(7)	C007	S1	1.766(2)
C1	C2A	1.464(19)	C7	C8	1.393(5)
C1	N1	1.486(5)	C7	C10	1.397(5)
C2	C3	1.523(7)	C8	N2	1.333(5)
C2A	C3	1.58(2)	C9	N2	1.335(4)
C3	C4	1.522(5)	C9	N3	1.317(5)
C3	C5	1.512(6)	C10	N3	1.351(6)
C3	C6	1.516(5)	N1	S1	1.624(2)
C4	N1	1.486(5)	O1	S1	1.446(3)
C5	C6	1.519(6)	O2	S1	1.437(3)
C6	C7	1.480(5)			

Table 5: Bond Angles for *cis*-191.

Atom	Atom	Atom	Angle/°	Atom	Atom	Atom	Angle/°
C2A	C1	N1	105.8(8)	C8	C7	C6	124.6(3)
N1	C1	C2	105.1(3)	C8	C7	C10	114.8(4)
C3	C2	C1	104.0(4)	C10	C7	C6	120.5(3)
C1	C2A	C3	104.3(12)	N2	C8	C7	123.2(3)
C4	C3	C2	105.6(4)	N3	C9	N2	127.6(4)
C4	C3	C2A	109.4(8)	N3	C10	C7	123.2(4)
C5	C3	C2	126.8(4)	C1	N1	C4	111.20(19)
C5	C3	C2A	107.9(10)	C1	N1	S1	119.6(3)
C5	C3	C4	118.8(4)	C4	N1	S1	117.6(2)
C5	C3	C6	60.2(3)	C8	N2	C9	115.8(3)
C6	C3	C2	119.9(4)	C9	N3	C10	115.2(3)
C6	C3	C2A	128.1(8)	N1	S1	C007	107.22(11)
C6	C3	C4	120.5(4)	O1	S1	C007	107.99(19)
N1	C4	C3	101.4(3)	O1	S1	N1	107.08(17)
C3	C5	C6	60.0(3)	O2	S1	C007	108.2(2)
C3	C6	C5	59.7(3)	O2	S1	N1	107.04(17)
C7	C6	C3	119.0(3)	O2	S1	O1	118.79(11)
C7	C6	C5	123.4(3)				

Table 6: Torsion Angles for *cis*-191.

A	B	C	D	Angle/°	A	B	C	D	Angle/°
C1	C2	C3	C4	-33.4(6)	C3	C6	C7	C8	70.4(5)
C1	C2	C3	C5	113.1(5)	C3	C6	C7	C10	-106.0(4)
C1	C2	C3	C6	-173.5(4)	C4	C3	C5	C6	-110.6(4)
C1	C2A	C3	C4	7.5(17)	C4	C3	C6	C5	107.9(4)

Table 6: Torsion Angles for *cis*-191.

A	B	C	D	Angle/°	A	B	C	D	Angle/°
C1	C2A	C3	C5	138.0(11)	C4	C3	C6	C7	-6.0(6)
C1	C2A	C3	C6	-156.2(7)	C4	N1	S1	C007	70.2(3)
C1	N1	S1	C007	-69.8(3)	C4	N1	S1	O1	-174.1(2)
C1	N1	S1	O1	45.9(2)	C4	N1	S1	O2	-45.7(2)
C1	N1	S1	O2	174.3(2)	C5	C3	C4	N1	-114.8(4)
C2	C1	N1	C4	4.0(4)	C5	C3	C6	C7	-113.9(4)
C2	C1	N1	S1	146.4(4)	C5	C6	C7	C8	-0.6(5)
C2	C3	C4	N1	34.9(5)	C5	C6	C7	C10	-177.1(3)
C2	C3	C5	C6	106.8(5)	C6	C3	C4	N1	174.7(3)
C2	C3	C6	C5	-117.9(5)	C6	C7	C8	N2	-173.7(3)
C2	C3	C6	C7	128.2(5)	C6	C7	C10	N3	174.6(3)
C2A	C1	N1	C4	30.3(11)	C7	C8	N2	C9	-0.7(5)
C2A	C1	N1	S1	172.6(11)	C7	C10	N3	C9	-0.7(5)
C2A	C3	C4	N1	9.6(11)	C8	C7	C10	N3	-2.2(5)
C2A	C3	C5	C6	124.3(8)	C10	C7	C8	N2	3.0(4)
C2A	C3	C6	C5	-90.0(13)	N1	C1	C2	C3	18.0(5)
C2A	C3	C6	C7	156.1(13)	N1	C1	C2A	C3	-21.6(15)
C3	C4	N1	C1	-24.1(3)	N2	C9	N3	C10	3.5(5)
C3	C4	N1	S1	-167.3(2)	N3	C9	N2	C8	-2.8(5)
C3	C5	C6	C7	106.7(4)					

Table 7: Hydrogen Atom Coordinates (Å×10^4) and Isotropic Displacement Parameters (Å^2×10^3) for *cis*-191.

Atom	*x*	*y*	*z*	U(eq)
H1AA	8308.6	9069.09	3545.73	27
H1AB	5431.61	9137.02	3571.02	27

Table 7: Hydrogen Atom Coordinates (Å×10^4) and Isotropic Displacement Parameters (Å^2×10^3) for *cis*-191.

Atom	*x*	*y*	*z*	U(eq)
H1BC	6007.57	9312.38	3792.57	27
H1BD	8443.07	8817.53	3255.14	27
H2A	5290.48	8568.75	1662.66	34
H2B	8028.01	7993.08	1780.82	34
H2AA	6109.42	8577.87	1627.81	34
H2AB	3714.51	8441.5	2304.68	34
H4A	5833.69	5072.58	3722.31	25
H4B	8433.09	5478.52	3299.59	25
H5A	1949.69	6531.35	1430.96	43
H5B	2428.81	5071.05	2279.52	43
H6	5399.42	5971.9	414.65	39
H00A	12636.58	7023.08	5744.98	30
H00B	11933.84	8048.74	4642.92	30
H00C	11828.02	6321.85	4497	30
H8	4231.44	2939.89	2247.36	28
H9	9746.43	611.66	1546.2	39
H10	9077.25	4475.39	185.31	43

Table 8: Atomic Occupancy for *cis*-191.

Atom	*Occupancy*	Atom	*Occupancy*	Atom	*Occupancy*
H1AA	0.740(15)	H1AB	0.740(15)	H1BC	0.260(15)
H1BD	0.260(15)	C2	0.740(15)	H2A	0.740(15)
H2B	0.740(15)	C2A	0.260(15)	H2AA	0.260(15)
H2AB	0.260(15)				

Experimental

Single crystals of $C_{11}H_{15}N_3O_2S$ **[*cis*-191]** were **[Crystallisation from acetone and hexane]**. A suitable crystal was selected and **[oil on 200 micrometre micromount]** on a **SuperNova, Dual, Cu at home/near, Eos** diffractometer. The crystal was kept at 110.00(10) K during data collection. Using Olex2 [1], the structure was solved with the SHELXT [2] structure solution program using Intrinsic Phasing and refined with the SHELXL [3] refinement package using Least Squares minimisation.

1. Dolomanov, O.V., Bourhis, L.J., Gildea, R.J, Howard, J.A.K. & Puschmann, H. (2009), J. Appl. Cryst. 42, 339-341.
2. Sheldrick, G.M. (2015). Acta Cryst. A71, 3-8.
3. Sheldrick, G.M. (2015). Acta Cryst. C71, 3-8.

Crystal structure determination of [*cis*-191]

Crystal Data for $C_{11}H_{15}N_3O_2S$ (M =253.32 g/mol): monoclinic, space group $P2_1$ (no. 4), a = 5.5821(2) Å, b = 9.2130(4) Å, c = 11.4922(5) Å, β = 95.183(4)°, V = 588.60(4) Å^3, Z = 2, T = 110.00(10) K, μ(Mo Kα) = 0.269 mm^{-1}, *Dcalc* = 1.429 g/cm^3, 3229 reflections measured (7.12° ≤ 2Θ ≤ 60.16°), 2312 unique (R_{int} = 0.0274, R_{sigma} = 0.0508) which were used in all calculations. The final R_1 was 0.0421 (I > 2σ(I)) and wR_2 was 0.1018 (all data).

Refinement model description

Number of restraints - 1, number of constraints - unknown.

Details:

```
1. Twinned data refinement
 Scales: 0.84(15)
 0.16(15)
2. Fixed Uiso
 At 1.2 times of:
  All C(H) groups, All C(H,H) groups, All C(H,H,H,H) groups
 At 1.5 times of:
  All C(H,H,H) groups
3. Uiso/Uaniso restraints and constraints
Uanis(C2) = Uanis(C2A)
4. Others
 Sof(H1BC)=Sof(H1BD)=Sof(C2A)=Sof(H2AA)=Sof(H2AB)=1-FVAR(1)
 Sof(H1AA)=Sof(H1AB)=Sof(C2)=Sof(H2A)=Sof(H2B)=FVAR(1)
5.a Ternary CH refined with riding coordinates:
 C6(H6)
5.b Secondary CH2 refined with riding coordinates:
 C1(H1AA,H1AB), C1(H1BC,H1BD), C2(H2A,H2B), C2A(H2AA,H2AB), C4(H4A,H4B),
 C5(H5A,H5B)
5.c Aromatic/amide H refined with riding coordinates:
 C8(H8), C9(H9), C10(H10)
5.d Idealised Me refined as rotating group:
 C007(H00A,H00B,H00C)
```

exo-**192**

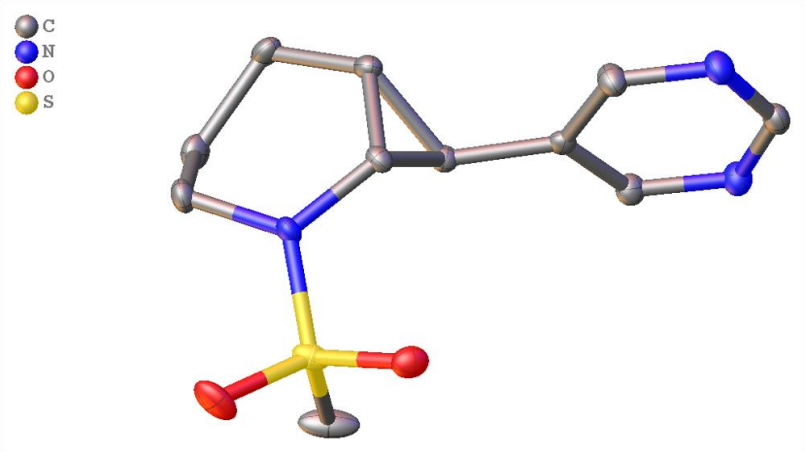

Table 1: Crystal data and structure refinement for *exo*-192.

Identification code	*exo*-**192**
Empirical formula	$C_{11}H_{15}N_3O_2S$
Formula weight	253.32
Temperature/K	110.00(10)
Crystal system	monoclinic
Space group	$P2_1/c$
a/Å	15.5461(6)
b/Å	5.2979(2)
c/Å	14.1558(6)
α/°	90
β/°	98.287(4)
γ/°	90
Volume/Å^3	1153.71(8)
Z	4
ρ_{calc}g/cm^3	1.458
μ/mm^{-1}	2.460
F(000)	536.0
Crystal size/mm^3	0.221 × 0.111 × 0.068
Radiation	Cu Kα (λ = 1.54184)

2Θ range for data collection/°	11.504 to 134.132
Index ranges	$-18 \leq h \leq 14$, $-6 \leq k \leq 6$, $-16 \leq l \leq 16$
Reflections collected	3900
Independent reflections	2061 [R_{int} = 0.0267, R_{sigma} = 0.0369]
Data/restraints/parameters	2061/0/215
Goodness-of-fit on F^2	1.058
Final R indexes [I>=2σ (I)]	R_1 = 0.0338, wR_2 = 0.0832
Final R indexes [all data]	R_1 = 0.0425, wR_2 = 0.0876
Largest diff. peak/hole / e $Å^{-3}$	0.31/-0.31

Data collected, solved, and refine by Adrian C Whitwood

Table 2: Fractional Atomic Coordinates (×10^4) and Equivalent Isotropic Displacement Parameters (Å^2×10^3) for *exo*-192. U_{eq} is defined as 1/3 of the trace of the orthogonalised U_{IJ} tensor.

Atom	*x*	*y*	*z*	U(eq)
C1	8465.2(12)	3545(4)	7750.4(13)	16.7(4)
C2	8201.1(12)	819(4)	7875.9(14)	17.9(4)
C3	7212.4(13)	578(4)	7707.3(14)	17.9(4)
C4	6803.2(11)	1915(4)	6808.8(13)	14.5(4)
C5	7305.5(11)	3814(4)	6325.2(13)	12.4(4)
C6	7080.8(11)	1251(4)	5854.0(13)	12.6(4)
C7	6433.0(11)	1097(4)	4982.0(12)	12.6(4)
C8	5734.4(12)	2754(4)	4797.3(14)	18.1(4)
C9	5292.5(12)	880(4)	3370.9(13)	15.8(4)
C10	6484.9(12)	-718(4)	4286.4(13)	15.7(4)
C11	9350.0(15)	2223(4)	5719(2)	30.0(6)
N1	8183.0(9)	4397(3)	6757.1(10)	13.3(3)
N2	5160.0(10)	2672(3)	3993.2(11)	18.3(4)

Table 2: Fractional Atomic Coordinates ($\times 10^4$) and Equivalent Isotropic Displacement Parameters ($Å^2 \times 10^3$) for *exo*-192. U_{eq} is defined as 1/3 of the trace of the orthogonalised U_{IJ} tensor.

Atom	*x*	*y*	*z*	U(eq)
N3	5921.9(10)	-856(3)	3477.8(11)	17.3(4)
O1	9591.9(8)	6420(3)	6639.1(11)	26.1(4)
O2	8443.8(8)	6278(3)	5238.6(9)	19.5(3)
S1	8902.1(3)	5073.4(8)	6073.0(3)	15.20(16)

Table 3: Anisotropic Displacement Parameters ($Å^2 \times 10^3$) for *exo*-192. The Anisotropic displacement factor exponent takes the form: $-2\pi^2[h^2a^{*2}U_{11}+2hka^*b^*U_{12}+\ldots]$.

Atom	U_{11}	U_{22}	U_{33}	U_{23}	U_{13}	U_{12}
C1	14.0(9)	20.3(10)	14.4(9)	0.2(8)	-3.4(7)	-0.4(8)
C2	20.8(10)	18.1(10)	13.9(9)	3.5(8)	-0.4(8)	1.2(8)
C3	20.6(10)	21.9(11)	11.8(9)	0.7(8)	4.9(8)	-5.7(8)
C4	11.4(9)	18.6(10)	14.1(9)	-1.1(8)	3.5(7)	-2.1(7)
C5	9.8(8)	12.2(9)	14.8(9)	-1.1(8)	0.6(7)	0.5(7)
C6	12.1(8)	13.1(9)	12.7(9)	-0.2(7)	1.7(7)	1.0(7)
C7	11.5(8)	14.1(9)	12.7(9)	0.6(7)	3.3(7)	-3.2(7)
C8	15.1(9)	20.5(10)	18.1(9)	-3.9(9)	0.0(7)	2.0(8)
C9	14.0(9)	17.7(10)	14.9(9)	0.6(8)	-0.5(7)	-3.3(8)
C10	16.1(9)	15.0(9)	15.7(9)	1.1(8)	0.9(7)	1.1(8)
C11	26.7(12)	13.2(10)	55.7(16)	3.1(11)	25.2(12)	4.4(9)
N1	9.6(7)	15.5(8)	14.2(8)	-0.2(6)	-0.3(6)	-1.9(6)
N2	15.2(8)	20.2(9)	18.7(8)	-1.2(7)	-0.6(6)	2.1(7)
N3	18.4(8)	16.9(8)	15.9(8)	-1.5(7)	0.2(6)	0.2(7)
O1	14.8(7)	21.4(8)	40.4(9)	3.8(7)	-1.3(6)	-7.4(6)
O2	20.6(7)	18.2(7)	20.6(7)	3.7(6)	6.2(6)	0.7(6)

Table 3: Anisotropic Displacement Parameters ($Å^2×10^3$) for *exo*-192. The Anisotropic displacement factor exponent takes the form: $-2\pi^2[h^2a^{*2}U_{11}+2hka^*b^*U_{12}+\ldots]$.

Atom	U_{11}	U_{22}	U_{33}	U_{23}	U_{13}	U_{12}
S1	12.3(2)	9.5(2)	24.5(3)	1.42(18)	5.37(18)	-0.58(17)

Table 4: Bond Lengths for *exo*-192.

Atom	Atom	Length/Å	Atom	Atom	Length/Å
C1	C2	1.519(3)	C7	C10	1.387(3)
C1	N1	1.482(2)	C8	N2	1.342(2)
C2	C3	1.526(3)	C9	N2	1.331(3)
C3	C4	1.514(3)	C9	N3	1.335(2)
C4	C5	1.498(3)	C10	N3	1.339(2)
C4	C6	1.518(2)	C11	S1	1.765(2)
C5	C6	1.531(2)	N1	S1	1.6211(15)
C5	N1	1.446(2)	O1	S1	1.4330(14)
C6	C7	1.479(2)	O2	S1	1.4379(14)
C7	C8	1.391(3)			

Table 5: Bond Angles for *exo*-192.

Atom	Atom	Atom	Angle/°	Atom	Atom	Atom	Angle/°
N1	C1	C2	110.65(15)	N2	C8	C7	123.01(18)
C1	C2	C3	110.15(17)	N2	C9	N3	126.65(17)
C4	C3	C2	112.59(16)	N3	C10	C7	123.17(17)
C3	C4	C6	120.04(16)	C1	N1	S1	119.93(12)
C5	C4	C3	120.96(15)	C5	N1	C1	117.93(15)
C5	C4	C6	60.99(12)	C5	N1	S1	118.99(12)

Table 5: Bond Angles for *exo*-192.

Atom	Atom	Atom	Angle/°	Atom	Atom	Atom	Angle/°
C4	C5	C6	60.15(12)	C9	N2	C8	115.90(16)
N1	C5	C4	118.20(15)	C9	N3	C10	115.92(16)
N1	C5	C6	121.06(15)	N1	S1	C11	108.34(10)
C4	C6	C5	58.86(12)	O1	S1	C11	106.89(11)
C7	C6	C4	120.61(15)	O1	S1	N1	107.51(8)
C7	C6	C5	119.85(16)	O1	S1	O2	118.72(9)
C8	C7	C6	122.78(17)	O2	S1	C11	108.40(11)
C10	C7	C6	121.91(16)	O2	S1	N1	106.63(8)
C10	C7	C8	115.31(17)				

Table 6: Torsion Angles for *exo*-192.

A	B	C	D	Angle/°	A	B	C	D	Angle/°
C1	C2	C3	C4	47.3(2)	C5	C6	C7	C10	148.56(17)
C1	N1	S1	C11	74.25(17)	C5	N1	S1	C11	-85.27(17)
C1	N1	S1	O1	-40.93(17)	C5	N1	S1	O1	159.55(14)
C1	N1	S1	O2	−169.26(14)	C5	N1	S1	O2	31.22(16)
C2	C1	N1	C5	46.1(2)	C6	C4	C5	N1	−111.55(18)
C2	C1	N1	S1	−113.67(16)	C6	C5	N1	C1	-83.9(2)
C2	C3	C4	C5	-15.8(3)	C6	C5	N1	S1	76.1(2)
C2	C3	C4	C6	56.4(2)	C6	C7	C8	N2	177.86(17)
C3	C4	C5	C6	109.6(2)	C6	C7	C10	N3	−178.05(17)
C3	C4	C5	N1	-2.0(3)	C7	C8	N2	C9	0.4(3)
C3	C4	C6	C5	−111.04(19)	C7	C10	N3	C9	0.0(3)

Table 6: Torsion Angles for *exo*-192.

A	B	C	D	Angle/°	A	B	C	D	Angle/°
C3	C4	C6	C7	140.41(18)	C8	C7	C10	N3	1.7(3)
C4	C5	C6	C7	109.83(18)	C10	C7	C8	N2	-1.9(3)
C4	C5	N1	C1	-13.5(2)	N1	C1	C2	C3	-63.0(2)
C4	C5	N1	S1	146.40(14)	N1	C5	C6	C4	106.88(18)
C4	C6	C7	C8	38.2(3)	N1	C5	C6	C7	−143.29(17)
C4	C6	C7	C10	−142.13(18)	N2	C9	N3	C10	-1.8(3)
C5	C4	C6	C7	−108.56(19)	N3	C9	N2	C8	1.6(3)
C5	C6	C7	C8	-31.1(3)					

Table 7: Hydrogen Atom Coordinates (Å×10^4) and Isotropic Displacement Parameters (Å^2×10^3) for *exo*-192.

Atom	*x*	*y*	*z*	U(eq)
H6	7539(13)	80(40)	5886(14)	11(5)
H10	6967(14)	-2000(40)	4373(15)	25(6)
H1A	9058(14)	3720(40)	7886(15)	18(5)
H9	4886(13)	820(40)	2826(15)	20(5)
H2A	8433(14)	270(40)	8514(16)	23(6)
H5	6988(12)	5290(40)	6032(14)	15(5)
H3A	7029(13)	-1060(50)	7679(14)	15(5)
H2B	8481(13)	-350(40)	7434(14)	18(5)
H1B	8184(13)	4620(40)	8200(15)	19(6)
H4	6199(14)	2330(40)	6772(15)	19(5)
H8	5598(13)	4040(50)	5233(15)	23(6)
H3B	6997(13)	1290(40)	8224(15)	17(5)

Table 7: Hydrogen Atom Coordinates (Å×10^4) and Isotropic Displacement Parameters (Å^2×10^3) for *exo*-192.

Atom	*x*	*y*	*z*	U(eq)
H11A	9800(20)	2670(60)	5350(20)	67(9)
H11B	8908(15)	1290(50)	5321(16)	28(6)
H11C	9617(17)	1240(60)	6292(19)	44(8)

Experimental

Single crystals of $C_{11}H_{15}N_3O_2S$ **[*exo*-192]** were **[crystallisation from dichloromethane and hexane]**. A suitable crystal was selected and **[oil on 200 micrometre micromount]** on a **SuperNova, Dual, Cu at home/near, Eos** diffractometer. The crystal was kept at 110.00(10) K during data collection. Using Olex2 [1], the structure was solved with the SHELXT [2] structure solution program using Intrinsic Phasing and refined with the SHELXL [3] refinement package using Least Squares minimisation.

1. Dolomanov, O.V., Bourhis, L.J., Gildea, R.J, Howard, J.A.K. & Puschmann, H. (2009), J. Appl. Cryst. 42, 339-341.
2. Sheldrick, G.M. (2015). Acta Cryst. A71, 3-8.
3. Sheldrick, G.M. (2015). Acta Cryst. C71, 3-8.

Crystal structure determination of [***exo***-192]

Crystal Data for $C_{11}H_{15}N_3O_2S$ (M =253.32 g/mol): monoclinic, space group $P2_1/c$ (no. 14), a = 15.5461(6) Å, b = 5.2979(2) Å, c = 14.1558(6) Å, β = 98.287(4)°, V = 1153.71(8) Å^3, Z = 4, T = 110.00(10) K, μ(Cu Kα) = 2.460 mm^{-1}, *Dcalc* = 1.458 g/cm^3, 3900 reflections measured (11.504° ≤ 2Θ ≤ 134.132°), 2061 unique (R_{int} = 0.0267, R_{sigma} = 0.0369) which were used in all calculations. The final R_1 was 0.0338 (I > 2σ(I)) and wR_2 was 0.0876 (all data).

Refinement model description

Number of restraints - 0, number of constraints - unknown.
Details:
N/A

exo-**193**

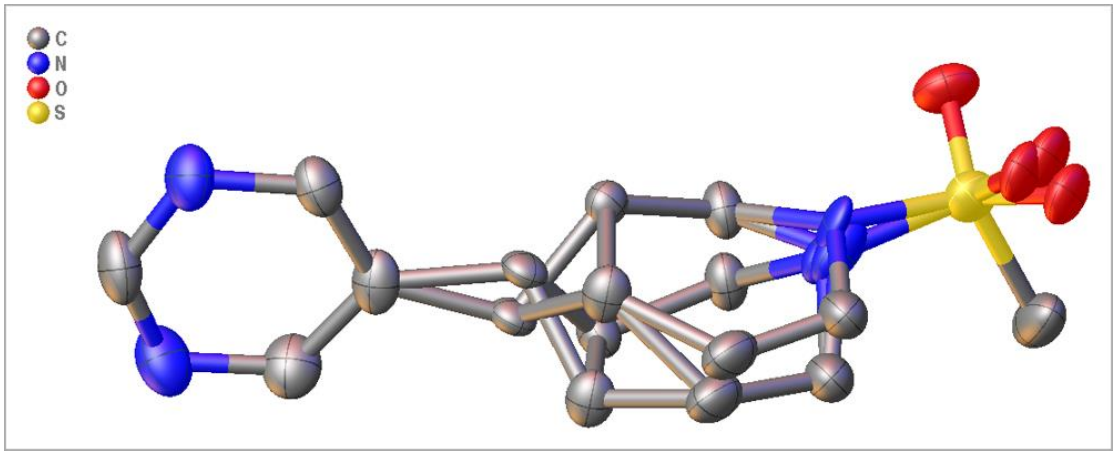

Table 1: Crystal data and structure refinement for *exo*-193.

Identification code	*exo*-**193**
Empirical formula	$C_{11.01}H_{15.02}N_3O_2S$
Formula weight	253.53
Temperature/K	110.05(10)
Crystal system	monoclinic
Space group	$P2_1/c$
a/Å	6.3622(4)
b/Å	24.9957(18)
c/Å	7.3870(5)
α/°	90
β/°	97.405(6)
γ/°	90
Volume/Å^3	1164.94(13)
Z	4
ρ_{calc}g/cm^3	1.446
μ/mm^{-1}	2.437
F(000)	536.0
Crystal size/mm^3	0.266 × 0.243 × 0.061
Radiation	Cu Kα (λ = 1.54184)

2Θ range for data collection/°	7.072 to 142.234
Index ranges	$-7 \leq h \leq 7, -29 \leq k \leq 30, -5 \leq l \leq 8$
Reflections collected	4010
Independent reflections	2193 [R_{int} = 0.0208, R_{sigma} = 0.0333]
Data/restraints/parameters	2193/37/213
Goodness-of-fit on F^2	1.036
Final R indexes [I>=2σ (I)]	R_1 = 0.0481, wR_2 = 0.1220
Final R indexes [all data]	R_1 = 0.0591, wR_2 = 0.1301
Largest diff. peak/hole / e $Å^{-3}$	0.31/-0.45

Data collected, solved, and refined by Adrian C Whitwood

Refinement Special Details

The bicyclic ring and one of the oxygens were disordered and modelled in 3 positions with refined occupancies of 0.464(3):0.277(5):0.261(6). There was close overlap of some atom positions in the various forms and for these the ADP and coordinates were constrained to be the same as follows:

C1B & C1C, C2B & C2C, C3B & C3C, C4B & C4C, C5A & C5C, C6A & C6C.

In addition, the ADP of other pairs were also constrained to be equal as follows C3A & C3B, C4A & C4B, C5A & C5B, C6A & C6B. The S-O bond lengths to the disordered oxygen were restrained to be equal and the ADP of the oxygens constrained to be equal. The C-N bond lengths in the disordered parts were also restrained to be equal.

Table 2: Fractional Atomic Coordinates (×10^4) and Equivalent Isotropic Displacement Parameters (Å^2×10^3) for *exo*-193. U_{eq} is defined as 1/3 of the trace of the orthogonalised U_{IJ} tensor.

Atom	*x*	*y*	*z*	U(eq)
C1A	4838(9)	5930(3)	2186(7)	30.2(12)
C1B	5745(8)	6147(2)	1951(6)	29.5(10)
C1C	5745(8)	6147(2)	1951(6)	29.5(10)
C2A	3536(7)	6305.7(19)	3180(6)	26.0(11)

Table 2: Fractional Atomic Coordinates ($\times 10^4$) and Equivalent Isotropic Displacement Parameters ($Å^2 \times 10^3$) for *exo*-193. U_{eq} is defined as 1/3 of the trace of the orthogonalised U_{IJ} tensor.

Atom	*x*	*y*	*z*	U(eq)
C2B	5443(6)	6679.3(16)	2878(5)	22.9(9)
C2C	5443(6)	6679.3(16)	2878(5)	22.9(9)
C3A	4305(10)	6848(3)	3784(10)	23.4(9)
C3B	3571(8)	6748(3)	3937(9)	23.4(9)
C3C	3571(8)	6748(3)	3937(9)	23.4(9)
C4A	4146(8)	6413(2)	5176(7)	30.7(7)
C4B	5775(7)	6680.3(18)	4934(6)	30.7(7)
C4C	5775(7)	6680.3(18)	4934(6)	30.7(7)
C5A	6172(7)	6149(2)	6018(7)	37.2(10)
C5B	6890(20)	6224(6)	5860(20)	37.2(10)
C5C	6172(7)	6149(2)	6018(7)	37.2(10)
C6A	6796(6)	5697.7(14)	4973(5)	37.2(8)
C6B	8033(16)	5883(4)	5068(12)	37.2(8)
C6C	6796(6)	5697.7(14)	4973(5)	37.2(8)
C7	2646(4)	7289.5(10)	3878(3)	32.8(5)
C8	483(4)	7281.1(11)	3961(4)	40.8(6)
C9	380(4)	8180.4(11)	4091(4)	39.4(6)
C10	3539(4)	7792.1(10)	3849(3)	32.4(5)
C11	7459(5)	4804.0(11)	2153(4)	53.6(8)
N1A	7015(16)	5831(11)	3065(14)	30(3)
N1B	7660(20)	5918(8)	3048(13)	25(3)
N1C	7310(40)	5820(20)	3120(30)	41(10)
N2	-673(3)	7721.6(10)	4067(3)	44.4(6)
N3	2430(3)	8244.5(8)	3955(3)	36.6(5)
O1A	10623(8)	5296(3)	3145(13)	43.3(14)

Table 2: Fractional Atomic Coordinates ($\times 10^4$) and Equivalent Isotropic Displacement Parameters ($Å^2 \times 10^3$) for *exo*-193. U_{eq} is defined as 1/3 of the trace of the orthogonalised U_{IJ} tensor.

Atom	*x*	*y*	*z*	U(eq)
O1B	10812(12)	5449(5)	2910(30)	43.3(14)
O1C	10597(13)	5526(5)	3233(19)	43.3(14)
O2C	8489(3)	5589.7(8)	184(2)	46.4(5)
S1	8634.7(10)	5428.3(3)	2052.1(9)	39.5(2)

Table 3: Anisotropic Displacement Parameters ($Å^2 \times 10^3$) for *exo*-193. The Anisotropic displacement factor exponent takes the form: $-2\pi^2[h^2a^{*2}U_{11}+2hka^*b^*U_{12}+\ldots]$.

Atom	U_{11}	U_{22}	U_{33}	U_{23}	U_{13}	U_{12}
C1A	30(3)	32(3)	28(3)	-3(2)	2(2)	10(2)
C1B	26(2)	28(3)	34(2)	-5(2)	3.4(19)	7(2)
C1C	26(2)	28(3)	34(2)	-5(2)	3.4(19)	7(2)
C2A	22(2)	27(2)	29(2)	-3(2)	5.4(18)	1.0(18)
C2B	22.4(19)	23(2)	22.4(19)	1.6(15)	1.3(15)	1.8(15)
C2C	22.4(19)	23(2)	22.4(19)	1.6(15)	1.3(15)	1.8(15)
C3A	17(3)	27(3)	27.4(17)	0.8(16)	8(2)	-3(2)
C3B	17(3)	27(3)	27.4(17)	0.8(16)	8(2)	-3(2)
C3C	17(3)	27(3)	27.4(17)	0.8(16)	8(2)	-3(2)
C4A	37.2(16)	30.9(17)	22.8(15)	-2.6(13)	-0.6(13)	5.3(13)
C4B	37.2(16)	30.9(17)	22.8(15)	-2.6(13)	-0.6(13)	5.3(13)
C4C	37.2(16)	30.9(17)	22.8(15)	-2.6(13)	-0.6(13)	5.3(13)
C5A	39(3)	34(2)	38.2(18)	13.5(14)	6(2)	1(2)
C5B	39(3)	34(2)	38.2(18)	13.5(14)	6(2)	1(2)
C5C	39(3)	34(2)	38.2(18)	13.5(14)	6(2)	1(2)
C6A	37.2(19)	33.1(19)	44.8(18)	6.5(15)	18.1(16)	6.2(14)

Table 3: Anisotropic Displacement Parameters ($Å^2×10^3$) for *exo*-193. The Anisotropic displacement factor exponent takes the form: $-2\pi^2[h^2a^{*2}U_{11}+2hka^*b^*U_{12}+\ldots]$.

Atom	U_{11}	U_{22}	U_{33}	U_{23}	U_{13}	U_{12}
C6B	37.2(19)	33.1(19)	44.8(18)	6.5(15)	18.1(16)	6.2(14)
C6C	37.2(19)	33.1(19)	44.8(18)	6.5(15)	18.1(16)	6.2(14)
C7	38.3(13)	32.6(13)	25.5(11)	-8.5(10)	-4.0(10)	8.0(10)
C8	39.1(14)	36.8(14)	45.1(15)	-5.5(12)	-0.9(11)	-2.4(11)
C9	35.3(13)	38.8(14)	42.1(14)	-13.4(11)	-2.4(11)	13.6(11)
C10	26.6(11)	38.0(13)	31.9(12)	-6.8(10)	0.9(9)	5.2(9)
C11	81(2)	30.9(14)	56.2(18)	11.6(13)	37.9(17)	16.5(14)
N1A	32(4)	25(5)	31(5)	7(4)	-4(3)	3(4)
N1B	41(7)	9(5)	26(5)	1(3)	0(4)	7(5)
N1C	52(12)	28(13)	40(12)	10(7)	-11(8)	4(9)
N2	31.5(11)	48.7(14)	52.0(14)	-11.5(11)	1.7(10)	3.0(10)
N3	37.6(11)	30.3(11)	40.6(12)	-9.5(9)	-0.6(9)	4.4(9)
O1A	46.6(13)	36(4)	47(2)	20(3)	5.6(15)	19.4(19)
O1B	46.6(13)	36(4)	47(2)	20(3)	5.6(15)	19.4(19)
O1C	46.6(13)	36(4)	47(2)	20(3)	5.6(15)	19.4(19)
O2C	57.7(12)	45.9(11)	37.3(10)	17.9(8)	13.3(9)	2.6(9)
S1	42.0(4)	40.6(4)	37.5(4)	15.1(3)	10.9(3)	11.2(3)

Table 4: Bond Lengths for *exo*-193.

Atom	Atom	Length/Å	Atom	Atom	Length/Å
C1A	C2A	1.505(7)	C5A	C6A	1.451(7)
C1A	N1A	1.472(8)	C5B	C6B	1.306(18)
C1B	C2B	1.520(6)	C5C	C6C	1.451(7)
C1B	N1B	1.486(8)	C6A	N1A	1.473(6)

Table 4: Bond Lengths for *exo*-193.

Atom	Atom	Length/Å	Atom	Atom	Length/Å
C1C	C2C	1.520(6)	C6B	N1B	1.483(7)
C1C	N1C	1.479(8)	C6C	N1C	1.479(8)
C2A	C3A	1.489(8)	C7	C8	1.386(4)
C2A	C4A	1.500(6)	C7	C10	1.380(3)
C2B	C3B	1.516(6)	C8	N2	1.332(3)
C2B	C4B	1.506(5)	C9	N2	1.327(4)
C2C	C3C	1.516(6)	C9	N3	1.331(3)
C2C	C4C	1.506(5)	C10	N3	1.340(3)
C3A	C4A	1.509(9)	C11	S1	1.736(3)
C3A	C7	1.535(8)	N1A	S1	1.684(17)
C3B	C4B	1.507(7)	N1B	S1	1.595(15)
C3B	C7	1.474(7)	N1C	S1	1.57(3)
C3C	C4C	1.507(7)	O1A	S1	1.449(2)
C3C	C7	1.474(7)	O1B	S1	1.449(3)
C4A	C5A	1.509(7)	O1C	S1	1.449(3)
C4B	C5B	1.464(16)	O2C	S1	1.4290(18)
C4C	C5C	1.555(6)			

Table 5: Bond Angles for *exo*-193.

Atom	Atom	Atom	Angle/°	Atom	Atom	Atom	Angle/°
N1A	C1A	C2A	115.8(9)	C8	C7	C3B	112.3(3)
N1B	C1B	C2B	103.5(7)	C8	C7	C3C	112.3(3)
N1C	C1C	C2C	110(2)	C10	C7	C3A	111.6(3)
C3A	C2A	C1A	122.3(5)	C10	C7	C3B	132.3(3)
C3A	C2A	C4A	60.6(4)	C10	C7	C3C	132.3(3)

Table 5: Bond Angles for *exo*-193.

Atom	Atom	Atom	Angle/°	Atom	Atom	Atom	Angle/°
C4A	C2A	C1A	120.1(4)	C10	C7	C8	115.3(2)
C3B	C2B	C1B	119.0(4)	N2	C8	C7	123.3(2)
C4B	C2B	C1B	116.5(4)	N2	C9	N3	127.0(2)
C4B	C2B	C3B	59.8(3)	N3	C10	C7	123.1(2)
C3C	C2C	C1C	119.0(4)	C1A	N1A	C6A	105.0(6)
C4C	C2C	C1C	116.5(4)	C1A	N1A	S1	119.9(13)
C4C	C2C	C3C	59.8(3)	C6A	N1A	S1	115.4(10)
C2A	C3A	C4A	60.0(4)	C1B	N1B	S1	112.6(8)
C2A	C3A	C7	117.8(4)	C6B	N1B	C1B	125.9(10)
C4A	C3A	C7	112.4(5)	C6B	N1B	S1	113.4(8)
C4B	C3B	C2B	59.8(3)	C1C	N1C	S1	114.6(16)
C7	C3B	C2B	115.2(4)	C6C	N1C	C1C	116.3(8)
C7	C3B	C4B	117.4(4)	C6C	N1C	S1	122(2)
C4C	C3C	C2C	59.8(3)	C9	N2	C8	115.7(2)
C7	C3C	C2C	115.2(4)	C9	N3	C10	115.5(2)
C7	C3C	C4C	117.4(4)	N1A	S1	C11	103.1(8)
C2A	C4A	C3A	59.3(4)	N1B	S1	C11	118.3(7)
C2A	C4A	C5A	115.2(4)	N1C	S1	C11	106.0(18)
C5A	C4A	C3A	117.8(5)	O1A	S1	C11	96.9(3)
C2B	C4B	C3B	60.4(3)	O1A	S1	N1A	115.4(6)
C5B	C4B	C2B	117.8(7)	O1B	S1	C11	114.0(5)
C5B	C4B	C3B	132.8(7)	O1B	S1	N1B	100.2(8)
C2C	C4C	C3C	60.4(3)	O1C	S1	C11	117.9(6)
C2C	C4C	C5C	120.7(4)	O1C	S1	N1C	94.0(16)
C3C	C4C	C5C	115.2(4)	O2C	S1	C11	108.71(14)
C6A	C5A	C4A	113.5(4)	O2C	S1	N1A	107.0(3)

Table 5: Bond Angles for *exo*-193.

Atom	Atom	Atom	Angle/°	Atom	Atom	Atom	Angle/°
C6B	C5B	C4B	124.3(12)	O2C	S1	N1B	104.4(4)
C6C	C5C	C4C	115.3(4)	O2C	S1	N1C	109.8(3)
C5A	C6A	N1A	113.5(11)	O2C	S1	O1A	123.1(4)
C5B	C6B	N1B	112.6(11)	O2C	S1	O1B	110.7(8)
C5C	C6C	N1C	116.2(19)	O2C	S1	O1C	118.5(7)
C8	C7	C3A	133.1(3)				

Table 6: Torsion Angles for *exo*-193.

A	B	C	D	Angle/°	A	B	C	D	Angle/°
C1A	C2A	C3A	C4A	-109.0(5)	C3C	C4C	C5C	C6C	86.2(5)
C1A	C2A	C3A	C7	149.9(5)	C3C	C7	C8	N2	174.8(3)
C1A	C2A	C4A	C3A	112.4(6)	C3C	C7	C10	N3	-174.0(4)
C1A	C2A	C4A	C5A	3.7(7)	C4A	C2A	C3A	C7	-101.1(6)
C1A	N1A	S1	C11	-66.9(13)	C4A	C3A	C7	C8	-47.6(7)
C1A	N1A	S1	O1A	-171.3(10)	C4A	C3A	C7	C10	133.3(4)
C1A	N1A	S1	O2C	47.6(15)	C4A	C5A	C6A	N1A	55.9(8)
C1B	C2B	C3B	C4B	105.5(4)	C4B	C2B	C3B	C7	108.3(5)
C1B	C2B	C3B	C7	-146.1(4)	C4B	C3B	C7	C8	-144.5(4)
C1B	C2B	C4B	C3B	-109.7(5)	C4B	C3B	C7	C10	31.7(7)
C1B	C2B	C4B	C5B	16.1(8)	C4B	C5B	C6B	N1B	-14.7(18)
C1B	N1B	S1	C11	-80.2(11)	C4C	C2C	C3C	C7	108.3(5)
C1B	N1B	S1	O1B	155.4(12)	C4C	C3C	C7	C8	-144.5(4)
C1B	N1B	S1	O2C	40.7(13)	C4C	C3C	C7	C10	31.7(7)
C1C	C2C	C3C	C4C	105.5(4)	C4C	C5C	C6C	N1C	9.5(17)
C1C	C2C	C3C	C7	-146.1(4)	C5A	C6A	N1A	C1A	-69.9(17)

Table 6: Torsion Angles for *exo*-193.

A	B	C	D	Angle/°	A	B	C	D	Angle/°
C1C	C2C	C4C	C3C	-109.7(5)	C5A	C6A	N1A	S1	155.8(11)
C1C	C2C	C4C	C5C	-6.2(6)	C5B	C6B	N1B	C1B	-21(2)
C1C	N1C	S1	C11	-100(3)	C5B	C6B	N1B	S1	-167.5(11)
C1C	N1C	S1	O1C	140(3)	C5C	C6C	N1C	C1C	-49(4)
C1C	N1C	S1	O2C	17(4)	C5C	C6C	N1C	S1	161(3)
C2A	C1A	N1A	C6A	49.6(19)	C6A	N1A	S1	C11	60.2(14)
C2A	C1A	N1A	S1	-178.6(9)	C6A	N1A	S1	O1A	-44.1(18)
C2A	C3A	C4A	C5A	104.3(5)	C6A	N1A	S1	O2C	174.8(11)
C2A	C3A	C7	C8	19.2(8)	C6B	N1B	S1	C11	70.5(13)
C2A	C3A	C7	C10	-159.8(4)	C6B	N1B	S1	O1B	-53.9(15)
C2A	C4A	C5A	C6A	-20.3(6)	C6B	N1B	S1	O2C	-168.5(10)
C2B	C1B	N1B	C6B	48.1(18)	C6C	N1C	S1	C11	50(4)
C2B	C1B	N1B	S1	-165.5(9)	C6C	N1C	S1	O1C	-70(4)
C2B	C3B	C4B	C5B	-101.8(10)	C6C	N1C	S1	O2C	167(3)
C2B	C3B	C7	C8	148.0(4)	C7	C3A	C4A	C2A	110.2(5)
C2B	C3B	C7	C10	-35.8(7)	C7	C3A	C4A	C5A	-145.5(4)
C2B	C4B	C5B	C6B	16.6(15)	C7	C3B	C4B	C2B	-104.6(5)
C2C	C1C	N1C	C6C	58(4)	C7	C3B	C4B	C5B	153.6(9)
C2C	C1C	N1C	S1	-150(3)	C7	C3C	C4C	C2C	-104.6(5)
C2C	C3C	C4C	C5C	-112.4(4)	C7	C3C	C4C	C5C	143.0(4)
C2C	C3C	C7	C8	148.0(4)	C7	C8	N2	C9	0.0(4)
C2C	C3C	C7	C10	-35.8(7)	C7	C10	N3	C9	0.0(4)
C2C	C4C	C5C	C6C	17.0(6)	C8	C7	C10	N3	2.1(4)
C3A	C2A	C4A	C5A	-108.7(5)	C10	C7	C8	N2	-2.1(4)
C3A	C4A	C5A	C6A	-87.5(6)	N1A	C1A	C2A	C3A	52.2(11)
C3A	C7	C8	N2	178.8(4)	N1A	C1A	C2A	C4A	-20.1(11)

Table 6: Torsion Angles for *exo*-193.

A	B	C	D	Angle/°	A	B	C	D	Angle/°
C3A	C7	C10	N3	-178.6(4)	N1B	C1B	C2B	C3B	-109.9(8)
C3B	C2B	C4B	C5B	125.7(7)	N1B	C1B	C2B	C4B	-41.4(8)
C3B	C4B	C5B	C6B	90.8(13)	N1C	C1C	C2C	C3C	-97.8(13)
C3B	C7	C8	N2	174.8(3)	N1C	C1C	C2C	C4C	-29.3(14)
C3B	C7	C10	N3	-174.0(4)	N2	C9	N3	C10	-2.6(4)
C3C	C2C	C4C	C5C	103.5(5)	N3	C9	N2	C8	2.6(4)

Table 7: Hydrogen Atom Coordinates (Å×10^4) and Isotropic Displacement Parameters (Å^2×10^3) for *exo*-193.

Atom	*x*	*y*	*z*	U(eq)
H1AA	4104.28	5589.06	2041.1	36
H1AB	4909.32	6072.17	974.52	36
H1BA	4522.82	5917.01	1984.08	35
H1BB	5978.47	6199.07	690.87	35
H1CA	4402.41	5958.94	1737.96	35
H1CB	6239.72	6208.62	780.07	35
H2A	2004.65	6283.45	2799.6	31
H2B	5908.32	6999.32	2274.44	27
H2C	5908.32	6999.32	2274.44	27
H3A	5723.03	6954.41	3537.7	28
H3B	2595.9	6445.05	3951.98	28
H3C	2595.9	6445.05	3951.98	28
H4A	2995.42	6441.74	5935.1	37
H4B	6362.42	7021.42	5419.15	37
H4C	6434.88	7001.66	5517.42	37
H5AA	7301.36	6412.18	6132.96	45

Table 7: Hydrogen Atom Coordinates (Å×10^4) and Isotropic Displacement Parameters (Å^2×10^3) for *exo*-193.

Atom	*x*	*y*	*z*	U(eq)
H5AB	5994.17	6027.73	7236.53	45
H5BA	7814.18	6370.62	6885.88	45
H5BB	5823.76	6015.45	6369.31	45
H5CA	7269.46	6210.48	7035.41	45
H5CB	4886.14	6054.49	6520.8	45
H6AA	5747.33	5416.38	4984.95	45
H6AB	8136.95	5559.67	5561.73	45
H6BA	7706.82	5523.39	5440.28	45
H6BB	9520.57	5949.31	5475.19	45
H6CA	5656.21	5437.22	4864.87	45
H6CB	8025.23	5531.07	5660.16	45
H8	-196.14	6951.32	3941.08	49
H9	-397.11	8490.14	4217.45	47
H10	4978.18	7818.14	3752.69	39
H11A	5991.52	4826.7	1655.22	80
H11B	7569.59	4688.3	3401.32	80
H11C	8165.34	4551.71	1459.65	80

Table 8: Atomic Occupancy for *exo*-193.

Atom	*Occupancy*	Atom	*Occupancy*	Atom	*Occupancy*
C1A	0.464(3)	H1AA	0.464(3)	H1AB	0.464(3)
C1B	0.277(5)	H1BA	0.277(5)	H1BB	0.277(5)
C1C	0.261(6)	H1CA	0.261(6)	H1CB	0.261(6)
C2A	0.464(3)	H2A	0.464(3)	C2B	0.277(5)
H2B	0.277(5)	C2C	0.261(6)	H2C	0.261(6)

Table 8: Atomic Occupancy for *exo*-193.

Atom	***Occupancy***	**Atom**	***Occupancy***	**Atom**	***Occupancy***
C3A	0.464(3)	H3A	0.464(3)	C3B	0.277(5)
H3B	0.277(5)	C3C	0.261(6)	H3C	0.261(6)
C4A	0.464(3)	H4A	0.464(3)	C4B	0.277(5)
H4B	0.277(5)	C4C	0.261(6)	H4C	0.261(6)
C5A	0.464(3)	H5AA	0.464(3)	H5AB	0.464(3)
C5B	0.277(5)	H5BA	0.277(5)	H5BB	0.277(5)
C5C	0.261(6)	H5CA	0.261(6)	H5CB	0.261(6)
C6A	0.464(3)	H6AA	0.464(3)	H6AB	0.464(3)
C6B	0.277(5)	H6BA	0.277(5)	H6BB	0.277(5)
C6C	0.261(6)	H6CA	0.261(6)	H6CB	0.261(6)
N1A	0.464(3)	N1B	0.277(5)	N1C	0.261(6)
O1A	0.464(3)	O1B	0.277(5)	O1C	0.261(6)

194

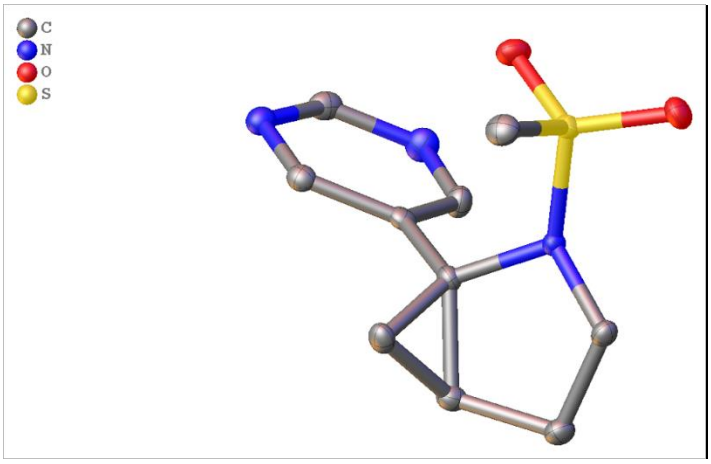

Table 1: Crystal data and structure refinement for 194.

Identification code	**194**
Empirical formula	$C_{10}H_{13}N_3O_2S$
Formula weight	239.29
Temperature/K	110.00(10)
Crystal system	orthorhombic
Space group	Pbca
a/Å	13.1333(4)
b/Å	10.4036(3)
c/Å	15.6547(5)
α/°	90
β/°	90
γ/°	90
Volume/Å^3	2138.96(11)
Z	8
ρ_{calc}g/cm^3	1.486
μ/mm^{-1}	2.620
F(000)	1008.0
Crystal size/mm^3	0.249 × 0.16 × 0.12
Radiation	Cu Kα (λ = 1.54184)

2Θ range for data collection/°	11.304 to 134.148
Index ranges	$-9 \leq h \leq 15, -12 \leq k \leq 12, -18 \leq l \leq 18$
Reflections collected	4781
Independent reflections	1917 [R_{int} = 0.0247, R_{sigma} = 0.0276]
Data/restraints/parameters	1917/0/198
Goodness-of-fit on F^2	1.048
Final R indexes [I>=2σ (I)]	R_1 = 0.0308, wR_2 = 0.0765
Final R indexes [all data]	R_1 = 0.0365, wR_2 = 0.0807
Largest diff. peak/hole / e $Å^{-3}$	0.33/-0.38

Data collected, solved and refined by Adrian C Whitwood

Table 2: Fractional Atomic Coordinates (×10^4) and Equivalent Isotropic Displacement Parameters (Å^2×10^3) for 194. U_{eq} is defined as 1/3 of the trace of the orthogonalised U_{IJ} tensor.

Atom	*x*	*y*	*z*	U(eq)
C1	8081.7(13)	5955.5(17)	7376.3(11)	13.1(4)
C2	8389.3(13)	5353.6(19)	6526.4(12)	16.0(4)
C3	7400.9(13)	4872.1(17)	6147.5(11)	14.9(4)
C4	6688.5(14)	4131.3(17)	6725.6(12)	14.9(4)
C5	6536.9(12)	5558.5(16)	6594.3(10)	12.2(4)
C6	5651.0(13)	6085.6(16)	6120.4(10)	12.1(4)
C7	4730.9(13)	5448.4(17)	6052.2(11)	13.8(4)
C8	4062.7(14)	7115.5(18)	5313.8(11)	16.6(4)
C9	5708.5(14)	7261.9(17)	5705.7(12)	16.3(4)
C10	6235.2(15)	5492.5(18)	8736.8(12)	18.2(4)
N1	7019.3(10)	6422.8(13)	7221.0(9)	11.1(3)
N2	3923.6(11)	5951.4(14)	5647.1(9)	15.6(3)
N3	4921.9(12)	7801.1(15)	5303.7(10)	18.5(4)

Table 2: Fractional Atomic Coordinates (×10^4) and Equivalent Isotropic Displacement Parameters (Å^2×10^3) for 194. U_{eq} is defined as 1/3 of the trace of the orthogonalised U_{IJ} tensor.

Atom	*x*	*y*	*z*	U(eq)
O1	5391.3(9)	7262.5(12)	7799.0(8)	18.7(3)
O2	7015.3(9)	7770.2(12)	8518.1(8)	18.6(3)
S1	6382.3(3)	6858.4(4)	8079.0(3)	12.40(15)

Table 3: Anisotropic Displacement Parameters (Å^2×10^3) for 194. The Anisotropic displacement factor exponent takes the form: -2π^2[h^{2}a*^{2}U$_{11}$+2hka*b*U$_{12}$+…].

Atom	U_{11}	U_{22}	U_{33}	U_{23}	U_{13}	U_{12}
C1	9.8(8)	13.4(8)	16.2(9)	0.2(7)	-1.1(7)	0.6(7)
C2	12.4(8)	17.9(9)	17.9(9)	-1.4(8)	0.6(7)	1.7(7)
C3	14.9(9)	15.5(9)	14.2(9)	-1.9(7)	-0.1(7)	2.4(7)
C4	15.5(9)	10.3(9)	19.0(9)	-0.5(7)	-2.8(7)	0.9(7)
C5	13.1(8)	10.4(8)	13.0(8)	-1.7(7)	0.2(7)	-0.6(7)
C6	14.8(8)	12.3(8)	9.3(8)	-2.5(7)	0.7(6)	1.4(7)
C7	15.5(8)	13.8(8)	12.1(8)	0.2(7)	1.5(7)	0.4(7)
C8	15.6(9)	21.6(9)	12.7(8)	-0.2(7)	-1.8(7)	4.0(8)
C9	14.4(9)	14.6(9)	19.8(9)	0.4(7)	-1.4(7)	-2.1(7)
C10	19.2(10)	18.4(9)	17.1(9)	2.8(8)	3.7(8)	-0.3(8)
N1	9.3(7)	11.5(7)	12.6(7)	-1.7(6)	-1.1(5)	0.1(6)
N2	14.1(7)	18.2(8)	14.4(7)	-1.2(6)	-0.4(6)	0.9(6)
N3	19.2(8)	17.0(8)	19.3(8)	3.4(6)	-1.4(6)	1.5(6)
O1	13.8(6)	21.5(7)	20.7(7)	-2.8(6)	-0.6(5)	5.1(5)
O2	19.1(7)	16.8(7)	20.0(6)	-6.8(5)	-2.3(5)	-1.0(5)
S1	12.0(2)	11.7(2)	13.5(2)	-2.11(16)	0.29(15)	0.96(16)

Table 4: Bond Lengths for 194.

Atom	Atom	Length/Å	Atom	Atom	Length/Å
C1	C2	1.525(2)	C6	C9	1.387(2)
C1	N1	1.497(2)	C7	N2	1.342(2)
C2	C3	1.513(2)	C8	N2	1.331(2)
C3	C4	1.513(2)	C8	N3	1.335(2)
C3	C5	1.512(2)	C9	N3	1.333(2)
C4	C5	1.512(2)	C10	S1	1.7656(19)
C5	C6	1.485(2)	N1	S1	1.6459(14)
C5	N1	1.474(2)	O1	S1	1.4362(13)
C6	C7	1.382(2)	O2	S1	1.4365(13)

Table 5: Bond Angles for 194.

Atom	Atom	Atom	Angle/°	Atom	Atom	Atom	Angle/°
N1	C1	C2	103.80(14)	N2	C7	C6	122.70(16)
C3	C2	C1	104.52(14)	N2	C8	N3	127.35(17)
C2	C3	C4	117.71(15)	N3	C9	C6	123.35(16)
C5	C3	C2	107.83(14)	C1	N1	S1	115.50(11)
C5	C3	C4	59.98(11)	C5	N1	C1	108.09(13)
C5	C4	C3	59.99(11)	C5	N1	S1	119.51(11)
C4	C5	C3	60.03(11)	C8	N2	C7	115.57(15)
C6	C5	C3	122.09(14)	C9	N3	C8	115.12(16)
C6	C5	C4	122.26(14)	N1	S1	C10	108.06(8)
N1	C5	C3	105.87(13)	O1	S1	C10	108.32(9)
N1	C5	C4	116.88(14)	O1	S1	N1	106.99(7)
N1	C5	C6	116.36(14)	O1	S1	O2	118.50(8)
C7	C6	C5	123.12(15)	O2	S1	C10	108.40(9)

Table 5: Bond Angles for 194.

Atom	Atom	Atom	Angle/°	Atom	Atom	Atom	Angle/°
C7	C6	C9	115.75(16)	O2	S1	N1	106.15(7)
C9	C6	C5	121.12(15)				

Table 6: Torsion Angles for 194.

A	B	C	D	Angle/°	A	B	C	D	Angle/°
C1	C2	C3	C4	-46.2(2)	C4	C5	C6	C9	−153.29(17)
C1	C2	C3	C5	18.67(19)	C4	C5	N1	C1	44.58(19)
C1	N1	S1	C10	-63.15(14)	C4	C5	N1	S1	-90.28(16)
C1	N1	S1	O1	−179.60(12)	C5	C6	C7	N2	177.69(15)
C1	N1	S1	O2	52.95(13)	C5	C6	C9	N3	−176.99(16)
C2	C1	N1	C5	30.98(17)	C5	N1	S1	C10	68.55(14)
C2	C1	N1	S1	167.87(11)	C5	N1	S1	O1	-47.89(14)
C2	C3	C4	C5	95.51(17)	C5	N1	S1	O2	−175.34(12)
C2	C3	C5	C4	−112.23(16)	C6	C5	N1	C1	−158.65(14)
C2	C3	C5	C6	136.33(16)	C6	C5	N1	S1	66.50(18)
C2	C3	C5	N1	0.02(18)	C6	C7	N2	C8	-0.2(2)
C3	C4	C5	C6	111.17(18)	C6	C9	N3	C8	-1.0(3)
C3	C4	C5	N1	-93.53(16)	C7	C6	C9	N3	3.7(3)
C3	C5	C6	C7	98.4(2)	C9	C6	C7	N2	-3.0(2)
C3	C5	C6	C9	-80.8(2)	N1	C1	C2	C3	-29.82(18)
C3	C5	N1	C1	-19.43(17)	N1	C5	C6	C7	−129.48(16)
C3	C5	N1	S1	−154.28(11)	N1	C5	C6	C9	51.3(2)

Table 6: Torsion Angles for 194.

A	B	C	D	Angle/°	A	B	C	D	Angle/°
C4	C3	C5	C6	−111.44(18)	N2	C8	N3	C9	-2.9(3)
C4	C3	C5	N1	112.25(15)	N3	C8	N2	C7	3.5(3)
C4	C5	C6	C7	25.9(2)					

Table 7: Hydrogen Atom Coordinates (Å×10^4) and Isotropic Displacement Parameters (Å^2×10^3) for 194.

Atom	*x*	*y*	*z*	U(eq)
H1A	8519(14)	6670(20)	7512(13)	16(5)
H1B	8074(14)	5304(19)	7828(12)	11(5)
H2A	8876(15)	4700(20)	6613(13)	18(5)
H2B	8693(15)	5980(20)	6159(13)	20(5)
H3	7314(14)	4748(19)	5554(13)	16(5)
H4A	6189(15)	3580(20)	6472(13)	18(5)
H4B	6941(15)	3807(18)	7272(12)	16(5)
H7	4627(14)	4631(19)	6318(12)	12(5)
H8	3465(15)	7500(20)	5029(13)	19(5)
H9	6318(16)	7700(20)	5700(14)	22(6)
H10A	6872(18)	5240(20)	8908(14)	28(6)
H10B	5882(15)	4870(20)	8425(13)	21(5)
H10C	5812(16)	5760(20)	9209(14)	26(6)

Experimental

Single crystals of $C_{10}H_{13}N_3O_2S$ **[194]** were **[Layered hexane on acetone]**. A suitable crystal was selected and **[oil on 200 micrometre micromount]** on a **SuperNova, Dual, Cu at home/near, Eos** diffractometer. The crystal was kept at 110.00(10) K during data collection. Using Olex2 [1], the structure was solved with the SHELXT [2] structure solution program using Intrinsic Phasing and refined with the SHELXL [3] refinement package using Least Squares minimisation.

1. Dolomanov, O.V., Bourhis, L.J., Gildea, R.J, Howard, J.A.K. & Puschmann, H. (2009), J. Appl. Cryst. 42, 339-341.
2. Sheldrick, G.M. (2015). Acta Cryst. A71, 3-8.
3. Sheldrick, G.M. (2015). Acta Cryst. C71, 3-8.

Crystal structure determination of [194]

Crystal Data for $C_{10}H_{13}N_3O_2S$ (*M* =239.29 g/mol): orthorhombic, space group Pbca (no. 61), *a* = 13.1333(4) Å, *b* = 10.4036(3) Å, *c* = 15.6547(5) Å, *V* = 2138.96(11) Å^3, *Z* = 8, *T* = 110.00(10) K, μ(Cu Kα) = 2.620 mm^{-1}, *Dcalc* = 1.486 g/cm^3, 4781 reflections measured (11.304° ≤ 2Θ ≤ 134.148°), 1917 unique (R_{int} = 0.0247, R_{sigma} = 0.0276) which were used in all calculations. The final R_1 was 0.0308 (I > 2σ(I)) and wR_2 was 0.0807 (all data).

Refinement model description

Number of restraints - 0, number of constraints - unknown.
Details:
N/A

196

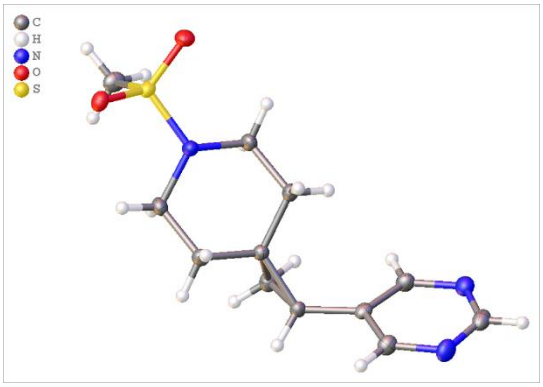

Table 1 Crystal data and structure refinement for 196.

Identification code	**196**
Empirical formula	$C_{12}H_{17}N_3O_2S$
Formula weight	267.34
Temperature/K	110.00(10)
Crystal system	orthorhombic
Space group	$Pna2_1$
a/Å	15.0120(4)
b/Å	8.3086(3)
c/Å	10.2868(3)
α/°	90
β/°	90
γ/°	90
Volume/Å^3	1283.06(7)
Z	4

ρ_{calc}g/cm^3	1.384
μ/mm^{-1}	2.241
F(000)	568.0
Crystal size/mm^3	0.33 × 0.33 × 0.246
Radiation	Cu Kα (λ = 1.54184)
2Θ range for data collection/°	11.79 to 141.53
Index ranges	-18 ≤ h ≤ 18, -8 ≤ k ≤ 9, -9 ≤ l ≤ 12
Reflections collected	2722
Independent reflections	1663 [R_{int} = 0.0191, R_{sigma} = 0.0272]
Data/restraints/parameters	1663/1/164
Goodness-of-fit on F^2	1.097
Final R indexes [I>=2σ (I)]	R_1 = 0.0285, wR_2 = 0.0722
Final R indexes [all data]	R_1 = 0.0297, wR_2 = 0.0734
Largest diff. peak/hole / e Å^{-3}	0.20/-0.36
Flack parameter	0.086(15)

Data collected and refined by Theo Tanner

Table 2: Fractional Atomic Coordinates (×10^4) and Equivalent Isotropic Displacement Parameters (Å^2×10^3) for 196. U_{eq} is defined as 1/3 of the trace of the orthogonalised U_{IJ} tensor.

Atom	*x*	*y*	*z*	U(eq)
S1	-4927.6(4)	-8803.1(7)	-4209.5(9)	16.15(16)
O1	-4030.7(12)	-8852(2)	-4699(2)	20.4(4)
O2	-5056.6(13)	-8566(3)	-2843(2)	23.2(5)
N3	-8681.2(16)	-1437(3)	-5324(2)	23.4(6)
N2	-7657.0(16)	311(3)	-6398(3)	24.0(6)
N1	-5429.0(15)	-7338(3)	-4964(2)	18.0(5)
C3	-6503.2(17)	-5158(3)	-6421(2)	15.2(6)
C9	-7240.2(19)	-989(4)	-6871(3)	20.8(6)

Table 2: Fractional Atomic Coordinates ($\times 10^4$) and Equivalent Isotropic Displacement Parameters ($Å^2 \times 10^3$) for 196. U_{eq} is defined as 1/3 of the trace of the orthogonalised U_{IJ} tensor.

Atom	*x*	*y*	*z*	U(eq)
C5	-6301.5(17)	-6816(3)	-4440(3)	19.1(6)
C11	-8247.3(17)	-2711(3)	-5824(3)	19.4(6)
C7	-7009.5(18)	-3914(3)	-7210(3)	16.2(6)
C4	-6522.1(18)	-5147(3)	-4954(3)	18.4(6)
C1	-5395.1(19)	-7387(4)	-6408(3)	19.4(6)
C10	-8357.4(18)	1(4)	-5641(3)	23.7(6)
C6	-7328.7(19)	-5642(4)	-7150(3)	21.2(6)
C2	-5612.3(17)	-5715(3)	-6941(3)	18.1(6)
C8	-7498.3(15)	-2559(3)	-6611(3)	15.2(6)
C12	-5445.9(19)	-10630(4)	-4653(3)	22.2(6)

Table 3: Anisotropic Displacement Parameters ($Å^2 \times 10^3$) for 196. The Anisotropic displacement factor exponent takes the form: $-2\pi^2[h^2a^{*2}U_{11}+2hka^*b^*U_{12}+\ldots]$.

Atom	U_{11}	U_{22}	U_{33}	U_{23}	U_{13}	U_{12}
S1	17.0(3)	15.6(3)	15.8(3)	0.4(3)	-1.6(3)	2.6(2)
O1	17.3(9)	19.2(10)	24.5(10)	-0.4(9)	-0.8(8)	3.1(8)
O2	27.4(10)	27.0(11)	15.2(10)	1.0(9)	-2.1(9)	5.7(9)
N3	22.7(11)	25.8(14)	21.8(13)	0.2(11)	-0.9(11)	5.6(11)
N2	25.7(12)	16.9(14)	29.4(14)	-2.7(11)	-2.5(11)	1.3(10)
N1	19.9(11)	19.8(13)	14.3(12)	2.5(9)	1.5(10)	5.4(10)
C3	15.7(12)	15.3(13)	14.7(14)	1.3(11)	1.0(10)	1.5(11)
C9	19.2(13)	18.6(15)	24.5(15)	0.2(12)	-1.8(12)	-0.6(11)
C5	19.5(12)	21.3(14)	16.5(15)	2.2(11)	5.4(11)	4.4(11)
C11	18.7(11)	18.4(14)	21.1(13)	2.5(12)	1.2(12)	-0.2(11)
C7	17.5(13)	15.0(14)	16.1(13)	1.9(11)	2.1(11)	2.1(11)

Table 3: Anisotropic Displacement Parameters ($Å^2×10^3$) for 196. The Anisotropic displacement factor exponent takes the form: $-2\pi^2[h^2a^{*2}U_{11}+2hka^*b^*U_{12}+\ldots]$.

Atom	U_{11}	U_{22}	U_{33}	U_{23}	U_{13}	U_{12}
C4	19.5(13)	17.9(14)	17.9(14)	0.4(11)	1.9(11)	4.5(12)
C1	21.4(12)	21.7(15)	15.2(12)	-2.4(12)	2.2(12)	4.9(12)
C10	25.9(13)	22.3(15)	22.9(15)	-5.6(13)	-7.8(13)	6.7(13)
C6	21.5(14)	17.1(15)	25.0(15)	-1.2(12)	1.0(12)	0.1(12)
C2	18.7(12)	18.9(14)	16.6(13)	1.6(11)	2.3(11)	1.3(11)
C8	14.2(11)	15.7(15)	15.7(14)	-0.2(11)	-5.3(10)	0.1(11)
C12	25.6(13)	16.9(14)	24.2(13)	0.1(12)	-3.9(12)	-4.1(12)

Table 4: Bond Lengths for 196.

Atom	Atom	Length/Å	Atom	Atom	Length/Å
S1	O1	1.4381(19)	C3	C7	1.518(4)
S1	O2	1.433(2)	C3	C4	1.510(4)
S1	N1	1.628(2)	C3	C6	1.503(4)
S1	C12	1.765(3)	C3	C2	1.513(3)
N3	C11	1.345(4)	C9	C8	1.386(4)
N3	C10	1.330(4)	C5	C4	1.521(4)
N2	C9	1.340(4)	C11	C8	1.391(4)
N2	C10	1.334(4)	C7	C6	1.515(4)
N1	C5	1.481(3)	C7	C8	1.479(3)
N1	C1	1.487(3)	C1	C2	1.529(4)

Table 5: Bond Angles for 196.

Atom	Atom	Atom	Angle/°	Atom	Atom	Atom	Angle/°
O1	S1	N1	106.70(12)	C2	C3	C7	117.5(2)

Table 5: Bond Angles for 196.

Atom	Atom	Atom	Angle/°	Atom	Atom	Atom	Angle/°
O1	S1	C12	107.31(13)	N2	C9	C8	123.9(3)
O2	S1	O1	118.30(12)	N1	C5	C4	109.5(2)
O2	S1	N1	107.59(12)	N3	C11	C8	122.8(3)
O2	S1	C12	108.21(14)	C6	C7	C3	59.40(17)
N1	S1	C12	108.41(14)	C8	C7	C3	123.0(2)
C10	N3	C11	115.9(3)	C8	C7	C6	123.2(2)
C10	N2	C9	115.1(3)	C3	C4	C5	109.7(2)
C5	N1	S1	117.03(18)	N1	C1	C2	109.0(2)
C5	N1	C1	113.7(2)	N3	C10	N2	127.2(3)
C1	N1	S1	116.1(2)	C3	C6	C7	60.40(18)
C4	C3	C7	121.4(2)	C3	C2	C1	109.9(2)
C4	C3	C2	111.8(2)	C9	C8	C11	115.1(3)
C6	C3	C7	60.19(18)	C9	C8	C7	119.8(2)
C6	C3	C4	119.0(2)	C11	C8	C7	125.1(2)
C6	C3	C2	118.1(2)				

Table 6: Torsion Angles for 196.

A	B	C	D	Angle/°	A	B	C	D	Angle/°
S1	N1	C5	C4	161.58(19)	C4	C3	C7	C6	-107.8(3)
S1	N1	C1	C2	161.62(17)	C4	C3	C7	C8	4.3(4)
O1	S1	N1	C5	-167.5(2)	C4	C3	C6	C7	111.6(3)
O1	S1	N1	C1	53.7(3)	C4	C3	C2	C1	57.0(3)
O2	S1	N1	C5	-39.6(2)	C1	N1	C5	C4	-58.7(3)
O2	S1	N1	C1	-178.4(2)	C10	N3	C11	C8	0.8(4)
N3	C11	C8	C9	-1.5(4)	C10	N2	C9	C8	-0.1(4)

Table 6: Torsion Angles for 196.

A	B	C	D	Angle/°	A	B	C	D	Angle/°
N3	C11	C8	C7	-178.5(3)	C6	C3	C7	C8	112.0(3)
N2	C9	C8	C11	1.1(4)	C6	C3	C4	C5	86.2(3)
N2	C9	C8	C7	178.3(2)	C6	C3	C2	C1	-86.7(3)
N1	C5	C4	C3	56.1(3)	C6	C7	C8	C9	-170.2(3)
N1	C1	C2	C3	-55.6(3)	C6	C7	C8	C11	6.6(4)
C3	C7	C8	C9	117.3(3)	C2	C3	C7	C6	108.3(3)
C3	C7	C8	C11	-65.9(4)	C2	C3	C7	C8	-139.7(3)
C9	N2	C10	N3	-0.6(4)	C2	C3	C4	C5	-57.1(3)
C5	N1	C1	C2	58.3(3)	C2	C3	C6	C7	-107.3(3)
C11	N3	C10	N2	0.3(5)	C8	C7	C6	C3	-111.6(3)
C7	C3	C4	C5	157.1(2)	C12	S1	N1	C5	77.2(2)
C7	C3	C2	C1	-155.7(2)	C12	S1	N1	C1	-61.6(3)

Table 7: Hydrogen Atom Coordinates (Å×10^4) and Isotropic Displacement Parameters (Å^2×10^3) for 196.

Atom	*x*	*y*	*z*	U(eq)
H9	-6748.55	-829.57	-7405.79	25
H5A	-6279.58	-6795.3	-3498.17	23
H5B	-6760.75	-7570.86	-4702.08	23
H11	-8457.19	-3737.54	-5635.58	23
H7	-6719.28	-3634.6	-8033.09	19
H4A	-7108.26	-4825.95	-4653.66	22
H4B	-6091.72	-4375.37	-4628.09	22
H1A	-5822.78	-8164.46	-6732.81	23
H1B	-4805.94	-7713.19	-6691.99	23
H10	-8651.93	888.16	-5296.07	28

Table 7: Hydrogen Atom Coordinates (Å×10^4) and Isotropic Displacement Parameters (Å^2×10^3) for 196.

Atom	*x*	*y*	*z*	U(eq)
H6A	-7861.05	-5867.5	-6647.5	25
H6B	-7255.5	-6300.62	-7921.24	25
H2A	-5151.39	-4961.52	-6684.24	22
H2B	-5630.8	-5750.87	-7883.12	22
H12A	-5136.26	-11512.61	-4255.64	33
H12B	-5429.24	-10747.38	-5581.4	33
H12C	-6053.9	-10622.11	-4364.34	33

Experimental

Single crystals of $C_{12}H_{17}N_3O_2S$ **[196]** were **[Acetone/hexane layering]**. A suitable crystal was selected and **[oil on 200um mount]** on a **SuperNova, Dual, Cu at home/near, Eos** diffractometer. The crystal was kept at 110.00(10) K during data collection. Using Olex2 [1], the structure was solved with the SHELXT [2] structure solution program using Intrinsic Phasing and refined with the SHELXL [3] refinement package using Least Squares minimisation.

1. Dolomanov, O.V., Bourhis, L.J., Gildea, R.J, Howard, J.A.K. & Puschmann, H. (2009), J. Appl. Cryst. 42, 339-341.
2. Sheldrick, G.M. (2015). Acta Cryst. A71, 3-8.
3. Sheldrick, G.M. (2015). Acta Cryst. C71, 3-8.

Crystal structure determination of [**196**]

Crystal Data for $C_{12}H_{17}N_3O_2S$ (*M* =267.34 g/mol): orthorhombic, space group $Pna2_1$ (no. 33), *a* = 15.0120(4) Å, *b* = 8.3086(3) Å, *c* = 10.2868(3) Å, *V* = 1283.06(7) Å^3, *Z* = 4, *T* = 110.00(10) K, μ(Cu Kα) = 2.241 mm^{-1}, *Dcalc* = 1.384 g/cm^3, 2722 reflections measured (11.79° ≤ 2Θ ≤ 141.53°), 1663 unique (R_{int} = 0.0191, R_{sigma} = 0.0272) which were used in all calculations. The final R_1 was 0.0285 (I > 2σ(I)) and wR_2 was 0.0734 (all data).

Refinement model description

Number of restraints - 1, number of constraints - unknown.
Details:

```
1. Fixed Uiso
 At 1.2 times of:
  All C(H) groups, All C(H,H) groups
 At 1.5 times of:
  All C(H,H,H) groups
2.a Ternary CH refined with riding coordinates:
 C7(H7)
2.b Secondary CH2 refined with riding coordinates:
 C5(H5A,H5B), C4(H4A,H4B), C1(H1A,H1B), C6(H6A,H6B), C2(H2A,H2B)
2.c Aromatic/amide H refined with riding coordinates:
 C9(H9), C11(H11), C10(H10)
2.d Idealised Me refined as rotating group:
 C12(H12A,H12B,H12C)
```

197

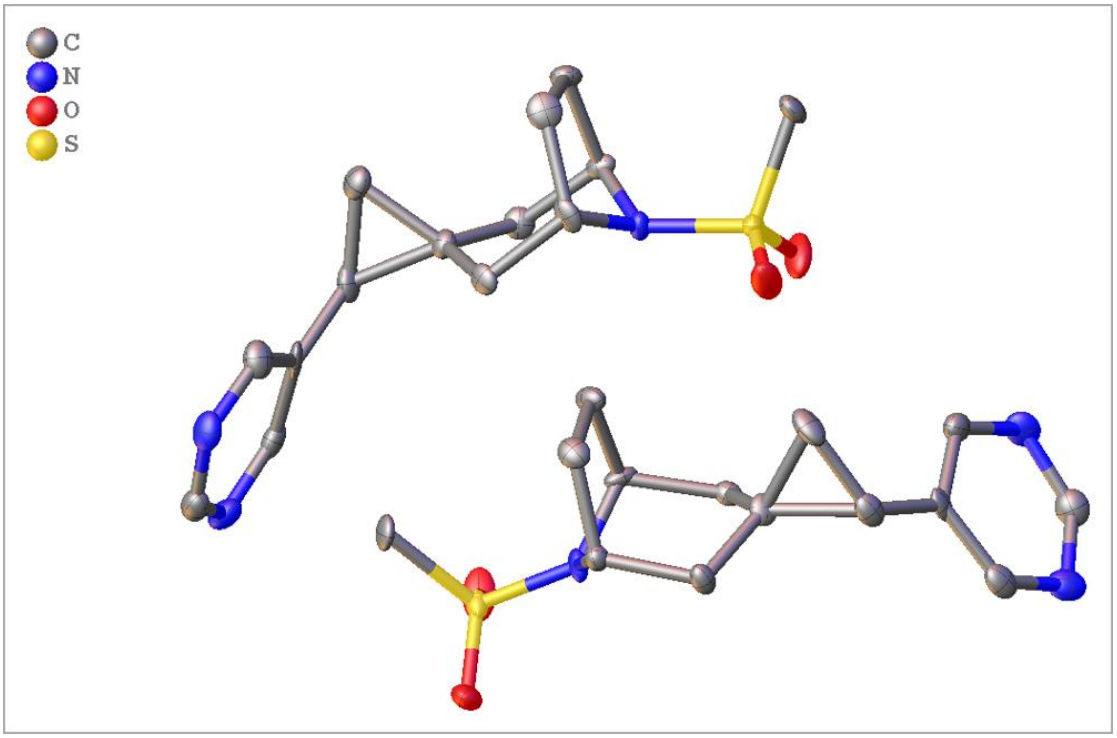

Table 1: Crystal data and structure refinement for 197.

Identification code	**197**
Empirical formula	$C_{14}H_{19}N_3O_2S$
Formula weight	293.38
Temperature/K	110.05(10)
Crystal system	orthorhombic
Space group	$Pna2_1$
a/Å	21.4998(8)
b/Å	5.94886(17)
c/Å	21.8797(9)
α/°	90
β/°	90
γ/°	90
Volume/Å^3	2798.39(17)
Z	8
ρ_{calc}g/cm^3	1.393

μ/mm^{-1}	2.106
F(000)	1248.0
Crystal size/mm^3	0.179 × 0.08 × 0.032
Radiation	Cu Kα (λ = 1.54184)
2Θ range for data collection/°	8.082 to 134.16
Index ranges	-25 ≤ h ≤ 24, -7 ≤ k ≤ 7, -12 ≤ l ≤ 26
Reflections collected	8921
Independent reflections	3577 [R_{int} = 0.0479, R_{sigma} = 0.0492]
Data/restraints/parameters	3577/1/364
Goodness-of-fit on F^2	1.029
Final R indexes [I>=2σ (I)]	R_1 = 0.0692, wR_2 = 0.1846
Final R indexes [all data]	R_1 = 0.0713, wR_2 = 0.1869
Largest diff. peak/hole / e $Å^{-3}$	1.59/-0.37
Flack parameter	0.23(5)

Data collected, solved, and refined by Adrian C Whitwood

Refinement Special Details

The crystals exhibited racemic twinning with a refined ratio of 0.77:0.23(5) of the two components. There was noticeable smearing of reflections along the c-axis, indicative of further twinning which could not be resolved. This is believed to be responsible for the large residual density peaks.

Table 2: Fractional Atomic Coordinates (×10^4) and Equivalent Isotropic Displacement Parameters ($Å^2$×10^3) for 197. U_{eq} is defined as 1/3 of the trace of the orthogonalised U_{IJ} tensor.

Atom	*x*	*y*	*z*	U(eq)
C1	5794(3)	7456(12)	5523(3)	18.1(14)
C2	5654(4)	9816(12)	5736(3)	23.0(16)
C3	5173(3)	9546(11)	6269(3)	18.0(15)

Table 2: Fractional Atomic Coordinates ($\times 10^4$) and Equivalent Isotropic Displacement Parameters ($Å^2 \times 10^3$) for 197. U_{eq} is defined as 1/3 of the trace of the orthogonalised U_{IJ} tensor.

Atom	*x*	*y*	*z*	U(eq)
C4	5072(3)	6986(11)	6327(3)	15.5(14)
C5	5549(3)	5903(11)	6744(3)	19.4(15)
C6	6210(3)	6530(11)	6558(3)	16.3(14)
C7	6330(3)	6332(12)	5883(3)	17.4(14)
C8	6529(3)	8362(12)	6907(3)	21.3(15)
C9	6722(3)	5939(12)	7028(4)	22.1(16)
C10	7331(3)	4983(14)	6857(3)	20.7(15)
C11	7520(3)	2980(12)	7105(3)	20.5(15)
C12	8429(3)	3068(12)	6628(4)	23.7(16)
C13	7778(3)	6002(13)	6484(4)	24.0(16)
C14	4215(3)	8118(11)	5105(4)	21.4(15)
N1	5226(2)	6160(9)	5696(3)	16.2(12)
N2	8051(3)	1952(10)	7004(3)	25.1(14)
N3	8331(3)	5074(11)	6364(3)	24.2(14)
O1	4964(3)	5155(11)	4636(3)	39.3(15)
O2	4272(3)	4044(9)	5486(3)	35.7(15)
S1	4671.0(8)	5684(3)	5204.4(9)	20.2(4)
C15	6487(3)	2536(10)	4403(3)	16.8(14)
C16	6642(3)	4980(11)	4210(4)	19.5(15)
C17	7121(3)	4739(11)	3687(4)	20.1(15)
C18	7203(3)	2173(11)	3605(3)	15.3(14)
C19	6716(3)	1200(12)	3168(3)	17.4(14)
C20	6061(3)	1850(11)	3363(3)	17.2(14)
C21	5940(3)	1547(11)	4040(3)	14.0(13)
C22	5740(3)	3770(13)	3039(4)	25.0(16)

Table 2: Fractional Atomic Coordinates ($\times 10^4$) and Equivalent Isotropic Displacement Parameters ($Å^2 \times 10^3$) for 197. U_{eq} is defined as 1/3 of the trace of the orthogonalised U_{IJ} tensor.

Atom	*x*	*y*	*z*	U(eq)
C23	5538(3)	1387(12)	2909(3)	20.1(15)
C24	4929(3)	434(12)	3092(3)	17.8(14)
C25	4763(4)	-1685(13)	2888(3)	22.6(16)
C26	3859(4)	-1578(13)	3408(4)	26.1(16)
C27	4489(3)	1473(12)	3466(3)	21.3(15)
C28	8019(3)	3112(12)	4863(3)	20.8(16)
N4	7045(3)	1239(10)	4218(3)	16.9(13)
N5	4239(3)	-2720(10)	3028(3)	25.3(14)
N6	3952(3)	473(10)	3621(3)	23.9(14)
O3	7282(3)	11(10)	5261(3)	34.7(14)
O4	7992(3)	-899(8)	4404(3)	33.1(14)
S2	7589.4(7)	672(2)	4706.4(9)	17.0(4)

Table 3: Anisotropic Displacement Parameters ($Å^2 \times 10^3$) for 197. The Anisotropic displacement factor exponent takes the form: $-2\pi^2[h^2a^{*2}U_{11}+2hka^*b^*U_{12}+\ldots]$.

Atom	U_{11}	U_{22}	U_{33}	U_{23}	U_{13}	U_{12}
C1	10(3)	30(3)	15(3)	4(3)	4(3)	2(3)
C2	26(4)	28(4)	15(4)	9(3)	4(3)	-3(3)
C3	21(3)	15(3)	18(4)	-3(3)	2(3)	5(3)
C4	16(3)	12(3)	18(4)	-1(3)	6(3)	-3(2)
C5	20(3)	23(3)	15(3)	2(3)	4(3)	-2(3)
C6	15(3)	16(3)	18(4)	0(3)	-1(3)	-4(3)
C7	9(3)	21(3)	22(4)	3(3)	4(3)	-3(3)
C8	17(3)	23(3)	23(4)	-3(3)	1(3)	-6(3)
C9	19(3)	33(4)	14(4)	1(3)	-6(3)	-4(3)

Table 3: Anisotropic Displacement Parameters ($Å^2 \times 10^3$) for 197. The Anisotropic displacement factor exponent takes the form: $-2\pi^2[h^2a^{*2}U_{11}+2hka^*b^*U_{12}+\ldots]$.

Atom	U_{11}	U_{22}	U_{33}	U_{23}	U_{13}	U_{12}
C10	10(3)	35(4)	17(4)	-10(3)	-4(3)	-7(3)
C11	23(3)	25(3)	14(3)	-4(3)	-2(3)	-10(3)
C12	17(3)	27(3)	27(4)	-9(3)	0(3)	0(3)
C13	23(4)	30(4)	18(4)	4(3)	-3(3)	-3(3)
C14	17(3)	26(3)	21(4)	-3(3)	-6(3)	9(3)
N1	11(3)	21(3)	16(3)	-5(3)	-2(2)	0(2)
N2	27(3)	20(3)	28(4)	-8(3)	1(3)	-4(3)
N3	18(3)	32(3)	22(3)	0(3)	2(3)	-9(3)
O1	27(3)	56(3)	35(4)	-29(3)	-10(3)	16(3)
O2	29(3)	28(3)	50(4)	9(3)	-17(3)	-15(2)
S1	16.0(8)	17.0(7)	27.8(10)	-9.1(7)	-9.0(7)	4.6(6)
C15	29(4)	9(3)	13(3)	-2(3)	1(3)	1(3)
C16	13(3)	16(3)	29(4)	-2(3)	4(3)	0(3)
C17	20(3)	18(3)	22(4)	7(3)	2(3)	-2(3)
C18	14(3)	17(3)	14(3)	-1(3)	-2(3)	1(3)
C19	14(3)	26(3)	12(3)	-2(3)	-1(3)	4(3)
C20	20(3)	20(3)	11(3)	6(3)	-2(3)	-1(3)
C21	14(3)	14(3)	14(3)	3(3)	2(3)	1(2)
C22	18(3)	29(3)	28(4)	15(3)	-2(3)	4(3)
C23	19(3)	30(3)	11(3)	1(3)	-1(3)	5(3)
C24	13(3)	31(4)	10(3)	-1(3)	-5(3)	5(3)
C25	22(4)	33(4)	13(4)	2(3)	-2(3)	7(3)
C26	24(4)	32(4)	22(4)	3(3)	2(3)	0(3)
C27	23(3)	22(3)	19(4)	-4(3)	-6(3)	3(3)
C28	11(3)	25(3)	26(4)	-2(3)	-4(3)	-8(3)
N4	11(3)	22(3)	19(3)	4(3)	-5(2)	-4(2)

Table 3: Anisotropic Displacement Parameters ($Å^2×10^3$) for 197. The Anisotropic displacement factor exponent takes the form: $-2\pi^2[h^2a^{*2}U_{11}+2hka^*b^*U_{12}+\ldots]$.

Atom	U_{11}	U_{22}	U_{33}	U_{23}	U_{13}	U_{12}
N5	33(3)	24(3)	19(3)	4(3)	1(3)	7(3)
N6	23(3)	33(3)	15(3)	-4(3)	6(3)	5(3)
O3	35(3)	42(3)	27(3)	22(3)	-8(3)	-20(3)
O4	28(3)	25(3)	46(4)	-13(3)	-17(3)	14(2)
S2	15.1(7)	14.1(7)	21.9(8)	3.5(7)	-7.4(7)	-2.7(6)

Table 4: Bond Lengths for 197.

Atom	Atom	Length/Å	Atom	Atom	Length/Å
C1	C2	1.510(10)	C15	C16	1.550(9)
C1	C7	1.548(9)	C15	C21	1.536(9)
C1	N1	1.494(8)	C15	N4	1.483(8)
C2	C3	1.566(9)	C16	C17	1.547(10)
C3	C4	1.544(9)	C17	C18	1.547(9)
C4	C5	1.516(10)	C18	C19	1.532(9)
C4	N1	1.502(8)	C18	N4	1.491(9)
C5	C6	1.525(9)	C19	C20	1.521(9)
C6	C7	1.504(10)	C20	C21	1.516(9)
C6	C8	1.498(9)	C20	C22	1.511(9)
C6	C9	1.546(9)	C20	C23	1.524(9)
C8	C9	1.523(10)	C22	C23	1.509(10)
C9	C10	1.476(10)	C23	C24	1.482(10)
C10	C11	1.371(11)	C24	C25	1.384(11)
C10	C13	1.399(10)	C24	C27	1.396(10)
C11	N2	1.314(9)	C25	N5	1.320(10)
C12	N2	1.334(10)	C26	N5	1.349(10)

Table 4: Bond Lengths for 197.

Atom	Atom	Length/Å	Atom	Atom	Length/Å
C12	N3	1.342(10)	C26	N6	1.321(10)
C13	N3	1.338(10)	C27	N6	1.342(10)
C14	S1	1.761(6)	C28	S2	1.754(7)
N1	S1	1.631(6)	N4	S2	1.620(6)
O1	S1	1.430(7)	O3	S2	1.437(6)
O2	S1	1.438(6)	O4	S2	1.436(6)

Table 5: Bond Angles for 197.

Atom	Atom	Atom	Angle/°	Atom	Atom	Atom	Angle/°
C2	C1	C7	113.1(6)	C21	C15	C16	112.6(5)
N1	C1	C2	103.8(5)	N4	C15	C16	103.9(5)
N1	C1	C7	104.9(5)	N4	C15	C21	106.2(5)
C1	C2	C3	105.5(5)	C17	C16	C15	105.0(5)
C4	C3	C2	104.8(5)	C18	C17	C16	104.6(5)
C5	C4	C3	112.0(6)	C19	C18	C17	111.6(6)
N1	C4	C3	102.5(5)	N4	C18	C17	103.8(6)
N1	C4	C5	105.4(5)	N4	C18	C19	105.4(5)
C4	C5	C6	111.4(6)	C20	C19	C18	111.2(5)
C5	C6	C9	115.5(6)	C19	C20	C23	117.0(6)
C7	C6	C5	113.8(6)	C21	C20	C19	113.7(6)
C7	C6	C9	120.8(6)	C21	C20	C23	119.3(6)
C8	C6	C5	117.9(6)	C22	C20	C19	118.9(6)
C8	C6	C7	118.6(6)	C22	C20	C21	118.1(6)
C8	C6	C9	60.0(5)	C22	C20	C23	59.6(5)
C6	C7	C1	109.8(5)	C20	C21	C15	109.2(5)

Table 5: Bond Angles for 197.

Atom	Atom	Atom	Angle/°	Atom	Atom	Atom	Angle/°
C6	C8	C9	61.6(4)	C23	C22	C20	60.6(5)
C8	C9	C6	58.4(4)	C22	C23	C20	59.7(4)
C10	C9	C6	123.4(6)	C24	C23	C20	122.9(6)
C10	C9	C8	124.2(6)	C24	C23	C22	124.2(6)
C11	C10	C9	119.8(7)	C25	C24	C23	119.3(7)
C11	C10	C13	113.9(6)	C25	C24	C27	114.6(7)
C13	C10	C9	126.2(7)	C27	C24	C23	126.0(7)
N2	C11	C10	126.5(7)	N5	C25	C24	124.8(7)
N2	C12	N3	127.7(6)	N6	C26	N5	126.2(7)
N3	C13	C10	123.1(7)	N6	C27	C24	122.3(6)
C1	N1	C4	104.1(5)	C15	N4	C18	103.6(5)
C1	N1	S1	121.4(5)	C15	N4	S2	120.9(5)
C4	N1	S1	120.1(4)	C18	N4	S2	120.4(4)
C11	N2	C12	113.7(6)	C25	N5	C26	115.1(7)
C13	N3	C12	115.0(6)	C26	N6	C27	116.8(6)
N1	S1	C14	110.2(3)	N4	S2	C28	109.7(3)
O1	S1	C14	108.5(4)	O3	S2	C28	107.6(4)
O1	S1	N1	106.8(3)	O3	S2	N4	106.4(3)
O1	S1	O2	119.1(4)	O4	S2	C28	108.1(3)
O2	S1	C14	106.2(3)	O4	S2	N4	105.6(3)
O2	S1	N1	105.8(3)	O4	S2	O3	119.2(4)

Table 6: Torsion Angles for 197.

A	B	C	D	Angle/°	A	B	C	D	Angle/°
C1	C2	C3	C4	0.4(7)	C15	C16	C17	C18	0.8(7)

Table 6: Torsion Angles for 197.

A	B	C	D	Angle/°	A	B	C	D	Angle/°
C1	N1	S1	C14	-76.9(6)	C15	N4	S2	C28	-73.4(6)
C1	N1	S1	O1	40.8(6)	C15	N4	S2	O3	42.8(6)
C1	N1	S1	O2	168.7(5)	C15	N4	S2	O4	170.4(5)
C2	C1	C7	C6	51.1(7)	C16	C15	C21	C20	51.7(7)
C2	C1	N1	C4	-42.9(6)	C16	C15	N4	C18	-42.2(6)
C2	C1	N1	S1	96.6(6)	C16	C15	N4	S2	96.6(6)
C2	C3	C4	C5	86.8(7)	C16	C17	C18	C19	86.8(7)
C2	C3	C4	N1	-25.8(7)	C16	C17	C18	N4	-26.2(7)
C3	C4	C5	C6	-52.1(8)	C17	C18	C19	C20	-53.1(8)
C3	C4	N1	C1	42.6(6)	C17	C18	N4	C15	42.8(6)
C3	C4	N1	S1	-97.5(6)	C17	C18	N4	S2	-96.2(6)
C4	C5	C6	C7	-46.2(8)	C18	C19	C20	C21	-45.8(8)
C4	C5	C6	C8	99.6(7)	C18	C19	C20	C22	100.2(7)
C4	C5	C6	C9	167.6(6)	C18	C19	C20	C23	168.7(6)
C4	N1	S1	C14	56.3(6)	C18	N4	S2	C28	58.7(6)
C4	N1	S1	O1	174.0(5)	C18	N4	S2	O3	174.8(5)
C4	N1	S1	O2	-58.1(6)	C18	N4	S2	O4	-57.6(6)
C5	C4	N1	C1	-74.8(6)	C19	C18	N4	C15	-74.6(6)
C5	C4	N1	S1	145.1(5)	C19	C18	N4	S2	146.4(5)
C5	C6	C7	C1	46.9(8)	C19	C20	C21	C15	46.2(7)
C5	C6	C8	C9	104.8(7)	C19	C20	C22	C23	106.1(7)
C5	C6	C9	C8	-108.9(7)	C19	C20	C23	C22	-109.3(7)
C5	C6	C9	C10	138.4(7)	C19	C20	C23	C24	137.3(7)
C6	C8	C9	C10	111.4(8)	C20	C22	C23	C24	111.3(8)
C6	C9	C10	C11	-123.3(8)	C20	C23	C24	C25	-114.1(8)
C6	C9	C10	C13	61.4(10)	C20	C23	C24	C27	65.5(10)

Table 6: Torsion Angles for 197.

A	B	C	D	Angle/°	A	B	C	D	Angle/°
C7	C1	C2	C3	-87.7(6)	C21	C15	C16	C17	-89.5(7)
C7	C1	N1	C4	76.1(6)	C21	C15	N4	C18	76.8(6)
C7	C1	N1	S1	-144.5(5)	C21	C15	N4	S2	-144.5(5)
C7	C6	C8	C9	-111.0(7)	C21	C20	C22	C23	-109.3(7)
C7	C6	C9	C8	107.4(7)	C21	C20	C23	C22	107.2(7)
C7	C6	C9	C10	-5.2(10)	C21	C20	C23	C24	-6.2(10)
C8	C6	C7	C1	-98.7(7)	C22	C20	C21	C15	-100.2(7)
C8	C6	C9	C10	-112.7(8)	C22	C20	C23	C24	-113.4(8)
C8	C9	C10	C11	164.7(7)	C22	C23	C24	C25	172.5(7)
C8	C9	C10	C13	-10.6(12)	C22	C23	C24	C27	-7.9(11)
C9	C6	C7	C1	-168.9(6)	C23	C20	C21	C15	-169.2(6)
C9	C10	C11	N2	-178.8(7)	C23	C24	C25	N5	178.9(7)
C9	C10	C13	N3	177.5(7)	C23	C24	C27	N6	-178.6(7)
C10	C11	N2	C12	1.3(11)	C24	C25	N5	C26	-1.4(11)
C10	C13	N3	C12	0.4(11)	C24	C27	N6	C26	0.9(11)
C11	C10	C13	N3	1.9(11)	C25	C24	C27	N6	1.0(11)
C13	C10	C11	N2	-2.9(11)	C27	C24	C25	N5	-0.7(11)
N1	C1	C2	C3	25.4(7)	N4	C15	C16	C17	25.0(7)
N1	C1	C7	C6	-61.3(7)	N4	C15	C21	C20	-61.3(7)
N1	C4	C5	C6	58.6(7)	N4	C18	C19	C20	58.9(7)
N2	C12	N3	C13	-2.4(12)	N5	C26	N6	C27	-3.3(12)
N3	C12	N2	C11	1.6(11)	N6	C26	N5	C25	3.6(12)

Table 7: Hydrogen Atom Coordinates (Å×10^4) and Isotropic Displacement Parameters (Å^2×10^3) for 197.

Atom	*x*	*y*	*z*	U(eq)
H1	5870.28	7403.32	5072.08	22
H2A	5475.42	10721.2	5399.66	28
H2B	6037.08	10563.95	5884.21	28
H3A	5339.45	10178.54	6653.81	22
H3B	4777.61	10316.61	6168.38	22
H4	4636.69	6604.95	6448.58	19
H5A	5500.86	4249.16	6729.05	23
H5B	5473.98	6395.55	7170.21	23
H7A	6361.47	4726.82	5767.66	21
H7B	6729.33	7071.86	5780.28	21
H8A	6287.82	9142.84	7228.74	26
H8B	6824.74	9331.82	6681.35	26
H9	6553.91	5324.69	7419.77	27
H11	7238.55	2263.52	7377.83	25
H12	8813.6	2357.54	6535.14	28
H13	7683.4	7419.05	6306.31	29
H14A	4475.15	9329.48	4940.48	32
H14B	4041.79	8579.88	5499.14	32
H14C	3876.06	7797.19	4818.57	32
H15	6413.01	2427.49	4853.13	20
H16A	6264.26	5768.67	4066.12	23
H16B	6822.13	5828.56	4556.95	23
H17A	6963.52	5436.29	3306.23	24
H17B	7521	5456.21	3798.07	24
H18	7635.51	1771.83	3478.42	18
H19A	6794.71	1764.84	2749.3	21

Table 7: Hydrogen Atom Coordinates (Å×10^4) and Isotropic Displacement Parameters (Å^2×10^3) for 197.

Atom	*x*	*y*	*z*	U(eq)
H19B	6752.44	-458.76	3160.2	21
H21A	5894.18	-70.97	4135.92	17
H21B	5549.48	2320.35	4155.64	17
H22A	5455.89	4727.95	3282.01	30
H22B	5975.13	4572.33	2716.98	30
H23	5690.09	809.69	2506.17	24
H25	5046.59	-2450.36	2628.14	27
H26	3490.25	-2320.28	3535.75	31
H27	4572.54	2940.64	3616.24	26
H28A	8381.68	2723.6	5113.26	31
H28B	7757.1	4183.55	5085.89	31
H28C	8157.85	3790.5	4478.86	31

endo-**220**

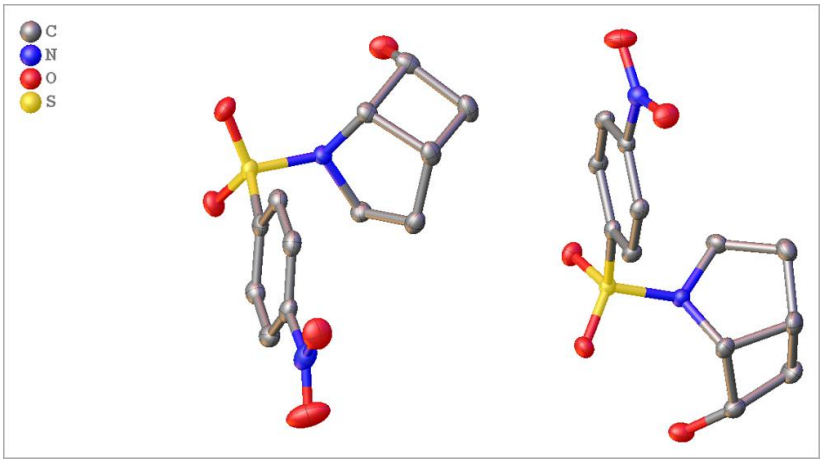

Table 1: Crystal data and structure refinement for *endo*-220.

Identification code	*endo*-**220**
Empirical formula	$C_{12}H_{14}N_2O_5S$

Formula weight	298.31
Temperature/K	110.00(10)
Crystal system	triclinic
Space group	P-1
a/Å	7.22716(15)
b/Å	13.1629(3)
c/Å	14.1120(3)
α/°	104.679(2)
β/°	90.8277(18)
γ/°	96.2347(18)
Volume/Å^3	1289.75(5)
Z	4
ρ_{calc}g/cm^3	1.536
μ/mm^{-1}	2.458
F(000)	624.0
Crystal size/mm^3	0.284 × 0.217 × 0.037
Radiation	Cu Kα (λ = 1.54184)
2Θ range for data collection/°	6.99 to 134.158
Index ranges	-8 ≤ h ≤ 6, -15 ≤ k ≤ 15, -14 ≤ l ≤ 16
Reflections collected	12385
Independent reflections	4607 [R_{int} = 0.0261, R_{sigma} = 0.0297]
Data/restraints/parameters	4607/0/473
Goodness-of-fit on F^2	1.053
Final R indexes [I>=2σ (I)]	R_1 = 0.0296, wR_2 = 0.0779
Final R indexes [all data]	R_1 = 0.0322, wR_2 = 0.0795
Largest diff. peak/hole / e Å^{-3}	0.33/-0.35

Data collected, solved, and refined by Adrian C Whitwood

Table 2: Fractional Atomic Coordinates ($\times 10^4$) and Equivalent Isotropic Displacement Parameters ($Å^2 \times 10^3$) for *endo*-220. U_{eq} is defined as 1/3 of the trace of the orthogonalised U_{IJ} tensor.

Atom	*x*	*y*	*z*	U(eq)
C1	4872(2)	4063.4(12)	2884.7(11)	19.7(3)
C2	5139(2)	3333.8(13)	3549.6(12)	22.6(3)
C3	3170(2)	3013.2(13)	3825.4(11)	21.7(3)
C4	2244(3)	3886.0(14)	4545.9(12)	27.5(4)
C5	801(2)	3897.0(12)	3737.4(12)	22.4(3)
C6	1866(2)	3114.6(12)	2974.3(11)	18.4(3)
C7	4413(2)	1943.3(12)	1115.8(10)	19.2(3)
C8	3531(2)	1006.0(12)	1270.4(11)	21.3(3)
C9	4571(2)	190.6(13)	1301.3(11)	22.4(3)
C10	6470(2)	336.3(12)	1175.7(11)	21.8(3)
C11	7365(2)	1251.5(13)	1002.0(11)	23.2(3)
C12	6315(2)	2065.0(13)	969.8(11)	21.5(3)
N1	3054.9(16)	3619.5(10)	2345.3(9)	17.2(3)
N2	7591(2)	-517.0(11)	1245.1(10)	27.6(3)
O1	539.9(17)	4877.8(9)	3546.6(9)	26.8(3)
O2	4133.9(16)	3744.8(9)	724.9(8)	25.2(2)
O3	1228.0(15)	2600.6(9)	852.2(8)	25.9(2)
O4	6775.6(19)	-1350.6(10)	1328.0(10)	36.0(3)
O5	9280.8(18)	-348.7(11)	1232.1(13)	49.8(4)
S1	3100.7(5)	3028.1(3)	1185.9(2)	18.61(10)
C13	6720(2)	3748.7(12)	7942.7(11)	20.1(3)
C14	7026(2)	3448.1(14)	8901.0(12)	24.6(3)
C15	9026(2)	3182.1(13)	8872.2(11)	23.8(3)
C16	10613(2)	4085.8(14)	8898.4(12)	26.7(4)
C17	11289(2)	3414.7(12)	7933.7(11)	21.2(3)

Table 2: Fractional Atomic Coordinates ($\times 10^4$) and Equivalent Isotropic Displacement Parameters ($Å^2 \times 10^3$) for *endo*-220. U_{eq} is defined as 1/3 of the trace of the orthogonalised U_{IJ} tensor.

Atom	*x*	*y*	*z*	U(eq)
C18	9394(2)	2703.3(12)	7780.2(11)	18.3(3)
C19	5465(2)	1558.8(11)	6144.9(10)	16.1(3)
C20	5933(2)	593.3(12)	6259.7(11)	18.0(3)
C21	4529(2)	-187.0(12)	6317.7(10)	17.7(3)
C22	2696(2)	16.7(11)	6243.4(10)	17.1(3)
C23	2213(2)	954.8(12)	6093.1(11)	18.3(3)
C24	3622(2)	1743.6(12)	6053.6(11)	18.5(3)
N3	7969.2(16)	3105.4(10)	7262.3(9)	16.5(3)
N4	1194.4(17)	-783.2(10)	6363.8(9)	19.8(3)
O6	11936.5(15)	3893.6(9)	7200.8(8)	24.1(2)
O7	6487.3(15)	3359.7(8)	5780.0(8)	21.2(2)
O8	8805.1(14)	2070.0(8)	5652.0(7)	20.5(2)
O9	1639.1(16)	-1541.5(9)	6632.9(9)	27.2(3)
O10	-418.5(15)	-647.2(9)	6205.0(10)	31.2(3)
S2	7294.5(5)	2571.5(3)	6143.4(2)	15.26(10)

Table 3: Anisotropic Displacement Parameters ($Å^2 \times 10^3$) for *endo*-220. The Anisotropic displacement factor exponent takes the form: $-2\pi^2[h^2a^{*2}U_{11}+2hka^*b^*U_{12}+\ldots]$.

Atom	U_{11}	U_{22}	U_{33}	U_{23}	U_{13}	U_{12}
C1	18.1(7)	19.7(8)	20.0(7)	4.4(6)	-0.7(6)	-1.4(6)
C2	24.4(8)	23.2(8)	20.5(8)	4.9(6)	-2.6(6)	6.1(6)
C3	29.0(8)	19.6(8)	19.9(7)	9.2(6)	3.3(6)	6.9(6)
C4	37.2(9)	28.1(9)	20.2(8)	8.0(7)	7.3(7)	10.7(7)
C5	23.0(8)	18.4(7)	28.7(8)	10.0(6)	8.8(6)	4.7(6)

Table 3: Anisotropic Displacement Parameters ($Å^2×10^3$) for *endo*-220. The Anisotropic displacement factor exponent takes the form: $-2\pi^2[h^2a^{*2}U_{11}+2hka^*b^*U_{12}+\ldots]$.

Atom	U_{11}	U_{22}	U_{33}	U_{23}	U_{13}	U_{12}
C6	19.8(7)	16.3(7)	20.7(7)	7.8(6)	3.4(6)	1.4(6)
C7	24.9(7)	19.5(7)	12.4(6)	2.6(6)	-0.7(5)	3.2(6)
C8	22.8(8)	22.9(8)	17.0(7)	4.2(6)	0.0(6)	-0.1(6)
C9	29.4(8)	20.0(8)	16.9(7)	4.6(6)	-2.2(6)	-0.8(6)
C10	27.3(8)	21.3(7)	15.9(7)	2.1(6)	-3.9(6)	5.4(6)
C11	22.8(8)	25.0(8)	19.8(7)	2.4(6)	-0.5(6)	2.3(6)
C12	25.2(8)	20.4(8)	17.6(7)	3.6(6)	1.2(6)	-0.5(6)
N1	16.7(6)	18.7(6)	17.1(6)	7.0(5)	1.4(5)	0.5(5)
N2	33.7(8)	22.9(7)	24.3(7)	1.8(6)	-6.6(6)	6.4(6)
O1	25.7(6)	19.4(6)	38.8(7)	12.0(5)	3.8(5)	6.5(5)
O2	31.6(6)	26.0(6)	22.0(5)	12.5(5)	5.5(5)	5.5(5)
O3	24.8(6)	30.1(6)	22.7(5)	7.4(5)	-6.5(4)	2.7(5)
O4	46.3(7)	25.5(6)	41.0(7)	15.0(5)	2.1(6)	8.9(5)
O5	28.5(7)	33.0(7)	87.1(12)	13.2(7)	-8.9(7)	7.4(6)
S1	20.91(18)	20.74(19)	15.41(18)	6.62(14)	-0.26(13)	3.17(14)
C13	18.3(7)	20.7(8)	20.2(7)	2.0(6)	2.9(6)	5.0(6)
C14	25.2(8)	28.3(8)	19.9(8)	6.4(7)	5.1(6)	0.4(7)
C15	27.0(8)	29.5(8)	17.1(7)	10.0(7)	-0.4(6)	2.8(7)
C16	22.7(8)	31.5(9)	22.1(8)	1.7(7)	-3.9(6)	-1.3(7)
C17	18.0(7)	23.5(8)	23.5(8)	8.6(6)	-0.9(6)	2.2(6)
C18	19.4(7)	18.4(8)	18.9(7)	7.7(6)	-2.0(6)	3.8(6)
C19	19.1(7)	16.1(7)	12.5(6)	2.6(5)	-0.6(5)	2.2(5)
C20	16.4(7)	19.5(7)	18.6(7)	4.4(6)	-1.2(5)	5.4(6)
C21	21.2(7)	15.4(7)	17.5(7)	4.7(6)	-0.9(5)	5.3(6)
C22	18.4(7)	17.3(7)	14.7(7)	2.4(5)	0.6(5)	1.8(5)

Table 3: Anisotropic Displacement Parameters ($Å^2×10^3$) for *endo*-220. The Anisotropic displacement factor exponent takes the form: $-2\pi^2[h^2a^{*2}U_{11}+2hka^*b^*U_{12}+\ldots]$.

Atom	U_{11}	U_{22}	U_{33}	U_{23}	U_{13}	U_{12}
C23	16.5(7)	19.7(7)	17.9(7)	1.9(6)	-0.5(5)	5.6(6)
C24	21.3(7)	17.1(7)	17.9(7)	4.2(6)	-1.1(6)	6.4(6)
N3	15.8(5)	18.5(6)	15.5(6)	3.6(5)	0.0(5)	4.2(5)
N4	19.7(6)	19.1(6)	19.5(6)	2.8(5)	1.9(5)	2.4(5)
O6	18.4(5)	26.3(6)	31.6(6)	13.9(5)	4.6(4)	3.5(5)
O7	25.2(5)	19.6(5)	21.4(5)	9.9(4)	-2.2(4)	3.5(4)
O8	21.5(5)	23.0(5)	17.1(5)	4.5(4)	4.1(4)	4.3(4)
O9	27.6(6)	23.9(6)	33.3(6)	13.7(5)	0.3(5)	1.6(5)
O10	17.3(5)	27.7(6)	48.9(7)	9.9(5)	2.6(5)	4.1(5)
S2	17.20(17)	15.48(17)	13.94(17)	4.94(13)	0.01(12)	2.83(13)

Table 4: Bond Lengths for *endo*-220.

Atom	Atom	Length/Å	Atom	Atom	Length/Å
C1	C2	1.527(2)	C13	C14	1.522(2)
C1	N1	1.4914(18)	C13	N3	1.4945(18)
C2	C3	1.524(2)	C14	C15	1.523(2)
C3	C4	1.548(2)	C15	C16	1.553(2)
C3	C6	1.557(2)	C15	C18	1.549(2)
C4	C5	1.538(2)	C16	C17	1.542(2)
C5	C6	1.564(2)	C17	C18	1.552(2)
C5	O1	1.4151(19)	C17	O6	1.4022(19)
C6	N1	1.4715(18)	C18	N3	1.4723(18)
C7	C8	1.395(2)	C19	C20	1.397(2)
C7	C12	1.391(2)	C19	C24	1.390(2)

Table 4: Bond Lengths for *endo*-220.

Atom	Atom	Length/Å	Atom	Atom	Length/Å
C7	S1	1.7813(15)	C19	S2	1.7732(15)
C8	C9	1.385(2)	C20	C21	1.382(2)
C9	C10	1.386(2)	C21	C22	1.388(2)
C10	C11	1.384(2)	C22	C23	1.384(2)
C10	N2	1.476(2)	C22	N4	1.4707(19)
C11	C12	1.387(2)	C23	C24	1.385(2)
N1	S1	1.6267(12)	N3	S2	1.6018(12)
N2	O4	1.2214(19)	N4	O9	1.2256(17)
N2	O5	1.218(2)	N4	O10	1.2244(17)
O2	S1	1.4293(11)	O7	S2	1.4395(11)
O3	S1	1.4325(11)	O8	S2	1.4335(10)

Table 5: Bond Angles for *endo*-220.

Atom	Atom	Atom	Angle/°	Atom	Atom	Atom	Angle/°
N1	C1	C2	104.18(12)	N3	C13	C14	103.34(12)
C3	C2	C1	104.16(12)	C13	C14	C15	104.04(12)
C2	C3	C4	115.89(14)	C14	C15	C16	118.05(14)
C2	C3	C6	105.50(12)	C14	C15	C18	106.39(12)
C4	C3	C6	89.80(12)	C18	C15	C16	89.09(11)
C5	C4	C3	90.45(12)	C17	C16	C15	88.74(12)
C4	C5	C6	89.91(11)	C16	C17	C18	89.37(11)
O1	C5	C4	118.42(14)	O6	C17	C16	120.39(13)
O1	C5	C6	117.78(12)	O6	C17	C18	120.21(13)
C3	C6	C5	89.17(11)	C15	C18	C17	88.49(11)
N1	C6	C3	106.09(12)	N3	C18	C15	102.75(12)

Table 5: Bond Angles for *endo*-220.

Atom	Atom	Atom	Angle/°	Atom	Atom	Atom	Angle/°
N1	C6	C5	114.28(12)	N3	C18	C17	112.79(12)
C8	C7	S1	119.09(12)	C20	C19	S2	118.22(11)
C12	C7	C8	121.13(14)	C24	C19	C20	121.75(14)
C12	C7	S1	119.66(12)	C24	C19	S2	120.02(11)
C9	C8	C7	119.53(14)	C21	C20	C19	119.23(13)
C8	C9	C10	118.43(15)	C20	C21	C22	118.31(14)
C9	C10	N2	118.47(14)	C21	C22	N4	118.69(13)
C11	C10	C9	122.92(15)	C23	C22	C21	123.00(14)
C11	C10	N2	118.61(14)	C23	C22	N4	118.27(13)
C10	C11	C12	118.37(15)	C22	C23	C24	118.60(13)
C11	C12	C7	119.59(15)	C23	C24	C19	119.04(14)
C1	N1	S1	117.62(10)	C13	N3	S2	120.06(10)
C6	N1	C1	108.67(11)	C18	N3	C13	112.88(11)
C6	N1	S1	118.85(10)	C18	N3	S2	123.07(10)
O4	N2	C10	118.16(14)	O9	N4	C22	117.61(12)
O5	N2	C10	118.42(14)	O10	N4	C22	118.46(13)
O5	N2	O4	123.41(15)	O10	N4	O9	123.92(13)
N1	S1	C7	106.05(6)	N3	S2	C19	107.28(6)
O2	S1	C7	107.32(7)	O7	S2	C19	106.66(7)
O2	S1	N1	107.40(6)	O7	S2	N3	107.21(6)
O2	S1	O3	120.48(7)	O8	S2	C19	107.14(6)
O3	S1	C7	107.45(7)	O8	S2	N3	107.94(6)
O3	S1	N1	107.31(6)	O8	S2	O7	120.01(6)

Table 6: Hydrogen Bonds for *endo*-220.

D	H	A	d(D-H)/Å	d(H-A)/Å	d(D-A)/Å	D-H-A/°
O1	H1	O7[1]	0.83(3)	2.13(3)	2.9398(17)	163(2)
O6	H6A	O1[1]	0.79(2)	2.12(2)	2.8930(17)	165(2)

Table 7: Torsion Angles for *endo*-220.

A	B	C	D	Angle/°	A	B	C	D	Angle/°
C1	C2	C3	C4	-71.78(16)	C13	C14	C15	C16	65.40(17)
C1	C2	C3	C6	25.72(15)	C13	C14	C15	C18	-32.53(16)
C1	N1	S1	C7	60.87(12)	C13	N3	S2	C19	-68.73(12)
C1	N1	S1	O2	-53.63(12)	C13	N3	S2	O7	45.52(12)
C1	N1	S1	O3	175.48(10)	C13	N3	S2	O8	176.11(11)
C2	C1	N1	C6	29.92(15)	C14	C13	N3	C18	-17.43(16)
C2	C1	N1	S1	-108.82(12)	C14	C13	N3	S2	140.78(11)
C2	C3	C4	C5	113.44(14)	C14	C15	C16	C17	-123.79(14)
C2	C3	C6	C5	-123.05(12)	C14	C15	C18	C17	134.59(13)
C2	C3	C6	N1	-7.97(15)	C14	C15	C18	N3	21.55(15)
C3	C4	C5	C6	-6.24(12)	C15	C16	C17	C18	15.61(12)
C3	C4	C5	O1	-128.18(14)	C15	C16	C17	O6	140.84(14)
C3	C6	N1	C1	-13.65(15)	C15	C18	N3	C13	-2.37(15)
C3	C6	N1	S1	124.51(11)	C15	C18	N3	S2	-159.83(10)
C4	C3	C6	C5	-6.16(12)	C16	C15	C18	C17	15.54(12)
C4	C3	C6	N1	108.91(13)	C16	C15	C18	N3	-97.50(12)
C4	C5	C6	C3	6.20(12)	C16	C17	C18	C15	-15.66(12)
C4	C5	C6	N1	-101.11(14)	C16	C17	C18	N3	87.55(14)
C5	C6	N1	C1	82.88(15)	C17	C18	N3	C13	-96.15(14)
C5	C6	N1	S1	-138.97(11)	C17	C18	N3	S2	106.39(13)

Table 7: Torsion Angles for *endo*-220.

A	B	C	D	Angle/°	A	B	C	D	Angle/°
C6	C3	C4	C5	6.26(12)	C18	C15	C16	C17	-15.65(12)
C6	N1	S1	C7	-73.62(12)	C18	N3	S2	C19	87.19(12)
C6	N1	S1	O2	171.88(10)	C18	N3	S2	O7	-158.56(11)
C6	N1	S1	O3	40.99(12)	C18	N3	S2	O8	-27.97(13)
C7	C8	C9	C10	0.0(2)	C19	C20	C21	C22	1.0(2)
C8	C7	C12	C11	-1.6(2)	C20	C19	C24	C23	1.0(2)
C8	C7	S1	N1	82.29(13)	C20	C19	S2	N3	-79.15(12)
C8	C7	S1	O2	-163.15(12)	C20	C19	S2	O7	166.23(11)
C8	C7	S1	O3	-32.23(13)	C20	C19	S2	O8	36.54(13)
C8	C9	C10	C11	-1.3(2)	C20	C21	C22	C23	1.4(2)
C8	C9	C10	N2	177.76(13)	C20	C21	C22	N4	-176.36(13)
C9	C10	C11	C12	1.2(2)	C21	C22	C23	C24	-2.6(2)
C9	C10	N2	O4	6.1(2)	C21	C22	N4	O9	7.99(19)
C9	C10	N2	O5	-172.82(16)	C21	C22	N4	O10	-173.08(14)
C10	C11	C12	C7	0.3(2)	C22	C23	C24	C19	1.4(2)
C11	C10	N2	O4	-174.83(14)	C23	C22	N4	O9	-169.91(13)
C11	C10	N2	O5	6.3(2)	C23	C22	N4	O10	9.02(19)
C12	C7	C8	C9	1.5(2)	C24	C19	C20	C21	-2.2(2)
C12	C7	S1	N1	-93.71(13)	C24	C19	S2	N3	99.56(12)
C12	C7	S1	O2	20.85(14)	C24	C19	S2	O7	-15.06(13)
C12	C7	S1	O3	151.77(12)	C24	C19	S2	O8	-144.75(11)
N1	C1	C2	C3	-33.95(15)	N3	C13	C14	C15	29.90(16)
N2	C10	C11	C12	-177.89(13)	N4	C22	C23	C24	175.16(13)
O1	C5	C6	C3	128.69(14)	O6	C17	C18	C15	-141.04(14)
O1	C5	C6	N1	21.4(2)	O6	C17	C18	N3	-37.83(19)
S1	C7	C8	C9	-174.48(11)	S2	C19	C20	C21	176.44(11)

Table 7: Torsion Angles for *endo*-220.

A	B	C	D	Angle/°	A	B	C	D	Angle/°
S1	C7	C12	C11	174.32(11)	S2	C19	C24	C23	-177.63(11)

Table 8: Hydrogen Atom Coordinates (Å×10^4) and Isotropic Displacement Parameters (Å^2×10^3) for *endo*-220.

Atom	*x*	*y*	*z*	U(eq)
H1A	4770(20)	4790(15)	3274(13)	20(4)
H1B	5850(30)	4096(15)	2419(14)	26(5)
H2A	5700(30)	2722(16)	3186(14)	28(5)
H2B	5980(30)	3704(16)	4106(15)	31(5)
H3	2990(20)	2347(16)	3969(13)	23(4)
H4A	3070(30)	4553(18)	4735(15)	35(5)
H4B	1740(30)	3720(17)	5131(16)	37(5)
H5	-460(30)	3557(15)	3816(13)	23(4)
H6	1130(20)	2497(14)	2603(13)	16(4)
H8	2190(30)	924(15)	1345(13)	23(4)
H9	4020(30)	-471(17)	1399(15)	31(5)
H11	8660(30)	1324(16)	890(14)	30(5)
H12	6920(30)	2694(17)	857(14)	28(5)
H1	1530(40)	5280(20)	3713(18)	48(7)
H13A	7120(30)	4492(16)	7987(14)	24(4)
H13B	5430(30)	3583(14)	7690(13)	22(4)
H14A	6160(30)	2819(17)	8925(15)	31(5)
H14B	6800(30)	4011(18)	9443(16)	36(5)
H15	9290(30)	2716(17)	9277(16)	37(5)
H16A	10110(30)	4746(17)	8800(15)	31(5)
H16B	11500(30)	4277(17)	9474(16)	39(6)
H17	12240(20)	2983(14)	8063(13)	19(4)

Table 7: Torsion Angles for *endo*-220.

A	B	C	D	Angle/°	A	B	C	D	Angle/°
H18		9350(20)				1955(15)		7551(12)	15(4)
H20		7190(30)				466(14)		6312(13)	19(4)
H21		4800(30)				-843(16)		6399(14)	26(5)
H23		940(30)				1067(14)		6032(12)	18(4)
H24		3330(30)				2414(16)		5984(14)	25(5)
H6A		11190(30)				4259(18)		7098(16)	35(6)

Experimental

Single crystals of $C_{12}H_{14}N_2O_5S$ **[*endo*-220]** were **[crystallisation from acetone and hexane]**. A suitable crystal was selected and **[oil on 200 micrometre micromount]** on a **SuperNova, Dual, Cu at home/near, HyPix** diffractometer. The crystal was kept at 110.00(10) K during data collection. Using Olex2 [1], the structure was solved with the SHELXT [2] structure solution program using Intrinsic Phasing and refined with the SHELXL [3] refinement package using Least Squares minimisation.

1. Dolomanov, O.V., Bourhis, L.J., Gildea, R.J, Howard, J.A.K. & Puschmann, H. (2009), J. Appl. Cryst. 42, 339-341.
2. Sheldrick, G.M. (2015). Acta Cryst. A71, 3-8.
3. Sheldrick, G.M. (2015). Acta Cryst. C71, 3-8.

Crystal structure determination of [***endo*-220**]

Crystal Data for $C_{12}H_{14}N_2O_5S$ (M =298.31 g/mol): triclinic, space group P-1 (no. 2), a = 7.22716(15) Å, b = 13.1629(3) Å, c = 14.1120(3) Å, α = 104.679(2)°, β = 90.8277(18)°, γ = 96.2347(18)°, V = 1289.75(5) Å^3, Z = 4, T = 110.00(10) K, μ(Cu Kα) = 2.458 mm^{-1}, *Dcalc* = 1.536 g/cm^3, 12385 reflections measured (6.99° ≤ 2Θ ≤ 134.158°), 4607 unique (R_{int} = 0.0261, R_{sigma} = 0.0297) which were used in all calculations. The final R_1 was 0.0296 (I > 2σ(I)) and wR_2 was 0.0795 (all data).

Refinement model description

Number of restraints - 0, number of constraints - unknown.
Details:
N/A

II. NMR Spectra

400 MHz ^{1}H NMR spectrum; 100.6 MHz ^{13}C NMR spectrum; $CDCl_3$ of **90**

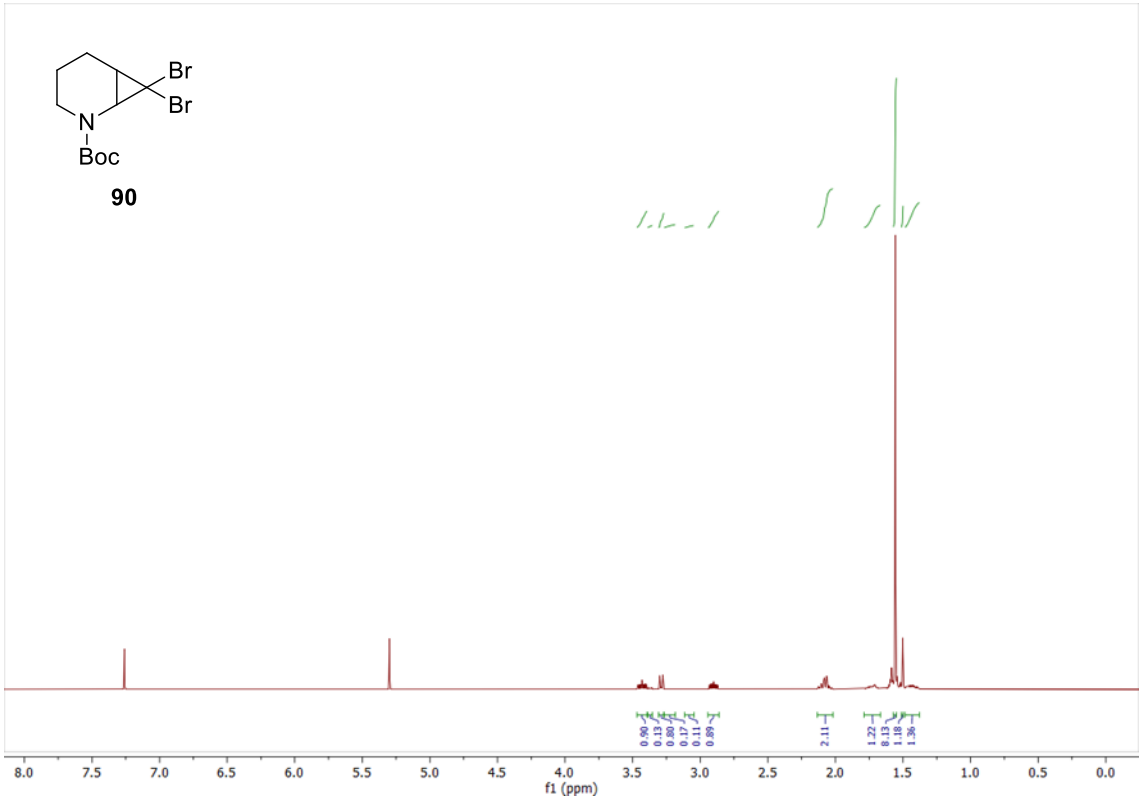

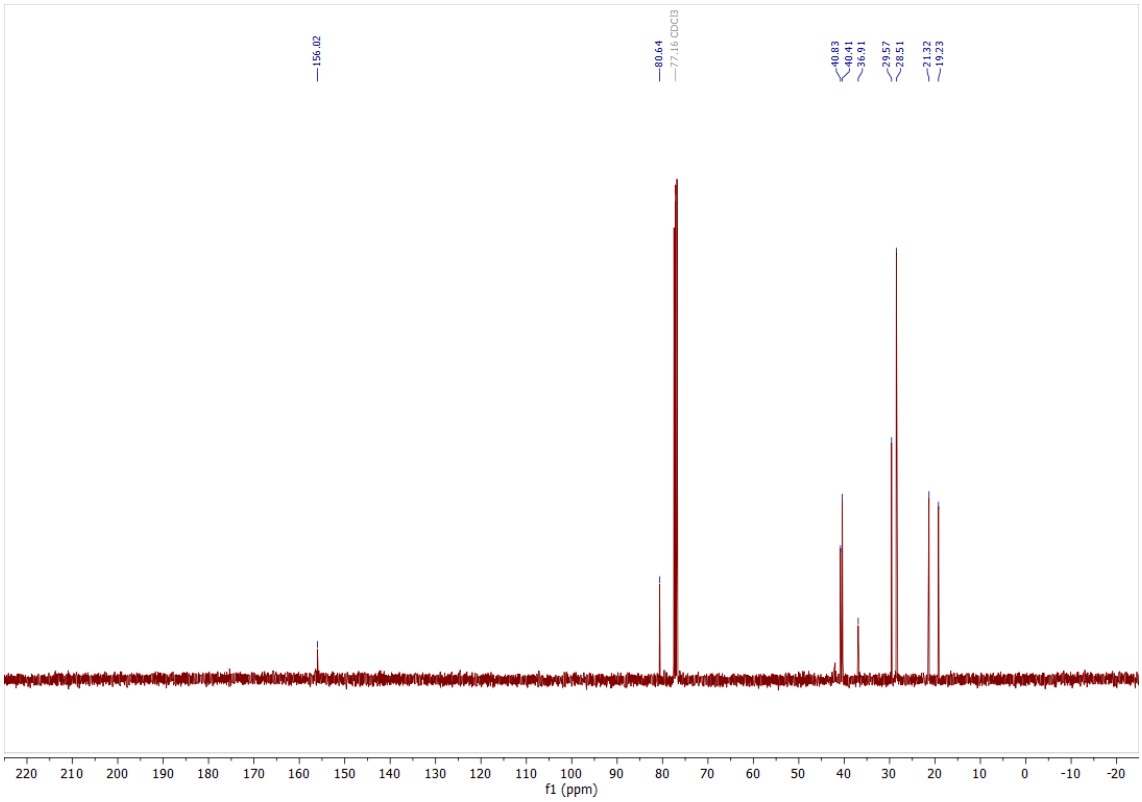

400 MHz ^{1}H NMR spectrum; 100.6 MHz ^{13}C NMR spectrum; $CDCl_3$ of *exo*-**91**

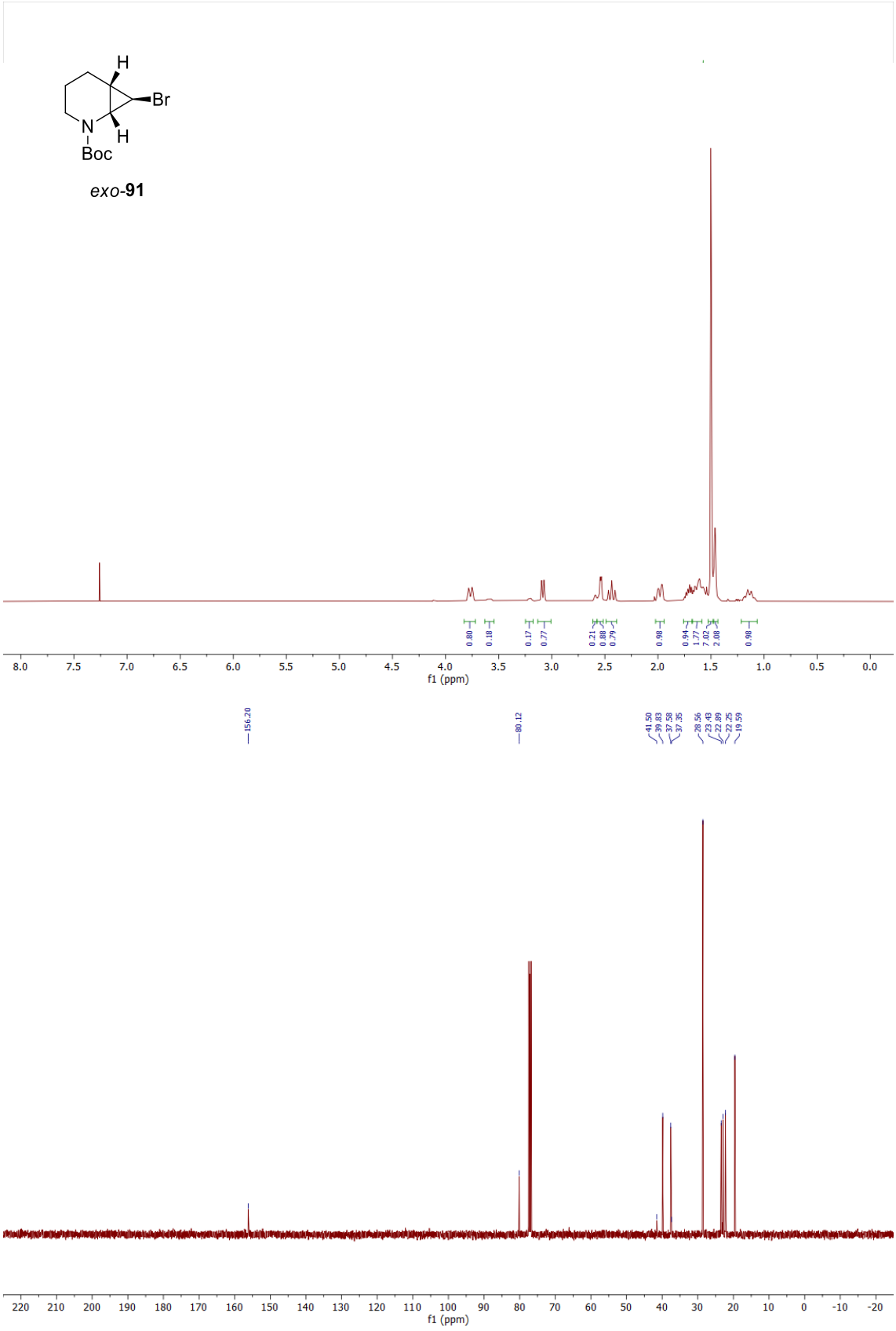

400 MHz ^{1}H NMR spectrum; 100.6 MHz ^{13}C NMR spectrum; 128.4 MHz ^{11}B spectrum; $CDCl_3$ of *exo*-**92**

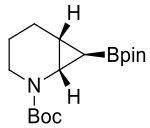

exo-**91**

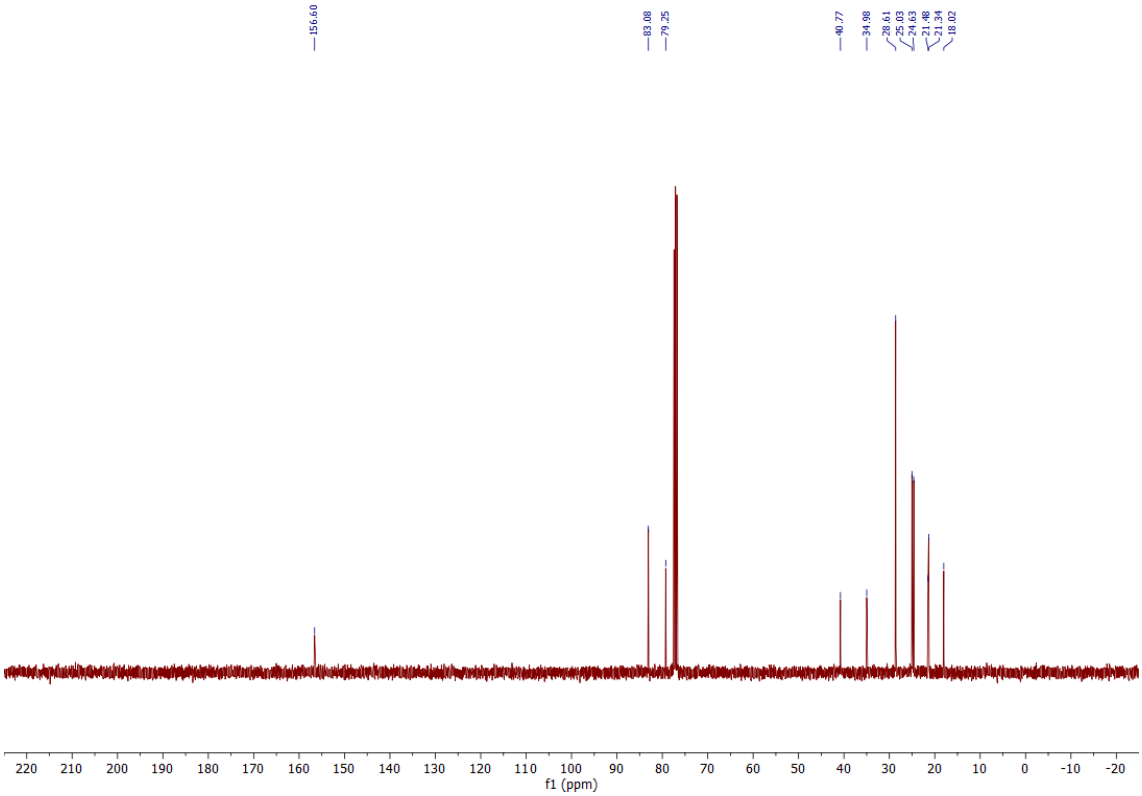

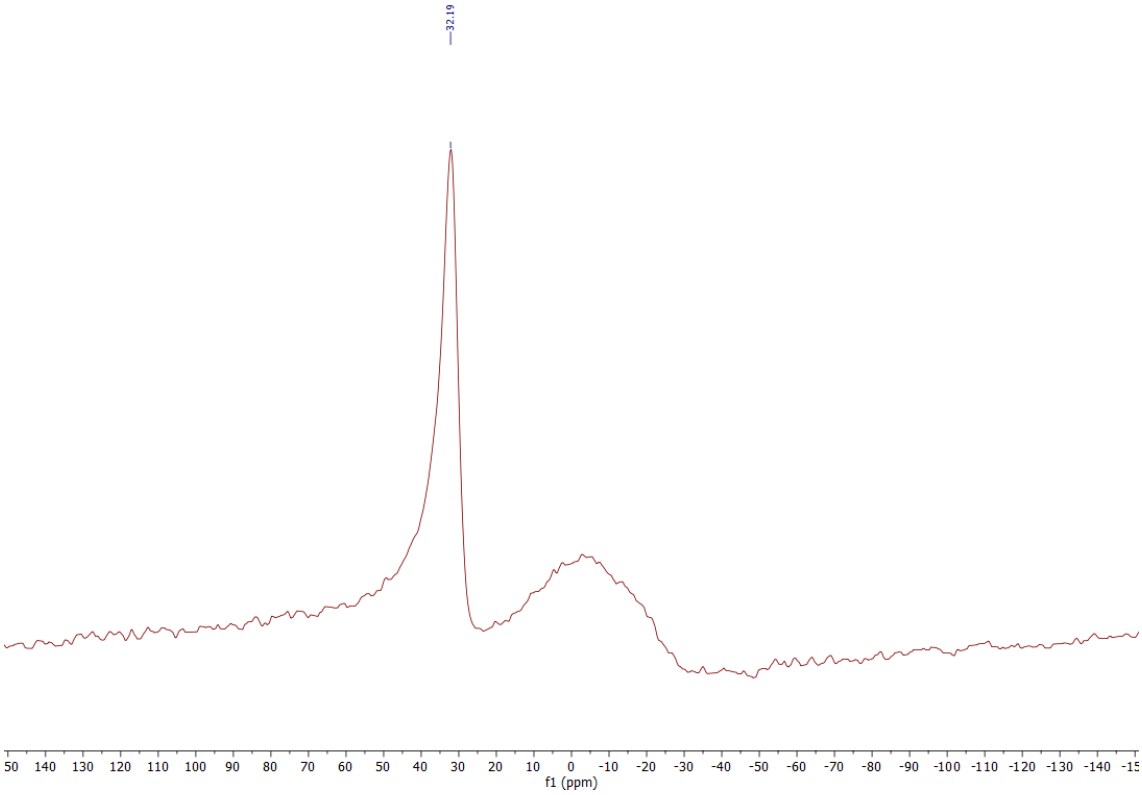
32.19
50 140 130 120 110 100 90 80 70 60 50 40 30 20 10 0 -10 -20 -30 -40 -50 -60 -70 -80 -90 -100 -110 -120 -130 -140 -15
f1 (ppm)

400 MHz ^{1}H NMR spectrum; 100.6 MHz ^{13}C NMR spectrum; 128.4 MHz ^{11}B spectrum; $CDCl_3$ of *exo*-**36**

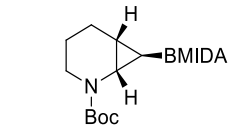

exo-**36**

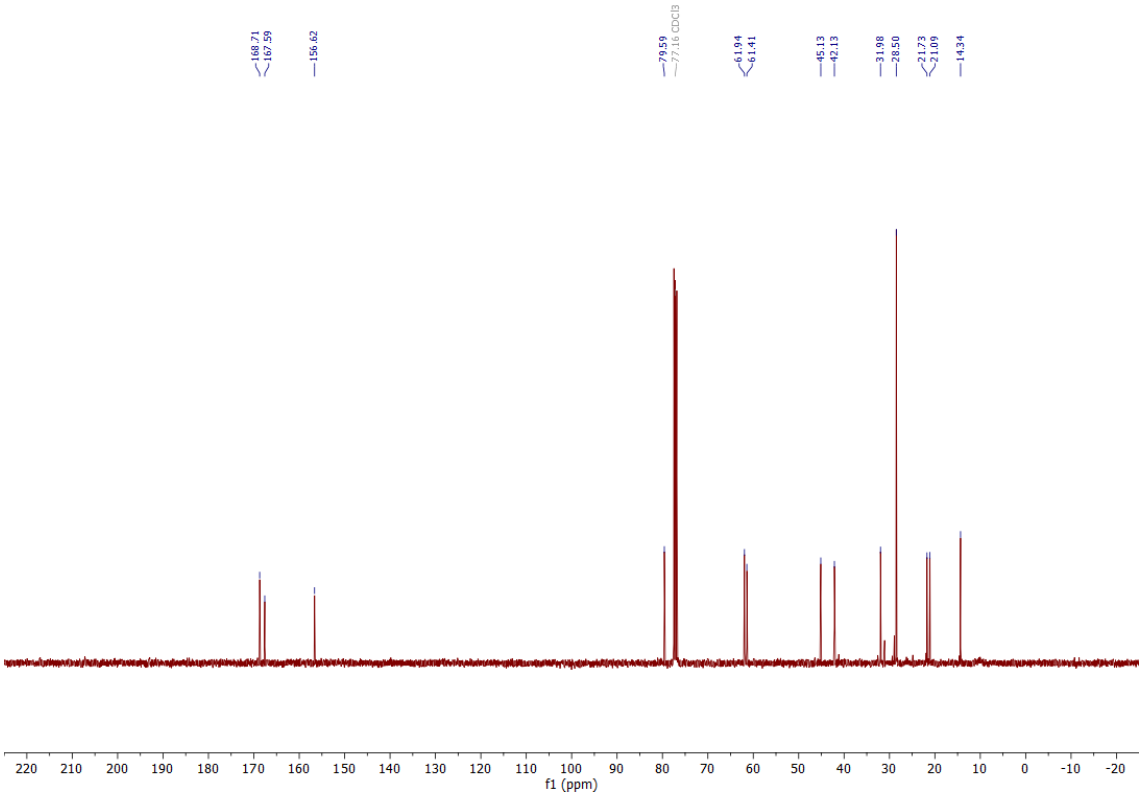

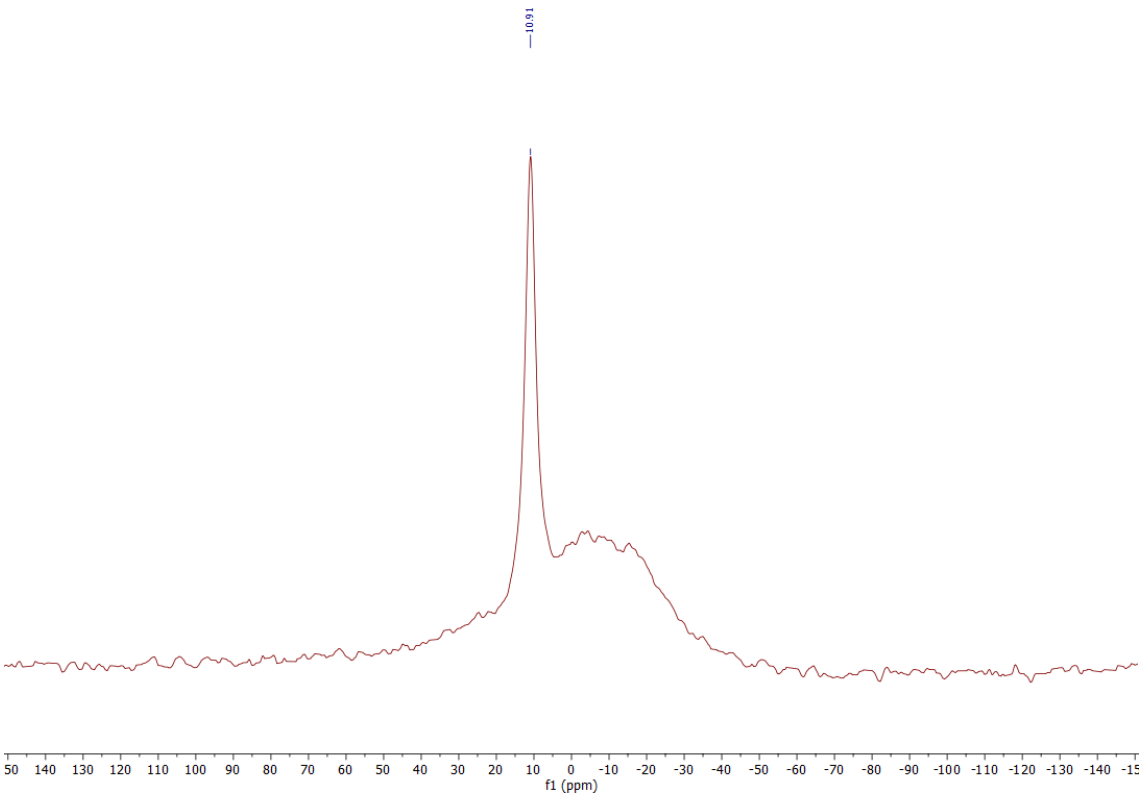
10.91
50 140 130 120 110 100 90 80 70 60 50 40 30 20 10 0 -10 -20 -30 -40 -50 -60 -70 -80 -90 -100 -110 -120 -130 -140 -15
f1 (ppm)

400 MHz ^{1}H NMR spectrum; 100.6 MHz ^{13}C NMR spectrum; $CDCl_3$ of **106**

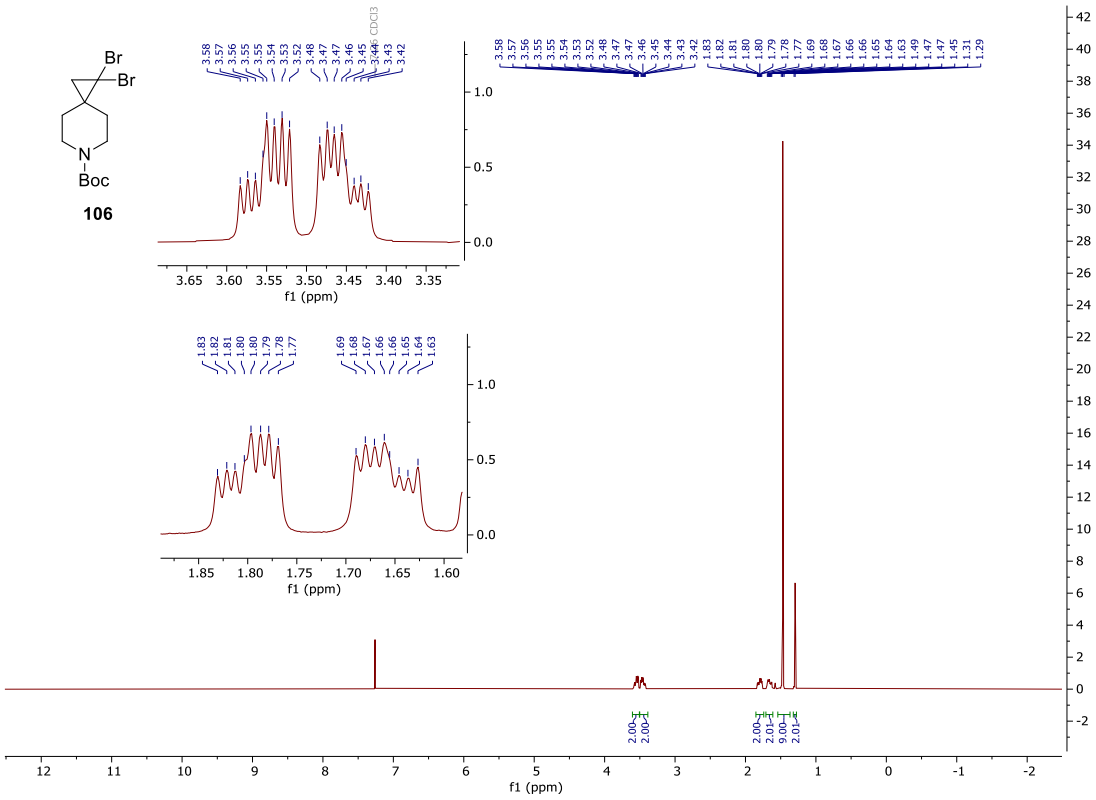

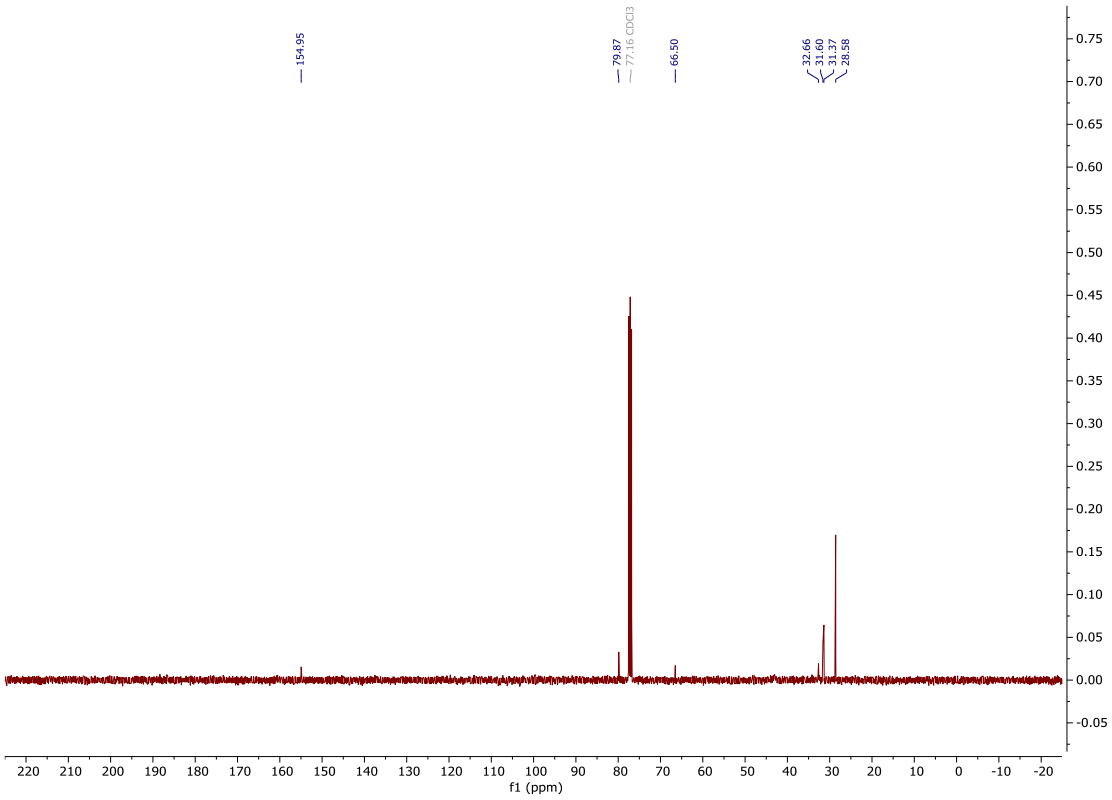

400 MHz ^{1}H NMR spectrum; 100.6 MHz ^{13}C NMR spectrum; $CDCl_3$ of **109**

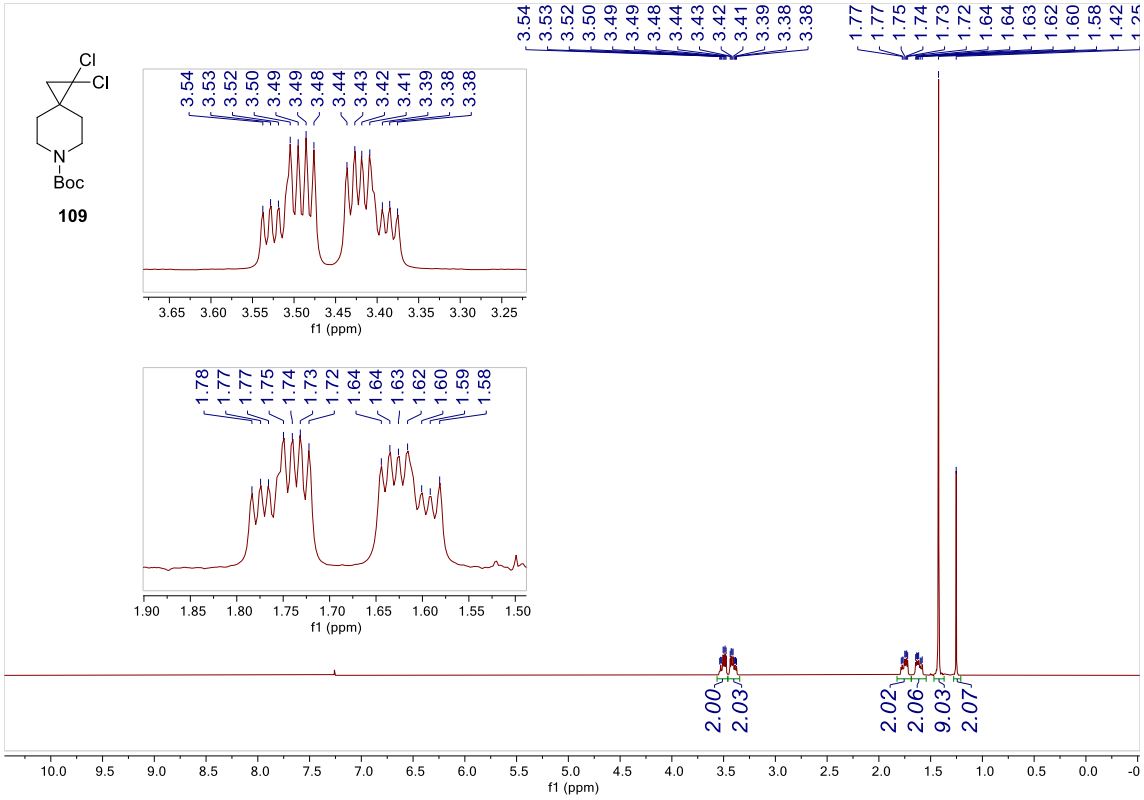

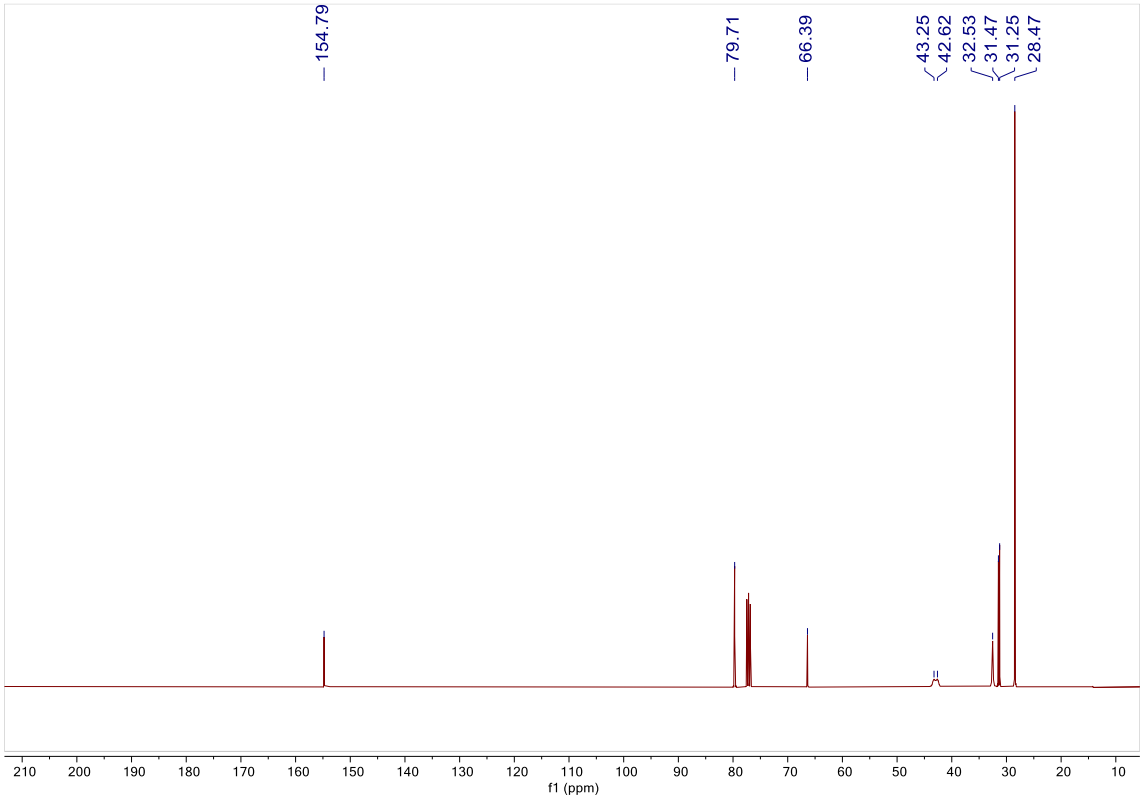

400 MHz ^{1}H NMR spectrum; $CDCl_3$ of **108**

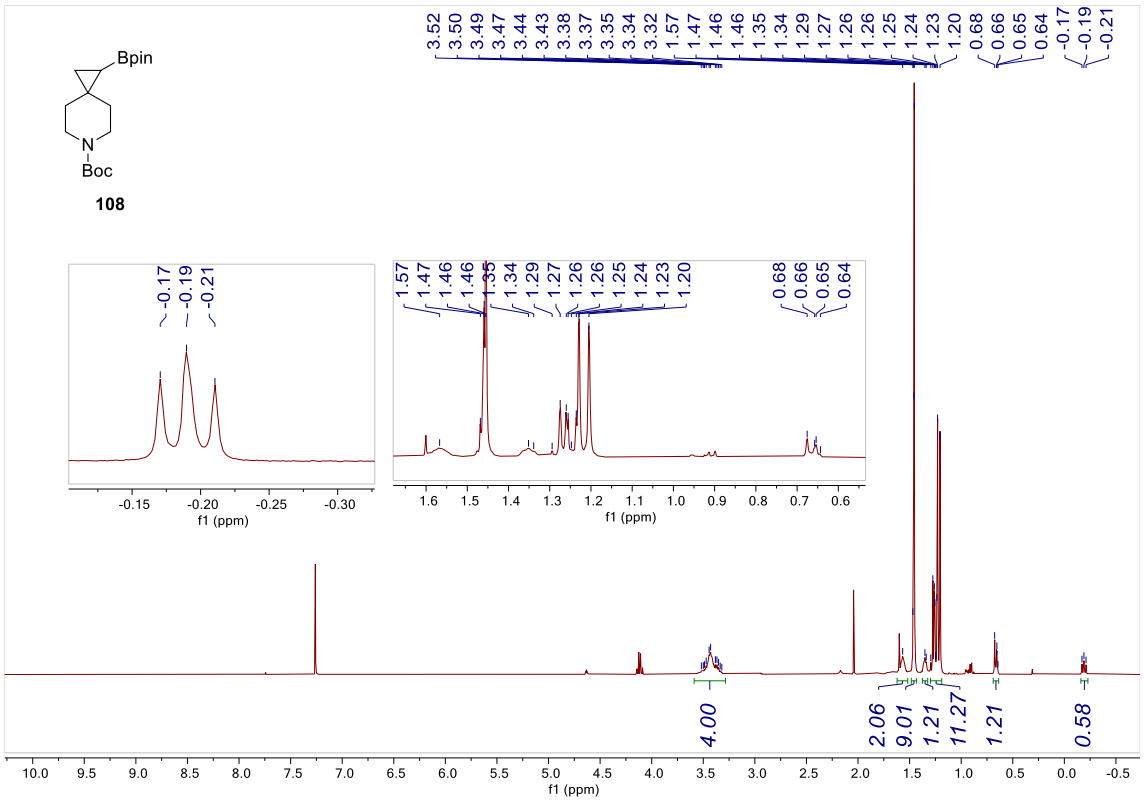

400 MHz ^{1}H NMR spectrum; 100.6 MHz ^{13}C NMR spectrum; 128.4 MHz ^{11}B NMR spectrum; acetone-d_6 of **37**

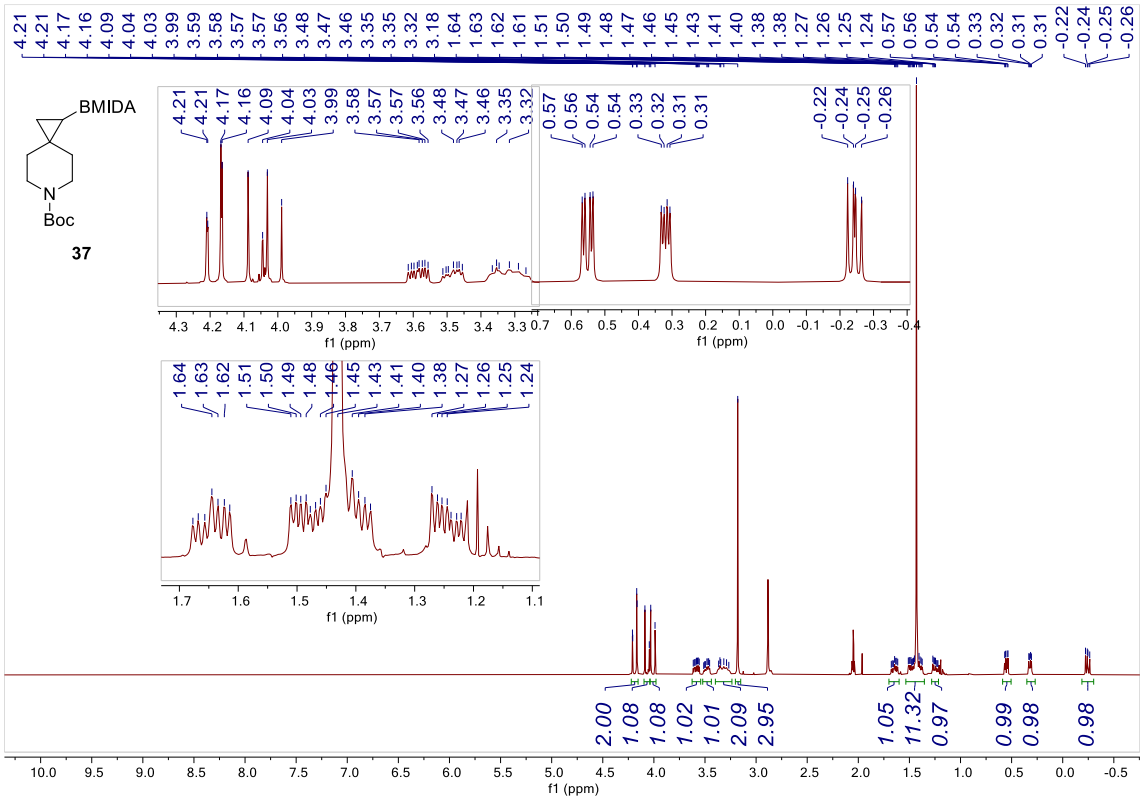

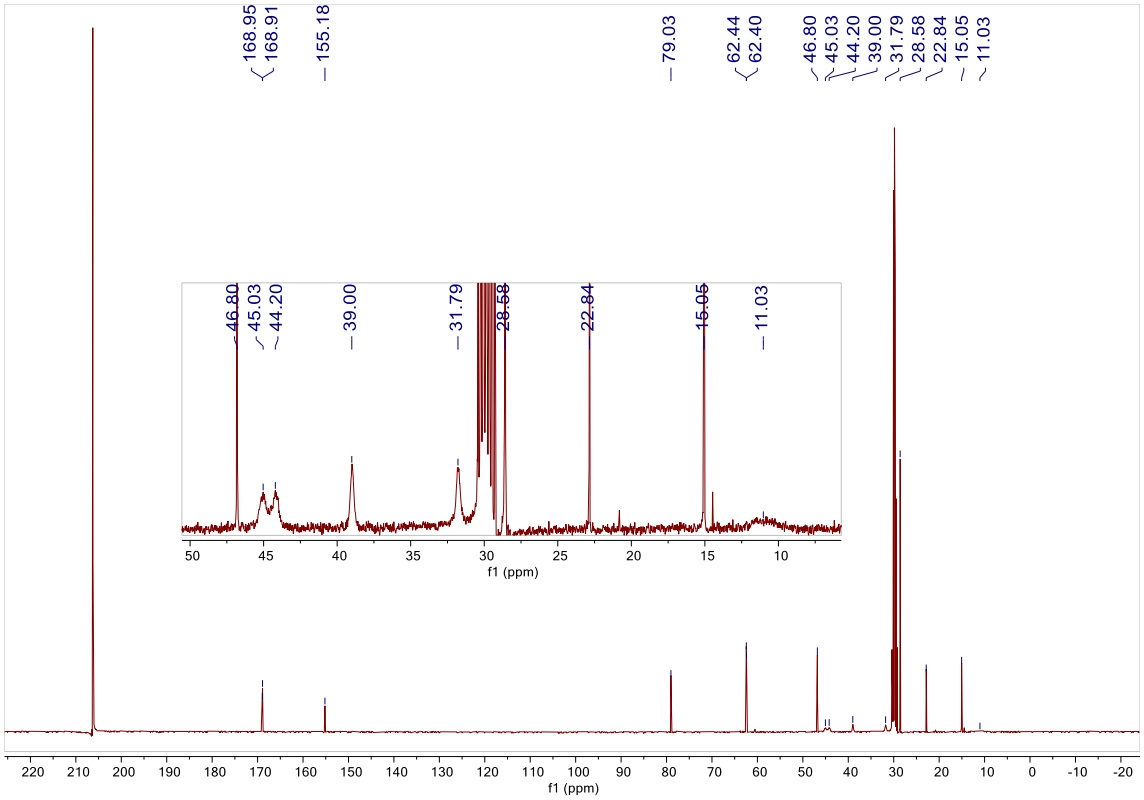

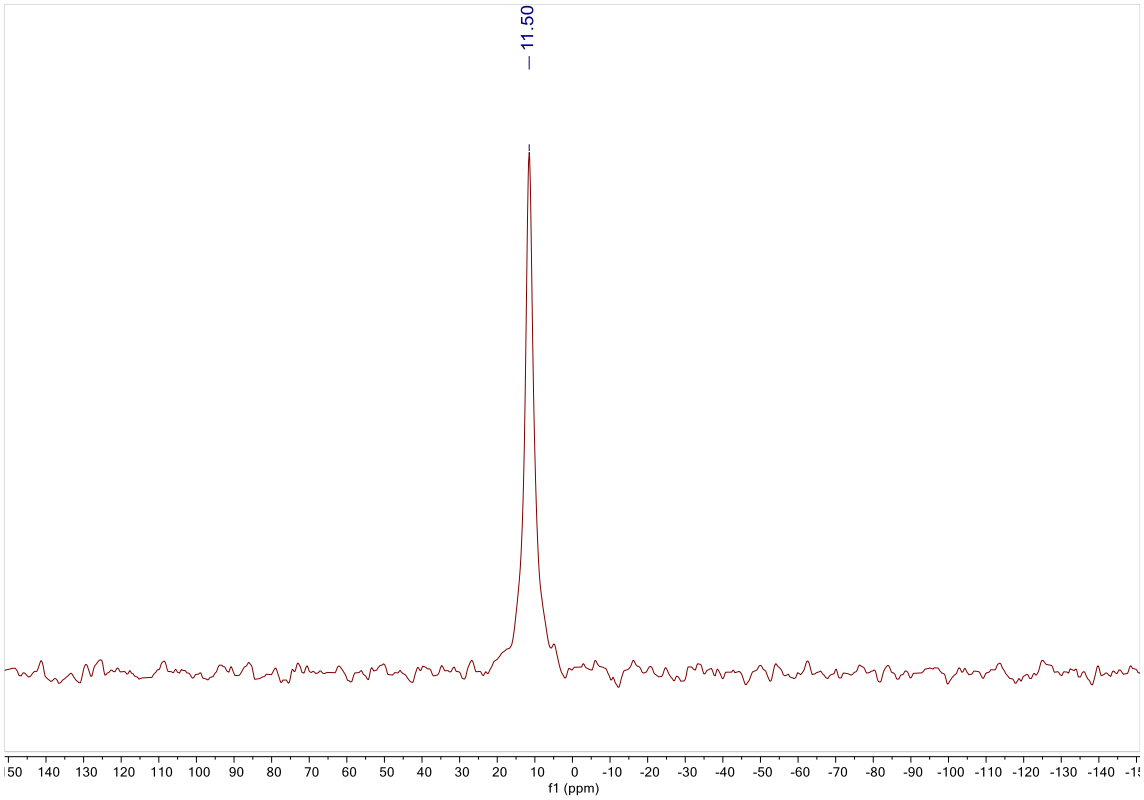
11.50
50 140 130 120 110 100 90 80 70 60 50 40 30 20 10 0 -10 -20 -30 -40 -50 -60 -70 -80 -90 -100 -110 -120 -130 -140
f1 (ppm)

400 MHz ^{1}H NMR spectrum; 100.6 MHz ^{13}C NMR spectrum; $CDCl_3$ of **74**

74

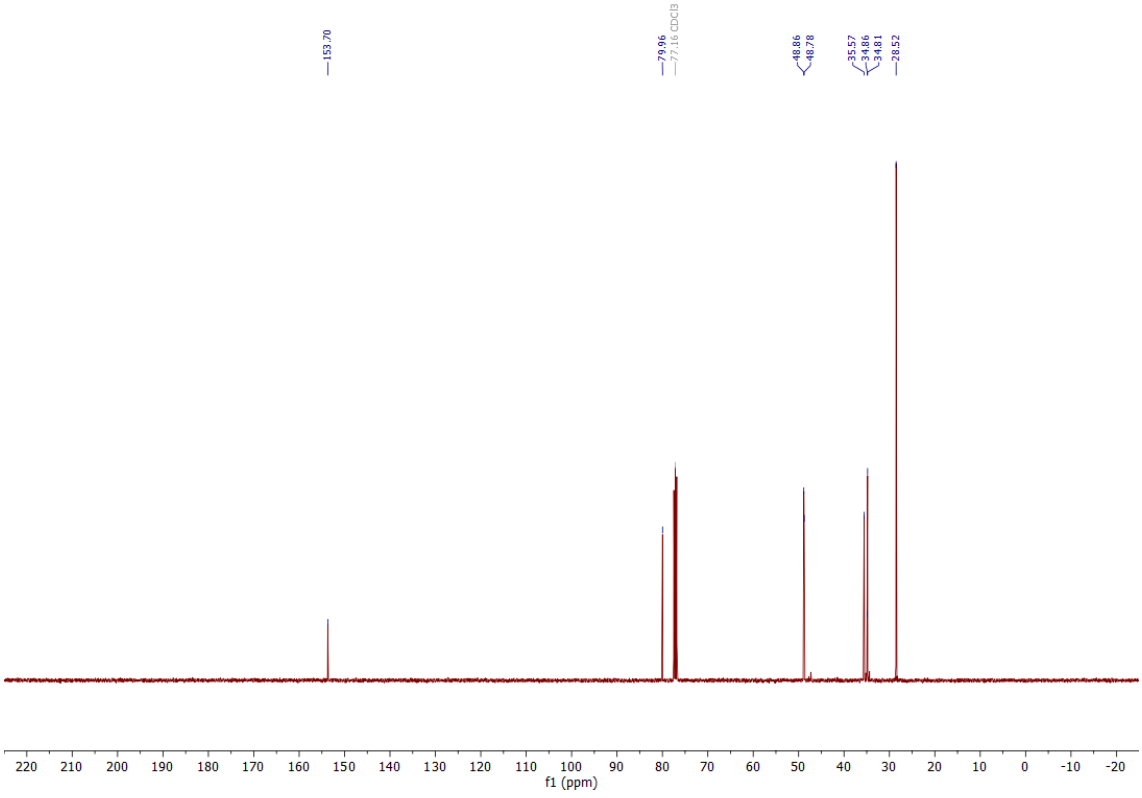

400 MHz ^{1}H NMR spectrum; 100.6 MHz ^{13}C NMR spectrum; $CDCl_3$ of *trans*-**111**

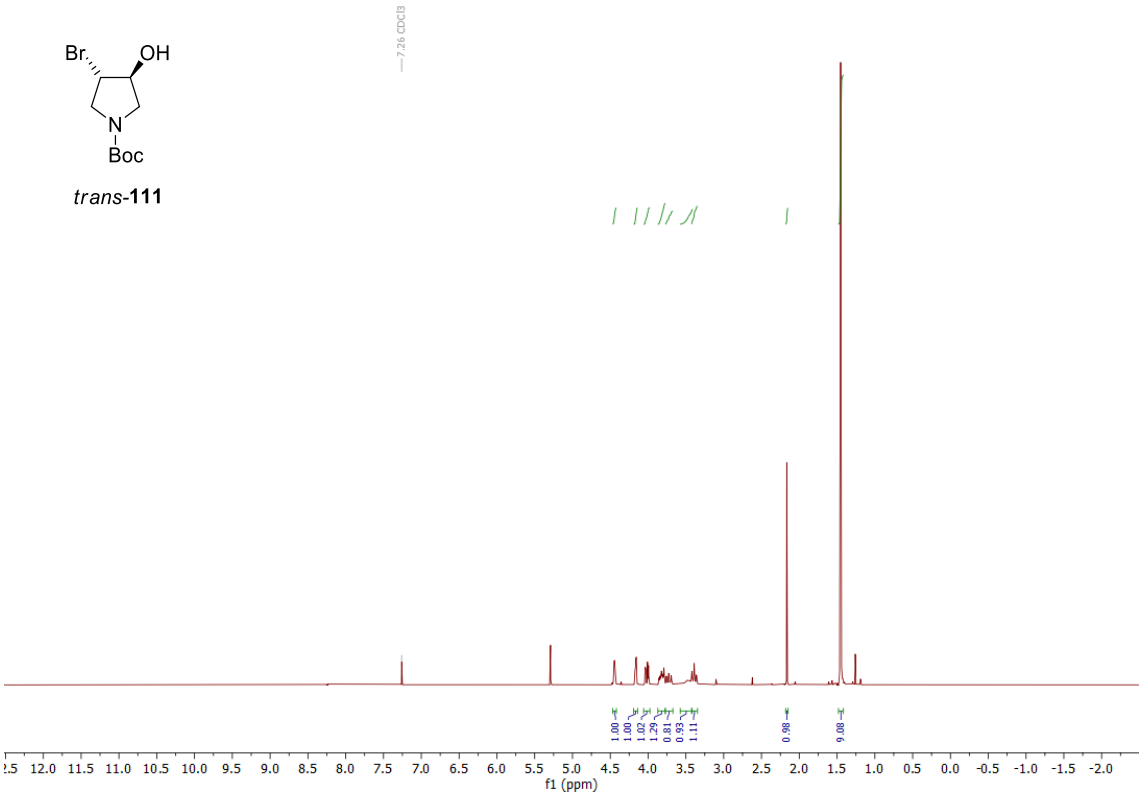

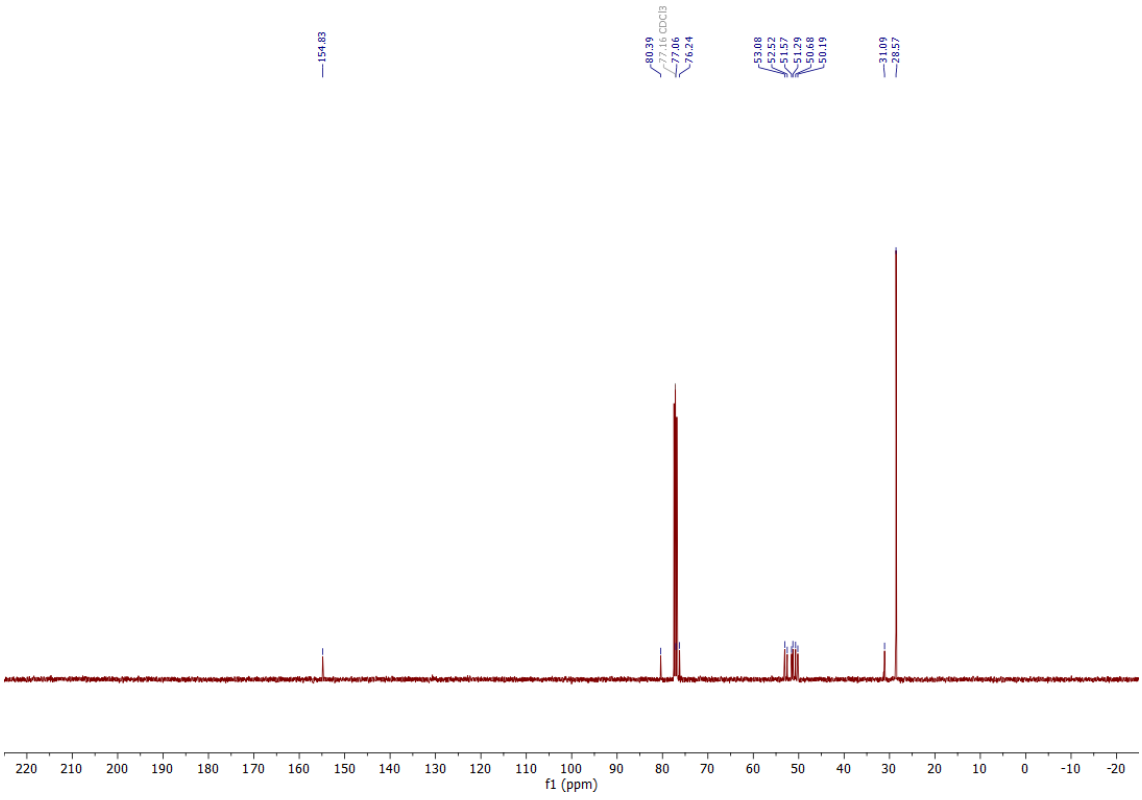

400 MHz ^{1}H NMR spectrum; 100.6 MHz ^{13}C NMR spectrum; $CDCl_3$ of *exo*-**110**

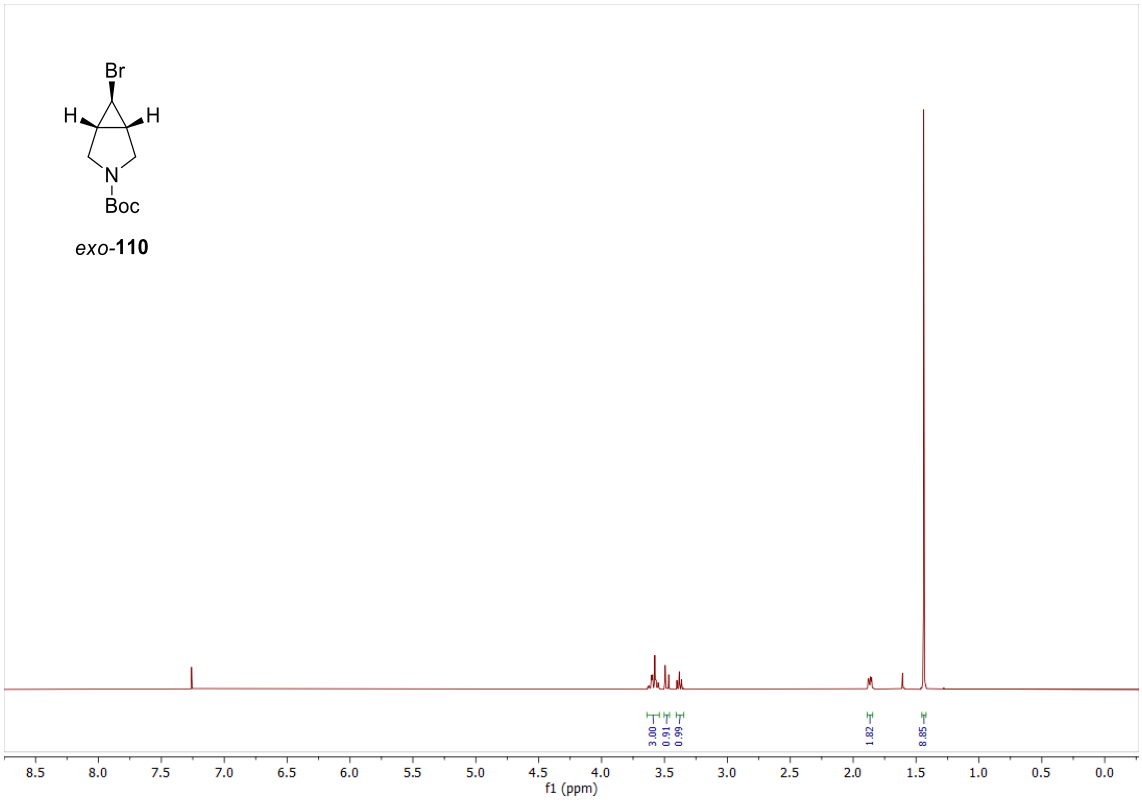

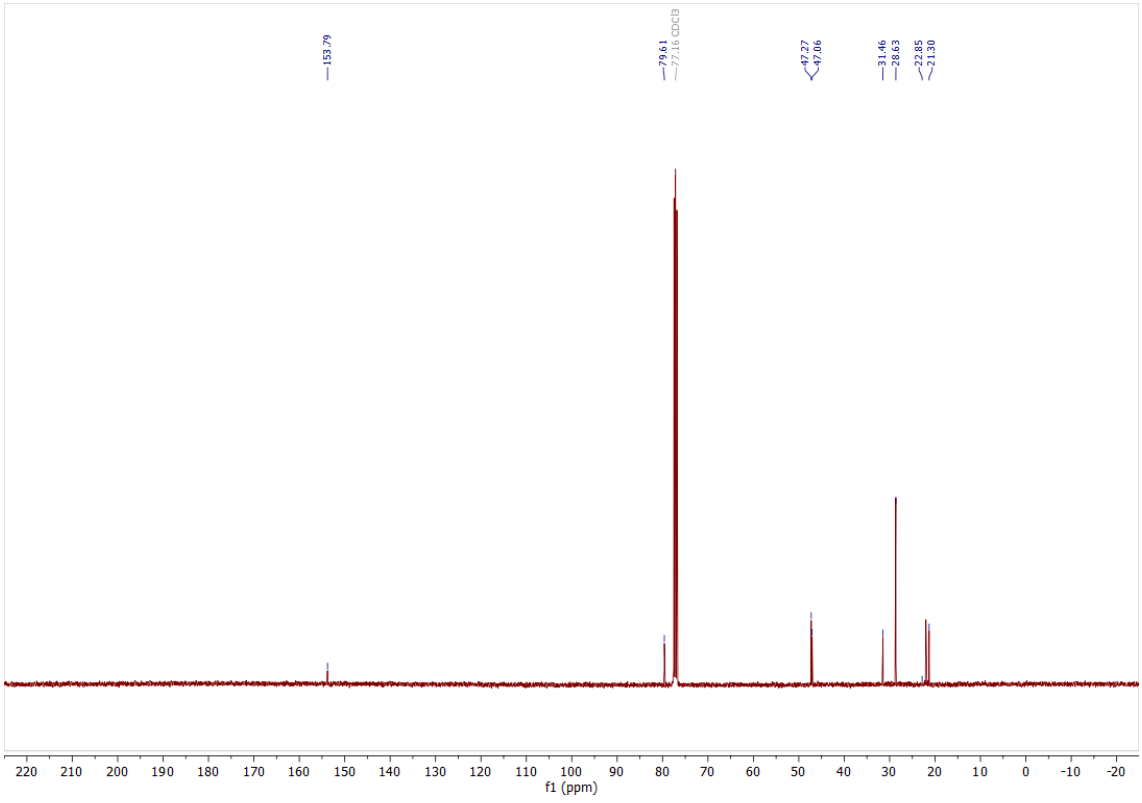

400 MHz ^{1}H NMR spectrum; 100.6 MHz ^{13}C NMR spectrum; $CDCl_3$ of *endo*-**110**

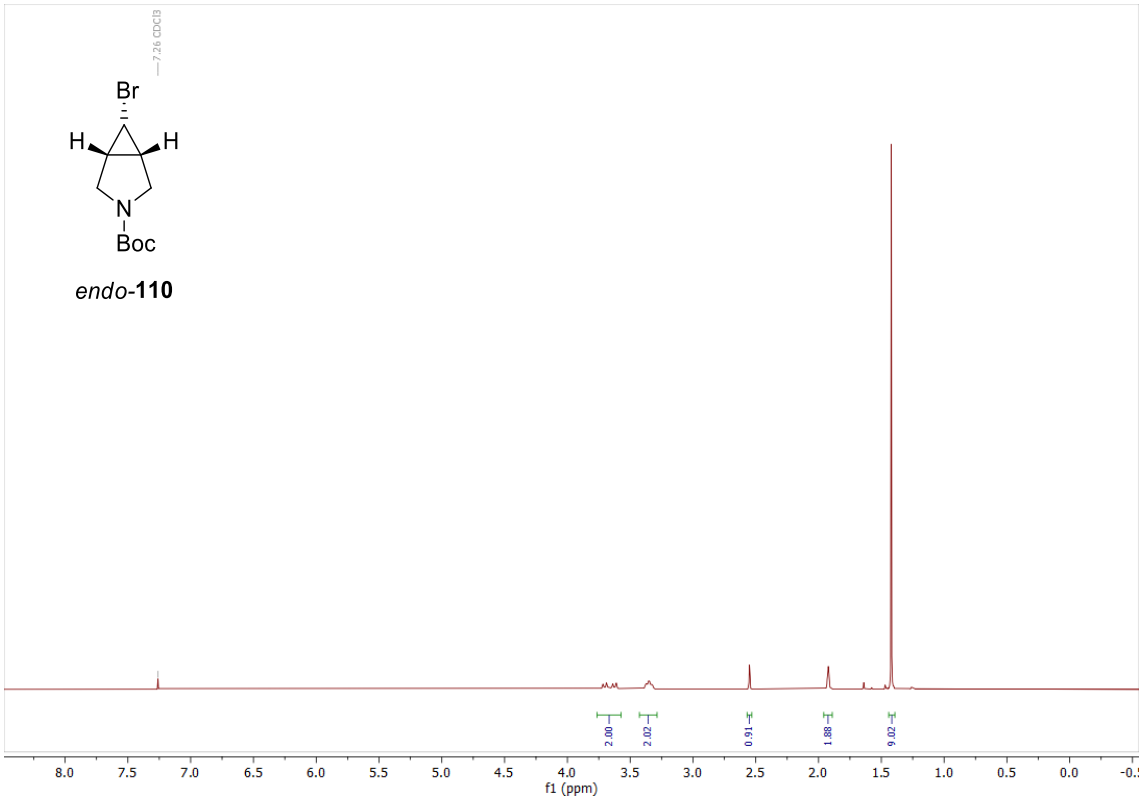

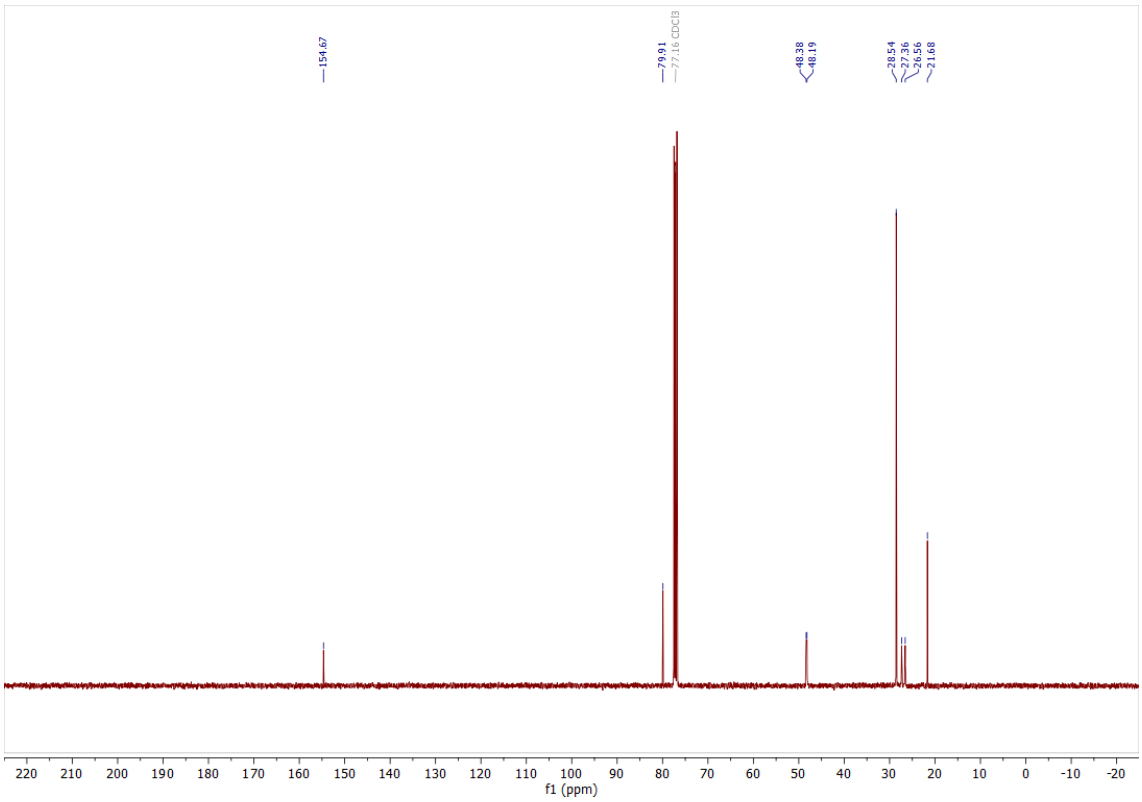

400 MHz ^{1}H NMR spectrum; 100.6 MHz ^{13}C NMR spectrum; 128.4 MHz ^{11}B NMR spectrum; $CDCl_3$ of *exo*-**112**

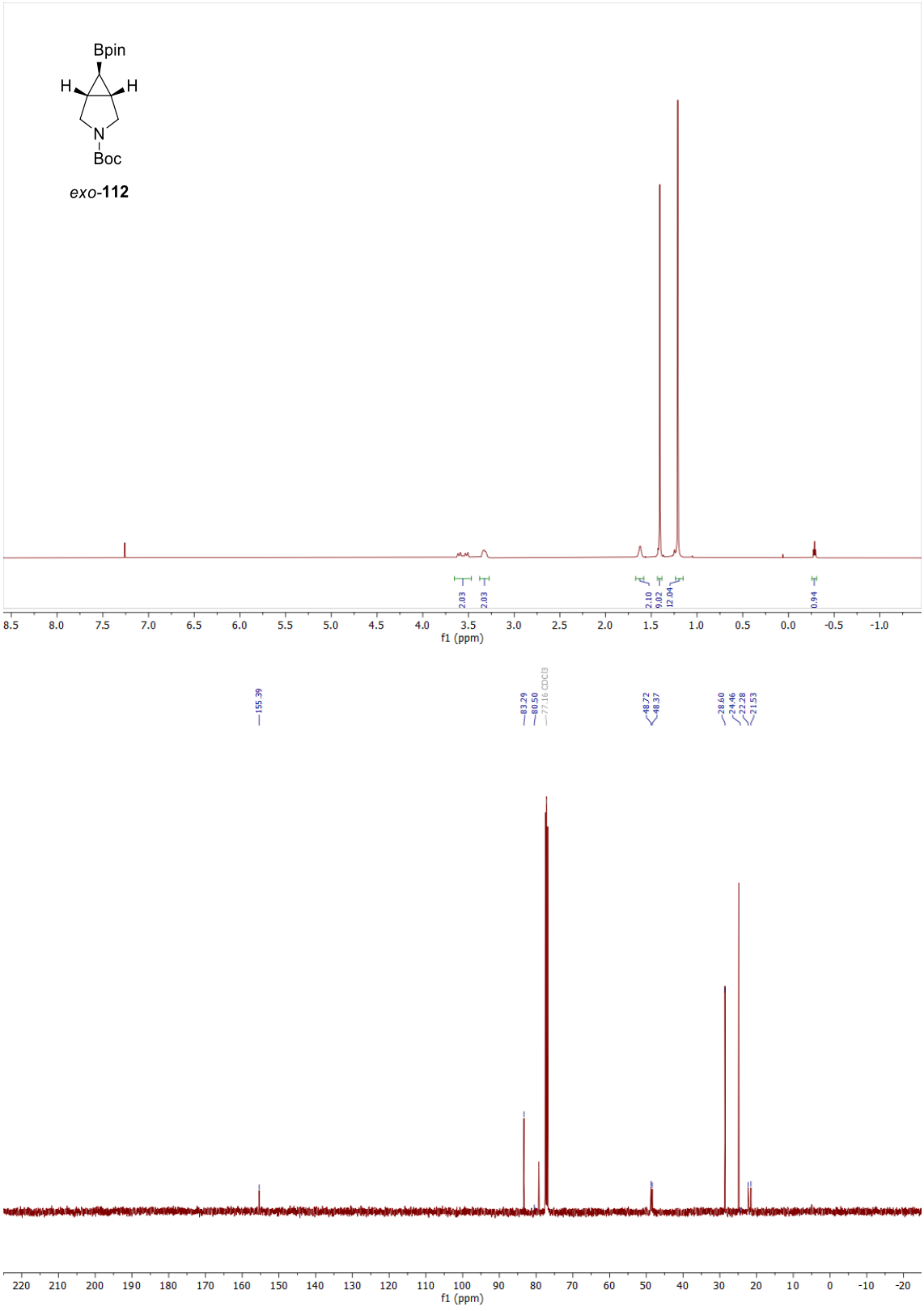

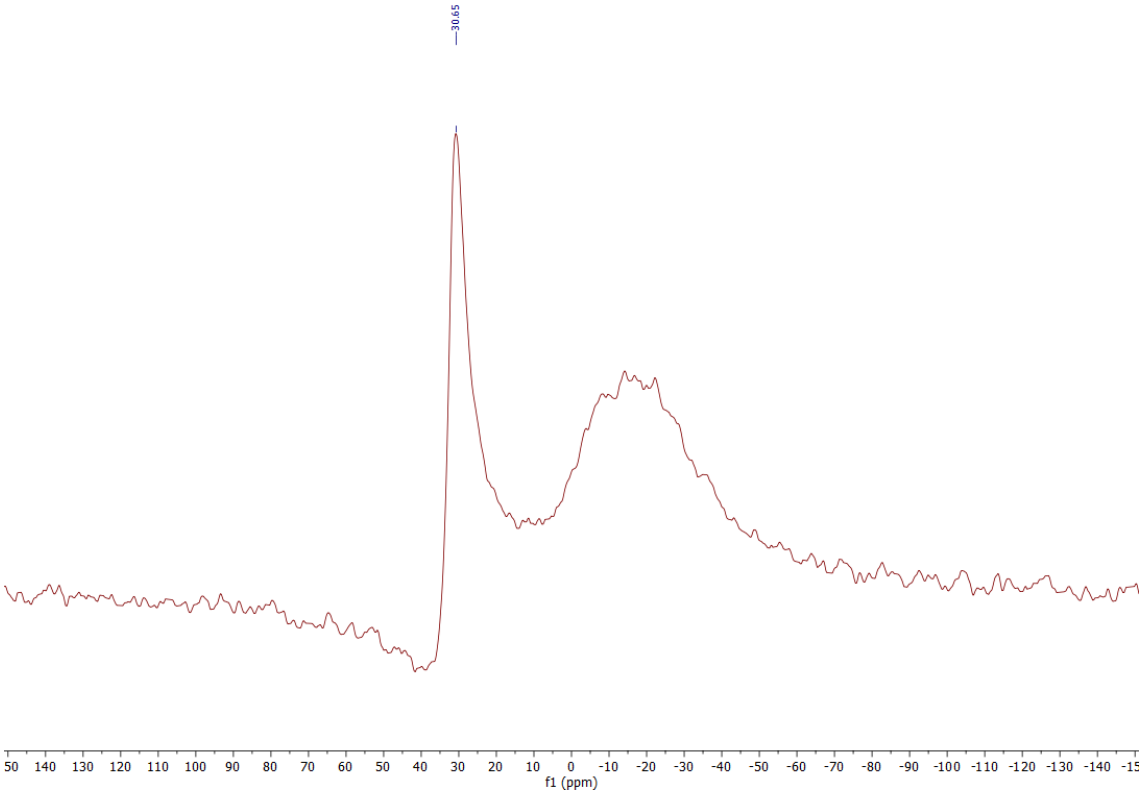
30.65
50 140 130 120 110 100 90 80 70 60 50 40 30 20 10 0 -10 -20 -30 -40 -50 -60 -70 -80 -90 -100 -110 -120 -130 -140 -15
f1 (ppm)

400 MHz ^{1}H NMR spectrum; 100.6 MHz ^{13}C NMR spectrum; 128.4 MHz ^{11}B NMR spectrum; $CDCl_3$ of *exo*-**39**

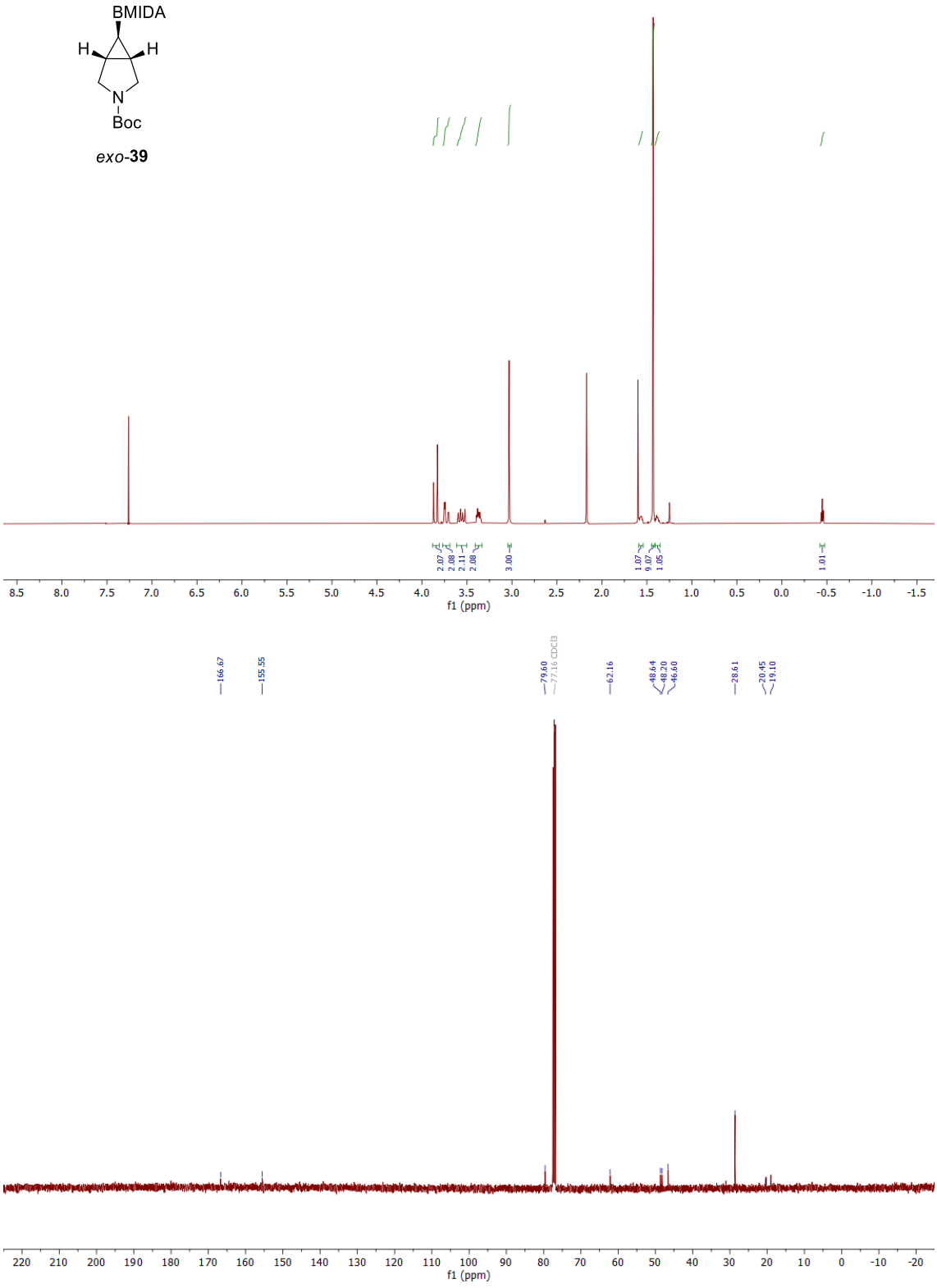

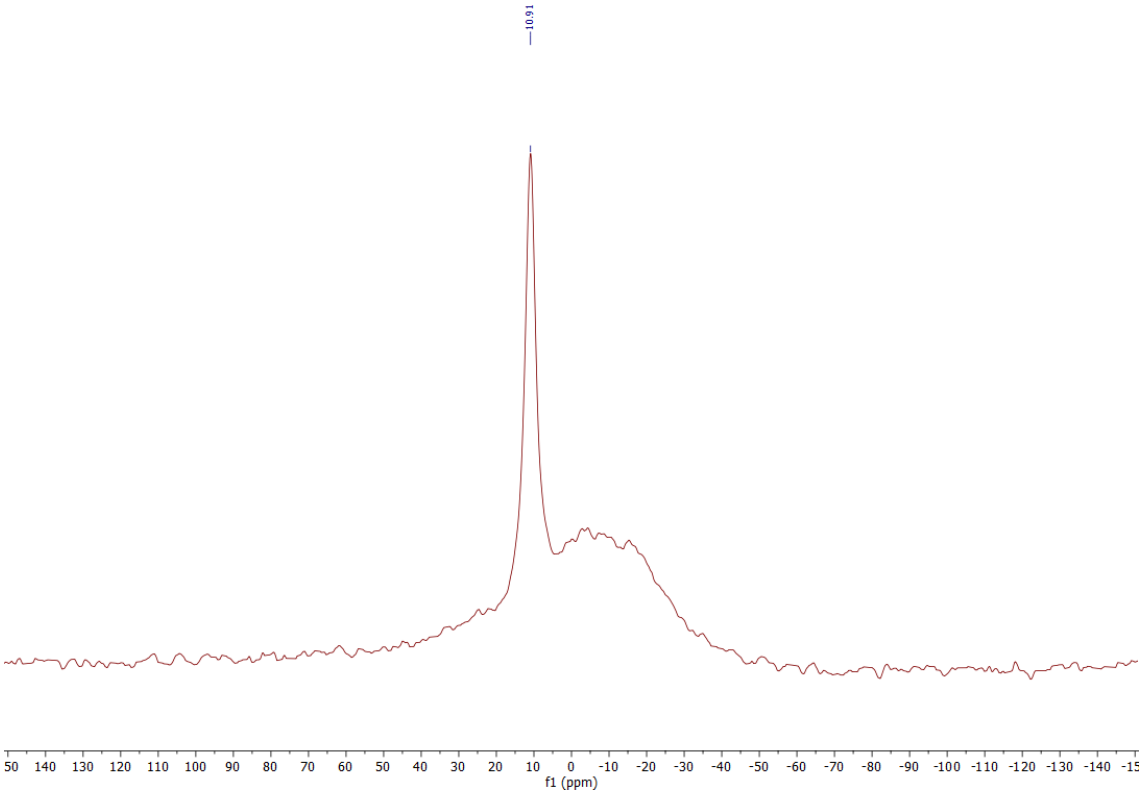
10.91
50 140 130 120 110 100 90 80 70 60 50 40 30 20 10 0 -10 -20 -30 -40 -50 -60 -70 -80 -90 -100 -110 -120 -130 -140 -15
f1 (ppm)

400 MHz ^{1}H NMR spectrum; 100.6 MHz ^{13}C NMR spectrum; $CDCl_3$ of **113**

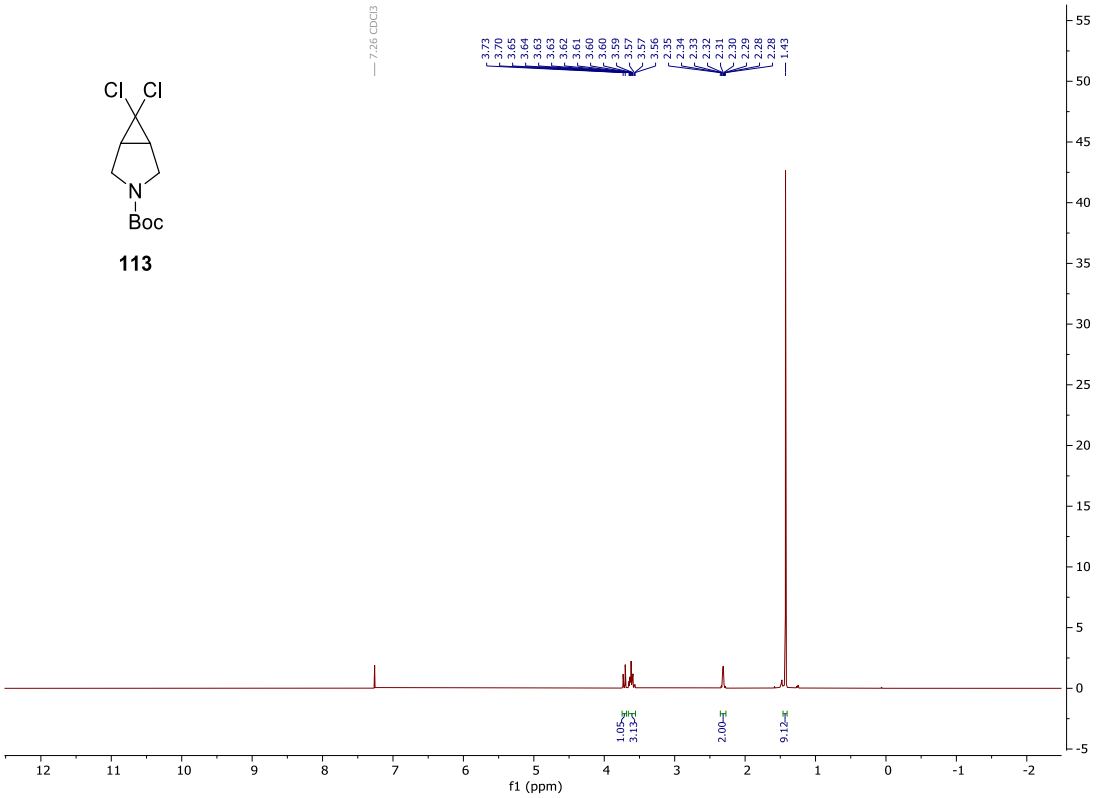

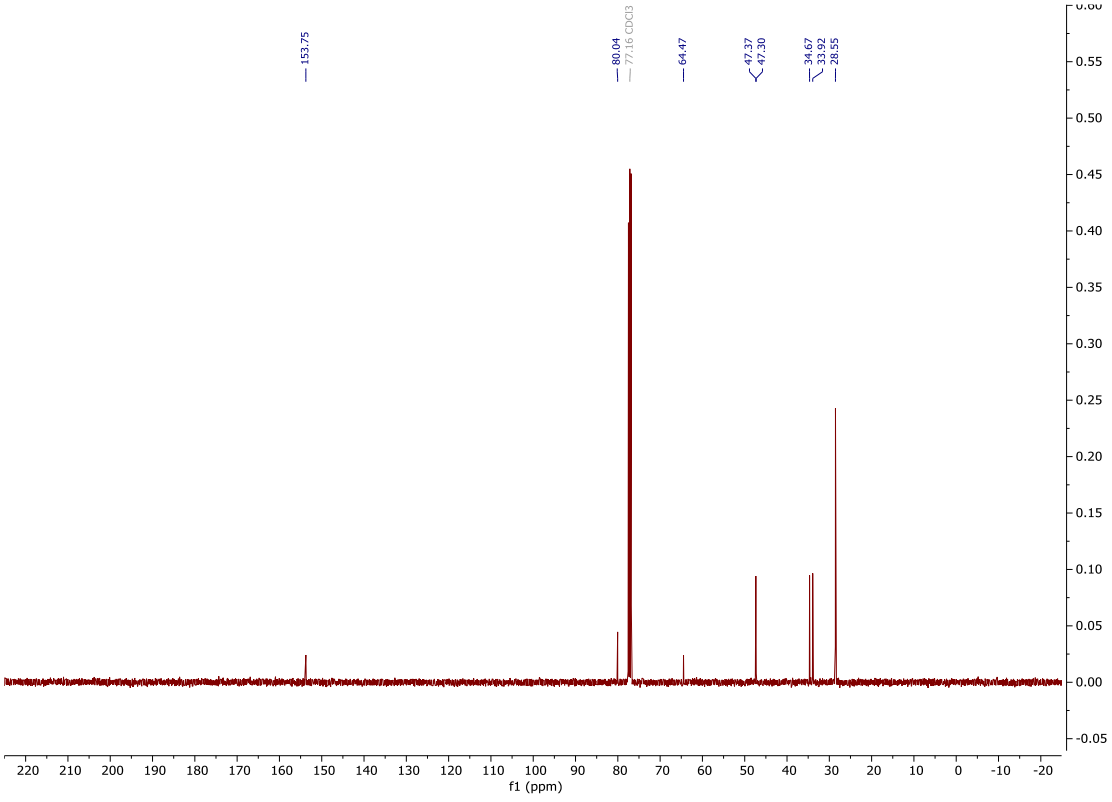

400 MHz ^{1}H NMR spectrum; 100.6 MHz ^{13}C NMR spectrum; $CDCl_3$ of **114**

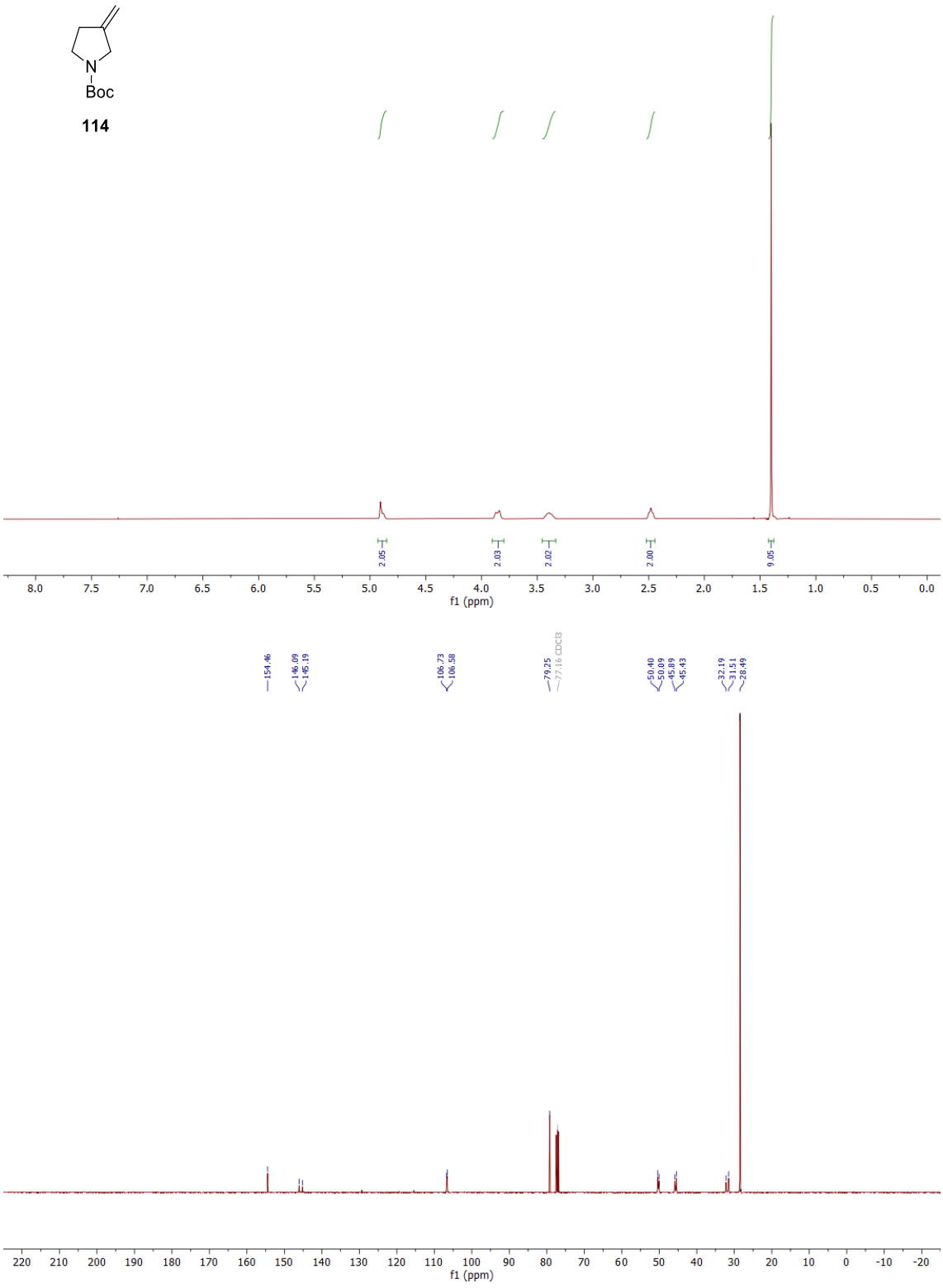

400 MHz ^{1}H NMR spectrum; 100.6 MHz ^{13}C NMR spectrum; $CDCl_3$ of **115**

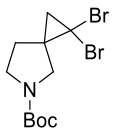

115

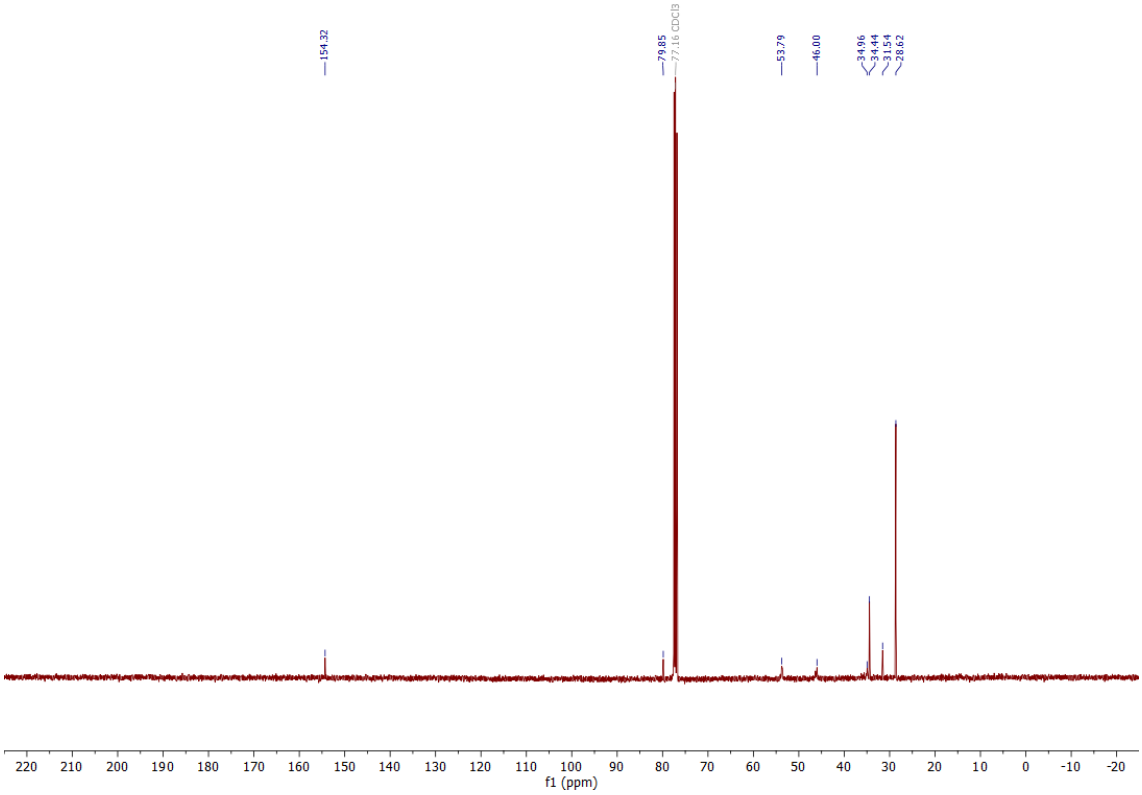

400 MHz ^{1}H NMR spectrum; 100.6 MHz ^{13}C NMR spectrum; $CDCl_3$ of *trans*-**116**

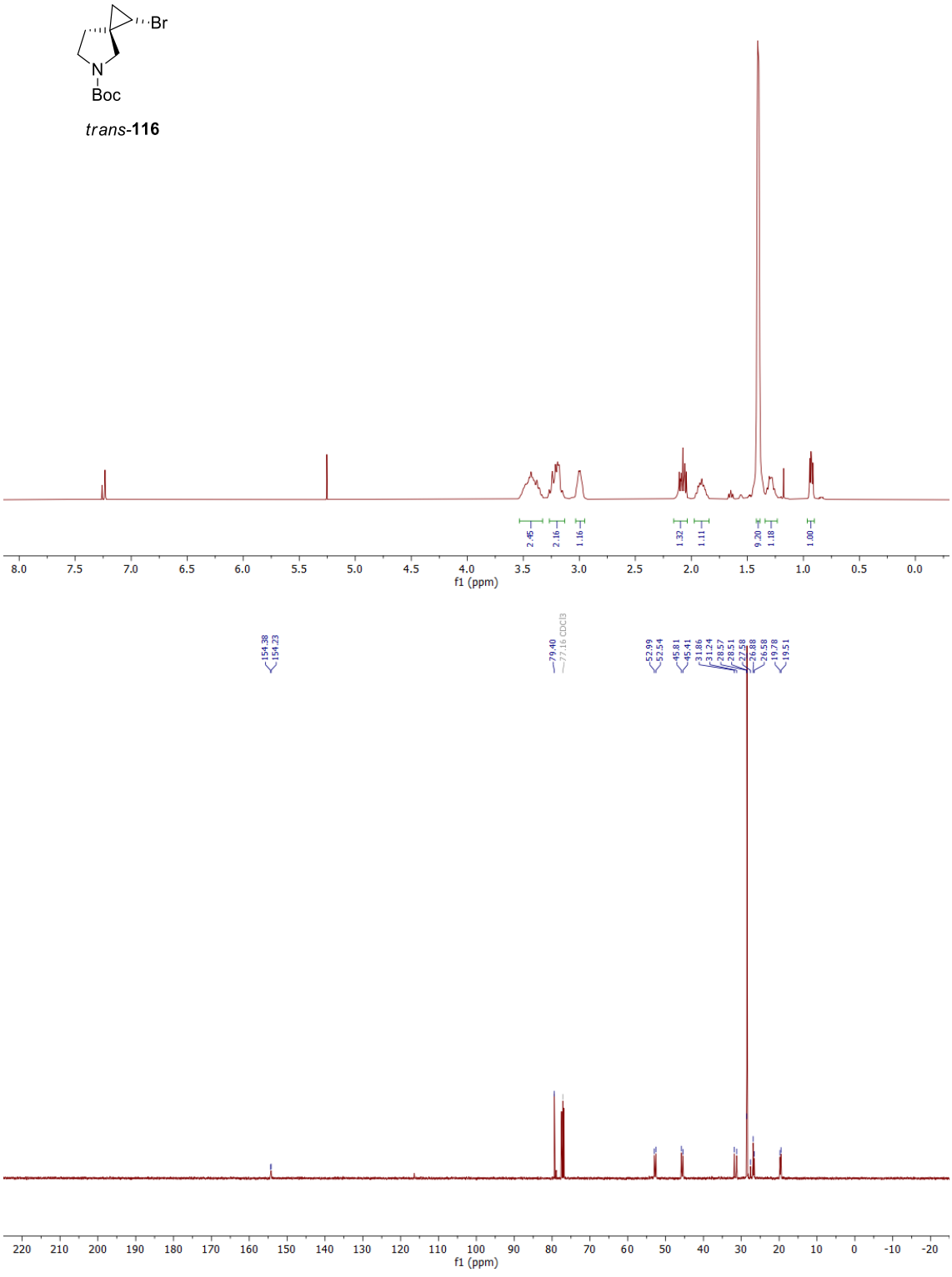

400 MHz ^{1}H NMR spectrum; 100.6 MHz ^{13}C NMR spectrum; $CDCl_3$ of *cis*-**116**

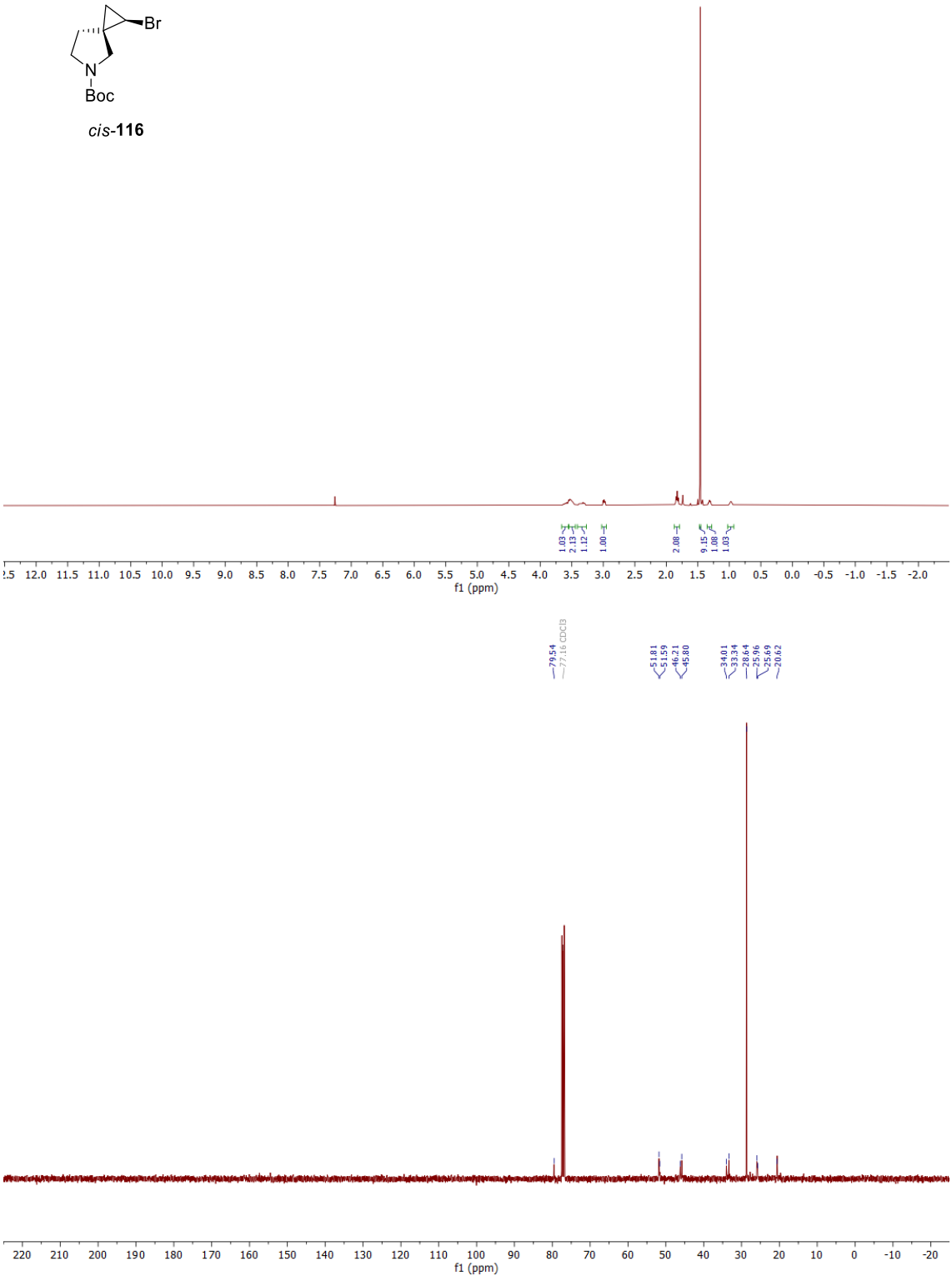

400 MHz ^{1}H NMR spectrum; 100.6 MHz ^{13}C NMR spectrum; 128.4 MHz ^{11}B NMR spectrum; $CDCl_3$ of *trans*-**119**

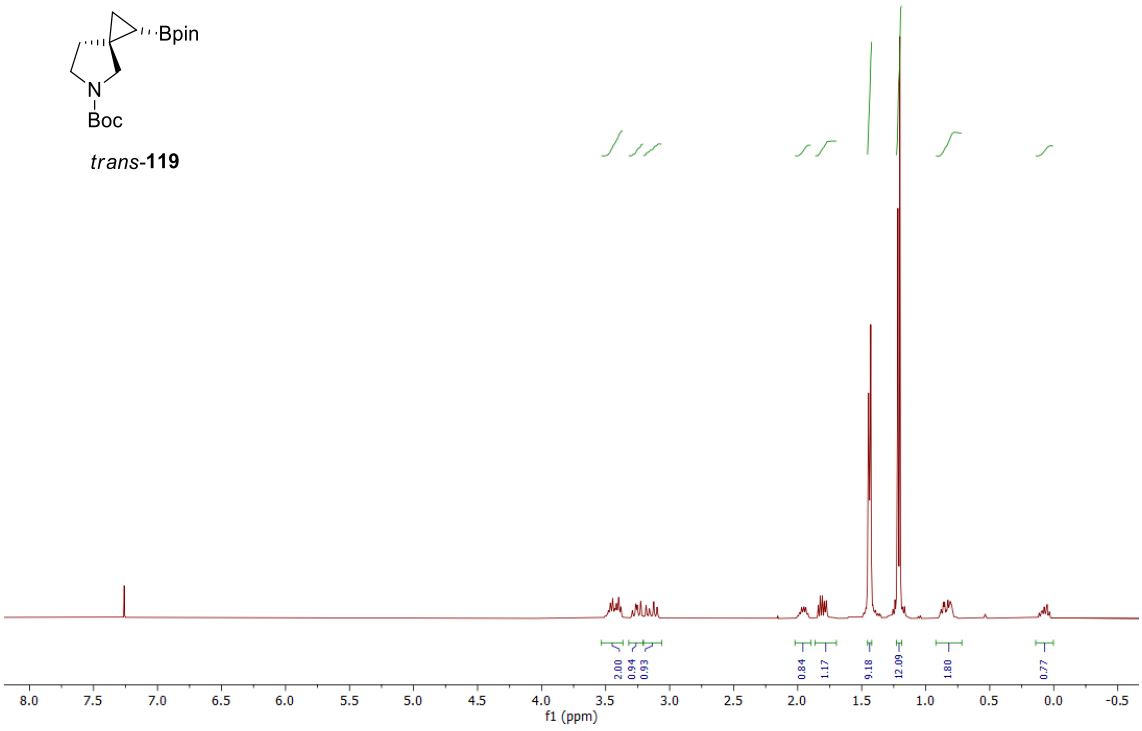

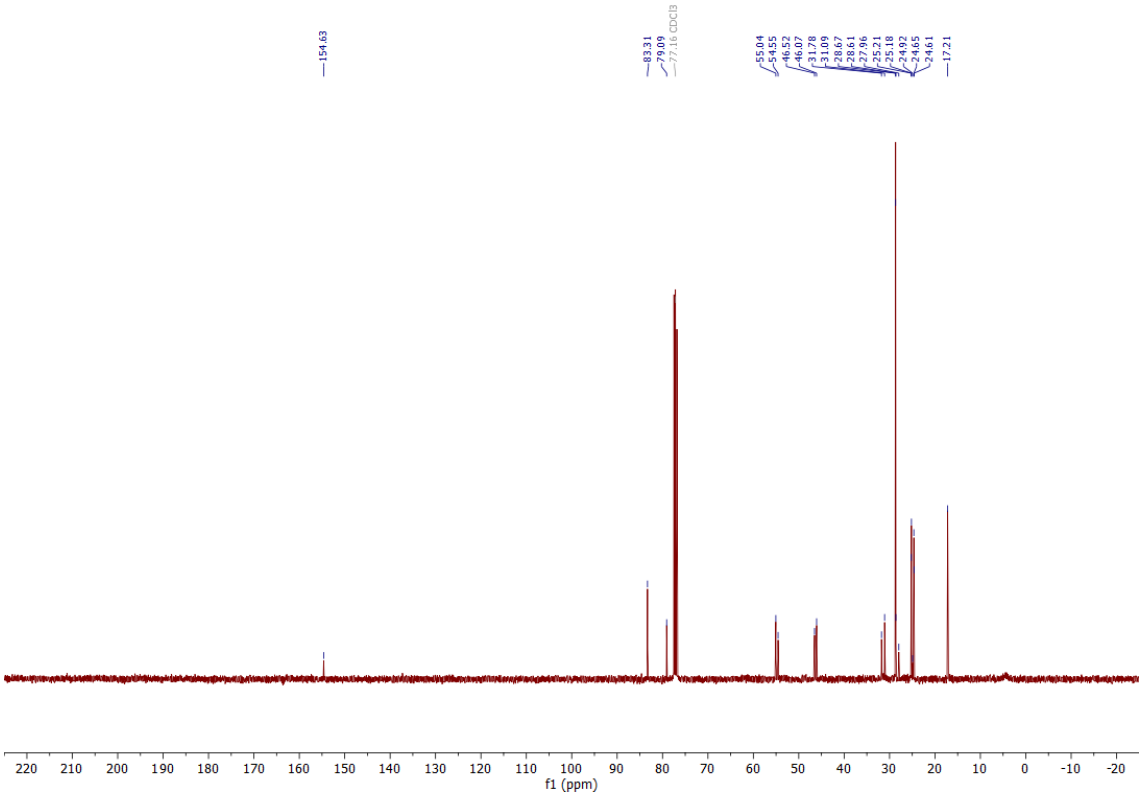

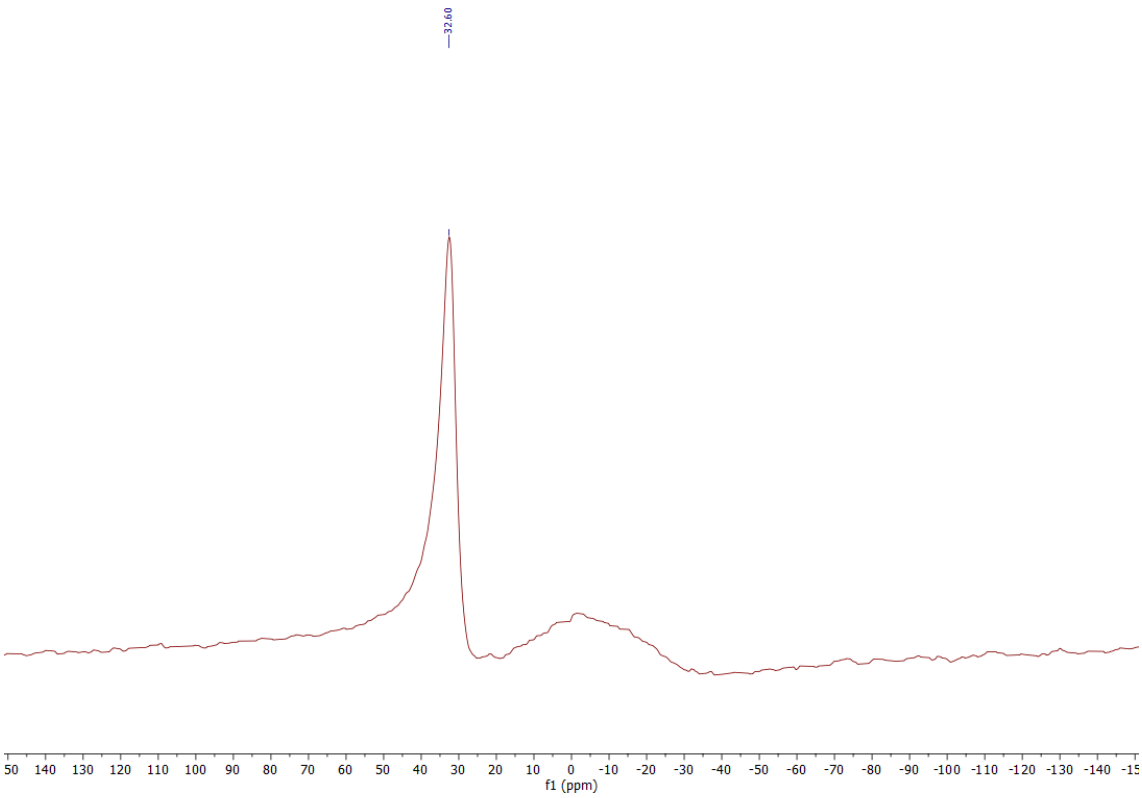
32.60
50 140 130 120 110 100 90 80 70 60 50 40 30 20 10 0 -10 -20 -30 -40 -50 -60 -70 -80 -90 -100 -110 -120 -130 -140 -15
f1 (ppm)

400 MHz ^{1}H NMR spectrum; 100.6 MHz ^{13}C NMR spectrum; 128.4 MHz ^{11}B NMR spectrum; $CDCl_3$ of *trans*-**38**

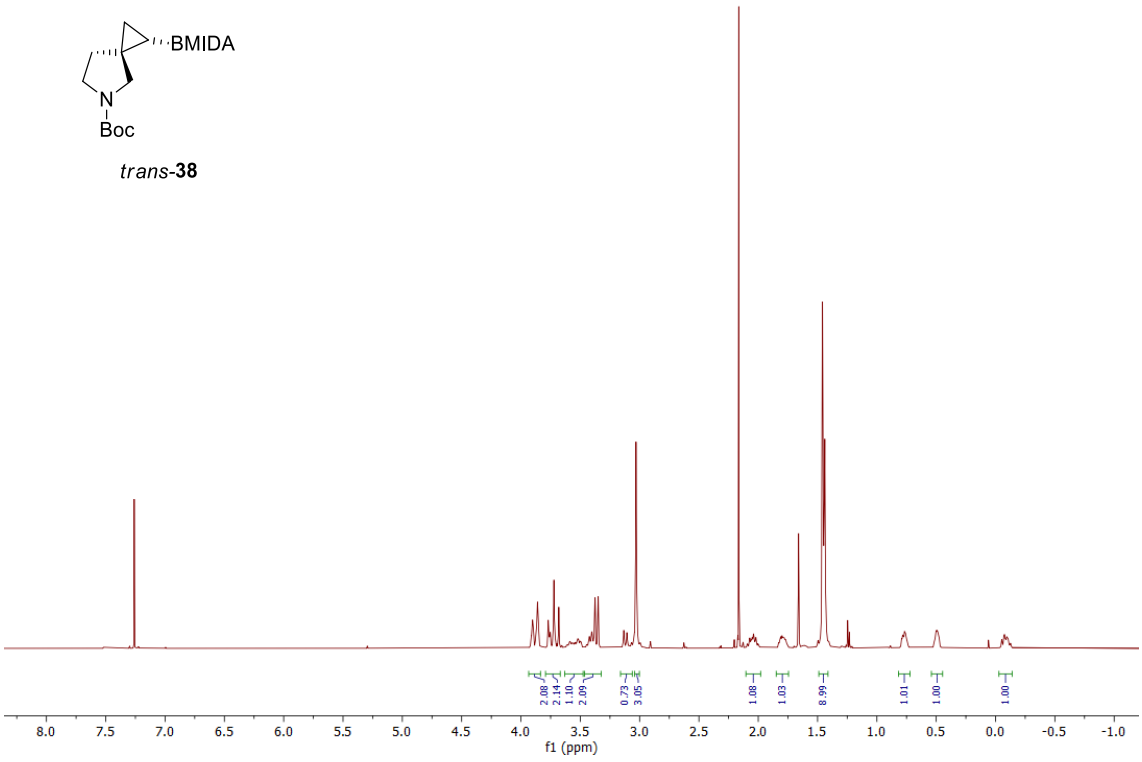

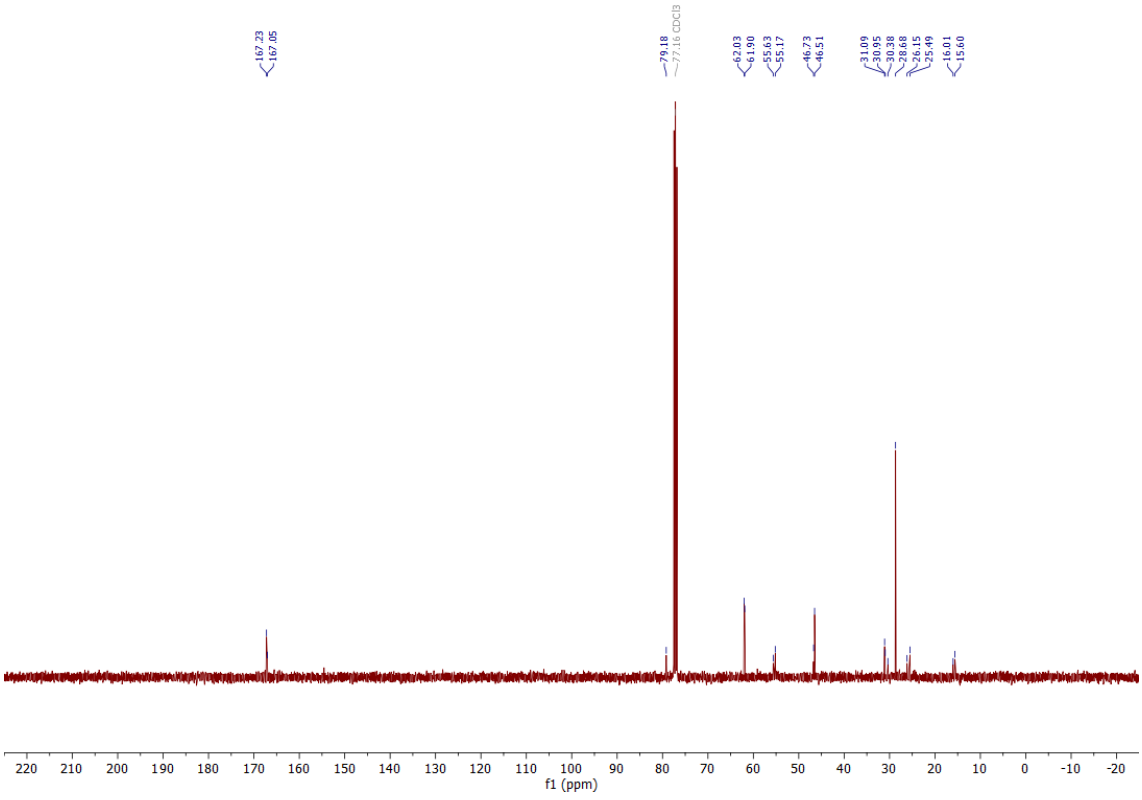

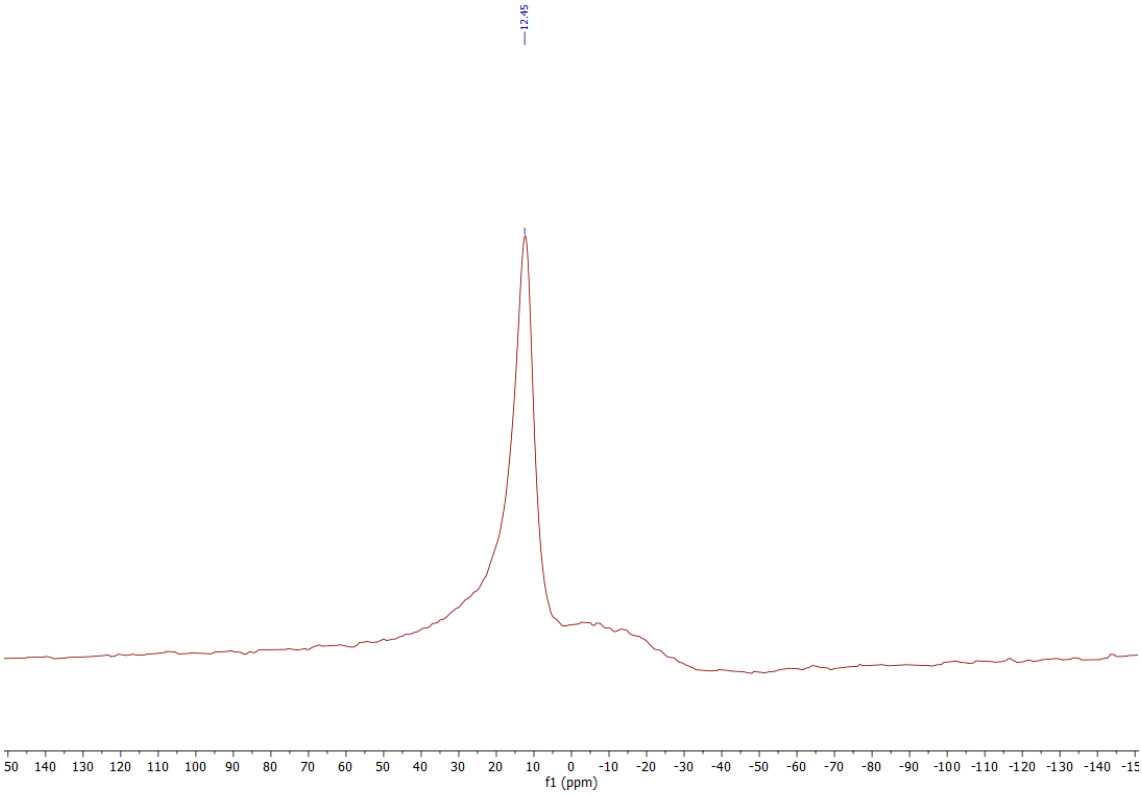
12.45
50 140 130 120 110 100 90 80 70 60 50 40 30 20 10 0 -10 -20 -30 -40 -50 -60 -70 -80 -90 -100 -110 -120 -130 -140 -15
f1 (ppm)

400 MHz ^{1}H NMR spectrum; 100.6 MHz ^{13}C NMR spectrum; 128.4 MHz ^{11}B NMR spectrum; $CDCl_3$ of *cis*-**119**

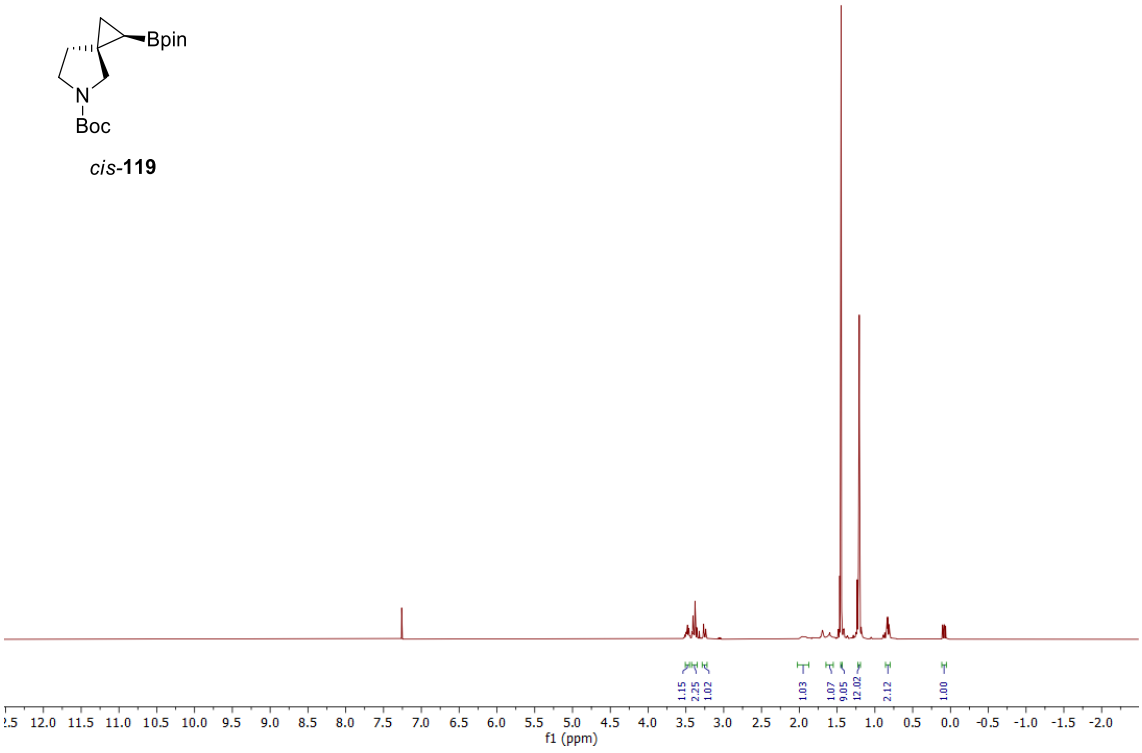

cis-**119**

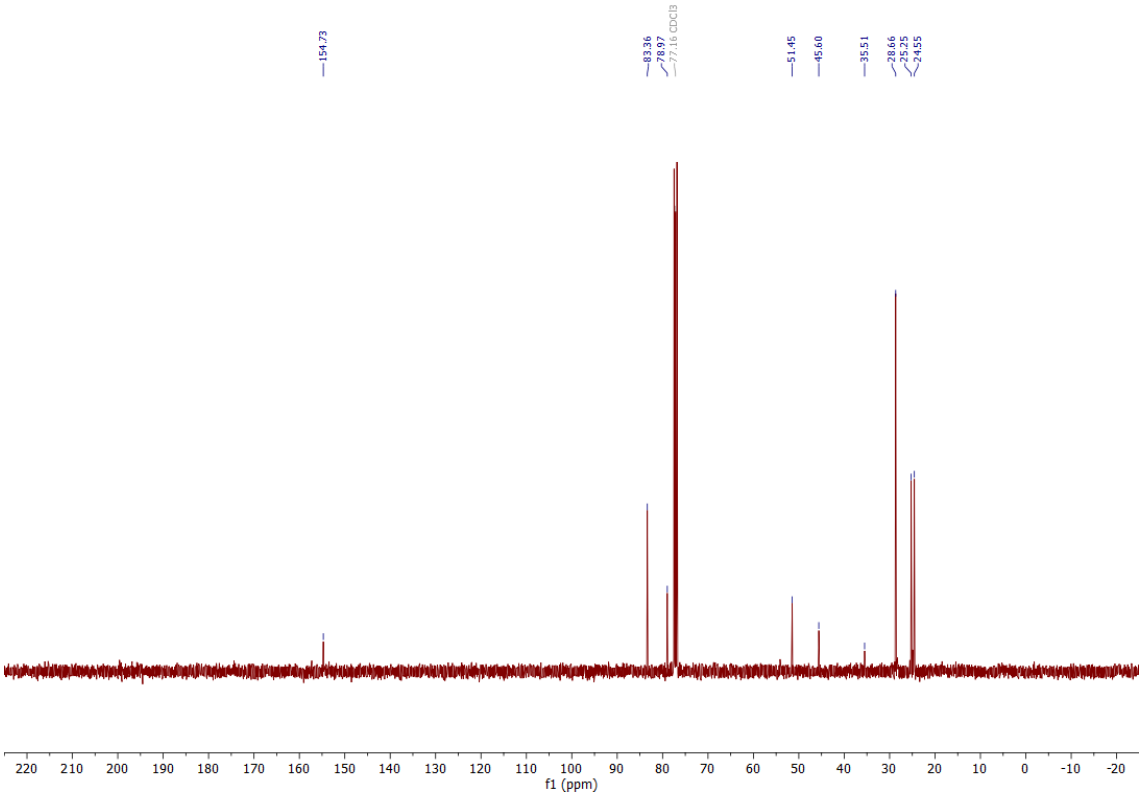

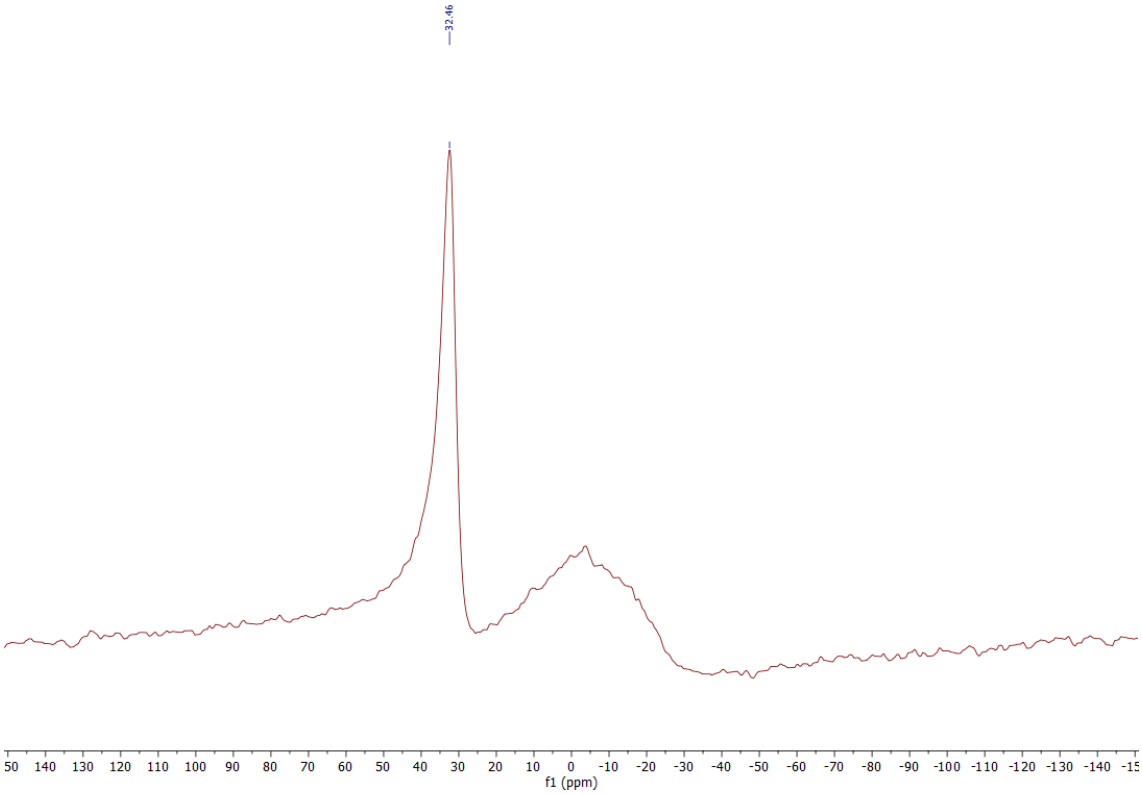
32.46
50 140 130 120 110 100 90 80 70 60 50 40 30 20 10 0 -10 -20 -30 -40 -50 -60 -70 -80 -90 -100 -110 -120 -130 -140 -15
f1 (ppm)

400 MHz ^{1}H NMR spectrum; 100.6 MHz ^{13}C NMR spectrum; 128.4 MHz ^{11}B NMR spectrum; $CDCl_3$ of *cis*-**38**

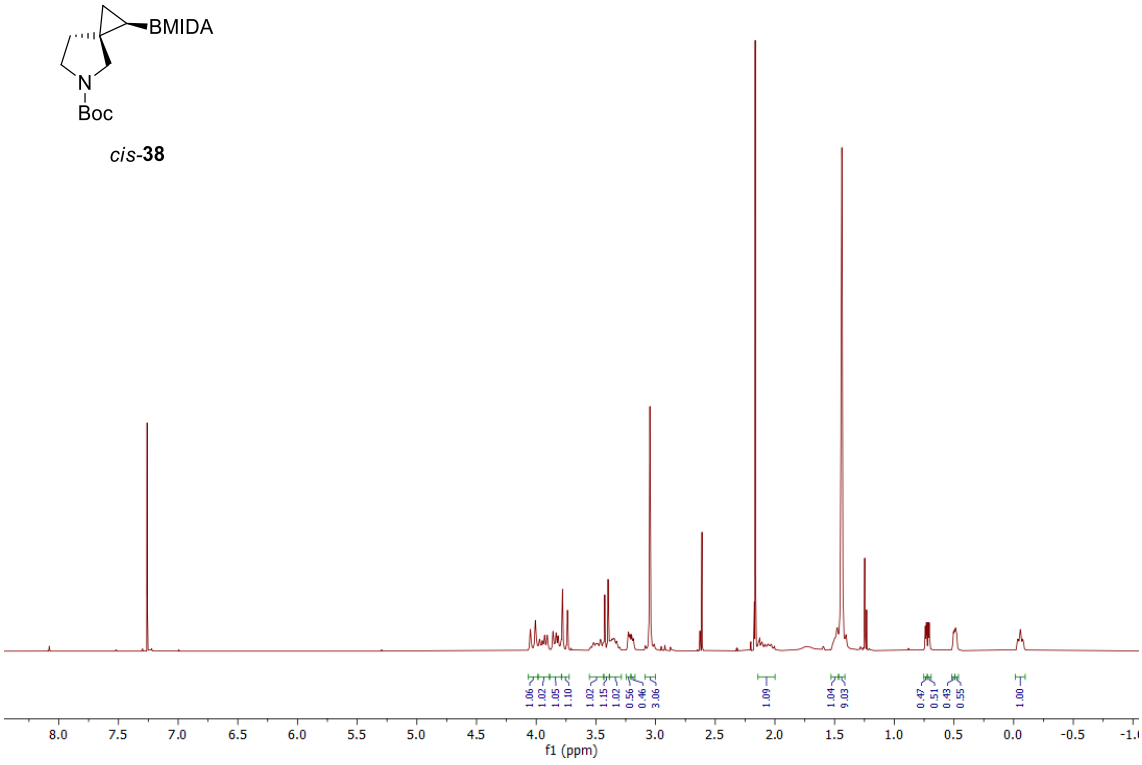

cis-**38**

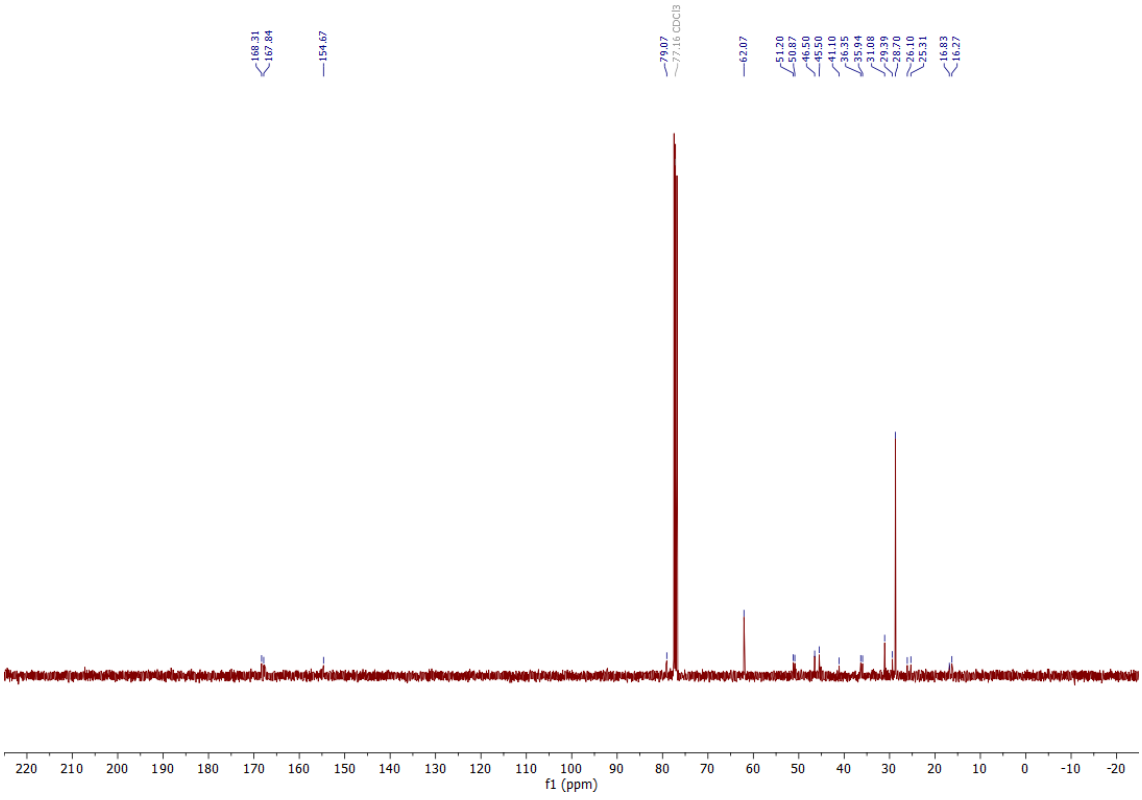

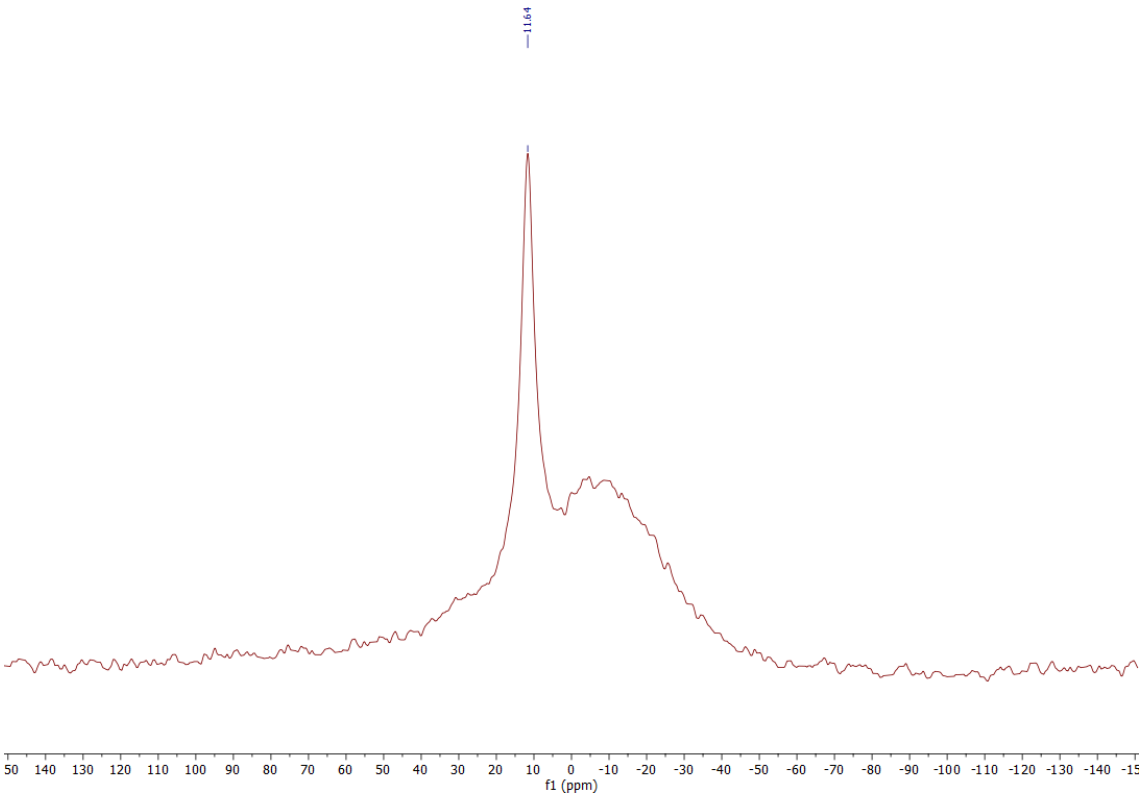
11.64
50 140 130 120 110 100 90 80 70 60 50 40 30 20 10 0 -10 -20 -30 -40 -50 -60 -70 -80 -90 -100 -110 -120 -130 -140 -15
f1 (ppm)

400 MHz ^{1}H NMR spectrum; 100.6 MHz ^{13}C NMR spectrum; $CDCl_3$ of *exo*-**116**

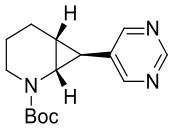

exo-**116**

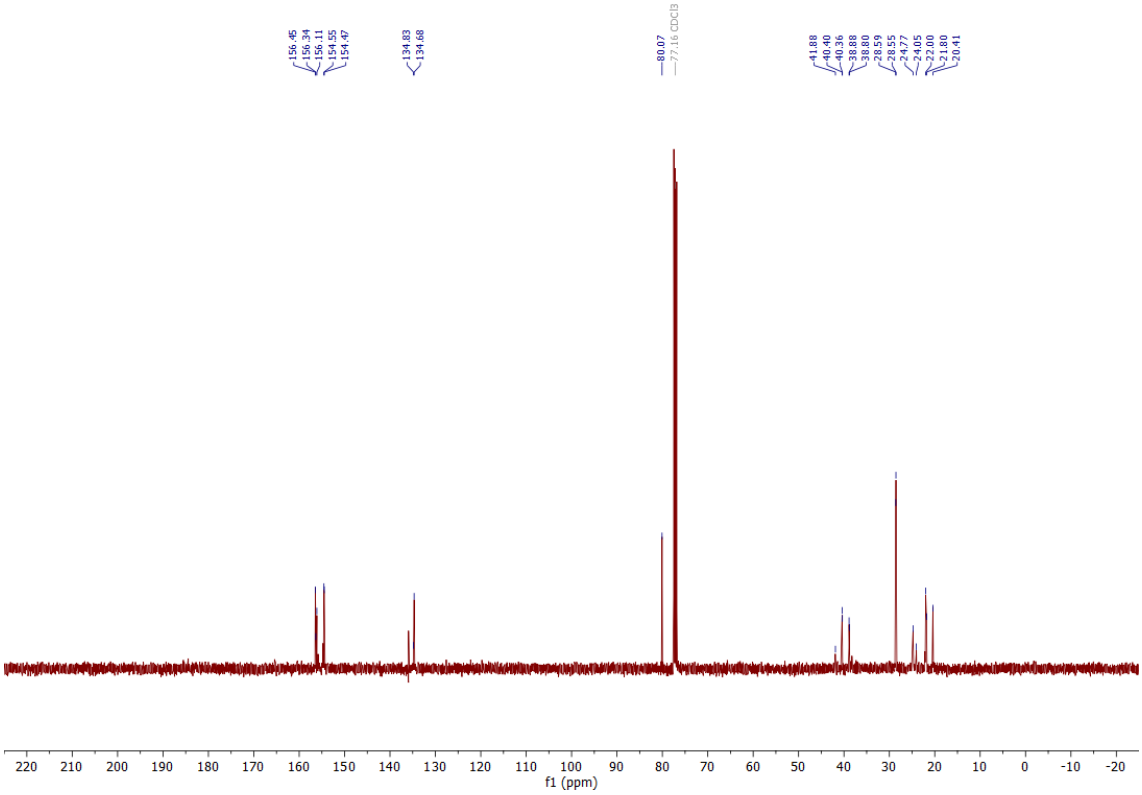

400 MHz ^{1}H NMR spectrum; 100.6 MHz ^{13}C NMR spectrum; $CDCl_3$ of *exo*-**170**

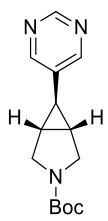

exo-**170**

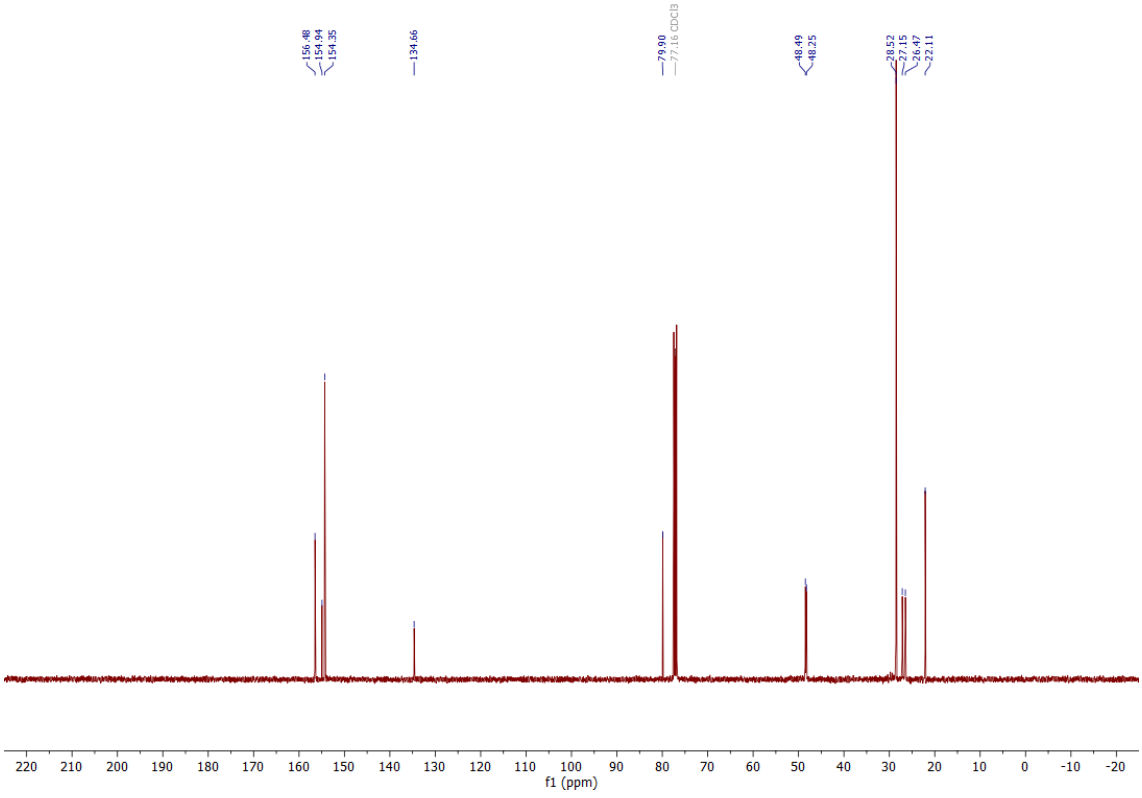

400 MHz ^{1}H NMR spectrum; 100.6 MHz ^{13}C NMR spectrum; $CDCl_3$ of *trans*-**171**

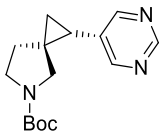

trans-**171**

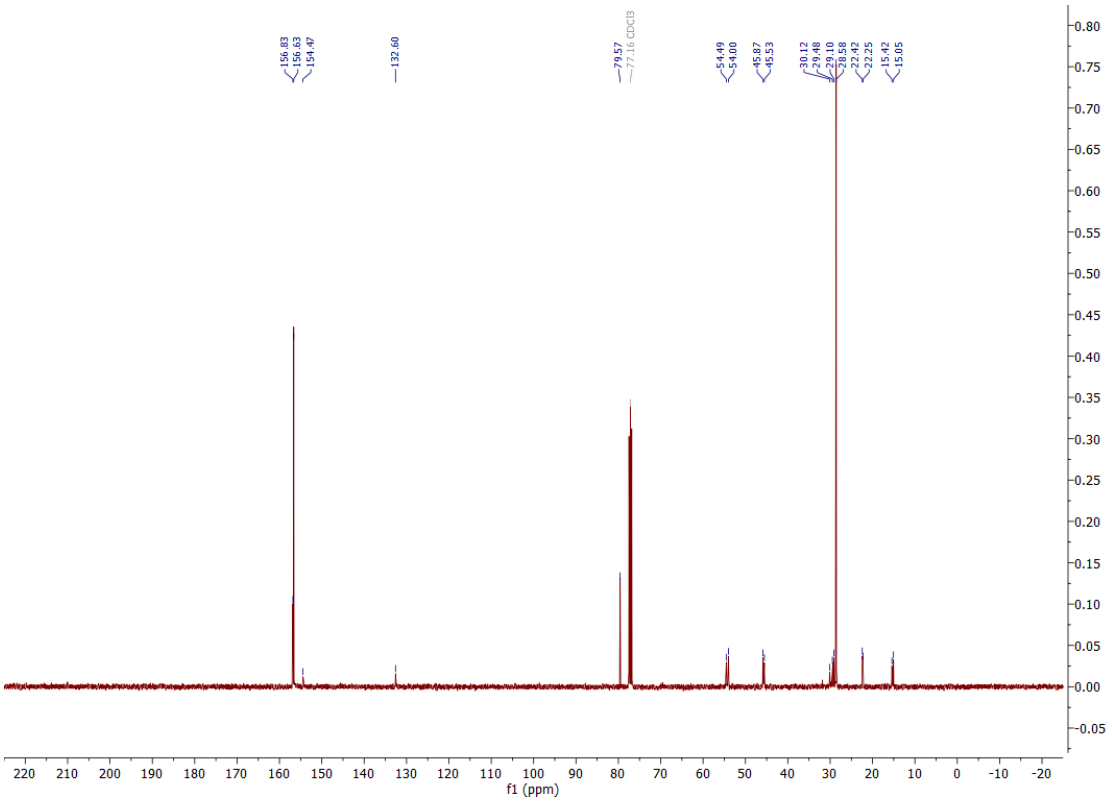

400 MHz ^{1}H NMR spectrum; 100.6 MHz ^{13}C NMR spectrum; $CDCl_3$ of *cis*-**171**

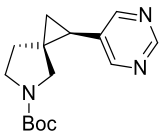

cis-**171**

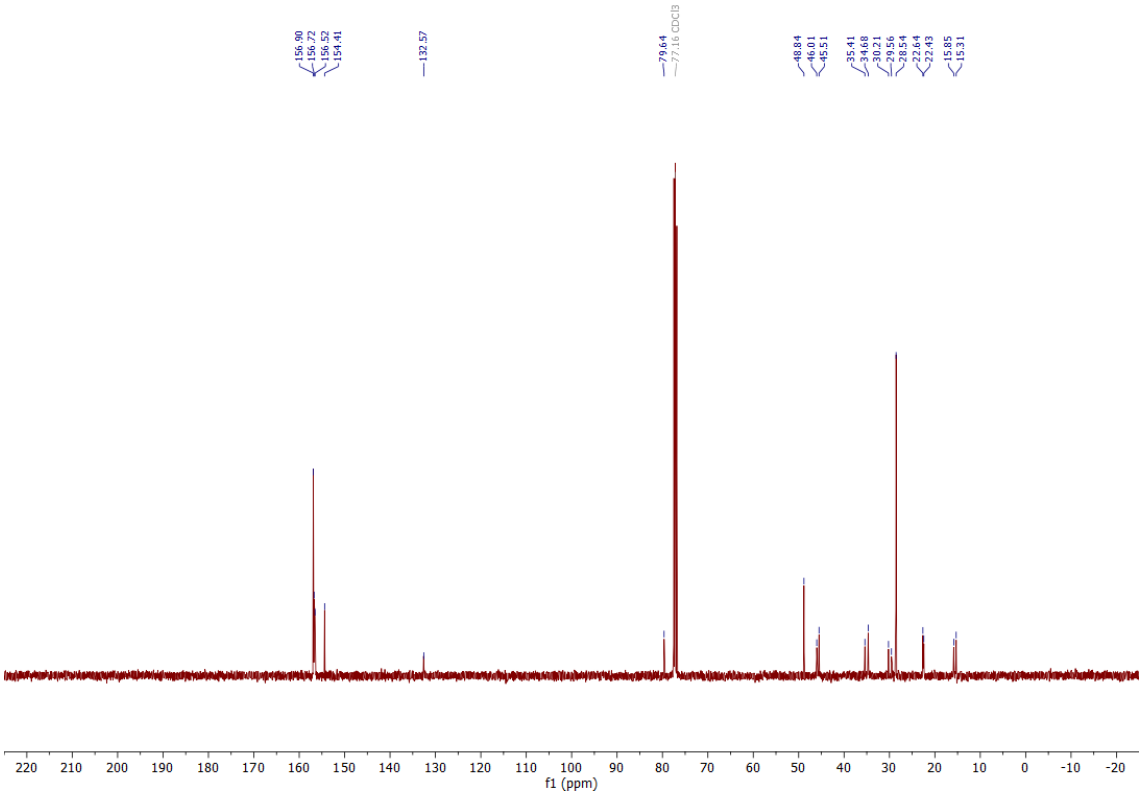

400 MHz ^{1}H NMR spectrum; 100.6 MHz ^{13}C NMR spectrum; $CDCl_3$ of *exo*-**173**

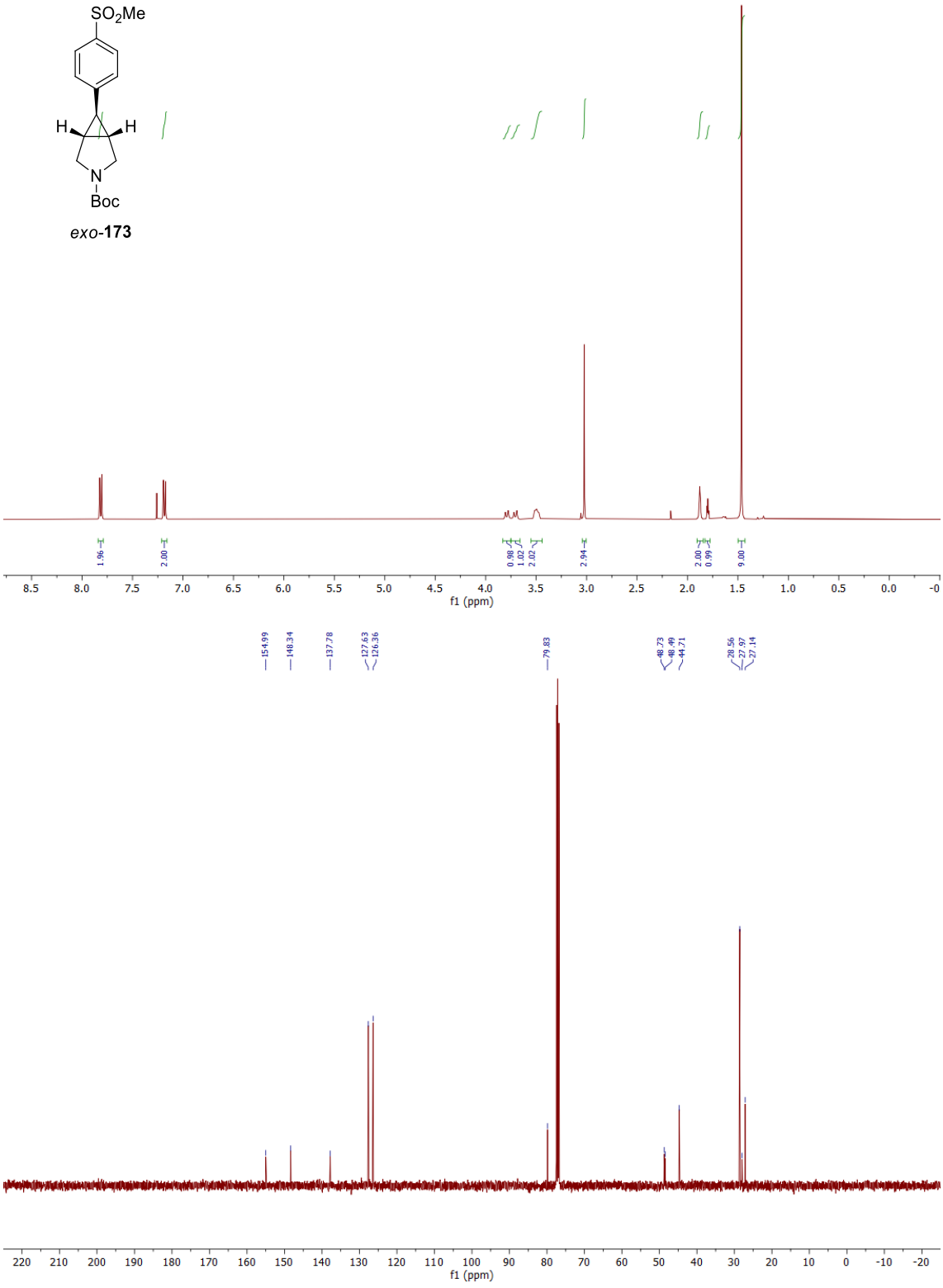

400 MHz ^{1}H NMR spectrum; 100.6 MHz ^{13}C NMR spectrum; $CDCl_3$ of *exo*-**174**

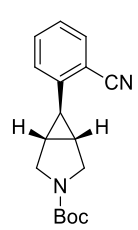

exo-**174**

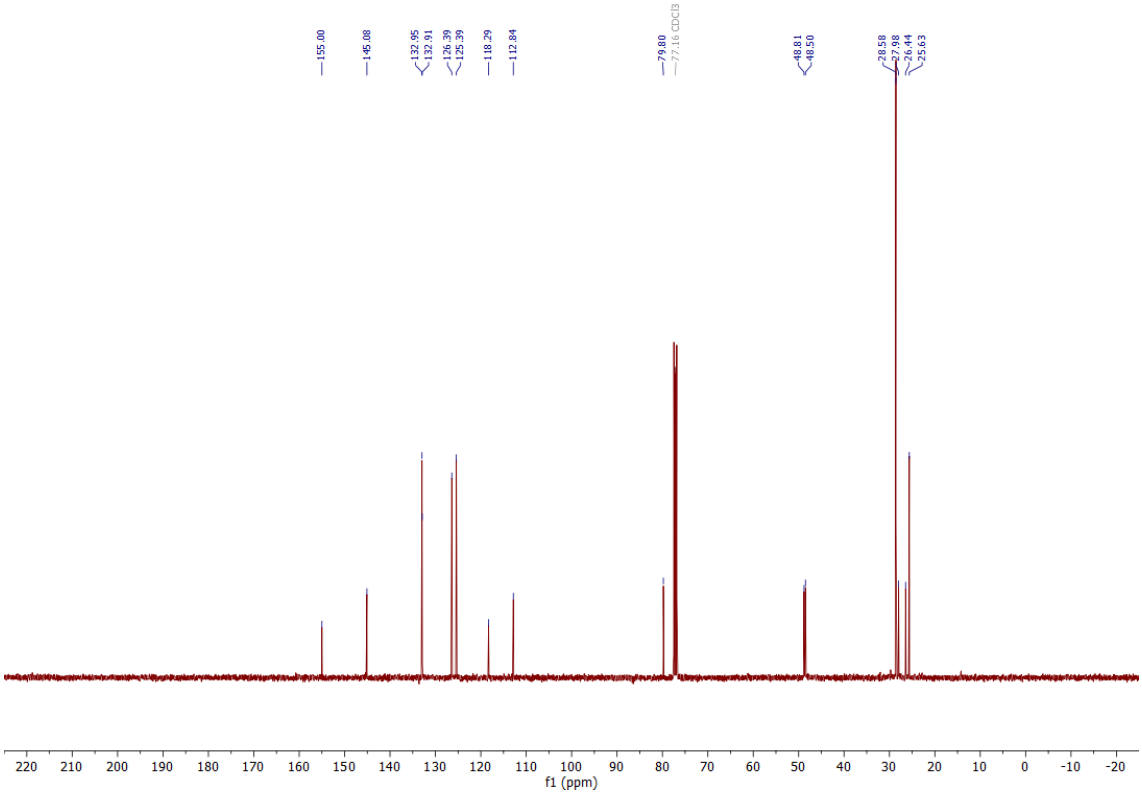

400 MHz ^{1}H NMR spectrum; 100.6 MHz ^{13}C NMR spectrum; $CDCl_3$ of *exo*-**175**

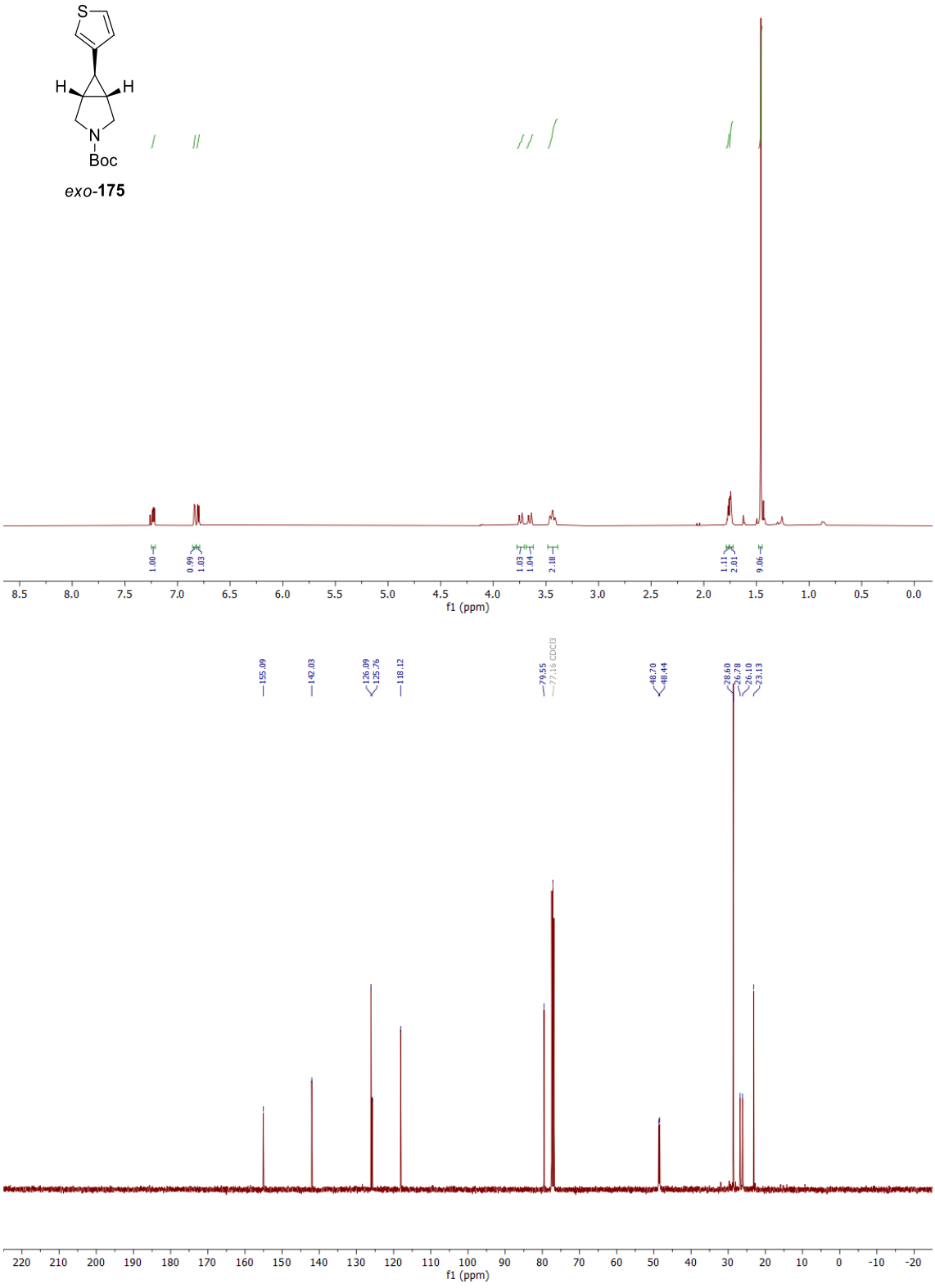

400 MHz ^{1}H NMR spectrum; 100.6 MHz ^{13}C NMR spectrum; $CDCl_3$ of *exo*-**176**

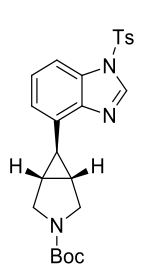

exo-**176**

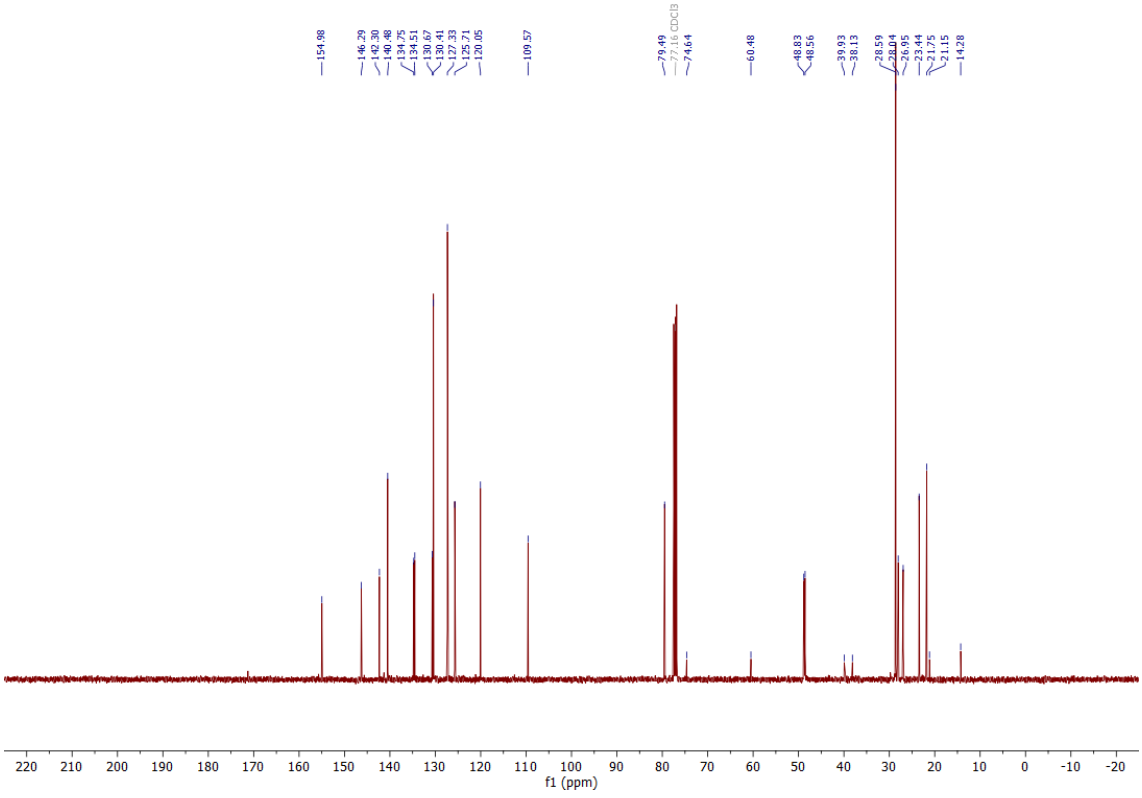

400 MHz ^{1}H NMR spectrum; 100.6 MHz ^{13}C NMR spectrum; $CDCl_3$ of *exo*-**177**

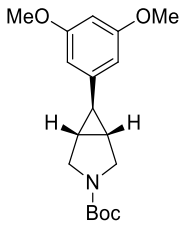

exo-**177**

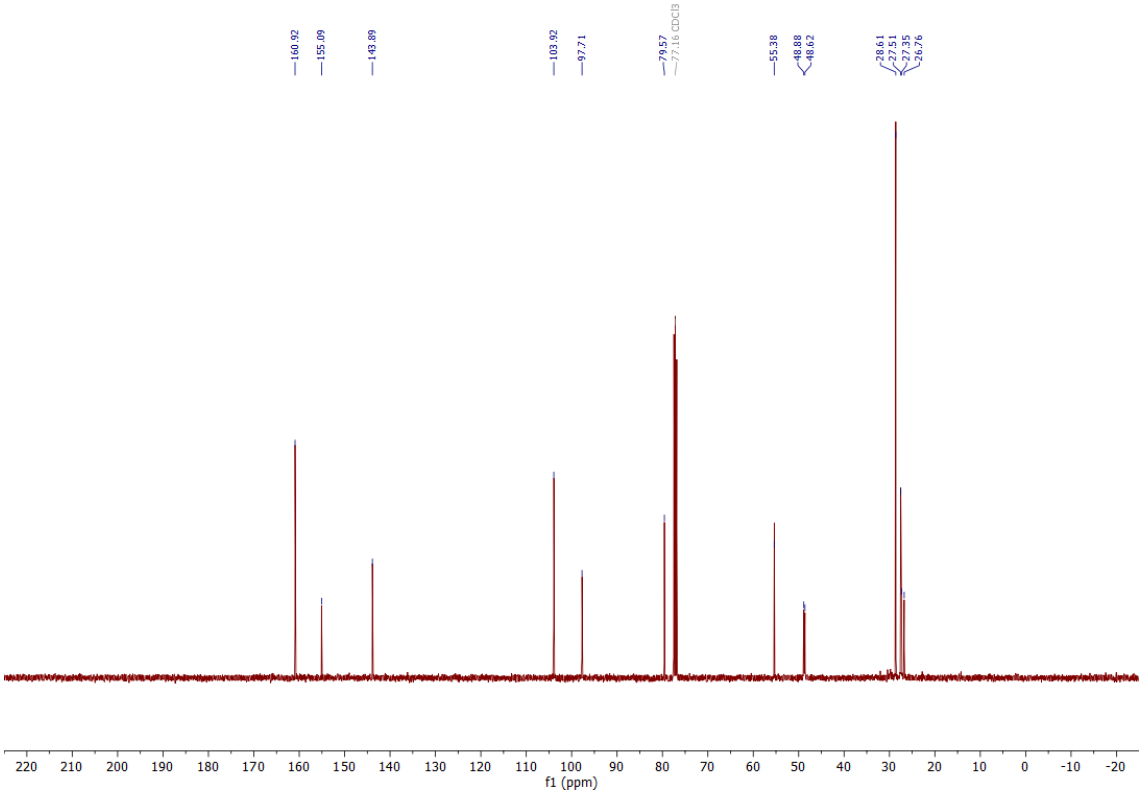

400 MHz ^{1}H NMR spectrum; 100.6 MHz ^{13}C NMR spectrum; $CDCl_3$ of *trans*-**178**

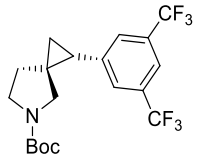

trans-**178**

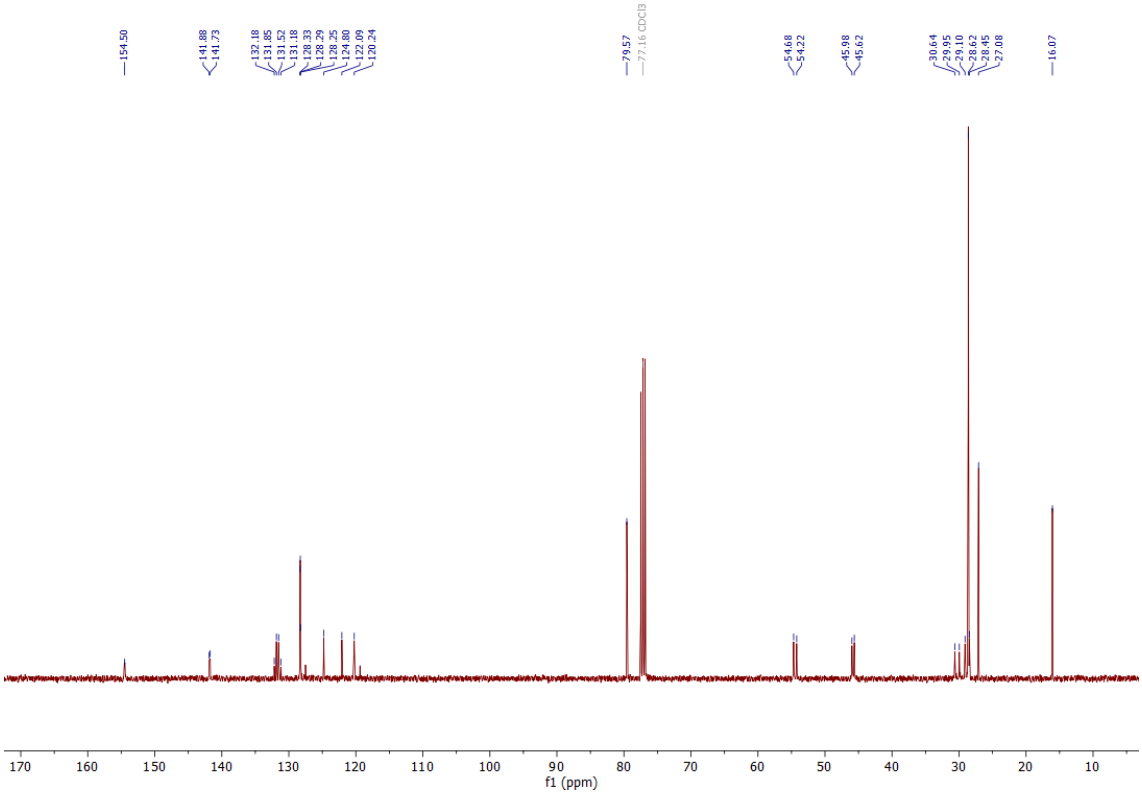

400 MHz ^{1}H NMR spectrum; 100.6 MHz ^{13}C NMR spectrum; $CDCl_3$ of *trans*-**179**

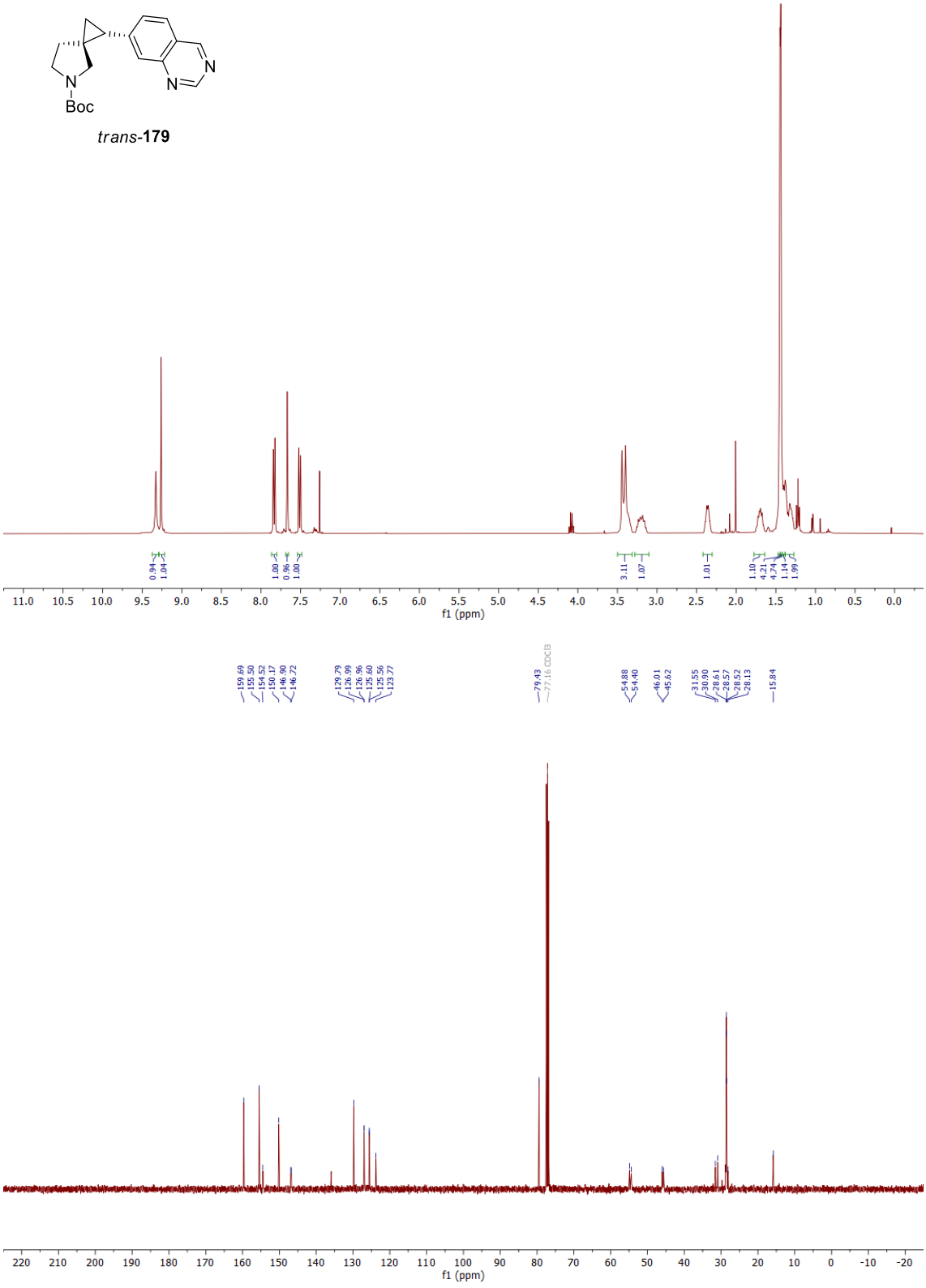

400 MHz ^{1}H NMR spectrum; 100.6 MHz ^{13}C NMR spectrum; $CDCl_3$ of *trans*-**180**

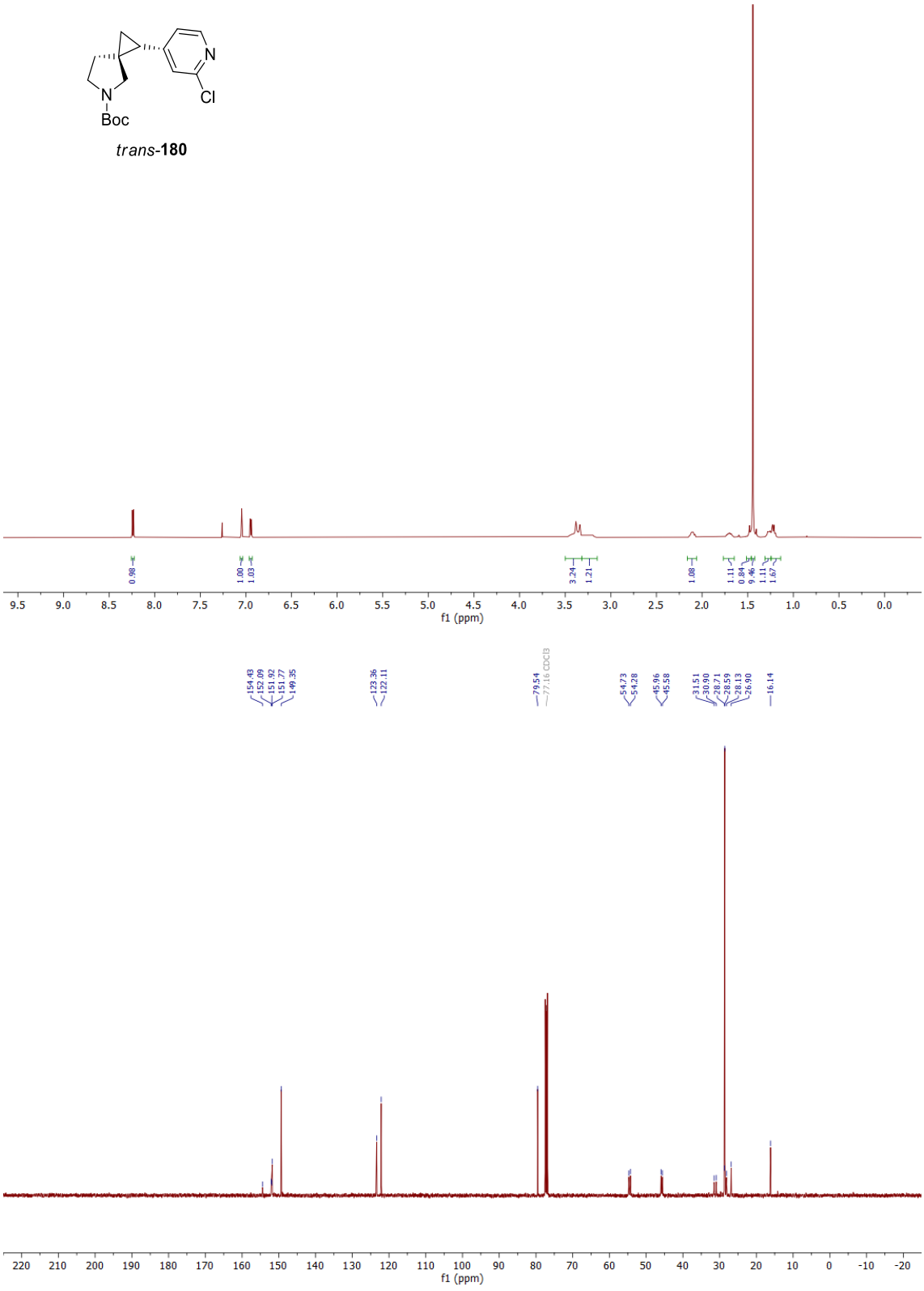

400 MHz ^{1}H NMR spectrum; 100.6 MHz ^{13}C NMR spectrum; $CDCl_3$ of *trans*-**181**

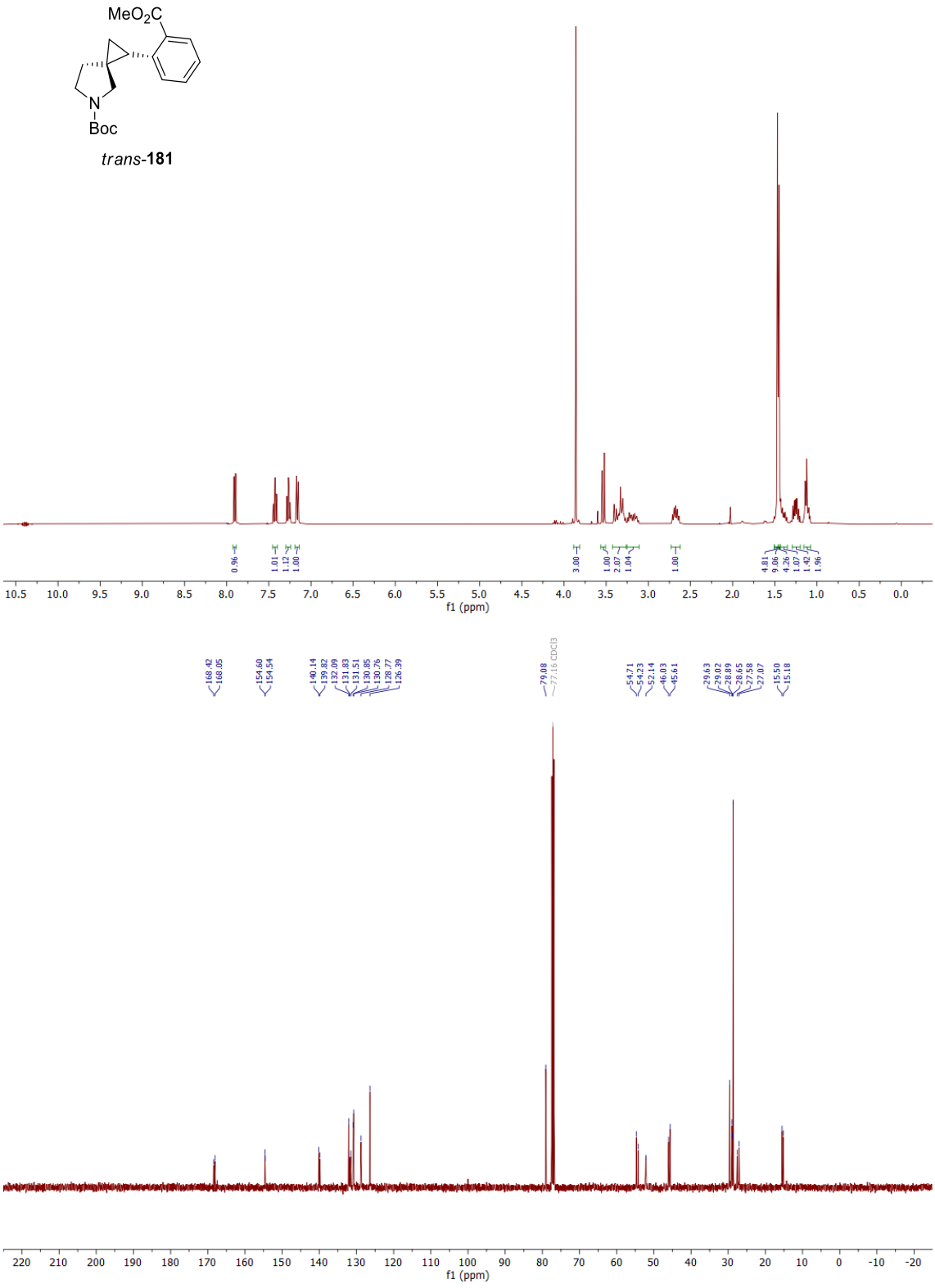

400 MHz ^{1}H NMR spectrum; 100.6 MHz ^{13}C NMR spectrum; $CDCl_3$ of *cis*-**182**

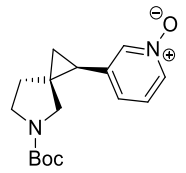

cis-**182**

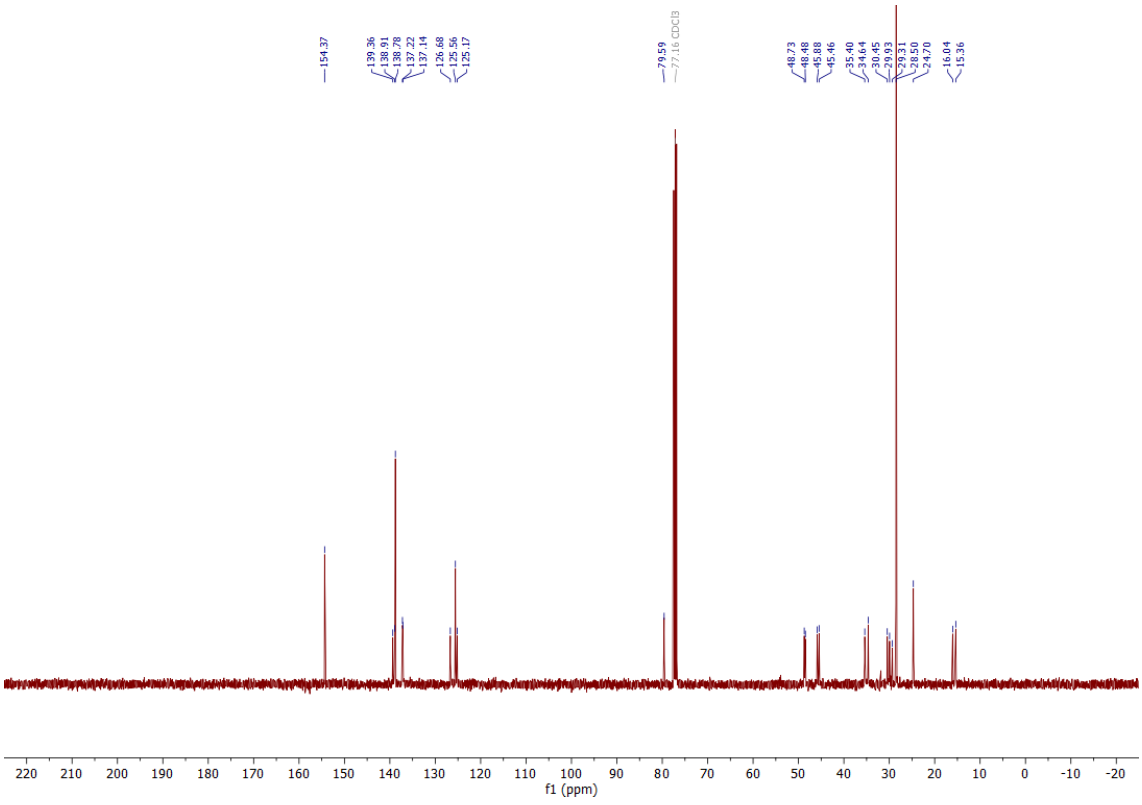

400 MHz ^{1}H NMR spectrum; 100.6 MHz ^{13}C NMR spectrum; $CDCl_3$ of *cis*-**183**

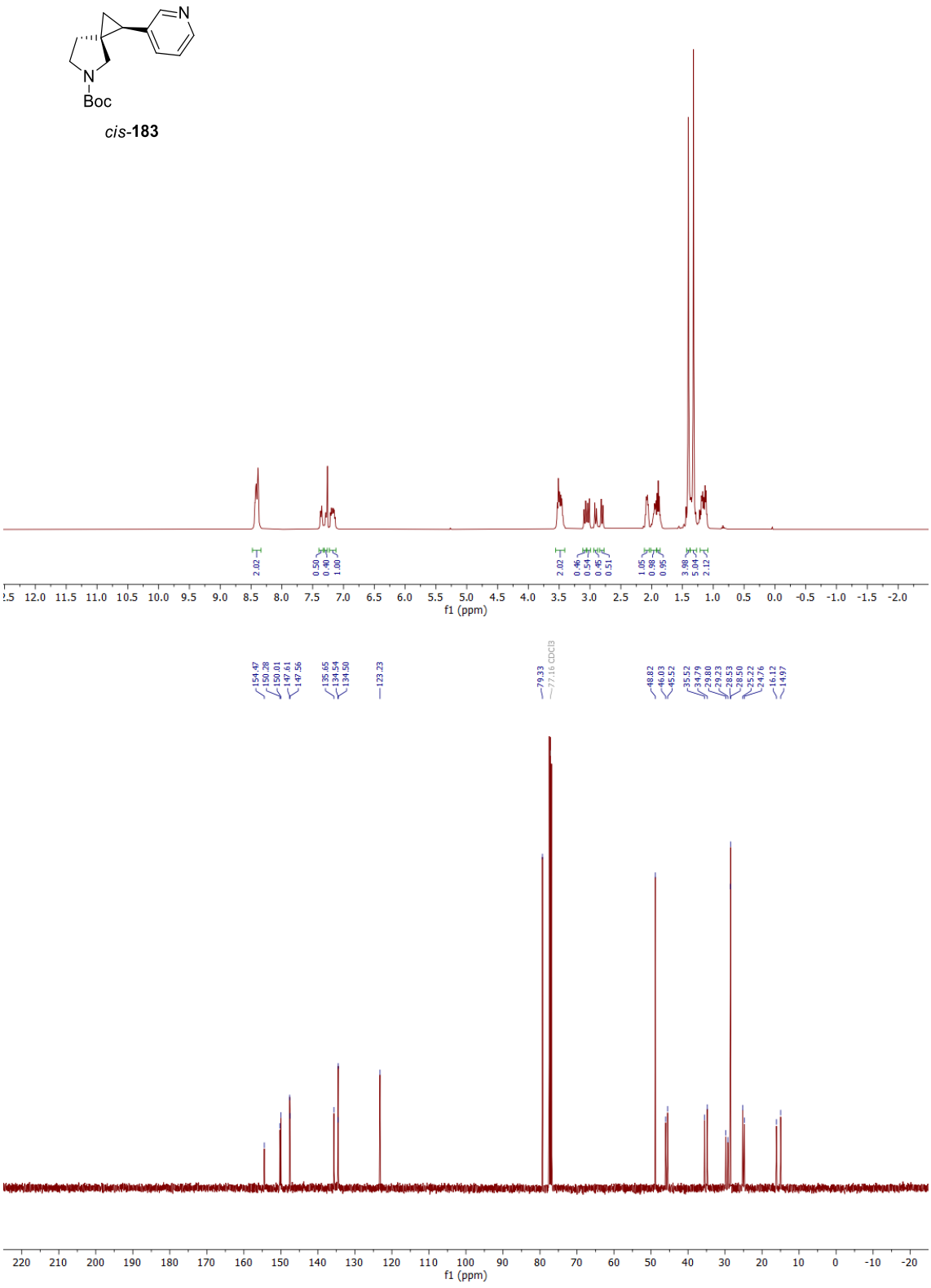

400 MHz ^{1}H NMR spectrum; 100.6 MHz ^{13}C NMR spectrum; $CDCl_3$ of *cis*-**184**

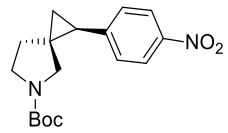

cis-**184**

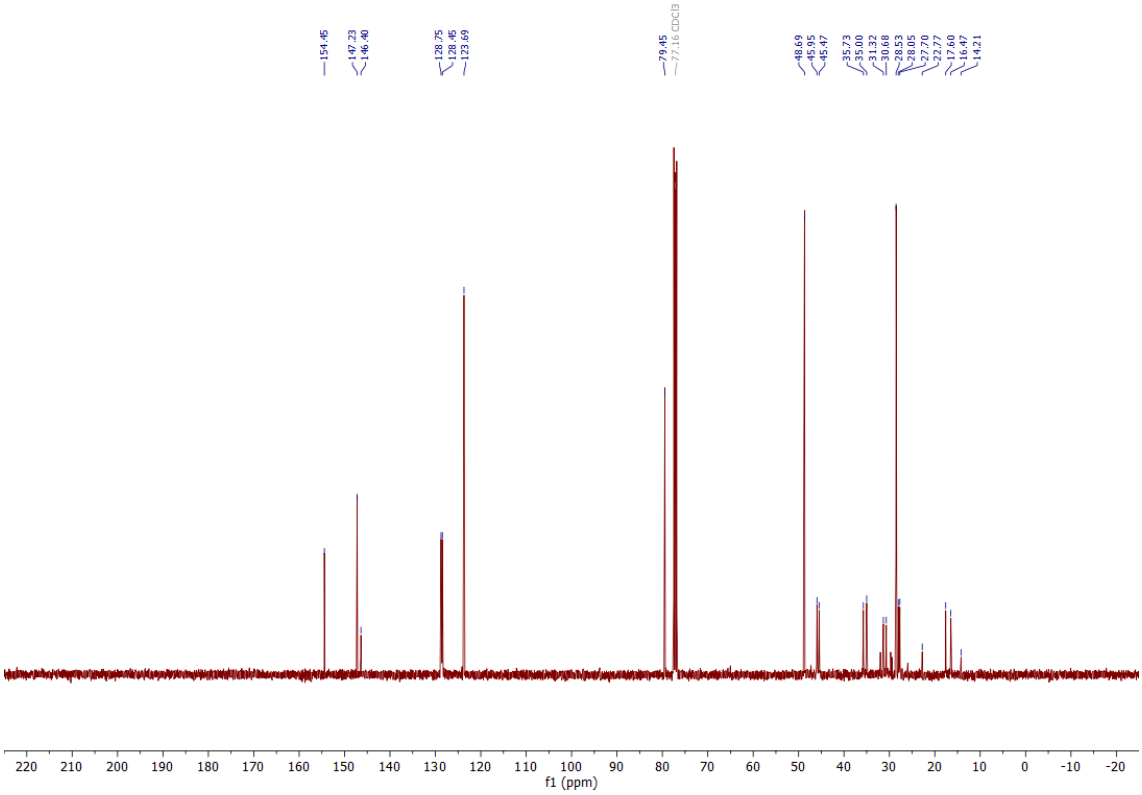

400 MHz ^{1}H NMR spectrum; 100.6 MHz ^{13}C NMR spectrum; $CDCl_3$ of *cis*-**185**

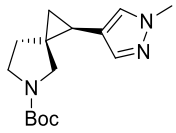

cis-**185**

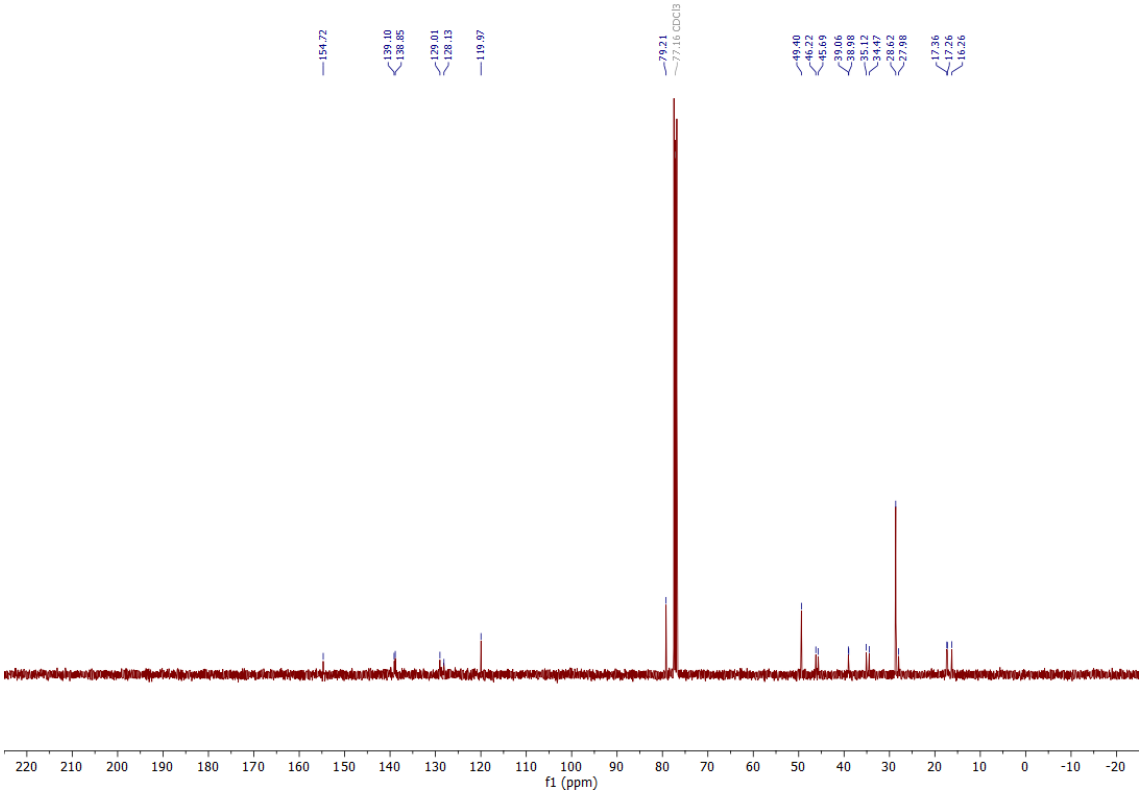

400 MHz ^{1}H NMR spectrum; 100.6 MHz ^{13}C NMR spectrum; $CDCl_3$ of *exo*-**186**

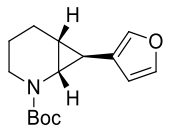

exo-**186**

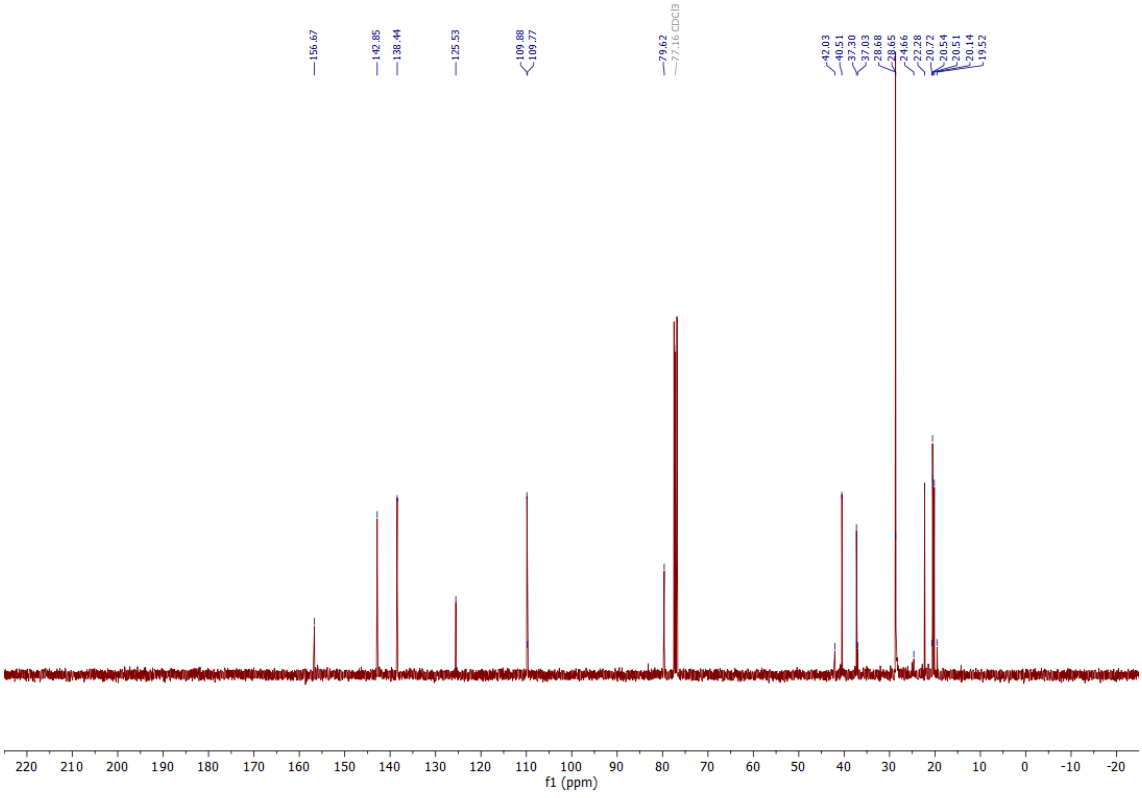

400 MHz ^{1}H NMR spectrum; 100.6 MHz ^{13}C NMR spectrum; $CDCl_3$ of *exo*-**187**

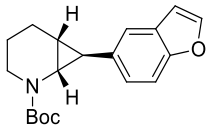

exo-**187**

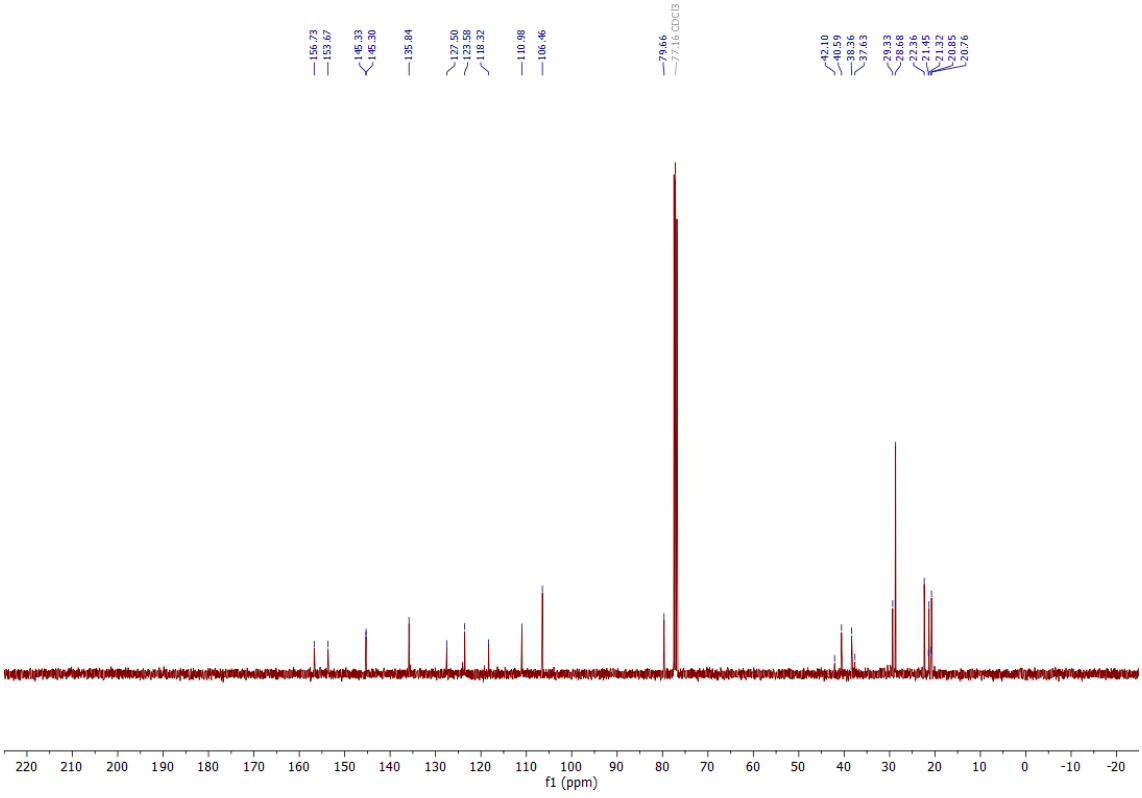

400 MHz ^{1}H NMR spectrum; 100.6 MHz ^{13}C NMR spectrum; $CDCl_3$ of *exo*-**188**

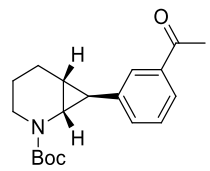

exo-**188**

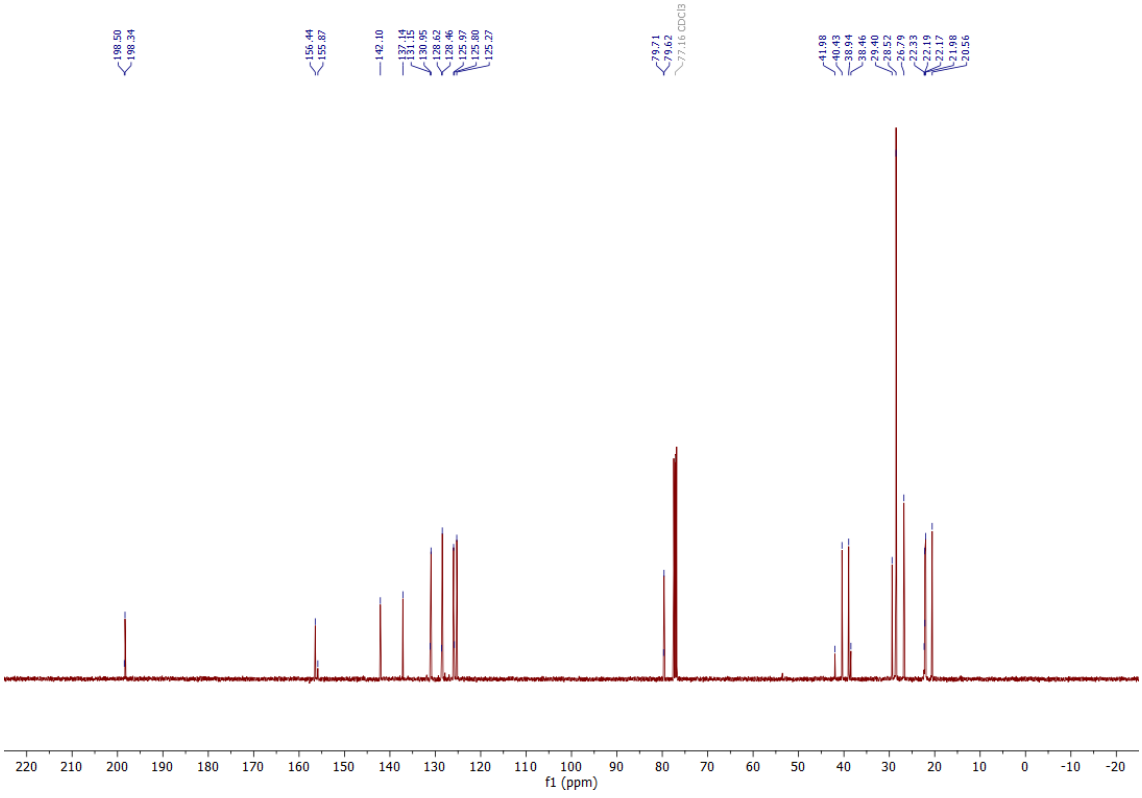

400 MHz ^{1}H NMR spectrum; 100.6 MHz ^{13}C NMR spectrum; $CDCl_3$ of *exo*-**189**

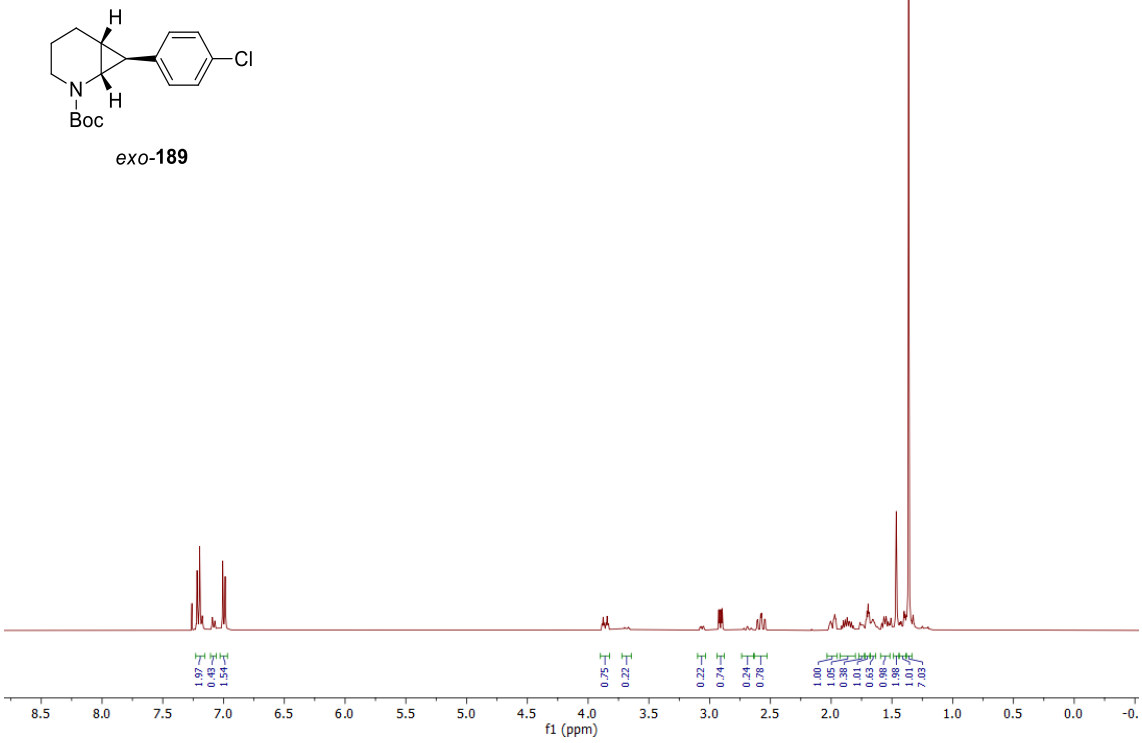

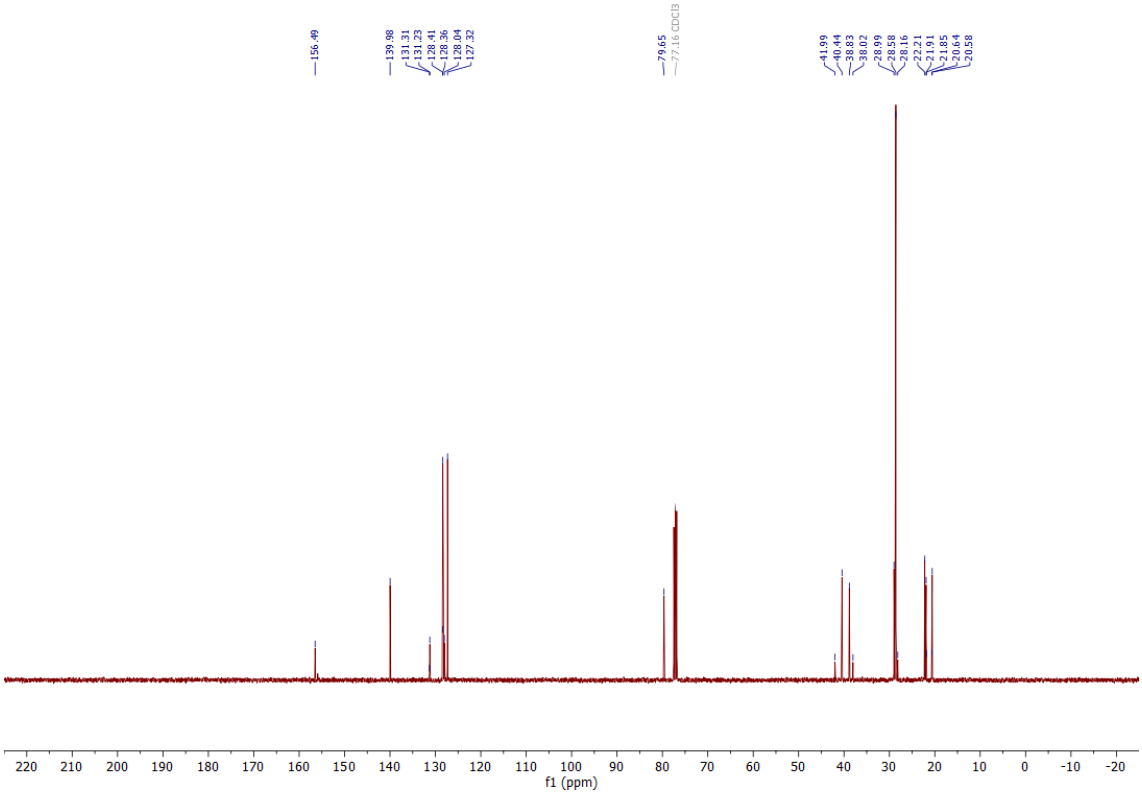

400 MHz ^{1}H NMR spectrum; 100.6 MHz ^{13}C NMR spectrum; $CDCl_3$ of *exo*-**190**

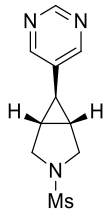

exo-**190**

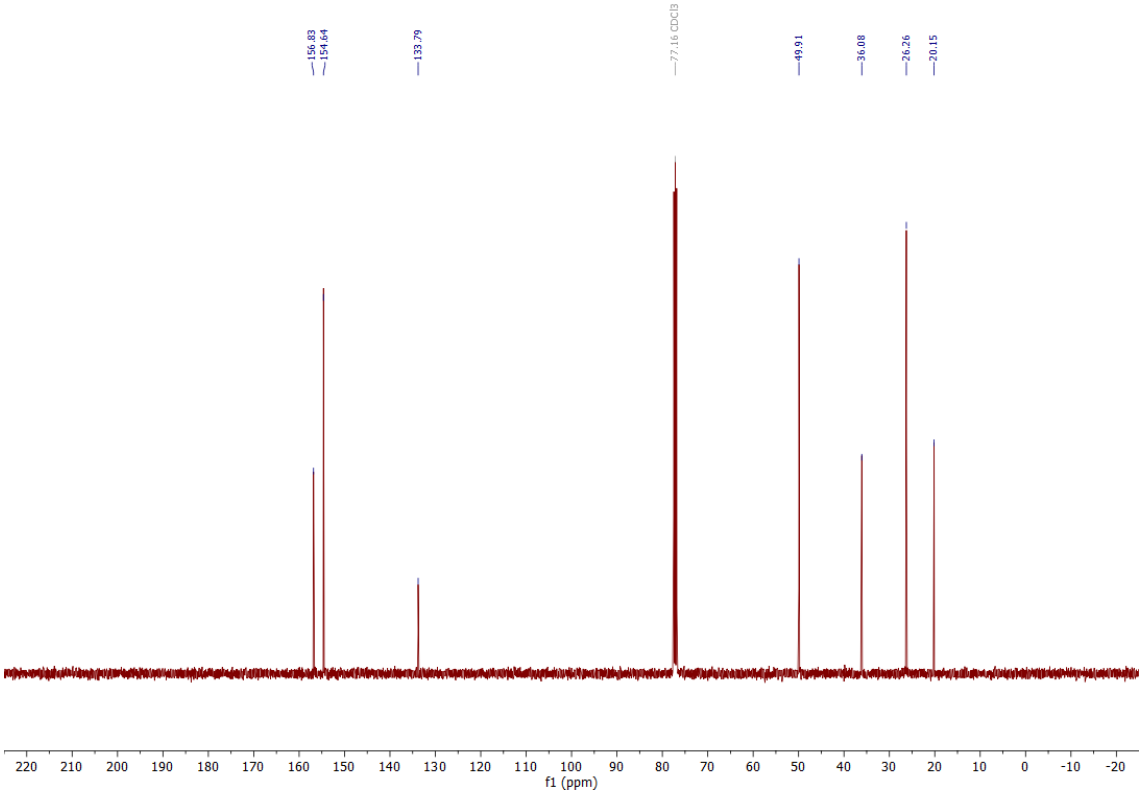

400 MHz ^{1}H NMR spectrum; 100.6 MHz ^{13}C NMR spectrum; $CDCl_3$ of *trans*-**191**

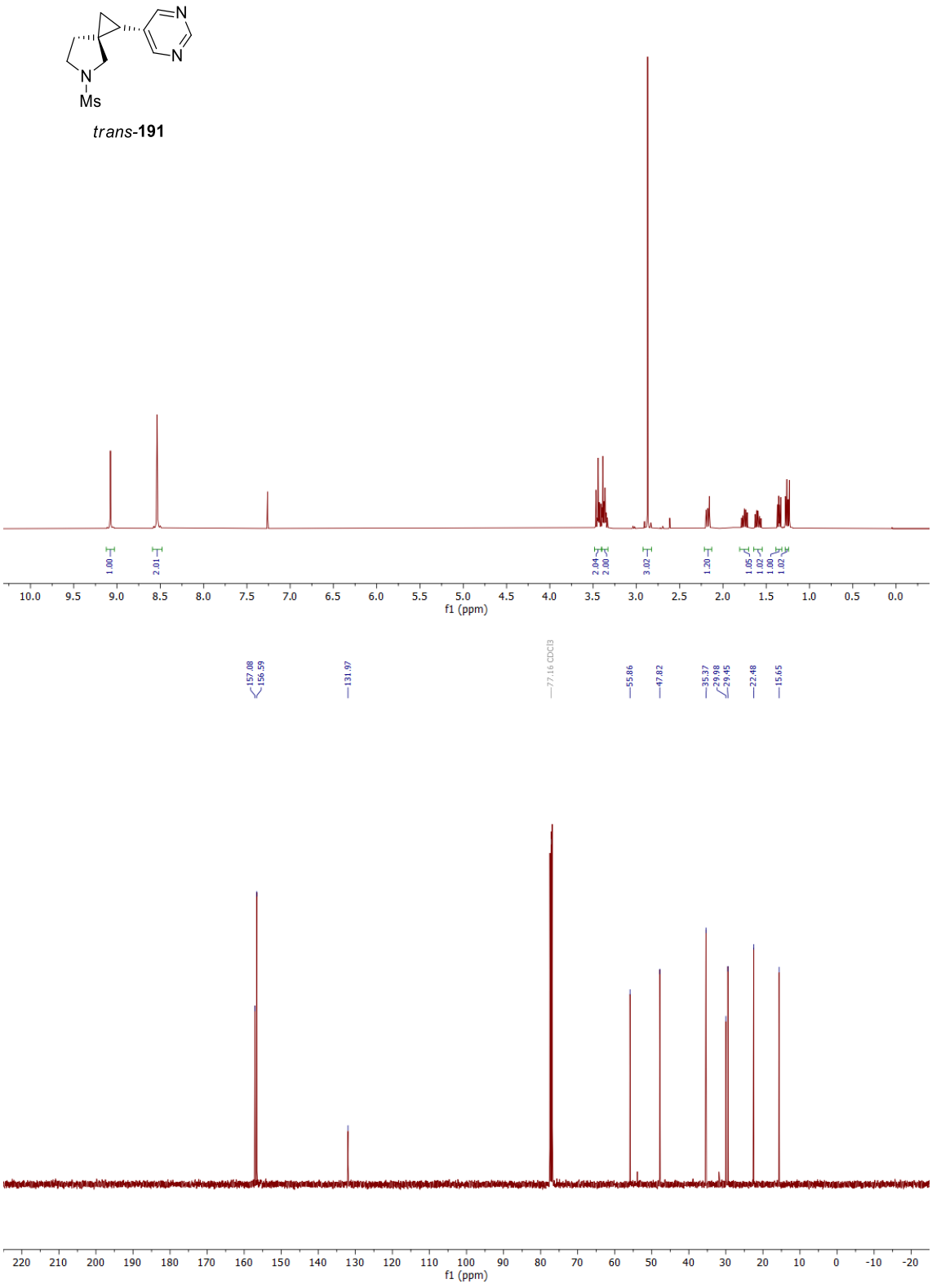

400 MHz ^{1}H NMR spectrum; 100.6 MHz ^{13}C NMR spectrum; $CDCl_3$ of *cis*-**191**

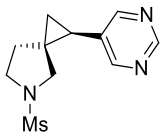

cis-**191**

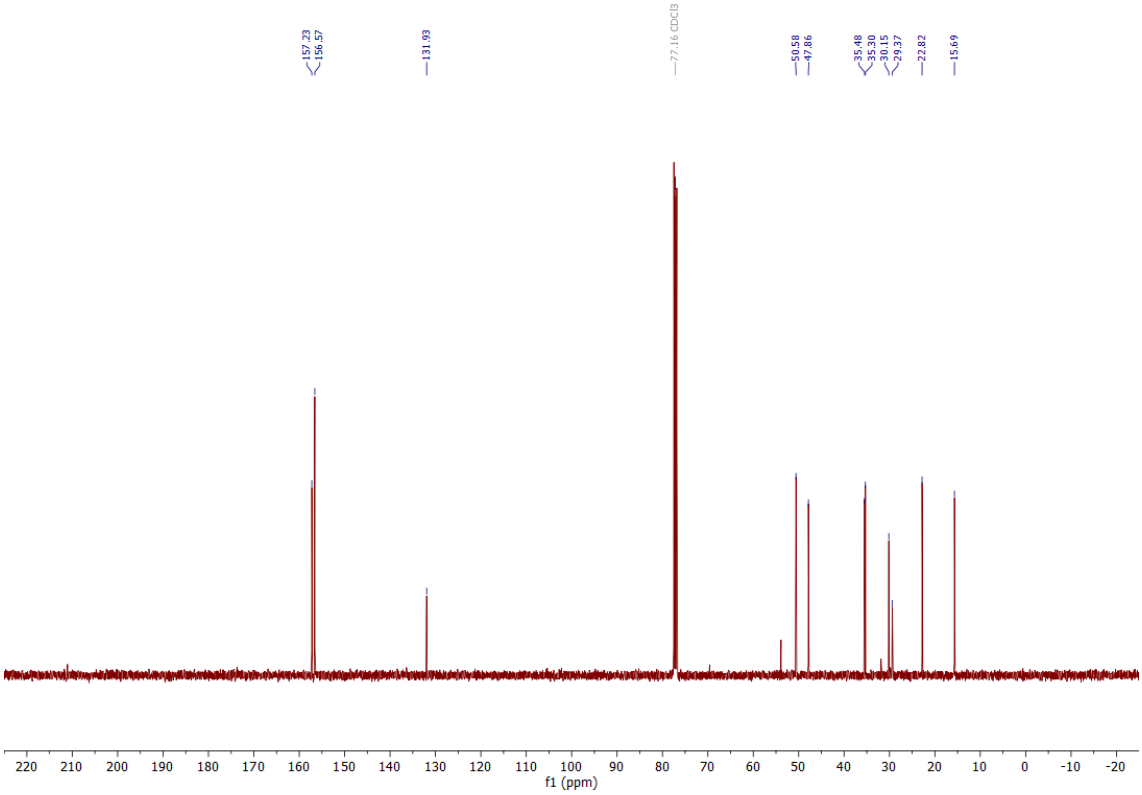

400 MHz ^{1}H NMR spectrum; 100.6 MHz ^{13}C NMR spectrum; $CDCl_3$ of *exo*-**192**

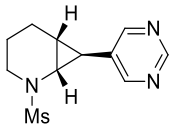

exo-**192**

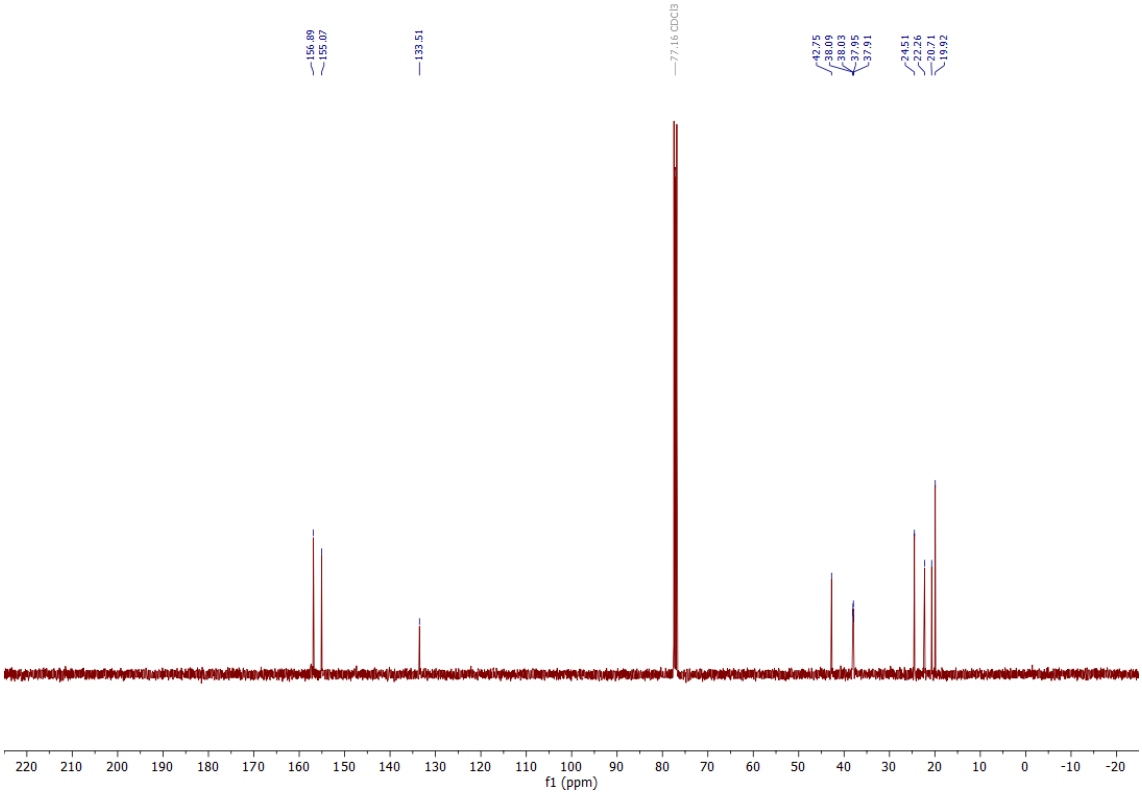

400 MHz ^{1}H NMR spectrum; 100.6 MHz ^{13}C NMR spectrum; $CDCl_3$ of **209**

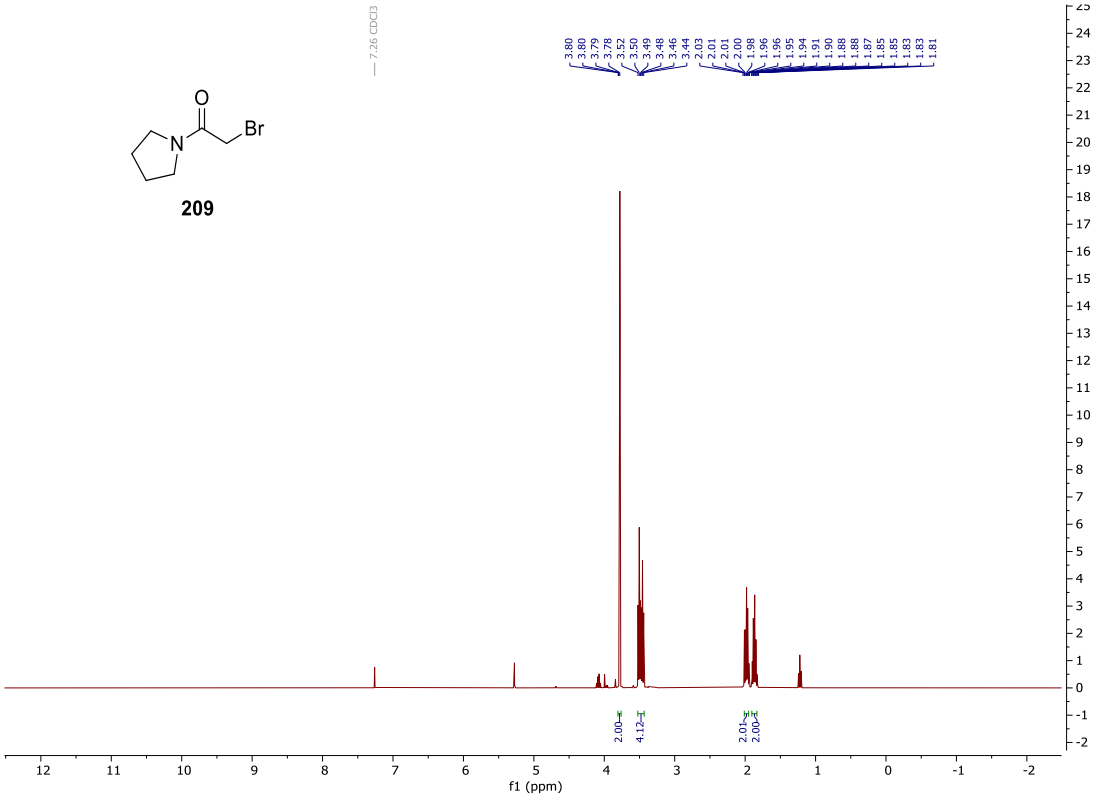

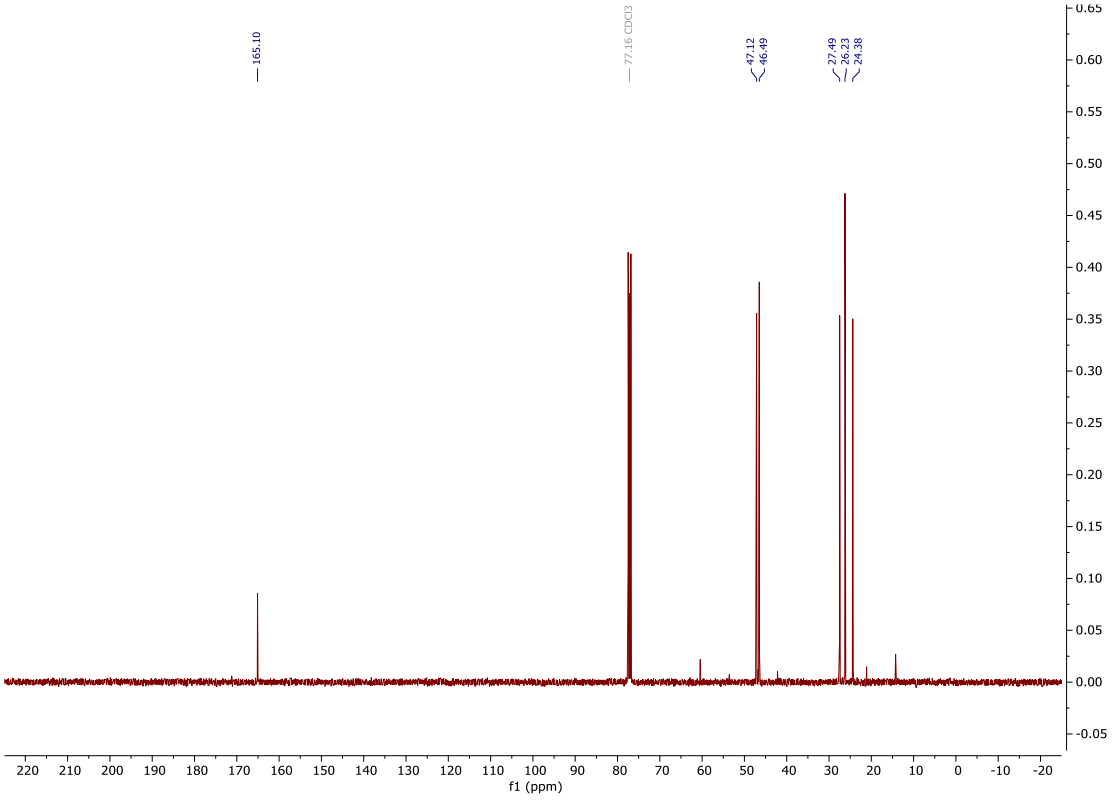

400 MHz ^{1}H NMR spectrum; 100.6 MHz ^{13}C NMR spectrum; $CDCl_3$ of **214**

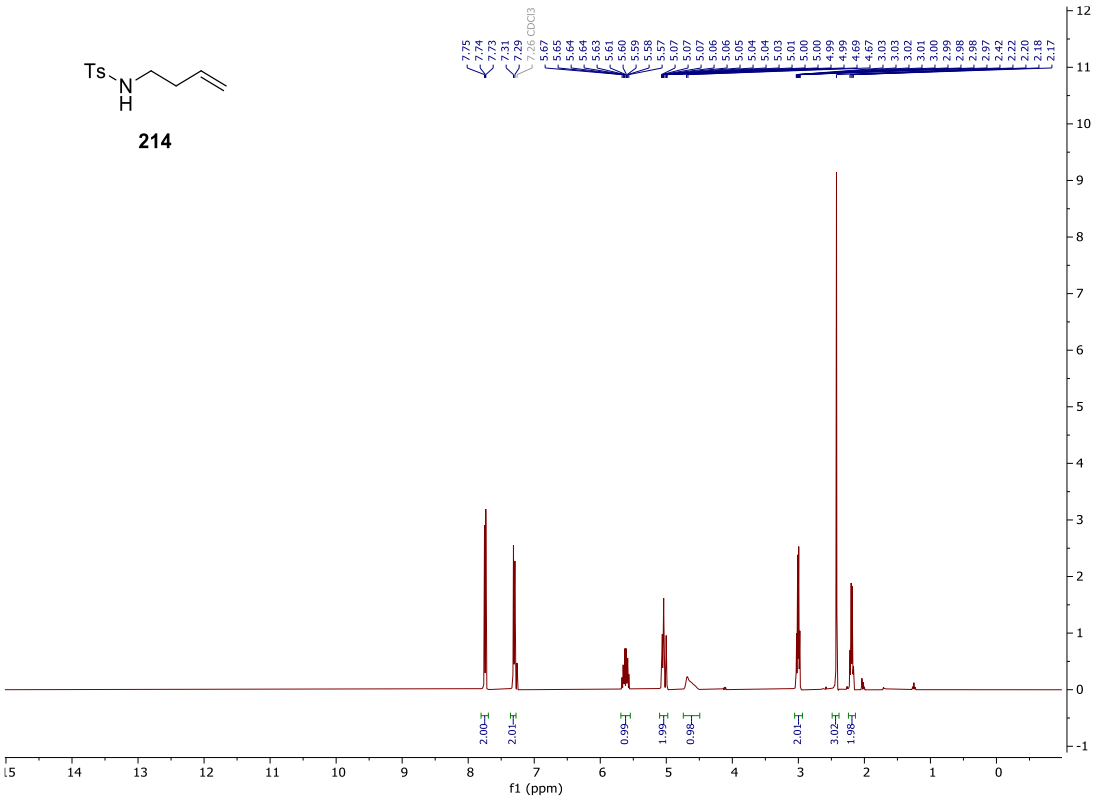

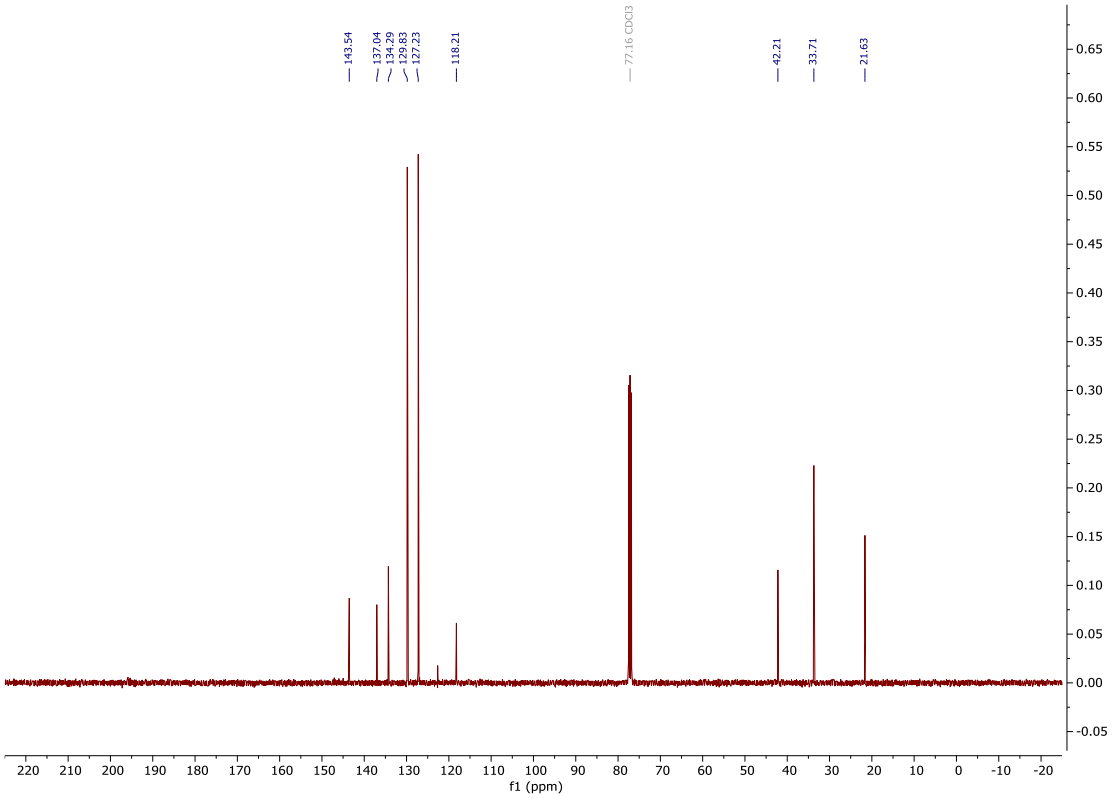

400 MHz ^{1}H NMR spectrum; 100.6 MHz ^{13}C NMR spectrum; $CDCl_3$ of **203**

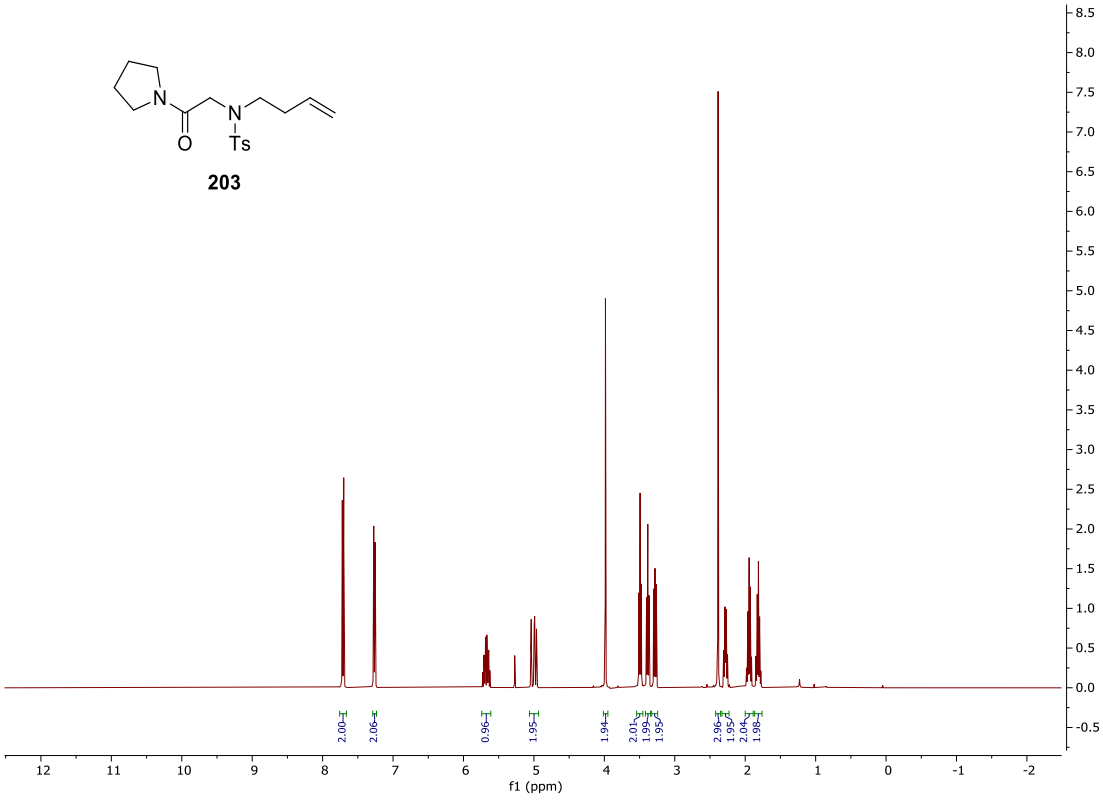

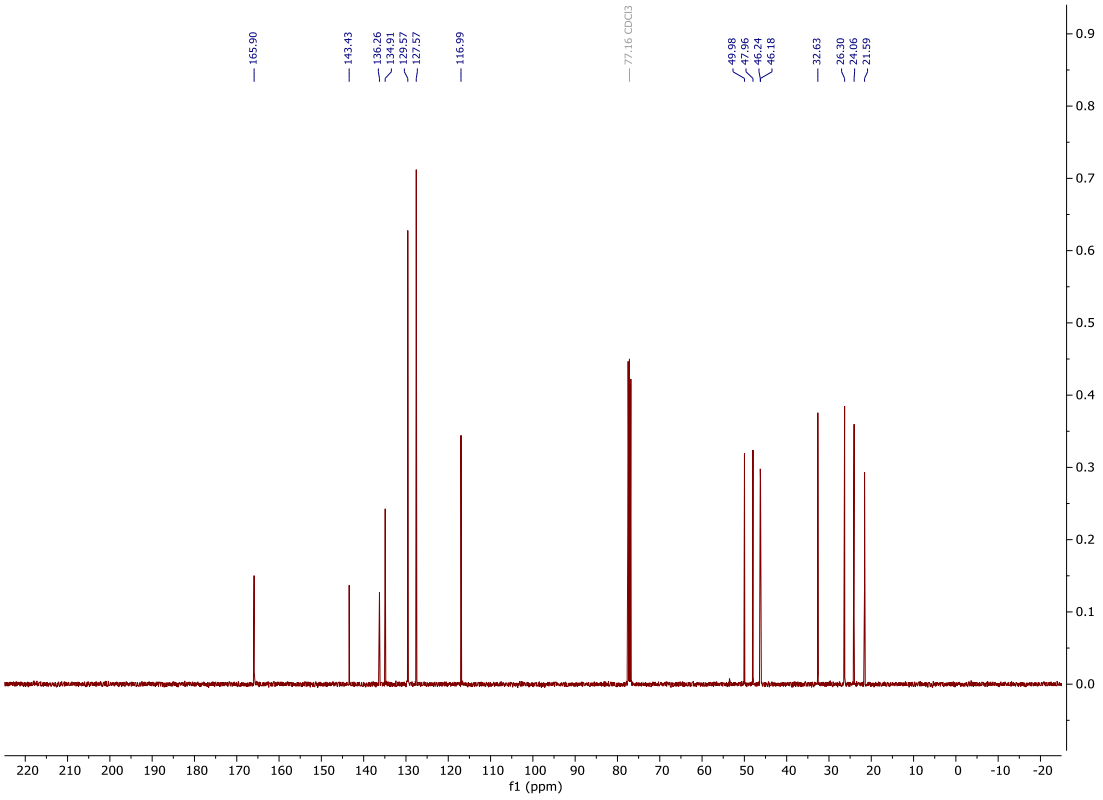

400 MHz ^{1}H NMR spectrum; 100.6 MHz ^{13}C NMR spectrum; $CDCl_3$ of **205**

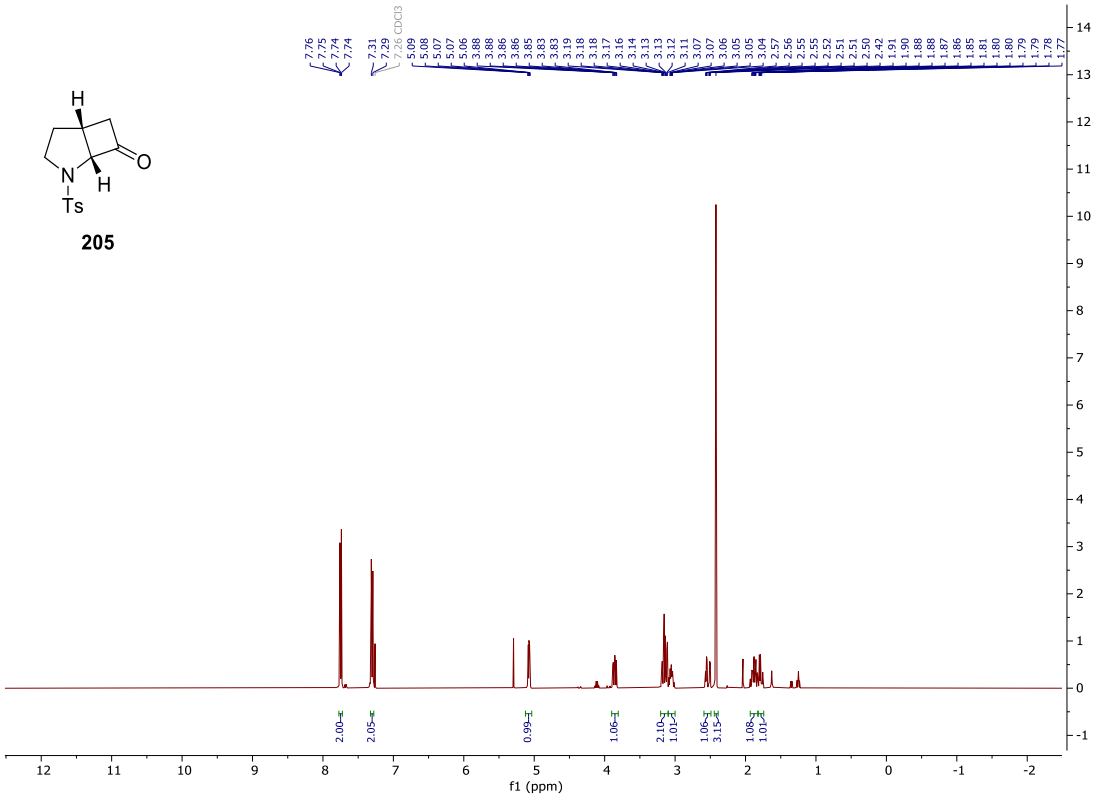

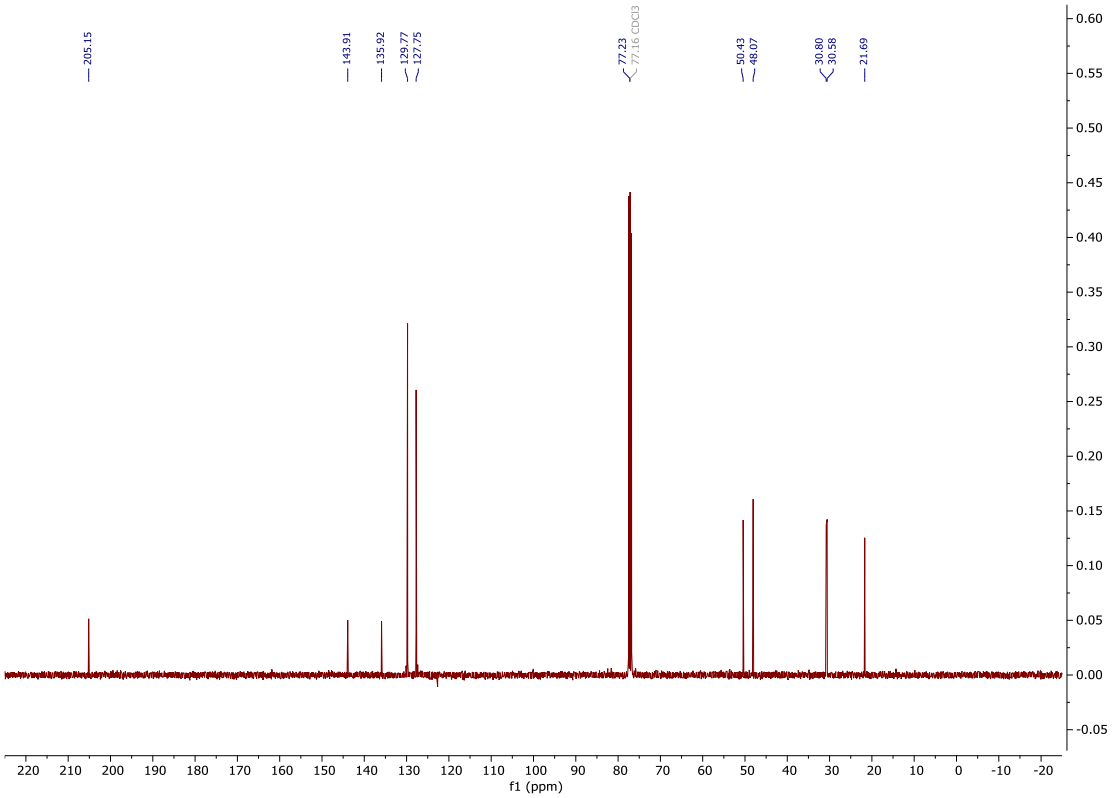

400 MHz ^{1}H NMR spectrum; 100.6 MHz ^{13}C NMR spectrum; $CDCl_3$ of *endo*-**215**

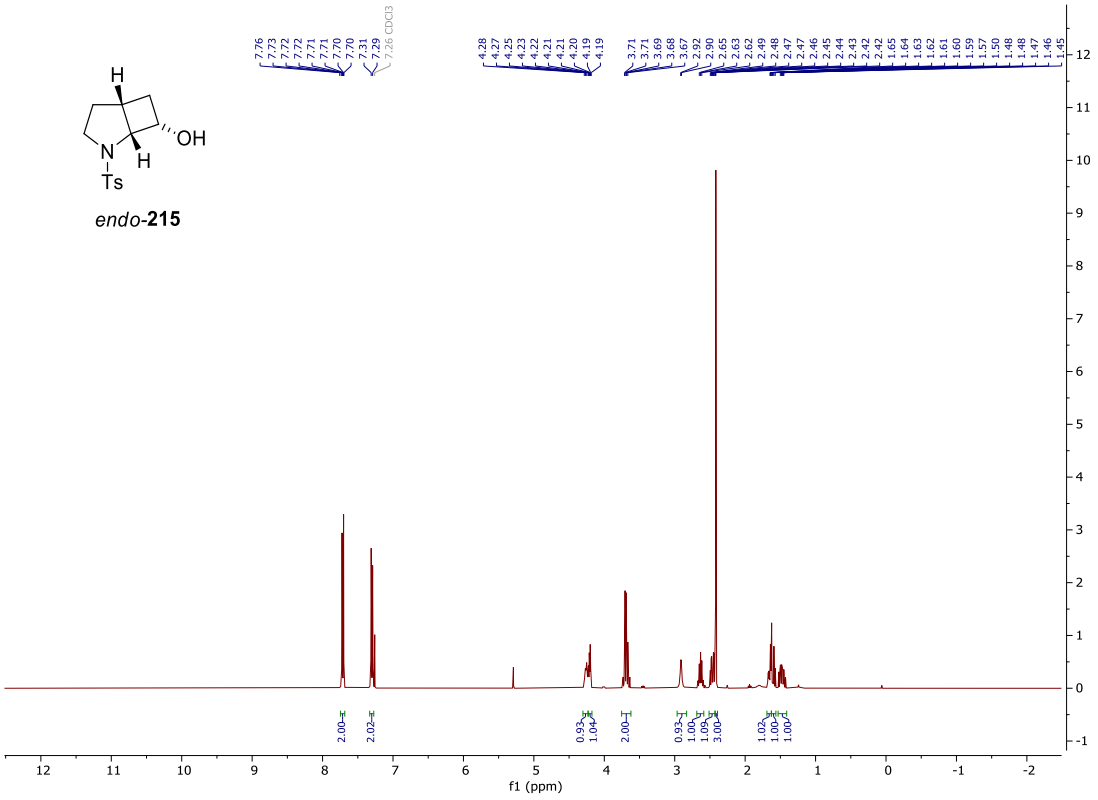

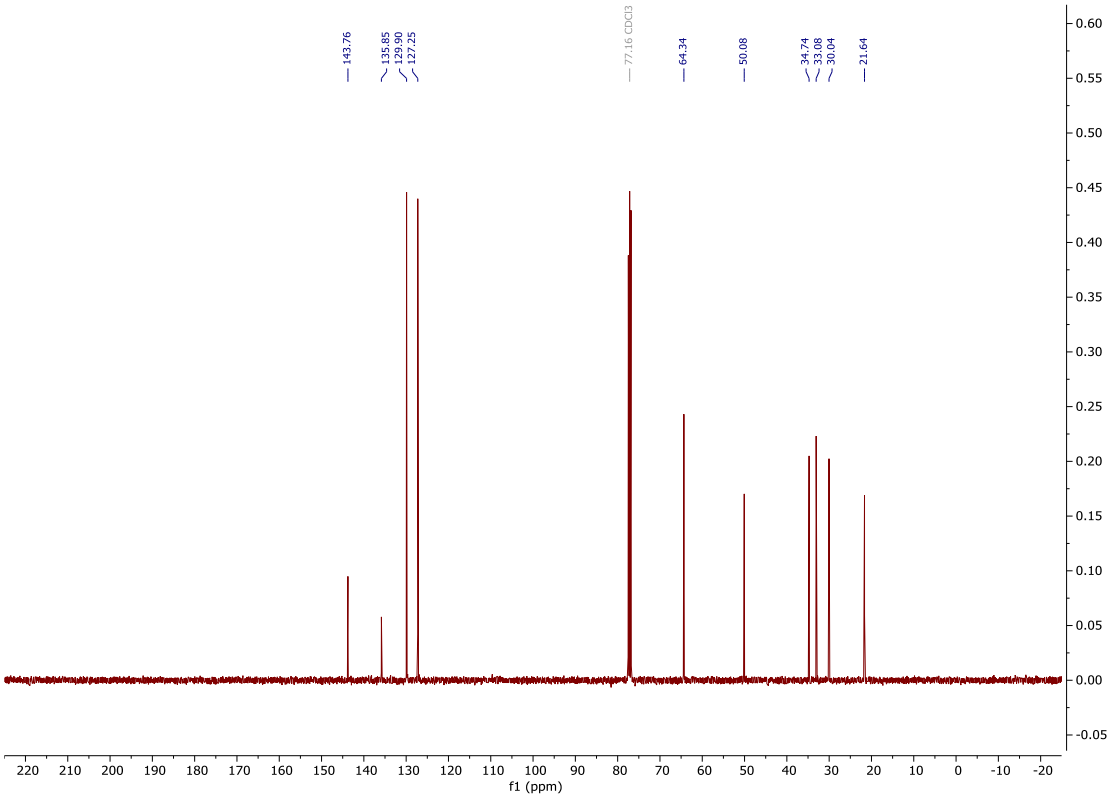

400 MHz ^{1}H NMR spectrum; 100.6 MHz ^{13}C NMR spectrum; $CDCl_3$ of **216**

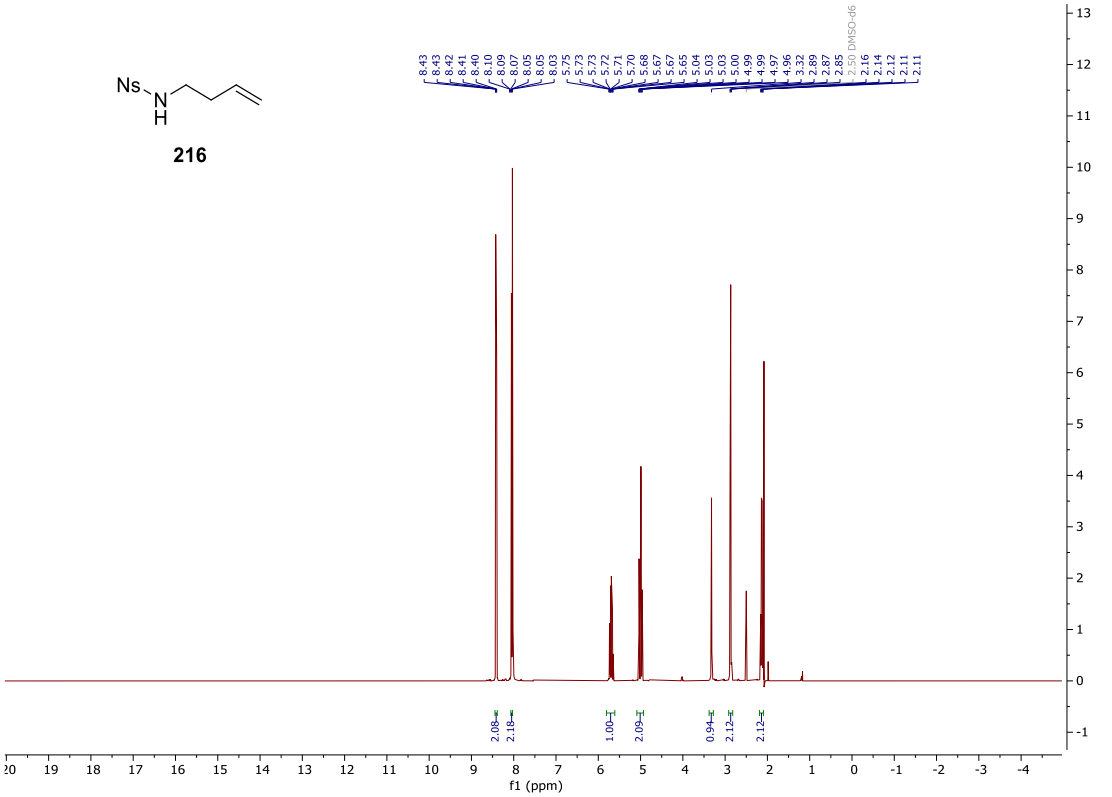

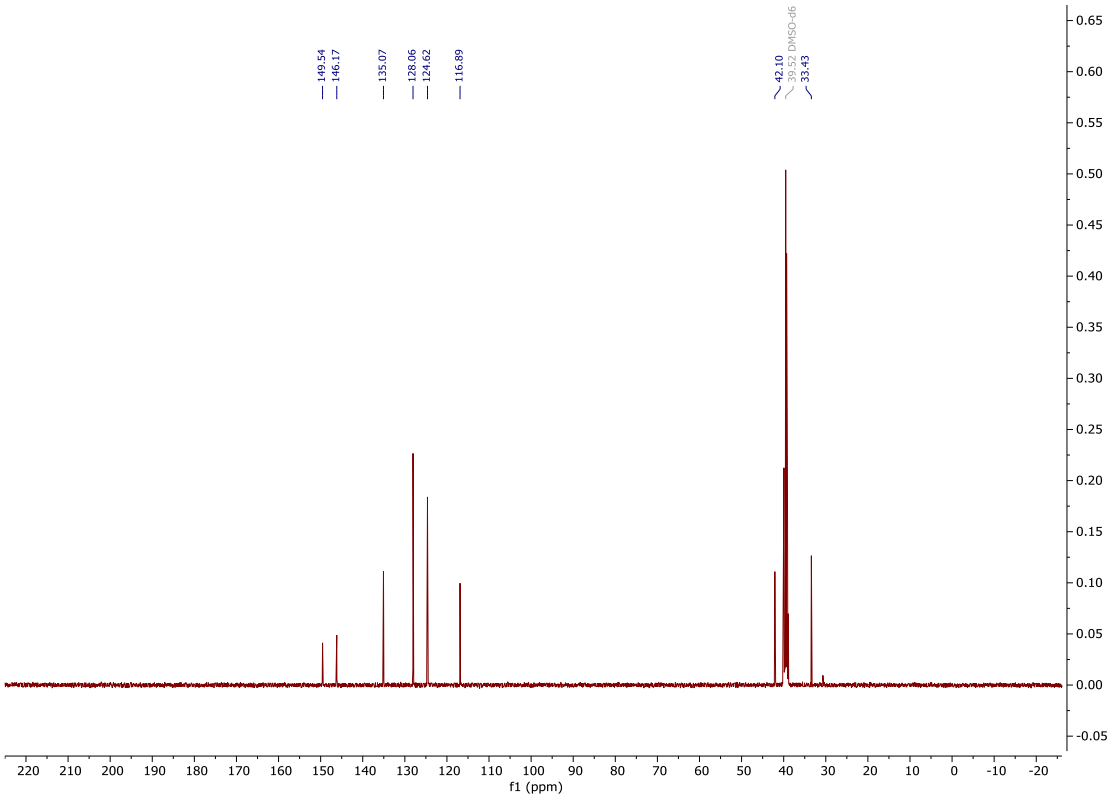

400 MHz ^{1}H NMR spectrum; 100.6 MHz ^{13}C NMR spectrum; $CDCl_3$ of **217**

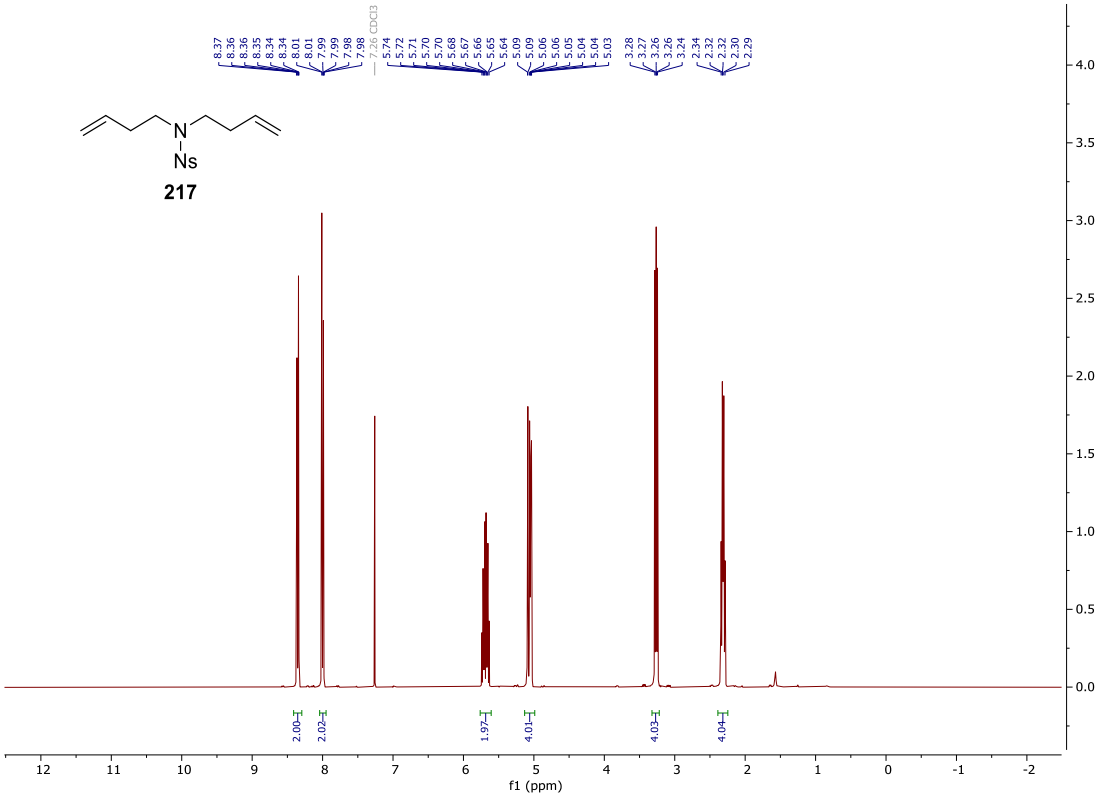

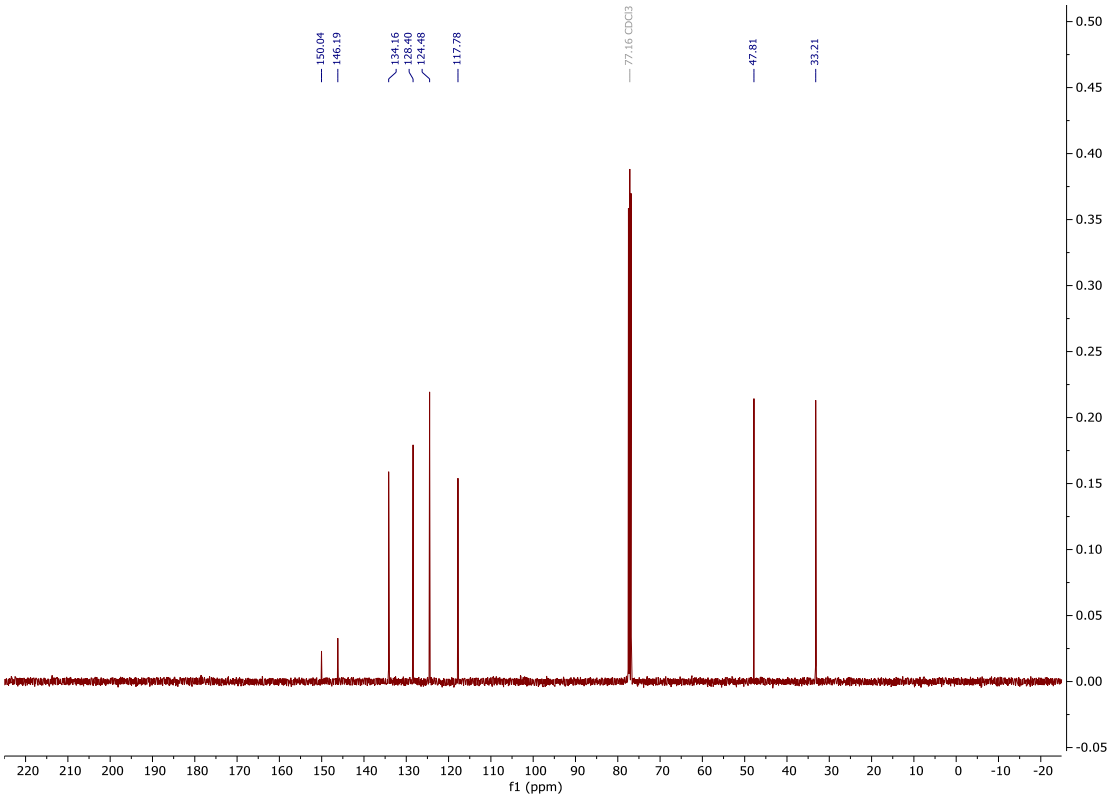

400 MHz ^{1}H NMR spectrum; 100.6 MHz ^{13}C NMR spectrum; $CDCl_3$ of **218**

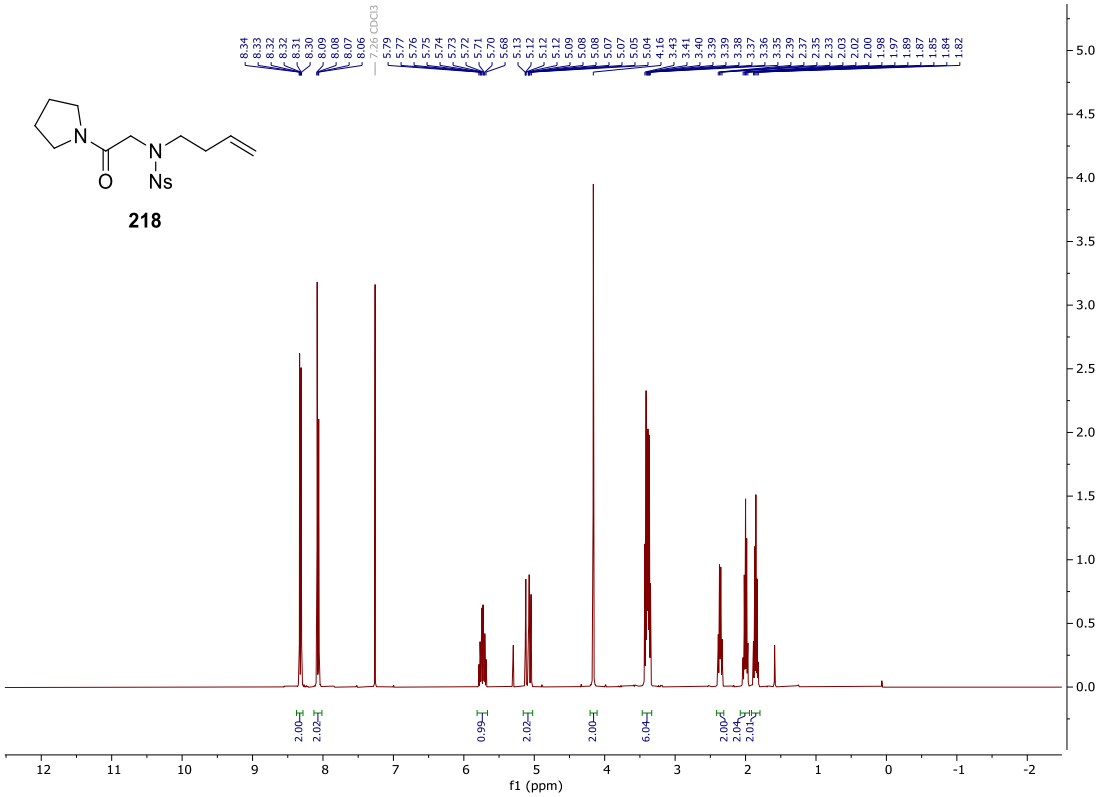

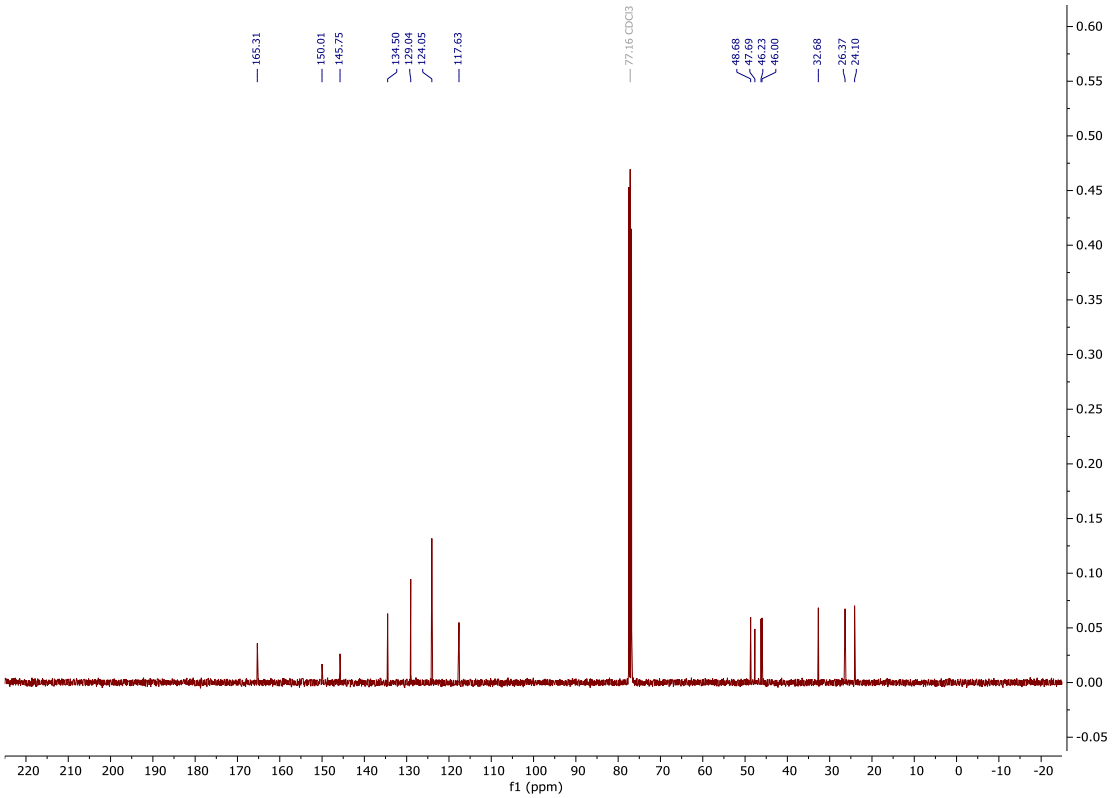

400 MHz ^{1}H NMR spectrum; 100.6 MHz ^{13}C NMR spectrum; $CDCl_3$ of **219**

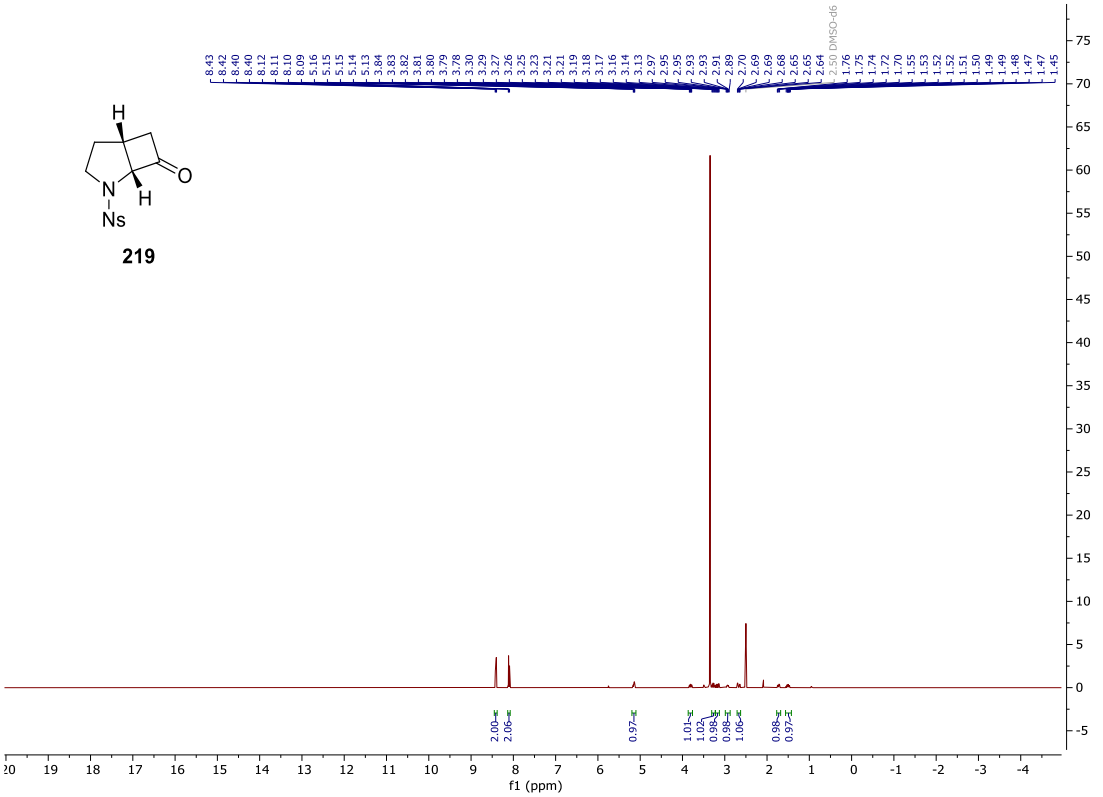

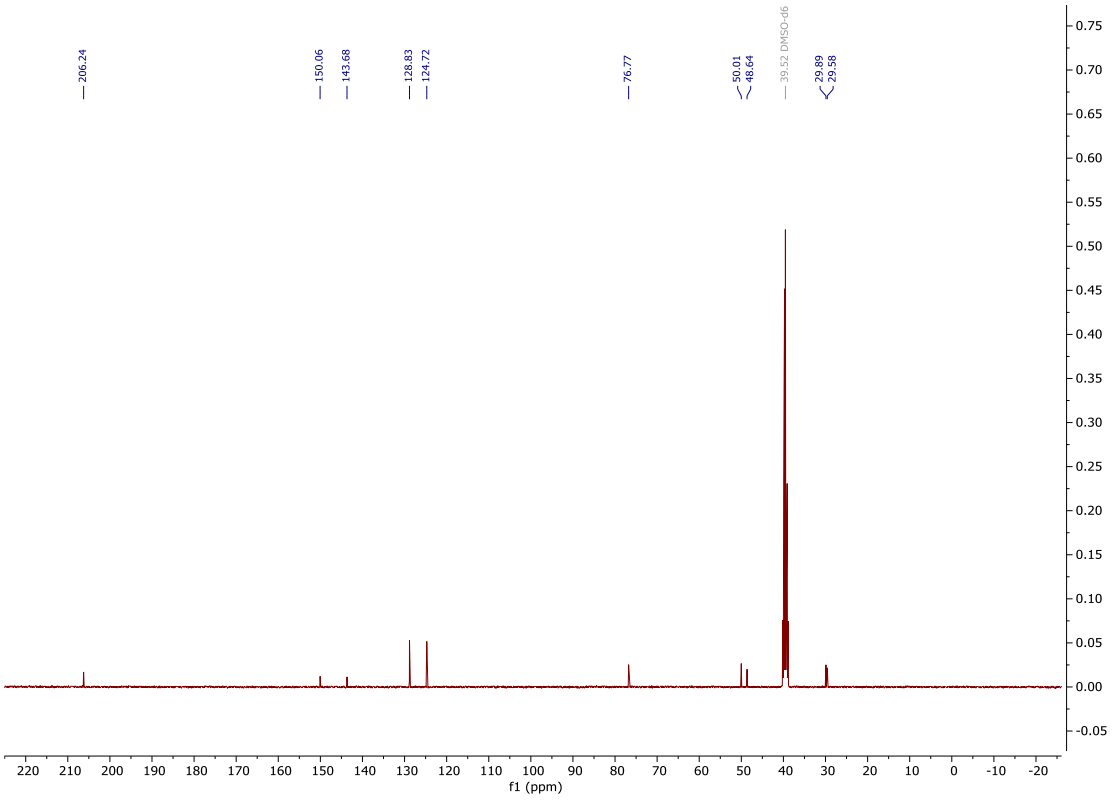

400 MHz ^{1}H NMR spectrum; 100.6 MHz ^{13}C NMR spectrum; $CDCl_3$ of *endo*-**220**

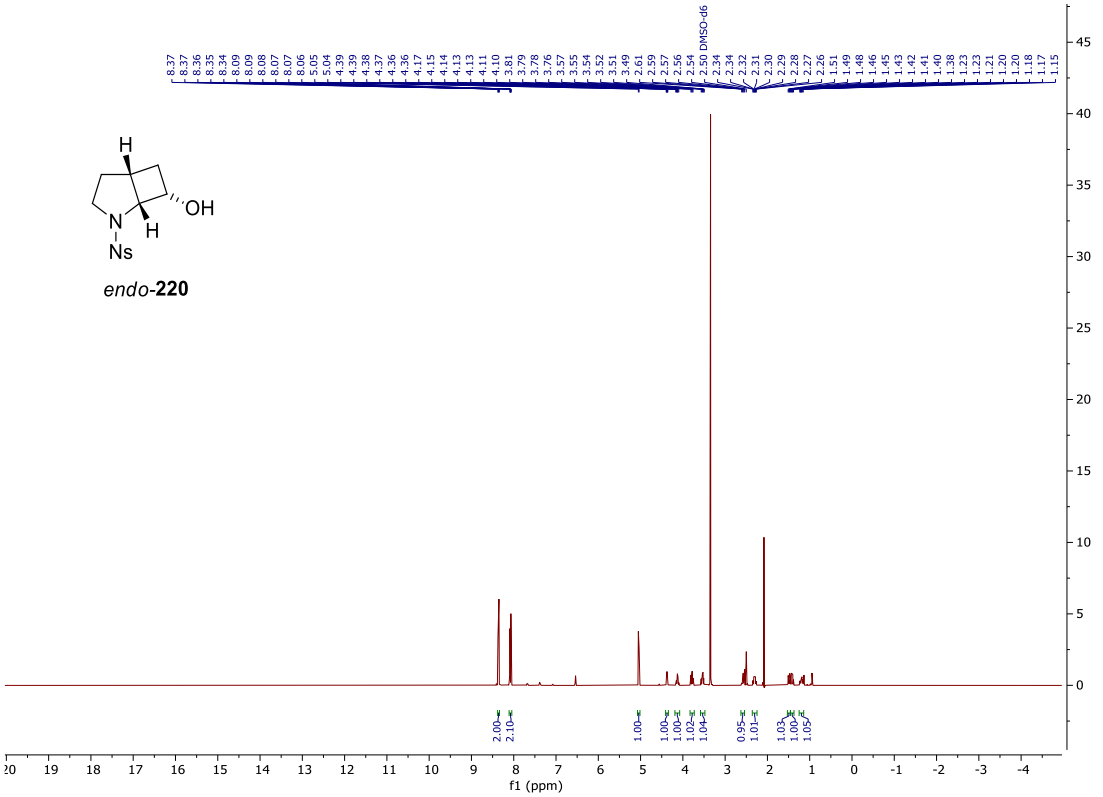

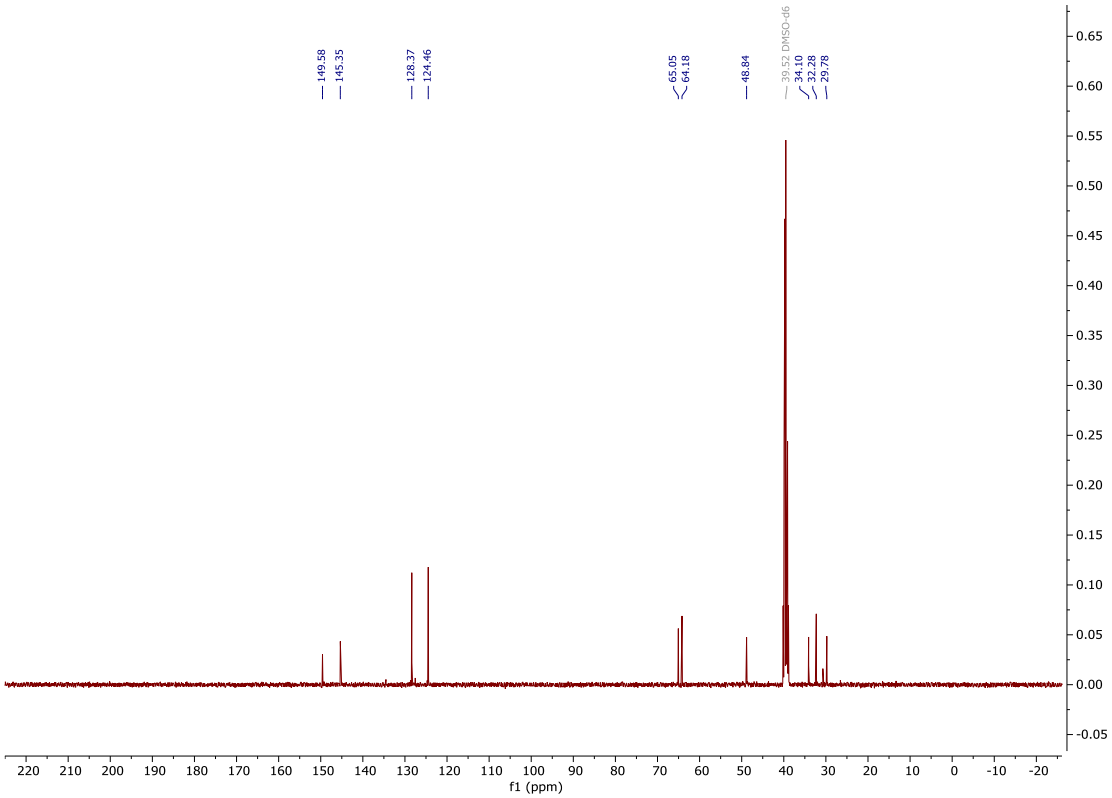

400 MHz ^{1}H NMR spectrum; 100.6 MHz ^{13}C NMR spectrum; $CDCl_3$ of **235**

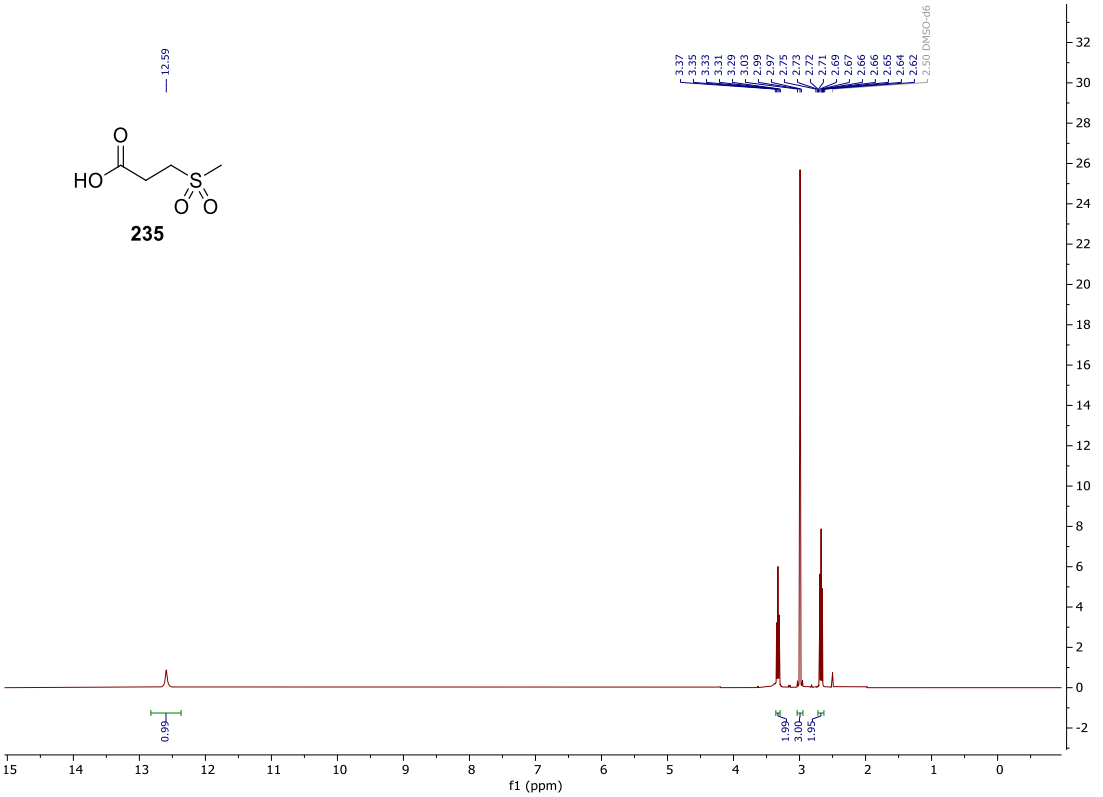

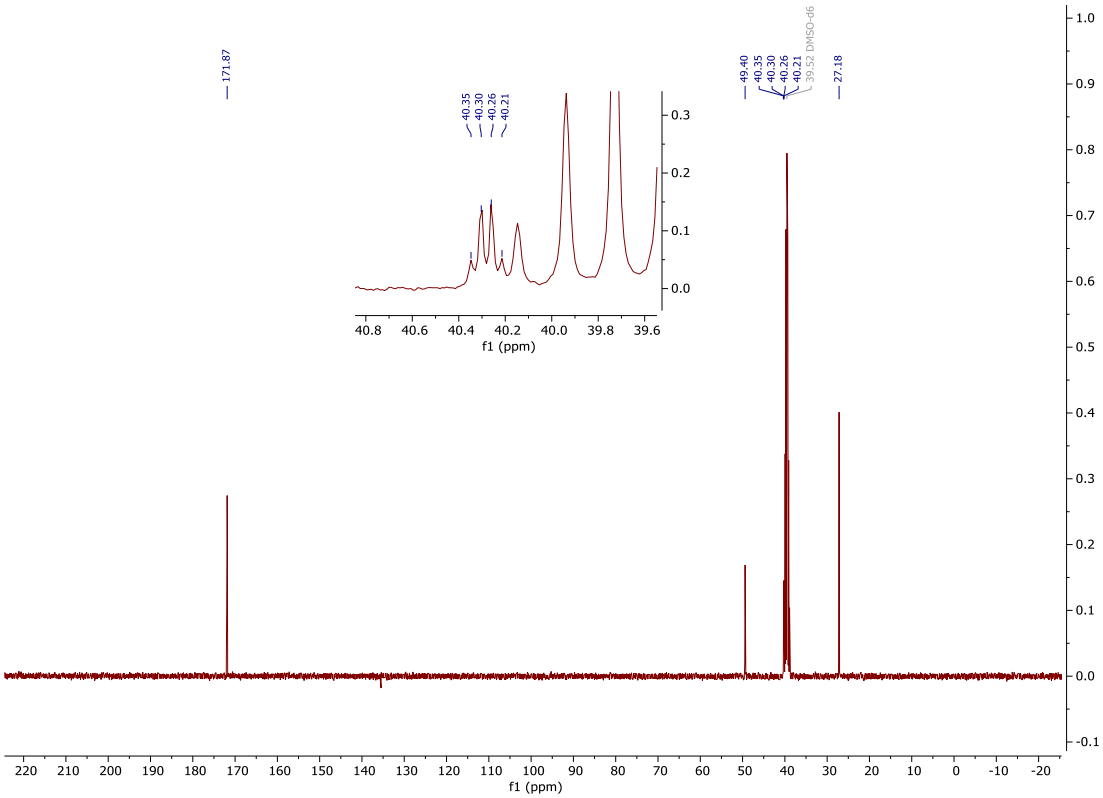

400 MHz ^{1}H NMR spectrum; 100.6 MHz ^{13}C NMR spectrum; $CDCl_3$ of *trans*-**253**

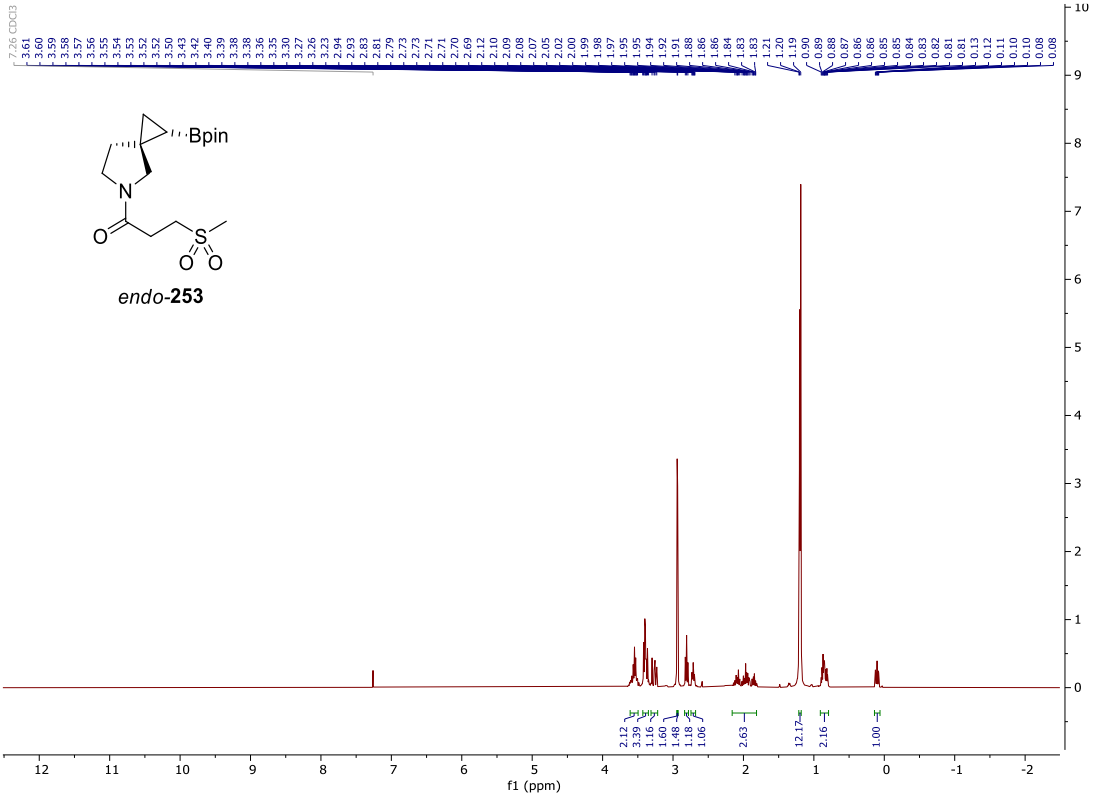

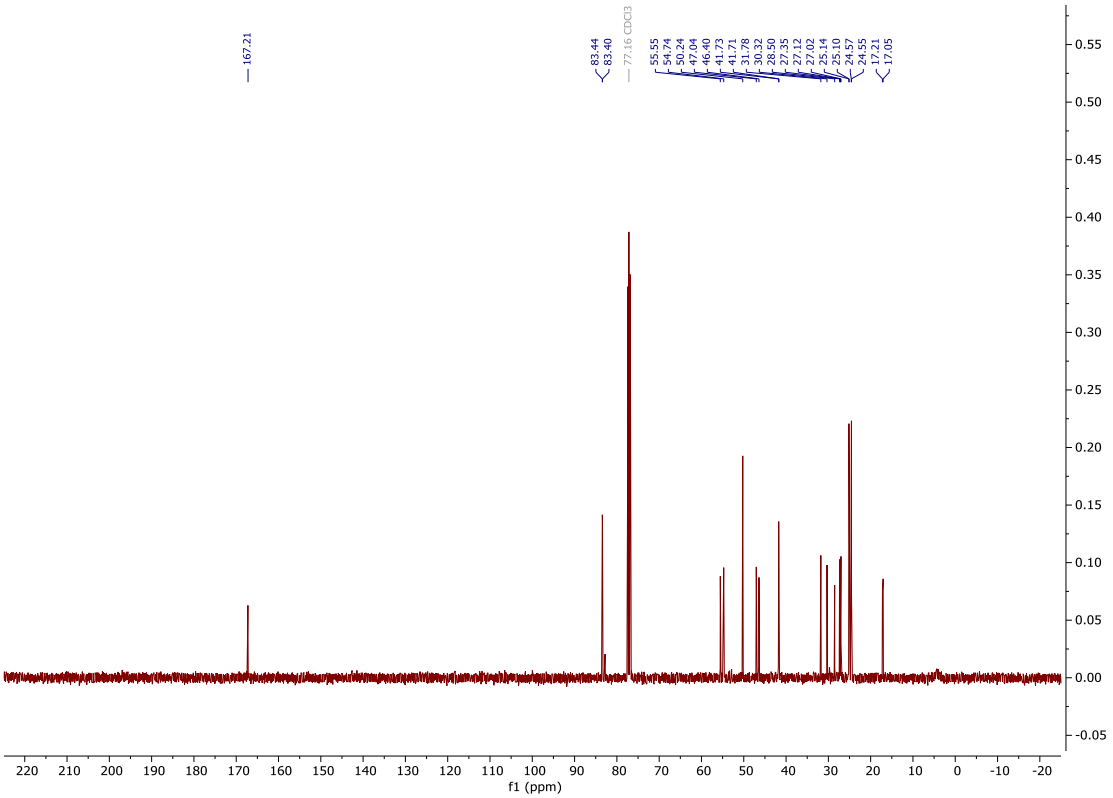

400 MHz ^{1}H NMR spectrum; 100.6 MHz ^{13}C NMR spectrum; $CDCl_3$ of **257**

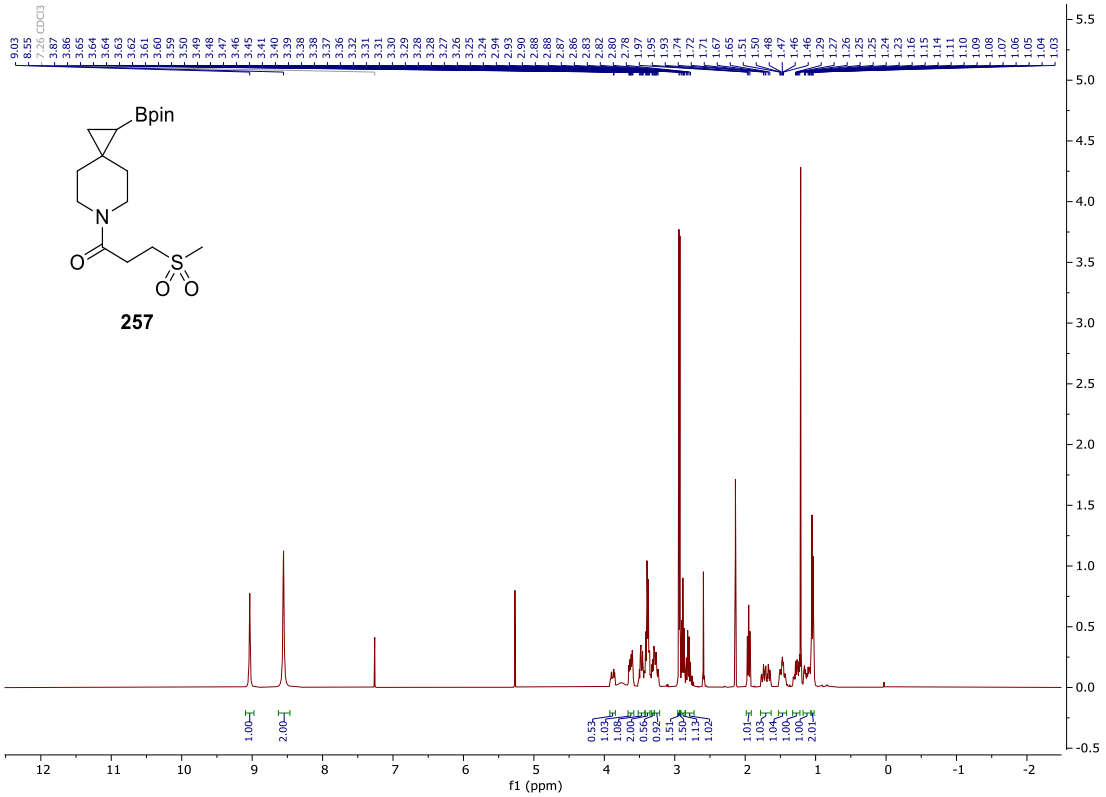

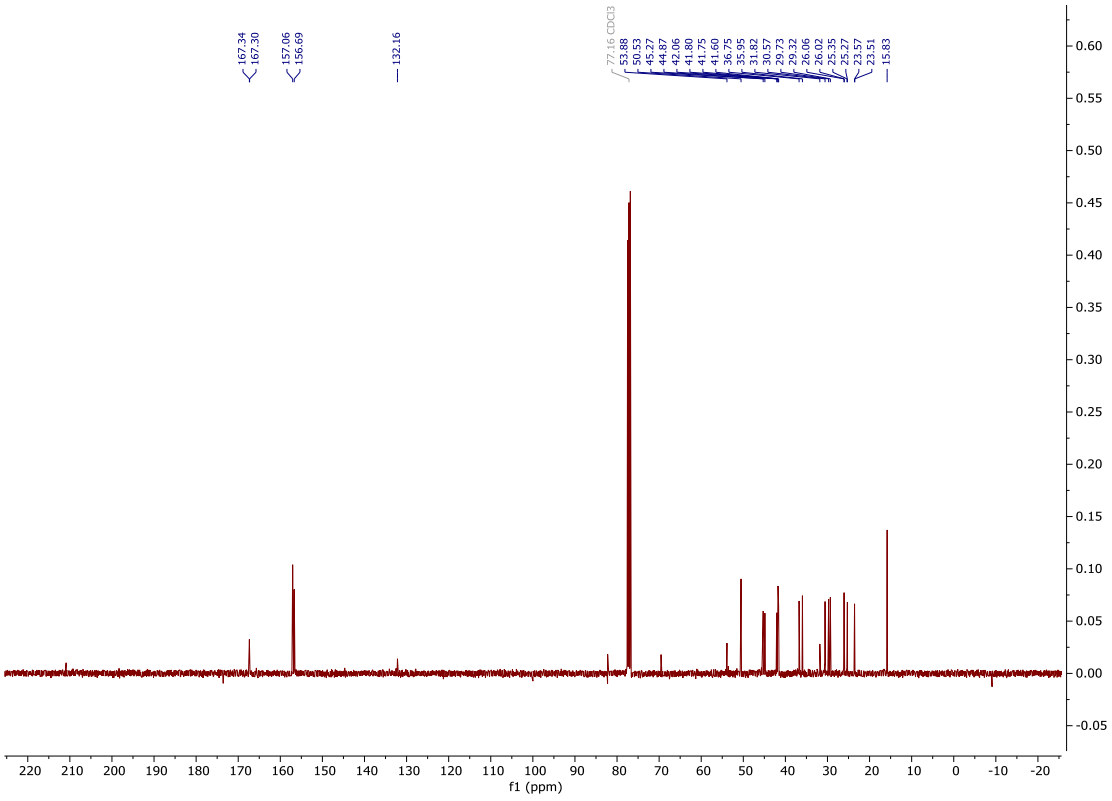

400 MHz ^{1}H NMR spectrum; 100.6 MHz ^{13}C NMR spectrum; $CDCl_3$ of **260**

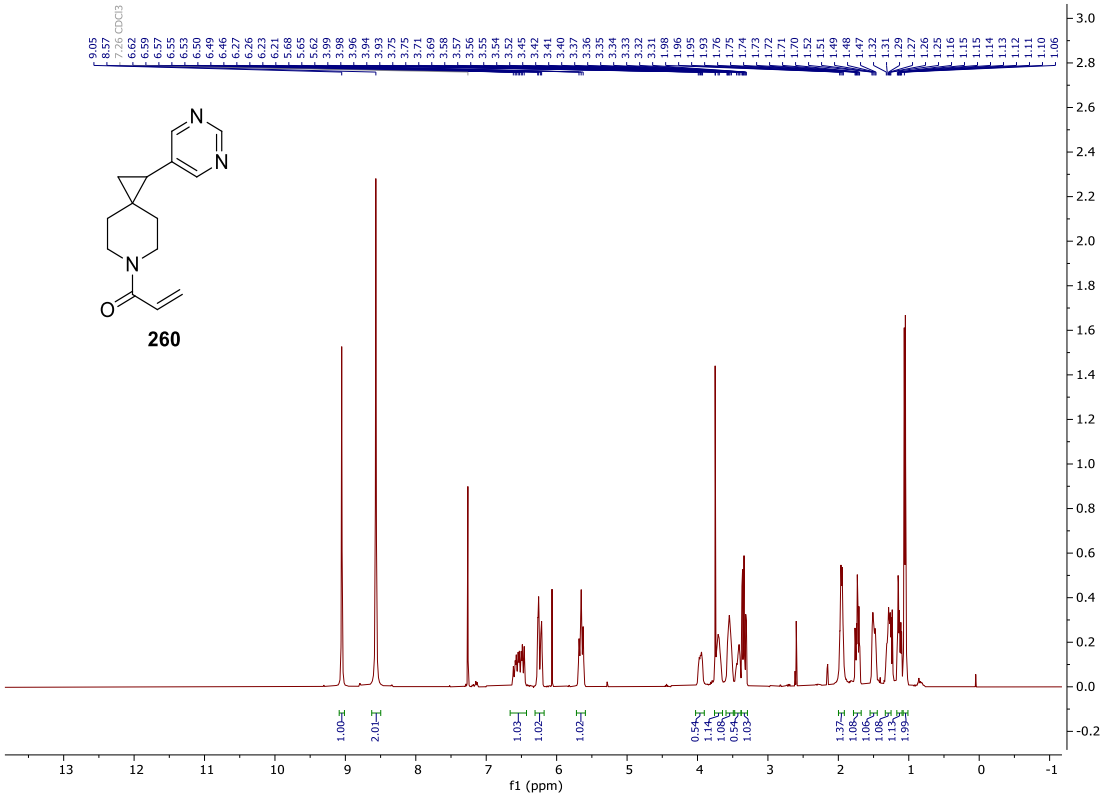

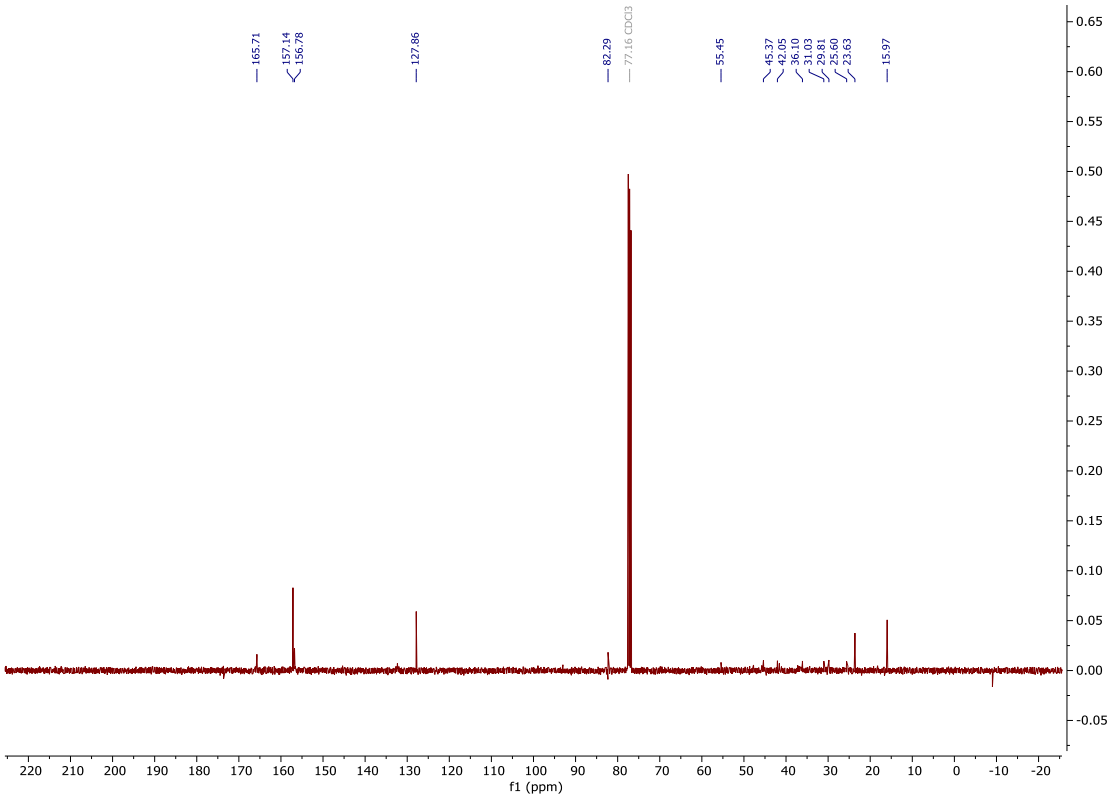

400 MHz ^{1}H NMR spectrum; 100.6 MHz ^{13}C NMR spectrum; $CDCl_3$ of **264**

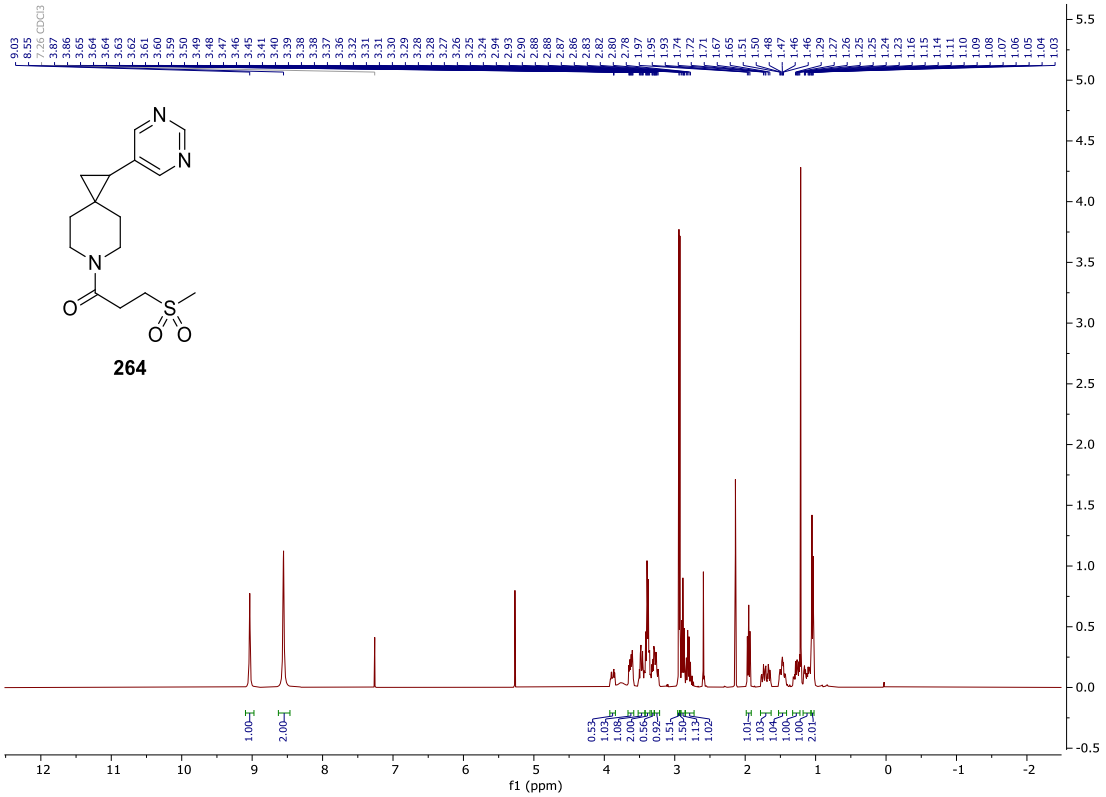

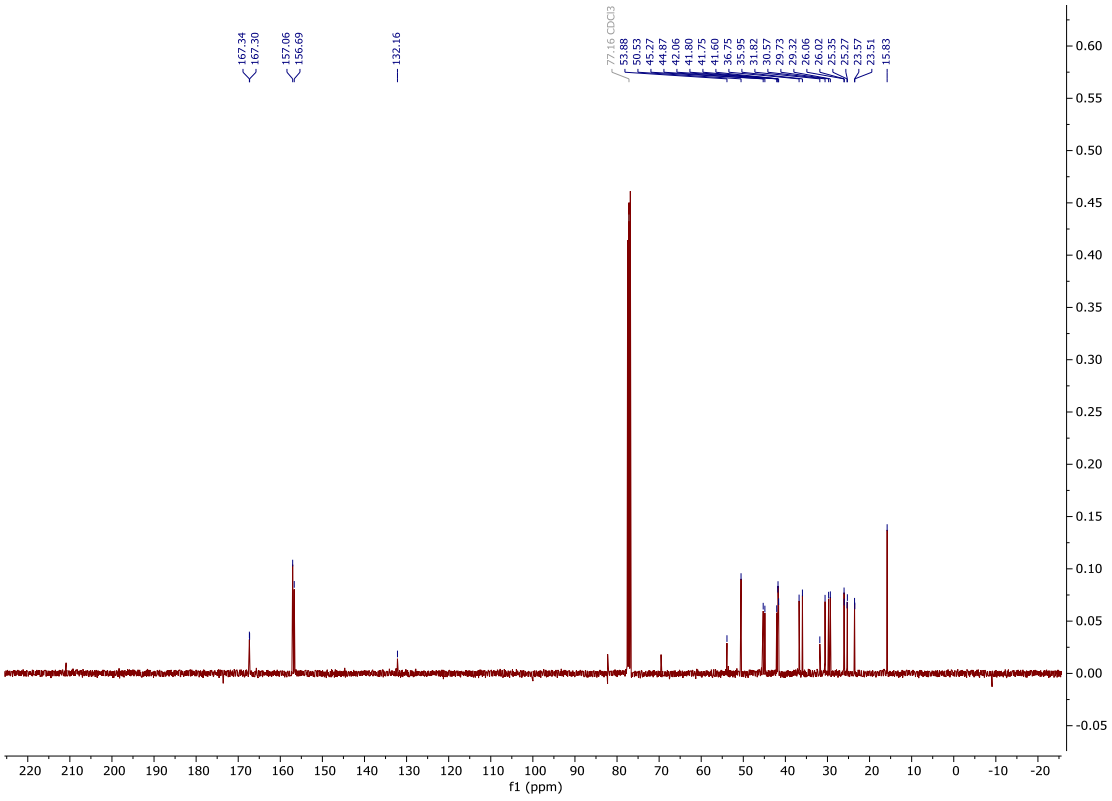

400 MHz ^{1}H NMR spectrum; 100.6 MHz ^{13}C NMR spectrum; $CDCl_3$ of **265**

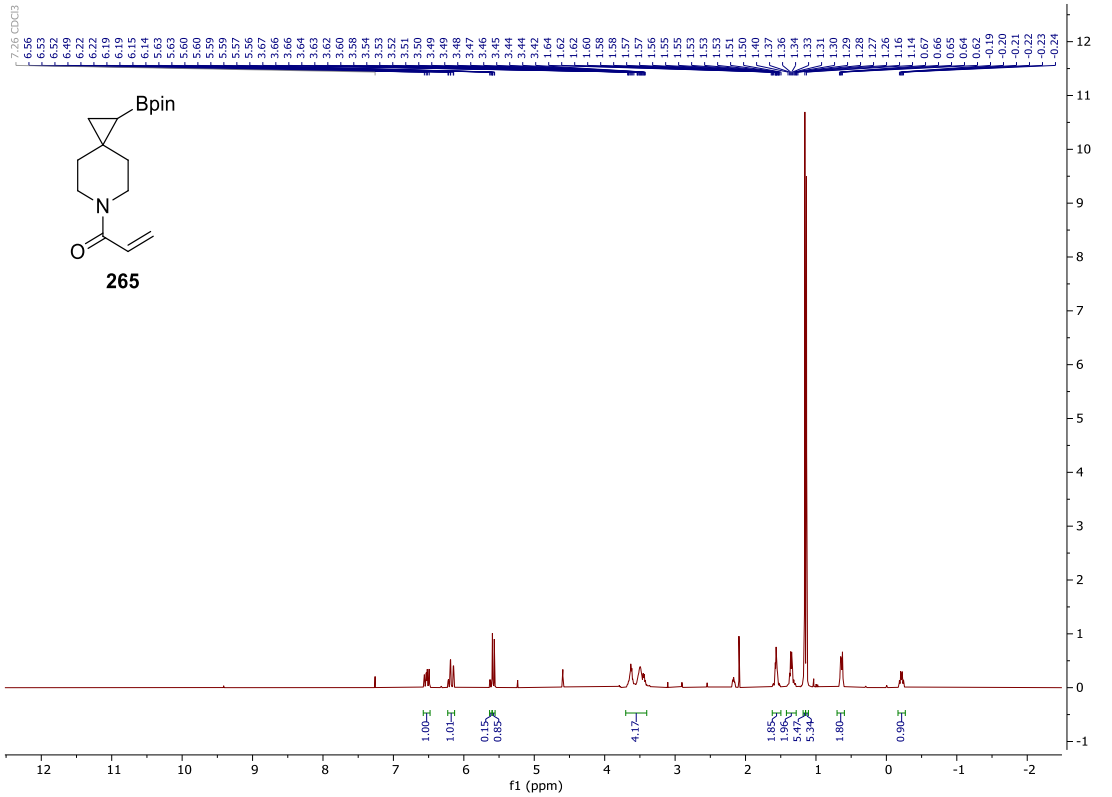

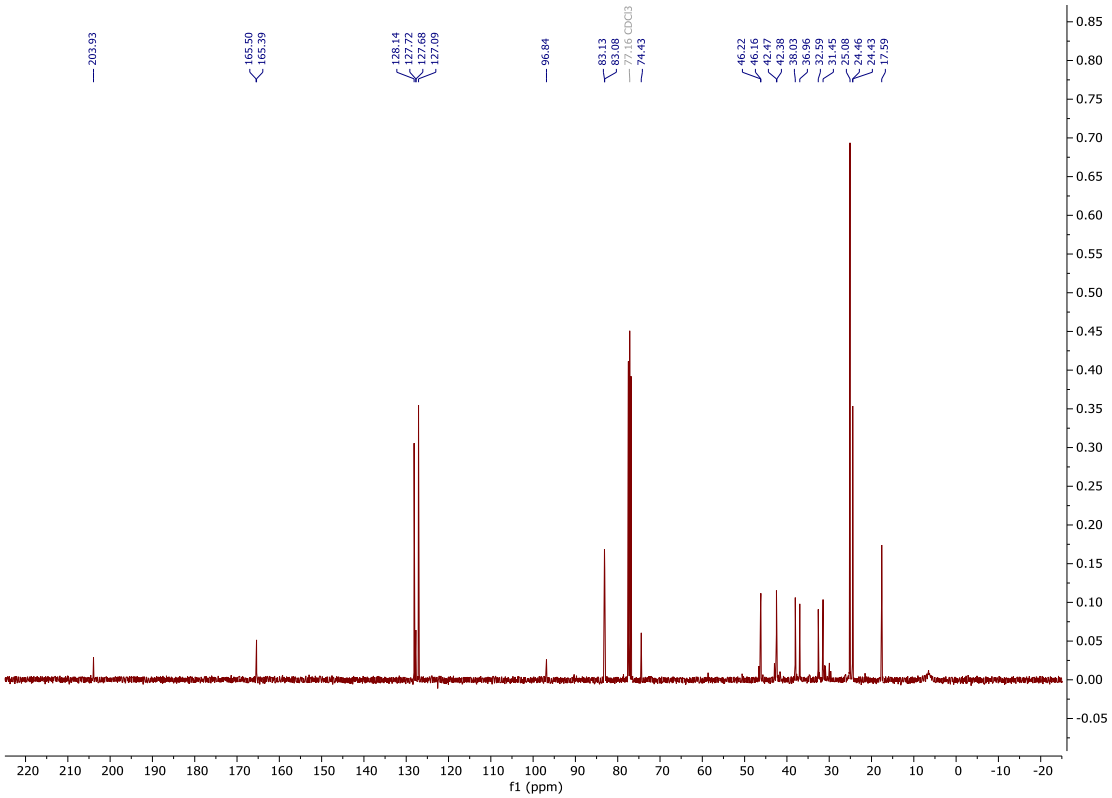

400 MHz ^{1}H NMR spectrum; 100.6 MHz ^{13}C NMR spectrum; $CDCl_3$ of **281**

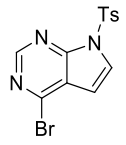

281

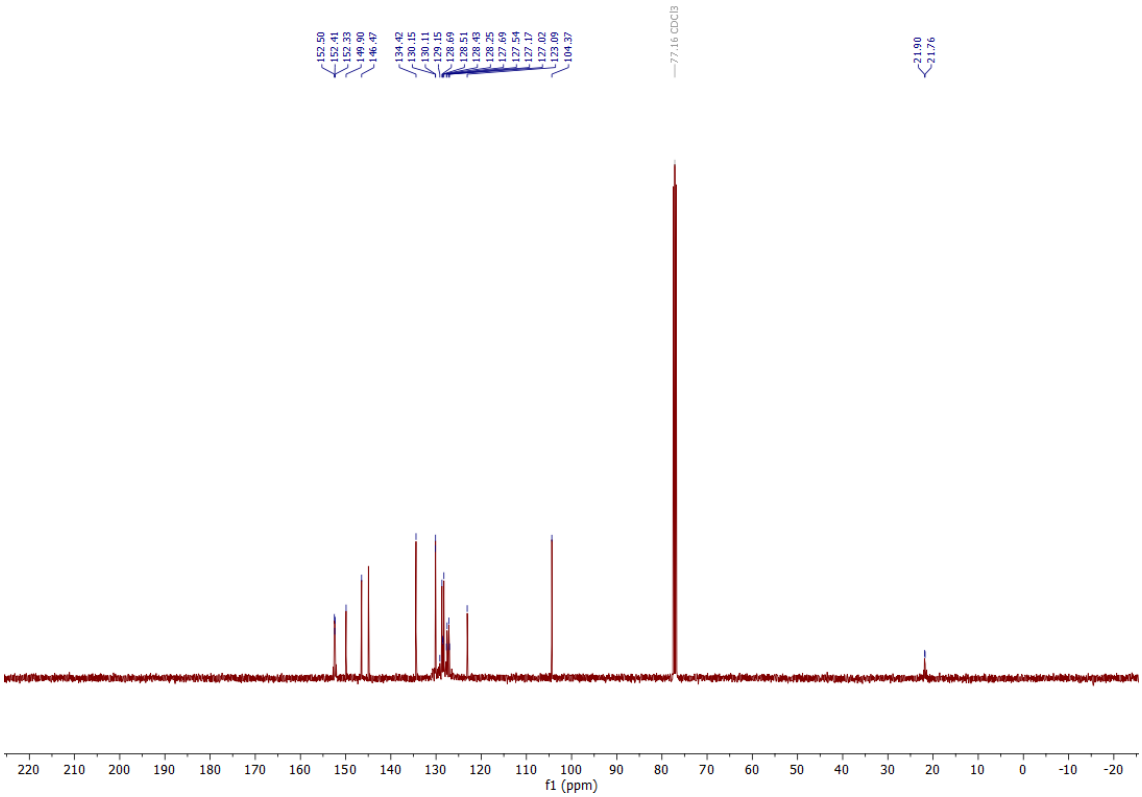

400 MHz ^{1}H NMR spectrum; 100.6 MHz ^{13}C NMR spectrum; $CDCl_3$ of *cis*-**282**

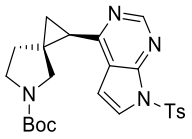

cis-**282**

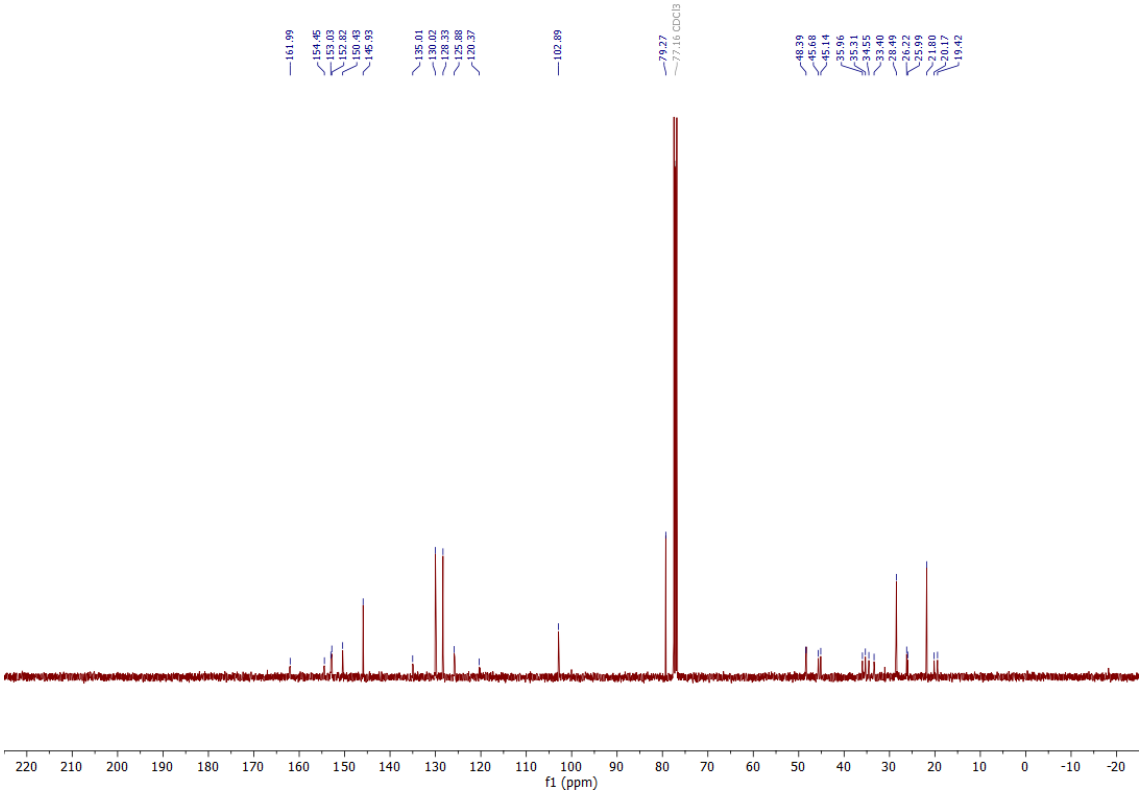

400 MHz ^{1}H NMR spectrum; 100.6 MHz ^{13}C NMR spectrum; $CDCl_3$ of *cis*-**284**

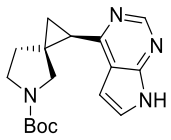

cis-**284**

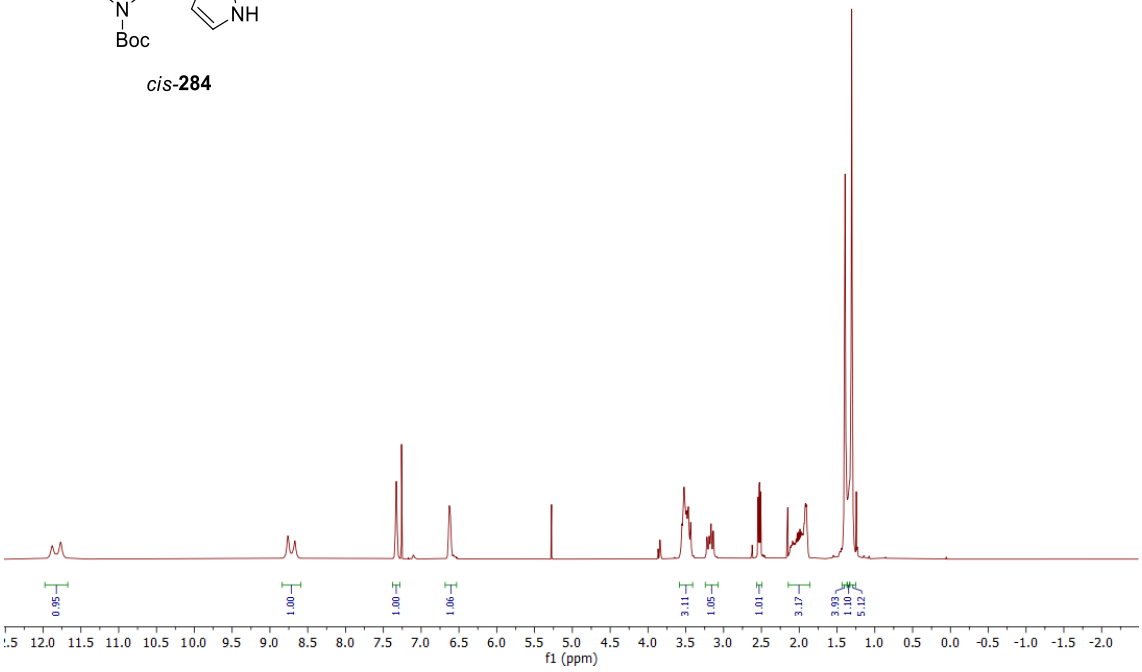

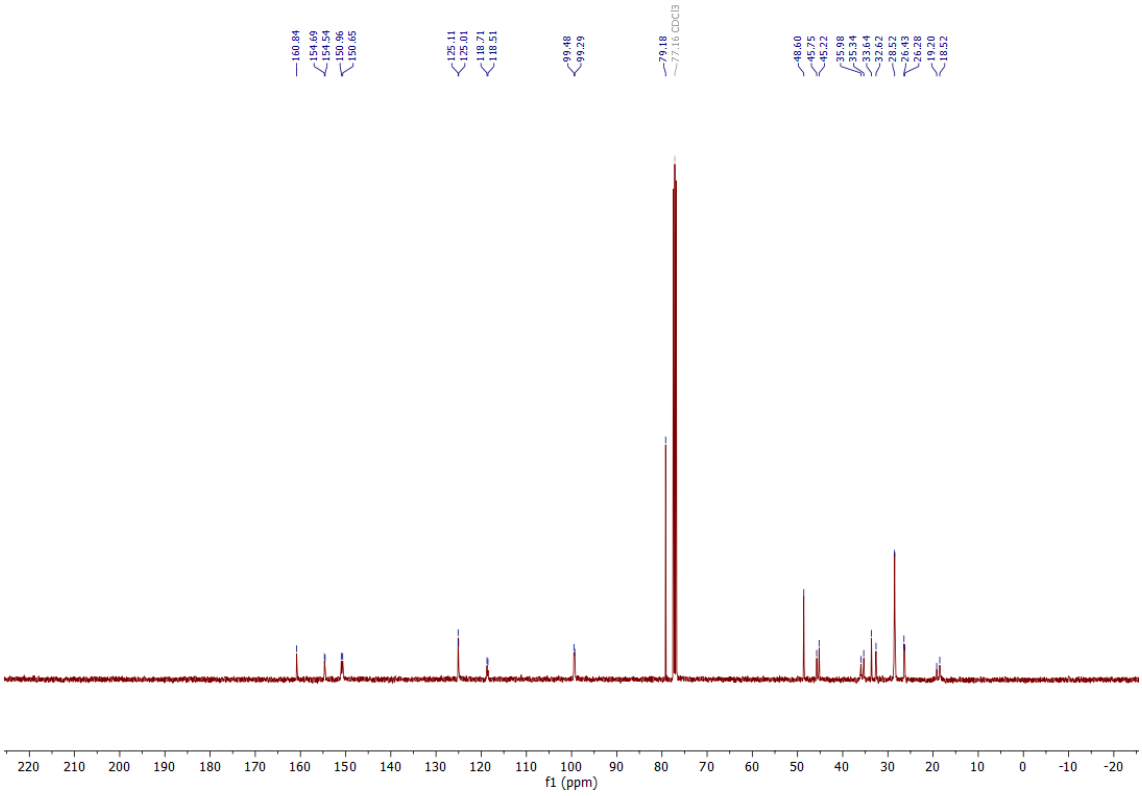

400 MHz ^{1}H NMR spectrum; 100.6 MHz ^{13}C NMR spectrum; $CDCl_3$ of *cis*-**285**

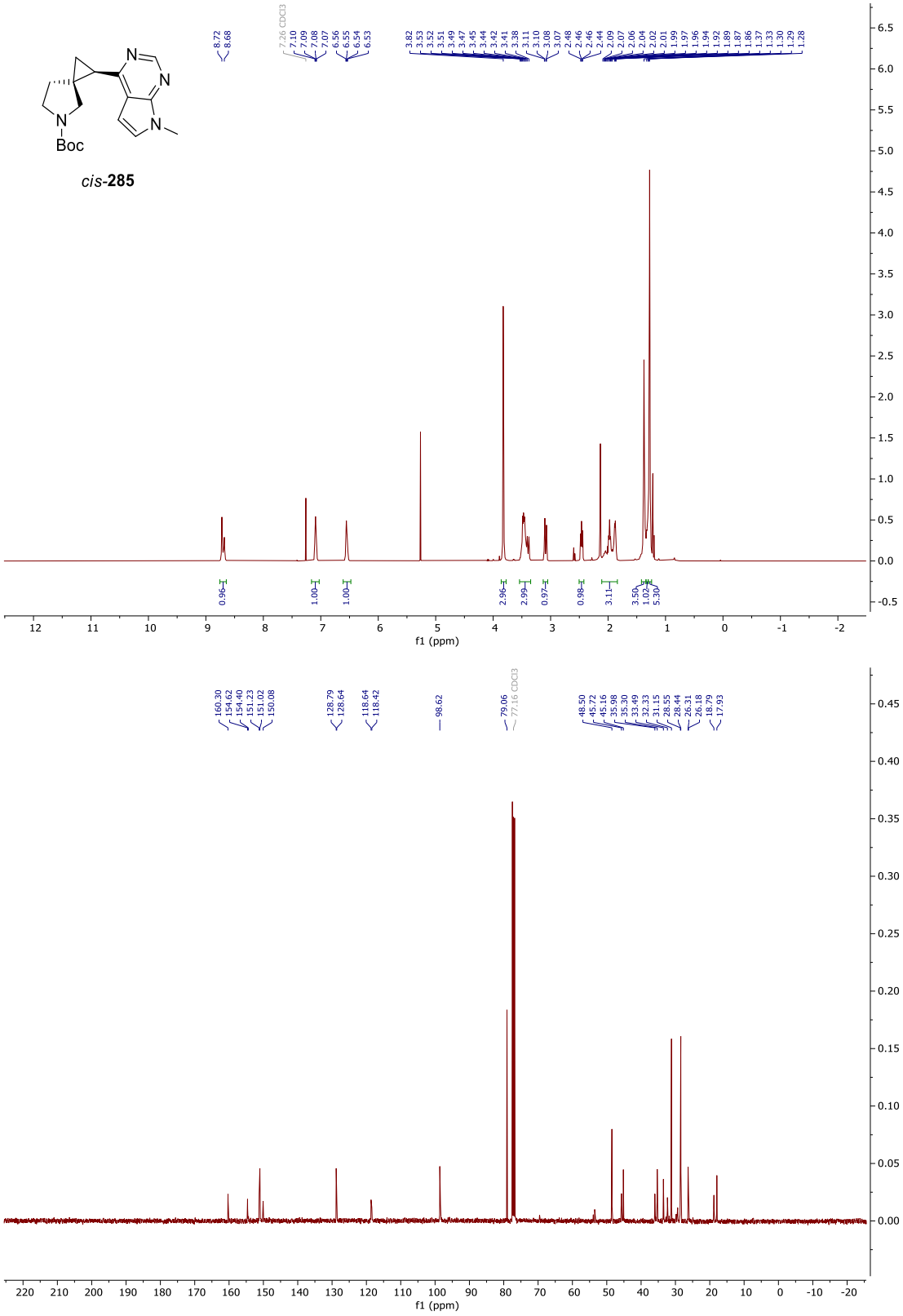

400 MHz ^{1}H NMR spectrum; 100.6 MHz ^{13}C NMR spectrum; $CDCl_3$ of *cis*-**266**

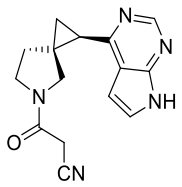

cis-**266**

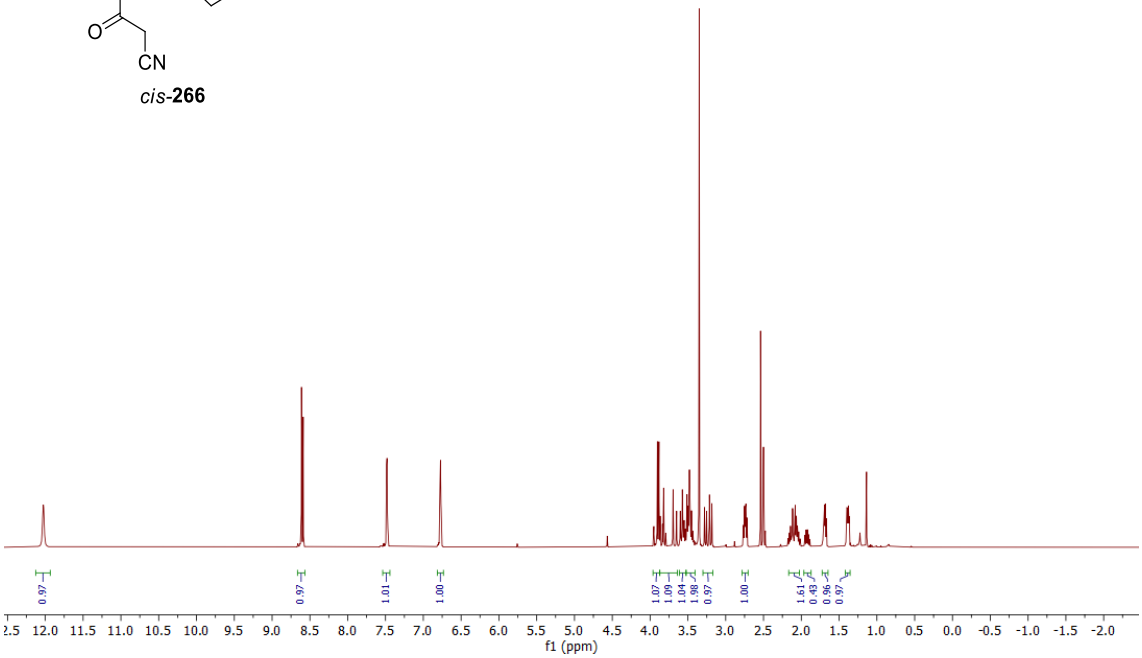

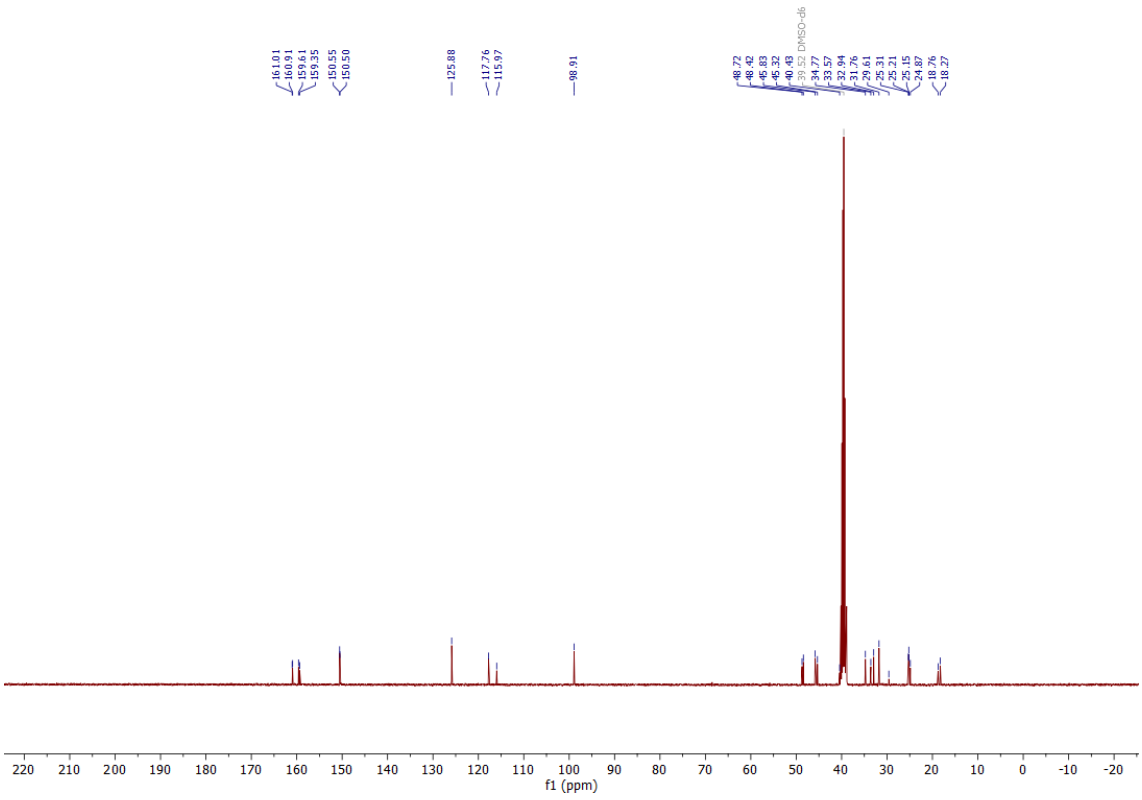

400 MHz ^{1}H NMR spectrum; 100.6 MHz ^{13}C NMR spectrum; $CDCl_3$ of *cis*-**267**

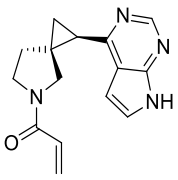

cis-**266**